FINAL REPORT
Project Activity ORD-FY04-006
Southern Great Basin Seismic Network Operations

The principal objective for Cooperative Agreement Project Activity ORD-FY04-006 was to continue the seismic monitoring of the Yucca Mountain region with networks of strong-motion and weak-motion instruments during the five-year period of the cooperative agreement (October 2003 through September 2008). Project personnel were to operate and maintain all the stations; the telemetry sites required for transmission of real-time data; and the computing facilities to collect, process and archive the seismic data. In addition, project personnel were to operate the array of nine borehole 3-component accelerometers at the pad of the north portal of the ESF and operate the 3-station ESF network.

The activity was designated *Quality Affecting* and was originally approved as a 60 month activity with a total budget of $9,117,998. However, per DOE, the workscope for this activity was transferred to a subcontract with Sandía National Laboratory 12 months prior to its originally scheduled end date. Project personnel were notified only eight weeks before the revised effective end date that the project was to be terminated prematurely. In addition, DOE's disbursements for the activity only totaled $6,198,188.10—$2,919,820.90 less than the total approved budget.

Because the activity was terminated 12 months early and experienced a 32% reduction in its overall budget, it was not possible to complete all components of the tasks as originally envisioned. However, all technical reports baselined for completion during the initial four years of the project activity were completed (table 1). Four of these technical reports have already been transmitted as qualified reports. The accompanying qualified technical report, TR-07-007, "Measurement of the Parameter Kappa, and Reevaluation of Kappa for Small to Moderate Earthquakes at Seismic Stations in the Vicinity of Yucca Mountain, Nevada," is the remaining report and constitutes the final technical report for this project activity.

In addition to these reports, the activity has produced more than one-half million data files and directories. All these files have been made available for incorporation into the Yucca Mountain Technical Data Management System (Table 2).

Table 1-Technical reports submitted from October 2003 through December 2007.

Report Number	Report Data	Title
TR-04-001	08/17/05	Initial Borehole Accelerometer Array Observations Near the North Portal of the ESF
TR-04-002	12/04/07	Seismicity in the Vicinity of Yucca Mountain, Nevada, for the Period October 1,2002 to September 30, 2003
TR-05-001	10/15/07	Seismicity in the Vicinity of Yucca Mountain, Nevada, for

		the Period October 1, 2003 to September 30, 2004
TR-07-002	11/26/07	Seismicity in the Vicinity of Yucca Mountain, Nevada, for the Period October 1,2004 to September 30, 2006
TR-07-007	12/05/07	Measurement of the Parameter Kappa, and Reevaluation of Kappa for Small to Moderate Earthquakes at Seismic Stations in the Vicinity of Yucca Mountain, Nevada

Table 2-Data submitted from October 2003 through December 2007.

NSHE DID #	YMP DTN (if assigned)	Title	Q Status	Submittal Date	Submittal size
006DV.001 Rev.2	MO0402UCC006DV.001	Earthquake catalog for the vicinity of Yucca Mountain, Nevada, for the period 10/01/2002 through 09/30/2003	Q	02/18/2004	78,497 bytes in 3 files/directories
006DV.002 Rev.2	MO0404UCC006DV.002	Focal mechanisms for earthquakes in the vicinity of Yucca Mountain, 10/01/2002 - 09/30/2003	Q	03/26/2004	4,163 bytes in 3 files/directories
006DV.003 Rev.3	MO0404UCC006DV.003	Accelerogram recordings in 2003 at three boreholes of the pad of the north portal of the ESF.	Q	03/30/2004	10,723,387 bytes in 215 files/directories
006DV.004 Rev.1	MO0404UCC006DV.004	Combined seismicity catalog for FY1996-2002 in the vicinity of Yucca Mountain.	Q	03/31/2004	463,153 bytes in 3 files/directories
006DV.005 Rev.1	MO0410UCC006DV.005	Independent Strong-Motion Site Locations	Q	10/05/2004	1,210 bytes in 2 files/directories
006DV.007 Rev.1	MO0505UCC006DV.007	Peak Ground Acceleration and Velocity for Selected 2003 Earthquakes at the ESF Pad Boreholes	Q	05/12/2005	2,845 bytes in 2 files/directories
006DV.008 Rev.0	MO0507UCC006DV.008	Hypocentral parameters for eight earthquakes used in the analysis of borehole accelerometer recordings on the pad of the north portal of the ESF.	UQ	07/08/2005	1,491 bytes in 2 files/directories
006DV.009 Rev.0	MO0507UCC006DV.009	Presumed blasts located within and near the Southern Great Basin Digital Seismic Network in the period 10/1/2003 to 9/30/2004.	UQ	07/25/2005	1,475 bytes in 2 files/directories
006DV.010 Rev.1	MO0508UCC006DV.010	Southern Great Basin Seismicity FY2004.	UQ	08/08/2005	79,458 bytes in 3 files/directories
006DV.011 Rev.2	MO0508UCC006DV.011	Hypocenters and magnitudes for earthquakes in the vicinity of Yucca Mountain, 10/1/2003 - 09/30/2004.	Q	08/22/2005	60,970 bytes in 3 files/directories
006DV.012 Rev.2	MO0508UCC006DV.012	Focal Mechanisms for Earthquakes in the vicinity of Yucca Mountain, 10/1/2003 - 9/30/2004.	Q	08/22/2005	3,474 bytes in 3 files/directories

006DV.013 Rev.2	MO0510UCC006DV.013	Southern Great Basin Digital Seismic Network (SGBDSN) waveform data for local earthquakes, 2000-2003.	Q	09/30/2005	8,295,576,392 bytes in 553,250 files/directories
006GB.001 Rev.0	MO0511UCC006GB.001	Yucca Mountain Free-Field Strong Motion Earthquake Recordings.	Q	10/20/2005	110,957,888 bytes in 5,237 files/directories
006GB.002 Rev.0	MO0601UCC006GB.002	AL5 Ratio Data: Seismic recordings of 13 magnitude 2 or larger earthquakes during 1999 at station AL5, in the Exploratory Studies Facilities (ESF) and station RPY on the ground surface above.	Q	01/09/2006	13,271,556 bytes in 260 files/directories
006GB.003 Rev.0	Pending	Seismic Attenuation Parameter Kappa and Seismic Spectral Fitting Results for Seismic Stations in the Vicinity of Yucca Mountain	Q	11/29/2007	955,629,223 bytes in 21,703 files/directories
006JL.001 Rev.1	MO0506UCC006JL.001	Preliminary Results for Refraction Microtremor Site Characterizations collected by UNR at Yucca Mountain Seismic Stations.	UQ	05/24/2005	519,876 bytes in 8 files/directories
006KS.001 Rev.0	MO0509UCC006KS.001	Vibrator Data Collected on the Pad at the Borehole UE-25 UZ #16.	UQ	09/20/2005	86,402,201 bytes in 66 files/directories
006KS.002 Rev.0	MO0711UCC006KS.002	Earthquake locations and magnitudes in the vicinity of Yucca Mountain, 10/1/2004 - 09/30/2006	Q	11/15/2007	92,994 bytes in 3 files/directories
006KS.003 Rev.0	MO0711UCC006KS.003	Presumed blasts located within 65 km of Yucca Mountain recorded on the Southern Great Basin Seismic Network, 10/1/2004 - 09/30/2006	UQ	11/15/2007	1385 bytes in 2 files/directories
006KS.004 Rev.0	MO0711UCC006KS.004	Presumed blasts recorded on the Southern Great Basin Seismic Network, 10/1/2002 - 09/30/2003	UQ	11/20/2007	1,087 bytes in 1 files/directories
000KS.001 Rev. 1	MO0507UCC000KS.001	Subset of 1996-1997 UE-25 UZ #16 Borehole Seismic Recordings.	UQ	07/14/2005	3,466,705 bytes in 161 files/directories

TECHNICAL REPORT

Measurement of the Parameter Kappa, and Reevaluation of Kappa for Small to Moderate Earthquakes at Seismic Stations in the Vicinity of Yucca Mountain, Nevada

Report Document Identifier:
TR-07-007
Task ORD-FY04-006

REVISION: 0

Originators:

Glenn Biasi, Nevada Seismological Laboratory

John G. Anderson, Nevada Seismological Laboratory

Approvals:

John G. Anderson, Principal Investigator — Approval Date: 12/5/2007

Amy Smiecinski, QA Manager, NSHE — Date: 12/5/07

EXECUTIVE SUMMARY

We address two primary questions. First, what are the values of seismic spectral decay parameter *kappa* at stations on and around Yucca Mountain. Second, can small and/or moderate earthquakes provide estimates of *kappa* that are valid for conditions of strong ground motion.

To address the first question we measured *kappa* for earthquake recordings of the Southern Great Basin Digital Seismic Network (SGBDSN) weak- and strong-motion stations. Over a period of approximately 7 years, 39 events triggered one or more stations of the permanent strong-motion network around Yucca Mountain. Weak-motion telemetered station data were gathered for these events and combined into a common database containing approximately 2400 interpretable recordings. Weak motion sensors have a 1-Hz free period, but were corrected for sensor response before fitting. Data from portable station recordings co-located with the permanent strong-motion network were also included to assess the ability of smallest earthquakes to measure *kappa* from the slopes of displacement spectra at low frequencies. Spectra were developed and fit using the qualified software package *kappaAH* (STN-UCCSN-003). The software creates tables containing results of individual spectral fits suitable for parametric study and plotting.

Qualified: New analyses of M2 to M4.7 earthquakes recorded with the SGBDSN provide estimates of *kappa* in the Yucca Mountain area. Our preferred estimates of *kappa* are found by treating *kappa* as a station constant out to an epicentral distance of 40 km. Station *kappa* estimates fall in a range generally ~20 to 40 msec, with a few distinct exceptions. The mean *kappa* at station RPY directly above the ESF is 39.7 msec. The mean of five SGBDSN stations on rock of Yucca Mountain itself is 30.4 msec. The mean kappa over all stations of the SGBDSN for which we have estimates is 24.9 msec.

Qualified: We explored two models of *kappa* variation with distance. The first model, where the *kappa* correction is linear from the origin to the recording station, strongly over-corrects station *kappa* estimates. Many stations would have unphysical, negative values, and predict positive high-frequency terminal slopes in spectral amplitude. The second model uses a bi-linear correction, with zero distance correction out to 40 km and a positive correction at greater distances. This model slightly improves the fit on a statistical basis, but also leads to improbable distance correction. The poor improvement appears to be caused by a high degree of irregularity in spectral roll-off with distance. As a tentative explanation of the lack of distance dependence out to ~40 km, we suggest that seismic energy from sources at typical earthquake depths stays in mid-crustal layers and consists primarily of direct and lightly scattered arrivals that have propagated in mid-crustal layers. Beyond ~40 km there is a clear trend toward increasing *kappa* values due to scattering and surface-wave processes, but the effects are highly variable. We also find that displacement slope *kappas* (*kds*) from earthquakes near M1 are biased, apparently by corner frequency effects. Displacement slope *kappas* from M<0.25 events appear to provide an approximate upper bound on *kappa* estimates.

Kappa estimates at individual stations strongly suggest a source contribution to *kappa*. Site measurements vary by 20 msec for events with very similar distances and back-azimuths. Were *kappa* purely a site effect, this variability should be much less. The conclusion that source terms contribute to *kappa* is reinforced by results of formal inversion by chi-squared significance ratios and by inspection of plots of fitting parameters. The source term is seen by comparing events in terms of their mean *kappas* over observing stations. Event mean *kappas* vary by ±10 msec around a mean of 27 msec. Event variations around this mean are used to correct station *kappa* estimates and develop our best estimate station *kappas.*

Unqualified: We analyzed a separate set of earthquake recordings from portable seismographs deployed shortly after the Little Skull Mountain (LSM) earthquake in 1992. These data were previously analyzed by Su et al. (1996) and by Anderson and Su (MOL.20071203.0134). Their results were influential in the YM Probabilistic Seismic Hazard Analysis (PSHA) because they were the only data at the time from which to estimate *kappa* in the Yucca Mountain area. Eighteen earthquakes with magnitudes from 2.5 to 4.5 were reanalyzed with *kappaAH.* We find similar, although somewhat higher values of *kappa*, with an average of 26.9 msec for the four stations actually on Yucca Mountain itself. This estimate is 11 msec greater than the most closely corresponding Anderson and Su (MOL.20071203.0134) case. Much of the difference in estimates traces to the aggressive distance correction applied by Anderson and Su (MOL.20071203.0134).

Unqualified: We also applied *kappaAH* to accelerograph records from the Blume strong motion network recordings of the Little Skull Mountain M5.6 mainshock and two M4+ aftershocks. These records are especially important for Yucca Mountain PSHA because they record the strongest ground motions of anywhere near the project area. The strongest Blume network shaking was recorded at the Lathrop Wells station (LWLB). This station was reoccupied as SGBDSN strong-motion station LWLS. This station thus provides a connection between the SGBDSN and the important Blume Lathrop Wells recording. Using 21 horizontal component LWLS recordings we find an average *kappa* of 34.3 msec, with a standard error of the mean of 1.8 msec. The mean of the four Blume accelerograms with stress drops below 300 bars (35.8 msec) are consistent with this value. Thus the limited data available tend to confirm that *kappa* estimates at M2 to M4.3 are similar to *kappa* estimates at M5.6. *Kappa* estimates at Blume station Control Point (CPTB) are distinctly lower than LWLB, despite the station epicentral distances being ~20 km greater than to the Lathrop Wells station.

Unqualified: As our primary approach to the second question of whether *kappa* estimates from M 3.5-5.0 records predict *kappa* values for larger earthquakes we analyzed a large set of Japanese data from the KiK-Net borehole array. We find mean *kappas* estimated from ensembles of M3.5 earthquakes generally predict *kappa* as measured from very strong (>500 gal peak ground acceleration) ground motions. This result is significant for Yucca Mountain ground motion predictions because it tends to confirm that *kappa* can be measured from moderate earthquakes and applied to large earthquakes and strong ground motions.

1.0 TABLE OF CONTENTS

EXECUTIVE SUMMARY…….. 2
1.0 TABLE OF CONTENTS……. 4
1.1 LIST OF FIGURES…….. 6
1.2 LIST OF TABLES…… 8
2.0 PURPOSE……. 9
3.0 QUALITY ASSURANCE…… 10
4.0 INTRODUCTION…… 11
5.0 METHODS AND MATERIALS…… 13
5.1 SEISMIC SPECTRAL MODELS AND METHODS OF ESTIMATING KAPPA 13
5.1.1 SPECTRAL MODELS AND KAPPA……. 13
5.1.2 NUMERICAL EVALUATION OF KAPPA……. 17
5.1.3 COMMENTS ON THREE-PARAMETER SPECTRAL ESTIMATION OF KAPPA…….. 17
5.1.4 DATA SELECTION BIAS……. 18
5.1.5 SMALL EVENT KAPPA ESTIMATES AND THE DISPLACEMENT KAPPA METHOD…… 18
5.2 INSTRUMENTATION AND DATA…… 19
5.2.1 SOUTHERN GREAT BASIN DIGITAL SEISMIC NETWORK…… 19
5.2.2 PORTABLE SEISMIC NETWORK, WEAK-MOTION RECORDINGS AT STRONG-MOTION SITES……. 20
5.2.3 LITTLE SKULLMOUNTAIN AFTERSHOCK PORTABLE NETWORK DEPLOYMENT…… 20
5.2.4 BLUME STRONG-MOTION NETWORK……. 21
5.3 RESULTS …… 22
5.3.1 SGBDSN SPECTRAL FITTING RESULTS…… 22
5.3.1.1 OVERVIEW OF SGBDSN CONFIGURATION AND FITTING… 22
5.3.1.2 FORMAL INVERSION MODEL FOR KAPPA RELATED TO SITE, DISTANCE AND SOURCE…… 23
5.3.1.3 STATION KAPPA ESTIMATES…… 26
5.3.1.4 SGBDSN M3 EARTHQUAKE SET STRESS DROPS AND CORNER FREQUENCIES……. 29
5.3.1.5 BEST ESTIMATE RESULTS COMPARED WITH FORMAL INVERSION …… 30

5.3.1.6 CONSIDERATION OF THE SILVA(F) AND Q(F) FUNCTIONS…30

5.3.2 PORTABLE STATION RECORDINGS OF LITTLE SKULL MOUNTAIN AFTERSHOCKS (UQ) …… 31

5.3.2.1 OVERVIEW OF THE LSM AFTERSHOCK ANALYSIS (UQ)… 31

5.3.2.2 LSM EARTHQUAKES: KAPPA, STRESS DROP, AND CORNER FREQUENCIES (UQ)……. 31

5.3.2.3 LSM STATION KAPPA ESTIMATES (UQ)…… 32

5.3.3 BLUME STRONG-MOTION NETWORK RESULTS (UQ)……. 32

5.3.3.1 OVERVIEW OF THE BLUME DATA ANALYSIS (UQ)……. 32

5.3.3.2 BLUME NETWORK EARTHQUAKES: KAPPA, STRESS DROP, AND CORNER FREQUENCIES (UQ)…….. 32

5.3.3.3 BLUME NETWORK STATION RESULTS (UQ)…….. 33

5.3.4 DEPENDENCE OF KAPPA ON MAGNITUDE FROM THE KIK-NET BOREHOLE DATA (UQ)……. 34

6.0 ASSUMPTIONS…… 35

7.0 DISCUSSION AND CONCLUSIONS…… 36

7.1 DISCUSSION: SGBDSN STATION MEASUREMENTS AND YUCCA MOUNTAIN APPLICATIONS…… 36

7.2 CONCLUSIONS BASED ON Q DATA…… 37

7.3 CORROBORATION FROM LSM, BLUME, AND KIK-NET ANALYSIS (UQ) 38

8.0 INPUTS AND REFERENCES…….. 39

8.1 Q INPUTS……. 39

8.2 NON-Q INPUTS……. 40

8.3 REFERENCES……. 40

9.0 SOFTWARE……. 42

10.0 ATTACHMENTS……. 43

TABLES……. 44

FIGURES…… 64

11.0 APPENDICES…….. 156

1.1 LIST OF FIGURES

Figure 5.1.1 Definition of *kappa* (from Anderson and Hough, 1984). (Unqualified)… 64

Figure 5.1.2 Model Fourier spectra of large and small earthquakes, showing intervention of corner frequency. (Unqualified)…….…… …… 65

Figure 5.1.3 (a, b, c). Explanation of *kappaAH* fitting plots. Captions are in the form of notes on the figures. (Unqualified) …… 66

Figure 5.2.1 Map of stations used in this study, in the vicinity of Yucca Mountain. (Qualified) ……. 69

Figure 5.2.2 is a detail of the central portion of Figure 5.2.1 near the ESF. The vertical line down the center of the figure is the Nevada Test Site boundary. (Qualified) ……. 70

Figure 5.2.3 Epicenters of SGBDSN "M3" earthquakes used in this study. Note the relatively good azimuthal coverage of well-recorded earthquakes. (Qualified)……. 71

Figure 5.2.4 Epicenters and station coverage from the Little Skull Mountain aftershock portable deployment. (Unqualified) …… 72

Figure 5.2.5 Epicenters and station coverage of the Blume strong-motion data set. (Unqualified)….. ……. 73

Figures 5.3.1.1-6 Example spectral fits for station CAF, *Case6a*. (Qualified)……. 74

Figures 5.3.2 (a) Event average *kappa* (solid) and average from event-station records less than 40 km. (dash) for each earthquake in the M3 set. The dashed line shows basis for event correction later. (b) *Kappa* measurements by event for the M3 set. *Case6a*. (Qualified) …… 80

Figure 5.3.3.1-37 Individual station summary plots for the M3 event set. *Case6a*. (Qualified) …….. 81

Figure 5.3.4.1-5 Stress drop is plotted versus corner frequency for SGBDSN M3 events, (Table 5.2), *Case6a*. Star symbol for event-station epicentral distances less than 40 km. (Qualified) ……. 118

Figure 5.3.5 Best estimate station *kappa* estimates shown with three sets of formal inversion results. (Qualified). …… 123

Figure 5.3.6 Base case station *kappa* and *kappa* if the *Silva(f)* and *Q(f)* functions are used. (Qualified) …… 124

Figure 5.3.7.1-12 Individual station plots for the LSM portable deployment. (Unqualified) …… 125

Figure 5.3.8 (a) Per-event average *kappa* and average from event-station records less than 40 km. (b) *Kappa* measurements by event for the LSM aftershocks. (Unqualified).. 137

Figure 5.3.9.1-2 Stress drop is plotted versus corner frequency for LSM aftershocks. Star symbol for event-station epicentral distances less than 40 km. (Unqualified)…….. 138

Figure 5.3.10 Comparison of *kappaAH* and Anderson and Su (MOL.20071203.0134) estimates. (Unqualified). …… 140

Figure 5.3.11.1-6 Blume station LWLB spectral fitting (Unqualified) ……... 141

Figure 5.3.12.1-4 Blume station CPTB spectral fits. (Unqualified). ……... 147

Figure 5.3.13 Blume network estimates of stress drop vs. corner frequency for the LSM mainshock and two aftershocks. Star symbol for event-station epicentral distances less than 40 km. (Unqualified). …… 151

Figure 5.3.14.1-3 Individual station plots for three Blume strong-motion network stations. (Unqualified) …… 152

Figure 5.3.15 (Upper) Acceleration slope *kappa* vs. *kappa* from *kappaAH* for three events recorded by the Blume strong-motion network. The general correspondence of the two is clear, although slope *kappas* are approximately 15% higher. (Lower) Stress drop vs. *kappa* for the three Blume strong-motion network recordings. (Unqualified)……. 155

APPENDIX B FIGURES

Figure B.1-72. Station parametric plots. Two plots per station, first with unconstrained stress drop, then with stress drop constrained to 45 bars. Spectral fits are shown only if the upper 95% bound on corner frequency is resolved. “Fail High Corner” value shows the number of spectral fits excluded. (Qualified) ……. 161

LIST OF TABLES

Table 5.1 Station Locations of the SGBDSN …… 44

Table 5.2 Earthquake Locations of the SGBDSN "M3" Data Set …… 47

Table 5.3 Earthquake Locations Recorded by a Portable Network at SGBDSN Strong Motion Sites …… 48

Table 5.4 Little Skull Mountain Portable Station Locations (UQ) …… 49

Table 5.5 Little Skull Mountain Portable Network Earthquake Locations (UQ)… 50

Table 5.6 Blume Strong Motion Network Station Locations (UQ) ……... 51

Table 5.7 Blume Strong Motion Seismic Network Earthquake Locations (UQ)….. 51

Table 5.8 Models tested in formal inversions to characterize the site, event, and distance dependence of *kappa* …… 52

Table 5.9 Improvements in fit for models in formal inversions. …… 53

Table 5.10 SGBDSN station parameter estimates for formal inversion models, *Case6a*. 54

Table 5.11 SGBDSN event terms for formal inversion models, *Case6a* …… 55

Table 5.12 SGBDSN event mean *kappa* and *kappa* for station-event distances less than 40 km, *Case6a* …….. 56

Table 5.13 SGBDSN event mean stress drop, corner frequency, and kappa, *Case6a* … 57

Table 5.14 SGBDSN station kappa estimates, *Case6a* …….. 58

Table 5.15 LSM network event mean *kappa* and *kappa* for station-event distances less than 40 km, *Caselsm4*, (UQ) …… 59

Table 5.16 LSM network event mean stress drop, corner frequency, and *kappa, Caselsm4* (UQ) …… 60

Table 5.17 LSM network station *kappa* estimates, *Caselsm4* (UQ)…… 61

Table 5.18 Blume strong motion network, LWLB and CPTB fitting parameters. (UQ) 62

Table 5.19 Blume network event mean stress drop, corner frequency, and *kappa* (UQ) 63

Table A-1, *KappaAH* input parameter list and example settings…… 157

2.0 PURPOSE

Seismic spectral decay can be characterized by a parameter *kappa*. It is normally associated in engineering practice with near-surface attenuation and scattering processes. *Kappa* is a key input parameter for adjusting ground motions from the Probabilistic Seismic Hazard Assessment. Presently that input is based mainly on an analysis of portable seismic network recordings of Little Skull Mountain aftershocks. In this report we expand the analysis to include data recorded by the permanent seismic network around Yucca Mountain. We address two primary questions.

(1) What are the values of seismic spectral decay parameter *kappa* at stations on and around Yucca Mountain.

(2) Can small and/or moderate earthquakes provide estimates of *kappa* that are valid for conditions of strong ground motion.

The project scope is to include available waveforms from the SGBDSN and any relevant collateral data. Discussions among the investigators identified as of potential use collateral portable network recordings, the previously analyzed LSM aftershock deployment data, and the Blume recordings of the LSM mainshock and aftershock strong ground motions. To investigate the dependence of *kappa* on earthquake magnitude data from the Kiban-Kyoshin Strong-Motion Network (KiK-Net) in Japan was best suited.

3.0 QUALITY ASSURANCE

This report is written in accordance with NSHE Quality Assurance program procedures, including:

QAP 3.0, Scientific Investigation Plan

QAP 3.2, Software Management

QAP 3.4, Technical Reports

QAP 3.1, Control of Electronic Data

Work on this project has been controlled under Scientific Notebook UCCSN-UNR-047, Vol. 1, "Improve the Physical Understanding of the Parameter *Kappa*" (MOL.20040323.0140) and Scientific Notebook UCCSN-UNR-097, Vol. 1. Fitting results for all spectra are included in the electronic media supplement of that notebook.

No conclusions of this Report are based on unqualified data.

4.0 INTRODUCTION

The parameter *kappa* was defined by Anderson and Hough (1984) to describe the high-frequency spectral roll-off of the strong motion seismic spectrum. In the work of Su et al., (1996) the numerical value of *kappa* estimated for sites near Yucca Mountain was small (~20 ms). The estimate obtained from these events has been applied through a rigorous methodology to develop design earthquake spectra with magnitude over 5.0. Smaller values of *kappa* lead to higher estimated ground motions in the methodology used by the Probabilistic Seismic Hazard Analysis (PSHA) for Yucca Mountain. An increase of 10 ms in *kappa* could result in a substantial decrease in the high frequency level of the predicted ground motions. Any parameter that plays such a critical role deserves close examination. Here, we study *kappa* and its associated uncertainties.

The data set used by Su et al (1996) consisted of 12 M 2.8 to 4.5 earthquakes recorded at temporary stations deployed after the June 1992 Little Skull Mountain earthquake. The *kappa* elements of that study were revisited by Anderson and Su (MOL.20071203.0134) and substantially confirmed. One weakness of those studies is the limited data used. Few of these stations were on tuff or on Yucca Mountain itself. A decade of Southern Great Basin Digital Seismic Network (SGBDSN) recording has now yielded a larger body of on-scale, well calibrated digital ground motion records suitable for investigating *kappa*. We use the SGBDSN data to check some of the original assumptions, improve the statistical confidence of the conclusions, and determine values of *kappa* for stations on or near Yucca Mountain.

The outstanding issues in *kappa* analysis, as they apply to Yucca Mountain, include:

1. The number itself. The *kappa* estimate near 20 msec from Su et al. (1996) and Anderson and Su (MOL.20071203.0134) is markedly smaller than is considered typical in California (Silva, 1995). The low *kappa* value has engineering consequences because when it is applied in ground motions analyses used in PSHA, it contributes to the extreme values of peak ground acceleration that the PSHA predicts. Also, in some areas precarious rock evidence indicates that no such accelerations have occurred.

2. The disagreement among analyses in the value of *kappa*. Previous reports indicate that smallest earthquakes yield *kappa* estimate 12-20 msec larger than average values from M3 to M4.5 aftershocks of Little Skull Mountain earthquake.

A critical assumption in most *kappa* models is that *kappa* characterizes seismic wave attenuation. If true, one should be able to measure *kappa* from earthquakes of any magnitude, but this has not been confirmed. Part of the reason is that the measurement is complicated by the corner frequency of the seismic spectrum, which falls within the frequency band where *kappa* is measured for events in the magnitude range from about M~2 to M~5. When Biasi and Smith (2001) measured *kappa* from the low frequency slopes of displacement spectra of M<1.0 earthquakes,

values from 22-56 ms for rock sites in the YM region. The studies of M2.6 to 4.5 earthquakes by Su et al. (1996) and Anderson and Su (MOL.20071203.0134) found mean estimates at YM stations of 20 msec or less. If the methods are equivalent, the differences might be attributed to different sets of stations, but many stations include stations sited on Yucca Mountain tuffs. Another difference is that Biasi and Smith assume that the corner frequencies of small earthquakes are above the measuring band (>25 Hz), or equivalently that their stress drops are similar in magnitude to those of larger earthquakes. Ide and Beroza (2001) lend indirect support to this assumption in their study showing that the stress drop of extremely small earthquakes is comparable to, and not orders of magnitude smaller than, stress drop for moderate to large earthquakes . However, the discrepancy between small and moderate earthquake *kappa* estimates remains unexplained.

3. The source of *kappa*. Classically and in engineering usage, *kappa* is attributed largely to the upper tens or hundreds of meters at the recording site. However, borehole recordings imply that a significant contribution to *kappa* originates below several hundred meters depth. Also, when earthquakes are considered from a small source region, a true site effect should be common to all recordings. In fact *kappa* observations of LSM aftershocks to stations on Yucca Mountain and at network stations appear to vary greatly, as though much of *kappa* actually derives from near the seismic source.

4. The repository overburden contribution to *kappa*. PSHA estimated ground motions to a free surface at 300 meters depth with properties of confined rock at that depth. Rock mechanical and borehole estimates suggest that several milliseconds of the total *kappa* accrue between 300 meters to the surface. If estimates of *kappa* are small at the surface, little is left to reduce incident ground accelerations from the seismic source to the repository level.

5. The variability of *kappa*. In most cases parametric estimates of *kappa* have some range of values that fit the data equally well in a statistical sense, so errors in *kappa* estimates must be addressed. As noted above, *kappa* at a station also varies significantly for events from the same source area.

6. Are *kappa* values from small to moderate magnitude earthquakes appropriately applied to the larger, potentially damaging earthquakes of engineering concern? Put another way, is there a significant magnitude dependence in *kappa*?

Questions 1 and 6 are of primary importance, but we find answers to several others in the course of our study.

Data from southern Nevada are capable of resolving only some of these questions. In a global search, we identified data from the Japanese borehole accelerometer array KiK-Net as most likely to address the questions of the shallow site structural contribution to *kappa* and the usefulness of moderate earthquake *kappa* estimates to predict strong ground motion.

5.0 METHODS AND MATERIALS

5.1 Seismic Spectral Models and Methods of Estimating *Kappa*

5.1.1 Spectral Models and *Kappa*

This section briefly reviews some of the main issues and methods for estimating *kappa*. *Kappa* was originally defined as an observational parameter describing the asymptotic high-frequency slope of large earthquake accelerograms (Anderson and Hough, 1984), as shown in Figure 5.1.1. This paper measured *kappa* in the frequency range 2 Hz < f < 12 Hz. This approach placed no assumptions on the source spectrum, the attenuation structure, or the site, but could be defined only for acceleration spectra from earthquakes that were large enough that an asymptote could be observed at frequencies higher than the corner frequency (limiting the low-frequency end of the band) and above the instrumental noise (limiting the high-frequency end of the band). A distance dependence on the *kappa* estimate was recognized, and attributed to attenuation (Q) effects.
A more complete model seismic spectrum *M(f)* may be modeled by seismic moment M_0, corner frequency f_0, and *kappa* κ:

$$M(f,r) = \left(\frac{\Phi M_0}{4\pi\rho\beta^3 r}\right)\left(\frac{(2\pi f)^\gamma}{1+\left(\frac{f}{f_0}\right)^2}\right)\exp\left(-\pi\kappa\ f\right) \qquad \text{(Equation 1)}$$

Φ is the average radiation pattern (0.85), β is the shear wave velocity at the source (350000 cm/sec), r is the hypocentral distance (cm), and ρ is the rock density at the source (2.6 gm/cm^3), and f is frequency in Hz. Variable *gamma* is set according to the data type, with γ = 0, 1, or 2 for displacement, velocity, or acceleration spectra, respectively. Corner frequency f_0 is an observational frequency parameter of seismic spectra related to the size of the fault rupture area and the time over which the rupture lasts. The Anderson and Hough (1984) estimate of *kappa* assumes, in effect, that γ=2 and the f_0 contribution can be neglected. Figure 5.1.2 shows that as the corner frequency increases attenuation effects cannot be neglected (Hanks, 1982; Anderson, 1986). In particular, the separate curvatures caused by f_0 and κ merge and the method of Anderson and Hough can no longer be used.
To estimate *kappa* from smaller earthquakes, Anderson and Humphrey (1991, abbreviated "AH-91") proposed that *kappa* be identified with the residual slope of an acceleration spectrum after removing a Brune-model source spectrum (the left two terms in Equation 1). When the earthquake source spectrum follows this shape, the AH-91 *kappa* definition is equivalent to the simple slope definition of Anderson and Hough (1984).

We solve for $M_{0'}$ and κ by least-squares fitting the observed spectrum to a version of Equation (1) at frequencies f_i:

$$\ln\left[M\left(f_i, r\right)\right] = \ln\left(M_0\right) + \ln A_0 - \pi\kappa \quad f_i + \ln\left(\frac{\left(2\pi f_i\right)^{\gamma}}{\left(1+\left(\frac{f_i}{f_0}\right)^{2}\right)}\right) \qquad \text{(Equation 2)}$$

This equation is linear in M_0 and κ if f_0 is known or assumed. A solution is found by trying a range of corner frequencies, solving for M_0 and κ assuming the trial f_0, and choosing the corner frequency that minimizes the squared error. In this formula, A_0 represents the several elements in the first square brackets of Equation 1, and γ is set according to the data type. The squared error of the fit is

$$E^2\left(f_0\right) = \frac{1}{NF}\sum_{i=1}^{NF}\left[\ln\left(A\left(f_i\right)\right) - \ln\left(M\left(f_i\right)\right)\right]^2 \qquad \text{(Equation 3)}$$

where *A(f)* is the S-wave spectrum estimated from the seismic time series and *NF* is the number of frequency bins in the spectrum.

Anderson and Hough (1984) recognized a site and distance dependence to *kappa*, which Anderson (1991) later generalized as:

$$\kappa = \kappa_0 + \tilde{\kappa}\left(R\right) \qquad \text{(Equation 4)}$$

where $\tilde{\kappa}\left(R\right)$ is a generalized distance-dependent shape depending on epicentral distance, and κ_0 is a site term that is unique for each site.

The AH-91 method was employed by Su et al. (1996) and Anderson and Su (MOL.20071203.0134). They modeled the observed values of κ with an approximate separation of site and distance related contributions to *kappa*:

$$\kappa = \kappa_0 + r\kappa_r \qquad \text{(Equation 5)}$$

In Equation 5, the general distance dependence in Equation 4 is approximated with a linear slope term κ_r and r is, in their studies, the hypocentral distance. The data in both studies came from portable seismographic stations around Little Skull Mountain from aftershocks shortly following the Little Skull Mountain earthquake. The use of the hypocentral distance instead of the epicentral distance was a decision that they used to adapt to data with predominantly short epicentral distances. This reduces all site *kappa* estimates by at least as much as κ_r times the average focal depth compared to the model proposed by Anderson (1991). The distance coefficient estimates κ_r = 0.53 msec/km and 0.69 msec/km from Su et al. (1996) and Anderson and Su (MOL.20071203.0134), respectively, correspond to a transfer of 5 to 9 msec from the site term to path effects. The κ_r estimates correspond to shear-wave quality factors Q_s of 54 and 41, respectively. Of significance to the project, the

only accepted estimates for engineering application at Yucca Mountain have come from these studies.
A related approach to estimating *kappa* from the acceleration spectrum of moderate-sized earthquakes has been proposed by Walt Silva. The modified equation is:

$$M(f,r) = S(f)\left(\frac{\Phi M_0}{4\pi\rho\beta^3 r}\right)\left(\frac{(2\pi f)^2}{1+\left(\frac{f}{f_0}\right)^2}\right)\exp\left(\frac{-\pi R f}{Q(f)\beta}\right)\exp(-\pi\kappa\ f) \qquad \text{(Equation 6)}$$

Function *S(f)* is intended to model the effects of shallow velocity layering on spectra. Dr. Silva estimates *S(f)* as a piecewise linear function that is smoothed from a calculated transfer function for a generic velocity model. The function *S(f)* can be defined separately for different regions and different surficial geologies. The model for the Yucca Mountain region used by Silva can be approximated reasonably by a fifth-order polynomial (Anderson and Su, MOL.20071203.0134). The term $\exp\left(\frac{-\pi R f}{Q(f)\beta}\right)$ is in the classic form of a distance correction for attenuation. For consistency with ground-motion modeling and the Yucca Mountain Probabilistic Seismic Hazard Analysis, $Q(f)=250f^{0.4}$. This term is intended to remove distance-related attenuation from A_0 (of Equation 2), so as to isolate the near-site spectral roll-off into parameter κ. While *S(f)* and *Q(f)* do address recognized non-site-specific attenuation sources, their use changes *kappa* from a simple observational property of the spectra to one that depends the particular values of *S(f)* and *Q(f)*. Furthermore, these functions can be regional variables, and thus values of *kappa* estimated by this method are subject to additional uncertainties deriving from uncertainties in *S(f)* and *Q(f)*.

Frequency-dependent site effects beyond the regional average *S(f)* are not considered in any models used in this report. Humphrey and Anderson (1992) and Su et al (1996) considered site effects as the average of residuals from Equation 1, and found that these residuals match the spectral amplifications determined from more traditional methods of estimating site response.

A related means of estimating *kappa* beginning from the displacement spectral version of Eqn 1 was proposed by K. Smith and applied by Biasi and Smith (2001). Taking the natural log of Equation 1 with γ = 0 and slightly rearranging,

$$\ln\left(M_d(f_i)\right) = \ln(M_0) + \ln\left[\frac{\Phi}{4\pi\rho\beta^3 R}\right] - \pi\kappa\ f - \ln\left[1+(f_i/f_0)^{\alpha}\right] \qquad \text{(Equation 7)}$$

A key property of this equation is that, for low enough frequencies relative to f_0, the term f_i/f_0 is small, making the spectral slope independent of the particular value of α. The

advantage of this approach is that, while $\alpha=2$ is a reasonable average, its value is unknown for any particular earthquake. Modeling by Madariaga (1976) suggests $1<\alpha<3$ as a realistic range for α. The key problem for the displacement slope method in Equation 7 is that *kappa* is overestimated in proportion to the corner-frequency contribution (from Equation 7, by $ln[1 + (f_i/f_0)^{\alpha}]$). When corner frequencies are sufficiently high that the last term in Equation 7 can be neglected, the least-squares fitting problem becomes:

$$\ln\left(M_d\left(f_i\right)\right) = \ln\left(M_0\right) + \ln\left[A\right] - \pi\kappa \; f \qquad \text{(Equation 8)}$$

Thus if $f<<f_0$, *kappa* may be estimated from the slope of the observed displacement spectrum. This condition might be met by small earthquakes having stress drops of tens of bars or more provided that they are recorded with sufficient bandwidth and signal-to-noise ratios. The Southern Great Basin Digital Seismic Network routinely records small earthquakes with clear shear-wave arrivals. Biasi and Smith (2001) applied the small earthquake method to SGBDSN data to estimate *kappa* at permanent and some portable seismic stations around Yucca Mountain. Corner frequency effects on *kappa* estimates from small earthquakes are explored quantitatively in a later section.

A key objective of this report is to attempt to reconcile the two main attempts to estimate *kappa* for engineering use at Yucca Mountain. *Kappa* values from Biasi and Smith (2001) average 36 msec on and around Yucca Mountain, and contrast significantly with the <20 msec average value from Anderson and Su.

The differences among spectral models in Equations 1, 6, and 8 highlight the fact that all *kappa* estimates are made relative to some model of spectral shape. Equation 1 measures *kappa* relative to the simple omega-squared model of Brune (1970), so distance dependence and velocity model effects are assigned primarily to *kappa*. Equation 6 allocates known velocity structure effects to *S(f)* and distance dependence to *Q(f)*. *Kappa* is measured relative to the omega-squared model after these factors have been removed, and thus is a different quantity from an estimate made from the same spectrum using Equation 1. The model expressed in Equation 8 is that corner-frequency contributions can be neglected – effectively an infinite corner-frequency approximation. Thus *kappa* is just the slope of the spectrum in a certain window (here, 5-25 Hz), but it still includes distance and velocity structure effects. The analogous zero Hz corner-frequency approximation is acceleration slope *kappa* estimate of Anderson and Hough (1984). Among the models discussed above the value of *kappa* differs numerically and in its detailed meaning. Other models might be proposed, dividing the distance, site, velocity, and path effects differently, or combining them in different ways. To maintain a definition of *kappa* based on the shape of the spectrum itself we proceed with the Anderson-Humphrey (1991) model, and measure *kappa* as the slope of the residual assuming an f^2 source spectral roll-off.

5.1.2 Numerical evaluation of *kappa*

Glenn Biasi, with assistance primarily from Debi Kilb of UCSD, developed computer code *kappaAH* (*kappaAH v1.0*, STN-UCCSN-003) to measure *kappa* and other relevant parameters and provide simple presentations of results. The code is written using the *MATLAB* programming language. The code is tailored to process data stored in a Center for Seismic Studies (CSS) 3.0 database, a widely known standard that is also integral to the Antelope Real-Time System. This system is used by the Nevada Seismological Laboratory to gather and process Southern Great Basin Digital Seismic Network data and to merge it with other stations not involved in Yucca Mountain seismic monitoring. The main elements of the processing method are presented in Appendix A.

A sample output figure from *kappaAH* (Figure 5.1.3a, b, c) presents several sub-plots that together summarize the basic analysis of a single seismogram. *KappaAH* computes signal spectra for windows around analyst-identified S-wave arrivals, and computes noise spectra from an equal time length in the pre-P-arrival portion of the time series. From these it estimates spectral fitting and slope parameters and a signal-to-noise ratio. For each seismogram we consider, a figure like Figure 5.1.3a is created. To ensure traceability and uniformity, all figures are automatically generated and each fitting result is assigned a unique identification number called a *fitid*. Each plot also shows the relevant configuration parameters of the spectral fit so these details cannot be separated from the parametric results. Criteria such as signal-to-noise ratio can be used at a later stage to decide which parametric estimates are included in station and event summaries. Further details of the analysis, and the definition of the various parameters, are presented in Figures 5.1.3a-c and in Appendix A.

5.1.3 Comments on Three-Parameter Spectral Estimation of *Kappa*.

The precision with which one may identify the "best fit" values of *kappa*, f_0, and M_0 using Equations 1 and 2 using the AH method can be greater than numerical models of noise and spectra warrant. That is, while a unique minimum may be found, in general a range of those values will be expected to fit the observed spectrum well enough that they cannot be rejected. If the misfit of *ln(A(f))* around *ln(M(f))* can be modeled by a normal distribution, then the normalized squared error E^2 (Equation 3) can be modeled by a chi-squared distribution with *NF-3* degrees of freedom. Standard tables of the chi-squared distribution give test values for various levels of confidence beyond which improvements in fit cannot be considered significant. These are the basis for the confidence bounds identified in Figure 5.1.3.

Numerical exploration of the AH fitting method had two notable aspects. First there is normally a fairly large range of corner frequency and *kappa* must be allowed if one uses the chi-squared estimates of the confidence intervals. The width of this interval increases with corner frequency, and thus with decreasing magnitude. There is also a steep tradeoff

between corner frequency and *kappa*, (e.g., Figure 5.1.3a, center-right), that can cause any systematic underestimation of corner frequency to map into an underestimate of *kappa*. In the fitting of Figure 5.1.3, as measured by the squared error, the *kappa* and corner frequency confidence bounds are not independent. Pairs with equivalent squared error allowed by the chi-squared test on E^2 form a elliptical or "banana-shaped" contours. . Plots isolating uncertainties in *kappa* or corner frequency alone neglect this correlation and if considered separately could suggest pairs that the data would not allow.

5.1.4 Data Selection Bias

Valid spectra that do not exhibit a minimum misfit for reasonable f_0 values might be discarded as null measurements. However, the do provide a lower bound on f_0 and thus on *kappa*. If excluded, the remaining records will be the fraction with smaller values of corner frequency and *kappa*, and thus will bias the overall results to smaller values. Fortunately the sampling bias effect is weakest on the largest and best-recorded events in the Little Skull Mountain aftershock data. A qualitative estimation data selection bias suggests data selection bias could cause 1-2 msec downward bias in the Su et al. (1996) and subsequent estimates.

5.1.5 Small Event *Kappa* Estimates and the Displacement *Kappa* Method

Kappa values from very small earthquakes are estimated with the assumption that spectral roll-off effects caused by the corner frequency (Equations 7 and 8) are negligible. The method of estimating *kappa* from the low-frequency portion of small earthquake displacement spectra was introduced in Biasi and Smith (2001). They examined data from approximately 263 earthquakes with a median magnitude M_L=0.3 recorded by Southern Great Basin Digital Seismic Network stations. Above it was shown that for earthquakes with magnitude M_L=0, stress drops would have to be systematically lower than 10 bars to affect the slope *kappa* estimates. However this assumption could not be tested directly. An indirect test was conducted, in which the earthquakes were divided by magnitude around the median, and the *kappa* estimates for the two halves were compared. On average the larger events, with mean M_L~0.8, *kappas* were larger by 3.1 msec than for the smaller event fraction with M_L~-0.1. Results of this split indicate that displacement *kappa* estimates in Biasi and Smith (2001) considering all events could be biased upward on average by 3 msec or more.

Both the displacement and acceleration slope *kappas* are estimated for every seismogram analyzed. They have the physical interpretations of the infinite and zero corner frequency asymptotic measurements, and thus represent outside bounds to any *kappa* estimate with a finite corner frequency. At most one of these estimates will approximate the true *kappa*. Neither estimate will be reliable for events with corner frequencies in or near the measurement window, here 5-25 Hz.

5.2. Instrumentation and Data

5.2.1 Southern Great Basin Digital Network

The Southern Great Basin Digital Seismic Network (SGBDSN) is focused on a 100 km diameter region centered on Yucca Mountain (Figures 5.2.1, 5.2.2; Table 5.1). It has been operated by the Nevada Seismological Laboratory since 1992, technically began with the upgrade in 1995 from analog to three-component digital instrumentation. Data from these stations is telemetered to the Nevada Seismological Laboratory in real time and recorded and analyzed there. The network also includes nine non-telemetered strong motion instruments.

SGBDSN instruments in this network fall into a few categories. The majority of the data have been recorded on 24-bit digital recorders with high-gain velocity sensors. The sensitivity of these stations is such that the apparent completeness threshold for earthquake detection in the vicinity of Yucca Mountain itself is about M_L -0.3. All telemetered stations have until 2006 recorded 100 sample-per-second (sps) data only in triggered mode, so the existence of a record for a given earthquake depends on there having been adequate signal to trigger the field recorder. At some stations (Table 5.1) recording began with CMG-40 broadband sensors. Broadband records were corrected only for their gain in the analysis because they are flat to velocity in the analysis frequency band. In the database they have channel codes beginning with "HH". In 2001 and 2002 these sensors were replaced with lower maintenance S-13 short-period sensors. All short-period data have "EH?" channel codes, where "?" is Z, N, or E. The S-13 sensors are flat to ground velocity inputs above ~2 Hz, but require sensor correction if amplitudes are of interest at lower frequencies. Since July 2000 ten stations on or near Yucca Mountain were augmented with 3-component Reftek-133-05 accelerometers. This was done to increase the number of on-scale recordings should a large earthquake occur. These instruments are flat to ground acceleration throughout the frequency band considered in this report. The data are recognized in the database by their station codes and HG? channel codes. The SGBDSN also includes nine Terratek digital strong motion recorders. The accelerometers themselves are the same type as at the telemetered stations. These stations record acceleration in triggered mode with 16 bit resolution, so the number of records for a given earthquake and the proportion with acceptable signal-to-noise ratios varies from event to event. Table 5.1 gives locations and a one or two word site description for each of these stations

Figure 5.2.3 shows a map of the epicenters of SGBDSN earthquakes used in this study. Earthquakes were selected if they had at least one triggered strong motion record. Our goal was to maximize the number of Terratek strong motion records, since there were relatively few of them compared to the more sensitive weak motion stations. Also, if a strong motion site recorded it, many weak motion stations were also sure to trigger and produce high signal-to-noise recordings. This selection strategy effectively guaranteed that all M3+ events would be included, but smaller events are allowed. The resulting dataset includes 39 earthquakes spanning in magnitude from M_L 1.98 to 4.70 and over 2400 useable recordings. As a short name we call this set the SGBDSN "M3" data. The study by Anderson and Su (MOL.20071203.0134) considered earthquakes as small as M3.0, but the higher dynamic range of (24 vs. 16 bits) of the permanent telemetered stations encouraged us to consider

smaller events. This dataset comprises the best available data from permanent SGBDSN stations for the period from October 1995 to the present. Earthquake locations and magnitudes are listed in Table 5.2.

Details of data selection and accession are given in Section 8. This is a Q dataset.

5.2.2 Portable Seismic Network, Weak-Motion Recording at Strong-Motion Sites

A temporary seismic array data set has been included in this report. These data were recorded in early 1997 and used in Biasi and Smith (2001). The portable recorders were co-located with Terratek strong motion sites for the purpose of characterizing *kappa* at those sites using the displacement *kappa* method. Station names match those in Table 5.1, with a "W" in place of the last "S" of the corresponding TerraTek recorder station codes. Refraction technologies 16-bit recorders and S-13 1-Hz sensors were used. The recorded earthquakes were all small. Nevertheless they contribute to understanding *kappa* because they fill event coverage in the magnitude range for which the accelerometer would not normally trigger.

The portable data were collected under scientific notebook SN0094, "Preliminary Data Gathering with the UNR/YMP Strong Motion Network", MOL 19980203.0705. The data themselves are accessible by MOUNR1998AUG26.001, "Seismic Data, Weak-Motion Portable Instrument Recordings at Strong-Motion Monitoring Sites Around Yucca Mountain, January – June 1997 Recording Period, With Supporting Data". Earthquakes actually used come from the January 1997 portion of the recordings. This period included 35 earthquakes in a magnitude range from Ml -0.42 to 1.45. After screening for quality of the spectra, over 400 recordings were used. This proved adequate for our intended use to interpret patterns in small events and relate them to the moderate event set. A catalog of the selected earthquakes is given in Table 5.3.

Details of data selection and accession are given in Section 8. This is a Q dataset.

5.2.3 Little Skull Mountain Aftershock Portable Network Deployment

Portable station data were collected from July through November 1992 (Sheehan et al., 1994), during the most active portion of the Little Skull Mountain aftershock sequence. Instrumentation included high and low gain accelerometers and active and passive velocity instruments. The recorders, sensors, and data are described in Sheehan et al. (1994; DTN GS940283117412.002, Q report, data in RPC only). Supplemental details of data selection are given in Scientific Notebook SN-UCCSN-UNR-097, v.1. Earthquake and station locations are shown in Figure 5.2.4 and Tables 5.4, and 5.5.

Details of data selection and accession are given in Section 8. We analyze this data as Unqualified.

5.2.4 Blume Strong Motion Network

The Little Skull Mountain mainshock and two M4+ aftershocks were recorded by a strong-motion network operated by John Blume Associates under contract to DOE (Lum and Honda, 1992; Lum and Honda, 1993). The Blume mainshock recordings at Lathrop Wells (LWLB) and Control Point (CPTB) are the strongest ground shaking records available near Yucca Mountain, and thus have been extremely important for Project use. Blume station locations are listed in Table 5.6 and shown with the earthquakes in Figure 5.2.5.

Details of data selection and accession are given in Section 8. These data are Unqualified.

5.3. RESULTS:

5.3.1 SGBDSN Spectral Fitting Results

5.3.1.1 Overview of SGBDSN Configuration and Fitting

SGBDSN station *kappas* are estimated using the combined permanent and weak-motion temporary network data. Individual waveform fits are included in DID 006GB.003, subdirectories *case6a/Figs* and *casewm1/Figs*. Database tables with all fitting results are in *case6a/db* and *casewm1/db*. All tables are in ASCII format and viewable with a plain text editor. Primary results for the SGBDSN station *kappa* estimates are developed using spectral fits from 0.9 to 35 Hz, the multi-taper spectral estimator, and sensor corrections for all passive instruments. All spectra are re-sampled to a uniform log spacing of points in order to balance data importance across the fitting band.

Basic data for understanding *kappa* at SGBDSN sites comes from individual spectral fits. Figures 5.3.1.1-6 shows north and east component recording pairs at station CAF that illustrate some of the types of input that must be summarized. Figure 5.3.1.1 (*fitid* 85174) has an apparent best fit at 50 Hz and an unphysical stress drop. This record has an average signal-to-noise ratio (*SNRmean*, center bottom between figures) of 217.5, so noise is not the cause. Examination of the squared error curve shows that a fit below 10 Hz would also fit as well, within the errors, and also have stress drop near a reasonable value (lower-right subplot) of 30 bars. To use this record we consider the lower bound of *kappa* to be fairly well constrained, and keep only the acceleration slope *kappa* estimate (21.4 msec, second value of *kal* in center right subplot). The east component record for the same earthquake (Figure 5.3.1.2, *fitid* 85173) is well constrained in both *kappa* (17.5 msec) and corner frequency (5.7 Hz). For one earthquake then, the two components give one best fit *kappa* of 17.5 and an estimate from *kal* that *kappa* should be greater than 21.4. Spectra in Figures 5.3.1.3 and 5.3.1.4 both have a formal squared error misfit near 15 Hz, but have stress drops of 350 and 183 bars, respectively (see title above waveforms). These estimates are high, but not impossible to exclude. The corner frequency fitting point is in a flat minimum that would admit a range of lower values, and a 95% confidence upper limit of 50 Hz. Spectra may not exhibit strong minima for a variety of reasons, including subtle source and frequency-dependent site effects. For reasons discussed below, source directivity is also likely to be important. The records in Figures 5.3.1.3 and 5.3.1.4 exemplify marginal fitting results which would be excluded if one requires the corner frequency to be bounded and below 50 Hz. Finally, Figures 5.3.1.5 and 5.3.1.6 show spectral fits with well-defined minima in squared error, reasonable stress drops, and *kappa* estimates in the mid-20's. Acceleration slope *kappas* are both slightly lower than the respective best *kappa* estimates, as they should be. Results from Figures 5.3.1.5 and 5.3.1.6 would be included in any estimate of *kappa* at this station.

The above discussion highlights two principal decisions that must be made in using fitting results from velocity spectra. First is how to treat spectral fits without a clear minimum in

squared error. On one hand we could say that parameter estimates are not unconstrained at the (say) 95% level, and not use the data. On the other hand, this practice is likely to introduce a sampling bias, since only spectra with low corner frequencies may be selected, even for earthquakes with a true corner frequency of a few Hz. For example, only less than 10% of horizontal component fits at station LSC on Little Skull Mountain would be admitted.

Appendix B shows all horizontal component fitting results developed by qualified *kappaAH* macros *getgood2* and *bysta9* for which the upper 95% range of corner frequency is resolved within the trial corner frequency range, that is, less than 50 Hz. These data are the subset one gets from the SGBDSN data if only "resolved" data are used for interpretation. Because of the (small) size of earthquakes considered, requiring fits to be "resolved" in this way creates a set biased toward the low corner frequency elements of any given earthquake. The introduction to Appendix B gives further details.

5.3.1.2 Formal Inversion Model for *Kappa* Related to Site, Distance, and Source.

Certain choices in developing our preferred *kappa* estimates in the next section were motivated by exploration of a formal inversion of the *kappa* measurements. We use a staged approach to test the significance of site, event, and distance correction terms. Each stage tests a small increment, so the value of each addition may be evaluated against a previous baseline. The inversion explores a generalization of Equation (4):

$$\kappa = \kappa_0 + \kappa_E + \tilde{\kappa}(R) \qquad (9)$$

where κ_0 is a per-station term, κ_E is a per-event term, and distance term $\tilde{\kappa}(R) = R\kappa_R$ uses epicentral distance R, and a linear slope κ_R. The staged inversions are implemented in *kappaAH* macro *k_summary*. We use the epicentral distance, in contrast to Su et al (1996) and Anderson and Su (MOL.20071203.0134) who used the hypocentral distance. Philosophically, this makes it easier to avoid double-counting of attenuation when modeling, because it is possible to choose Q values in a layered medium for which t^* equals κ_0.

For Equation 9 we use a series of linear inversions of the form:

$$\mathbf{Gm=d} \qquad (10)$$

In Equation 10, **m** is a column vector of model parameters, variously containing κ_0 rows for each station, κ_E rows for each event, and a row for κ_R which is the same for all stations. The column vector **d** contains the *kappa* estimates from all the seismograms. **G** is a sparsely populated matrix relating the data to the model with a value of 1.0 to select the station and event terms, and one (R) with the epicentral distance to multiply by κ_R in the model matrix. We add the constraint that the event terms sum to zero to resolve the ambiguity of the event mean from trading off with the station mean.

We implemented a series of models, as listed in Table 5.8. Each model was tested to determine if the added complexity of additional parameters was justified. Table 5.9 summarizes the results. In Table 5.9 variance reduction ratios ("Ratio" column) greater than ~1.10 are significant at the 95% level.

Model 1 assumes *kappa* is a universal constant, independent of distance, station, and source. *Kappa* for this model is 26±15 msec (Table 5.10, M1_k and M1_s, respectively). All of the other models are significantly better than Model 1.

Model 2 (Table 5.8) considers *kappa* as only a station term, independent of distance or source terms. Model 3 adds event terms, but does not include distance dependence. Model 4 uses station, event, and linear distance terms to Model 3.

Considering Models 2, 3, and 4, the station terms are a significant improvement over *kappa* as a universal constant (Table 5.9, Model 2). Event and station terms together significantly reduce residual variance (the normalized square of the data minus the model prediction) over Model 2 with station terms alone. Interestingly, the addition of the linear $R\kappa_R$ term to station and event terms (Model 4) does not reduce residual variance. The lack of significant improvement is not because of the number of new variables, since only one new variable is being added. Rather it appears to indicate that the distance correction improves fits at some sites and degrades it at others. The smaller value of station *kappa* estimates between Model 3 and Model 4 (M3_k and M4_k columns, respectively, in Table 5.10) shows that the distance correction is absorbing 10-15 msec of site *kappa*.

Model 5 tests the significance of κ_0 and $R\kappa_r$ without event terms. It tests the assumption that *kappa* increases with distance. Model 6 tests whether event terms by themselves are a significant improvement over the case of *kappa* as a universal constant.

We find (Table 5.9) that Model 5 with site *kappas* plus a distance term significantly improve residual misfit. Model 5 finds $\kappa_r = 0.483$ msec/km (Table 5.11, A5_k). Like Model 4 the distance correction reduces site *kappas* roughly by κ_r times the average station-event distance. Model 6 also significantly reduces residual misfits, but does so by increasing event terms by the average of the station term (Table 5.11, compare E6_k with E3_k or E4_k). Thus site and event terms are significant separately (Models 5 and 6) or together (Model 3), but not improved by the further addition of a distance term (Model 4).

Models 7 and 8 test for internal trade-offs among station, event, and distance terms. Model 7 is Model 4 but with the κ_r term constrained to the value found in Model 5, where no event terms were used. Model 8 is like Model 7, but additionally constrains the site *kappa* terms to the values found without event terms (Model 5). Results (Table 5.9) confirm that the event terms significantly reduce the variance relative to Model 5. Station *kappa* estimates for both models are low, with only four and five stations above 20 msec for Models 7 and 8, respectively.

Models 9 and 10 include *kappa* variation with distance as a bilinear function. Model 9 is similar to Model 4, differing only in the bi-linear distance model. Model 10 follows Model

5 with station terms and a bi-linear distance term. A review of station *kappa* versus distance plots (Appendix B) shows little convincing evidence that *kappa* has a distance dependence in the range $0 < R < 40$ km, thus motivating this bilinear function:

$$\tilde{\kappa}(R) = \begin{cases} 0 & R < R_C \\ \kappa_R (R - R_C) & R > R_C \end{cases} \qquad (11)$$

We find that the bilinear model does somewhat better than the full linear correction of Model 4, but the improvement is not statistically significant. Station and event parameters for all models are given in Tables 5.10 and 5.11.

We make the following observations about these results:

1. Station and event terms separately (Models 2 and 6, respectively) or together (Model 3) significantly reduce residual misfit, while Model 4, with one more free parameter, does not. The difference has to be in how the distance correction prescribes tradeoffs between site and event terms. It means at least that the distance dependence term $\exp\left(\frac{-\pi R f}{Q(f)\beta}\right)$ in Equation 6 and its representation by Equation 4 are not compelling.

2. Model results strongly confirm the importance of event terms even though they are not explicitly in the spectral models of Equations 1 or 6. The source of event variability could include deviations in source spectral shape from the assumed log slope of -2, or perhaps a near-source condition that would affect the average spectrum seen at all stations.

3. The bilinear distance term seems to have some basis in the data, but its physical basis is not clear. A possible explanation is related to the deeper penetration of seismic body wave ray paths with increasing distance. For short epicentral distances ray paths are entirely upward through brittle crust. Attenuation and apparent site *kappa* will be dominated by scattering within brittle crustal layers. At some distance ray paths for typical hypocentral depths will begin to dive into the aseismic lower crust. Attenuation in lower crust is likely to be higher due especially to temperature effects. Horizontal paths through the attenuating lower crust would appear as a linear distance dependence in *kappa* beginning at 30-40 km epicentral distance. Hough and Anderson (1988) made a similar suggestion to explain the distance dependence at Anza. The bilinear dependence in $\tilde{\kappa}(R)$ should be regarded as a hypothesis pending development of a more adequate physical explanation.

4. Both the linear and bilinear distance dependence models constrain the shape of the *kappa*-distance relationship, one as a line and the other as a hockey-stick shape. Both shapes permit distant events to affect, and for some stations, control the site *kappa*. Given the uncertainty in the distance term and its variability, we consider it safer to confine events contributing to best estimate *kappas* to those near recording stations. Based on inversion results we adopt the distance of 40 km, and recognize the need for event term corrections.

5.3.1.3 Station *Kappa* Estimates

After considering the problems created by forcing a single distance correction on all station data we developed an alternative approach that does not depend on distance correction. Our preferred approach instead uses only relatively short station-epicentral distances and neglects the distance correction. We took this approach for two reasons. First, *kappa* matters more for the ground motion hazard component caused by moderate earthquakes near the repository than for larger, more distant earthquakes that control the hazard at lower frequencies. Thus the most relevant measure of *kappa* is whatever is observed from nearby earthquakes. Second, a review of Appendix B plots shows that out to a distance of 30-40 km *kappa* is often relatively constant. This observation motivated the bi-linear fit implemented in formal inversion Model 9. The essential problem with the bi-linear fit is that distant earthquakes influence, and can control site *kappa* estimates even when short station-event measurements of *kappa* are available. Restricting station estimates to earthquakes within 40 km has certain negative consequences that are discussed below.

To develop station *kappa* estimates we first estimate average differences among events. The event average *kappa* is computed as the arithmetic mean of *kappa* estimates for that earthquake. The event means seem to vary primarily because of true source variations (events richer or poorer in high frequencies), but station coverage relative to the focal mechanism, and/or variations in mean distance from the event to the station probably also contribute. Figures 5.3.2 shows event mean *kappas* (upper plot) and the individual measurements (lower plot). For most events the scatter of individual measurements around the mean is similar, suggesting that whatever causes the scatter of *kappa* estimates is relatively consistent from event to event. This is confirmed in Table 5.12, where the standard deviation of *kappa* estimates is listed (*sd k* column). Table 5.12 includes a second event *kappa* estimate formed only from fitting results at epicentral distances less than 40 km. Event mean *kappas* for epicentral distances less than 40 km are similar but somewhat smaller than the unrestricted set (Figure 5.3.2, upper, dashed and solid lines, respectively).

Figures 5.3.3.1-37 present station *kappa* estimates based on spectral fits for epicentral distances less than 40 km. Figure 5.3.3.1 shows data from station AL5. In the upper-right, Brune stress drop is plotted against *kappa*. To be on these plots at all, we select horizontal components, the corner frequency must be less than 20 Hz, and fits must pass a weak maximum squared error misfit of 0.151 units. Green dots are *kappa*-stress drop estimates after a further subset requiring stress drops<300 bars. Horizontally displaced from them are diamonds showing same values after correction for a mean event *kappa* bias (*dk*, Table 5.12). As may be seen, the event corrections are typically a few msec. In most cases event correction improves the central tendency of *kappa* measurements. Red dots show fits with values greater than 300 bar stress drops but less than 1000. This distinction allows the reader to assess the consequences of excluding data over 300 bars from the station estimate. AL5 shows a weak trend to increasing stress drop with *kappa*. In Figure 5.3.3.1, lower-right, corner frequency is plotted versus *kappa*. Green dots are the <1000 bar stress drop data. In the upper-left, *kappa* (green dots) and event-corrected *kappa* (red diamonds) are shown versus local magnitude.

We were motivated to investigate ways to use the acceleration slope *kappa* estimates because of the number of *kappaAH* fits that lacked a formally bounded estimate of corner frequency. For example, at station LSC only 4 of 56 horizontal component corner frequency measurements (Appendix B) are bounded at the 95% level below 45 Hz. *Kacc2* gives a useful inequality relationship bearing on the true value of *kappa* even when the spectral fit does not have a formal minimum squared error misfit, or the stress drop exceeds 300 bars. Parameter *kacc2* should generally be smaller or equal to the station *kappa* depending on how close the corner frequency is to the 10-30 Hz band for *kacc2* estimation. The line descending to the right in Figure 5.3.3.1 is the fraction *n/N* (*n* is the count to the right, *N* is the total) of the total *kacc2* measurements consistent with a given value on the *kappa* axis. In the case of AL5, about 80% of *kacc2* measurements would be inconsistent with a *kappa* estimate of 10 msec, and 70% prefer a site *kappa* greater than the event corrected mean of 14.1 msec. A weighted site *kappa* is developed by multiplying each measured *kappa* value by the fraction *n/N* for the point, then normalizing. This has the effect of up-weighting data that agree with the majority of *kacc2* inequality data, and reducing the weight of estimates contradicted by most *kacc2* data. Thus the weighted site *kappa* may be interpreted qualitatively as being consistent with more of the data than the mean or event-corrected mean *kappas*. It is not our recommended site *kappa* estimate, however, because the meaning of the *n/N* weighting is not consistent from one site to the next. For example, if the *kacc2* estimates are reliable and unaffected by corner frequency, the 50% *n/N* point will correspond to the median *kappa*. On the other hand, if most data are excluded because the corner frequencies are not resolved, the median *kacc2* (50% point on the solid curve) is an approximate lower bound of the likely *kappa*. The value of the weighted *kappa* estimate is shown in the field of the plot.

In Figures 5.3.3.1-37, lower-left, is a simple map showing all events recorded by that site (green dots), and events used to develop the site *kappa* estimates (diamonds: 300 bar stress drop, f_c<20Hz, epicentral distance<40 km). A few stations are shown on all maps to provide a consistent reference from map to map. Station RPY is on Yucca Mountain above the Exploratory Studies Facility.

Station BTW (Figure 5.3.3.3) is exceptional among SGBDSN stations for its low values of *kappa*. This station is centrally located relative to the available M3 earthquake set, and thus constrained by a better than average data set. The plot of Brune stress drop versus *kappa* (upper-right) shows that the upper cutoff of 300 bars is excluding a significant number of the artificially high *kappa* estimates, as it was intended to do. The site *kappa* estimate is dominated by a large number of negative *kappa* estimates, resulting in an event-corrected site mean of 5.4 msec. There is no obvious bias in *kappa* with event magnitude (Figure 5.3.3.3, upper-left).

One of the objectives of this study is to relate the small-event displacement slope *kappa* estimates (*kds*) of site *kappa* introduced by Biasi and Smith (2001) to estimates constrained by larger earthquakes. If validated, the *kds* estimate of *kappa* would be valuable for site study where very small earthquakes are available but strong ground motion records are not. Figure 5.3.3.3 shows *kds* for small earthquakes (left-pointing triangles) measured from the spectral slopes in the 5-25 Hz band. These data are from spectral fitting of the *casewm1*

earthquake set. Best-fit values of *kappa* are shown as diamonds. Small earthquake best-fit *kappa* estimates are not included in the station estimate. For most stations the best-fit values are significantly smaller than the estimates from the M3+ event set; BTW is an exception in this case. The solid line descending to the left shows the *kds* measurements interpreted as an inequality relation analogous to the *kacc2* line. In this case the site *kappa* will be smaller or similar to (plot to the left of) the *kds* measurement. Numerically the fraction of *kds* measurements contradicting a given value of *kappa* is given by n/N, where n in this case is the number of *kds* measurements to the left and N is the total number of measurements. In the limit of infinite corner frequency the median *kds* would be the site *kappa* provided that the true spectrum behaves like the reference model spectrum (Equation 2) and has a median spectral falloff of ω^{-2} above the corner frequency. For site BTW the *kds* measurements are not strongly constraining, but consistent with a site *kappa* less than ~35 msec.

Station BYMS shows a more typical relationship of *kds* and small earthquake best fits to the best estimates from the M3 earthquake set. Constrained small earthquake best-fit estimates are systematically smaller, and *kds* is systematically larger than mean or event-corrected mean *kappas*. For station BYMS *kappa* from the M3 set form a reasonably constrained group centered on ~25 msec. Stress drops are in a normal range, from ~8 to 200 bars, with most in the range of 20 to 120 bars.

Station CAF exhibits a clear linear trend of increasing stress drop with increasing *kappa*. Some other stations also show this trend (DOM, FMW, FRG, LWLS, RED, RPY, SCF, SPC, STO, SYM, WLD, YCW). Corner frequency trades off with *kappa* in the fitting process, but this does not seem to account for the trend in stress drop, because trends in corner frequency versus *kappa* (lower-right plots) tend to be more subdued where they are present at all. For these stations there also does not seem to be a magnitude dependence to *kappa*, so the trend in stress drop is not a simple fitting tradeoff with moment.

Measurements for station LSC show that some magnitude dependence does seem to affect the *kds* measurement above M ~0.5. Only below M 0.2 do the *kds* estimates begin to compare favorably with the site *kappa* of 36 msec. Apparent stress drops for LSC are relatively high. Only five component measurements of *kappa* among the horizontals have upper 95% limits of corner frequency resolved below 50 Hz. It is possible that the siting and geology of station LSC may contribute to this. Station LSC is near the top of the west-facing cliff of Little Skull Mountain, and the NNE dip of the bedded tuff at the site would tend to focus energy toward the station.

Station LWLS reoccupies the site of the Blume strong-motion station at Lathrop Wells. This station recorded the Little Skull Mountain mainshock, which is the strongest recorded earthquake-induced ground motion anywhere near Yucca Mountain. LWLS event-corrected mean *kappa* is of 34.3 msec is slightly above the average for SGBDSN sites, perhaps reflecting its siting on deep alluvium. There is no clear trend in *kappa* versus magnitude among the available earthquake recordings.

Site conditions at station RED (Figure 5.3.3.18) are clearly anomalous. The largest recorded *kappa* among the accepted subset is 18 msec, and the event-corrected mean is 1.9 msec. At face value this implies that there is virtually no attenuation for paths to station RED. Inspection of the waveforms suggests that some form of site effect is responsible.

Station RPY (Figure 5.3.3.19) is above the Exploratory Surface Facility on Yucca Mountain. The event-corrected mean of 39.7 msec is above average for SGBDSN stations. The average does not appear to be magnitude dependent, and is, if anything, smaller than it would be if only the largest events were used.

Site estimates stations SGR, STC, and TYM exhibit the negative side of using only earthquakes within 40 km of the station. TYM has only one small earthquake in the set within 40 km; STC and SGR have only two. We consider *kappa* for these stations to be undetermined. These stations are in the outermost ring of the SGBDSN, and thus farthest from Yucca Mountain.

Station *kappa* fitting results are tabulated in Table 5.14.

Kappa for stations on Yucca Mountain is a specific interest of this project. Station RPY (39.7 msec) is on Yucca Mountain approximately centered above the repository. Nearby rock stations on Yucca Mountain (Figure 5.2.2, Table 5.1) include STO (31.2 msec), TYMS (27.6 msec), SYMS (27.3 msec), and EXHS (26.2 msec). The mean of these five stations is 30.4 msec. This estimate may be considered most representative of surface rock sites on Yucca Mountain. Station FRG (20.6 msec) somewhat separated from the Yucca Mountain rock group, but it is on the tuffs that comprise Yucca Mountain. If included, the mean *kappa* on rock from these six stations is 28.8 msec. If only stations of the main Yucca Mountain block are considered (RPY, STO, TYMS, and SYMS) the mean of YM rock stations is 31.45 msec. Stations BYMS and MDVS are on alluvium. BYMS (25.4 msec) is in the bottom of Solitario Canyon in what is likely to be relatively thin alluvium. MDVS (30.4 msec) is in Midway Valley, just east of the ESF pad. The mean of the two, 27.9 msec, is not significantly different from the mean of six Yucca Mountain rock sites.

Station AL5 (Alcove 5) is the one station in the ESF with enough records in the M3 set for a constrained *kappa* estimate. Based on eight component measurements from earthquakes within 40 km, AL5 has a mean *kappa* of 14.1 msec. Station RPY (39.7 msec) is approximately above AL5, so the 25.6 msec difference in *kappa* between them is one measure of the attenuation of the ESF overburden. If RPY is considered anomalous, even the difference from AL5 to the mean of main YM block stations (31.45 msec) is still a substantial 17.35 msec. While cited to four place precision to make the value explicit, the standard errors of station mean estimates (Table 5.14, *kcor_SE*) show that accuracy at the millisecond-level is optimistic.

5.3.1.4 SGBDSN M3 Earthquake Set Stress Drops and Corner Frequencies

Stress drop is plotted versus corner frequency in Figure 5.3.4 for every event used in the station *kappa* estimates above. On the plots, star patterns show measurements from the

same subset as the station estimates. Points with only "X"s are component measurements not used because of the station-event distance. Earthquakes e_150432-150437 occurred at the southeastern edge of the SGBDSN in Frenchman Flat, and thus had more stations beyond 40 km. Events clearly differ from one another. Event e_150294 has magnitude of 3.09 and a mean stress drop of 71.3 bars; event e_150406 has a magnitude of 2.87 (equivalent within the resolution), and a mean stress drop of 8.8 bars, or almost an order of magnitude smaller. These plots have the interesting characteristic that measurements spread in a fairly linear trend over 1½ to 2 orders of magnitude in stress drop, corresponding to a factor of ~4 in corner frequency for virtually all earthquakes from M2 to M4.3. Stress drop is proportional to the moment times the cube of the corner frequency, so the slope of the trend is approximately 3:1. The spectral fit quality is similar among measurements, so we conclude that the spread is typical of this type of data, but do not resolve whether it is a source property or a numerical artifact. Effects of directivity or focal mechanism would be the most likely explanation as a source property. Event average corner frequency, stress drop, and *kappa* are given in Table 5.13. Average event stress drops span from 4.0 to 91.8 bars, and the average of all event stress drops is 31.8 bars (Table 5.13).

5.3.1.5 Best Estimate Results Compared With Formal Inversion

Problems with the formal inversion method were noted in an earlier section as motivation to estimate the site *kappa* using only near-station earthquakes. Figure 5.3.5 compares site *kappa* from three formal inversion models to best estimates based on station-earthquake distances <40 km. Formal Model 3 used only site and event terms; Models 4 and 9 add linear and bilinear distance terms. Figure 5.3.5 (upper) shows that among formal models, Model 3 most closely matches best estimate results. Models 4 and 9 both exhibit large excursions from Model 3 and best estimates. The excursions reflect the variable reliability of the distance correction. Model 4 station *kappas* are smaller than any other model at virtually all stations because, compared with the others, it subtracts an additional amount roughly equal to κ_r times the distance to the nearest events. The histogram in Figure 5.3.5 compares formal inversion Model 9 to best estimate results. This figure makes two points. First, the mode of the difference is small, indicating that the Model 9 results are not strongly biased. Second, the width of the distribution confirms our impression that the distance correction destabilizes *kappa* estimation. In this case, "destabilize" means the distance correction moves many station *kappa* estimates far from what one would infer from using measurements from <40 km epicentral distances.

5.3.1.6 Consideration of the *Silva(f)* and *Q(f)* Functions (Qualified)

The alternative approach to measuring *kappa* has been proposed by Silva (1995; Equation 6). The *Silva(f)* and *Q(f)* function programmed into the qualified version of *kappaAH* were exercised as Case 7. Data inputs are identical to those of previous cases. From Equation 6 it may be seen that the *Silva(f)* function and *Q(f)* functions can be accommodated by

subtracting them from the observed spectrum in the spectral domain. The net effect is shown in Figure 5.3.6. On average station *kappas* are 4.5 msec smaller (Figure 5.3.6) than mean values without it. The effects on *kappa* are due to the frequency-dependent nature of *Silva(f)* and *Q(f)*. Other than a small shift toward smaller values there is little on which to comment.

5.3.2 Portable Station Recordings of Little Skull Mountain Aftershocks (Unqualified)

5.3.2.1 Overview of the LSM Aftershock Analysis (UQ)

We used a slightly modified version of *kappaAH* to analyze data from the small network of portable seismic stations deployed following the Little Skull Mountain earthquake (Figure 5.2.4). The deployment included a mix of accelerometers and velocity sensors recorded with 16-bit Refraction Technologies dataloggers. Recording was in triggered mode only, so not all stations recorded every event. Eighteen events with magnitudes between 2.7 and 4.5 (Table 5.5) were recorded between July 25 and November 6, 1992. The primary description of the deployment is Sheehan et al. (1994). Scientific Notebook SN-UCCSN-UNR-097, pages 52-59 supplement that description with details of waveforms and database preparation. Station locations from Su et al. (1996) are listed in Table 5.4. Event locations and magnitudes (Su et al., 1996) are listed in Table 5.5. Anderson and Su (MOL.20071203.0134) analyzed only 12 of these events. Earthquakes are concentrated the vicinity of the Little Skull Mountain aftershock zone, so all station-event distances are less than 40 km. The modification to *kappaAH* consisted of taking the noise portion of the time series from the end of the record if there was not sufficient length before the first P arrival. This lowers the signal-to-noise ratio in some cases. No modifications were made to the analysis or fitting subroutines. Details of the modification are given in SN-UCCSN-UNR-097. The modified code was kept in a separate directory and applied only to LSM and Blume network analysis. All results are unqualified, and labeled accordingly.

5.3.2.2 LSM Earthquakes: *Kappa*, Stress Drop, and Corner Frequencies (UQ)

Event mean *kappas* are shown for each earthquake in Figure 5.3.8. With one exception event mean *kappa* deviations are less than about 8.6 msec (Table 5.15, *dk*), and similar to the range seen with the SGBDSN data. Individual event stress drops are plotted versus corner frequency by earthquake in Figure 5.3.9.1-2. Like the SGBDSN data, the individual measurements span 1.5 to 2 orders of magnitude in stress drop for a given event scalar moment. Earthquake mean stress drop, corner frequency, and mean *kappa* are shown in Table 5.16. Mean corner frequencies range from 1.5 to 11.4 Hz, and mean stress drops range from 2.8 to 94.6 bars. This range is similar to that found in the SGBDSN M3 dataset. Differences in events appear to be resolved by the data.

5.3.2.3 LSM Station *Kappa* Estimates (UQ)

Individual station plots are shown in Figure 5.3.7. The cumulative *kacc2* curves (blue solid line) are generally consistent with site means with the median *kacc2* value a bit lower, as expected.

Station *kappa* estimates are shown in Table 5.17. Individual *kappa* measurements have a standard deviation of 5.6-8.9 msec for the event-corrected estimates (*kcor sd* column, Table 5.17). Station RLSM has four measurements not used in the station *kappa* estimate because of high stress drops – more than any other site (Figure 5.3.7.6, red dots in stress drop vs. *kappa* panel). The average stress drop measured at the site is also among the highest in the station set. These high values are interesting because site LSC, which is about a kilometer farther west of RLSM on Little Skull Mountain also recorded high individual and average values. RLSM is sited on the capping basalt layer of Little Skull Mountain, while LSC is slightly down-section in tuff, and on the brow of a cliff. Since both sites record high values it seems likely that the cause is a systematic relationship to the Little Skull Mountain aftershock zone perhaps relating to directivity.

Stations RES2, RSFC, RYMT, and RYMM are actually on Yucca Mountain, so the mean *kappa* of these stations has been of special interest. Station RES2 is on Exile Hill (Figure 5.2.4; compare with Figure 5.2.2), and thus close to the ESF. The average *kappa* for these four stations using the *mean_k* station estimate (Table 5.17) is 27.1; using the event corrected station estimates the average is 26.85 msec (*kcor* column, Table 5.17). These values are based on 52 total component measurements (Table 5.17). The most comparable SGBDSN station set (Yucca Mountain rock: RPY, STO, EXHS, SYMS, and TYMS, Table 5.14, *k_cor* column) gives a comparable mean of 30.4 msec. Anderson and Su (MOL.20071203.0134) previously studied these records. Their most comparable result using only horizontal components yielded station estimates on average 11 msec smaller than from the present study (Figure 5.3.10). Most of the difference between estimates traces to the distance correction applied by Anderson and Su that is not used in the present study.

5.3.3 Blume Strong Motion Network Results (Unqualified)

5.3.3.1 Overview of the Blume Data Analysis (UQ)

Accelerometers operated by Blume Associates for the Nevada Test Site recorded the Little Skull Mountain earthquake and two M4+ aftershocks. Data are from Lum and Honda (1992, 1993). These data were not collected for the Yucca Mountain program, and thus not qualified. The records were nevertheless extremely important for Yucca Mountain Probabilistic Seismic Hazard Analysis because they were the strongest ground shaking records from anywhere near Yucca Mountain. The stations at Lathrop Wells (LWLB) and Control Point (CPTB) were the closest to the earthquake.

Because of the importance of the records, we included the Blume accelerometer data in analysis with *kappaAH*. The data available cover three triggers.

-- LSM June 29, 1992 M5.6 mainshock
-- LSM July 5, 1992 M4.4 aftershock
-- LSM Sep 13, 1992 M4.1 aftershock

Data sources for this section are described in Section 8.

5.3.3.2 Blume Network Earthquakes: *Kappa*, Stress Drop, and Corner Frequencies (UQ)

Individual fits for horizontal component recordings by the Lathrop Wells and Control Point stations are shown in Figures 5.3.11and 5.3.12. For station LWLB three events are available; for CPTB only two events triggered. Based on scoping work we fit the spectra from 0.9 to 35 Hz for the two M4 events and 0.2 to 35 Hz for the LSM mainshock. A review of the fit quality (Figures 5.3.11 and 5.3.12) shows that fitting minima are clear and the corner frequencies of all component fits have resolved 95% ranges.

5.3.3.3 Blume Network Station Results (UQ)

The LWLB mainshock records have high stress drops – 105.9 MPa (1059 bars) based on the average of two horizontal components (Table 5.18). The high values seem to be required by the data. For example, for the stress drop to be a more typical 100 bars, the corner frequency would be less than 0.5 Hz. The spectra (Figure 5.3.11.5 and 6) are half a decade higher in frequency near the peak amplitudes. We speculate that the source spectrum is more complex than in Equation 2 due to the large source dimension or that some sort of directivity may have distorted the apparent source-time function of the earthquake. The average stress drop for all stations recording the mainshock (e_5, Figure 5.3.13) is about a factor of 4 lower, but the moment is similar, so the high stress drop at LWLB is due almost entirely to the site-specific observation of higher corner frequency ($\Delta\sigma \sim M_o f_c^3$). A source term is also suggested from the difference between the M4 aftershocks (e_4 and e_6, Table 5.19), since these events have nearly identical back-azimuths and distances.

Station CPTB (Figure 5.3.12.1-4) also recorded high stress drops for the LSM mainshock, although not as high as station LWLB. CPTB is ~31 km from the Little Skull Mountain mainshock and aftershocks. CPTB has a lower *kappa* value, despite being over twice as far from the hypocenter than LWLB (Table 5.18). A difference in site conditions seems to be one of the causes; CPTB is on weathered limestone, while LWLB is on alluvium. A source term correction appears necessary from CPTB data as well; like LWLB there is about 20 msec difference in *kappa* estimates between events 4 and 5. Event 4 seems to have been richer in high frequencies than events 5 and 6. Summaries for stations LWLB, CPTB, and BTYB are provided in Figure 5.3.14.1-3.

Blume station events are large enough to test the acceleration slope *kappa* estimate to that of fitting. Figure 5.3.15 *kappa* from *kappaAH* versus *kacc1* (the 5-25 Hz estimate) for the three available earthquakes. Noise above 25 Hz made the 10-30 Hz estimate, *kacc2*, unsuitable. There is a clear linear correspondence, but for these data *kacc1* is systematically larger by about 15%. The reason for this is not known.

5.3.4. Dependence of *Kappa* on Magnitude from the KiK-Net borehole data (UQ)

Anderson et al. (MOL.20071203.0132) present non-Q measurements of *kappa* on KiK-Net stations in Japan. These data are ideal for the study of *kappa* since KiK-Net stations have recorded thousands of earthquakes on scale with the largest greater than M7. KiK-Net data also permit the study of how much of *kappa* can be attributed to the shallow geology. The data are freely available on the internet.

At each site surface and downhole 3-component accelerometers are separated by ~100 m. Velocity and lithologic logs are also available. Data were selected for closely similar source-receiver paths and the availability of strong ground motions. As a descriptive device acceleration spectra were divided into three regimes, where the transition from one to the next is gradational. In the low frequency band the free-surface effect controls amplitudes both at the surface and downhole. In an intermediate band the free-surface downhole and the up-hole velocity structure dominates ground motion amplifications. In the high-frequency band attenuation is typically strong and can match or exceed amplifications from the velocity structure. For the ~100 meter boreholes and velocities of the KiK-Net stations analyzed, the low, intermediate, and high frequency behaviors were recognized at frequencies of approximately <1 Hz, 1-10 Hz, and 10-30 Hz, respectively (Anderson et al., MOL.20071203.0132).

Slope *kappas* for KiK-Net data are measured in the frequency band from 10-30 Hz. The earthquakes studied have magnitudes between 3.5 and 7.0. *Kappa* is generally highly scattered at smaller magnitudes. Some of this scatter is likely caused by source terms, which are not separated. In most cases, the measured values of *kappa* in the largest earthquakes at a station are consistent with the distribution of *kappa* measured from events with $3.5<M<5$. Due to the high scatter, a large number of measurements from small events are generally required. With this caveat, Anderson et al. (MOL.20071203.0132) suggest that it is acceptable to use the average value of *kappa* for earthquakes under magnitude 4.0 for estimates of the spectral falloff of ground motions of earthquakes with $M>6$.

6. ASSUMPTIONS

Technical assumptions have been discussed above. Briefly they include:

-- Site effects are linear in the range of the earthquakes studied. Linearity should be satisfied for seismic records with accelerations limited to a small fraction of gravity. The highest accelerations other than the LSM mainshock are less than ~2% of gravity, where linearity is not seriously questioned. The Blume mainshock accelerometer recordings at Lathrop Wells peak have a high-frequency peak at 0.21 g, which is at the low end of where non-linearity might be a factor. For that record, however, a non-linear shift to longer periods is the opposite of what is observed, so non-linearity is unlikely to affect any of the data used here.

-- We assume that the low frequency branch of spectra of displacement seismograms is flat, and use that feature when estimating *kappa* for smallest earthquakes. At low enough frequencies the displacement must reach a constant, or the earth would continue to move after the earthquake. We use the displacement *kappa* measurement as confirmatory only, so our results do not depend on resolving this assumption. On average we expect the displacement spectrum to fall off as f^{-2} above the corner frequency, and accept that if individual earthquakes have other shapes in the 5-25 Hz band, the difference will map the into some perturbation to *kappa*.

7. DISCUSSION AND CONCLUSIONS

7.1 Discussion: SGBDSN Station Measurements and Yucca Mountain Applications (Q)

(Q) Rock stations on Yucca Mountain: Station RPY (39.7 msec, Table 5.14, Figure 5.2.2) is on Yucca Mountain, approximately centered above the repository. Other nearby rock stations (Figure 5.2.2) with sufficient records to obtain estimates of *kappa* are STO (31.2 msec), TYMS (27.6 msec), SYMS (27.3 msec), and EXHS (26.2 msec). The mean is of these five, 30.4 msec, is considered most representative of rock sites on Yucca Mountain. The median, 27.6 msec, is smaller because of the relatively large value at RPY. Station FRG (Fran Ridge, 20.6 msec, Table 5.14) is also on Yucca Mountain tuff, but somewhat removed from the other stations. If included with the previous five, the median is 27.45 msec and the mean is 28.75 msec. Station AL5 (14.1 msec) has not been included in these estimates because it is underground, in the ESF tunnel.

(Q) ESF Overburden Attenuation, RPY and AL5: Station RPY and AL5 form an approximate surface-underground pair. The increase in kappa from AL5 to RPY, 25.6 msec, suggests significant attenuation in the ESF overburden. Even if AL5 is compared with the 30.4 msec mean of Yucca Mountain rock sites, the difference is 16.3 msec. The simple interpretation is that the ESF overburden is strongly attenuating, a conclusion consistent with previous analyses.

(Q) Other stations in the Yucca Mountain area: Stations BYMS (25.4 msec) is on an unknown thickness of alluvium in the bottom of Solitario Canyon west of the main Yucca Mountain block (Figure 5.2.2). Station MDVS (30.4 msec) is east of the ESF in deeper alluvium. As a gross average of surface stations around Yucca Mountain, stations RPY, STO, TYMS, SYMS, EXHS, FRG, BYMS, and MDVS yield a mean of 28.6 msec. The mean of all SGBDSN station kappa estimates is 24.9 msec (Table 5.14, *k_cor* column, "Means" row).

(Q) Alluvium vs. Rock Stations: Stations CAF (25.7 msec), MDVS (30.4 msec), FOCS (26.9 msec), BYMS (25.4 msec), and LWLS (34.3 msec) on alluvium do not stand out from other stations (Table 5.14), and yield a mean of 28.54 msec. The similarity of this value to the mean values above for Yucca Mountain rock is somewhat unexpected.

(Q) Paleozoic vs. other rock: Stations on Paleozoic rock (AMD, HEL, LEC, PUV, RED, SPC, STH, TAR, WLD, YFT, SPRS, and WCTS; Tables 5.1 and 5.14) are undistinguished as a group from *kappa* values of the Yucca Mountain tuff sites. The exceptionally low *kappa* estimate at station RED (1.9 msec) appears to be due to unusual local conditions at the site.

(Q) Necessity of source terms: The addition of event terms results in a very significant improvement in the fit of the model. The RMS misfit in Table 5.9 improves from 11.3 msec of model 2 to 6.7 msec of model 3. As discussed in Section 5.3.3, the relationship of

this source term to earthquake source physics is unknown. The importance of the source term seems to imply that the spectral falloff assumed for Equations 1 and 6, and illustrated in Figure 5.1.2, may be reasonable on average, but that individual earthquakes deviate from it significantly. The variation of individual component measurements around the mean even for the larger earthquakes suggests an additional role for directivity or focal mechanism effects.

7.2 Conclusions Based on Q Data

KappaAH analysis of SGBDSN recordings of M2 to M4+ earthquakes provides for the following conclusions:

1. The available SGBDSN data provide stable and reasonably constrained estimates of *kappa* in the Project area.

2. *Kappa* for rock stations on Yucca Mountain itself has a mean value of 30.4 msec. Mean alluvial station *kappa* is similar but based on a two-station sample.

3. The repository overburden appears to contribute significantly to the total *kappa* estimate at the surface. Mean *kappa* for rock stations on Yucca Mountain is greater by than observed *kappa* at station AL5 in the ESF by 16.3 msec. This estimate is a based on a single ESF station, and would be improved by a larger sample of ESF-surface station pairs.

4. Linear and bi-linear distance correction of station *kappas* from the SGBDSN data does not sufficiently improve fits of *kappa* vs. distance to justify its use. *Kappa* does increase with distance beyond 40 km but present data are too variable to recommend that the rate of increase in kappa beyond 40 km be used to "correct" recordings with short epicentral distances.

5. An event contribution to the variability in *kappa* is suggested by two findings. First, *kappa* varies by 15-25 msec at individual sites for earthquakes with similar epicentral distances and source locations. Since the ray paths near the station are very similar, the station-side contribution to kappa should not vary strongly enough to account for the variation. Second, event mean *kappa* values vary significantly from one event to another with no alternative explanations such as systematic path or station coverage patterns.

6. The displacement slope *kappa* method can provide an upper bound on site *kappa* but the measurements are highly variable, and mean values even for M<0.5 earthquakes tend to be inflated by corner frequency or other effects.

7.3 Corroboration from LSM, Blume, and KiK-Net Analysis (Unqualified)

(UQ) 1. The Little Skull Mountain portable network data yield similar average *kappas* overall to those from SGBDSN stations and the M3 data set. The mean *kappa* from four LSM network stations on rock on Yucca Mountain is 26.85 msec. This average compares favorably with the mean of SGBDSN rock stations on Yucca Mountain.

(UQ) 2. The Lathrop Wells strong motion site provides a connection between the SGBDSN and Blume network recordings. The mean *kappa* for LSM mainshock and two large aftershocks is 40 msec. Within uncertainties this estimate is consistent with the 34.3 msec *kappa* estimate obtained from SGBDSN M3 events. This agreement indicates that M3 earthquakes can provide a useful estimate of *kappa* for events up to at least M5.6. Thus in the magnitude range available in Yucca Mountain area recordings, *kappa* does not depend on magnitude.

(UQ) 3. *KappaAH* analysis of Blume strong-motion network recordings at Lathrop Wells indicate stress drops over 1000 bars. The mean stress drop for the LSM M5.6 mainshock for all stations is a relatively high 236 bars.

(UQ) KiK-Net strong-motion recordings from earthquakes with magnitudes between 3.5 and 7.0 indicate that *kappa* is not an obvious function of magnitude. Scatter in *kappa* is higher in the magnitude range $3.5<M<5$, but the mean reasonably predicts *kappa* estimated from larger earthquakes. Due to the high scatter, a large number of measurements from small events need to be obtained.

8. INPUTS AND REFERENCES

8.1 Q Inputs:

DID 012DV.013 Southern Great Basin Digital Seismic Network (SGBDSN) waveform data for local earthquakes, 1995-1999. Waveforms from directories 1996/{051,062,173,191,193,208,244,249,291}/wf, 1997/{165,239,255,260,316,349}/wf, 1998/{069,084,092,104,167,342}/wf, 1999/{011,023,025,027,131,174}/wf.

DID 006DV.004 (MO0404UCC006DV.004), Combined seismicity catalog for FY1996-2002 in the vicinity of Yucca Mountain., file sgbdsn.hypo

DID 006DV.005 (MO0410UCC006DV.005) Independent Strong-Motion Site Locations, file strong_motion_locs.txt.

DID 012DV.010, Locations of stations in the Southern Great Basin Digital Seismic Network, DID 006DV.010, file sgbdsn_locations.dat

DID 006DV.013 Southern Great Basin Digital Seismic Network (SGBDSN) waveform data for local earthquakes, 2000-2003. Data from 2000/{131,253,294,326}/wf, and 2002/{145,165,169}/wf.

DID 006GB.001, Yucca Mountain Free-Field Strong Motion Earthquake Recordings, files in SAC directory, data in sub-directories sm_9602.SAC, sm_9606.SAC, sm_9701.SAC, sm_9703.SAC, sm_9709.SAC, sm_9711.SAC, sm_9803.SAC, sm_9804.SAC, sm_9811.SAC, sm_9901.SAC, sm_9902.SAC, sm_9904.sac sm_9908.SAC, sm_9910.SAC, sm_0002.SAC, sm_0004.SAC, sm_0008.SAC, sm_0101.SAC, and sm_0206.SAC

DID 006GB.003, Seismic Attenuation Parameter Kappa and Seismic Spectral Fitting Results for Seismic Stations in the Vicinity of Yucca Mountain. Under top directory kappawrap, files in subdirectories: case6a/Figs_summary (tabulated results have extensions .tbl - 4 files; developed data in files F* and T*), case6a/kappa_out, case2a/Figs_summary/*.tbl, case3a/Figs_summary/*.tbl, and case7/Figs_summary/*.tbl.

MOUNR1998AUG26.001 SEISMIC DATA, WEAK-MOTION PORTABLE INSTRUMENT RECORDINGS AT STRONG-MOTION MONITORING SITES AROUND YUCCA MOUNTAIN, JANUARY - JUNE 1997 RECORDING PERIOD, WITH SUPPORTING DATA (C), Files on electronic media: cdrom/jan97.ev/R023.01 through R031.01, all.

8.2 Non-Q Inputs:

Anderson, J. G. and Su, F. (2001) Reevaluation of *Kappa* for Little Skull Mountain Earthquakes, University of Nevada Report, reference Work Plan WP# 14012210M3, Table 9. (MOL.20071203.0134)

Anderson, J. G., Tibuleac, I. M., and Biasi, G. (2007). "An Evaluation of the Kappa Model for the Seismic Spectrum in the Context of Data from Kiban-Kyoshin Strong-Motion Network, Japan", Draft report, ORD-FY04-006, 140 p. (MOL.20071203.0132).

Lum, P.K. and K. K. Honda, 1992. Processed seismic motion records from the Little Skull Mountain, Nevada, earthquake of June 29, 1992, recorded at stations in southern Nevada, Report # JAB-10733-TM6 UC-703 National Technical Information Service, 206 p. DE93013314. HQO.940520.0008; Files: Table 1; and all data.

Lum, P.K. and K. K. Honda, 1993, Processed seismic motion records from Little Skull Mountain aftershocks, Nevada earthquakes of July 5 and September 13, 1992 recorded at seismic stations in southern Nevada, DOE Report JAB-10733-TM8. 10-53. DE93018074. Files: All data

Sheehan, A.F., S.L. Gillett, Kenneth D. Smith and M.K. Savage (1994), "Data report on seismological field investigations of the 29 June 1992 Little Skull Mountain earthquake", University of Nevada, Reno, Seismological Laboratory. DTN GS940283117412.002, Waveform data unqualified. Waveforms: Files from DVD 5, directories jd207.92_222.92.dir/R{207,210,212}.01; DVD 6, directories jd223.92_254.92.dir/R{229,231,236,237,242,243}.01; DVD 7, directories jd255.92_308.92.dir/R{257,258,269,282,283}.01; DVD 8, directories jd309.92_006.93.dir/R{309,311}.01

Su, F., J. G. Anderson, J. N. Brune, and Y. Zeng. (1996). A comparison of direct S-wave and coda wave site amplification determined from aftershocks of the Little Skull Mountain earthquake, Bulletin of the Seismological Society of America, 86, 1006-1018. Tables 1 and 2.

8.3 References

Anderson, J. G. (1986). Implication of attenuation for studies of the earthquake source, *Earthquake Source Mechanics, Geophysical Monograph 37, (Maurice Ewing Series 6)*, American Geophysical Union, Washington, D.C. 311-318.

Anderson, J.G. (1991). A preliminary descriptive model for the distance dependence of the spectral decay parameter in southern California, *Bulletin of the Seismological Society of America 81*, 2186-2193.

Anderson, J. G. and S. Hough (1984). A model for the shape of the Fourier amplitude spectrum of acceleration at high frequencies, *Bulletin of the Seismological Society of America, 74,* 1969-1994.

Anderson, J. G. and J. R. Humphrey, Jr. (1991). A least-squares method for objective determination of earthquake source parameters, *Seismological Research Letters, 62,* 201-209.

Ide, S. and G. C. Beroza, (2001). Does apparent stress vary with earthquake size?, *Geophysical Research Letters, 28,* 3349-3352.

Biasi, G. and K. D. Smith (2001) Final Project Report, "Site effects for seismic monitoring stations in the vicinity of Yucca Mountain, Nevada", Prepared for the US DOE/UCCSN Cooperative Agreement Number DE-FC08-98NV12081, Task 12, Southern Great Basin Seismic Network Operations (SGBSN), MOL.20011204.0045

Brune, J. N. (1970). Tectonic stress and the spectra of seismic shear waves from earthquakes, *Journal of Geophysical Research, 75*, 4997-5009.
MOL 19980203.0705. Scientific Notebook SN0094, "Preliminary Data Gathering with the UNR/YMP Strong Motion Network".

Hanks, T. C. (1982) fmax, *Bulletin of the Seismological Society of America, 72*, 1867-1880.

Hough, S.E. and J. G. Anderson (1988). High-frequency spectra observed at Anza, California: implications for Q structure, *Bulletin of the Seismological Society of America, 78*, 692-707.

Humphrey, J. R. Jr. and J. G. Anderson (1992). Shear wave attenuation and site response in Guerrero, Mexico, *Bulletin of the Seismological Society of America 82*, 1622-1645.

Madariaga, R. (1976). Dynamics of an expanding circular fault, *Bulletin of the Seismological Society of America, 66,* 639-667.

Silva, W. (1995). Engineering characterization of strong ground motion recorded at rock sites, *Electric Power Research Institute Topical Report TR-102262, Project 2556-48, Final Report, June 1995.*

Scientific Notebook UCCSN-UNR-047 v. 1, Yucca Mountain Kappa Subtask, John Anderson, P.I., MOL.20040323.0141.

9. SOFTWARE

Analysis in this report was conducted with the following:

kappaAH v 1.0 (qualified, STN-UCCSN-003).

For the Little Skull Mountain and Blume network analysis a copy of *kappaAH* was modified to read the noise time series from the end of the record. The modified version is unqualified, and the Blume and Little Skull Mountain analyses are unqualified.

Matlab v. 6 (exempt under QAP 3.2 Rev. 8)

Work was conducted on Sun Workstation "*wonder*" (hostid 838c1811), running *Solaris 9*.

No quality-affecting models were used in this report.

10. ATTACHMENTS

None.

Table 5.1 Station Locations and Description for the SGBDSN and Strong-Motion Sites
Qualified – DID 012DV.010, File sgbdsn_locations.dat

Permanent Network Monitoring Sites

code	station name and area	latitude north	longitude west	elevation km	on date	seismometer	strong motion+	site geology
AL5	Alcove 5, ESF	36.8596	116.4547	1.0660	1998252	Mark_Products L4	y	YM tuff
AMD	Amargosa Desert	36.4526	116.2809	0.7754	1997115	Geotech S-13&	n	Paleozoic
BTW	Beatty Wash	36.9978	116.5665	1.3910	1995230	Geotech S-13	n	Tuff**
CAF	Calico Fan	36.8391	116.3377	1.1100	1995034	Geotech S-13	y	Alluvium
CRF	Crater Flat	36.8118	116.5340	1.0320	1995165	Geotech S-13	y	Tuff
DOM	Dome Mountain	37.0021	116.4086	1.7110	1995333	Geotech S-13	n	Tuff**
ECO	Echo Peak	37.2108	116.3296	2.2320	1999197	Geotech GS-13	n	Tuff**
FMW	Forty Mile Wash	36.9021	116.3688	1.1460	1995165	Geotech S-13	n	Tuff**
FRG	Fran Ridge	36.8169	116.4195	1.1550	1995165	Geotech S-13	y	YM tuff**
HEL	Hell's Gate	36.7246	116.9750	0.7470	2002175	Geotech S-13	n	Paleozoic
LEC	Lee's Camp	36.5627	116.6896	1.1130	2002057	Geotech S-13	n	Paleozoic
LSC	Little Skull Cliff	36.7307	116.3255	1.2380	1995034	Geotech S-13	y	Tuff
NCF	North Crater Flat	36.8899	116.5682	1.1510	1995034	Geotech S-13	n	Alluvium
PUV	Plutonium Valley	36.9494	115.9633	1.2530	1995258	Geotech S-13	n	Paleozoic
PIT	Cinder Pit	36.6798	115.4937	0.0850	2000334	Geotech S-13	n	YM tuff
RED	Red Mountain	36.6895	116.0930	1.1430	1996037	Geotech S-13	n	Paleozoic^
RPY	Repository	36.8515	116.4563	1.3010	1996038	Geotech S-13%	y	YM tuff
SCF	South Crater Flat	36.7568	116.5440	0.9090	1995034	Geotech S-13	y	Basalt
SGR	South Grapevine	36.9805	117.0327	1.5600	1998127	Geotech S-13	n	TBS
SPC	Specter Range	36.6746	116.2030	1.0640	1996075	Geotech S-13$	n	Paleozoic
STC	Silent Canyon	37.2939	116.4358	1.9600	1995209	Geotech S-13	n	Tuff
STH	Stripped Hills	37.6457	116.3375	1.0500	2000179	Geotech S-13	n	Paleozoic
STO	Solitario Canyon	36.8603	116.4742	1.3590	1995165	Geotech S-13	y	YM tuff
SYM	South Yucca Mountain	36.7416	116.4460	0.9950	1995034	Geotech S-13	y	YM tuff

TAR	Tarantula Canyon	36.8680	116.6322	1.2310	1996023	Geotech	S-13	n	Paleozoic
TIM	Timber Mountain	37.0667	116.4694	1.8710	1996143	Geotech	S-13#	n	Tuff
TPW	Topopah Wash	36.9016	116.2519	1.5730	1995258	Geotech	S-13	n	Tuff
TWP	Twin Peaks	37.2047	116.1234	1.5760	1995205	Geotech	S-13	n	TBS
TYM	Thirsty Mountain	37.1441	116.7208	1.4570	1996275	Geotech	S-13*	n	Tuff**
WLD	Wildcat Mountain	36.7927	116.6257	0.9300	1995193	Geotech	S-13	n	Paleozoic@
YCW	Yucca Wash	36.9224	116.4756	1.4980	1996032	Geotech	S-13	y	YM Tuff
YFT	Yucca Flat	37.0762	115.9735	1.3540	1999197	Geotech	GS-13	n	Paleozoic

---

+ “y” indicates that a RefTek 133-05 strong-motion instrument has been added at the site
&station AMD used a Guralp CMG-40 until 03/06/2002
%station RPY used a Guralp CMG-40 until 05/02/2001
$station SPC used a Guralp CMG-40 until 02/27/2002
#station TIM used a Guralp CMG-40 until 05/01/2002
*station TYM used a Guralp CMG-40 until 04/10/2002
^Local alteration may be responsible for the known unusual site effects at RED
@Colocated with WCTS
**Very thin alluvial cover

SGBDSN Independent Strong-Motion Sites:

Source: DID 006DV.005, File strong_motion_locs.txt

code	station name and area	latitude north	longitude west	elevation km	site geology
SPRS	Specter Range	36.6882	-116.1772	1.0710	Paleozoic
LWLS	Lathrop Wells	36.6445	-116.3976	0.8250	Alluvium
BYMS	Bottom Yucca Mountain	36.8393	-116.4767	1.2510*	Alluvium
SYMS	Side Yucca Mountain	36.8377	-116.4723	1.3280	YM tuff
WCTS	Wildcat Canyon	36.7929	-116.6256	0.9660	Paleozoic
MDVS	Midway Valley	36.8519	-116.4214	1.1120	Alluvium
TYMS	Top Yucca Mountain	36.8394	-116.4675	1.5060	YM tuff
FOCS	Field Operations Center	36.7779	-116.2867	1.0420	Alluvium
EXHS	Exile Hill	36.8495	-116.4294	1.1780	YM tuff

*BYMS station was removed in January 2002.

Table 5.2. Earthquake Locations of the SGBDSN “M3” Data Set
Source: DID 006DV004, file sgbdsn.hypo
Origin and event id's are for identification within this report, and have no numerical or other significance.

Lat deg	Lat min	Lon deg	Lon min	Depth km	Origin YYYYMMDD	Time HHMM	Time SS.SS	Ml	Origin Id	Event Id
36	44.51	116	17.48	14.14	19960220	1737	27.29	2.69	150405	687
36	45.10	116	17.23	11.92	19960302	1142	40.39	2.87	150406	726
36	44.42	116	17.45	9.63	19960621	32	57.32	2.37	150407	1273
36	44.21	116	17.36	10.18	19960709	2348	51.36	2.41	150408	1429
36	44.34	116	17.79	11.02	19960711	720	41.00	2.32	150409	1438
36	44.19	116	17.56	10.97	19960726	1252	38.36	3.08	150410	1542
36	43.19	116	18.17	11.11	19960831	2258	41.73	2.98	150411	1803
36	43.70	116	18.24	9.90	19960905	721	43.42	2.60	150412	1846
36	43.79	116	17.90	9.55	19960905	816	55.60	3.55	150413	1853
36	43.68	116	18.00	9.68	19960905	820	49.58	2.96	150414	1854
36	38.07	115	51.29	2.50	19970614	1948	19.73	3.58	150416	3429
36	39.90	116	15.57	9.16	19970827	1451	23.22	2.12	150417	3833
36	42.89	116	18.30	11.74	19970912	1332	24.99	1.98	150418	3947
36	50.54	116	15.91	11.61	19970912	1336	54.63	3.87	150419	3942
36	50.58	116	15.73	11.55	19970912	1400	47.41	2.43	150420	3986
36	50.32	116	16.08	11.69	19970917	456	59.56	2.55	150421	4044
36	50.35	116	15.71	11.26	19971112	841	33.37	3.02	150422	4819
36	49.40	116	44.94	1.99	19971215	2114	18.36	2.23	150423	5065
37	10.05	116	36.00	5.46	19980310	1421	4.86	3.19	150424	5516
36	57.62	116	43.67	2.46	19980325	1255	53.34	3.04	150425	5605
36	57.49	116	41.39	3.47	19980325	1308	46.34	2.54	150426	5598
37	10.45	116	36.29	5.91	19980402	1920	16.45	3.57	150427	5665
36	42.15	116	18.32	12.93	19980414	105	52.05	2.29	150428	5796
36	43.03	116	18.26	11.64	19980616	954	19.71	2.09	150429	6316
36	47.94	115	56.85	11.45	19981208	514	6.03	2.75	150430	7221
36	42.52	116	18.43	11.67	19990111	1109	28.69	2.39	150431	7391
36	48.25	115	57.51	0.01	19990123	300	32.61	3.85	150432	7482
36	49.34	115	58.73	10.53	19990123	700	19.92	0.34	150433	7483
36	47.48	115	58.53	0.04	19990125	1852	5.15	4.03	150434	7566
36	46.98	115	58.67	9.36	19990127	1044	21.78	4.70	150435	7738
36	45.42	115	58.95	10.79	19990511	534	25.02	3.01	150436	9179
37	12.20	116	49.40	6.40	19990623	703	15.09	3.33	150437	9446
36	47.64	116	13.78	7.40	20000510	717	40.53	2.93	150286	25383
36	44.01	116	17.74	10.11	20000909	1912	11.78	3.16	150289	33302
36	35.25	116	15.65	1.43	20001020	1402	49.57	3.43	150292	35382
36	29.52	116	13.03	4.89	20001121	2039	41.97	3.42	150293	37259
36	43.14	116	18.21	10.52	20020525	1203	32.90	3.09	150294	9497
36	42.95	116	17.96	13.02	20020614	1240	44.50	4.42	150302	31
36	42.74	116	18.60	11.30	20020618	1624	31.63	3.13	150303	11730

Table 5.3 Earthquake Locations Recorded by a Portable Network at SGBDSN Strong Motion Sites

Lat Deg	Lat min	Lon Deg	Lon min.	Depth km	Origin time YYYYMMDD	Origin HHMM	Origin SS.SS	Ml	Origin Id	Event Id
36	44.21	116	13.31	6.15	19970123	2215	32.39	0.56	2786	2742
36	58.55	116	51.13	1.41	19970124	204	4.03	0.23	2791	2743
36	44.6	116	17.44	9.56	19970124	745	23.27	0.10	2794	2744
36	44.71	116	14.21	8.81	19970124	1638	51.05	0.31	2745	2745
36	44.38	116	14.43	9.05	19970124	1821	12.98	0.86	2746	2746
36	44.94	116	14.45	8.43	19970124	2235	50.7	0.26	2747	2747
36	44.08	116	18.2	9.69	19970125	40	22.27	-0.27	2757	2757
36	44.81	116	14.03	7.75	19970125	124	1.96	0.00	2756	2756
36	44.29	116	14.41	9.32	19970125	307	13.25	0.65	2755	2755
36	44.83	116	16.89	12.44	19970125	1105	44.83	0.02	2754	2754
36	43.6	116	17.82	10.23	19970125	1521	48.67	0.03	2752	2752
37	10.33	116	34.04	2.71	19970125	1535	12.52	0.78	2753	2753
36	42.63	116	45.34	1.27	19970125	1924	20.27	0.62	2751	2751
36	42.74	116	17.49	12.75	19970125	1955	59.14	1.44	2749	2749
36	43.15	116	17.9	11.74	19970125	1956	20.17	1.45	2750	2750
36	46.35	116	15.7	9.01	19970125	2028	55.39	0.20	2748	2748
36	43.29	116	18.02	9.82	19970126	729	48.21	0.14	2758	2758
36	43.62	116	17.88	11.06	19970126	1232	11.86	-0.06	2759	2759
36	44.51	116	17.53	8.9	19970126	1932	8.6	0.03	2760	2760
36	49.37	116	14.3	10.15	19970126	2347	38.2	-0.03	2761	2761
36	42.5	116	18.61	11.25	19970127	605	52.22	0.28	2762	2762
36	57.98	116	7.24	9.13	19970127	829	33.89	-0.07	2763	2763
36	43.61	116	18.57	8.97	19970128	615	46.06	-0.02	2764	2764
36	41.18	116	16.59	9.14	19970128	1041	39.52	0.71	2766	2766
36	44.61	116	17.32	10.09	19970129	315	13.41	-0.04	2767	2767
36	42.99	116	17.48	10.92	19970130	549	56.36	-0.37	2768	2768
36	42.36	116	18.22	12.96	19970130	553	27.95	0.02	2770	2770
36	42.17	116	18.35	13.15	19970130	643	52.98	0.14	2771	2771
36	42.5	116	18.5	10.48	19970130	649	5.54	0.37	2772	2772
36	42.53	116	18.32	12.15	19970130	708	9.79	0.03	2773	2773
36	43	116	18.51	11.52	19970130	715	16.71	-0.17	2774	2774
36	42.99	116	18.69	11.14	19970130	715	43.76	-0.42	2775	2775
36	49.07	116	12.38	6.21	19970130	1543	5.69	-0.10	2769	2769
36	51.19	116	16.56	9.78	19970131	854	15.11	-0.34	2776	2776
36	44.06	116	17.77	10.47	19970131	1331	39.52	-0.28	2777	2777

Source: DID 006DV.004 (MO0404UCC006DV.004), Combined seismicity catalog for FY1996-2002 in the vicinity of Yucca Mountain.

Table 5.4 Little Skull Mountain Portable Station Locations

Unqualified, included for information only. Do not use for quality-affecting work.

sta	lat	lon	elev
	deg.	deg.	km
rbnd	36.6646	-116.2041	1.157
ryuc	36.6206	-116.2117	0.847
rdun	36.6865	-116.5363	0.824
res2	36.8543	-116.4520	1.293
rxtn	36.7261	-116.3275	1.054
rfoc	36.7779	-116.2868	1.006
rlsm	36.7339	-116.3161	1.215
rsfc	36.8531	-116.4237	1.092
rcom	36.7285	-116.2223	1.136
rymm	36.8310	-116.4688	1.529
rymt	36.8371	-116.4683	1.549
rtpp	36.7229	-116.1288	1.132

Source: Su, F., J. G. Anderson, J. N. Brune, and Y. Zeng. (1996). A comparison of direct S-wave and coda wave site amplification determined from aftershocks of the Little Skull Mountain earthquake, Bulletin of the Seismological Society of America, 86, 1006-1018. Table 1

Table 5.5 Little Skull Mountain Portable Network Earthquake Locations
Unqualified, included for information only; not for use
in any quality-affecting work.

lat	lon	depth	time	orid	evid	ml
36.7195	-116.283	10.7	7/25/1992 (207) 2:16:35.550	392	392	2.7
36.7465	-116.2593	9	7/28/1992 (210) 10:37:41.800	401	401	3.2
36.7077	-116.2978	9.9	7/30/1992 (212) 8:13:35.560	409	409	3.2
36.7558	-116.2657	11.1	8/16/1992 (229) 16:36:36.010	419	419	3.3
36.7573	-116.2487	12.3	8/18/1992 (231) 8:00:05.330	430	430	3.5
36.7317	-116.2967	9.9	8/23/1992 (236) 7:47:21.240	442	442	2.8
36.7337	-116.2762	12.1	8/24/1992 (237) 20:55:59.940	454	454	2.7
36.7095	-116.2718	10.6	8/29/1992 (242) 1:18:31.430	466	466	3
36.8085	-116.2483	10.2	8/30/1992 (243) 15:37:16.490	477	477	3
36.7243	-116.3047	9.3	9/13/1992 (257) 11:46:20.820	488	488	4.5
36.7193	-116.3088	8.7	9/14/1992 (258) 5:35:52.000	502	502	3.2
36.6877	-116.3112	12.3	9/25/1992 (269) 21:12:24.000	515	515	3.7
36.7313	-116.3075	9.4	9/25/1992 (269) 21:16:39.100	524	524	3.7
36.7612	-116.2727	10.4	10/08/1992 (282) 12:23:56.880	533	533	3.8
36.7313	-116.2505	10.1	10/09/1992 (283) 0:16:17.830	546	546	3.4
36.7215	-116.3037	9.7	11/01/1992 (306) 8:35:07.420	558	558	3.2
36.6972	-116.2107	9.9	11/04/1992 (309) 1:00:14.510	561	561	3.4
36.7043	-116.3037	11.3	11/06/1992 (311) 20:24:03.150	573	573	3.5

Source:

Su, F., J. G. Anderson, J. N. Brune, and Y. Zeng. (1996). A comparison of direct S-wave and coda wave site amplification determined from aftershocks of the Little Skull Mountain earthquake, Bulletin of the Seismological Society of America, 86, 1006-1018. Table 2. Unqualified.

Table 5.6: Blume Strong Motion Network Station Locations
Unqualified, to support corroborating results only. Not for use in quality-affecting work

sta	lat	lon	staname
CPTB	36.93	-116.06	Blume Control Point SM site
LWLB	36.64	-116.40	Blume Lathrop Wells
BTYB	36.91	-116.76	Blume Beatty
LVNB	36.26	-115.31	Blume NW Las Vegas, Ann Road, W of Hwy 95
NDVB	37.03	-117.34	Blume NE Death Valley
DTWB	36.17	-115.19	Blume W. of old Downtown
DTCB	36.17	-115.14	Blume Central old Downtown
DTSB	36.11	-115.14	Blume S. of old Downtown btw Trop & Flamingo
FMNB	36.24	-115.02	Blume Frenchman Mntn
GFDB	37.71	-117.23	Blume Goldfield
TNPB	38.07	-117.23	Blume Tonopah
MN_4	36.23	-116.07	Pahrump Site 2
MN_5	36.21	-115.98	Pahrump Site 1
MN_6	36.15	-115.41	Las Vegas
MN_9	36.22	-115.22	Las Vegas
MN10	36.21	-115.16	Las Vegas
MN12	37.65	-115.63	Tempiute
MN14	37.27	-115.12	Alamo
MN17	36.18	-115.02	Las Vegas
MN18	36.06	-115.07	Las Vegas
MN20	35.15	-114.58	Laughlin

Source: Lum, P.K. and K. K. Honda, 1992. Processed seismic motion records from the Little Skull Mountain, Nevada, earthquake of June 29, 1992, recorded at stations in southern Nevada, Report # JAB-10733-TM6 UC-703 National Technical Information Service, 206 p. DE93013314. HQO.940520.0008. Files: Table 1.
Station names added for reference. LWLB site was reoccupied by SGBDSN station LWLS.

Table 5.7. Blume Event Locations and Times
This table is Unqualified, for corroboration purposes only. Do not use for quality-affecting work.

lat	lon	depth (km)	event time	orid	Ml
36.718	-116.289	9.0000	6/29/1992 (181) 10:14:22.000	5	5.60
36.674	-116.265	8.0000	7/05/1992 (187) 6:54:13.000	4	4.40
36.665	-116.324	8.0000	9/13/1992 (257) 11:46:20.000	6	4.10

Sources:
orid #5: Lum and Honda (1992), reference as above on this page. Data on their page 2.
orid #4 and 6: Lum, P.K. and K. K. Honda, 1992. Processed seismic motion records from the Little Skull Mountain, Nevada, earthquake of June 29, 1992, recorded at stations in southern Nevada, Report # JAB-10733-TM6 UC-703, data on page 1. Depth for these events is not given in this source. Nominal depth of 8 km inserted. KappaAH results for Blume network events do not depend on depth.

Table 5.8. Models tested in formal inversions to characterize the site, event, and distance dependence of *kappa* (Qualified)

Case #	Station terms	Event terms	*dk/dR*		Notes
1				$\kappa = \bar{\kappa}$	Base case assumes *kappa* is a universal constant
2	✓			$\kappa = \kappa_0$	Assumes *kappa* only depends on station
3	✓	✓		$\kappa = \kappa_0 + \kappa_E$	Assumes *kappa* depends on station and event. Constrains average of event terms to zero.
4	✓	✓	✓	$\kappa = \kappa_0 + \kappa_E + \kappa_R R$	Adds a linear distance term to Model 3. Constrains average of event terms to zero.
5	✓		✓	$\kappa = \kappa_0 + \kappa_R R$	Assumes *kappa* only depends on station and distance
6		✓		$\kappa = \kappa_E$	Assumes *kappa* only depends on the event. Average event term is unconstrained.
7	✓	✓	✓ constrained	$\kappa = \kappa_0 + \kappa_E + \kappa_R R$	Sets *dk/dR* to the value found in Model 5. Constrains average of event terms to zero.
8	✓cons trained	✓	✓ constrained	$\kappa = \kappa_0 + \kappa_E + \kappa_R R$	Sets *dk/dR* and all station terms to values in case 5. Constrains average of event terms to zero.
9	✓	✓	✓modified	$\kappa = \kappa_0 + \kappa_E + \tilde{\kappa}(R)$	Distance dependence is *dk/dR=0, R*<40 km, *dk/dR* determined by data, *R*>40 km.
10	✓		✓modified	$\kappa = \kappa_0 + \tilde{\kappa}(R)$	Distance dependence is *dk/dR=0, R*<40 km, *dk/dR* determined by data, *R*>40 km.

Table 5.9. Improvements in models for formal inversions. Model testing matrix for spectral fits with constrained upper corner frequency estimates. Entries s1, s2, etc., are the RMS misfits for Models 1, 2, etc. Ratios greater than 1.0 indicate some improvement in fit; a chi-squared test determines significance. Source for RMS misfit and Ratio data in DID 006GB.003, file kappawrap/case6a/kappa_out, with RMS in units of seconds. This table as displayed below in DID 006GB.003, file kappawrap/case6a/Figs_summary/T5.9_formal_invers_results.doc

Model	RMS Misfit (ms)	Compari-son model	Ratio basis	Ratio	Significant at level	Comments
1	14.8	base				Base model is κ=26.0 ms
2	11.3	1	s1/s2	1.3107	>95%	Station terms are important.
3	6.7	2	s2/s3	1.6720	>95%	Event terms improve the model.
4	7.2	3	s3/s4	0.9327	low	A linear distance term addition slightly degrades the fit.
5	9.8	2	s2/s5	1.1570	>95%	Distance dependence improves model when there are no event terms.
6	11.5	1	s1/s6	1.2915	>95%	Event terms by themselves are significant, and reduce the misfit by more than the station terms.
7	7.5	5	s5/s7	1.3021	>95%	
8	7.7	5	s5/s8	1.2649	>95%	
9	6.6	3	s3/s9	1.0168	low	Improvement with bilinear distance dependence has low significance, but is better than the linear Model 4.
10	9.9	2	s2/s10	1.1375	>95%	Bilinear distance dependence is an improvement over the station-terms-only model (2), but not quite as good as Model 5.

Table 5.10 SGBDSN station parameter estimates for formal inversion models, Case 6a.
Source: DID 006GB.003, file kappawrap/case6a, files kappa_out and Figs_summary/T10_formal_inv_station_part.xls

Sta	M1_k	M1_s	M2_k	M2_s	M3_k	M3_s	M4_k	M4_s	M5_k	M5_s	M6_k	M6_s	M7_k	M7_s	M8_k	M8_s	M9_k	M9_s	M10_k	M10_s
	msec	msec	msec	msec	msec	msec	msec	msec	msec	msec	msec	msec	msec	msec	msec	msec	msec	msec	msec	msec
AL5	25.98	14.79	18.15	1.75	9.28	1.89	-1.65	1.84	2.43	1.78	-999	-999	-3.43	1.89	2.43	1.78	9.02	1.89	14.41	1.76
AMD	25.98	14.79	25.15	2.47	21.37	2.66	10.05	2.64	10.2	2.48	-999	-999	7.64	2.66	10.2	2.48	20.95	2.66	22.34	2.48
BTW	25.98	14.79	6.12	1.7	2.53	1.81	-12.29	1.78	-12.73	1.75	-999	-999	-15.61	1.81	-12.73	1.75	0.95	1.85	0.68	1.72
BYMS	25.98	14.79	22.88	2.65	23	2.8	12.63	2.77	13.17	2.65	-999	-999	10.96	2.8	13.17	2.65	22.64	2.8	22.88	2.65
CAF	25.98	14.79	23.44	1.81	18.85	1.92	11.13	1.88	13.21	1.82	-999	-999	10.36	1.92	13.21	1.82	19.18	1.92	23.04	1.81
CRF	25.98	14.79	32.74	1.11	30.63	1.23	19.28	1.21	18.39	1.16	-999	-999	16.67	1.23	18.39	1.16	29.95	1.24	30.02	1.12
DOM	25.98	14.79	34.78	1.22	31.48	1.34	19.12	1.32	18.55	1.28	-999	-999	16.23	1.34	18.55	1.28	31.03	1.35	32.56	1.22
EXHS	25.98	14.79	26.24	2.02	19.31	2.16	9.67	2.11	13.88	2.03	-999	-999	8.46	2.16	13.88	2.03	19.28	2.16	24.45	2.02
FMW	25.98	14.79	18.98	1.46	16.66	1.57	6.4	1.56	5.84	1.49	-999	-999	3.81	1.57	5.84	1.49	15.99	1.58	16.5	1.47
FOCS	25.98	14.79	25.42	3.13	21.78	3.39	15.79	3.36	19.62	3.13	-999	-999	15.82	3.39	19.62	3.13	21.71	3.39	25.42	3.13
FRG	25.98	14.79	20.25	1.11	17.58	1.23	8.31	1.21	8.08	1.15	-999	-999	6.21	1.23	8.08	1.15	17.22	1.23	18.12	1.11
LSC	25.98	14.79	53.5	3.5	41.36	3.72	32.08	3.69	33.96	3.47	-999	-999	31.07	3.72	33.96	3.47	42.28	3.73	48.4	3.51
LWLS	25.98	14.79	31.6	2.33	30.62	2.48	22.08	2.45	23.95	2.34	-999	-999	21.15	2.48	23.95	2.34	30.32	2.49	31.6	2.33
MDVS	25.98	14.79	34.8	3.5	25.6	3.64	14.58	3.58	20.83	3.49	-999	-999	14.46	3.64	20.83	3.49	25.75	3.64	32.64	3.5
NCF	25.98	14.79	26.76	1.94	25.97	2.07	12.8	2.04	11.81	1.96	-999	-999	9.93	2.07	11.81	1.96	25.53	2.07	26.42	1.94
PUV	25.98	14.79	20.7	2.86	15.98	3.01	3.91	2.98	4.1	2.86	-999	-999	1.7	3.01	4.1	2.86	16.02	3.01	18.45	2.86
RED	25.98	14.79	-1.29	1.46	-4.1	1.6	-11.55	1.58	-10.85	1.48	-999	-999	-12.89	1.6	-10.85	1.48	-3.82	1.6	-1.29	1.46
RPY	25.98	14.79	36.16	1.35	34.73	1.46	24.81	1.42	23.86	1.38	-999	-999	22.85	1.46	23.86	1.38	34.43	1.46	34.52	1.35
SCF	25.98	14.79	30.59	2.11	34.26	2.25	23.16	2.22	18.95	2.12	-999	-999	20.92	2.25	18.95	2.12	33.88	2.25	30.59	2.11
SGR	25.98	14.79	23.64	1.81	13.75	1.93	-15.11	1.99	-16.32	1.99	-999	-999	-22.98	1.93	-16.32	1.99	3.39	3.17	-14.41	2.77
SPC	25.98	14.79	33.78	1.7	29.37	1.85	18.97	1.84	19.72	1.72	-999	-999	16.79	1.85	19.72	1.72	28.4	1.86	28.78	1.72
SPRS	25.98	14.79	29.38	2.02	23.95	2.14	17.6	2.1	21.18	2.03	-999	-999	17.47	2.14	21.18	2.03	24.35	2.14	29.38	2.02
STC	25.98	14.79	31.68	1.7	23.8	1.82	2.5	1.82	3.23	1.8	-999	-999	-2.64	1.82	3.23	1.8	18.44	2.23	11.92	2.02
STH	25.98	14.79	19.5	4.04	10.76	4.5	5.81	4.48	14.86	4.04	-999	-999	5.93	4.5	14.86	4.04	10.63	4.5	19.5	4.04
STO	25.98	14.79	30.79	1.46	25.3	1.58	14.42	1.54	15.98	1.5	-999	-999	12.26	1.58	15.98	1.5	24.87	1.58	27.71	1.47
SYM	25.98	14.79	24.79	1.61	21.76	1.73	13.15	1.72	12.53	1.63	-999	-999	10.9	1.73	12.53	1.63	21.23	1.73	21.68	1.62
SYMS	25.98	14.79	27.62	2.47	24.86	2.6	14.67	2.56	16.61	2.48	-999	-999	13.36	2.6	16.61	2.48	24.57	2.6	26.53	2.48
TAR	25.98	14.79	26.5	3.13	15.94	3.23	-1.55	3.15	2.87	3.11	-999	-999	-4.35	3.23	2.87	3.11	13.37	3.29	14.61	3.2
TIM	25.98	14.79	37.99	1.24	33.65	1.36	19.1	1.36	19.09	1.32	-999	-999	15.6	1.36	19.09	1.32	32.12	1.41	32.34	1.28
TPW	25.98	14.79	17.2	1.81	16.85	1.95	8.67	1.92	7.47	1.82	-999	-999	7.43	1.95	7.47	1.82	16.96	1.95	17.2	1.81
TWP	25.98	14.79	23.33	2.21	18.86	2.4	-0.6	2.34	-0.15	2.25	-999	-999	-3.92	2.4	-0.15	2.25	15.85	2.5	12.42	2.29
TYM	25.98	14.79	23.74	3.13	19.22	3.24	-5.76	3.14	-8.24	3.1	-999	-999	-10.82	3.24	-8.24	3.1	12.46	3.63	-1.4	3.42
TYMS	25.98	14.79	25.27	2.47	27.18	2.65	17.63	2.62	15.95	2.48	-999	-999	16.23	2.65	15.95	2.48	26.98	2.65	25.27	2.47
WCTS	25.98	14.79	6.84	3.5	6	3.66	-8.75	3.59	-8.35	3.48	-999	-999	-10.49	3.66	-8.35	3.48	5.81	3.67	6.84	3.5
WLD	25.98	14.79	15.83	2.47	11.85	2.6	-3.86	2.55	-4.77	2.49	-999	-999	-7.04	2.6	-4.77	2.49	10.13	2.63	8.43	2.51
YCW	25.98	14.79	25.04	1.24	24.58	1.34	12.97	1.35	10.45	1.28	-999	-999	10.04	1.34	10.45	1.28	23.98	1.35	23.05	1.24

Notes
1. M#_k and M#_s are the kappa estimate and standard deviation, respectively for Model #.
2. -999 values mean "not applicable" (e.g., no station terms for model 6)

Table 5.11 SGBDSN event terms for formal inversion models, Case 6a
Source: DID 006GB.003, file kappawrap/case6a/kappa_out, and this table in Figs_summary/T11_formal_inv_events_case6a.xls

Evid	E1_k	E2_k	E2_s	E3_k	E3_s	E4_k	E4_s	E5_k	E5_s	E6_k	E6_s	E7_k	E7_s	E8_k	E8_s	E9_k	E9_s	E10_k	E10_s
31	-999	-999	-999	-0.44	1.31	1.93	1.29	-999	-999	22.85	1.12	0.58	1.31	-2.54	1.12	-0.42	1.31	-999	-999
687	-999	-999	-999	-5.09	4.06	-4	4.06	-999	-999	22.32	4.04	-3.09	4.06	-4.02	4.04	-4.8	4.06	-999	-999
726	-999	-999	-999	-2.96	1.73	-0.54	1.71	-999	-999	15.81	1.61	-1.11	1.73	-2.95	1.61	-2.73	1.73	-999	-999
1273	-999	-999	-999	-2.48	1.57	0.24	1.55	-999	-999	21.14	1.46	-0.25	1.57	-1.99	1.46	-1.93	1.57	-999	-999
1429	-999	-999	-999	-3.12	2.55	-2.42	2.55	-999	-999	23.13	2.47	-3.21	2.55	-5.76	2.47	-2.69	2.55	-999	-999
1438	-999	-999	-999	-13.4	3.54	-11.3	3.55	-999	-999	16.63	3.5	-10.62	3.54	-11.09	3.5	-12.82	3.55	-999	-999
1542	-999	-999	-999	3	1.69	5.15	1.68	-999	-999	24.08	1.61	4.48	1.69	2.41	1.61	3.45	1.69	-999	-999
1803	-999	-999	-999	-0.86	1.49	1.17	1.48	-999	-999	21.02	1.4	0.35	1.49	-2.02	1.4	-0.63	1.49	-999	-999
1846	-999	-999	-999	-4.55	2.08	-2.1	2.07	-999	-999	21.23	2.02	-2.3	2.08	-4.43	2.02	-4.05	2.08	-999	-999
1853	-999	-999	-999	-0.98	1.27	1.82	1.25	-999	-999	21.5	1.14	1.07	1.27	-1.68	1.14	-0.55	1.28	-999	-999
1854	-999	-999	-999	-2.8	2.76	0.4	2.75	-999	-999	12.73	2.65	0.79	2.76	-1.48	2.65	-2.45	2.76	-999	-999
3429	-999	-999	-999	13.86	2.11	5.95	2.17	-999	-999	33.96	1.94	2.22	2.11	-0.03	1.94	10.85	2.23	-999	-999
3833	-999	-999	-999	-11.66	4.13	-11.27	4.14	-999	-999	7.18	4.04	-10.28	4.13	-12.38	4.04	-11.29	4.14	-999	-999
3942	-999	-999	-999	2.12	1.51	4.31	1.5	-999	-999	25.79	1.35	3.32	1.51	1.03	1.35	2.48	1.52	-999	-999
3947	-999	-999	-999	-17.92	4.03	-16.95	4.03	-999	-999	10.01	4.04	-15.95	4.03	-17.68	4.04	-17.55	4.03	-999	-999
3986	-999	-999	-999	-13.66	7.03	-21.6	6.95	-999	-999	8.1	7	-12.69	7.03	-14.31	7	-13.13	7.03	-999	-999
4044	-999	-999	-999	-4.09	4.07	-4.17	4.07	-999	-999	10.23	4.04	-3.2	4.07	-5.67	4.04	-3.87	4.07	-999	-999
4819	-999	-999	-999	-18.48	3.55	-17.03	3.55	-999	-999	2.12	3.5	-16.57	3.55	-17.36	3.5	-18.27	3.55	-999	-999
5065	-999	-999	-999	-15.85	6.95	-21.49	6.92	-999	-999	8.73	7	-14.1	6.95	-14.51	7	-15.26	6.95	-999	-999
5516	-999	-999	-999	2.05	2.98	8.62	2.64	-999	-999	27.47	2.65	4.67	2.98	1.11	2.65	2.87	2.98	-999	-999
5598	-999	-999	-999	-7.19	2.51	-6.77	2.51	-999	-999	19.98	2.47	-7.34	2.51	-9.15	2.47	-7.19	2.51	-999	-999
5605	-999	-999	-999	-1.73	1.89	1.58	1.88	-999	-999	23.46	1.81	1.11	1.89	-1.31	1.81	-1.18	1.9	-999	-999
5665	-999	-999	-999	9.32	1.73	8.5	1.74	-999	-999	34.31	1.65	6.86	1.73	4.6	1.65	8.85	1.74	-999	-999
5796	-999	-999	-999	-0.45	2.28	0.59	2.28	-999	-999	23.9	2.21	-0.09	2.28	-1.72	2.21	-0.22	2.28	-999	-999
6316	-999	-999	-999	0.79	7	-4.77	6.94	-999	-999	17.45	7	3.44	7	1.41	7	1.47	7	-999	-999
7221	-999	-999	-999	-19.3	4.07	-17.99	4.07	-999	-999	10.53	4.04	-16.96	4.07	-17.01	4.04	-18.75	4.07	-999	-999
7391	-999	-999	-999	-0.86	2.31	1.79	2.3	-999	-999	19.84	2.21	1.16	2.31	-1.78	2.21	-0.24	2.32	-999	-999
7482	-999	-999	-999	10.41	1.2	6.46	1.28	-999	-999	31.62	1.06	3.05	1.2	0.01	1.06	8.6	1.28	-999	-999
7483	-999	-999	-999	25.54	1.57	21.31	1.64	-999	-999	48.44	1.46	17.91	1.57	14.38	1.46	23.45	1.65	-999	-999
7566	-999	-999	-999	19.78	1.55	15.45	1.61	-999	-999	41.88	1.43	11.93	1.55	8.25	1.43	17.58	1.63	-999	-999
7738	-999	-999	-999	18.85	1.34	15.97	1.43	-999	-999	40.73	1.15	11.82	1.34	7.37	1.15	17.26	1.39	-999	-999
9179	-999	-999	-999	5.01	4.97	0.03	4.94	-999	-999	36.52	4.95	1.1	4.97	-2.11	4.95	3.76	4.97	-999	-999
9446	-999	-999	-999	7.91	2.11	10.13	2.1	-999	-999	29.33	2.02	9.38	2.11	6.2	2.02	9.56	2.15	-999	-999
9497	-999	-999	-999	5.64	2.43	8.21	2.42	-999	-999	29.4	2.33	7.69	2.43	4.52	2.33	6.12	2.43	-999	-999
11730	-999	-999	-999	-2.02	1.86	-0.2	1.86	-999	-999	19.05	1.75	-1.08	1.86	-3.76	1.75	-2	1.86	-999	-999
25383	-999	-999	-999	-6.28	1.26	-4.15	1.24	-999	-999	15.31	1.12	-5.38	1.26	-7.97	1.12	-6.01	1.26	-999	-999
33302	-999	-999	-999	0.91	1.88	4	1.86	-999	-999	21.96	1.7	3.61	1.88	1.05	1.7	1.23	1.88	-999	-999
35382	-999	-999	-999	12.66	2.73	12.51	2.73	-999	-999	26.01	2.33	11.46	2.73	7.38	2.33	12.7	2.73	-999	-999
37259	-999	-999	-999	18.31	4.13	15.86	4.13	-999	-999	37.15	4.04	16.23	4.13	14.13	4.04	17.79	4.14	-999	-999

A1_k	A1_s	A2_k	A2_s	A3_k	A3_s	A4_k	A4_s	A5_k	A5_s	A6_k	A6_s	A7_k	A7_s	A8_k	A8_s	A9_k	A9_s	A10_k	A10_s
-999	-999	-999	-999	-999	-999	0.3514	0.0164	0.483	0.0125	-999	-999	0.483	0.0125	0.483	0.0125	0.2315	0.056	0.789	0.0435

Notes
1. E#_k and E#_s are the kappa estimate and standard deviation, respectively for Model #.
2. A#_k and A#_s are auxilliary results - distance correction and standard deviation (msec)
3. -999 values mean "not applicable" (e.g., no event terms for models 1, 2, and 5)

Table 5.12 SGBDSN event mean kappa and mean kappa with r<40km
Case 6a, SGBDSN "M3" data
Source: DID 006GB.003, file kappawrap/case6a/Figs_summary/event_kappa_case6a.tbl.
Reduced data in kappawrap/case6a/Figs_summary/T12event_kappas_case6a.xls

origin_id	depth	k_(ms)	dk_(ms)	sd_k	k40_(ms)	dk40_(ms)	_d k40
e_150286	7.4	17.2	-10	11.3	16.9	-9	11.8
e_150289	10.11	24.2	-3	13.9	24.2	-1.7	13.9
e_150292	1.43	30	2.8	11.7	30	4.2	11.7
e_150293	4.89	36.6	9.4	11.8	35.6	9.7	13.4
e_150294	10.52	33.8	6.6	11.2	33	7.1	10.8
e_150302	13.02	22.6	-4.7	9.8	21.3	-4.6	9.6
e_150303	11.3	25.6	-1.7	12.5	25.6	-0.3	13
e_150405	14.14	24.3	-2.9	12	24.3	-1.5	12
e_150406	11.92	17.9	-9.4	13.7	17.9	-8	13.7
e_150407	9.63	23.7	-3.5	13.3	23.7	-2.1	13.3
e_150408	10.18	26.1	-1.1	14.1	26.1	0.2	14.1
e_150409	11.02	20.8	-6.5	14.7	20.8	-5.1	14.7
e_150410	10.97	29.2	2	13.4	28.9	3	13.7
e_150411	11.11	24.3	-2.9	12.4	25.1	-0.7	12.9
e_150412	9.9	20.6	-6.6	12.4	20.2	-5.7	12.7
e_150413	9.55	21.7	-5.6	13.1	22.1	-3.7	13.7
e_150414	9.68	16.4	-10.8	12.1	16.4	-9.4	12.1
e_150416	2.5	32.7	5.4	13.1	23.6	-2.3	16.8
e_150417	9.16	23.8	-3.4	17.6	24	-1.9	18.4
e_150418	11.74	17.3	-9.9	14.9	16.8	-9.1	15.8
e_150419	11.61	25.9	-1.3	11.6	25.9	0	11.6
e_150420	11.55	23.8	-3.4	12.9	23.7	-2.2	13.4
e_150421	11.69	24.8	-2.4	14.8	24.5	-1.4	15
e_150422	11.26	13.9	-13.4	12.9	14	-11.9	13.3
e_150423	1.99	19.6	-7.6	12.1	19	-6.9	11.9
e_150424	5.46	35.5	8.3	10.7	33.5	7.6	10
e_150425	2.46	28.3	1	13.3	29.1	3.2	12.1
e_150426	3.47	23.9	-3.3	13.8	22.8	-3.1	13.3
e_150427	5.91	35.1	7.8	12.9	32.1	6.2	13.1
e_150428	12.93	26.1	-1.1	10.3	25.1	-0.8	10.3
e_150429	11.64	29.9	2.7	10.4	29.1	3.2	9.8
e_150430	10.67	16.8	-10.4	12.6	16.8	-9.1	13.1
e_150431	11.67	25.9	-1.3	10.8	26.2	0.4	10.8
e_150432	0.01	34.4	7.1	10.2	34.2	8.3	14.3
e_150433	0.7	49.9	22.6	10.8	44.8	18.9	15.7
e_150434	0.04	42.5	15.2	11.5	37.8	11.9	16.6
e_150435	9.36	42.6	15.4	10.3	35.9	10	7.4
e_150436	10.79	36.4	9.2	11.3	32.5	6.6	10.4
e_150437	6.4	37.8	10.6	14.6	25.7	-0.2	12.7
Mean		27.23	0.00	12.48	25.88	-0.01	12.89

Notes:
(1) Data subset
sqerr<0.151 && bst<100 MPa && bfc < 20 Hz && SNRpct>0.50 && chan!~/..Z/
input: Case6a database
k40 has additional subset: epicentral distance edist<40000 (40 km)
(2) k and k40 are arithmetic means of kappa values passing respective subsets
(3) sd_k and sd_k40 are standard deviations of contributing measurements
(4) dk and dk40 are event differences from bottom row Mean k and k40, resp.
(5) Mean dk and dk40 are mean(absolute value(dk or dk40))

Table 5.13 SGBDSN event mean stress drop, corner frequency, and median kappa
Source: DID 006GB.003, file kappawrap/case6a/Figs_summary/T13case6aEventBfcBstFinal.xls
base table values in Figs_summary/event_bfc_bst.tbl

Event Id	fc (Hz)	fc_low (Hz)	fc_high (Hz)	Str-Drp bars	SD_low bars	SD_high bars	Kappa msec	SD_kappa msec
e_150286	3.3	2.2	5.1	4	1.3	12.5	16	11.3
e_150289	4.1	2.5	6.8	33.4	8.9	125.3	25.1	13.9
e_150292	4.9	3.2	7.6	59.4	22.2	158.8	33	11.7
e_150293	6	3.7	9.7	75.4	21.1	269.4	37.7	11.8
e_150294	8.2	5.4	12.4	71.3	17.2	295.3	34.2	11.2
e_150302	2.7	1.7	4.3	90.6	28.5	288.2	21.2	9.8
e_150303	6.9	4.1	11.7	59.3	14.6	241.3	26.4	12.5
e_150405	8.2	4.6	14.4	38.6	9.2	161.9	25.5	12
e_150406	4.4	3	6.5	8.8	2.7	28.7	15.7	13.7
e_150407	4.8	3.1	7.4	5	1	25.3	25.9	13.3
e_150408	8.3	5.1	13.7	18.3	3.9	85.3	29.2	14.1
e_150409	8.6	5	14.7	21.3	3.8	118.8	18.3	14.7
e_150410	5.7	3.6	9.2	39.6	10.8	146.2	29.9	13.4
e_150411	4.7	3.4	6.6	16.8	5.9	47.9	25.5	12.4
e_150412	6.1	4.1	8.9	13.2	3.8	46.1	23.3	12.4
e_150413	2.4	1.4	4.1	13	3.3	50.6	21.8	13.1
e_150414	3.3	2.1	5.1	8.3	2.2	30.9	21.1	12.1
e_150416	2	1.1	3.6	6.5	2.4	17.6	36.6	13.1
e_150417	8.7	5	15.2	10.1	1.7	59.2	24.8	17.6
e_150418	9	5.6	14.5	8.2	1.6	41.3	16.9	14.9
e_150419	2.5	1.9	3.3	40.5	18.9	86.7	29	11.6
e_150420	10.5	6.8	16.4	44.2	12.6	154.6	24.9	12.9
e_150421	8.9	5.9	13.6	34.2	7.8	150.9	28.5	14.8
e_150422	4.1	2.6	6.4	14.3	3.7	55.7	14.2	12.9
e_150423	9.9	6.3	15.4	11	2.9	41.4	20.4	12.1
e_150424	8.3	5	14	71.3	19.1	266.1	35.1	10.7
e_150425	5.4	3.1	9.5	16.7	3.1	89.5	29.5	13.3
e_150426	7.2	4.3	12.2	13.5	2.7	68.7	27.7	13.8
e_150427	4.4	2.9	6.6	30.6	8.8	106.8	34.2	12.9
e_150428	8.1	5.3	12.3	12.9	4.4	37.9	23.9	10.3
e_150429	11	7	17.3	22.6	4.7	109.4	29.1	10.4
e_150430	9.9	5.6	17.6	15.9	2.9	87.4	16.9	12.6
e_150431	7.9	5.5	11.4	11.9	3.7	38.1	27.4	10.8
e_150432	2.4	1.4	4	13.5	4.1	44.6	32.6	10.2
e_150433	5.6	3.7	8.6	32.1	8.9	115.9	49.5	10.8
e_150434	4.3	2.7	6.7	91.8	26.5	318.4	42.9	11.5
e_150435	3.4	2	5.5	59.8	14.3	250.1	42.2	10.3
e_150436	9.9	6.7	14.8	64.2	16.4	250.8	35.8	11.3
e_150437	7.5	4.7	12.2	39.5	9.8	159.9	39.4	14.6
			Mean:	31.84	8.75	120.09	27.98	12.48

Notes:
(1) Data subset
sqerr<0.151 && bst<100 MPa && bfc < 20 Hz && SNRpct>0.50 && chan!~/..Z/
input: Case6a database
(2) Mean corner frequency fc and stress drop Str-Drp from log-average:
10^mean(log10(.))
Std deviations from 10^std(log10(.))
(3) Kappa is median value

Table 5.14 SGBDSN station kappa estimates.
Case 6a, SGBDSN "M3" data; k_cor is the best station kappa estimate.
Source: DID 006GB.003, directory kappawrap/case6a/Figs_summary, files
T14_case6aStationKappaFinal.xls (this file) and station_kappas_case6a.tbl

sta	mean_k	k_std	k_SE	k_cor	kcor_sd	kcor_SE	k_wtd	n_used	N
AL5	0.0133	0.0062	0.002192	0.0141	0.006	0.0021	0.0162	8	15
AMD	0.0227	0.0049	0.001359	0.0232	0.0062	0.0017	0.0252	13	23
BTW	0.0036	0.0143	0.002489	0.0054	0.0132	0.0023	0.0112	33	50
CAF	0.0258	0.011	0.001976	0.0257	0.0065	0.0012	0.0315	31	50
CRF	0.0279	0.0066	0.000963	0.0307	0.0068	0.0010	0.0315	47	60
DOM	0.028	0.01	0.001562	0.0306	0.0072	0.0011	0.0334	41	53
FMW	0.0172	0.0104	0.001501	0.0198	0.0079	0.0011	0.0228	48	54
FRG	0.0176	0.0109	0.001607	0.0206	0.0098	0.0014	0.0236	46	58
LEC	0.0342	0.0022	0.00127	0.0309	0.0057	0.0033	0.0349	3	4
LSC	0.036	0.013	0.003064	0.0361	0.0088	0.0021	0.0422	18	37
NCF	0.0295	0.0071	0.001096	0.0319	0.0054	0.0008	0.0332	42	52
PUV	0.0226	0.0081	0.001909	0.0236	0.0071	0.0017	0.0268	18	34
RED	0.001	0.0117	0.001638	0.0019	0.0086	0.0012	0.0075	51	59
RPY	0.0364	0.008	0.00118	0.0397	0.0062	0.0009	0.0408	46	53
SCF	0.0401	0.0106	0.001598	0.0436	0.0102	0.0015	0.0456	44	57
SGR	0.0166	0.0008	0.000566	0.0059	0.0008	0.0006	0.0167	2	19
SPC	0.034	0.0128	0.00205	0.035	0.0103	0.0016	0.0409	39	53
STC	0.0371	0.0033	0.002333	0.0281	0.0056	0.0040	0.0379	2	34
STH	0.0247	0.0074	0.003021	0.0221	0.0053	0.0022	0.0278	6	7
STO	0.0292	0.0082	0.001297	0.0312	0.0065	0.0010	0.0336	40	56
SYM	0.0199	0.009	0.001342	0.0228	0.009	0.0013	0.0248	45	61
TAR	0.016	0.0078	0.002252	0.0212	0.0062	0.0018	0.0198	12	27
TIM	0.0322	0.0105	0.002409	0.0328	0.0067	0.0015	0.0374	19	48
TPW	0.0215	0.0109	0.00206	0.0214	0.0088	0.0017	0.0273	28	41
TYM	0.0228	0	0	0.0121	0	0.0000	0.0228	1	23
WLD	0.021	0.0074	0.001288	0.024	0.007	0.0012	0.0249	33	52
YCW	0.025	0.01	0.001715	0.0265	0.0079	0.0014	0.0303	34	42
YFT	0.0117	0	0	0.0222	0	0.0000	0.0117	1	3
BYMS	0.0219	0.0068	0.001649	0.0254	0.0064	0.0016	0.0254	17	18
EXHS	0.0249	0.0061	0.001929	0.0262	0.006	0.0019	0.0278	10	14
FOCS	0.0258	0.0153	0.004613	0.0269	0.0108	0.0033	0.0334	11	11
LWLS	0.0321	0.0078	0.001702	0.0343	0.0084	0.0018	0.0362	21	21
MDVS	0.0269	0.0034	0.001521	0.0304	0.0036	0.0016	0.0282	5	10
SPRS	0.0263	0.0094	0.001919	0.0246	0.0096	0.0020	0.0312	24	26
SYMS	0.0234	0.0063	0.001314	0.0273	0.0065	0.0014	0.0267	23	31
TYMS	0.0243	0.0067	0.00202	0.0276	0.0051	0.0015	0.0273	11	15
WCTS	0.0124	0.0096	0.0032	0.0163	0.0092	0.0031	0.017	9	9
Means	0.0239	0.0080	0.0018	0.0249	0.0069	0.0016	0.0280	23.8	34.6

Notes:
(1) Data: Case6a database. Subset for k and k_cor:
sqerr<0.151 && bst<100 MPa && bfc < 20 Hz && SNRpct>0.50 && ...
chan!~/..Z/ && epicentral distance edist<40000 (40 km)
Only station-event distance < 40 km measurements are used.
(2) mean_k: Mean of estimates from fitting (sec.) k_std: Standard deviation
(3) k_cor: k corrected for event mean estimates (sec); kcor_std: Standard deviation
(4) k_wtd: Mean of (station k weighted by acceration-slope kappa) (sec)
(5) n: Number of events within 40 km; N: Number at all distances.
(6) k SE and kcor SE: standard error of mean; e.g. k_std/sqrt(n)

Table 5.15 LSM network event mean kappa and kappa for station-event distances less than 40 km, Caselsm4

Source: SN-UCCSN-UNR-097 v.1, atch 2, directory kappawrap/caselsm4/Figs_summary
File: event_kappa_caselsm4.tbl

Unqualified, included for corroboration only. Not for use in quality-affecting work

origin id	k (ms)	dk (ms)	sd k	k40 (ms)	dk40 (ms)	sd k40
e_392	26.8	4.9	9	26.8	4.9	9
e_401	26.1	4.1	9.1	26.1	4.1	9.1
e_409	20.8	-1.1	12.9	20.8	-1.1	12.9
e_419	20.4	-1.5	10.3	20.4	-1.5	10.3
e_430	21.1	-0.9	6.9	21.1	-0.9	6.9
e_442	8.7	-13.2	7	8.7	-13.2	7
e_454	21.4	-0.5	5.3	21.4	-0.5	5.3
e_466	19.6	-2.3	9.3	19.6	-2.3	9.3
e_477	15	-7	12.4	15	-7	12.4
e_488	24.5	2.6	8.8	24.5	2.6	8.8
e_502	23.9	2	10.4	23.9	2	10.4
e_515	26.9	5	13.8	26.9	5	13.8
e_524	19.4	-2.6	13	19.4	-2.6	13
e_533	30.6	8.6	10.8	30.6	8.6	10.8
e_546	24.4	2.5	11.7	24.4	2.5	11.7
e_558	22.5	0.5	10.3	22.5	0.5	10.3
e_561	27.7	5.8	9	27.7	5.8	9
e_573	15.1	-6.8	11.4	15.1	-6.8	11.4

Table 5.16 LSM network event mean stress drop, corner frequency, and median kappa, Caselsm4 (UQ)

Source: SN-UCCSN-UNR-097 v.1, Atch. 2, directory kappawrap/caselsm4/Figs_summary
File: event_bfc_bst.tbl
Unqualified, included for corroboration only. Not for use in any quality-affecting work

Event Id	fc (Hz)	fc low (Hz)	fc high (Hz)	Str-Drp bars	SD low bars	SD high bars	Kappa msec	SD kappa msec
e_392	9.9	7.2	13.6	23.6	8.9	62.2	23.9	9
e_401	11.4	8.6	15.2	87.1	33.6	225.7	22.9	9.1
e_409	6.8	4	11.7	9.5	0.7	136.3	21.4	12.9
e_419	4.9	3.2	7.5	31.5	10.8	91.8	18.6	10.3
e_430	4.3	2.9	6.4	18.6	7.4	46.7	21.6	6.9
e_442	4.3	3.2	5.9	2.8	1.5	5.4	9.7	7
e_454	7.1	4.3	11.5	5.9	1.7	19.9	22	5.3
e_466	5.9	4.4	7.9	12.3	4.8	31.8	18.4	9.3
e_477	6.4	4	10.1	10.6	2.8	39.5	15.4	12.4
e_488	1.5	0.8	2.8	49.1	14.9	161.6	21.6	8.8
e_502	3.8	2.4	6	12	3.7	39.2	26.3	10.4
e_515	5.8	3.7	9	89.2	27.5	289.3	25.8	13.8
e_524	2.9	1.7	5	16.9	4.5	62.9	23.4	13
e_533	6.5	4.3	9.7	94.6	33.5	266.9	28.9	10.8
e_546	5.1	3.2	8	15.4	3.2	74.6	20.1	11.7
e_558	5.3	2.1	13.3	24.7	2.1	290.6	22.2	10.3
e_561	7.5	4.9	11.6	62.2	17	227.3	26.5	9
e_573	2.8	2	3.9	6.2	2.6	14.5	15.7	11.4

Notes:
(1) Data subset
sqerr<0.151 && bst<100 MPa && bfc < 20 Hz && ...
SNRpct>0.50 && chan!~/..Z/
input: caselsm4 database
(2) Kappa is median value

Table 5.17 LSM network station kappa estimates, Caselsm4 (Unqualified)

Source: SN-UCCSN-UNR-097 v.1, Atch 2, directory kappawrap/caselsm4/Figs_summary
Unqualified, included for corroboration only. Not for use in quality-affecting work

File: station_kappas_lsm.tbl

sta	mean k sec	k std sec	kcor sec	kcor sd sec	n used	N
rbnd	0.0240	0.0072	0.0245	0.0058	25	25
ryuc	0.0096	0.0088	0.0131	0.0068	13	14
rdun	0.0160	0.0069	0.0174	0.0060	20	20
res2	0.0353	0.0092	0.0342	0.0068	8	8
rxtn	0.0119	0.0101	0.0119	0.0076	23	24
rfoc	0.0185	0.0105	0.0194	0.0075	11	11
rlsm	0.0171	0.0110	0.0173	0.0089	8	12
rsfc	0.0255	0.0099	0.0246	0.0071	20	20
rcom	0.0186	0.0082	0.0192	0.0080	27	28
rymm	0.0296	0.0038	0.0298	0.0056	5	7
rymt	0.0179	0.0078	0.0188	0.0084	19	19
rtpp	0.0318	0.0081	0.0322	0.0068	31	32

Notes:

(1) Data: Caselsm4 database. Subset for k and k_cor:
sqerr<0.151 && bst<100 MPa && bfc < 20 Hz && SNRpct>0.50 && ...
chan!~/..Z/ && epicentral distance edist<40000 (40 km)
Only station-event distance < 40 km measurements are used.

(2) k_cor: k corrected for event mean estimates (sec); kcor_std: Standard deviation

(3) k_wtd: Mean of (station k weighted by acceration-slope kappa) (sec)
(4) n: Number of events within 40 km; N: Number at all distances.

Table 5.18 Blume strong motion network, LWLB and CPTB
fitting parameters.

Sources: SN-UCCSN-UNR-097, v.1, Atch. 2, top directory kappawrap/blume2,

(1) parametric data in file db/blume.srckappa. Columns in this file indicated below with labels C.x for column #x.

(2) file Figs_summary/station_kappas_blume.tbl

(3) File Figs_summary/station_kappas_blume_open.tbl

(4) Match orid in row to file db/blume.origin (col 5) then read ml in col 21.

Unqualified, included for corroboration only. Not for use in quality-affecting work

Individual fitting estimates for horizontal component records (W1, W2, N1, N2 chan fields)
bfc (bfcl, bfcu): corner frequency and 95% bounds
bst (bstl, bstu): stress drop (MPa) and 95% bounds. bars = 10xMPa
kappa (kappal, kappau): kappa and 95% bounds (sec)

orid	fitid	sta	chan	bfc	bfcl	bfcu	bst	bstl	bstu	mo	ml
				Hz	Hz	Hz	MPa	MPa	Mpa	N-m	
C.1	C.2	C.3	C.4	C.6	C.7	C.8	C.22	C.23	C.24	C.19	(4)
4	195	LWLB	W2	1.48	0.73	2.73	5.322	1.594	19.73	8.31E+15	4.4
4	197	LWLB	N2	1.28	0.58	2.33	3.824	1.084	12.97	9.23E+15	4.4
5	227	LWLB	W2	1.48	0.73	3.08	110.5	27.064	632.91	1.73E+17	5.6
5	228	LWLB	N2	1.78	0.98	3.48	101.21	28.493	526.58	9.08E+16	5.6
6	271	LWLB	N1	2.83	1.23	7.73	23.266	4.077	333	5.20E+15	4.1
6	273	LWLB	W1	1.73	0.68	3.93	13.153	2.603	87.448	1.29E+16	4.1
4	178	CPTB	W1	1.48	0.88	2.43	1.429	0.571	4.052	2.23E+15	4.4
4	179	CPTB	N1	1.88	0.98	3.58	3.382	0.995	14.942	2.58E+15	4.4
5	208	CPTB	W2	0.53	0.28	0.83	17.535	6.9	38.279	5.96E+17	5.6
5	210	CPTB	N2	0.78	0.33	1.63	33.856	8.548	151.81	3.61E+17	5.6

orid	fitid	sta	chan	kappa	kappal	kappau	sqerr	edist
				sec	sec	sec		meters
C.1	C.2	C.3	C.4	C.12	C.13	C.14	C.28	C.37
4	195	LWLB	W2	0.0284	0.0200	0.0397	0.137	14234
4	197	LWLB	N2	0.0273	0.0194	0.0375	0.119	14234
5	227	LWLB	W2	0.0498	0.0377	0.0664	0.212	12566
5	228	LWLB	N2	0.0467	0.0353	0.0625	0.154	12566
6	271	LWLB	N1	0.0433	0.0286	0.0670	0.229	12121
6	273	LWLB	W1	0.0443	0.0328	0.0612	0.256	12121

orid	fitid	sta	chan	kappa	kappal	kappau	sqerr	edist
				sec	sec	sec		meters
C.1	C.2	C.3	C.4	C.12	C.13	C.14	C.28	C.37
4	178	CPTB	W1	0.0014	-0.005	0.0103	0.065	30024
4	179	CPTB	N1	0.0181	0.0086	0.0313	0.109	30024
5	208	CPTB	W2	0.0234	0.0182	0.0293	0.096	31581
5	210	CPTB	N2	0.0379	0.0287	0.051	0.207	31581

sta	mean k	k std	kcor	kcor sd	n used	N	Data Source
	sec	sec	sec	sec			
CPTB	0.0143	0.0115	0.0169	0.0099	3	4	(2)
LWLB	0.0358	0.0092	0.036	0.0047	4	6	(2)

Mean kappa with subset applied: stress drop <300 bars

sta	mean k	k std	kcor	kcor sd	n used	N	Data source
	sec	sec	sec	sec			
CPTB	0.0202	0.0151	0.0221	0.0132	4	4	(3)
LWLB	0.04	0.0097	0.04	0.0073	6	6	(3)
BTYB	0.0232	0.0023	0.0232	0.003	6	6	(3)

Mean kappa, edist<50 km, bfc<20 Hz, no constraint on stress drop

Table 5.19 Blume network event mean stress drop, corner frequency, and kappa

Source: SN-UCCSN-UNR-097, v1, attachment 2, directory kappawrap/blume2/Figs_summary
File event_bfc_bst_blume.tbl

Unqualified, for corroboration only. Not for use in quality-affecting work.

Event Id	fc (Hz)	fc low (Hz)	fc high (Hz)	Str-Drp bars	SD low bars	SD high bars	Kappa msec	SD kappa msec
e_4	1.1	0.3	4.4	41.6	7.8	220.7	48.6	19.3
e_5	0.7	0.3	1.4	235.7	84.3	659.3	46.7	19.8
e_6	1.9	0.9	4.1	89.6	22.2	361.8	55.6	14.3

Subset: Horizontal components, no subset on stress drop or corner frequency. blume2 case

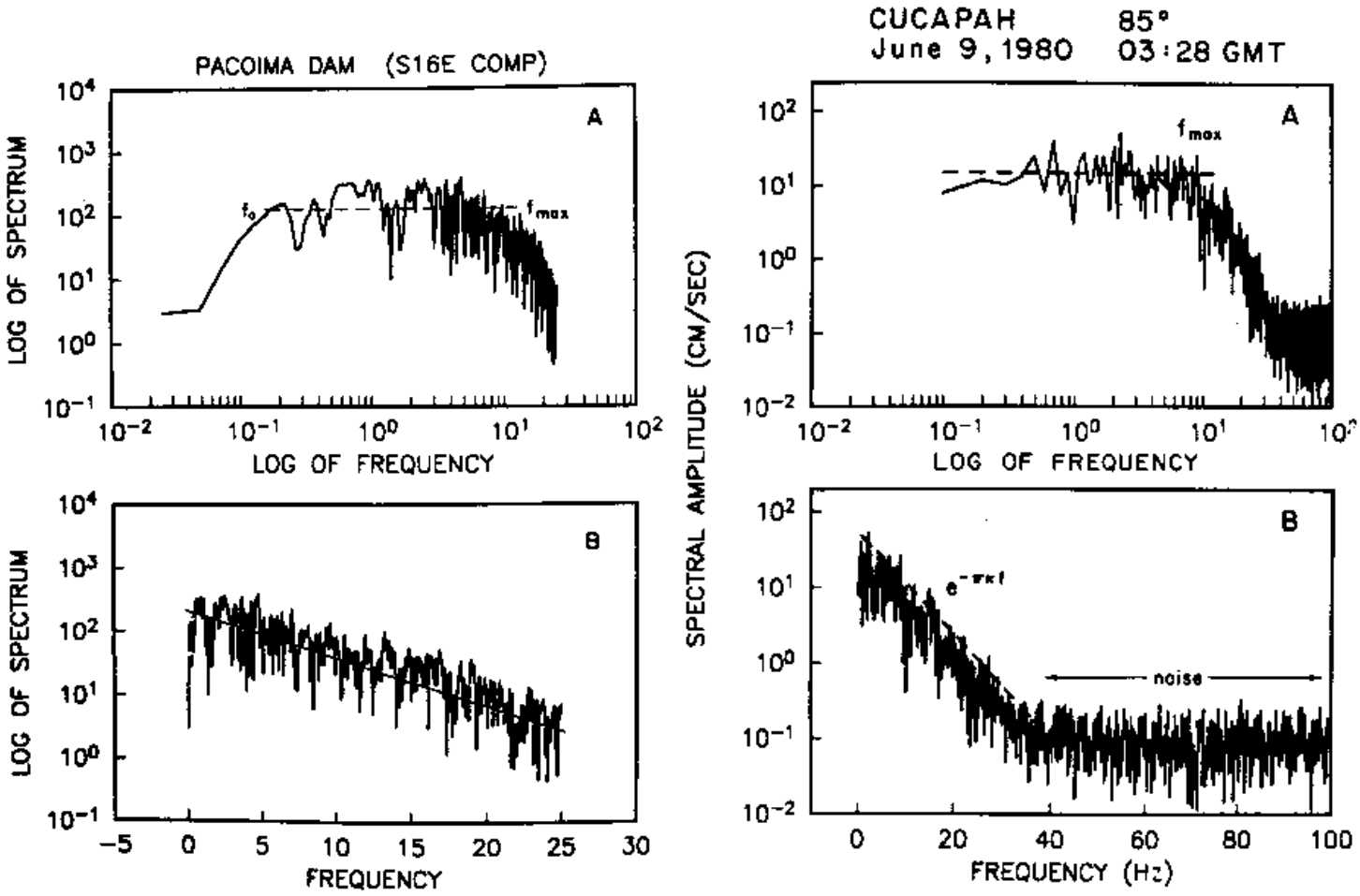

Figure 5.1.1. Definition of kappa (figure scanned from Anderson, J. G. and S. Hough, (1984), A model for the shape of the Fourier amplitude spectrum of acceleration at high frequencies, Bulletin of the Seismological Society of America, 74, p. 1969-1994. Unqualified, for illustration only. Not for use in any quality-affecting work.

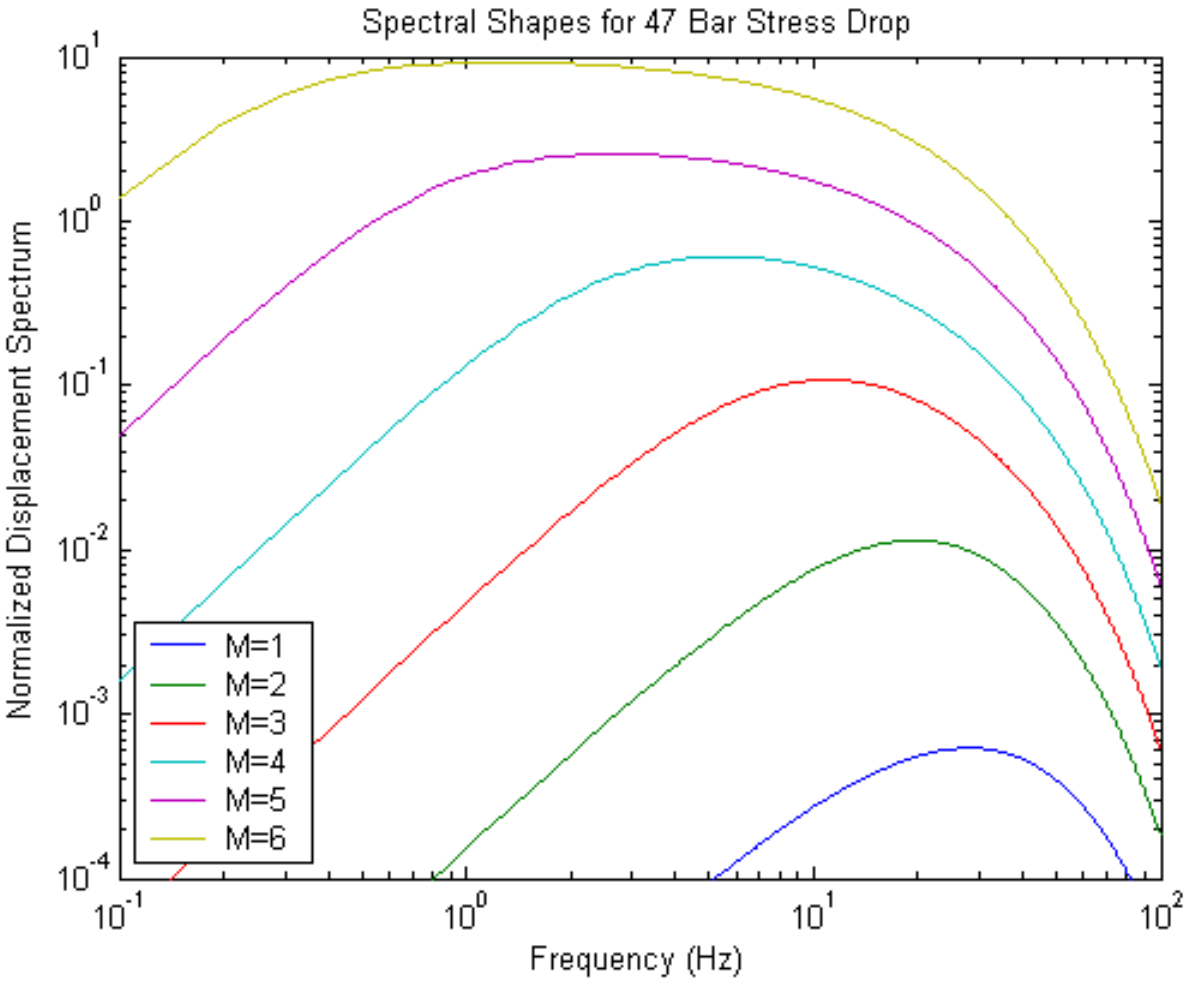

Figure 5.1.2. Model Fourier spectra of large and small earthquakes, showing intervention of corner frequency. Source: SN-UCCSN-UNR-047, v.1, p. 71 Unqualified, shown for illustration only, not for use in any quality-affecting work.

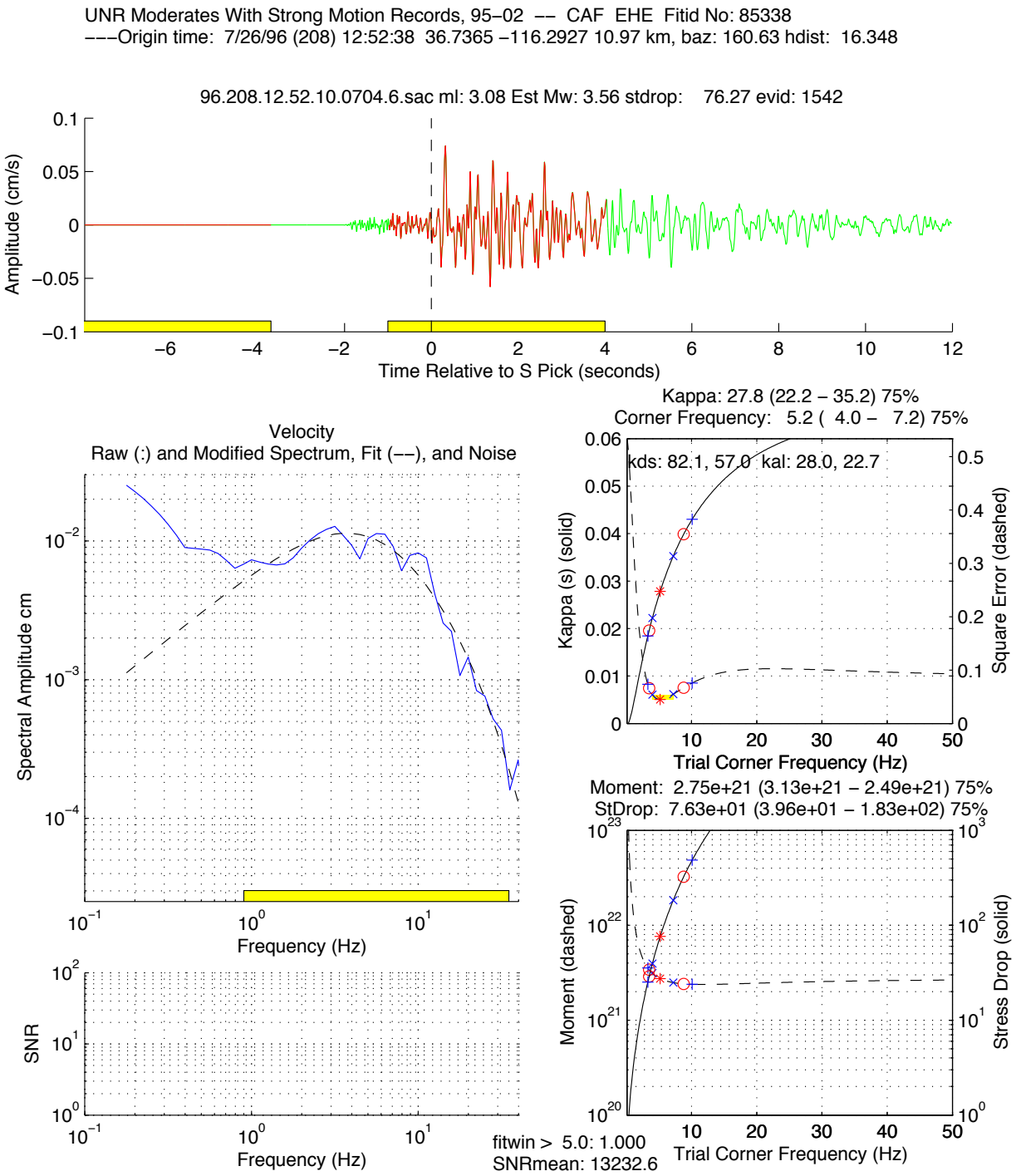

Kappa: 27.8 (22.2 – 35.2, 19.6–39.9, 18.4–43.0) Corner: 5.2 (4.0 – 7.2, 3.5– 8.8, 3.3–10.1)
Mo: 2.75e+21 (3.13e+21– 2.49e+21, 3.41e+21– 2.41e+21, 3.56e+21– 2.39e+21) calib: 1.000e+00, silva: n
LF Spec: 1.02e–03 (1.16e–03– 9.23e–04, 1.27e–03– 8.95e–04, 1.32e–03– 8.86e–04) hdist: 16.3, logsp: y, 20.0
stress drop: 7.63e+01 (3.96e+01 – 1.83e+02, 2.89e+01– 3.25e+02, 2.52e+01– 4.86e+02) type: 1 scorr: y
mu: 3.20e+11 rho: 2.60 beta: 3.50e+05 Mwslope: 1.50 Mwint: 16.10 radf : 0.85 tocm: 1.00e–07 mtm: y nw: 4.0
siglvls: 1.230 1.500 1.700 dof: 40 prepk: 1.00 postpk: 4.00 minerr: 0.045 filter: n lo,hi,nr,ftype: 0.3 9999.0 2 high
taperlen: 0.05 smooth: 0 pass, 0.10 0.20 0.40 0.20 0.10, 2 Dbase: db/zz

Figure 5.1.3 a. Example of a summary figure that is produced for each seismogram considered in this study. The time series is at the top, spectra and signal-to-noise on the left, parameter estimation and error plots are on the right, and the configuration and tabulated results are in the text field at the bottom. Further details are given in Figures 5.1.3 b and 5.1.3 c. Source: SN-UCCSN-UNR-097, v. 1, Attachment 2 Electronic Supplement, file case6a/Figs/S85338_96208125243_CAF_EHE.pdf. Unqualified, shown for illustration only. Not for use in any quality-affecting work.

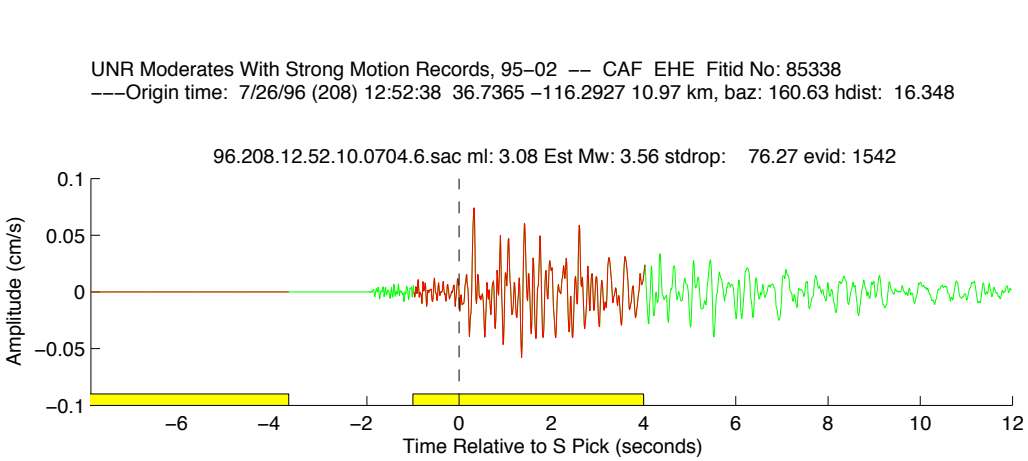

Title, station name, component name, and fitid, a unique identification number (here, 85338). Second line: Data file name, network magnitude, data-derived Mw and stress drop (bars), and database earthquake number.

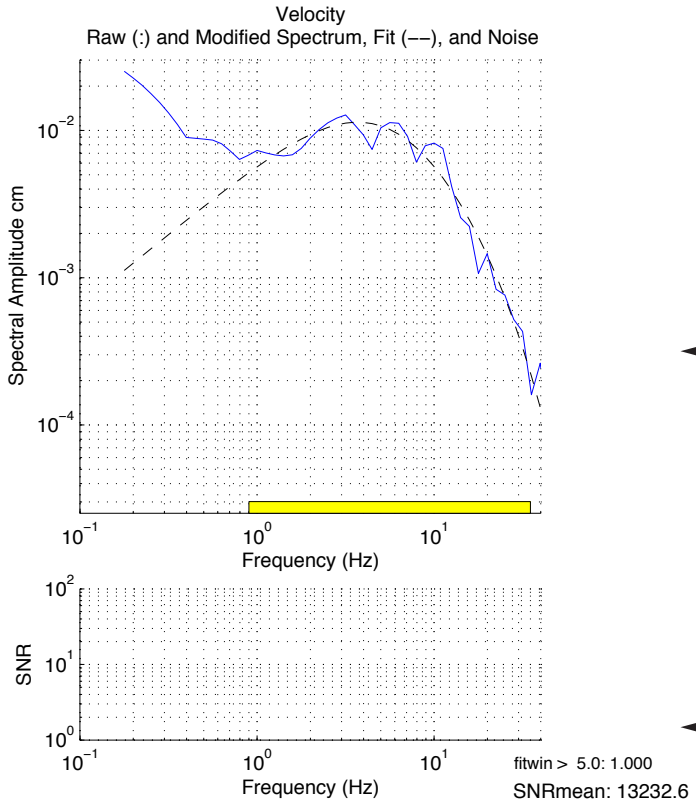

Red overprint and yellow underbar show the time series segment used for analysis - here S-wave arrival minus 1 to plus 4 seconds. An equal length noise segment (right underbar) is also extracted but not always fully displayed.

Raw and sensor-corrected spectra (blue and red lines, resp.) from above time series, calculated fit (dashed black line). The noise spectrum will be in green if it will plot on the axis set by the signal (not here). The spectrum is determined using either a multitaper or FFT is configurable by the user. The yellow bar indicates the frequency band used to fit the spectrum.

Signal-to-noise (SNR) ratio. Values above 100:1 are so good as to not need display. Within the fitting window (fitwin) the SNR threshold of 5.0:1 (in this case >100:1) is exceeded by 100 percent of the signal spectrum. The yellow bar indicates the frequency window used to make these measurements and for parameter estimation. Average SNR in this case is 13232:1.

Figure 5.1.3 b. Detailed description of three summary figure subplots: the original time series (top), the frequency spectra of the data (original signal, sensor corrected, best fitting model, and noise) and measurement of the signal to noise ratio (SNR). Most features are configurable by the user, including the length and starting point of the time series, the spectral estimation method, pre-filtering, the spectral range to fit, signal-to-noise ratio for quality estimation, and display in log or linear frequency. Sensor correction is also selectable. All parameters are configured in advance and applied to every seismogram in a batch calculation. The parameters can be easily changed and the batch calculation rerun to test parameter sensitivity, Results are Unqualified.

Source: SN-UCCSN-UNR-097, v. 1, Attachment 2 Electronic Supplement, file case6a/Figs/S85338_96208125243_CAF_EHE.pdf. Unqualified, for illustration purposes only. Not for use in any quality-affecting work.

Figure 5.1.3c, Explanation of kappaAH fitting plots. Source: UCCSN-UNR-097, v.1, Attachment 2 Electronic Supplement, file kappawrap/case6a/Figs/S85338_96208125243_CAF_EHE.pdf. Unqualified., shown for illustration only, not for use in any quality-affecting work.

Trial corner frequency versus kappa (solid line, left scale) and the square error fit (dashed line, right scale). The smallest squared error is considered the best fit and marked with stars on all parametric plots. The 75% (x), 90% (circles) and 95% (+) confidence levels are estimated with a chi-squared criteria and 40 degrees of freedom. The title lists the best estimate and 75% confidence ranges. The yellow box is included for visual emphasis and highlights the 75% range of squared error and corner frequency. The actual error ranges of corner frequency and kappa when considered together form an elliptical or banana-shaped contours along the kappa plot line. In this example the fit is well constrained in frequency-kappa space. For most small earthquakes the squared error plot is much flatter with increasing frequency. In such cases error bounds on kappa may be wide and are often not constrained by the data. Kds and kal refer to the displacement and acceleration slope estimates, corresponding to the infinite and zero corner-frequency asymptotes, respectively. Kds should approximate the best fit value for smallest earthquakes, and kal, the largest.

Dependence of the seismic moment (dashed line, left scale) and stress drop (solid line, right scale) on the trial corner frequency. Best fit values (stars) and 75% (x), 90% (circles) and 95% (+) confidence levels are indicated. The title lists the best fit and 75% confidence ranges.

A detailed listing of input parameter values (e.g., mu, rho, beta, mtm, mw, dof, prepk, postpk, taperlen, smooth, radf), information pertaining to the seismogram (e.g., calib, hdist, type, Dbase) and output results (e.g., Kappa, corner, Mo, stress drop, Mwslope, Mwint).

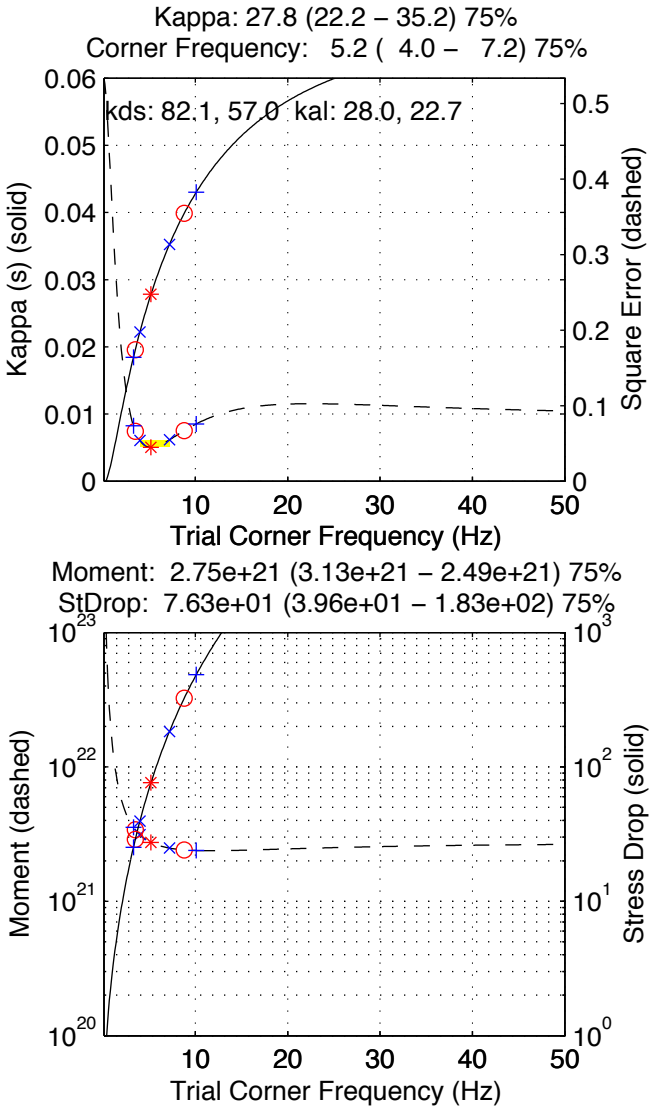

Kappa: 51.6 (17.8 – 51.6, 14.0–51.6, 12.3–51.6) Corner: 50.0 (6.4 – 50.0, 5.4–50.0, 5.0–50.0)
Mo: 3.43e+20 (3.32e+20– 3.43e+20, 3.50e+20– 3.43e+20, 3.62e+20– 3.43e+20) calib: 1.000e+00, silva: n
LF Spec: 1.38e–04 (1.33e–04– 1.38e–04, 1.41e–04– 1.38e–04, 1.45e–04– 1.38e–04) hdist: 15.1, logsp: y, 20.0
stress drop: 8.48e+03 (1.72e+01 – 8.48e+03, 1.09e+01– 8.48e+03, 8.93e+00– 8.48e+03) type: 1 scorr: y
mu: 3.20e+11 rho: 2.60 beta: 3.50e+05 Mwslope: 1.50 Mwint: 16.10 radf : 0.85 tocm: 1.00e–07 mtm: y nw: 4.0
siglvls: 1.230 1.500 1.700 dof: 40 prepk: 1.00 postpk: 4.00 minerr: 0.039 filter: n lo,hi,nr,ftype: 0.3 9999.0 2 high
taperlen: 0.05 smooth: 0 pass, 0.10 0.20 0.40 0.20 0.10, 2 Dbase: db/zz

Figure 5.2.1 Map of stations used in this study, in the vicinity of Yucca Mountain. Station dots left but station names removed in center. Station RPY is above the Exploratory Studies Facility tunnel. See Figure 5.2.2 for details around Yucca Mountain. Locations listed in Table 5.1. Source: DID 012DV.010, file sgbdsn_locations.dat and DID 006DV.005, file strong_motion_locs.txt.

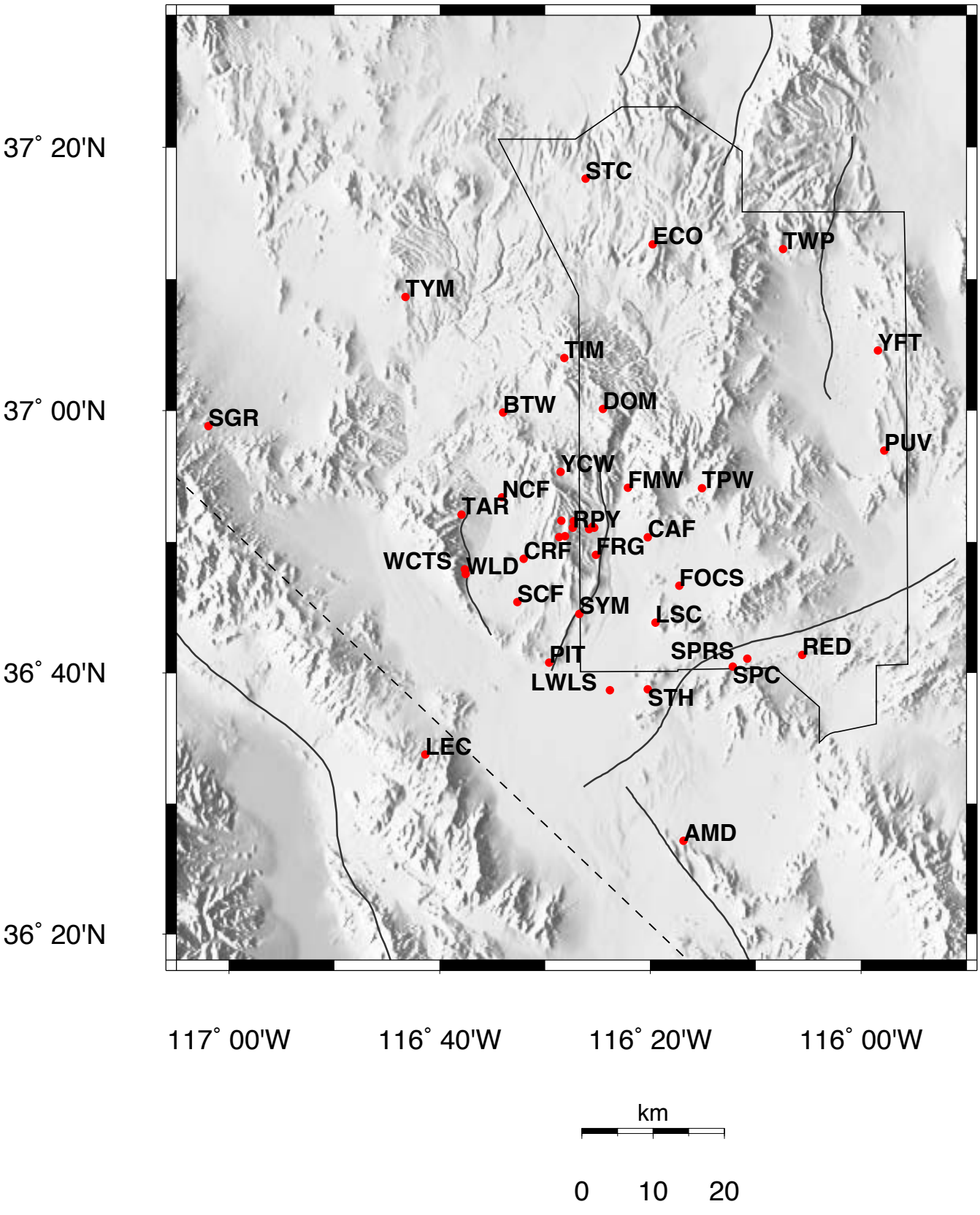

Figure 5.2.2 Close-up of SGBDSN stations in the vicinity of Yucca Mountain. Locations listed in Table 5.1. Source: DID 012DV.010, file sgbdsn_locations.dat and DID 006DV.005, file strong_motion_locs.txt.

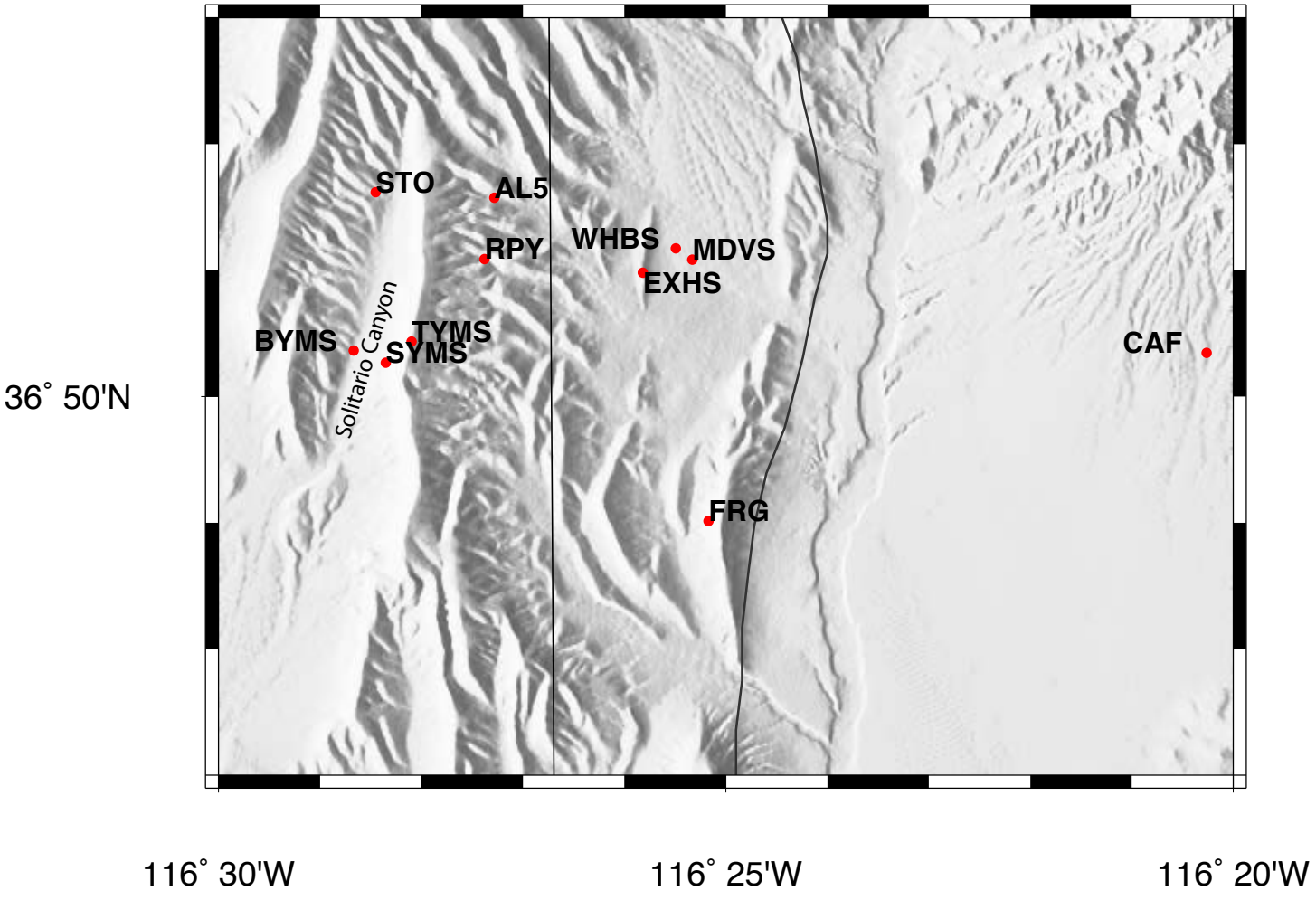

Figure 5.2.3. Epicenters of SGBDSN earthquakes used in this study (stars). Solid line polygon: Nevada Test Site; curved solid lines: schematic trace of larger faults. Source: DID 006DV.004, File sgbdsn.hypo. Specific earthquakes listed in Table 5.2.

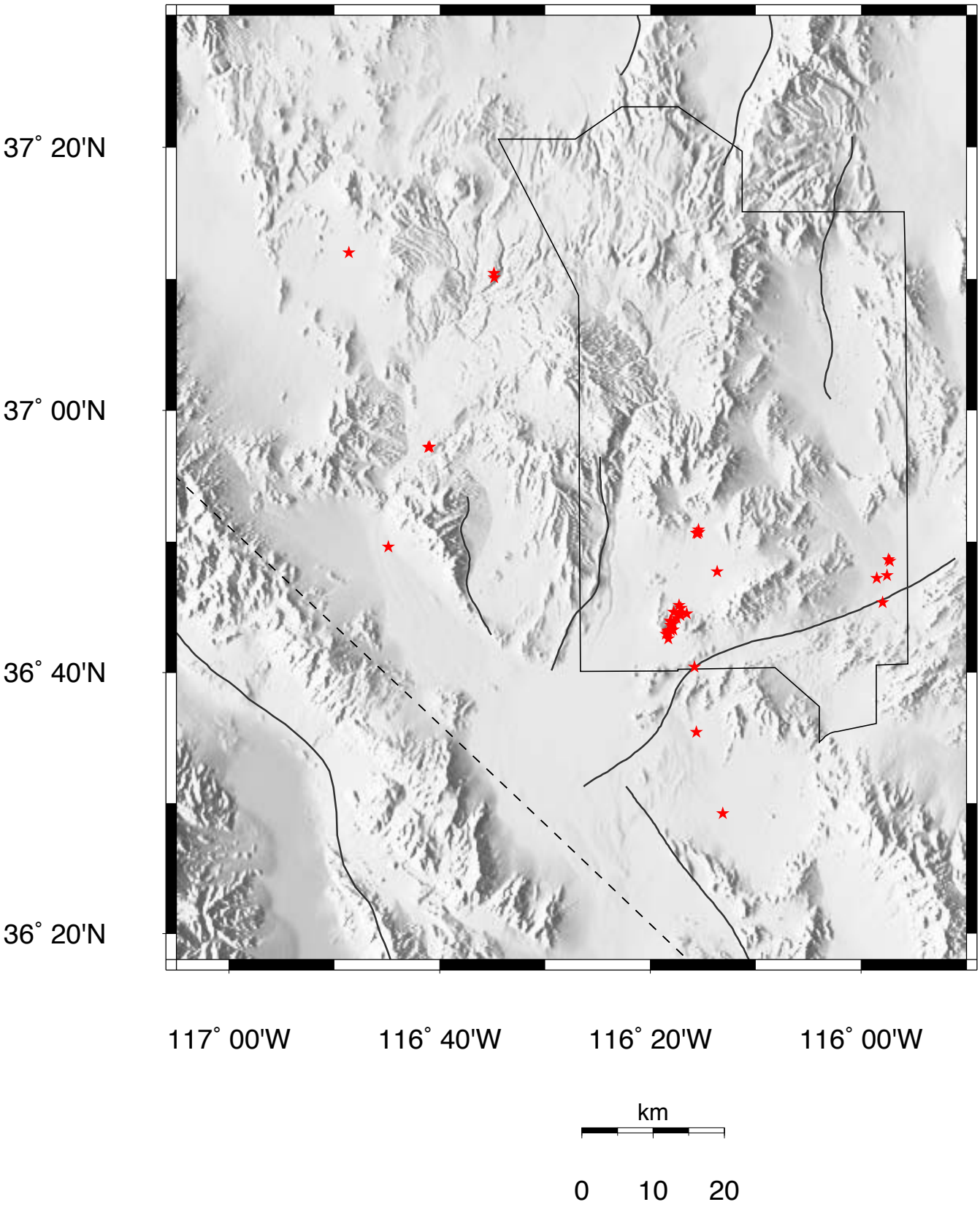

Figure 5.2.4 Earthquake picenters (stars) and station coverage (dots and labels) from the Little Skull Mountain aftershock portable deployment.
Source: Su, F., J. G. Anderson, J. N. Brune, and Y. Zeng. (1996). A comparison of direct S-wave and coda wave site amplification determined from aftershocks of the Little Skull Mountain earthquake, Bulletin of the Seismological Society of America, 86, 1006-1018. Tables 1 and 2. Unqualified, for information only. Do not use in quality-affecting work.

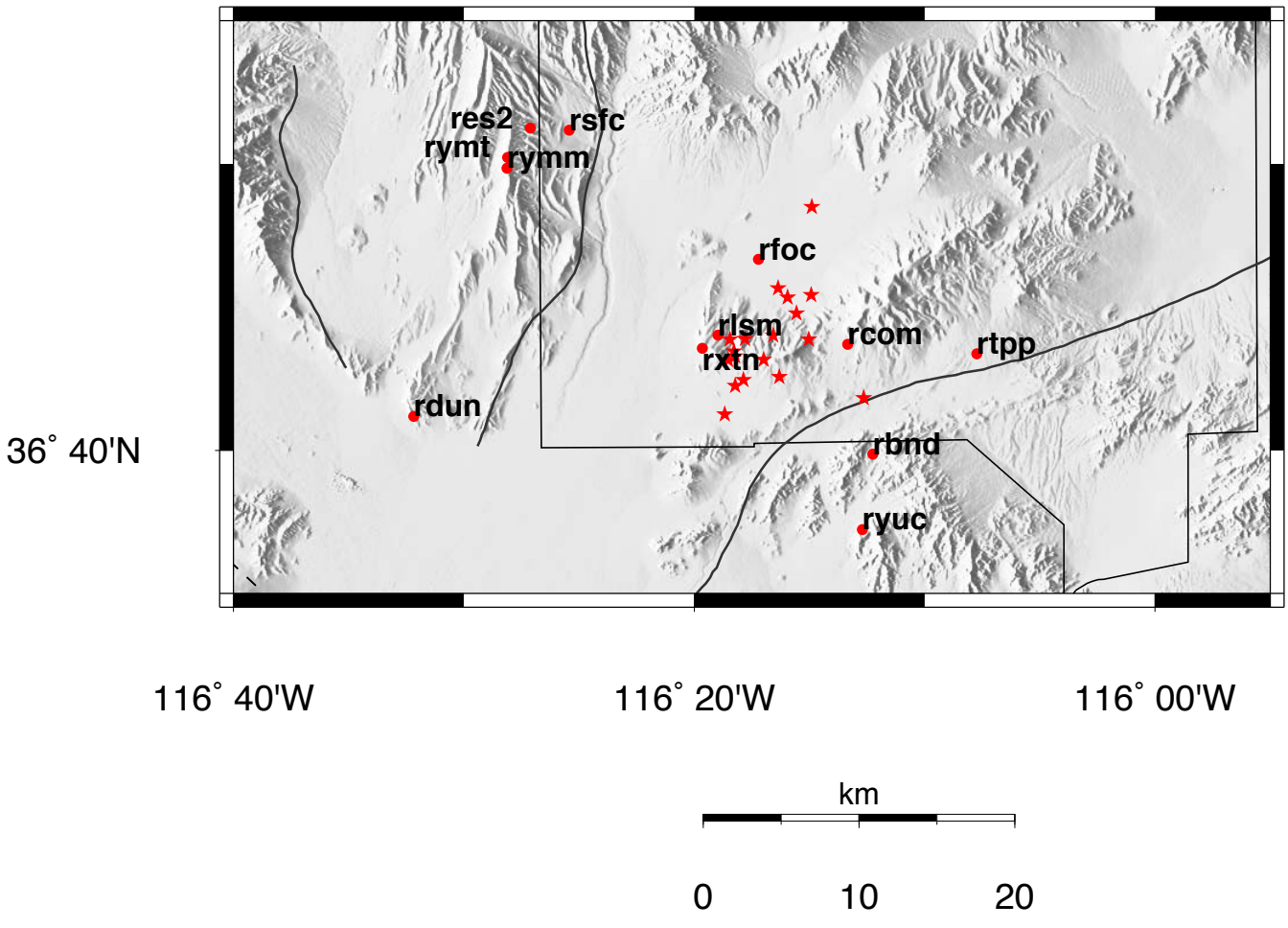

Figure 5.2.5. Epicenters and station coverage of the Blume strong-motion data set. Below: three closest stations. LWLB: Lathrop Wells; CPTB: Control Point; BTYB: Beatty. Inset: Dots show more distant stations. Stars: Little Skull Mountain mainshock and two aftershocks.
Source of station and earthquake locations:
Lum, P.K. and K. K. Honda, 1992. Processed seismic motion records from the Little Skull Mountain, Nevada, earthquake of June 29, 1992, recorded at stations in southern Nevada, Report # JAB-10733-TM6 UC-703 National Technical Information Service, 206 p. mainshock location: p. 1 and 2, stations: Table 1; and Lum, P.K. and K. K. Honda, 1993, Processed seismic motion records from Little Skull Mountain aftershocks, Nevada earthquakes of July 5 and September 13, 1992 recorded at seismic stations in southern Nevada, DOE Report JAB-10733-TM8. 10-53., page 1.
This page is Unqualified, and included for corroboration only. Do not use for quality-affecting work.

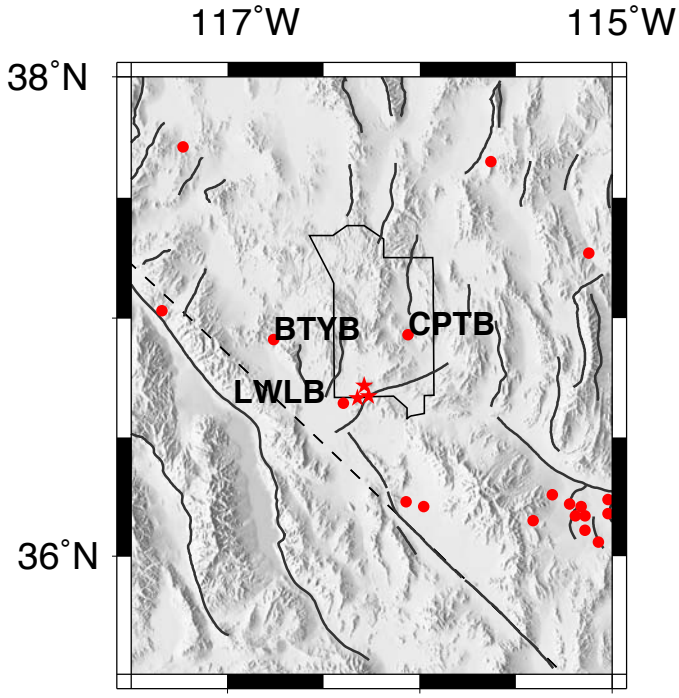

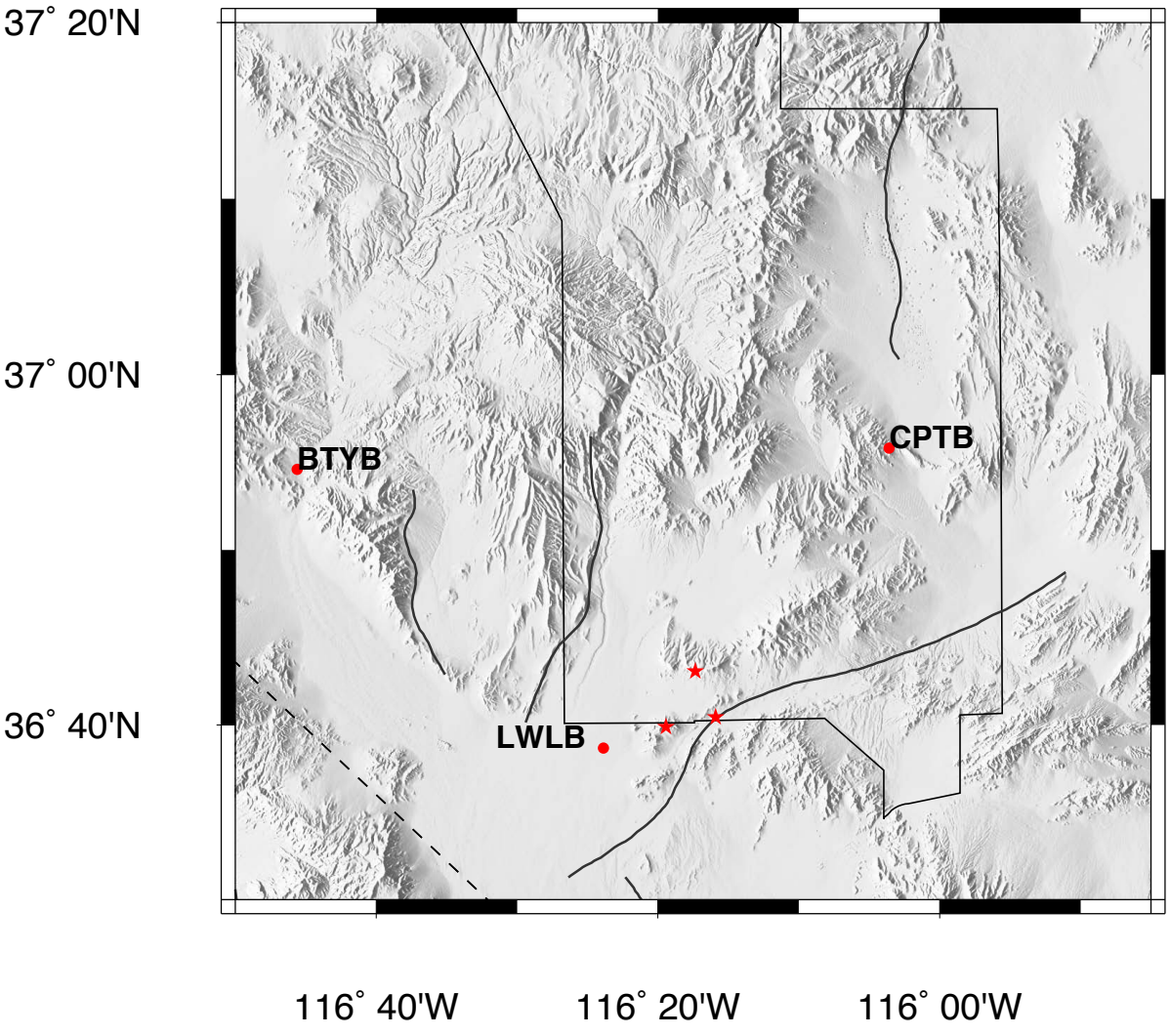

Figure 5.3.1.1. Example spectral fits for station CAF, case6a. See Figure 5.1.3a-c for an explanation of the plot elements. The N-S component of the same earthquake as Fig. 5.3.1.2, but the kappa estimate not constrained (center right subplot). Source: DID 006GB.003, file kappawrap/case6a/Figs/S85174_96173003302_CAF_EHN.eps.

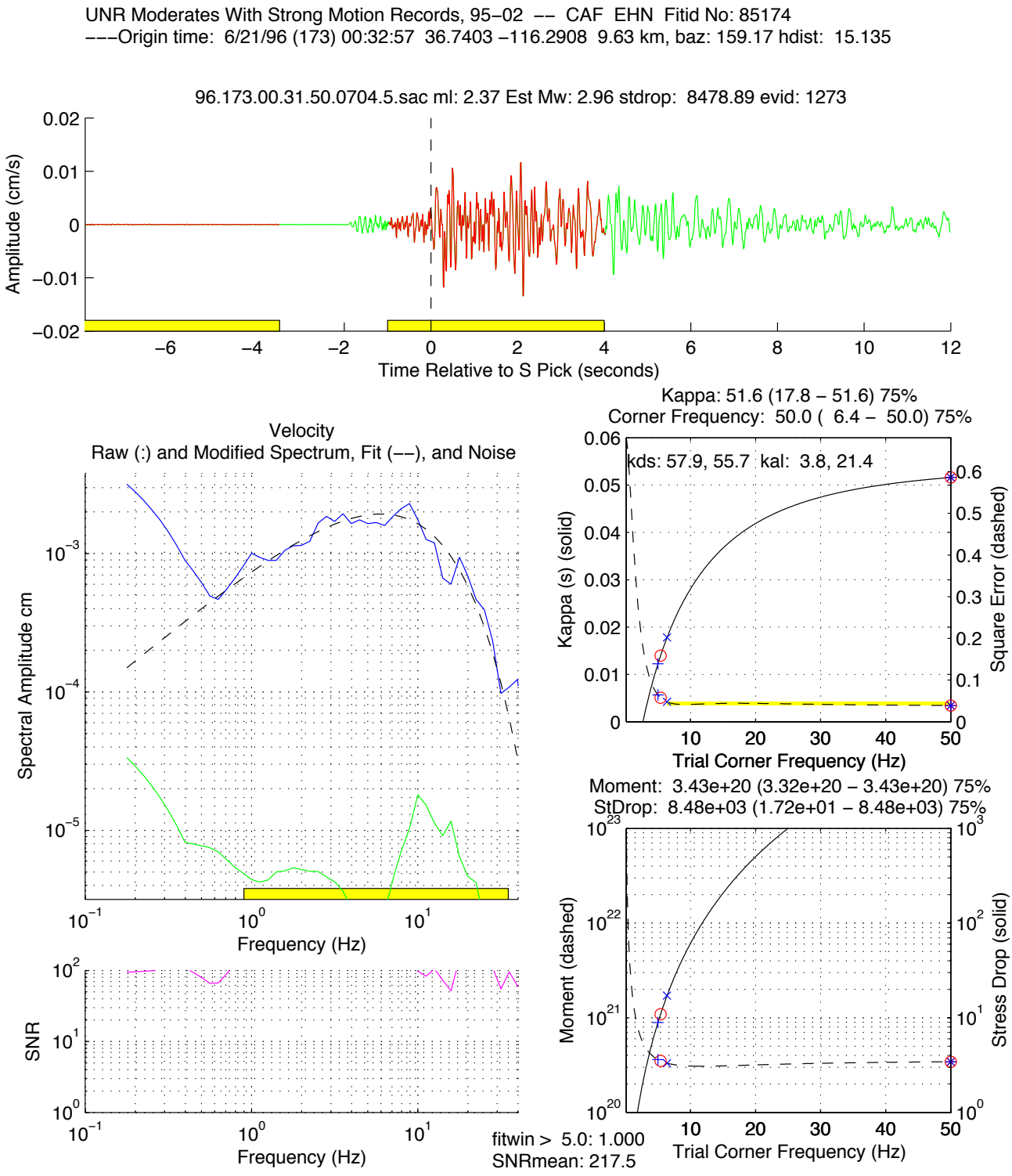

Kappa: 51.6 (17.8 – 51.6, 14.0–51.6, 12.3–51.6) Corner: 50.0 (6.4 – 50.0, 5.4–50.0, 5.0–50.0)
Mo: 3.43e+20 (3.32e+20– 3.43e+20, 3.50e+20– 3.43e+20, 3.62e+20– 3.43e+20) calib: 1.000e+00, silva: n
LF Spec: 1.38e–04 (1.33e–04– 1.38e–04, 1.41e–04– 1.38e–04, 1.45e–04– 1.38e–04) hdist: 15.1, logsp: y, 20.0
stress drop: 8.48e+03 (1.72e+01 – 8.48e+03, 1.09e+01– 8.48e+03, 8.93e+00– 8.48e+03) type: 1 scorr: y
mu: 3.20e+11 rho: 2.60 beta: 3.50e+05 Mwslope: 1.50 Mwint: 16.10 radf : 0.85 tocm: 1.00e–07 mtm: y nw: 4.0
siglvls: 1.230 1.500 1.700 dof: 40 prepk: 1.00 postpk: 4.00 minerr: 0.039 filter: n lo,hi,nr,ftype: 0.3 9999.0 2 high
taperlen: 0.05 smooth: 0 pass, 0.10 0.20 0.40 0.20 0.10, 2 Dbase: db/zz

Figure 5.3.1.2. Example spectral fits for station CAF, case6a. See Figure 5.1.3a-c for an explanation of the plot elements. The kappa estimate for this component (EW) and this earthquake is reasonably constrained (center right subplot). Source: DID 006GB.003, file kappawrap/case6a/Figs/S85173_96173003302_CAF_EHE.eps.

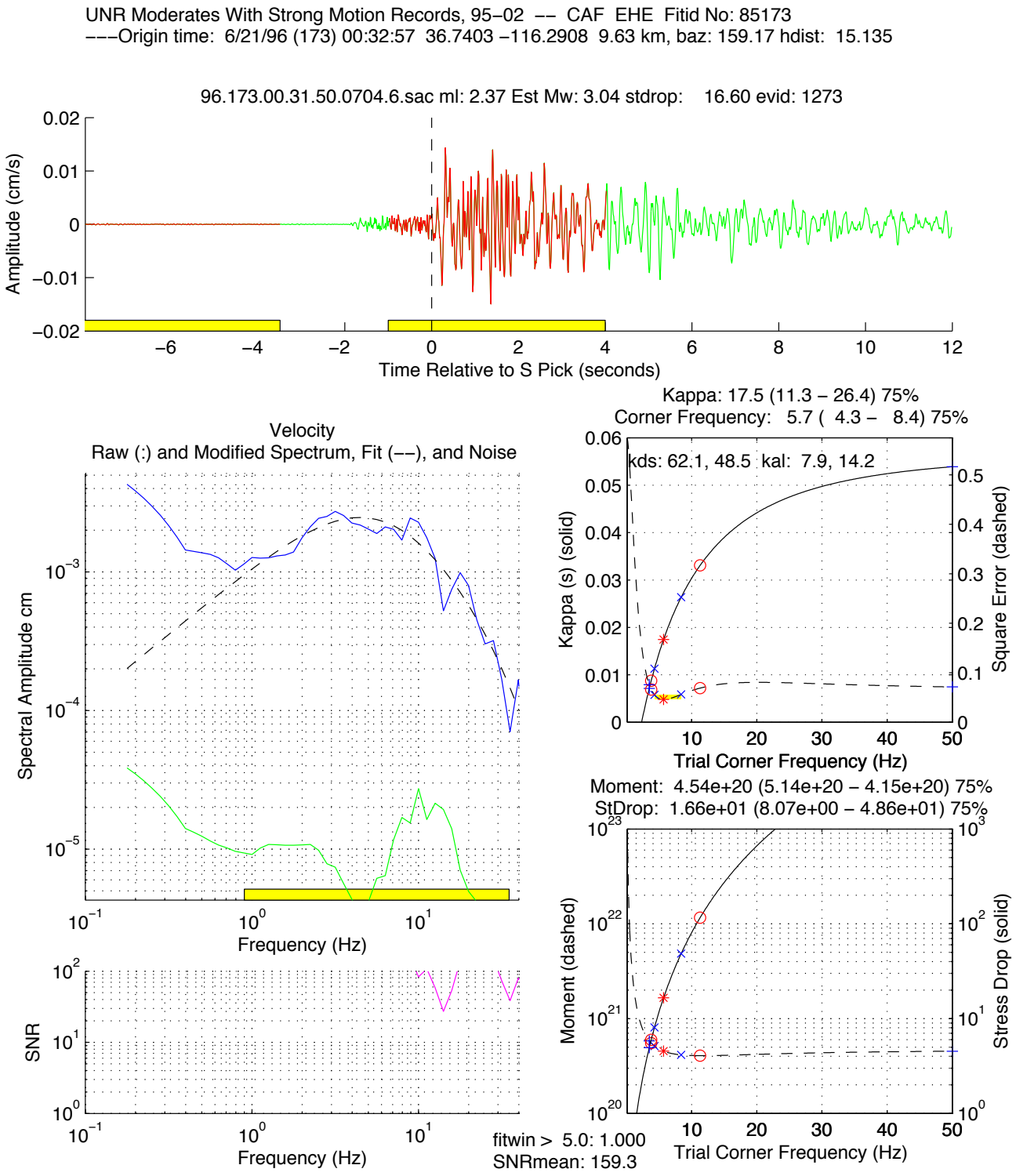

Kappa: 17.5 (11.3 – 26.4, 8.7–33.1, 7.1–53.9) Corner: 5.7 (4.3 – 8.4, 3.8–11.3, 3.5–50.0)
Mo: 4.54e+20 (5.14e+20– 4.15e+20, 5.52e+20– 4.07e+20, 5.83e+20– 4.53e+20) calib: 1.000e+00, silva: n
LF Spec: 1.82e–04 (2.06e–04– 1.66e–04, 2.21e–04– 1.63e–04, 2.34e–04– 1.82e–04) hdist: 15.1, logsp: y, 20.0
stress drop: 1.66e+01 (8.07e+00 – 4.86e+01, 5.98e+00– 1.16e+02, 4.94e+00– 1.12e+04) type: 1 scorr: y
mu: 3.20e+11 rho: 2.60 beta: 3.50e+05 Mwslope: 1.50 Mwint: 16.10 radf : 0.85 tocm: 1.00e–07 mtm: y nw: 4.0
siglvls: 1.230 1.500 1.700 dof: 40 prepk: 1.00 postpk: 4.00 minerr: 0.046 filter: n lo,hi,nr,ftype: 0.3 9999.0 2 high
taperlen: 0.05 smooth: 0 pass, 0.10 0.20 0.40 0.20 0.10, 2 Dbase: db/zz

Figure 5.3.1.3. Example spectral fits for station CAF, case6a. See Figure 5.1.3a-c for an explanation of the plot elements. Kappa estimate is poorly constrained and potentially biased to by the weak minimum squared error at 15 Hz (center right subplot). Source: DID 006GB.003, file kappawrap/case6a/Figs/S85224_96191234856_CAF_EHE.eps.

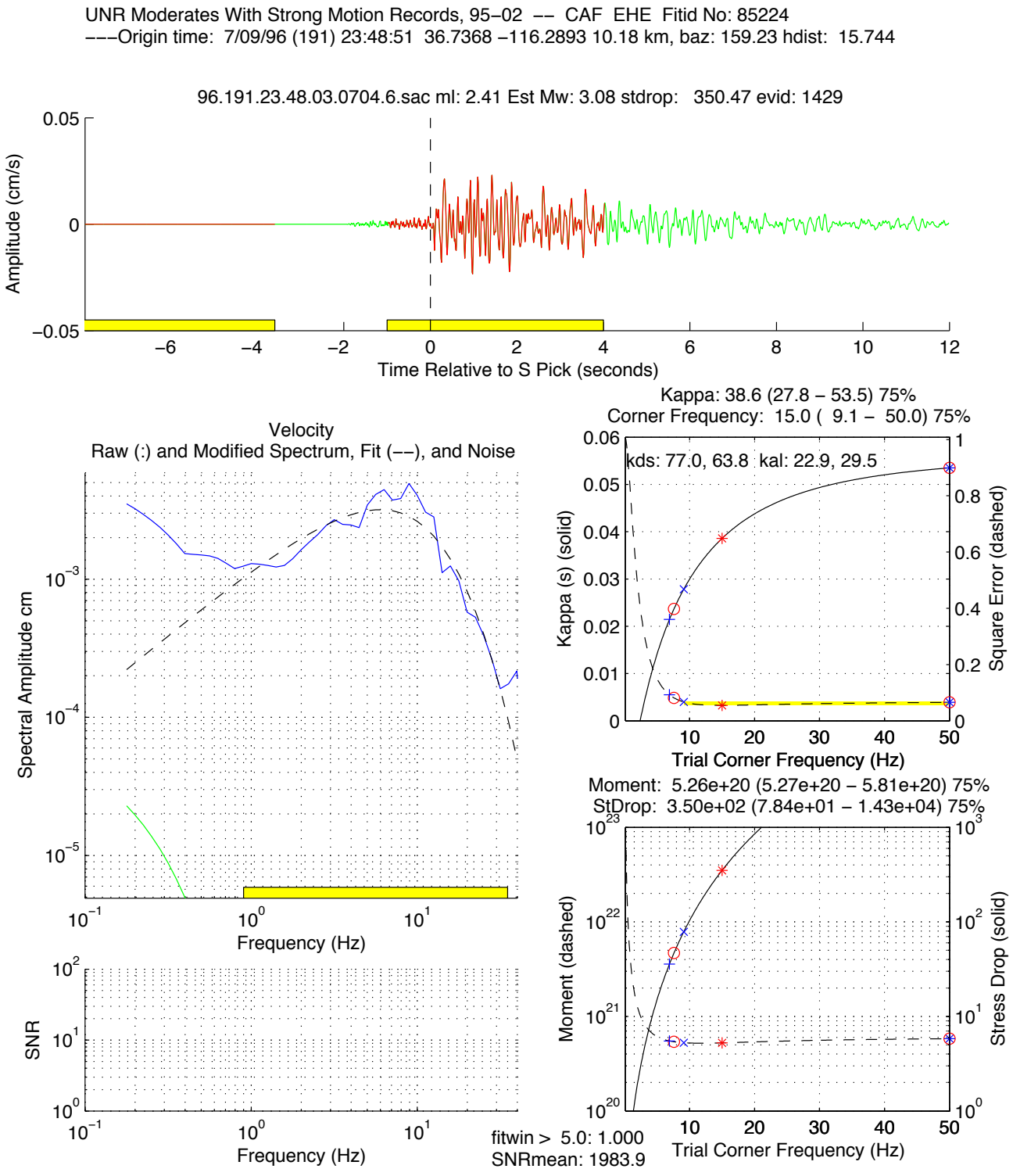

Kappa: 38.6 (27.8 – 53.5, 23.7–53.5, 21.4–53.5) Corner: 15.0 (9.1 – 50.0, 7.6–50.0, 6.9–50.0)
Mo: 5.26e+20 (5.27e+20– 5.81e+20, 5.40e+20– 5.81e+20, 5.51e+20– 5.81e+20) calib: 1.000e+00, silva: n
LF Spec: 2.03e–04 (2.03e–04– 2.24e–04, 2.08e–04– 2.24e–04, 2.12e–04– 2.24e–04) hdist: 15.7, logsp: y, 20.0
stress drop: 3.50e+02 (7.84e+01 – 1.43e+04, 4.68e+01– 1.43e+04, 3.57e+01– 1.43e+04) type: 1 scorr: y
mu: 3.20e+11 rho: 2.60 beta: 3.50e+05 Mwslope: 1.50 Mwint: 16.10 radf : 0.85 tocm: 1.00e–07 mtm: y nw: 4.0
siglvls: 1.230 1.500 1.700 dof: 40 prepk: 1.00 postpk: 4.00 minerr: 0.055 filter: n lo,hi,nr,ftype: 0.3 9999.0 2 high
taperlen: 0.05 smooth: 0 pass, 0.10 0.20 0.40 0.20 0.10, 2 Dbase: db/zz

Figure 5.3.1.4. Example spectral fits for station CAF, case6a. See Figure 5.1.3a-c for an explanation of the plot elements. Kappa estimate is poorly constrained but the weak minimum squared error at 13.9 Hz (center right subplot) is similar to the EW component, Figure 5.3.1.3. Source: DID 006GB.003, file kappawrap/case6a/Figs/S85225_96191234856_CAF_EHN.eps.

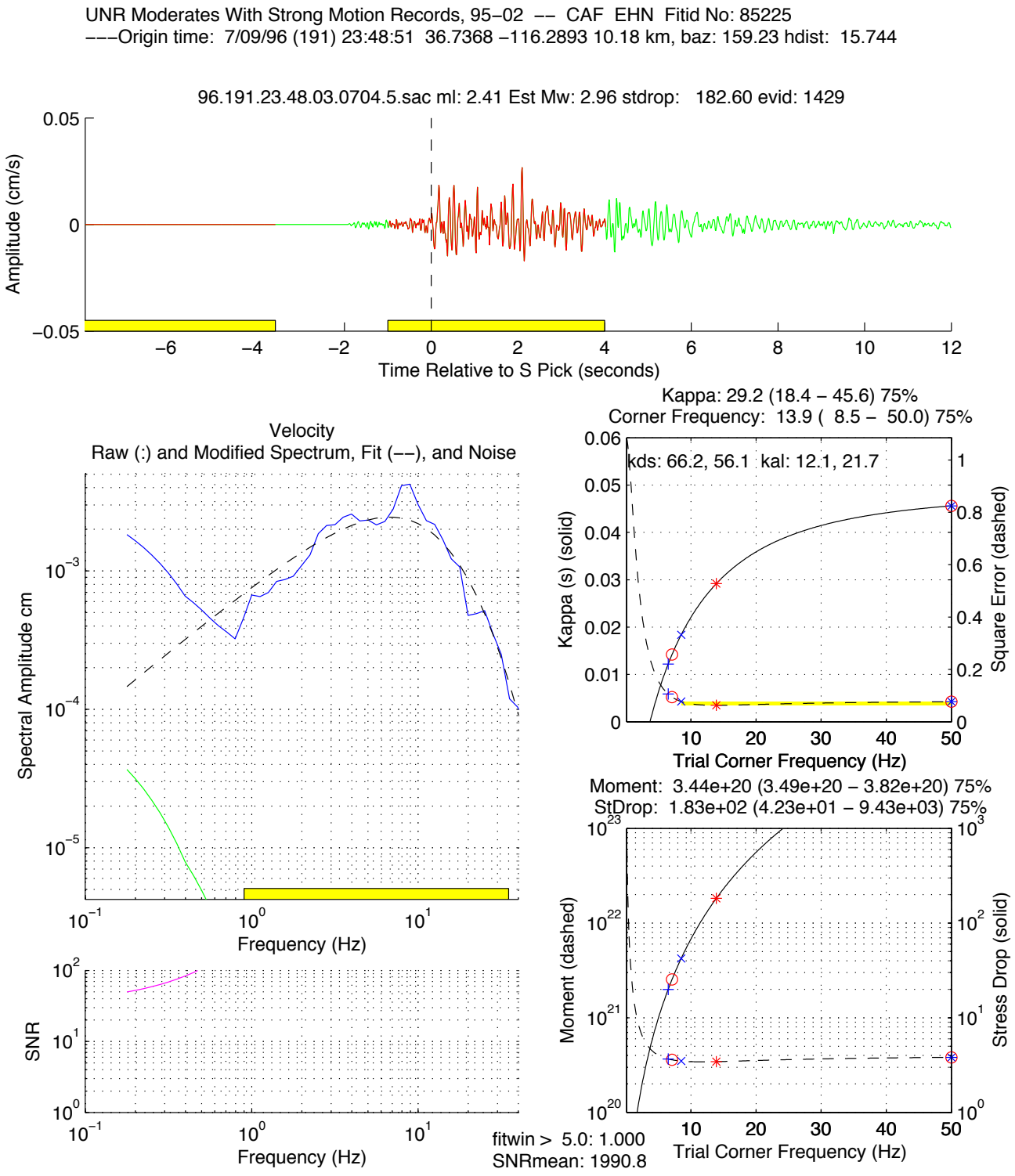

Kappa: 29.2 (18.4 – 45.6, 14.2–45.6, 12.2–45.6) Corner: 13.9 (8.5 – 50.0, 7.1–50.0, 6.5–50.0)
Mo: 3.44e+20 (3.49e+20– 3.82e+20, 3.60e+20– 3.82e+20, 3.67e+20– 3.82e+20) calib: 1.000e+00, silva: n
LF Spec: 1.33e–04 (1.35e–04– 1.47e–04, 1.39e–04– 1.47e–04, 1.42e–04– 1.47e–04) hdist: 15.7, logsp: y, 20.0
stress drop: 1.83e+02 (4.23e+01 – 9.43e+03, 2.54e+01– 9.43e+03, 1.99e+01– 9.43e+03) type: 1 scorr: y
mu: 3.20e+11 rho: 2.60 beta: 3.50e+05 Mwslope: 1.50 Mwint: 16.10 radf : 0.85 tocm: 1.00e–07 mtm: y nw: 4.0
siglvls: 1.230 1.500 1.700 dof: 40 prepk: 1.00 postpk: 4.00 minerr: 0.063 filter: n lo,hi,nr,ftype: 0.3 9999.0 2 high
taperlen: 0.05 smooth: 0 pass, 0.10 0.20 0.40 0.20 0.10, 2 Dbase: db/zz

Figure 5.3.1.5. Example spectral fit for station CAF, case6a. See Figure 5.1.3a-c for an explanation of the plot elements. Kappa estimate is well constrained (center right subplot). Source: DID 006GB.003, file kappawrap/case6a/Figs/S85338_96208125243_CAF_EHE.eps.

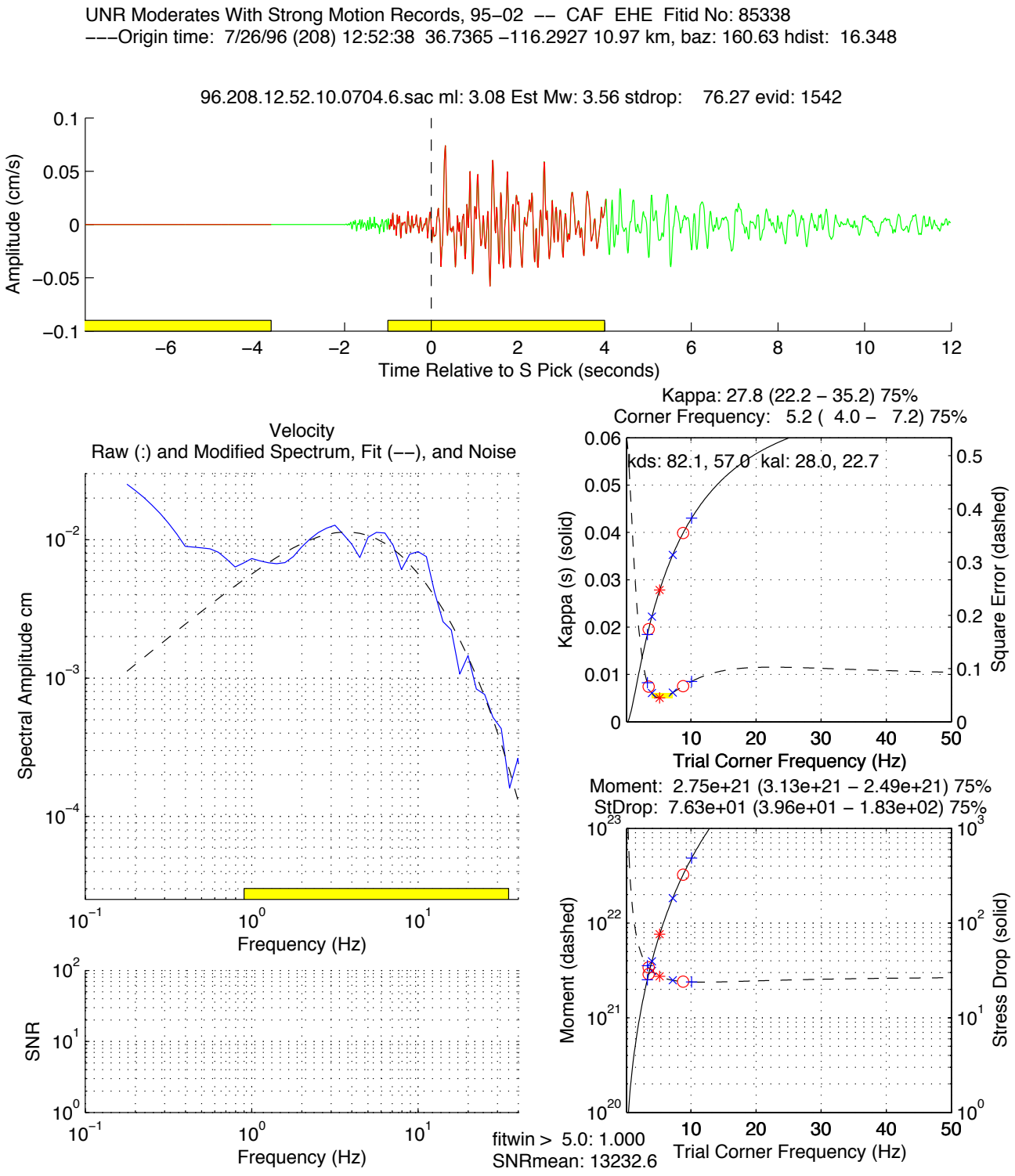

Kappa: 27.8 (22.2 – 35.2, 19.6–39.9, 18.4–43.0) Corner: 5.2 (4.0 – 7.2, 3.5– 8.8, 3.3–10.1)
Mo: 2.75e+21 (3.13e+21– 2.49e+21, 3.41e+21– 2.41e+21, 3.56e+21– 2.39e+21) calib: 1.000e+00, silva: n
LF Spec: 1.02e–03 (1.16e–03– 9.23e–04, 1.27e–03– 8.95e–04, 1.32e–03– 8.86e–04) hdist: 16.3, logsp: y, 20.0
stress drop: 7.63e+01 (3.96e+01 – 1.83e+02, 2.89e+01– 3.25e+02, 2.52e+01– 4.86e+02) type: 1 scorr: y
mu: 3.20e+11 rho: 2.60 beta: 3.50e+05 Mwslope: 1.50 Mwint: 16.10 radf : 0.85 tocm: 1.00e–07 mtm: y nw: 4.0
siglvls: 1.230 1.500 1.700 dof: 40 prepk: 1.00 postpk: 4.00 minerr: 0.045 filter: n lo,hi,nr,ftype: 0.3 9999.0 2 high
taperlen: 0.05 smooth: 0 pass, 0.10 0.20 0.40 0.20 0.10, 2 Dbase: db/zz

Figure 5.3.1.6. Example spectral fit for station CAF, case6a. See Figure 5.1.3a-c for an explanation of the plot elements. Kappa estimate is well constrained (center right subplot) and consistent with the EW estimate. Source: DID 006GB.003, file kappawrap/case6a/Figs/S85339_96208125243_CAF_EHN.eps.

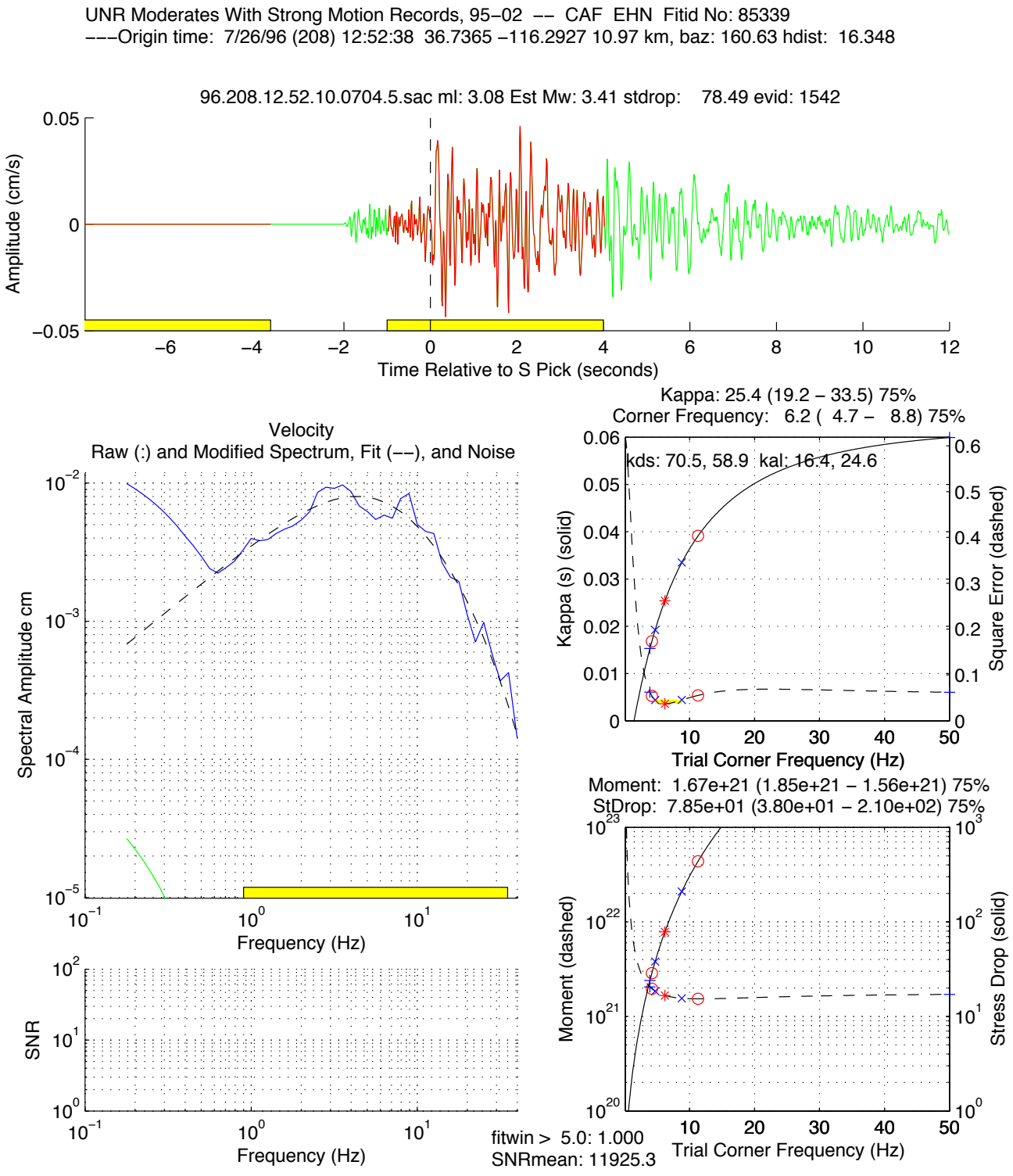

Kappa: 25.4 (19.2 – 33.5, 16.8–39.1, 15.3–59.9) Corner: 6.2 (4.7 – 8.8, 4.2–11.3, 3.9–50.0)
Mo: 1.67e+21 (1.85e+21– 1.56e+21, 1.96e+21– 1.54e+21, 2.05e+21– 1.71e+21) calib: 1.000e+00, silva: n
LF Spec: 6.19e–04 (6.88e–04– 5.78e–04, 7.29e–04– 5.70e–04, 7.61e–04– 6.35e–04) hdist: 16.3, logsp: y, 20.0
stress drop: 7.85e+01 (3.80e+01 – 2.10e+02, 2.87e+01– 4.38e+02, 2.40e+01– 4.22e+04) type: 1 scorr: y
mu: 3.20e+11 rho: 2.60 beta: 3.50e+05 Mwslope: 1.50 Mwint: 16.10 radf : 0.85 tocm: 1.00e–07 mtm: y nw: 4.0
siglvls: 1.230 1.500 1.700 dof: 40 prepk: 1.00 postpk: 4.00 minerr: 0.037 filter: n lo,hi,nr,ftype: 0.3 9999.0 2 high
taperlen: 0.05 smooth: 0 pass, 0.10 0.20 0.40 0.20 0.10, 2 Dbase: db/zz

Figure 5.3.2 Event average kappa (solid) and average from event-station records less than 40 km (dashed) for each earthquake in the "M3" set; SGBDSN data, case6a.

Source: DID 006GB.003, file kappawrap/case6a/Figs_summary/event_kappa_case6a.tbl. (upper figure), kappawrap/case6a/db/zz.srckappa (lower). event origin-id=col. 1, kappa=col. 12, epicentral distance=col. 37.

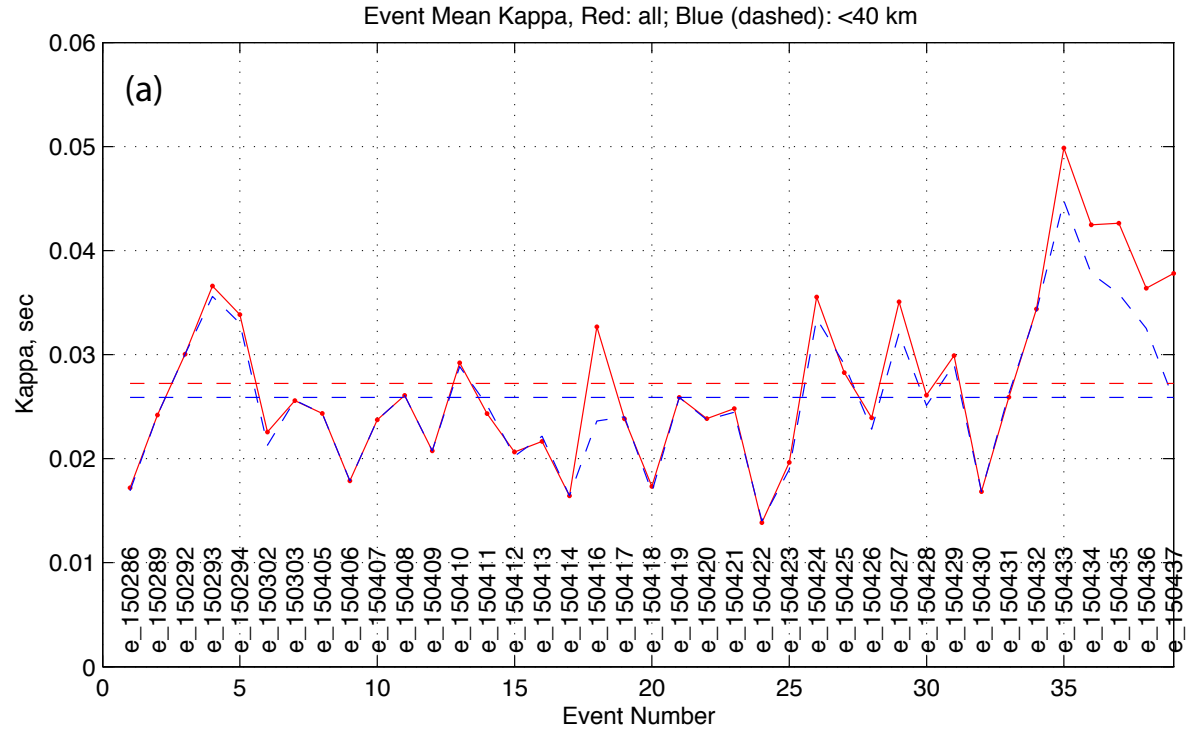

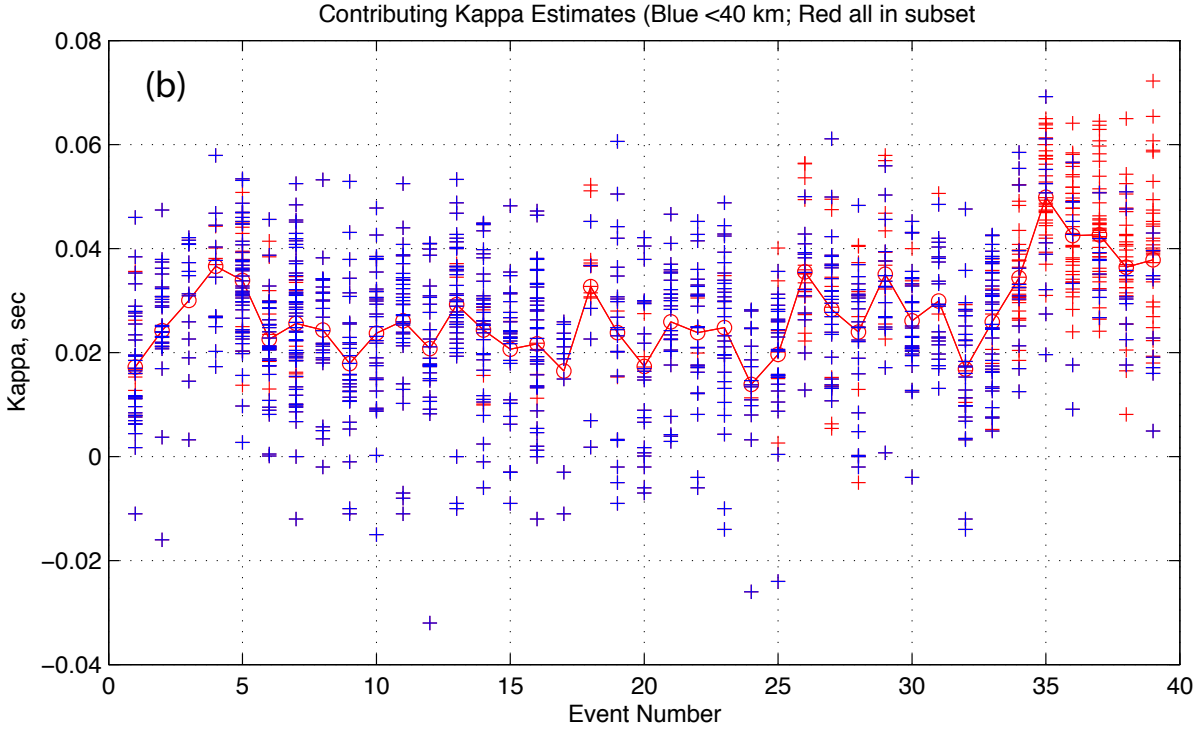

Figure 5.3.3.1 Station AL5. Source: DID 006GB.003, this figure: file kappawrap/case6a/Figs_summary/ml_vs_kcorr_40xsta.eps, where sta is the station name below. Ml, latitude, longitude in 006DV.004; kappa, stress drop, corner frequency, epicentral distance in DID 006GB.003, kappawrap/case6a/db/zz.srckappa columns 12, 22, 6, 37, and 18, respectively. Other subset details in Table 5.14. Small event kappa and displacement slope kappa from DID 006GB.003, kappawrap/casewm1/db/goodjan97.srckappa, columns 12 and 15, resp.

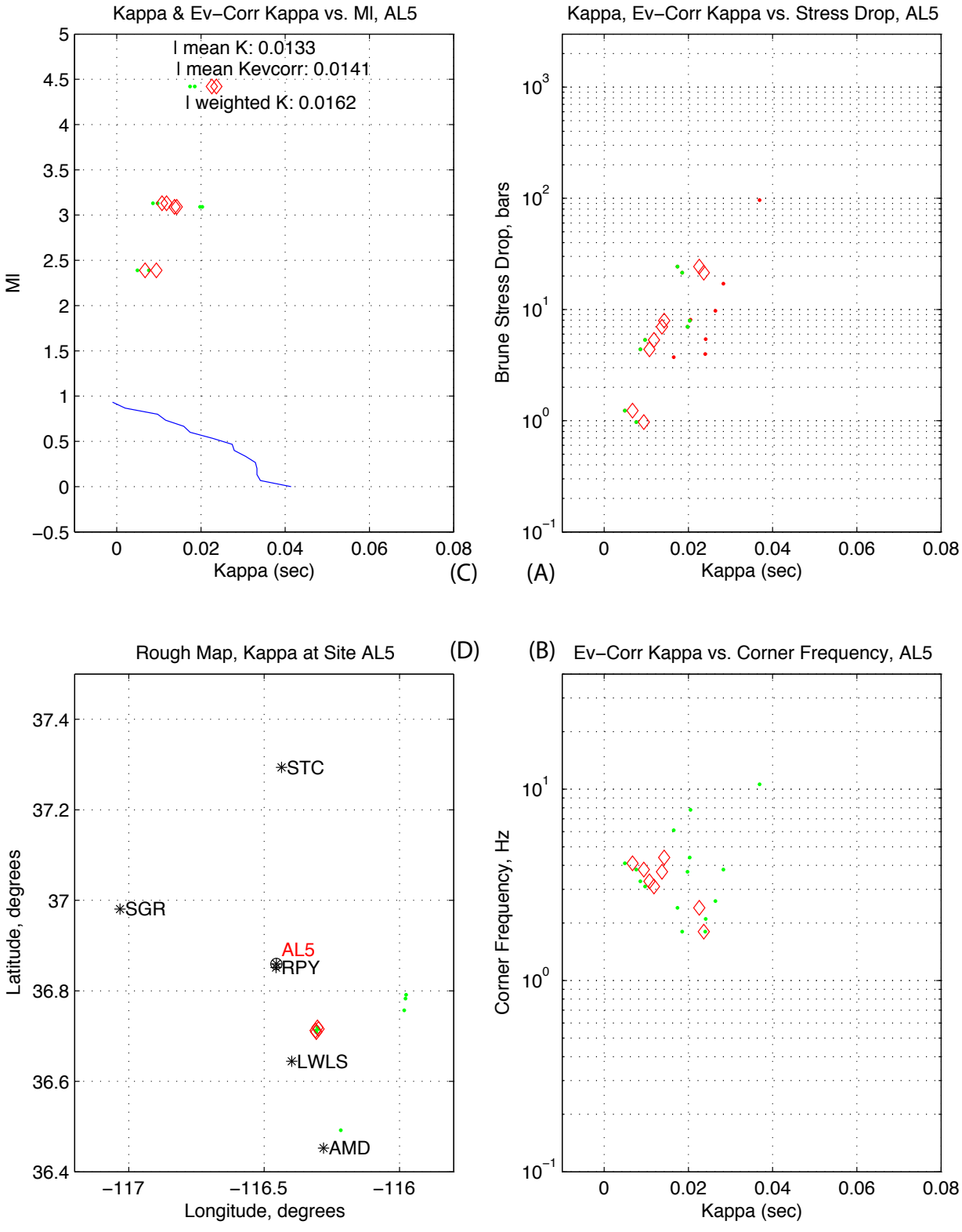

Figure 5.3.3.2. Station AMD. Source: DID 006GB.003, this figure: file kappawrap/case6a/Figs_summary/ml_vs_kcorr_40xsta.eps, where sta is the station name. Ml, latitude, longitude in 006DV.004; kappa, stress drop, corner frequency, epicentral distance in DID 006GB.003, kappawrap/case6a/db/zz.srckappa columns 12, 22, 6, 37, and 18, respectively. Other subset details in Table 5.14. Small event kappa and displacement slope kappa from DID 006GB.003, kappawrap/casewm1/db/goodjan97.srckappa, columns 12 and 15, resp.

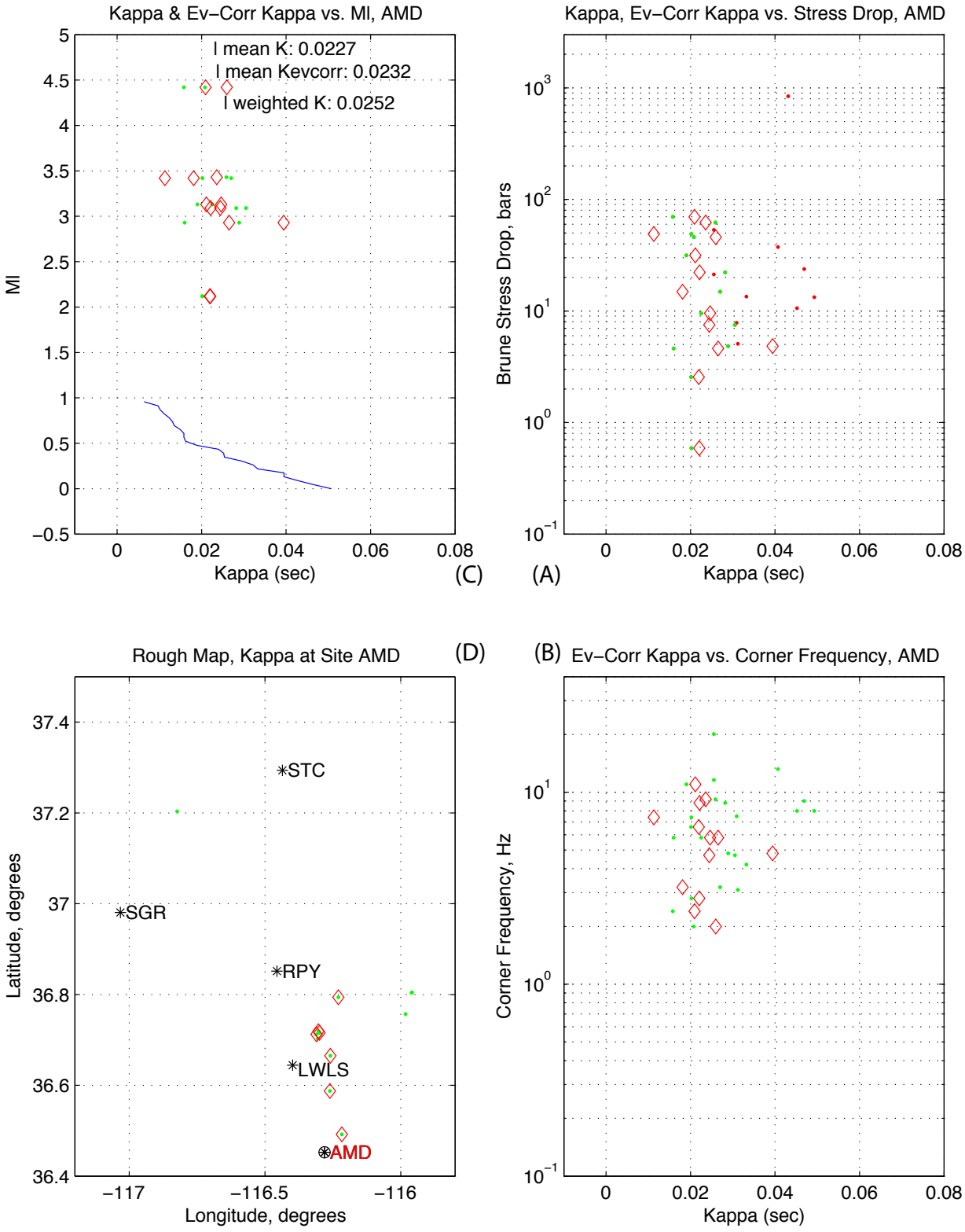

Figure 5.3.3.3. Station BTW. Source: DID 006GB.003, this figure: file kappawrap/case6a/Figs_summary/ml_vs_kcorr_40xsta.eps, where sta is the station name. Ml, latitude, longitude in 006DV.004; kappa, stress drop, corner frequency, epicentral distance in DID 006GB.003, kappawrap/case6a/db/zz.srckappa columns 12, 22, 6, 37, and 18, respectively. Other subset details in Table 5.14. Small event kappa and displacement slope kappa from DID 006GB.003, kappawrap/casewm1/db/goodjan97.srckappa, columns 12 and 15, resp.

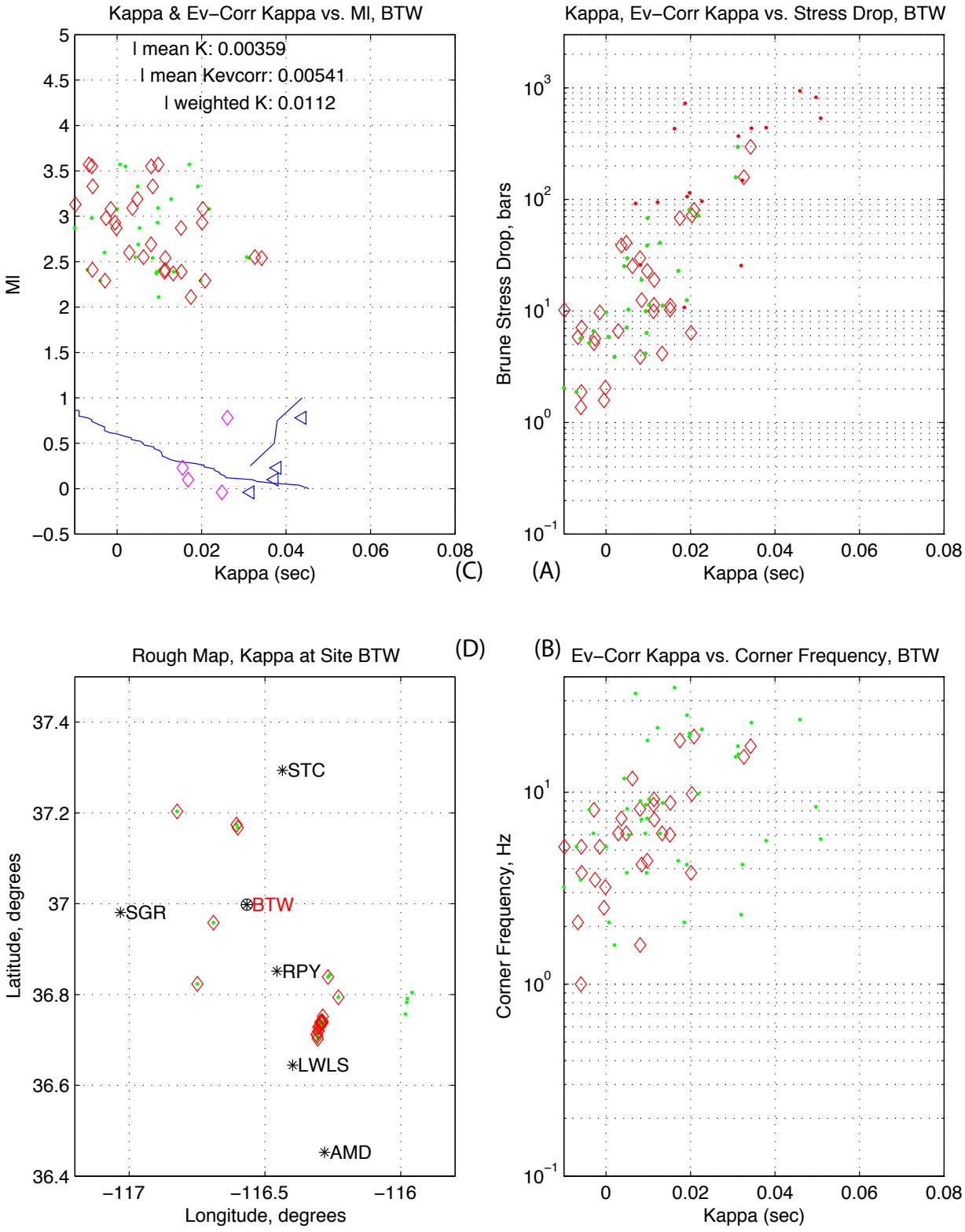

Figure 5.3.3.4. Station BYMS. Source: DID 006GB.003, this figure: file kappawrap/case6a/Figs_summary/ml_vs_kcorr_40xsta.eps, where sta is the station name. Ml, latitude, longitude in 006DV.004; kappa, stress drop, corner frequency, epicentral distance in DID 006GB.003, kappawrap/case6a/db/zz.srckappa columns 12, 22, 6, 37, and 18, respectively. Other subset details in Table 5.14. Small event kappa and displacement slope kappa from DID 006GB.003, kappawrap/casewm1/db/goodjan97.srckappa, columns 12 and 15, resp.

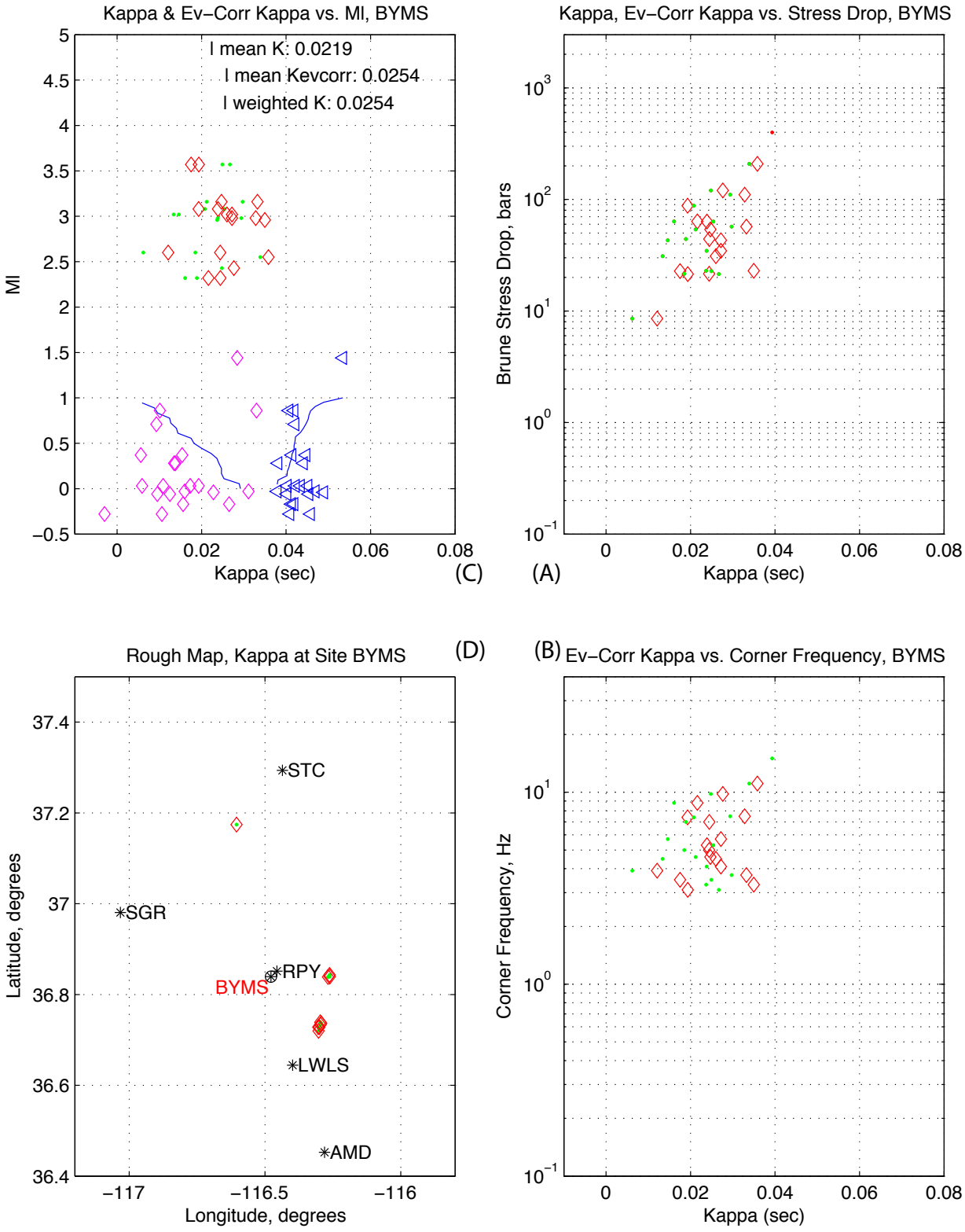

Figure 5.3.3.5 Station CAF. Source: DID 006GB.003, this figure: file kappawrap/case6a/Figs_summary/ml_vs_kcorr_40xsta.eps, where sta is the station name. Ml, latitude, longitude in 006DV.004; kappa, stress drop, corner frequency, epicentral distance in DID 006GB.003, kappawrap/case6a/db/zz.srckappa columns 12, 22, 6, 37, and 18, respectively. Other subset details in Table 5.14. Small event kappa and displacement slope kappa from DID 006GB.003, kappawrap/casewm1/db/goodjan97.srckappa, columns 12 and 15, resp.

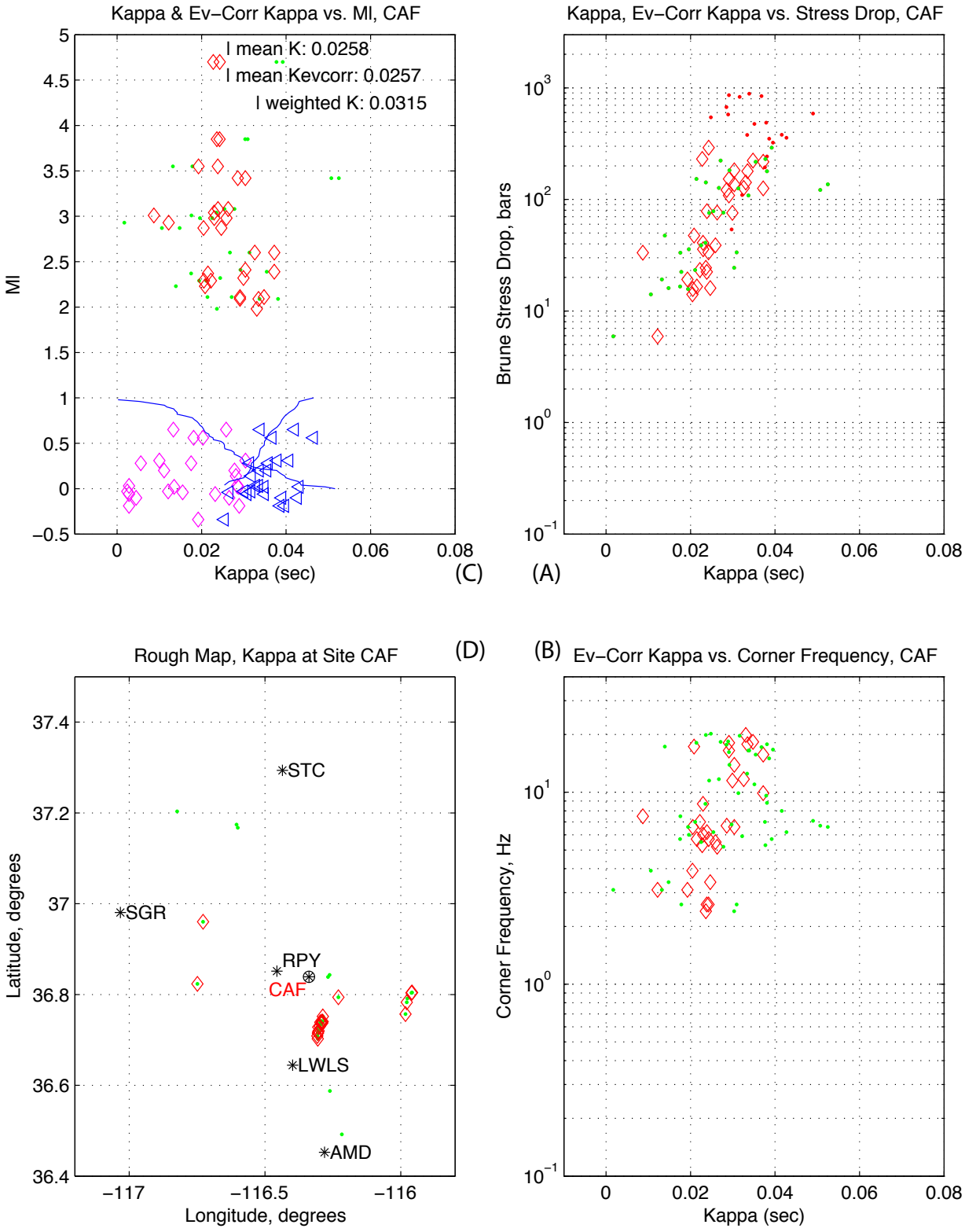

Figure 5.3.3.6. Station CRF. Source: DID 006GB.003, this figure: file kappawrap/case6a/Figs_summary/ml_vs_kcorr_40xsta.eps, where sta is the station name. Ml, latitude, longitude in 006DV.004; kappa, stress drop, corner frequency, epicentral distance in DID 006GB.003, kappawrap/case6a/db/zz.srckappa columns 12, 22, 6, 37, and 18, respectively. Other subset details in Table 5.14. Small event kappa and displacement slope kappa from DID 006GB.003, kappawrap/casewm1/db/goodjan97.srckappa, columns 12 and 15, resp.

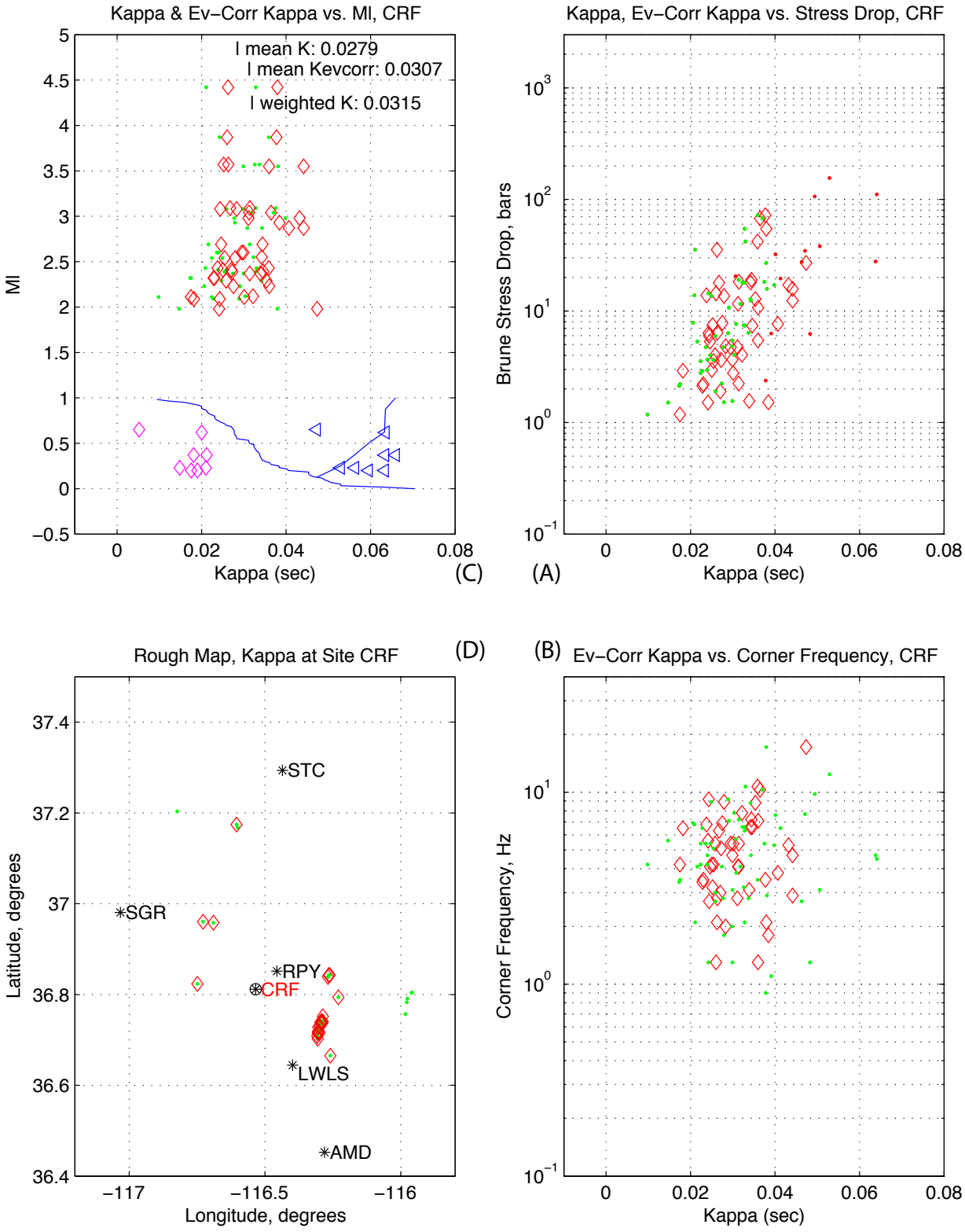

Figure 5.3.3.7. Station DOM. Source: DID 006GB.003, this figure: file kappawrap/case6a/Figs_summary/ml_vs_kcorr_40xsta.eps, where sta is the station name. Ml, latitude, longitude in 006DV.004; kappa, stress drop, corner frequency, epicentral distance in DID 006GB.003, kappawrap/case6a/db/zz.srckappa columns 12, 22, 6, 37, and 18, respectively. Other subset details in Table 5.14. Small event kappa and displacement slope kappa from DID 006GB.003, kappawrap/casewm1/db/goodjan97.srckappa, columns 12 and 15, resp.

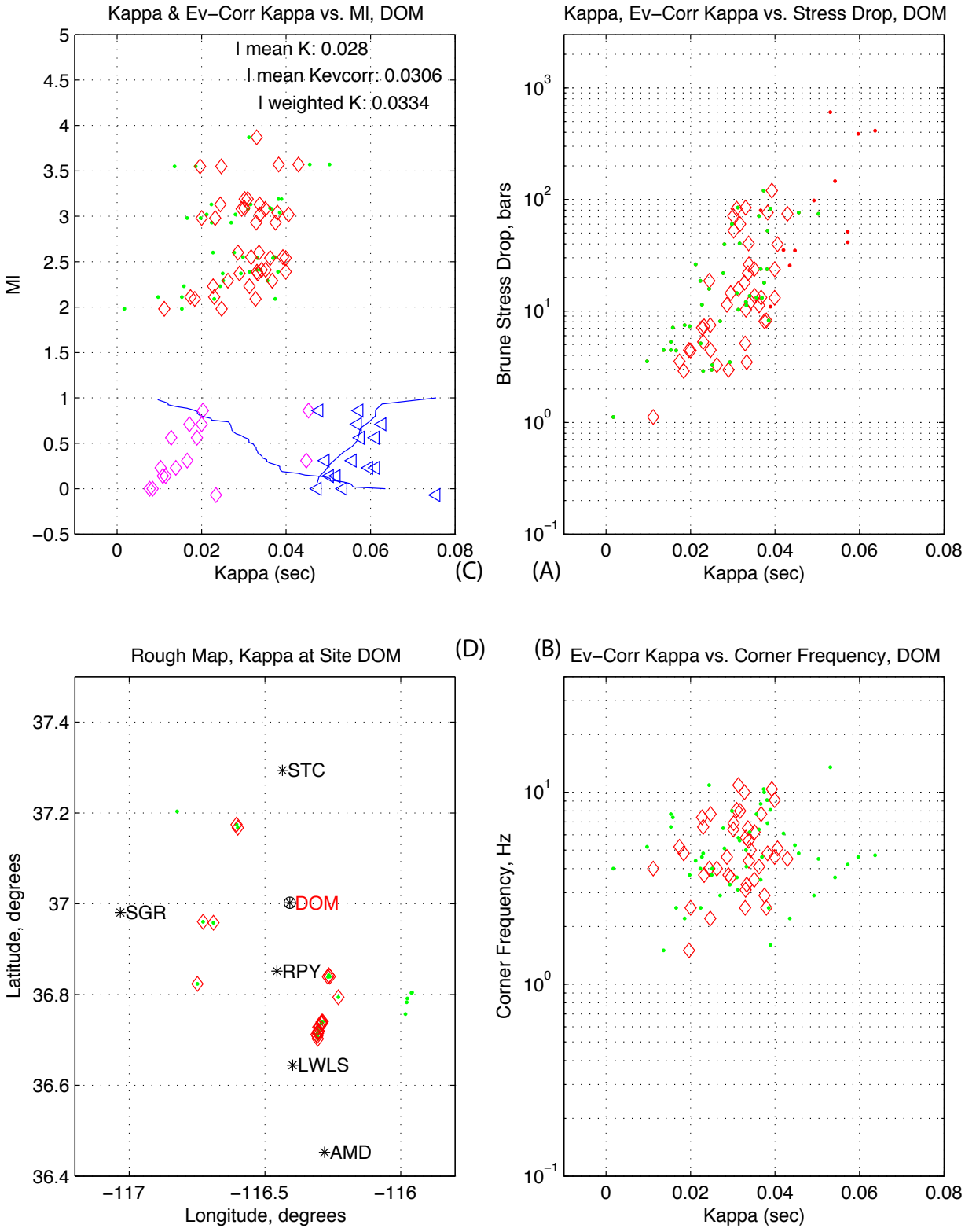

Figure 5.3.3.8. Station EXHS. Source: DID 006GB.003, this figure: file kappawrap/case6a/Figs_summary/ml_vs_kcorr_40xsta.eps, where sta is the station name. Ml, latitude, longitude in 006DV.004; kappa, stress drop, corner frequency, epicentral distance in DID 006GB.003, kappawrap/case6a/db/zz.srckappa columns 12, 22, 6, 37, and 18, respectively. Other subset details in Table 5.14. Small event kappa and displacement slope kappa from DID 006GB.003, kappawrap/casewm1/db/goodjan97.srckappa, columns 12 and 15, resp.

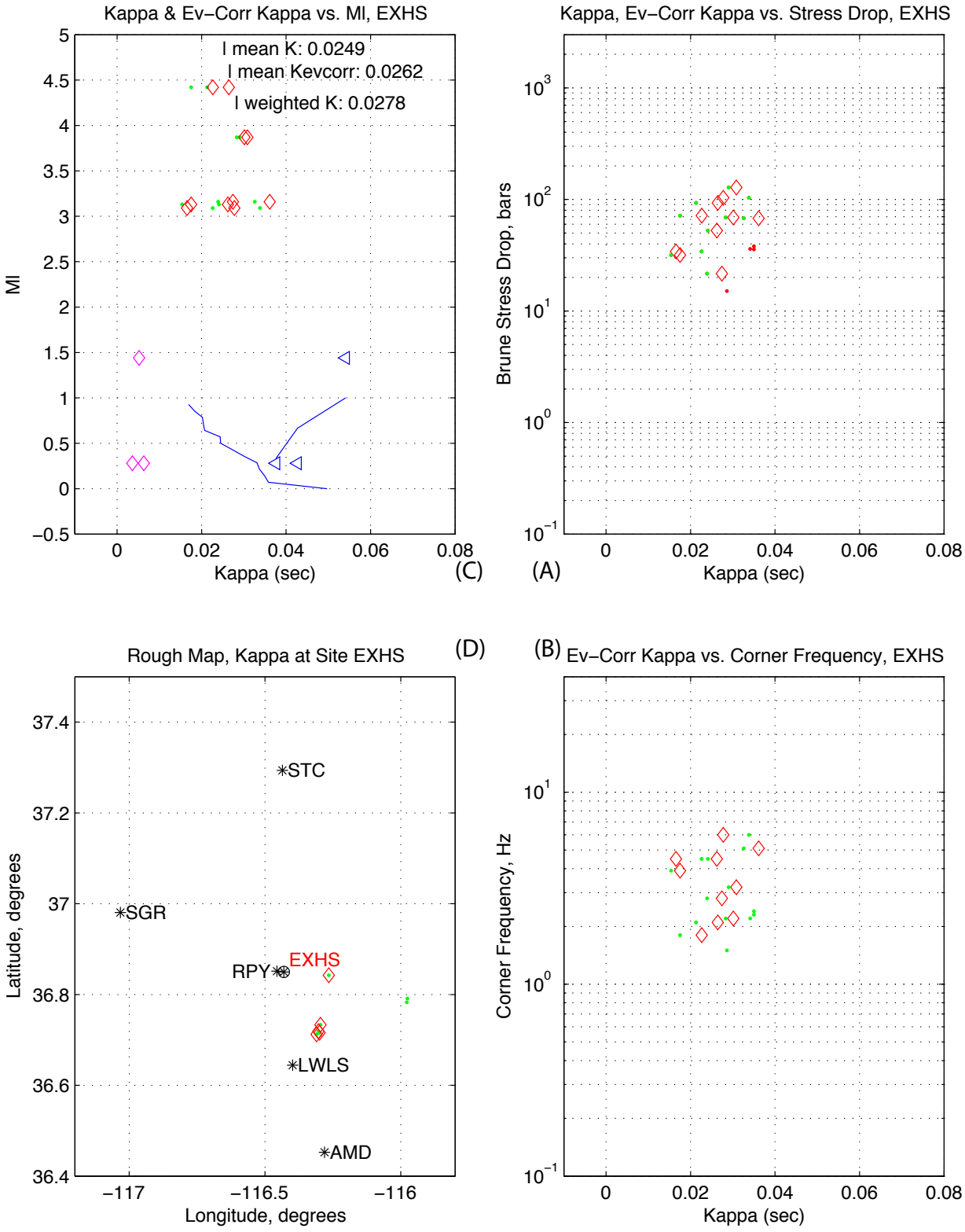

Figure 5.3.3.9. Station FMW. Source: DID 006GB.003, this figure: file kappawrap/case6a/Figs_summary/ml_vs_kcorr_40xsta.eps, where sta is the station name. Ml, latitude, longitude in 006DV.004; kappa, stress drop, corner frequency, epicentral distance in DID 006GB.003, kappawrap/case6a/db/zz.srckappa columns 12, 22, 6, 37, and 18, respectively. Other subset details in Table 5.14. Small event kappa and displacement slope kappa from DID 006GB.003, kappawrap/casewm1/db/goodjan97.srckappa, columns 12 and 15, resp.

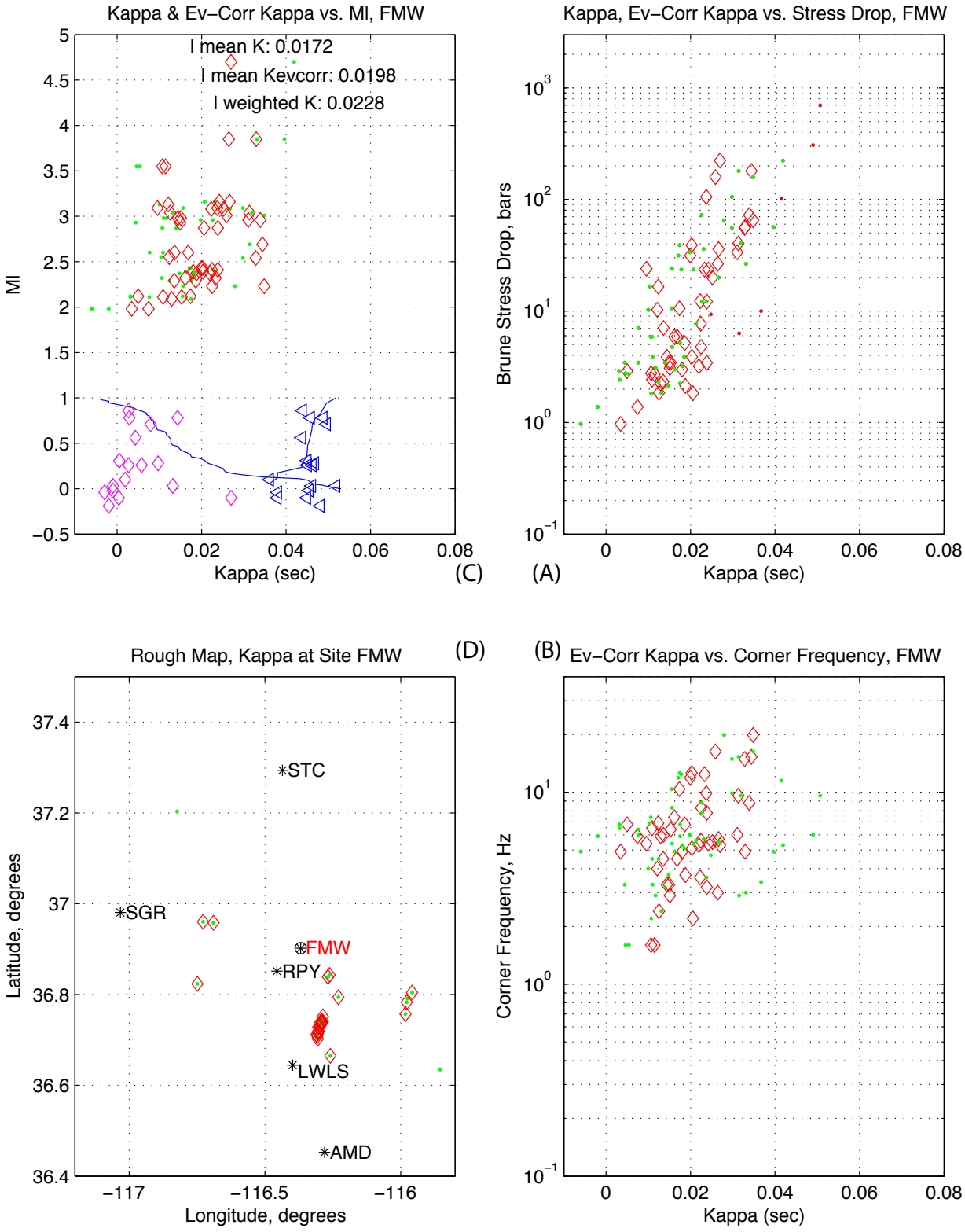

Figure 5.3.3.10. Station FOCS. Source: DID 006GB.003, this figure: file kappawrap/case6a/Figs_summary/ml_vs_kcorr_40xsta.eps, where sta is the station name. Ml, latitude, longitude in 006DV.004; kappa, stress drop, corner frequency, epicentral distance in DID 006GB.003, kappawrap/case6a/db/zz.srckappa columns 12, 22, 6, 37, and 18, respectively. Other subset details in Table 5.14. Small event kappa and displacement slope kappa from DID 006GB.003, kappawrap/casewm1/db/goodjan97.srckappa, columns 12 and 15, resp.

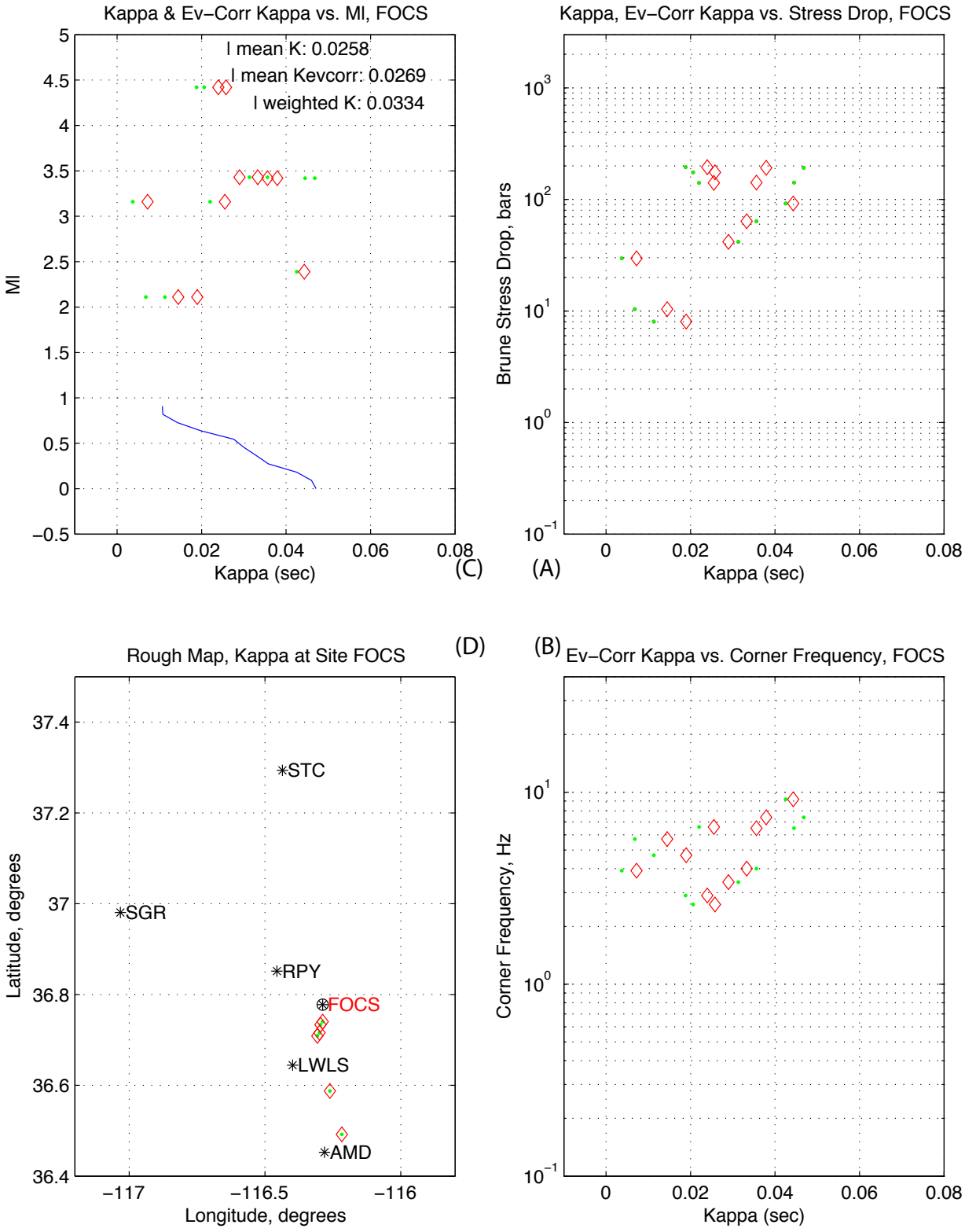

Figure 5.3.3.11. Station FRG. Source: DID 006GB.003, this figure: file kappawrap/case6a/Figs_summary/ml_vs_kcorr_40xsta.eps, where sta is the station name. Ml, latitude, longitude in 006DV.004; kappa, stress drop, corner frequency, epicentral distance in DID 006GB.003, kappawrap/case6a/db/zz.srckappa columns 12, 22, 6, 37, and 18, respectively. Other subset details in Table 5.14. Small event kappa and displacement slope kappa from DID 006GB.003, kappawrap/casewm1/db/goodjan97.srckappa, columns 12 and 15, resp.

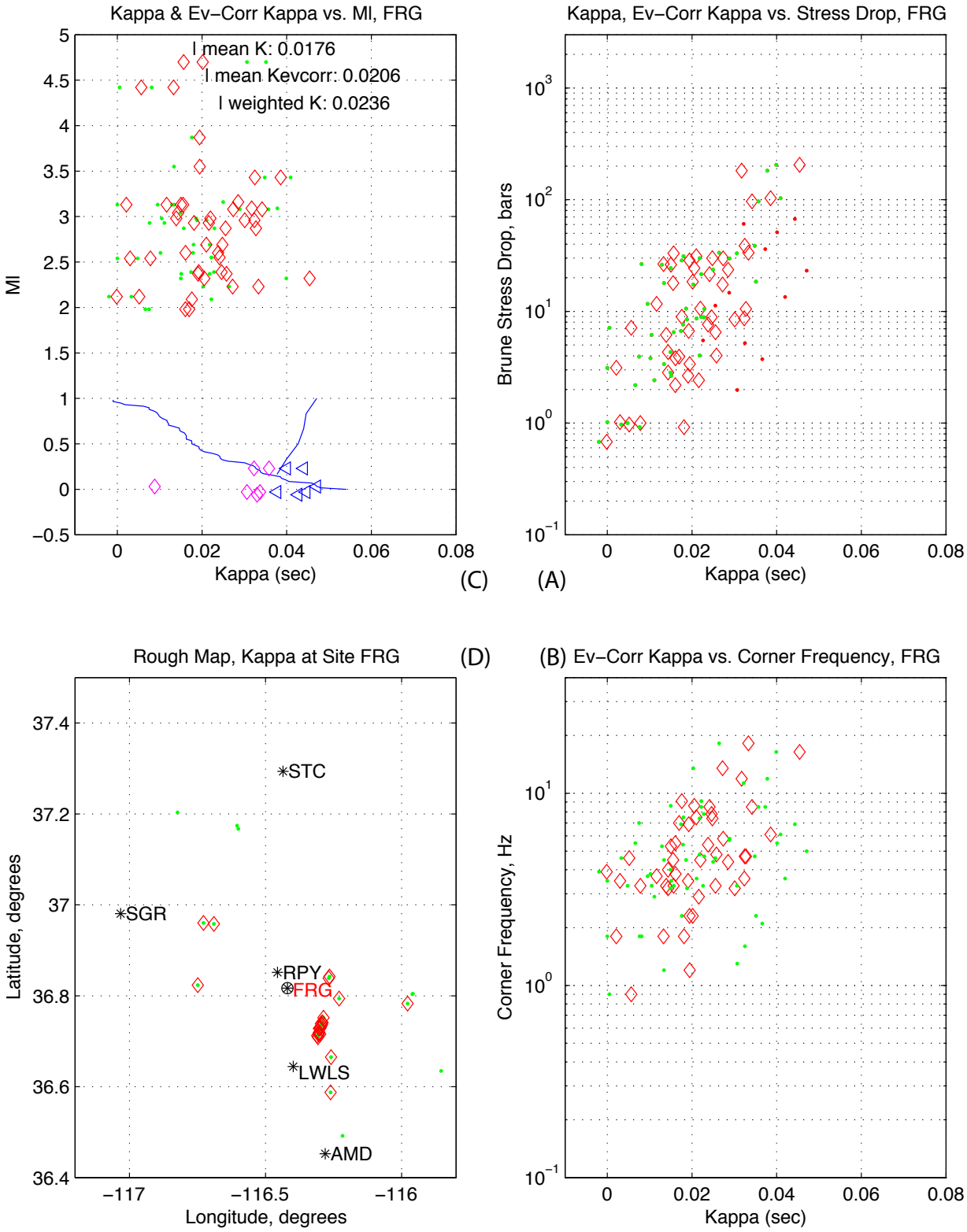

Figure 5.3.3.12. Station LEC. Source: DID 006GB.003, this figure: file kappawrap/case6a/Figs_summary/ml_vs_kcorr_40xsta.eps, where sta is the station name. Ml, latitude, longitude in 006DV.004; kappa, stress drop, corner frequency, epicentral distance in DID 006GB.003, kappawrap/case6a/db/zz.srckappa columns 12, 22, 6, 37, and 18, respectively. Other subset details in Table 5.14. Small event kappa and displacement slope kappa from DID 006GB.003, kappawrap/casewm1/db/goodjan97.srckappa, columns 12 and 15, resp.

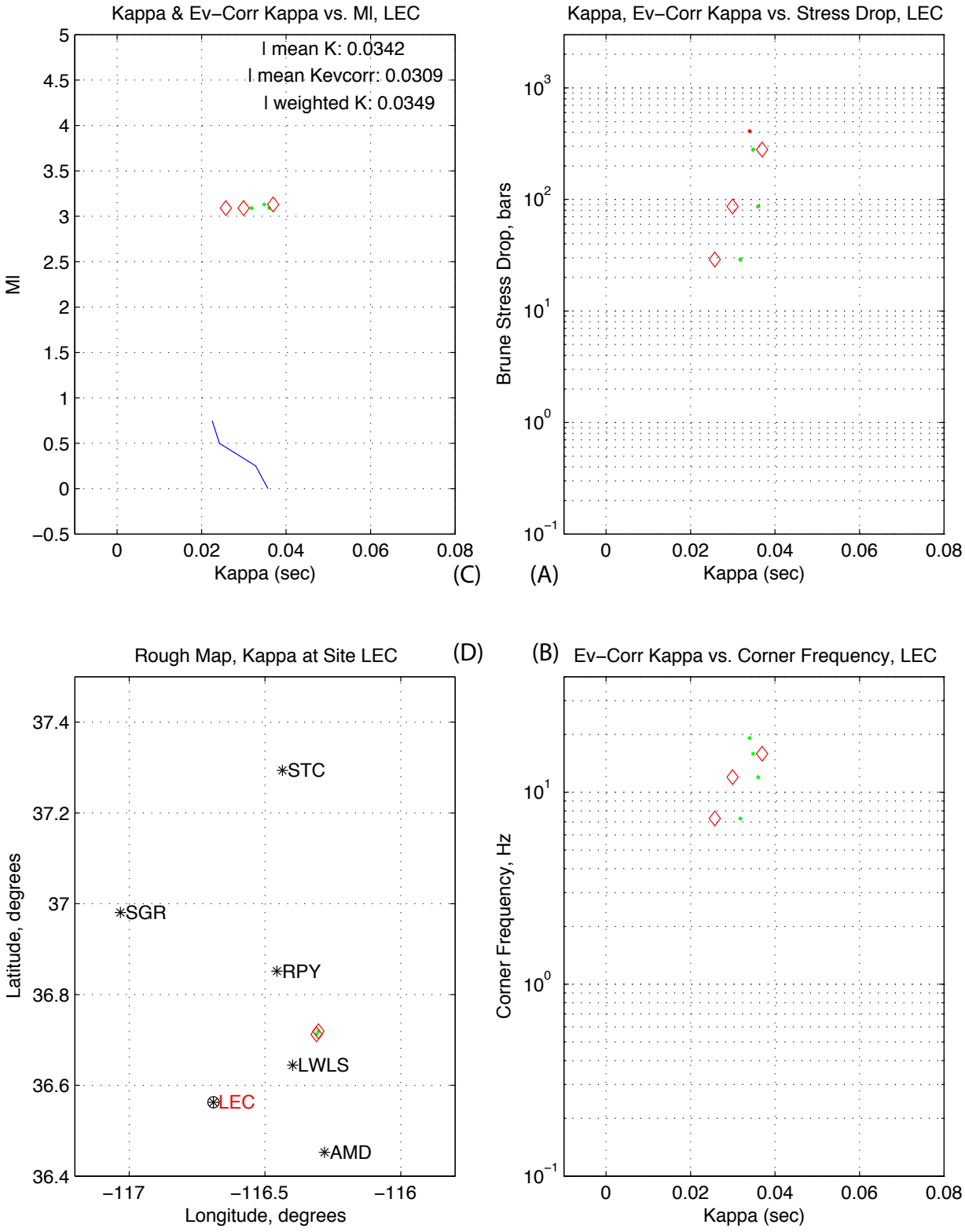

Figure 5.3.3.13. Station LSC. Source: DID 006GB.xxx, this figure: file kappawrap/case6a/Figs_summary/ml_vs_kcorr_40xsta.eps, where sta is the station name. Ml, latitude, longitude in 006DV.004; kappa, stress drop, corner frequency, epicentral distance in DID 006GB.003, kappawrap/case6a/db/zz.srckappa columns 12, 22, 6, 37, and 18, respectively. Other subset details in Table 5.14. Small event kappa and displacement slope kappa from DID 006GB.003, kappawrap/casewm1/db/goodjan97.srckappa, columns 12 and 15, resp.

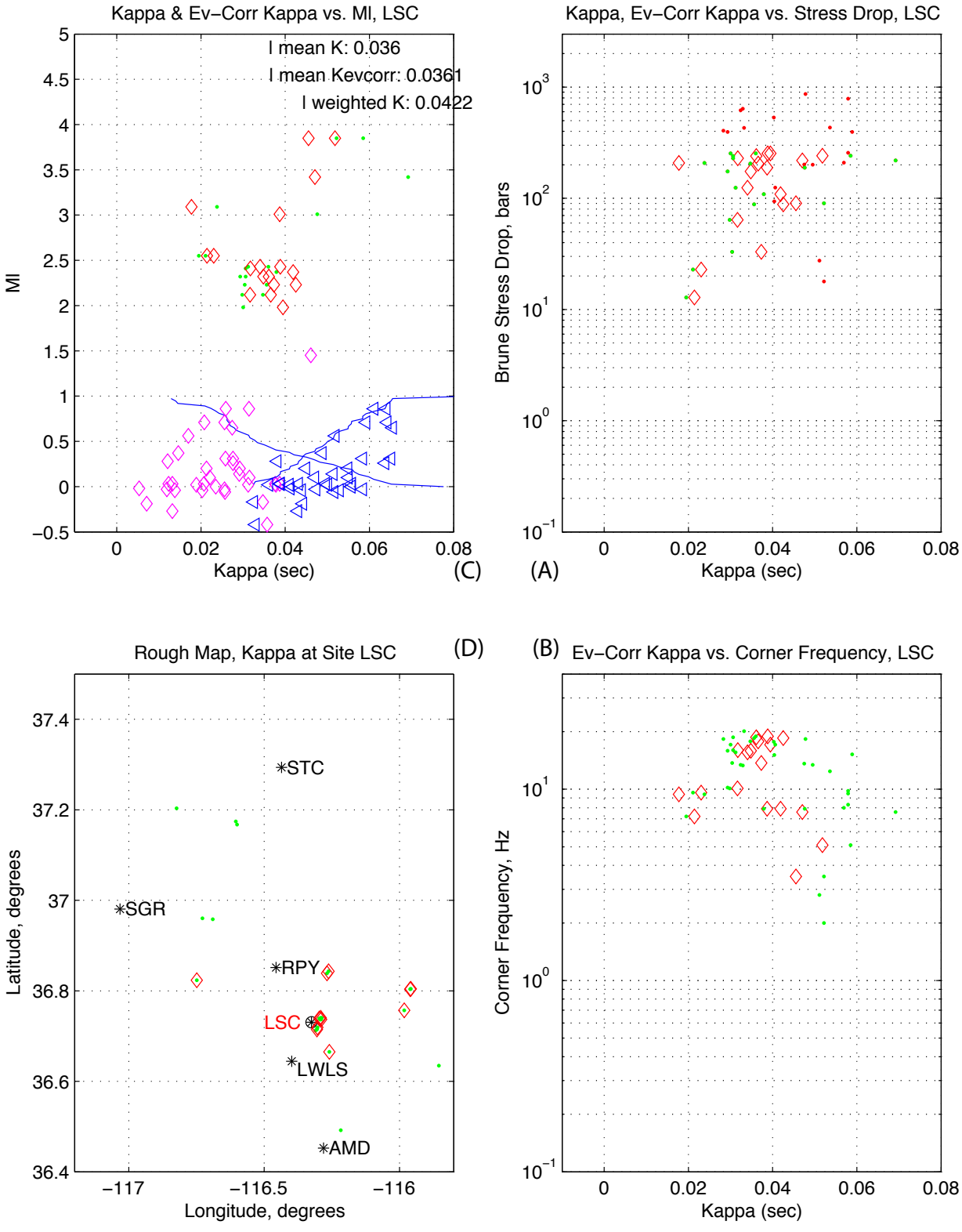

Figure 5.3.3.14. Station LWLS. Source: DID 006GB.003, this figure: file kappawrap/case6a/Figs_summary/ml_vs_kcorr_40xsta.eps, where sta is the station name. Ml, latitude, longitude in 006DV.004; kappa, stress drop, corner frequency, epicentral distance in DID 006GB.003, kappawrap/case6a/db/zz.srckappa columns 12, 22, 6, 37, and 18, respectively. Other subset details in Table 5.14. Small event kappa and displacement slope kappa from DID 006GB.003, kappawrap/casewm1/db/goodjan97.srckappa, columns 12 and 15, resp.

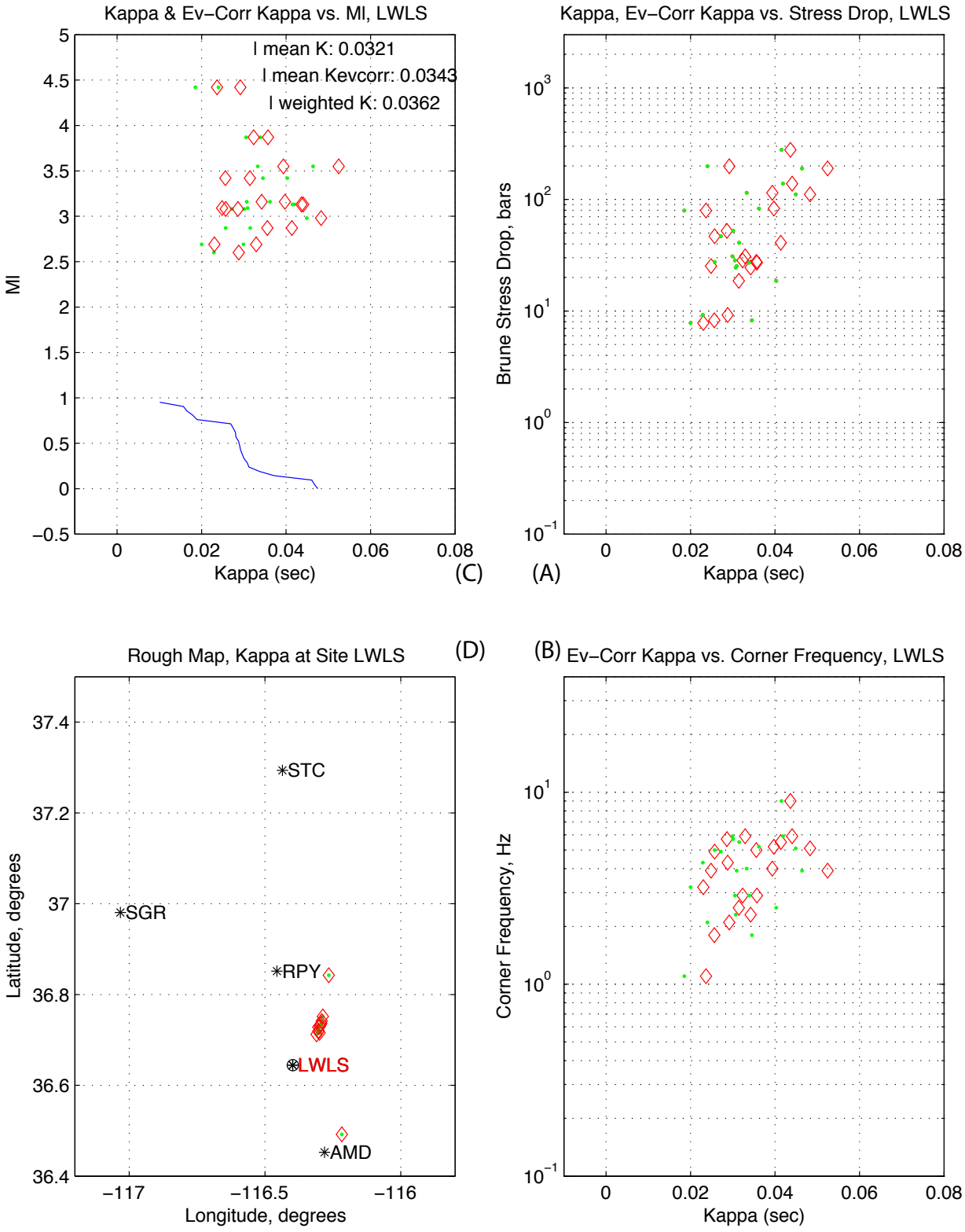

Figure 5.3.3.15. Station MDVS. Source: DID 006GB.003, this figure: file kappawrap/case6a/Figs_summary/ml_vs_kcorr_40xsta.eps, where sta is the station name. Ml, latitude, longitude in 006DV.004; kappa, stress drop, corner frequency, epicentral distance in DID 006GB.003, kappawrap/case6a/db/zz.srckappa columns 12, 22, 6, 37, and 18, respectively. Other subset details in Table 5.14. Small event kappa and displacement slope kappa from DID 006GB.003, kappawrap/casewm1/db/goodjan97.srckappa, columns 12 and 15, resp.

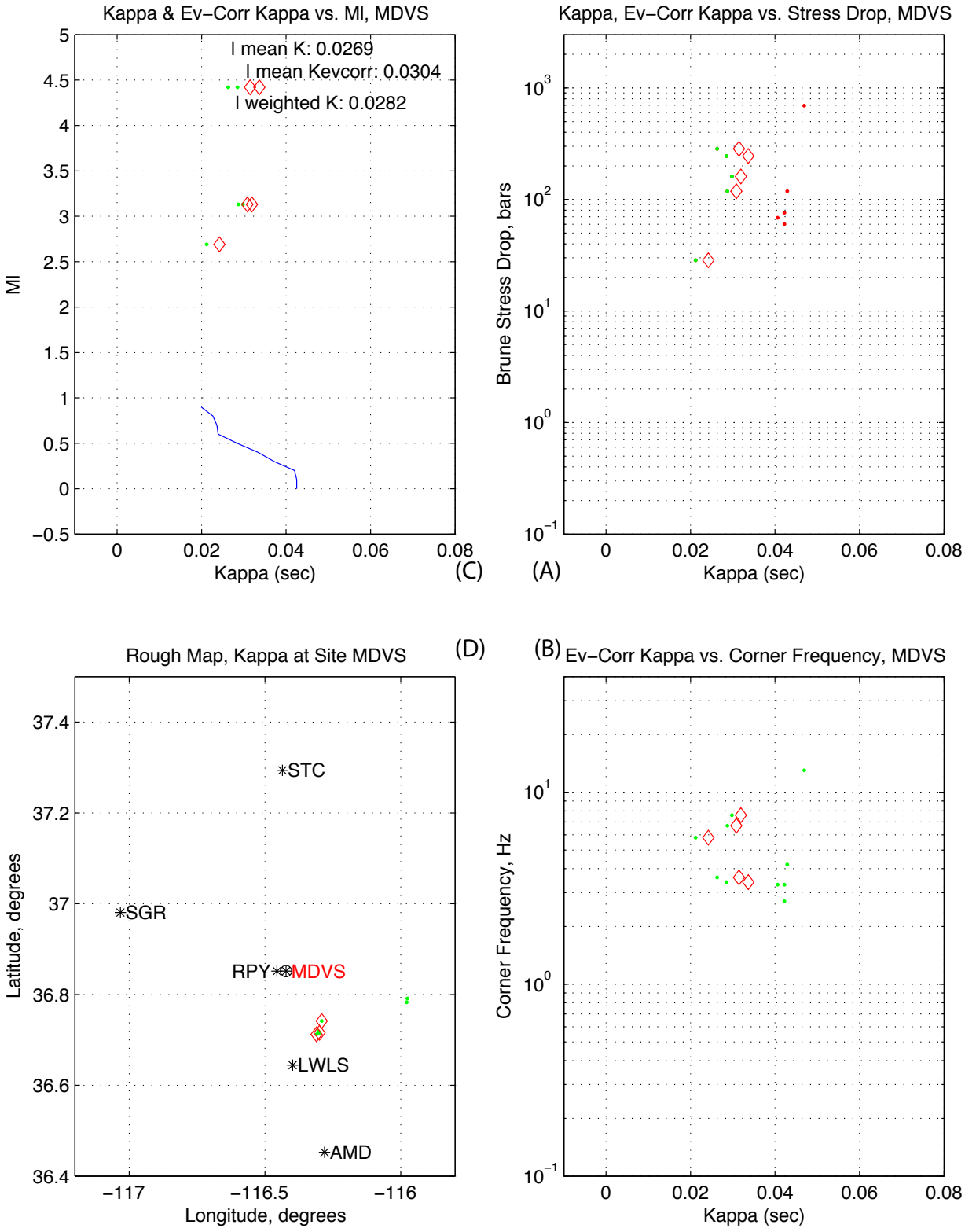

Figure 5.3.3.16. Station NCF. Source: DID 006GB.003, this figure: file kappawrap/case6a/Figs_summary/ml_vs_kcorr_40xsta.eps, where sta is the station name. Ml, latitude, longitude in 006DV.004; kappa, stress drop, corner frequency, epicentral distance in DID 006GB.003, kappawrap/case6a/db/zz.srckappa columns 12, 22, 6, 37, and 18, respectively. Other subset details in Table 5.14. Small event kappa and displacement slope kappa from DID 006GB.003, kappawrap/casewm1/db/goodjan97.srckappa, columns 12 and 15, resp.

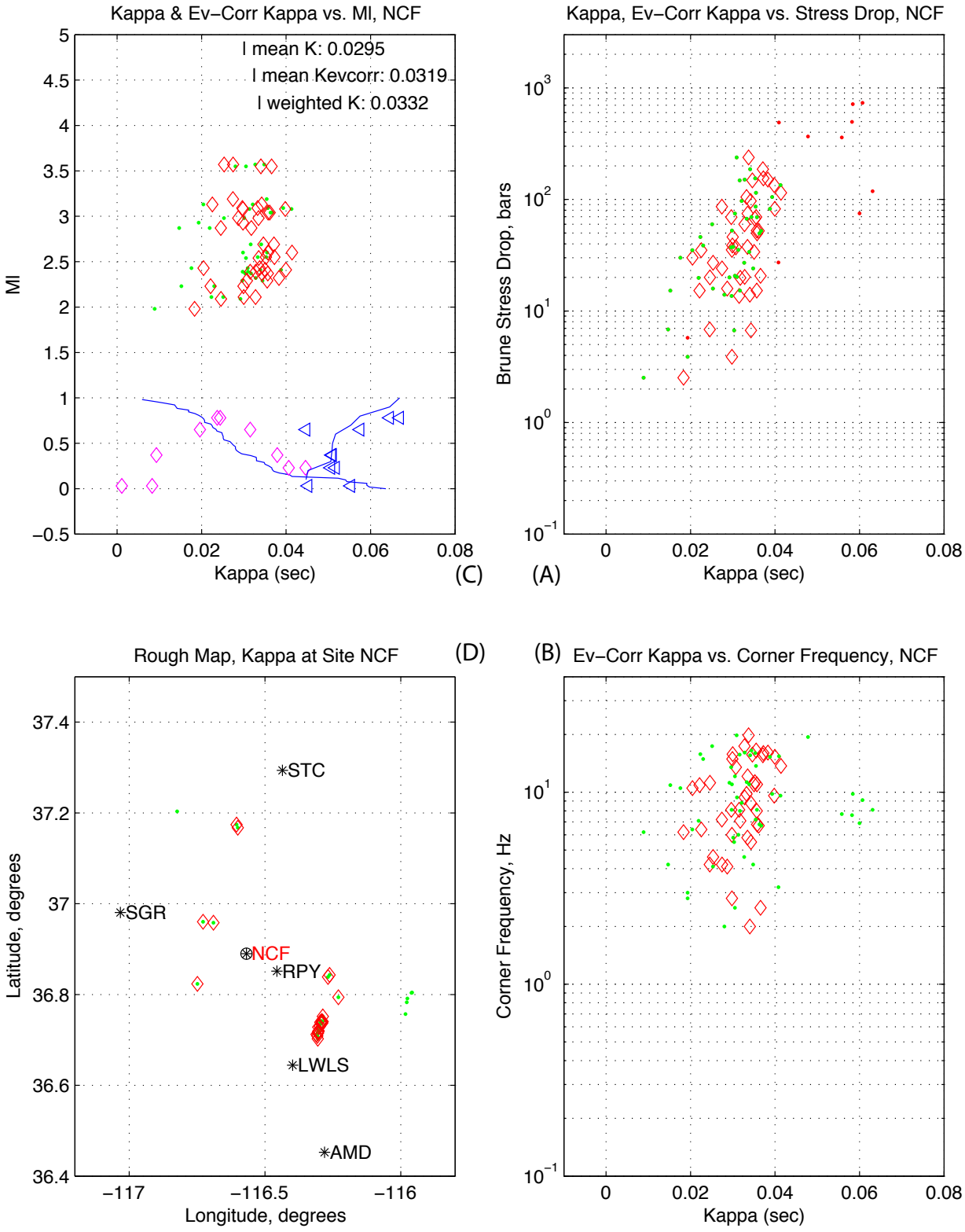

Figure 5.3.3.17. Station PUV. Source: DID 006GB.003, this figure: file kappawrap/case6a/Figs_summary/ml_vs_kcorr_40xsta.eps, where sta is the station name. Ml, latitude, longitude in 006DV.004; kappa, stress drop, corner frequency, epicentral distance in DID 006GB.003, kappawrap/case6a/db/zz.srckappa columns 12, 22, 6, 37, and 18, respectively. Other subset details in Table 5.14. Small event kappa and displacement slope kappa from DID 006GB.003, kappawrap/casewm1/db/goodjan97.srckappa, columns 12 and 15, resp.

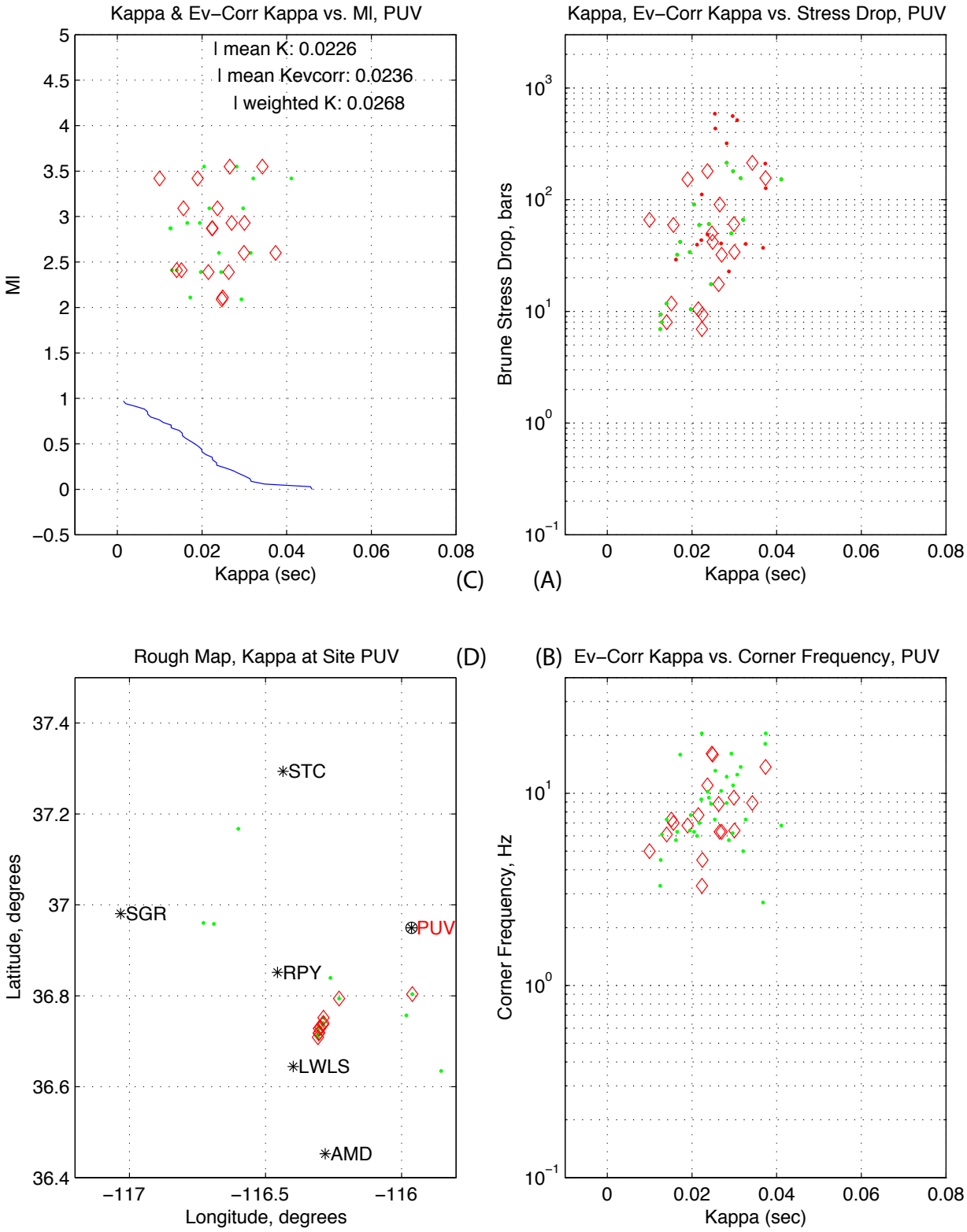

Figure 5.3.3.18. Station RED. Source: DID 006GB.003, this figure: file kappawrap/case6a/Figs_summary/ml_vs_kcorr_40xsta.eps, where sta is the station name. Ml, latitude, longitude in 006DV.004; kappa, stress drop, corner frequency, epicentral distance in DID 006GB.003, kappawrap/case6a/db/zz.srckappa columns 12, 22, 6, 37, and 18, respectively. Other subset details in Table 5.14. Small event kappa and displacement slope kappa from DID 006GB.003, kappawrap/casewm1/db/goodjan97.srckappa, columns 12 and 15, resp.

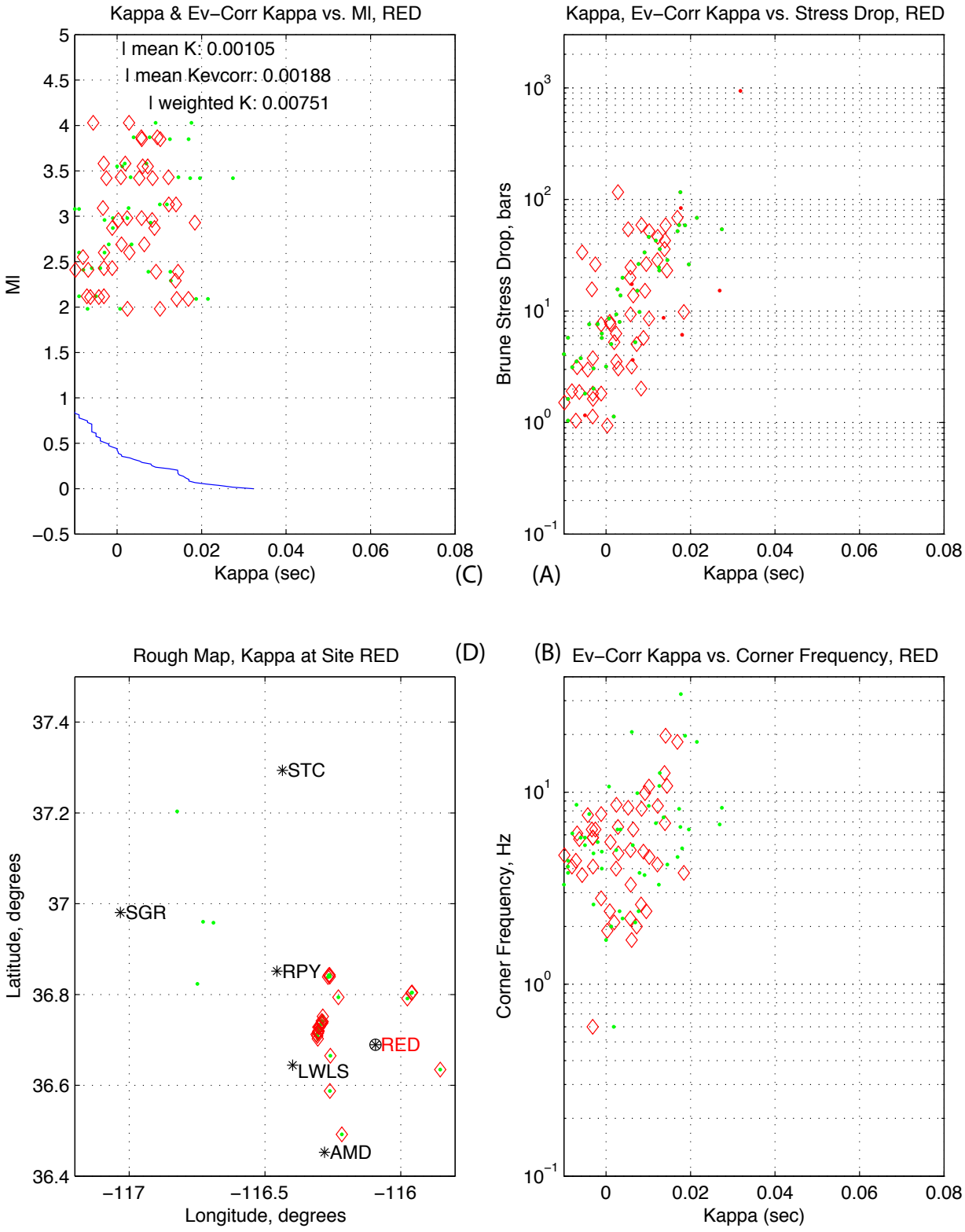

Figure 5.3.3.19. Station RPY. Source: DID 006GB.003, this figure: file kappawrap/case6a/Figs_summary/ml_vs_kcorr_40xsta.eps, where sta is the station name. Ml, latitude, longitude in 006DV.004; kappa, stress drop, corner frequency, epicentral distance in DID 006GB.003, kappawrap/case6a/db/zz.srckappa columns 12, 22, 6, 37, and 18, respectively. Other subset details in Table 5.14. Small event kappa and displacement slope kappa from DID 006GB.003, kappawrap/casewm1/db/goodjan97.srckappa, columns 12 and 15, resp.

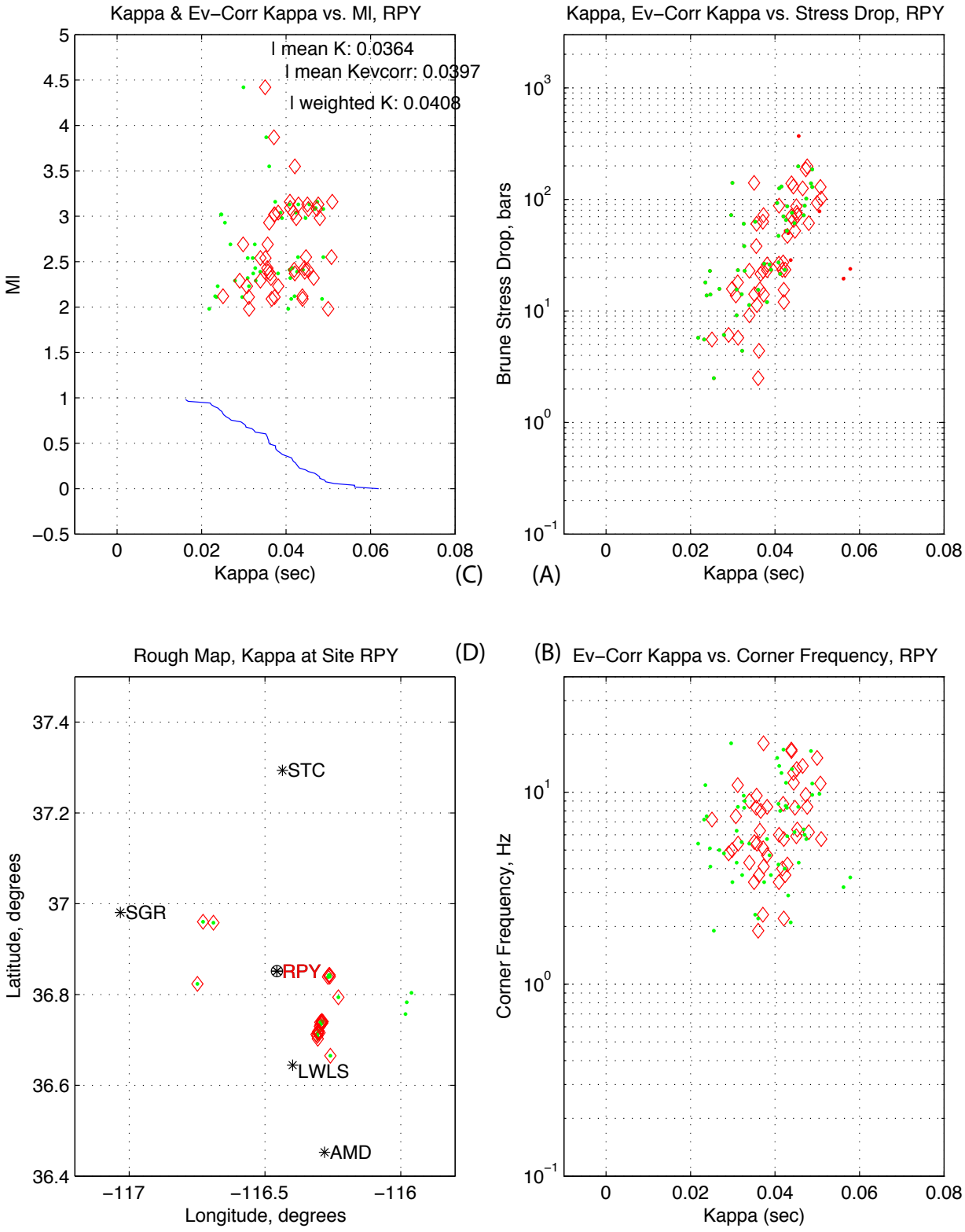

Figure 5.3.3.20. Station SCF. Source: DID 006GB.003, this figure: file kappawrap/case6a/Figs_summary/ml_vs_kcorr_40xsta.eps, where sta is the station name. Ml, latitude, longitude in 006DV.004; kappa, stress drop, corner frequency, epicentral distance in DID 006GB.003, kappawrap/case6a/db/zz.srckappa columns 12, 22, 6, 37, and 18, respectively. Other subset details in Table 5.14. Small event kappa and displacement slope kappa from DID 006GB.003, kappawrap/casewm1/db/goodjan97.srckappa, columns 12 and 15, resp.

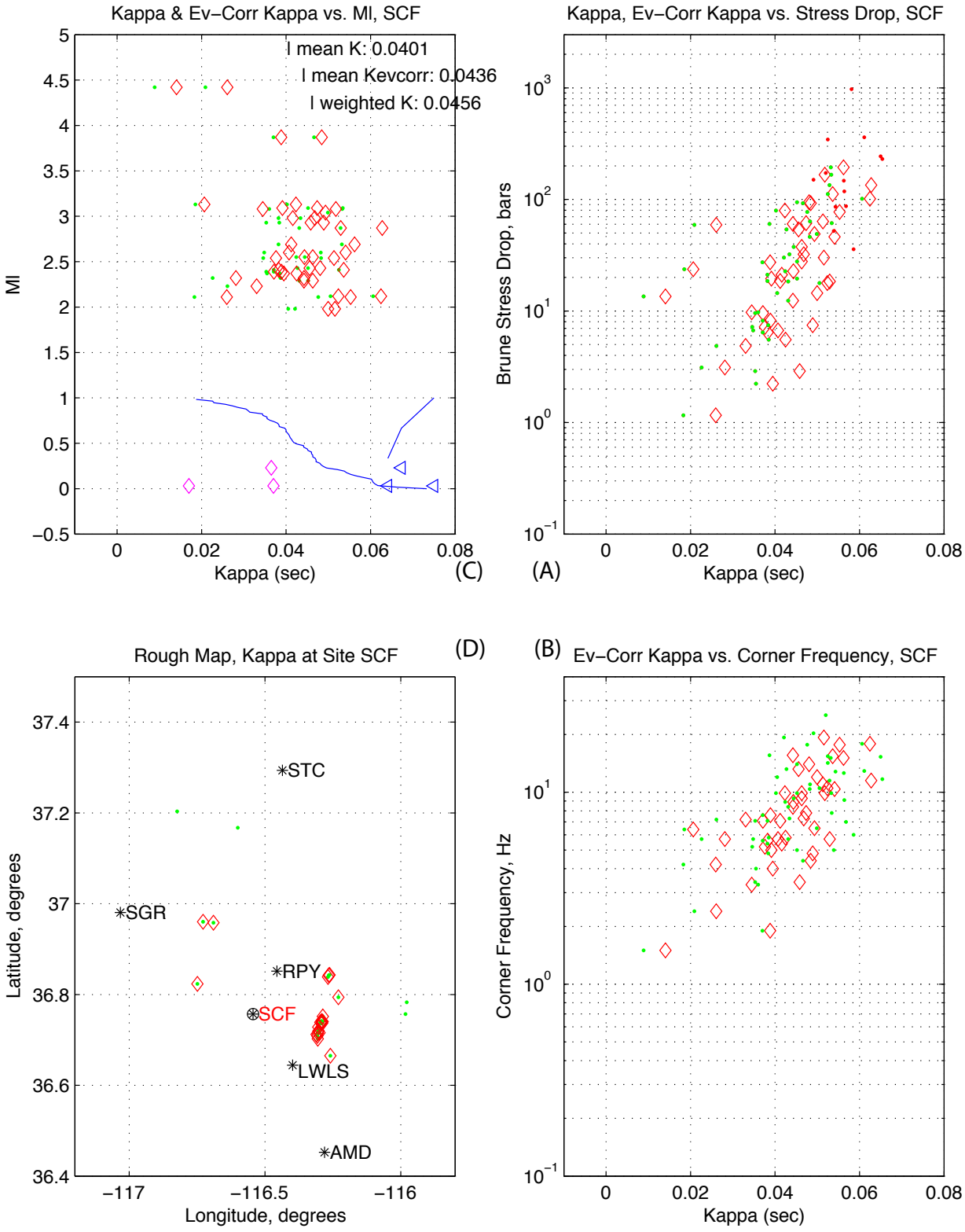

Figure 5.3.3.21. Station SGR. Source: DID 006GB.003, this figure: file kappawrap/case6a/Figs_summary/ml_vs_kcorr_40xsta.eps, where sta is the station name. Ml, latitude, longitude in 006DV.004; kappa, stress drop, corner frequency, epicentral distance in DID 006GB.003, kappawrap/case6a/db/zz.srckappa columns 12, 22, 6, 37, and 18, respectively. Other subset details in Table 5.14. Small event kappa and displacement slope kappa from DID 006GB.003, kappawrap/casewm1/db/goodjan97.srckappa, columns 12 and 15, resp.

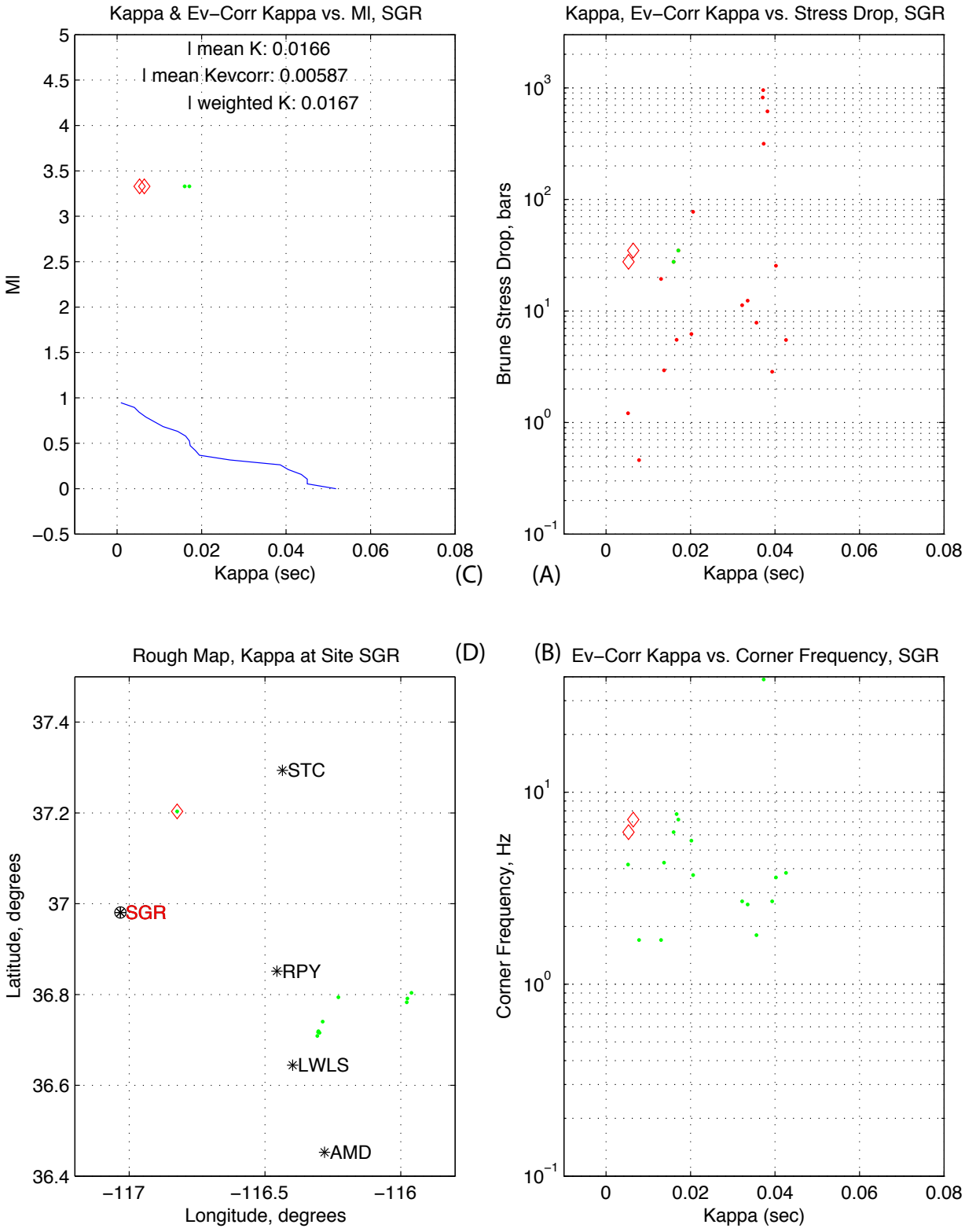

Figure 5.3.3.22. Station SPC. Source: DID 006GB.003, this figure: file kappawrap/case6a/Figs_summary/ml_vs_kcorr_40xsta.eps, where sta is the station name. Ml, latitude, longitude in 006DV.004; kappa, stress drop, corner frequency, epicentral distance in DID 006GB.003, kappawrap/case6a/db/zz.srckappa columns 12, 22, 6, 37, and 18, respectively. Other subset details in Table 5.14. Small event kappa and displacement slope kappa from DID 006GB.003, kappawrap/casewm1/db/goodjan97.srckappa, columns 12 and 15, resp.

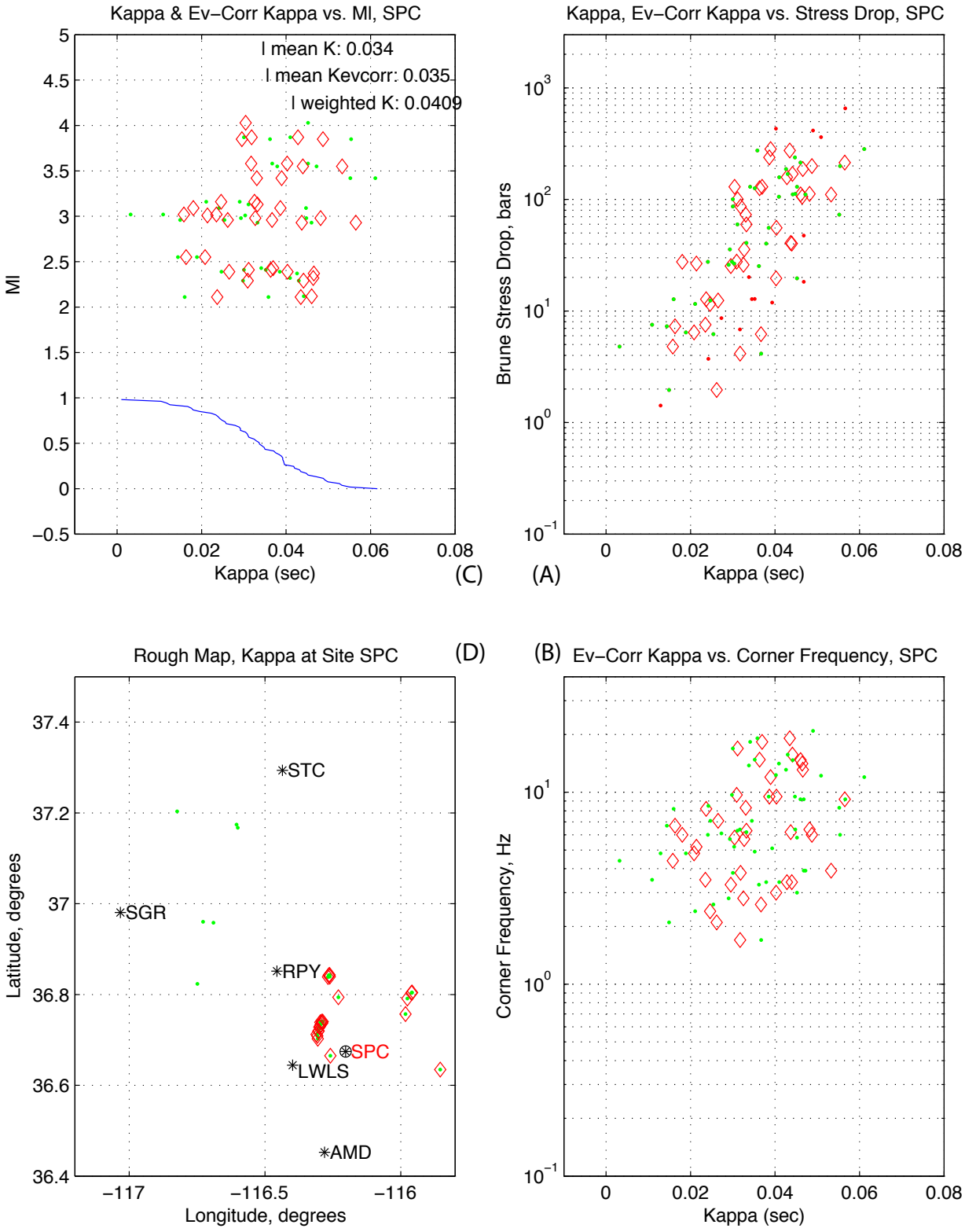

Figure 5.3.3.23. Station SPRS. Source: DID 006GB.003, this figure: file kappawrap/case6a/Figs_summary/ml_vs_kcorr_40xsta.eps, where sta is the station name. Ml, latitude, longitude in 006DV.004; kappa, stress drop, corner frequency, epicentral distance in DID 006GB.003, kappawrap/case6a/db/zz.srckappa columns 12, 22, 6, 37, and 18, respectively. Other subset details in Table 5.14. Small event kappa and displacement slope kappa from DID 006GB.003, kappawrap/casewm1/db/goodjan97.srckappa, columns 12 and 15, resp.

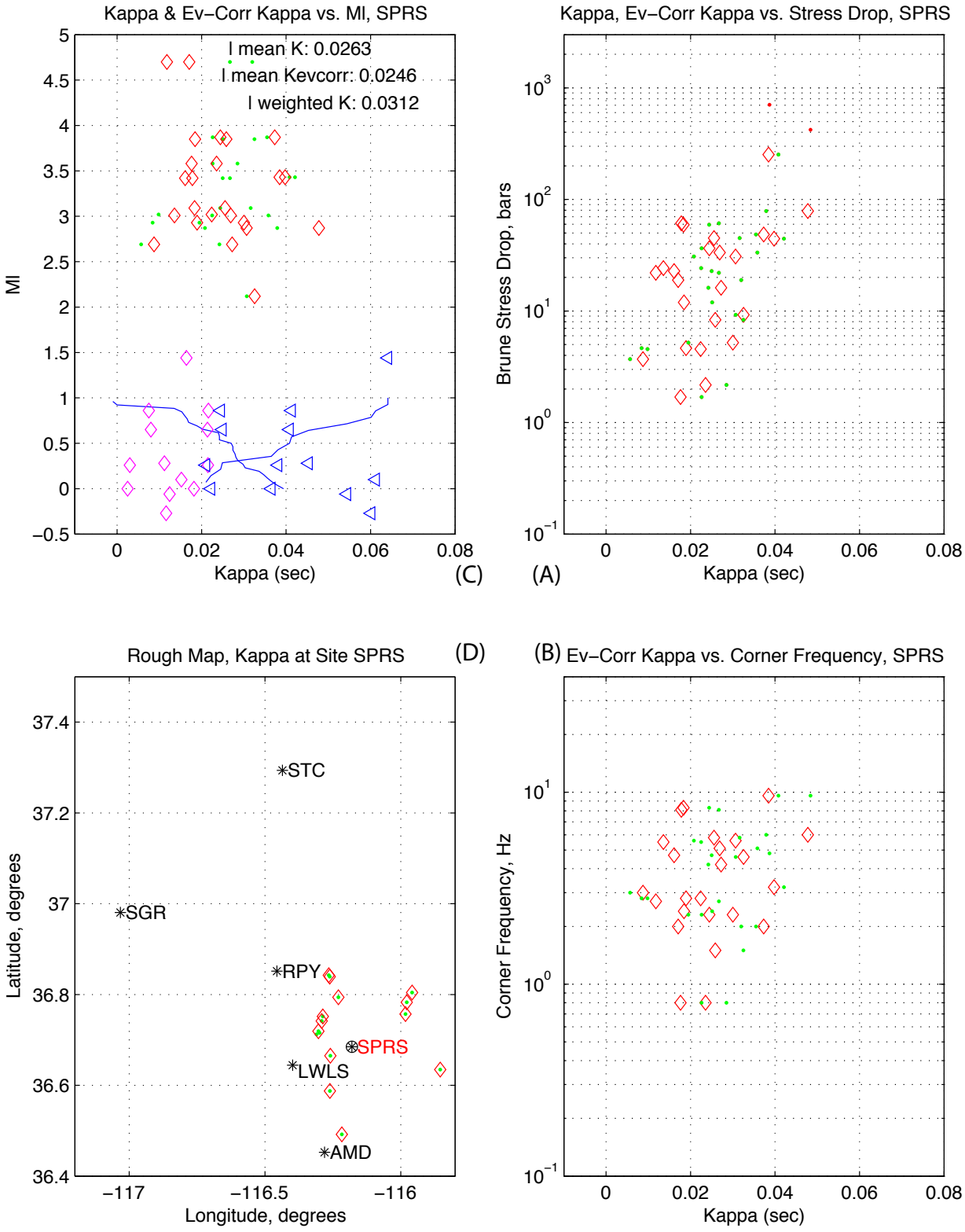

Figure 5.3.3.24. Station STC. Source: DID 006GB.003, this figure: file kappawrap/case6a/Figs_summary/ml_vs_kcorr_40xsta.eps, where sta is the station name. Ml, latitude, longitude in 006DV.004; kappa, stress drop, corner frequency, epicentral distance in DID 006GB.003, kappawrap/case6a/db/zz.srckappa columns 12, 22, 6, 37, and 18, respectively. Other subset details in Table 5.14. Small event kappa and displacement slope kappa from DID 006GB.003, kappawrap/casewm1/db/goodjan97.srckappa, columns 12 and 15, resp.

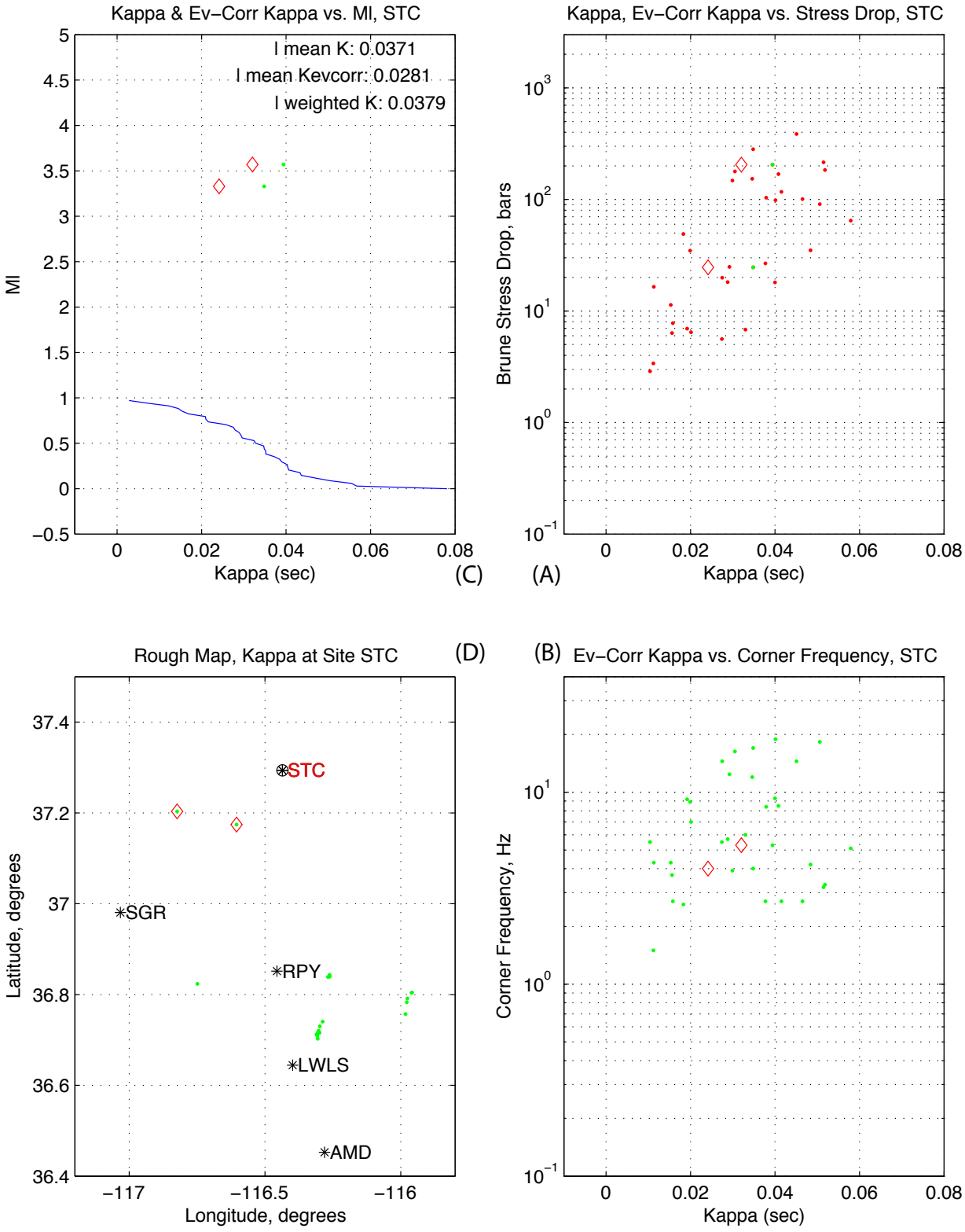

Figure 5.3.3.25. Station STH. Source: DID 006GB.003, this figure: file kappawrap/case6a/Figs_summary/ml_vs_kcorr_40xsta.eps, where sta is the station name. Ml, latitude, longitude in 006DV.004; kappa, stress drop, corner frequency, epicentral distance in DID 006GB.003, kappawrap/case6a/db/zz.srckappa columns 12, 22, 6, 37, and 18, respectively. Other subset details in Table 5.14. Small event kappa and displacement slope kappa from DID 006GB.003, kappawrap/casewm1/db/goodjan97.srckappa, columns 12 and 15, resp.

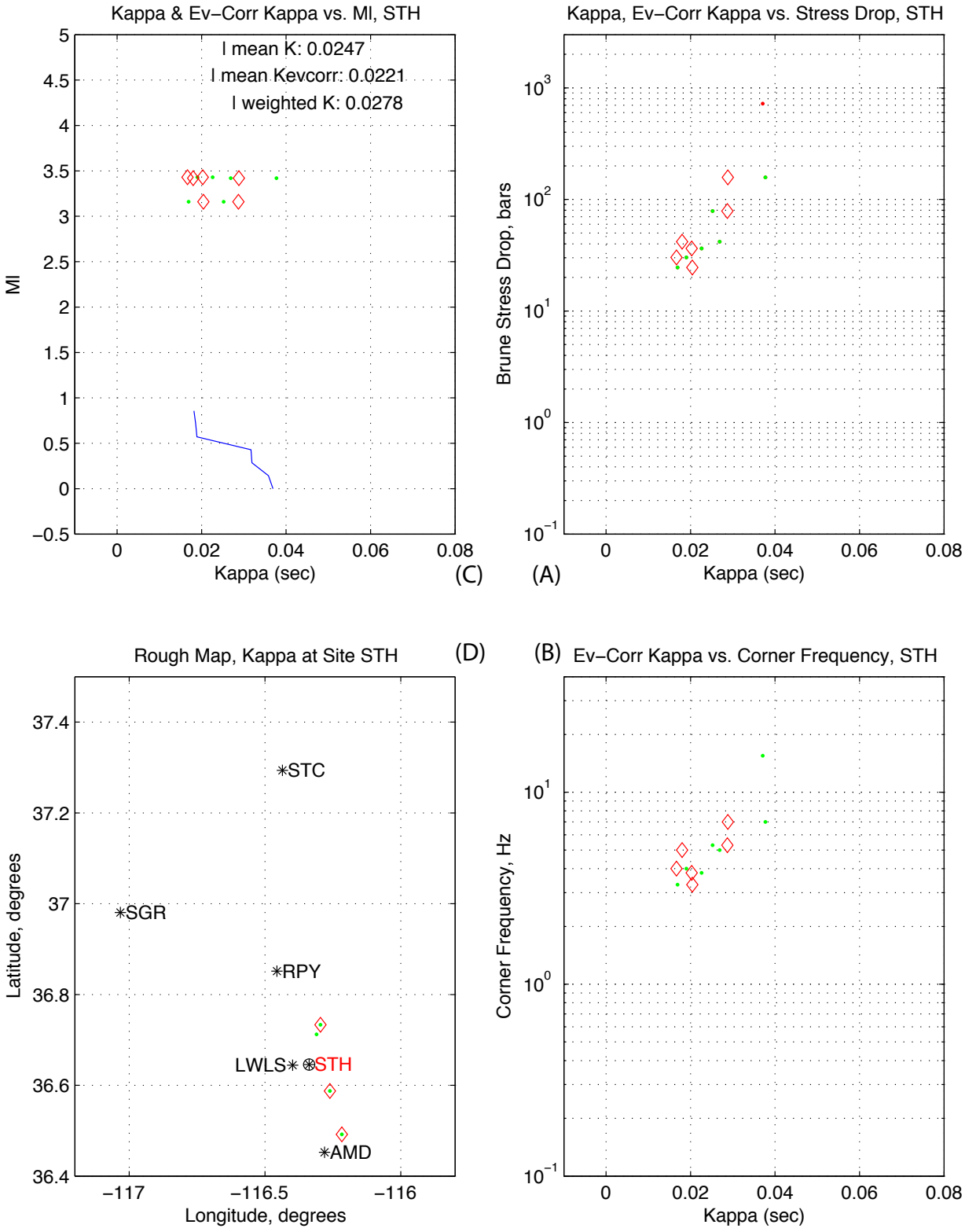

Figure 5.3.3.26. Station STO. Source: DID 006GB.003, this figure: file kappawrap/case6a/Figs_summary/ml_vs_kcorr_40xsta.eps, where sta is the station name. Ml, latitude, longitude in 006DV.004; kappa, stress drop, corner frequency, epicentral distance in DID 006GB.003, kappawrap/case6a/db/zz.srckappa columns 12, 22, 6, 37, and 18, respectively. Other subset details in Table 5.14. Small event kappa and displacement slope kappa from DID 006GB.003, kappawrap/casewm1/db/goodjan97.srckappa, columns 12 and 15, resp.

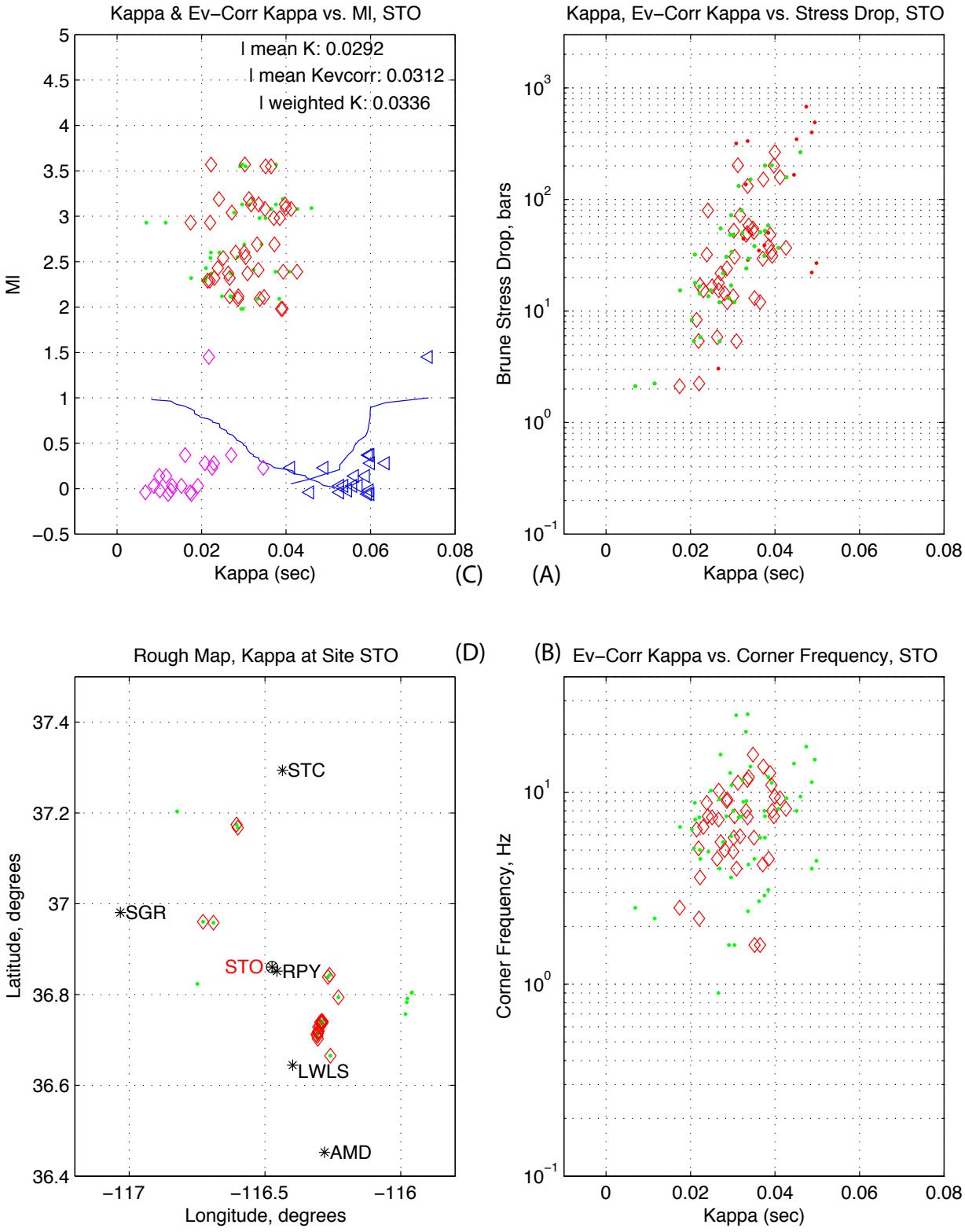

Figure 5.3.3.27. Station SYM. Source: DID 006GB.003, this figure: file kappawrap/case6a/Figs_summary/ml_vs_kcorr_40xsta.eps, where sta is the station name. Ml, latitude, longitude in 006DV.004; kappa, stress drop, corner frequency, epicentral distance in DID 006GB.003, kappawrap/case6a/db/zz.srckappa columns 12, 22, 6, 37, and 18, respectively. Other subset details in Table 5.14. Small event kappa and displacement slope kappa from DID 006GB.003, kappawrap/casewm1/db/goodjan97.srckappa, columns 12 and 15, resp.

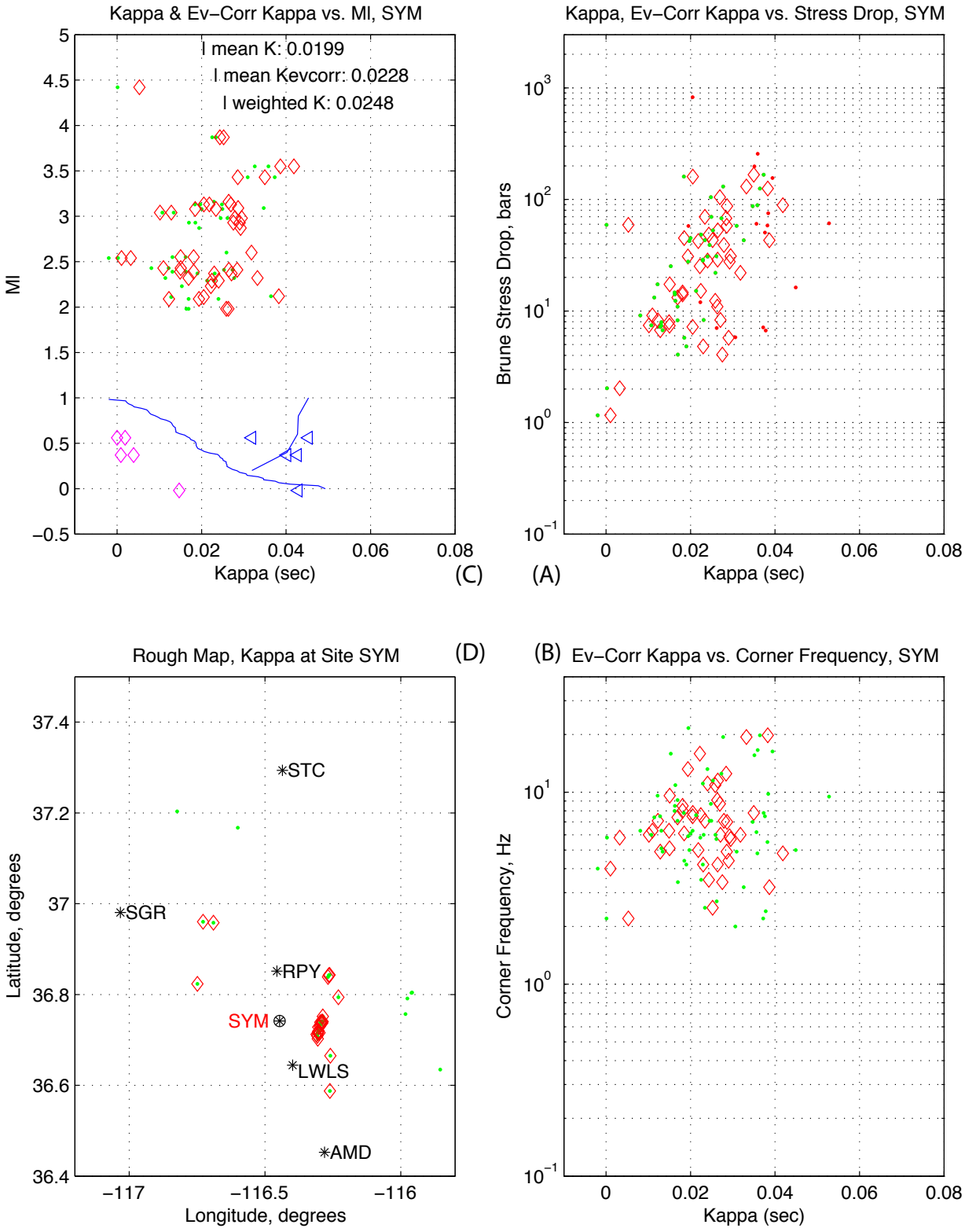

Figure 5.3.3.28. Station SYMS. Source: DID 006GB.003, this figure: file kappawrap/case6a/Figs_summary/ml_vs_kcorr_40xsta.eps, where sta is the station name. Ml, latitude, longitude in 006DV.004; kappa, stress drop, corner frequency, epicentral distance in DID 006GB.003, kappawrap/case6a/db/zz.srckappa columns 12, 22, 6, 37, and 18, respectively. Other subset details in Table 5.14. Small event kappa and displacement slope kappa from DID 006GB.003, kappawrap/casewm1/db/goodjan97.srckappa, columns 12 and 15, resp.

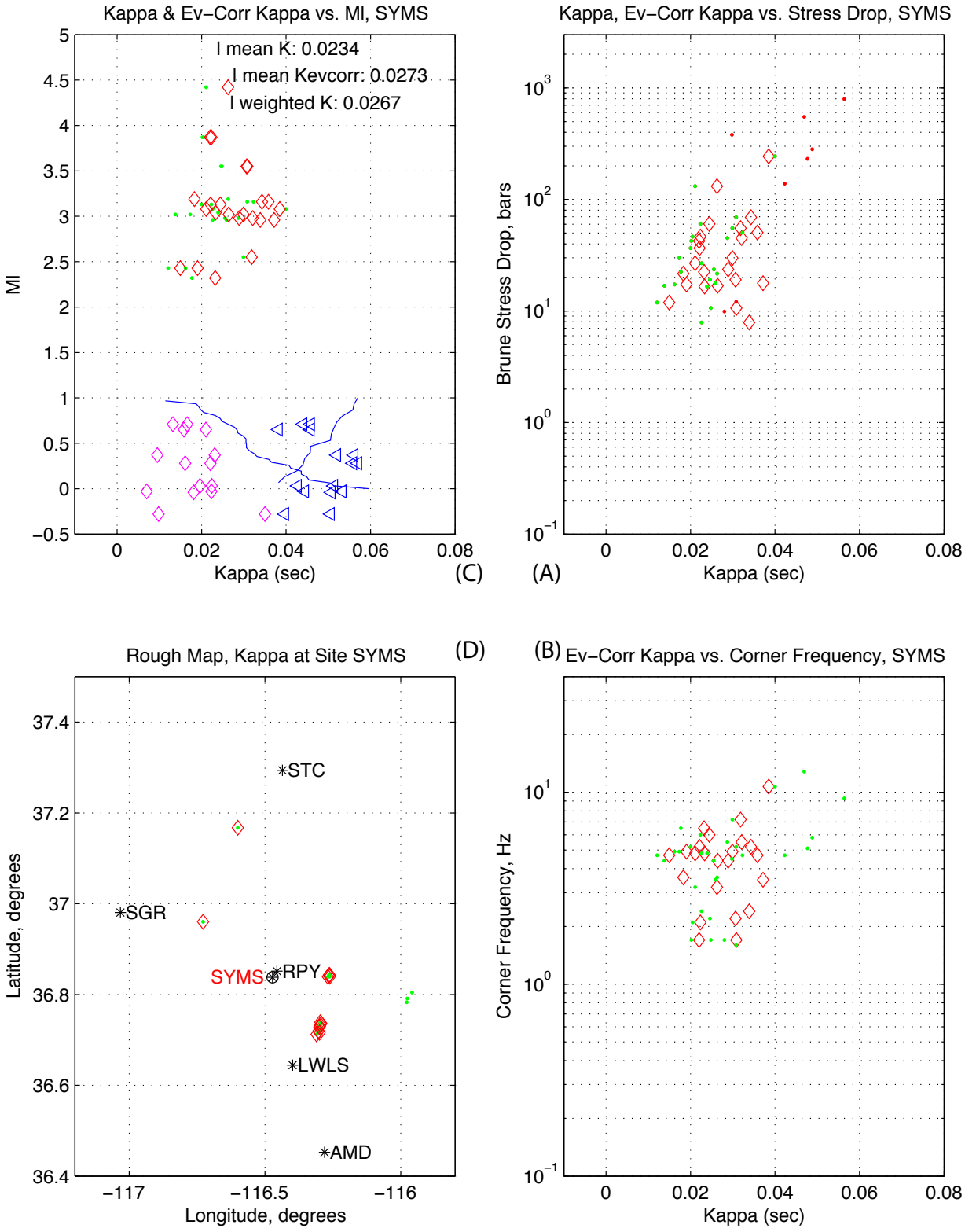

Figure 5.3.3.29. Station TAR. Source: DID 006GB.003, this figure: file kappawrap/case6a/Figs_summary/ml_vs_kcorr_40xsta.eps, where sta is the station name. Ml, latitude, longitude in 006DV.004; kappa, stress drop, corner frequency, epicentral distance in DID 006GB.003, kappawrap/case6a/db/zz.srckappa columns 12, 22, 6, 37, and 18, respectively. Other subset details in Table 5.14. Small event kappa and displacement slope kappa from DID 006GB.003, kappawrap/casewm1/db/goodjan97.srckappa, columns 12 and 15, resp.

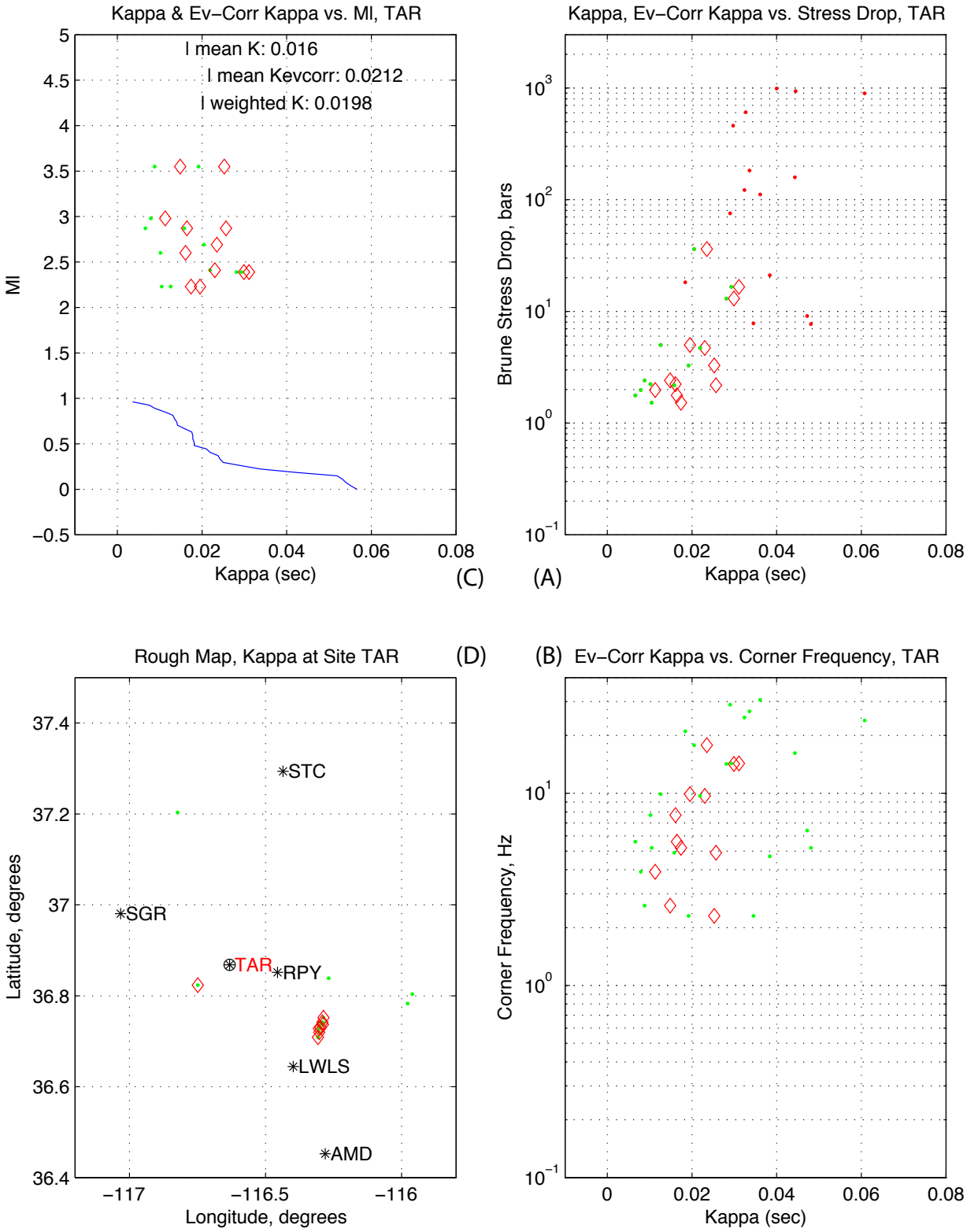

Figure 5.3.3.30 Station TIM. Source: DID 006GB.TIM, this figure: file kappawrap/case6a/Figs_summary/ml_vs_kcorr_40xsta.eps, where sta is the station name. Ml, latitude, longitude in 006DV.004; kappa, stress drop, corner frequency, epicentral distance in DID 006GB.003, kappawrap/case6a/db/zz.srckappa columns 12, 22, 6, 37, and 18, respectively. Other subset details in Table 5.14. Small event kappa and displacement slope kappa from DID 006GB.003, kappawrap/casewm1/db/goodjan97.srckappa, columns 12 and 15, resp.

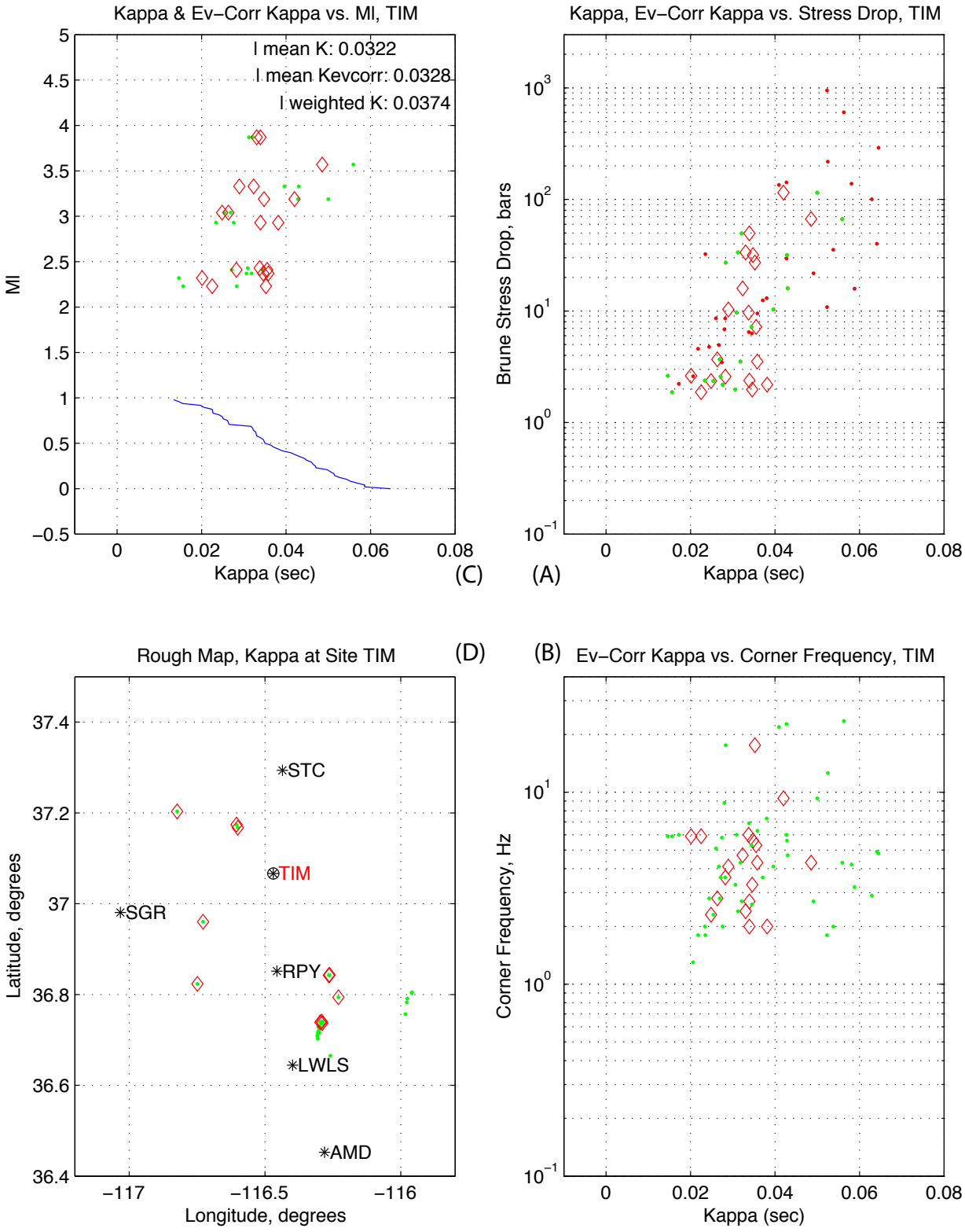

Figure 5.3.3.31. Station TPW. Source: DID 006GB.003, this figure: file kappawrap/case6a/Figs_summary/ml_vs_kcorr_40xsta.eps, where sta is the station name. Ml, latitude, longitude in 006DV.004; kappa, stress drop, corner frequency, epicentral distance in DID 006GB.003, kappawrap/case6a/db/zz.srckappa columns 12, 22, 6, 37, and 18, respectively. Other subset details in Table 5.14. Small event kappa and displacement slope kappa from DID 006GB.003, kappawrap/casewm1/db/goodjan97.srckappa, columns 12 and 15, resp.

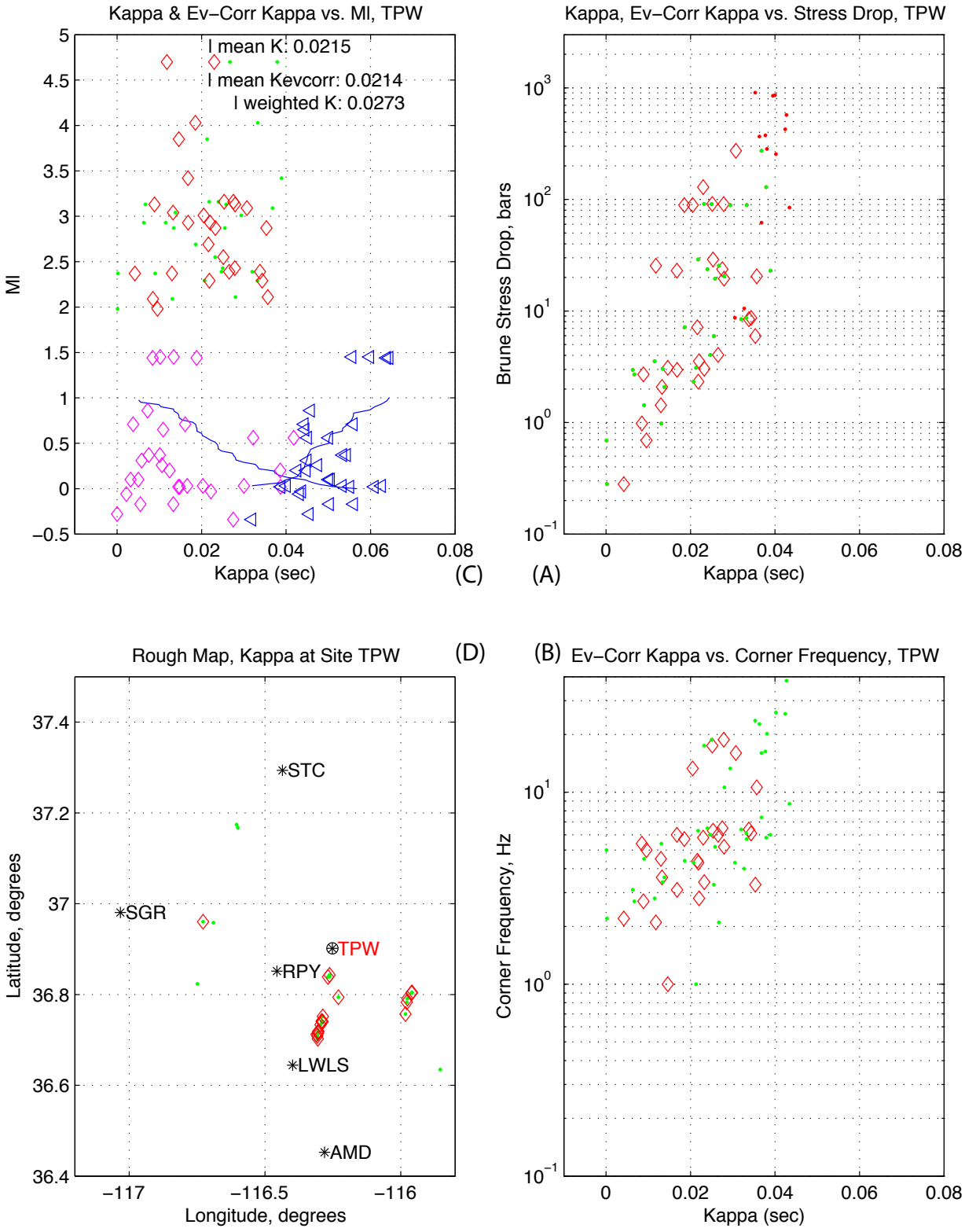

Figure 5.3.3.32. Station TYM. Source: DID 006GB.003, this figure: file kappawrap/case6a/Figs_summary/ml_vs_kcorr_40xsta.eps, where sta is the station name. Ml, latitude, longitude in 006DV.004; kappa, stress drop, corner frequency, epicentral distance in DID 006GB.003, kappawrap/case6a/db/zz.srckappa columns 12, 22, 6, 37, and 18, respectively. Other subset details in Table 5.14. Small event kappa and displacement slope kappa from DID 006GB.003, kappawrap/casewm1/db/goodjan97.srckappa, columns 12 and 15, resp.

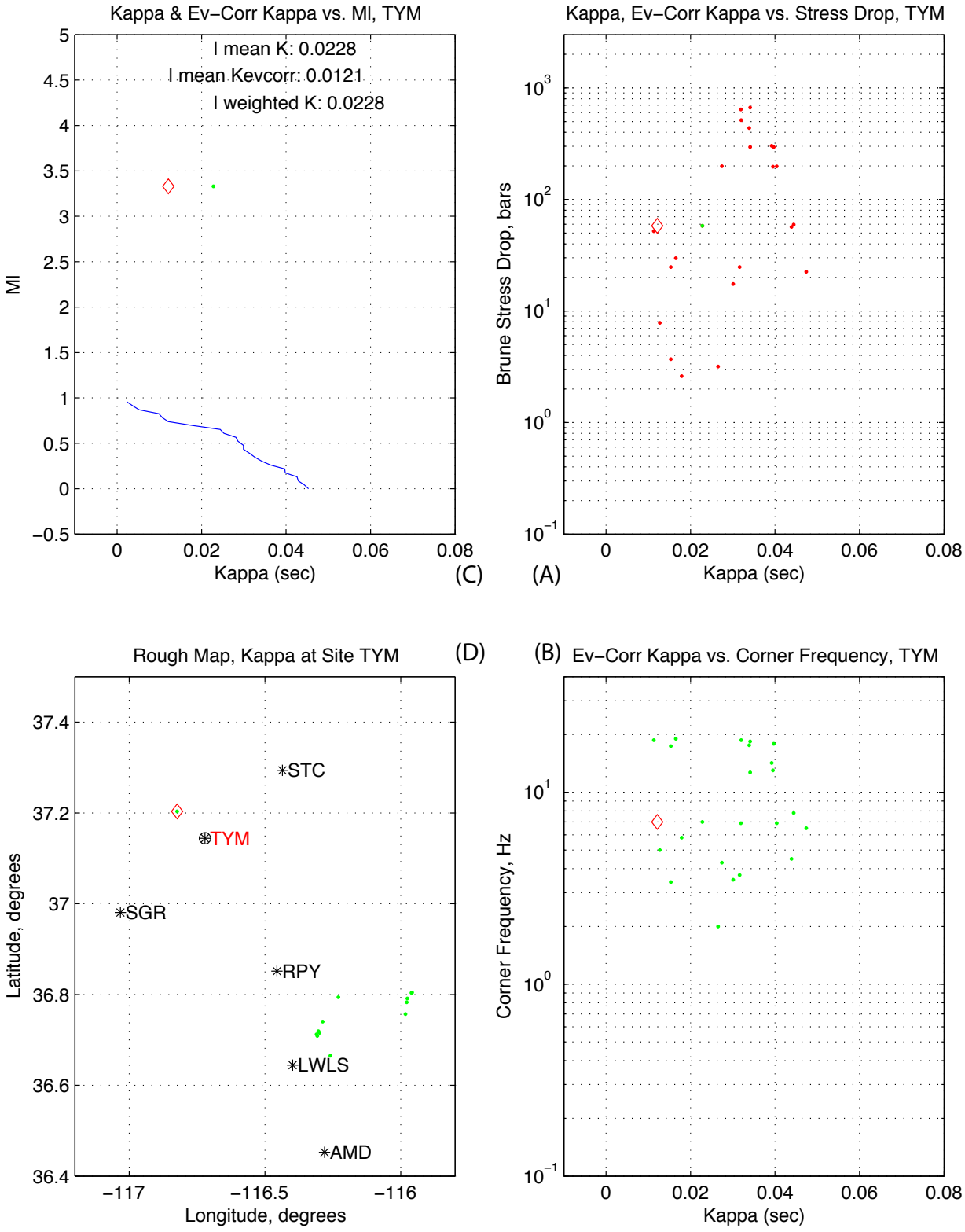

Figure 5.3.3.33. Station TYMS. Source: DID 006GB.003, this figure: file kappawrap/case6a/Figs_summary/ml_vs_kcorr_40xsta.eps, where sta is the station name. Ml, latitude, longitude in 006DV.004; kappa, stress drop, corner frequency, epicentral distance in DID 006GB.003, kappawrap/case6a/db/zz.srckappa columns 12, 22, 6, 37, and 18, respectively. Other subset details in Table 5.14. Small event kappa and displacement slope kappa from DID 006GB.003, kappawrap/casewm1/db/goodjan97.srckappa, columns 12 and 15, resp.

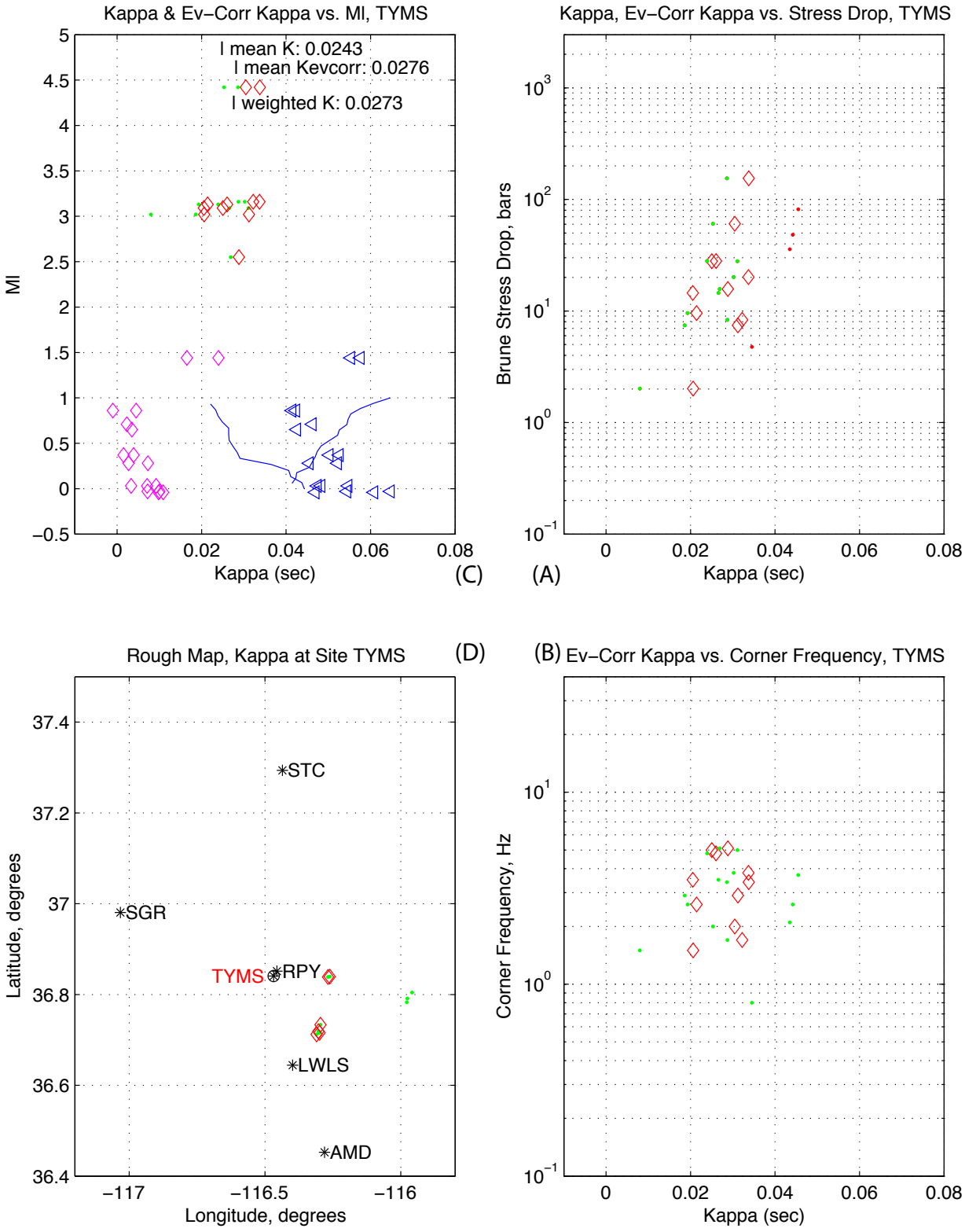

Figure 5.3.3.34. Station WCTS. Source: DID 006GB.003, this figure: file kappawrap/case6a/Figs_summary/ml_vs_kcorr_40xsta.eps, where sta is the station name. Ml, latitude, longitude in 006DV.004; kappa, stress drop, corner frequency, epicentral distance in DID 006GB.003, kappawrap/case6a/db/zz.srckappa columns 12, 22, 6, 37, and 18, respectively. Other subset details in Table 5.14. Small event kappa and displacement slope kappa from DID 006GB.003, kappawrap/casewm1/db/goodjan97.srckappa, columns 12 and 15, resp.

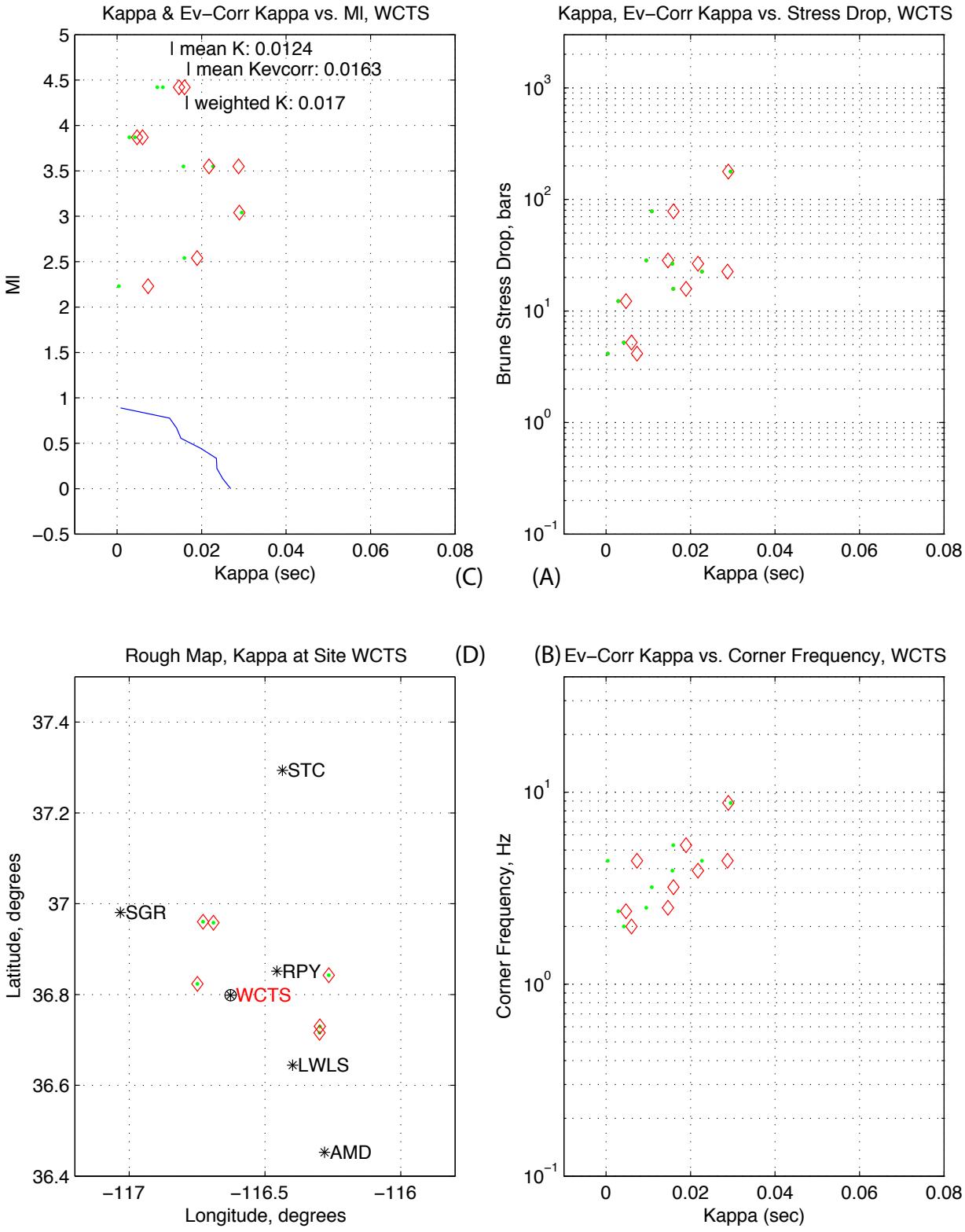

Figure 5.3.3.35. Station WLD. Source: DID 006GB.003, this figure: file kappawrap/case6a/Figs_summary/ml_vs_kcorr_40xsta.eps, where sta is the station name. Ml, latitude, longitude in 006DV.004; kappa, stress drop, corner frequency, epicentral distance in DID 006GB.003, kappawrap/case6a/db/zz.srckappa columns 12, 22, 6, 37, and 18, respectively. Other subset details in Table 5.14. Small event kappa and displacement slope kappa from DID 006GB.003, kappawrap/casewm1/db/goodjan97.srckappa, columns 12 and 15, resp.

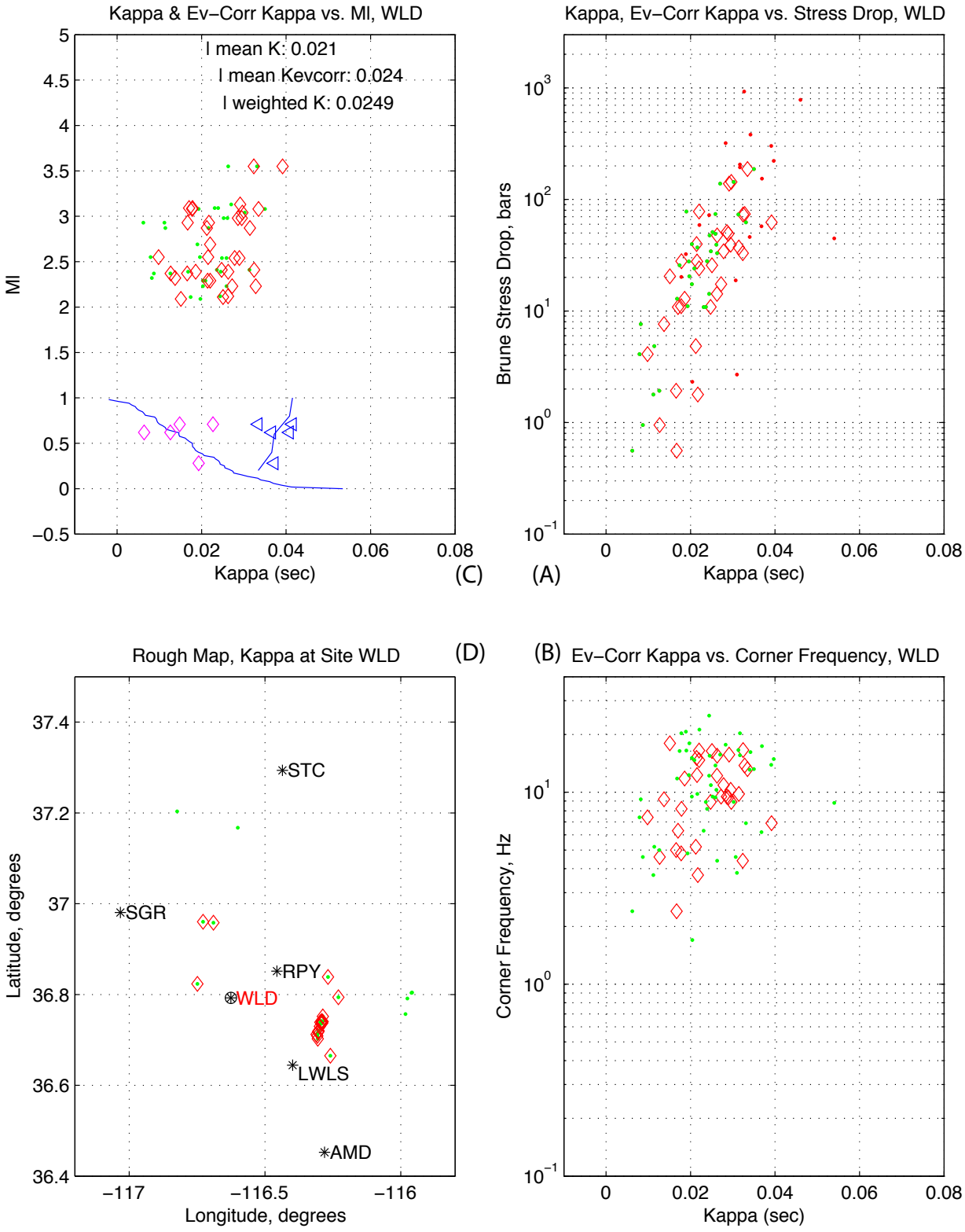

Figure 5.3.3.36. Station YCW. Source: DID 006GB.003, this figure: file kappawrap/case6a/Figs_summary/ml_vs_kcorr_40xsta.eps, where sta is the station name. Ml, latitude, longitude in 006DV.004; kappa, stress drop, corner frequency, epicentral distance in DID 006GB.003, kappawrap/case6a/db/zz.srckappa columns 12, 22, 6, 37, and 18, respectively. Other subset details in Table 5.14. Small event kappa and displacement slope kappa from DID 006GB.003, kappawrap/casewm1/db/goodjan97.srckappa, columns 12 and 15, resp.

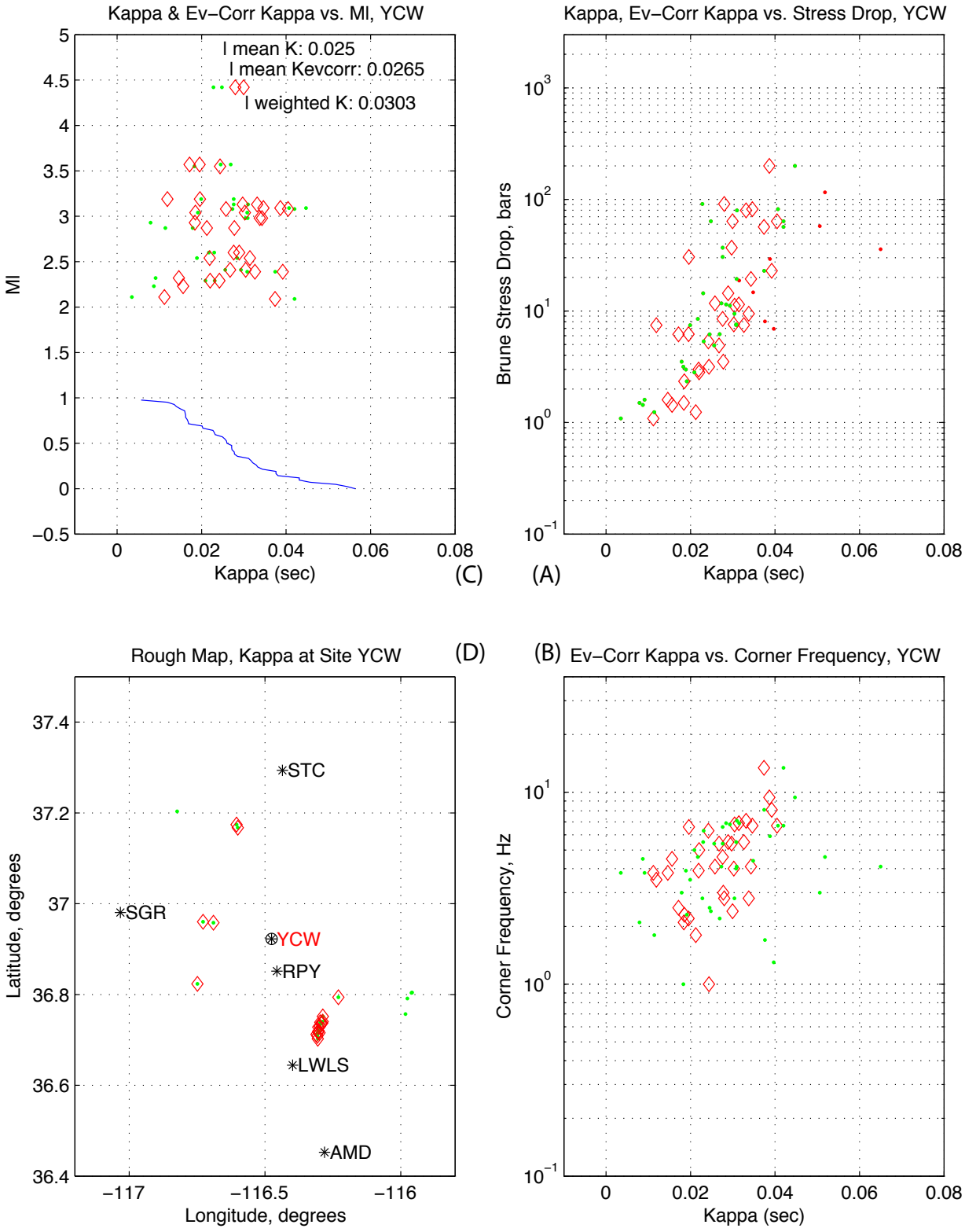

Figure 5.3.3.37. Station YFT. Source: DID 006GB.003, this figure: file kappawrap/case6a/Figs_summary/ml_vs_kcorr_40xsta.eps, where sta is the station name. Ml, latitude, longitude in 006DV.004; kappa, stress drop, corner frequency, epicentral distance in DID 006GB.003, kappawrap/case6a/db/zz.srckappa columns 12, 22, 6, 37, and 18, respectively. Other subset details in Table 5.14. Small event kappa and displacement slope kappa from DID 006GB.003, kappawrap/casewm1/db/goodjan97.srckappa, columns 12 and 15, resp.

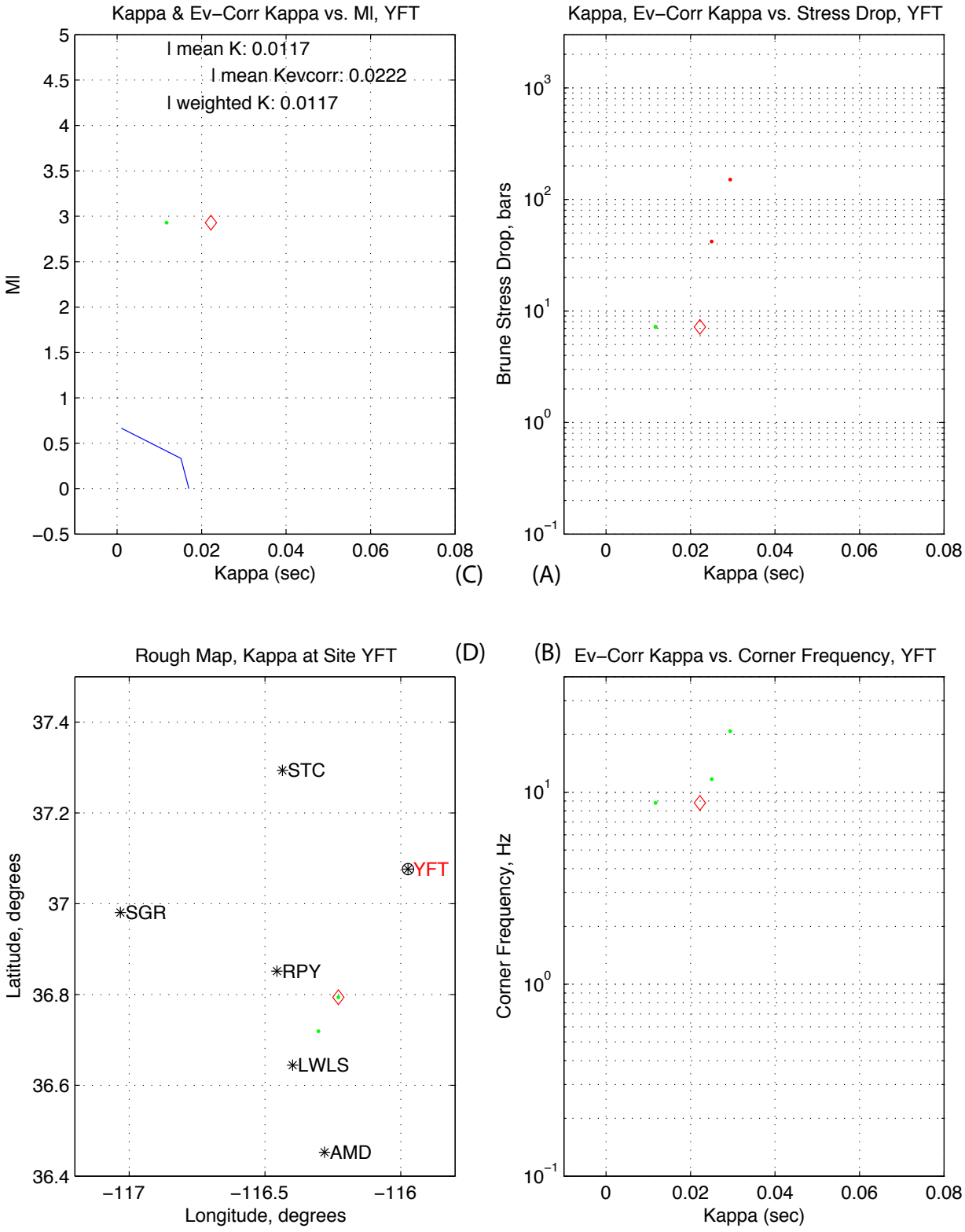

Figure 5.3.4.1 Stress drop is plotted versus corner frequency for SGBDSN M3 events (Table 5.2), case6a. X=epicentral distance>40 km
Source: DID 006GB003, file kappawrap/case6a/Figs_summary/event_kappas1.eps, data in file kappawrap/case6a/db/zz.srckappa. Stress drop=col 22, corner frequency= col 6; subset by event in col. 1, stress drop<100 MPa, squared error (col. 28)<0.151, SNRpct (col 43) >0.5; horizontal channels. Ml values from Table 5.2 (DID 006DV.004)

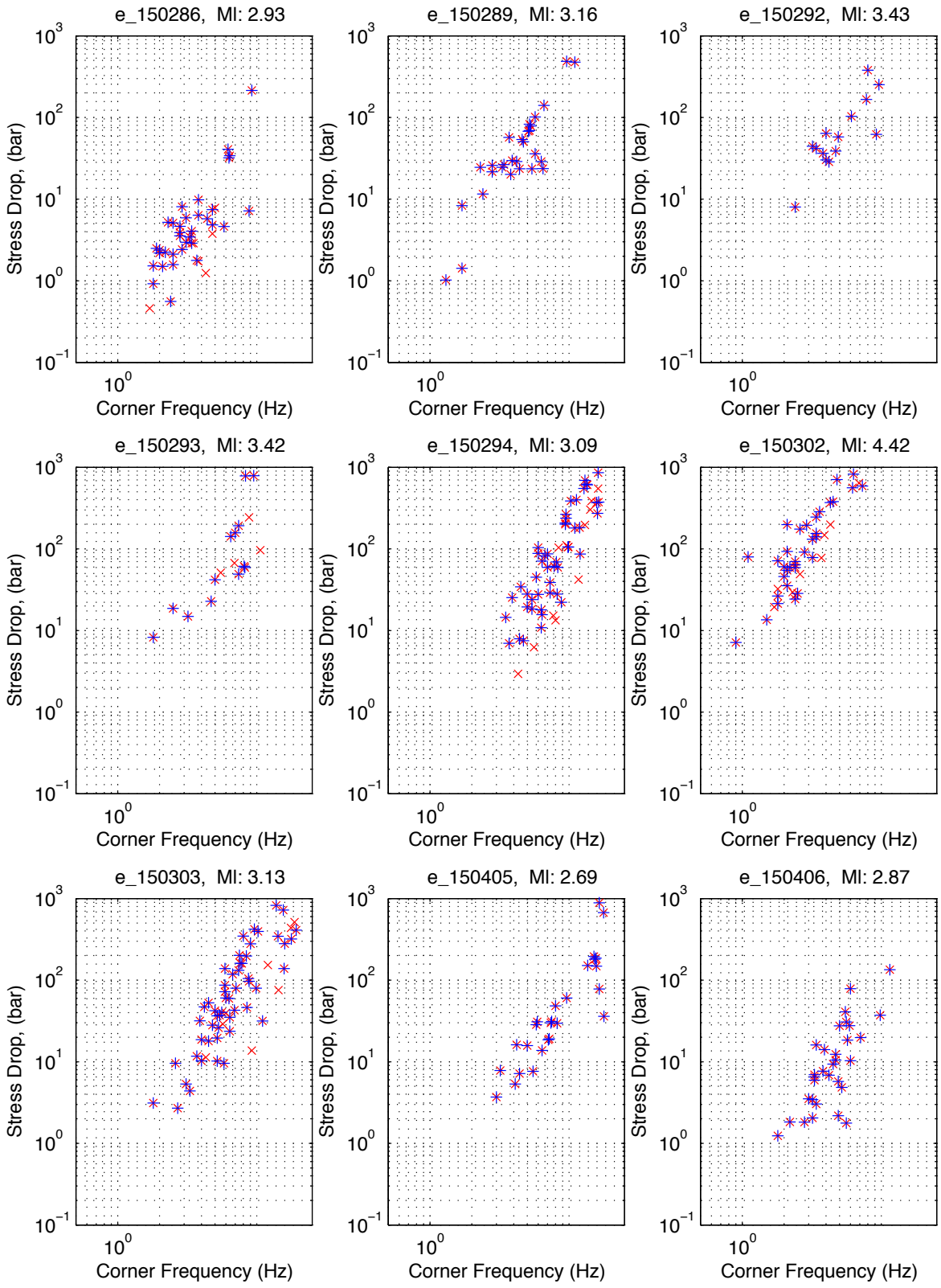

Figure 5.3.4.2 Stress drop is plotted versus corner frequency for SGBDSN M3 events (Table 5.2), case6a. X=epicentral distance>40 km
Source: DID 006GB003, data in file kappawrap/case6a/db/zz.srckappa. Ml values from Table 5.2 (DID 006DV.004). Subset details in Figure 5.3.4.1

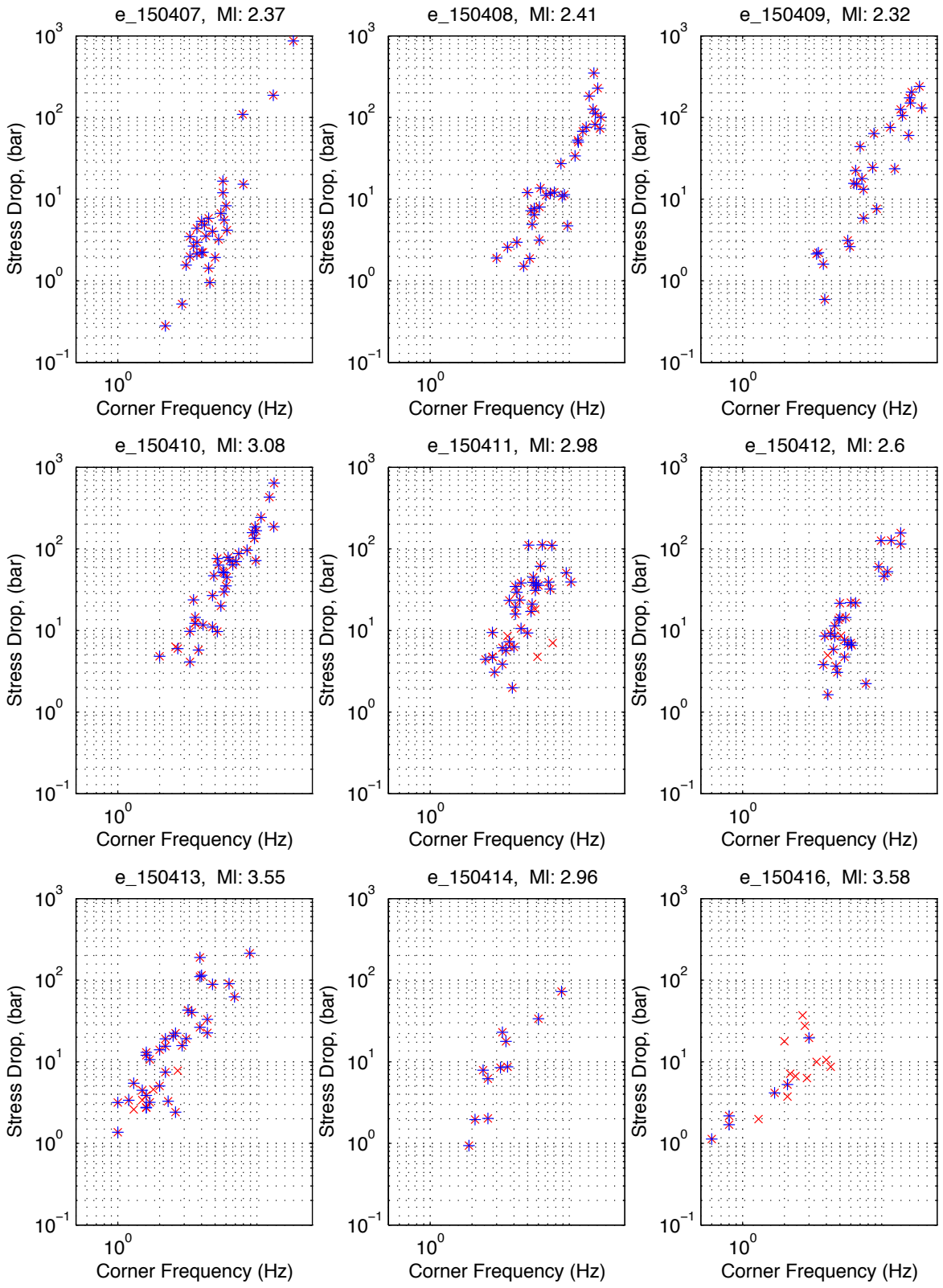

Figure 5.3.4.3 Stress drop is plotted versus corner frequency for SGBDSN M3 events (Table 5.2), case6a. X=epicentral distance>40 km
Source: DID 006GB003, data in file kappawrap/case6a/db/zz.srckappa. Ml values from Table 5.2 (DID 006DV.004). Subset details in Figure 5.3.4.1

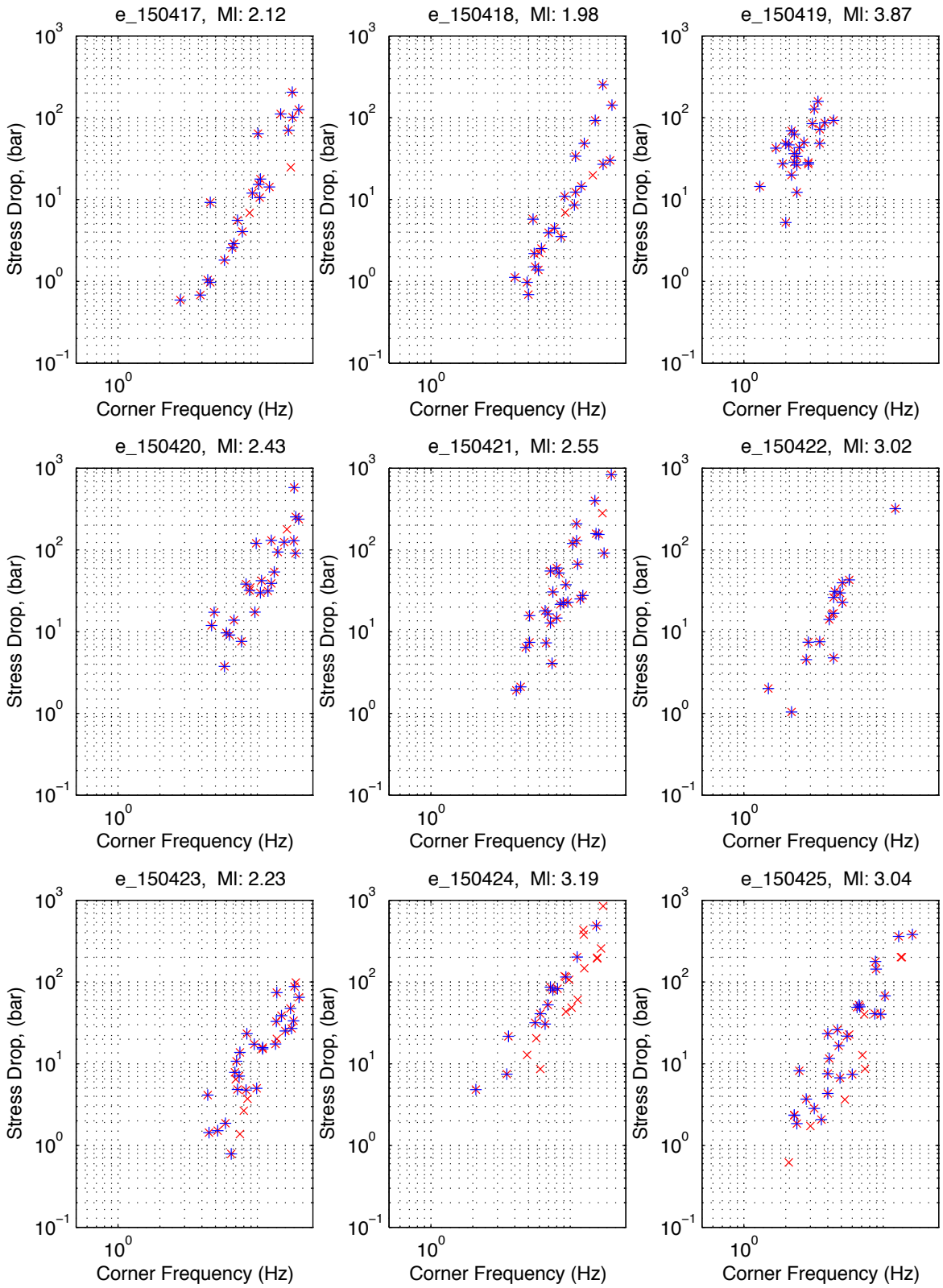

Figure 5.3.4.4 Stress drop is plotted versus corner frequency for SGBDSN M3 events (Table 5.2), case6a. X=epicentral distance>40 km
Source: DID 006GB003, data in file kappawrap/case6a/db/zz.srckappa. Ml values from Table 5.2 (DID 006DV.004). Subset details in Figure 5.3.4.1

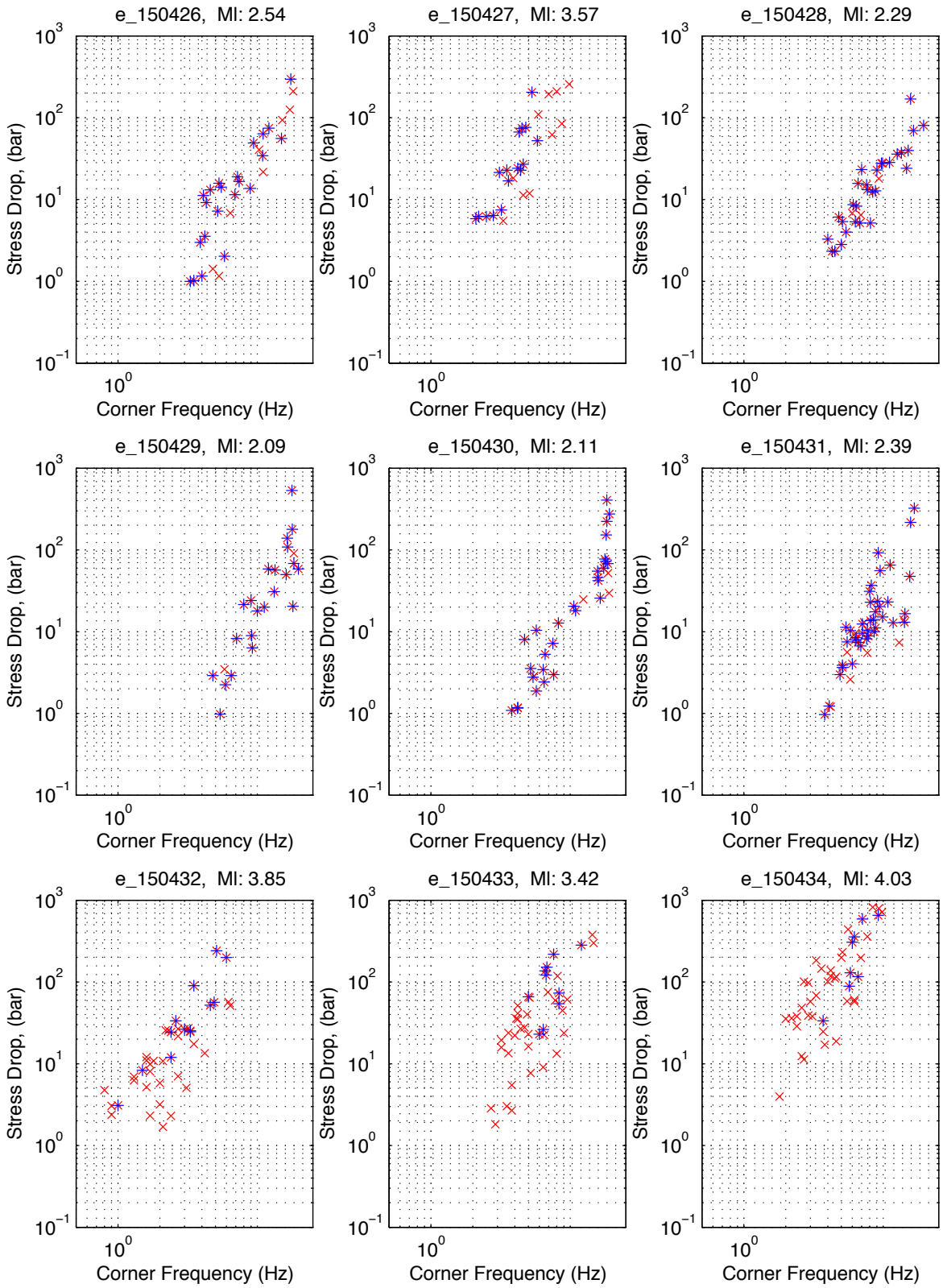

Figure 5.3.4.5 Stress drop is plotted versus corner frequency for SGBDSN M3 events (Table 5.2), case6a. X=epicentral distance>40 km
Source: DID 006GB003, data in file kappawrap/case6a/db/zz.srckappa. Ml values from Table 5.2 (DID 006DV.004). Subset details in Figure 5.3.4.1

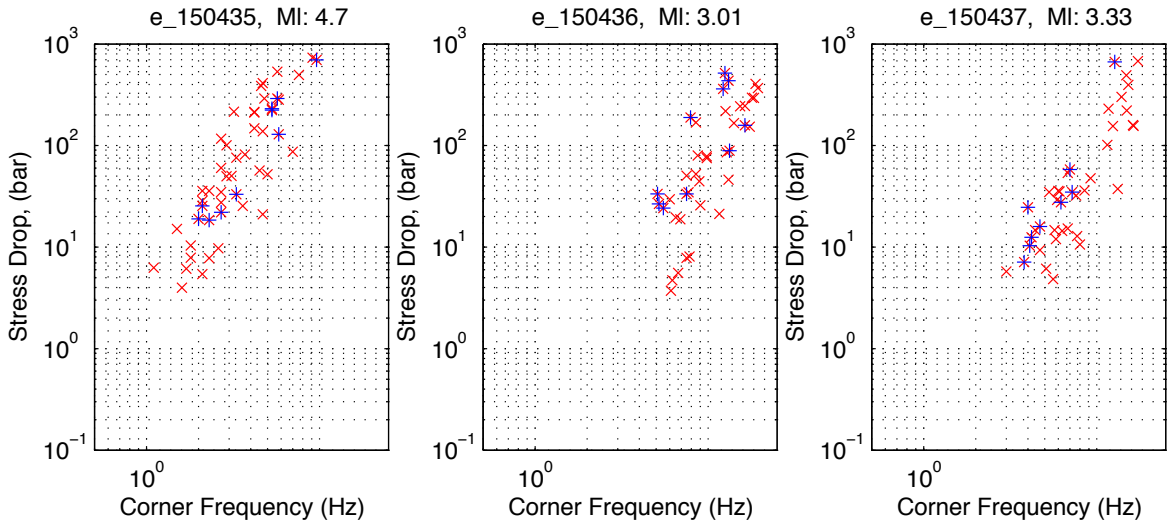

Figure 5.3.5, Best estimate station kappa estimates shown with three sets of formal inversion results. Formal inversion models 3, 4, and 9 are compared with kappa as a site term from epicentral distances less than 40 km. Histogram compares "Site only, Ev<40 km" and "km-9, bi-linear" models.
Source: DID 006GB.003. Case 6a station kappas from kappawrap/case6a/Figs_summary/station_kappas_case6a.tbl. Formal inversion models 3, 4, and 9 from corresponding stations in kappawrap/case6a/kappa_out, M3_k, M4_k, and M9_k columns, respectively. This plot: kappawrap/case6a/Figs_summary/fitting_v_byevent.pdf

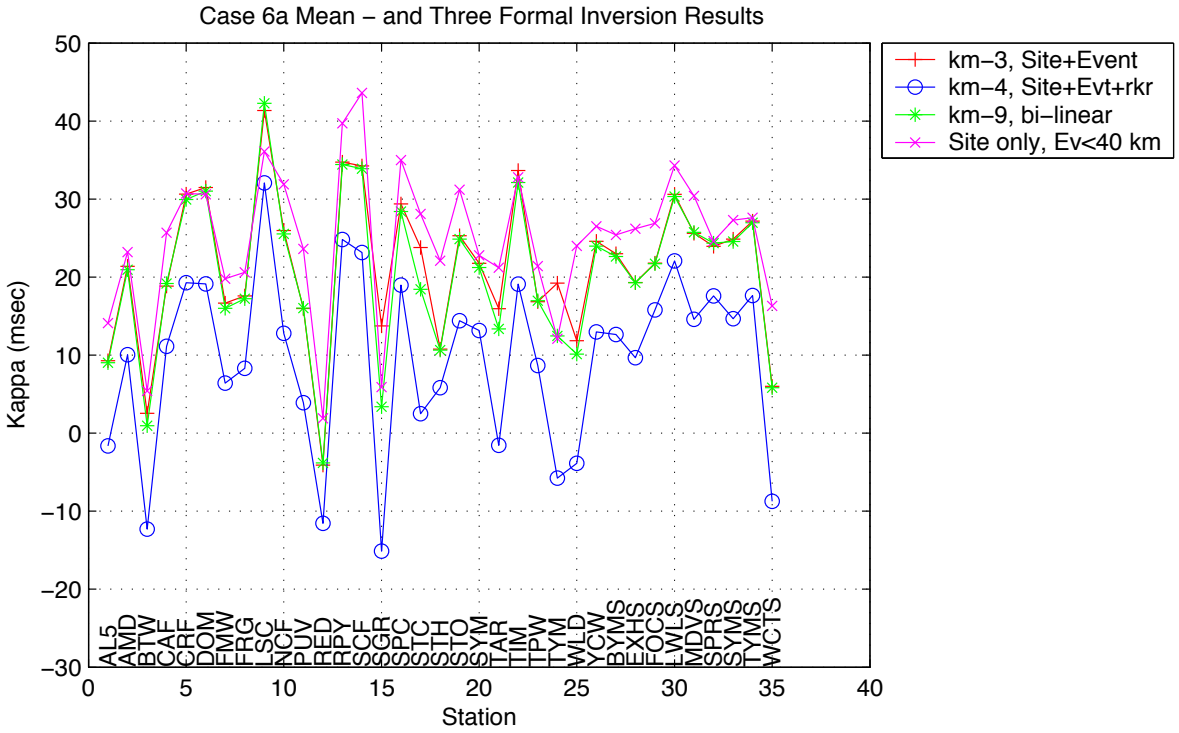

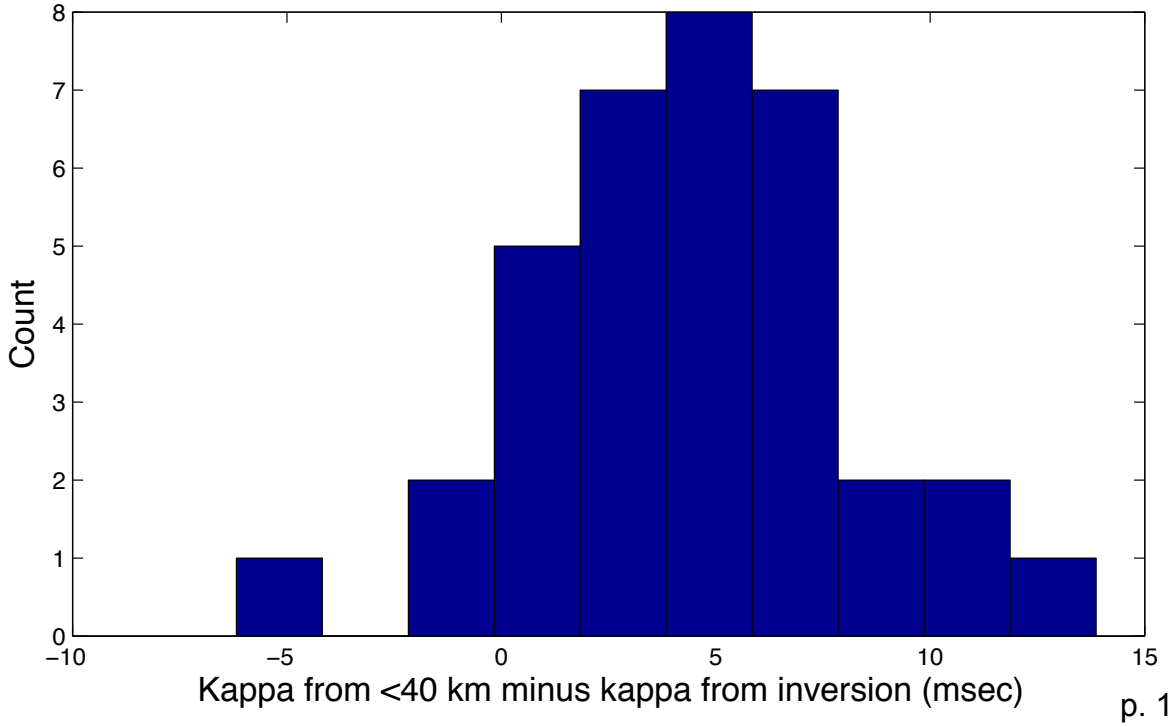

Figure 5.3.6 – Base case station kappa and kappa if the Silva(f) and Q(f) functions are used.

Source: DID 006GB003, files kappawrap/case6a/Figs_summary/station_kappas_case6a.tbl and kappawrap/case7/Figs_summary/station_kappas_case7.tbl. This plot in kappawrap/case6a/Figs_summary/silva_diffs.pdf.

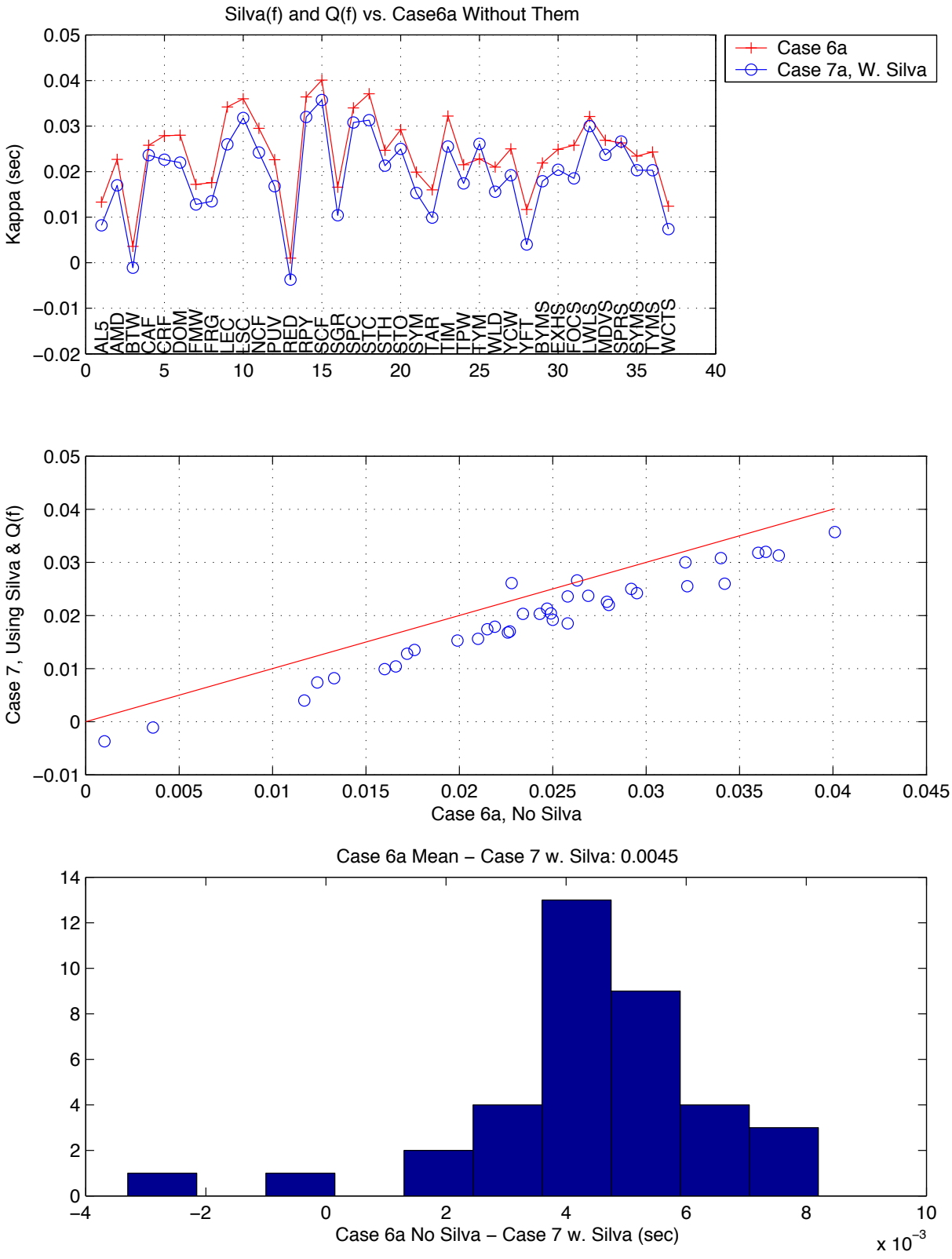

Figure 5.3.7.1 Station rbnd. Source: SN-UCCSN-UNR-097 v.1, Atch. 2, this figure: file kappawrap/caselsm4/Figs_summary/ml_vs_kcorr_40xsta.eps, where sta is the station name. Ml, latitude, longitude in 006DV.004; kappa, stress drop, corner frequency, epicentral distance in kappawrap/caselsm4/db/lsm_8.srckappa columns 12, 22, 6, 37, and 18, respectively. Other subset details in Table 5.17. Unqualified, for corroboration only; not for use in quality-affecting work.

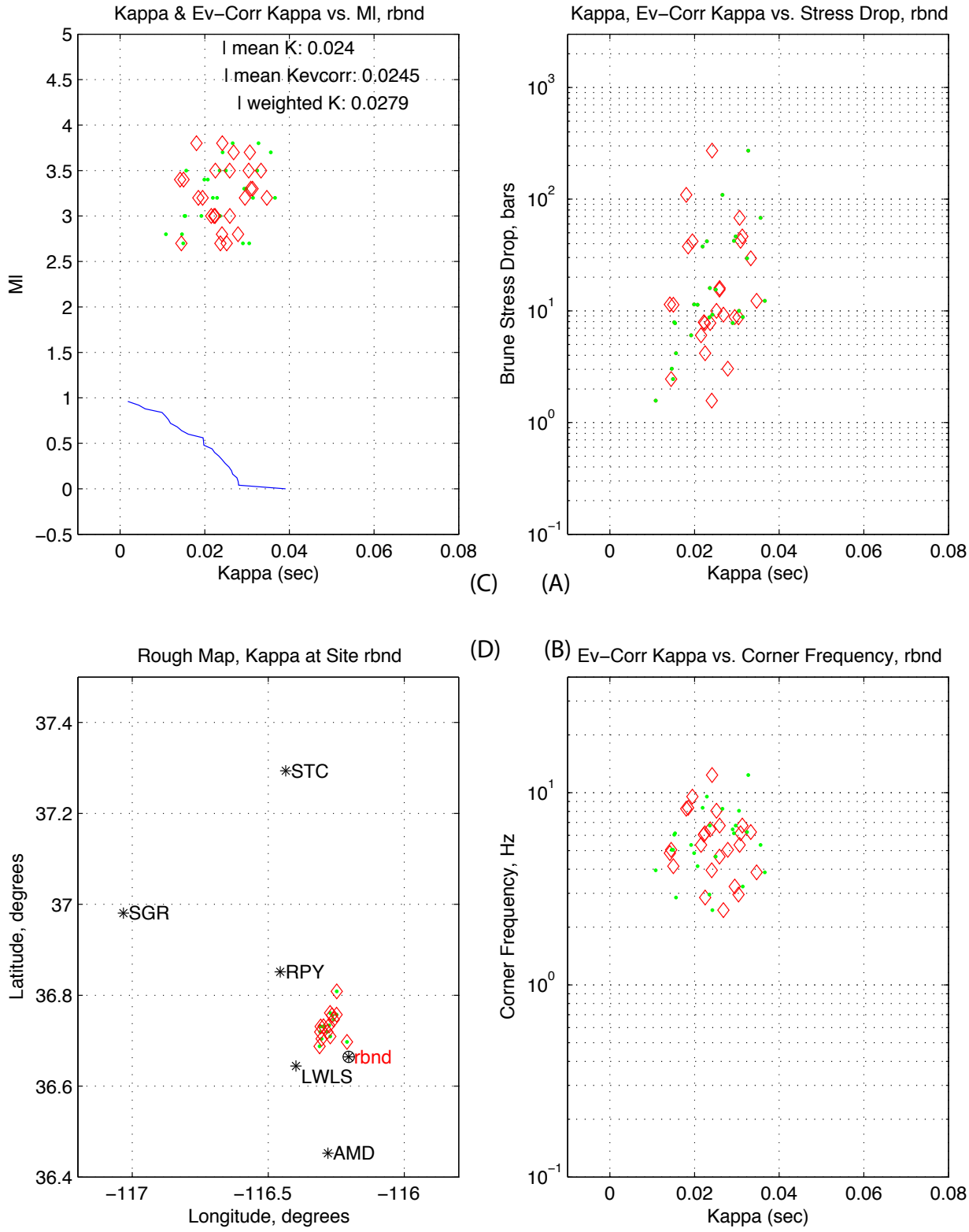

Figure 5.3.7.2. Station rcom. Source: SN-UCCSN-UNR-097 v.1, Atch. 2, this figure: file kappawrap/caselsm4/Figs_summary/ml_vs_kcorr_40xsta.eps, where sta is the station name. Ml, latitude, longitude in 006DV.004; kappa, stress drop, corner frequency, epicentral distance in kappawrap/caselsm4/db/lsm_8.srckappa columns 12, 22, 6, 37, and 18, respectively. Other subset details in Table 5.17. Unqualified, for corroboration only; not for use in quality-affecting work.

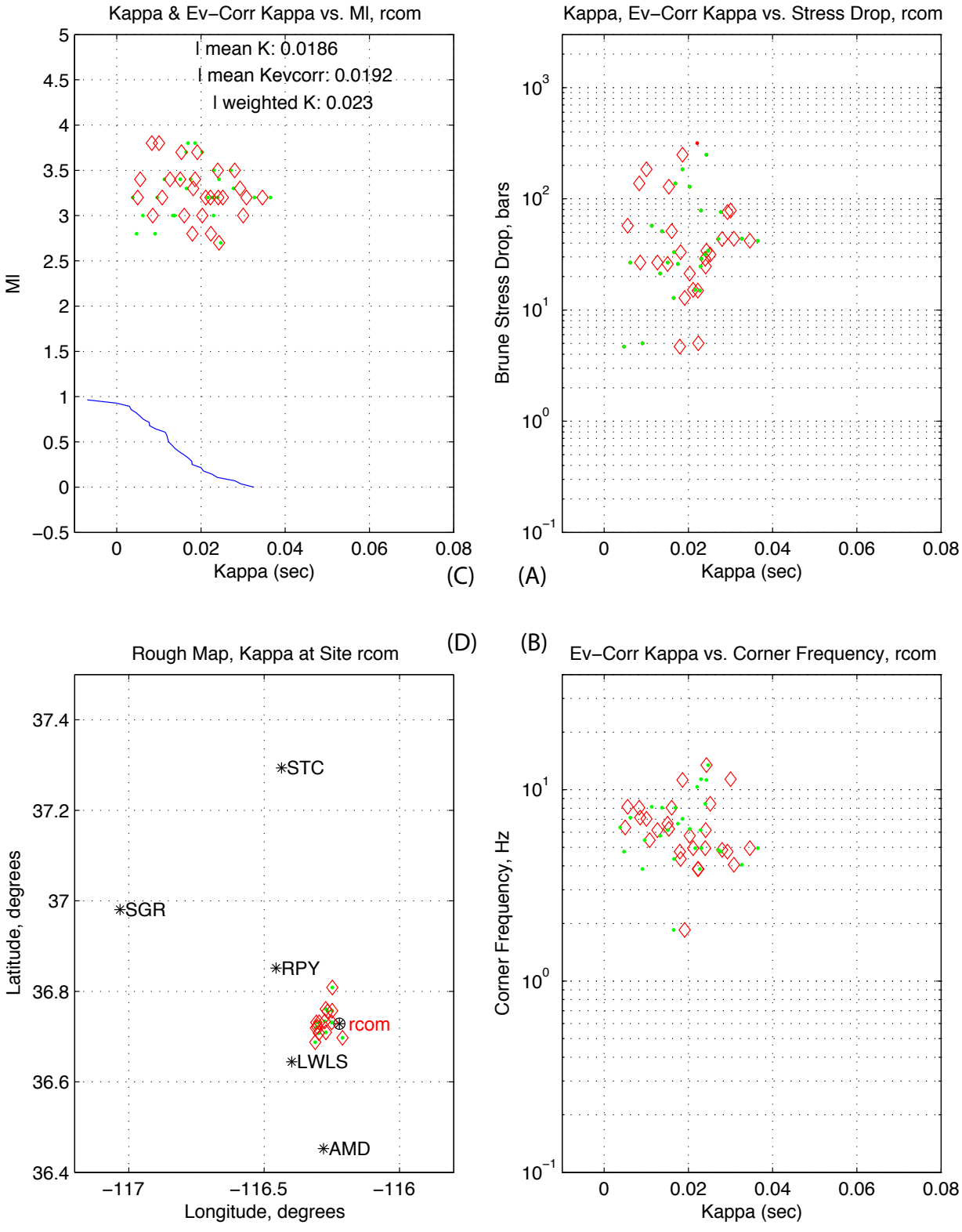

Figure 5.3.7.3. Station rdun. Source: SN-UCCSN-UNR-097 v.1, Atch. 2, this figure: file kappawrap/caselsm4/Figs_summary/ml_vs_kcorr_40xsta.eps, where sta is the station name. Ml, latitude, longitude in 006DV.004; kappa, stress drop, corner frequency, epicentral distance in kappawrap/caselsm4/db/lsm_8.srckappa columns 12, 22, 6, 37, and 18, respectively. Other subset details in Table 5.17. Unqualified, for corroboration only; not for use in quality-affecting work.

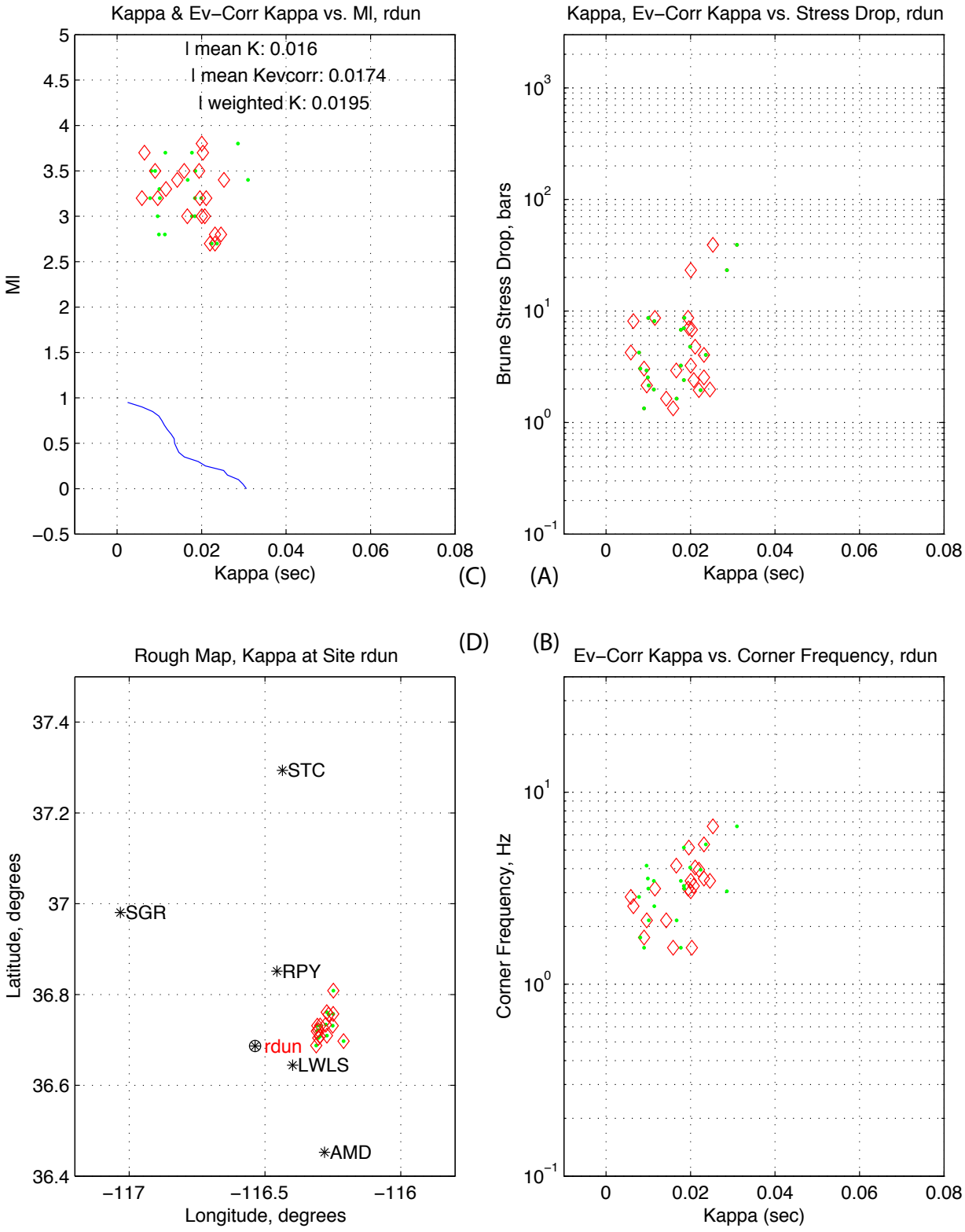

Figure 5.3.7.4. Station res2. Source: SN-UCCSN-UNR-097 v.1, Atch. 2, this figure: file kappawrap/caselsm4/Figs_summary/ml_vs_kcorr_40xsta.eps, where sta is the station name. Ml, latitude, longitude in 006DV.004; kappa, stress drop, corner frequency, epicentral distance in kappawrap/caselsm4/db/lsm_8.srckappa columns 12, 22, 6, 37, and 18, respectively. Other subset details in Table 5.17. Unqualified, for corroboration only; not for use in quality-affecting work.

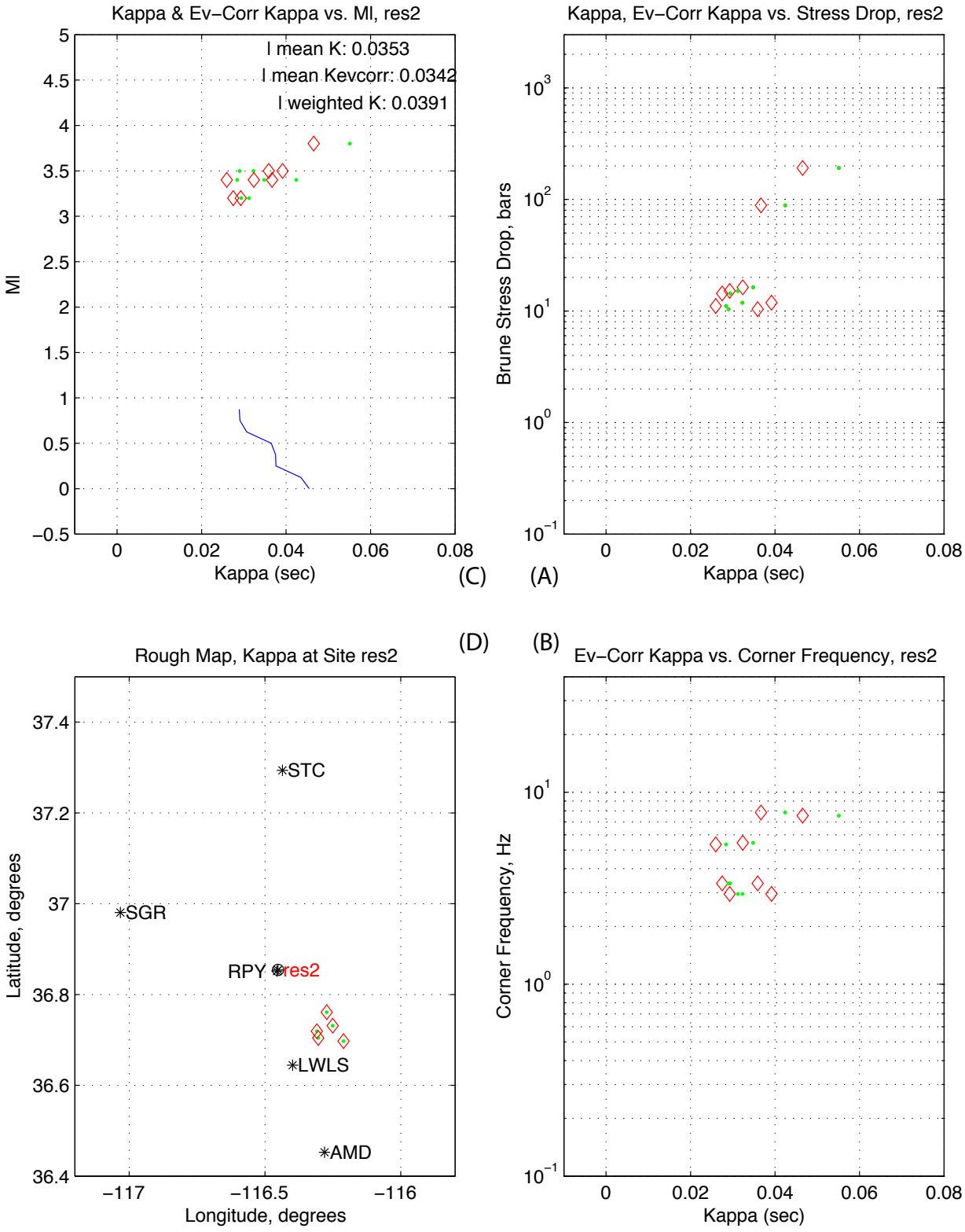

Figure 5.3.7.5. Station rfoc. Source: SN-UCCSN-UNR-097 v.1, Atch. 2, this figure: file kappawrap/caselsm4/Figs_summary/ml_vs_kcorr_40xsta.eps, where sta is the station name. Ml, latitude, longitude in 006DV.004; kappa, stress drop, corner frequency, epicentral distance in kappawrap/caselsm4/db/lsm_8.srckappa columns 12, 22, 6, 37, and 18, respectively. Other subset details in Table 5.17. Unqualified, for corroboration only; not for use in quality-affecting work.

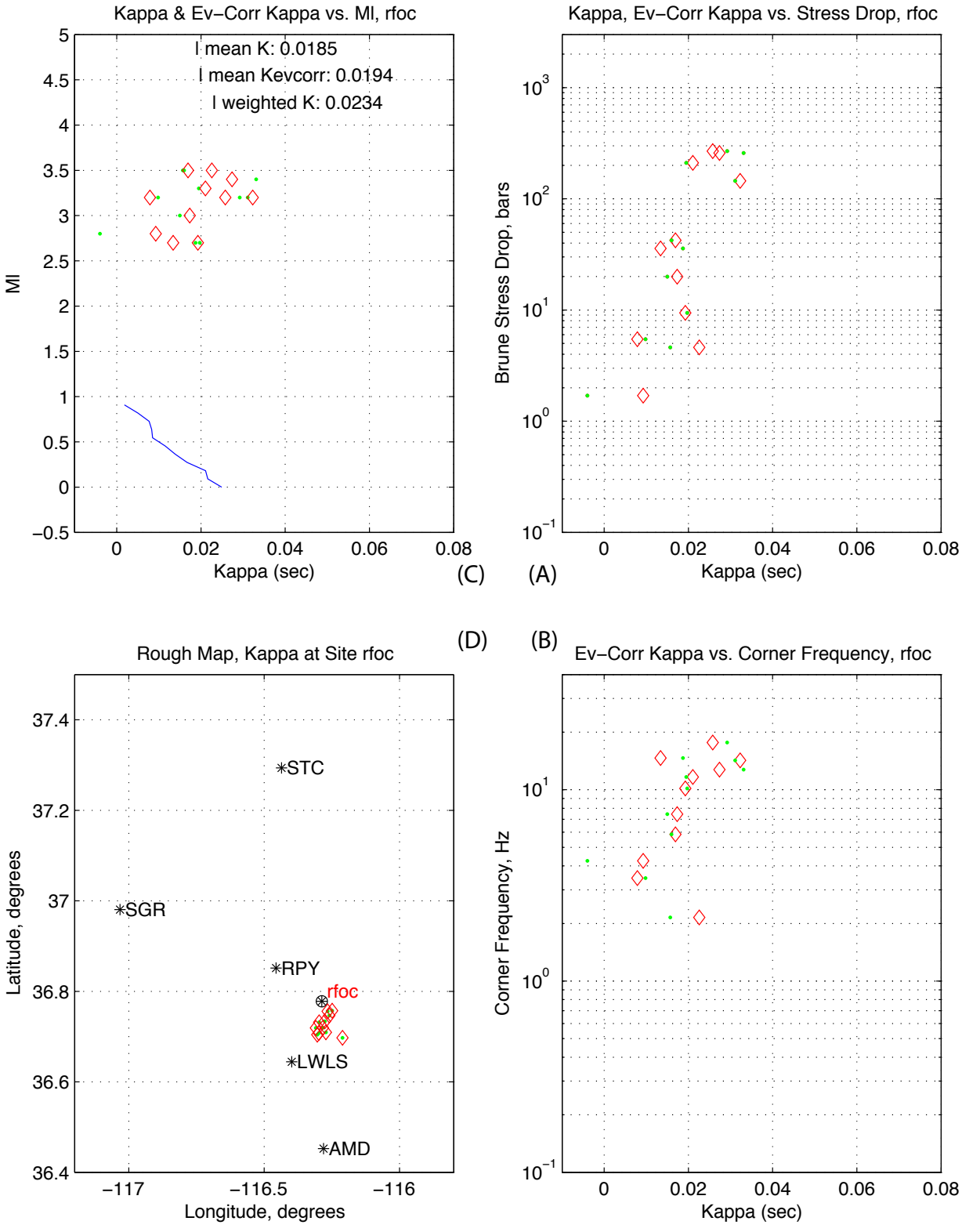

Figure 5.3.7.6. Station rlsm. Source: SN-UCCSN-UNR-097 v.1, Atch. 2, this figure: file kappawrap/caselsm4/Figs_summary/ml_vs_kcorr_40xsta.eps, where sta is the station name. Ml, latitude, longitude in 006DV.004; kappa, stress drop, corner frequency, epicentral distance in kappawrap/caselsm4/db/lsm_8.srckappa columns 12, 22, 6, 37, and 18, respectively. Other subset details in Table 5.17. Unqualified, for corroboration only; not for use in quality-affecting work.

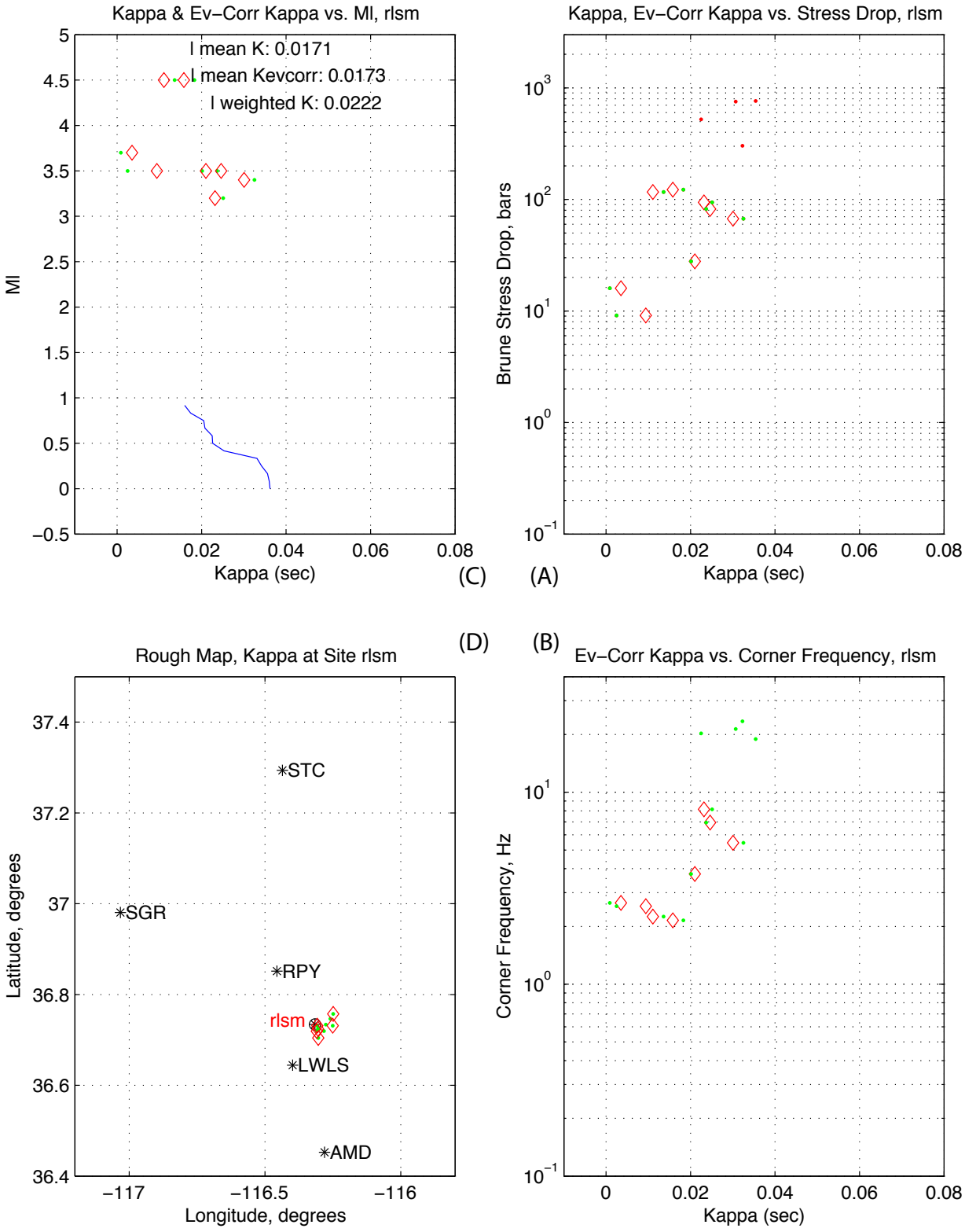

Figure 5.3.7.7. Station rsfc. Source: SN-UCCSN-UNR-097 v.1, Atch. 2, this figure: file kappawrap/caselsm4/Figs_summary/ml_vs_kcorr_40xsta.eps, where sta is the station name. Ml, latitude, longitude in 006DV.004; kappa, stress drop, corner frequency, epicentral distance in kappawrap/caselsm4/db/lsm_8.srckappa columns 12, 22, 6, 37, and 18, respectively. Other subset details in Table 5.17. Unqualified, for corroboration only; not for use in quality-affecting work.

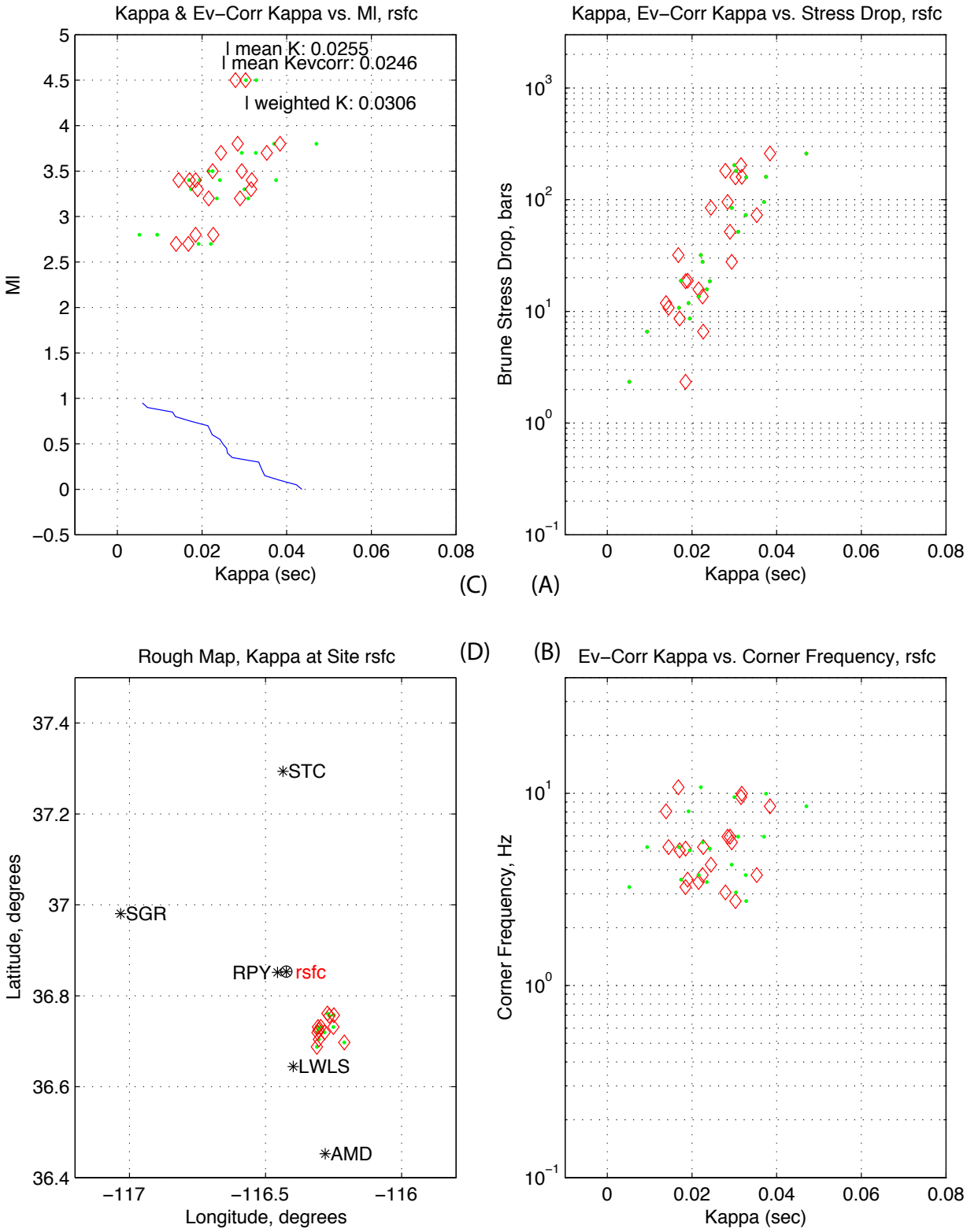

Figure 5.3.7.8. Station rtpp. Source: SN-UCCSN-UNR-097 v.1, Atch. 2, this figure: file kappawrap/caselsm4/Figs_summary/ml_vs_kcorr_40xsta.eps, where sta is the station name. Ml, latitude, longitude in 006DV.004; kappa, stress drop, corner frequency, epicentral distance in kappawrap/caselsm4/db/lsm_8.srckappa columns 12, 22, 6, 37, and 18, respectively. Other subset details in Table 5.17. Unqualified, for corroboration only; not for use in quality-affecting work.

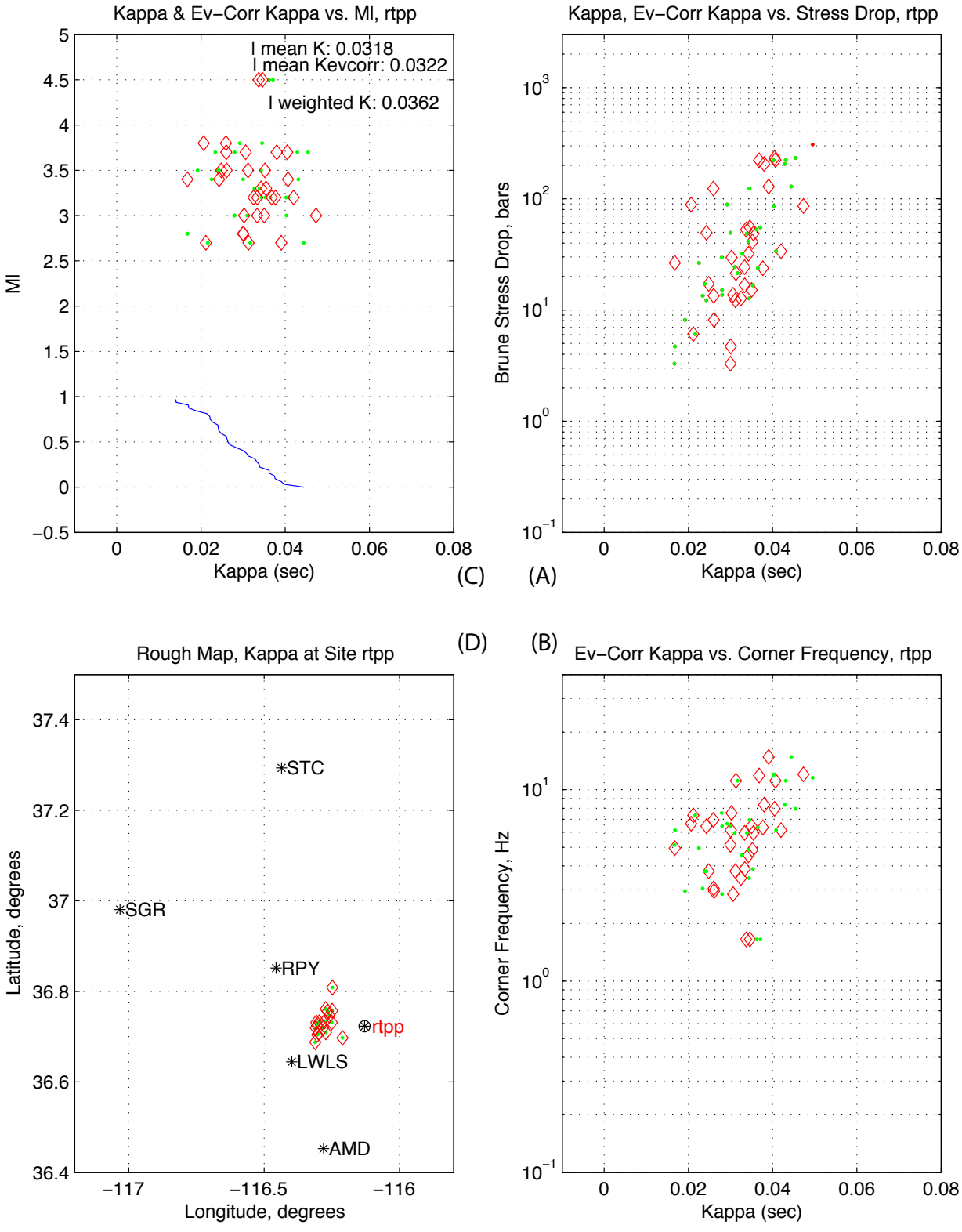

Figure 5.3.7.9. Station rxtn. Source: SN-UCCSN-UNR-097 v.1, Atch. 2, this figure: file kappawrap/caselsm4/Figs_summary/ml_vs_kcorr_40xsta.eps, where sta is the station name. Ml, latitude, longitude in 006DV.004; kappa, stress drop, corner frequency, epicentral distance in kappawrap/caselsm4/db/lsm_8.srckappa columns 12, 22, 6, 37, and 18, respectively. Other subset details in Table 5.17. Unqualified, for corroboration only; not for use in quality-affecting work.

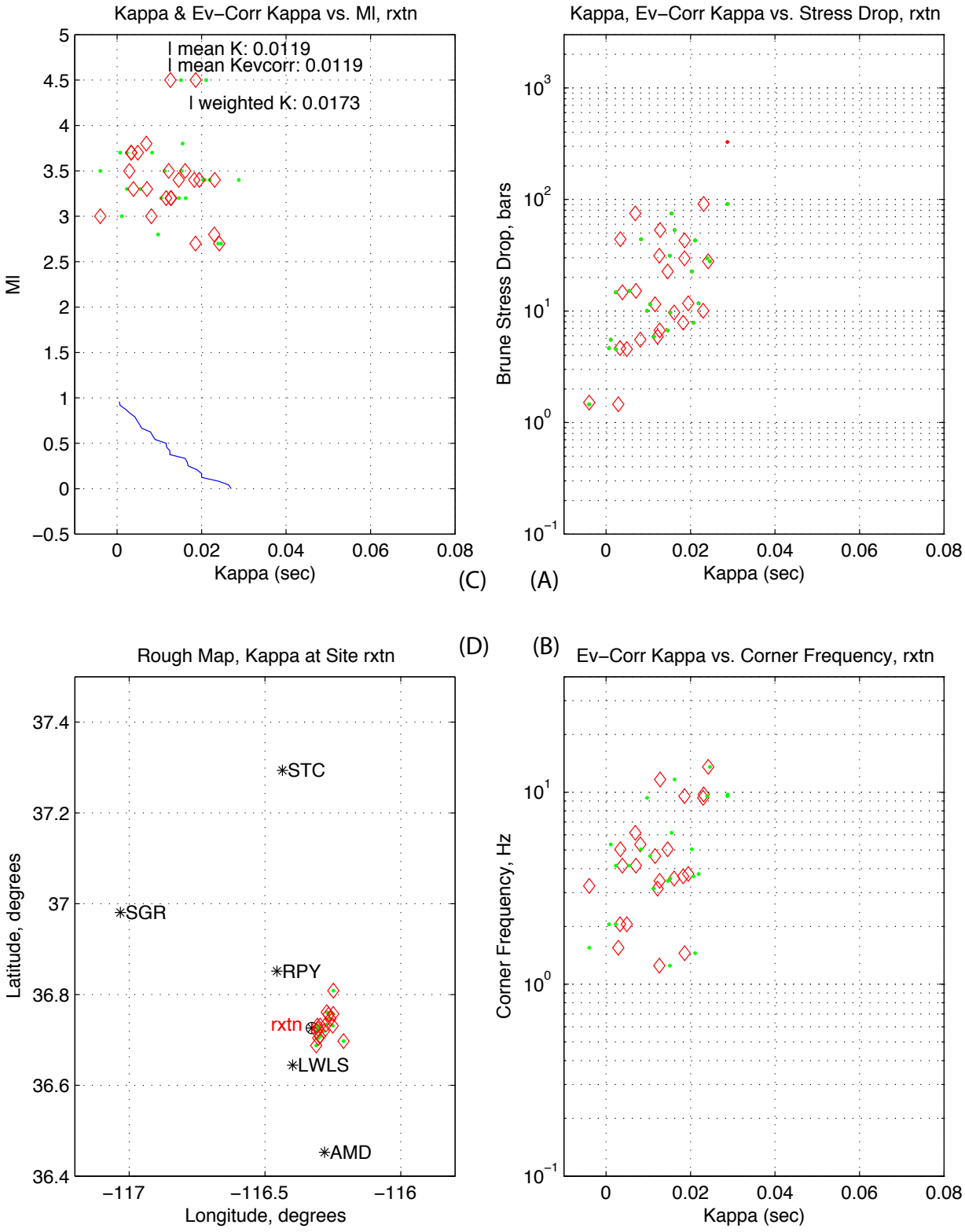

Figure 5.3.7.10. Station rymm. Source: SN-UCCSN-UNR-097 v.1, Atch. 2, this figure: file kappawrap/caselsm4/Figs_summary/ml_vs_kcorr_40xsta.eps, where sta is the station name. Ml, latitude, longitude in 006DV.004; kappa, stress drop, corner frequency, epicentral distance in kappawrap/caselsm4/db/lsm_8.srckappa columns 12, 22, 6, 37, and 18, respectively. Other subset details in Table 5.17. Unqualified, for corroboration only; not for use in quality-affecting work.

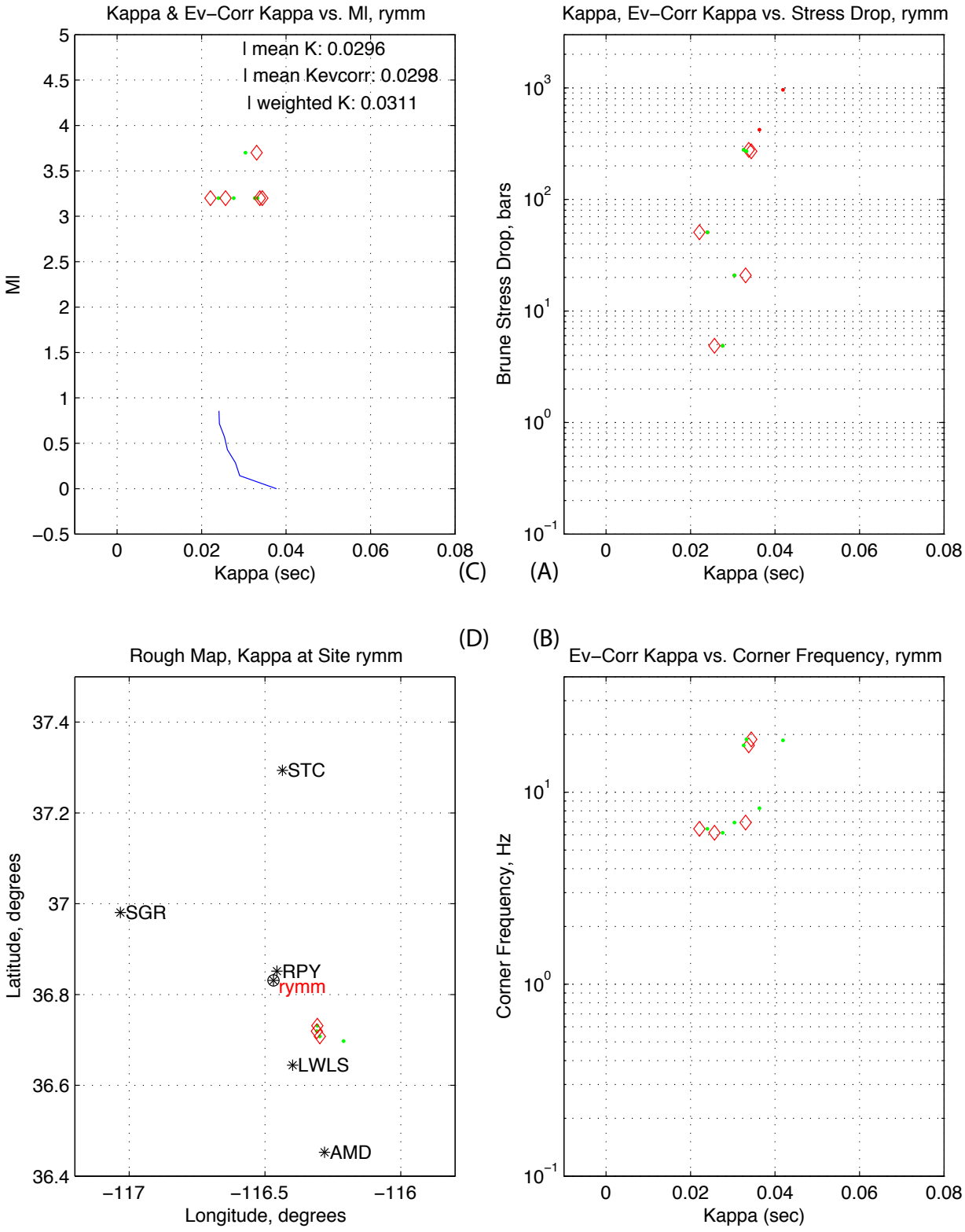

Figure 5.3.7.11. Station rymt. Source: SN-UCCSN-UNR-097 v.1, Atch. 2, this figure: file kappawrap/caselsm4/Figs_summary/ml_vs_kcorr_40xsta.eps, where sta is the station name. Ml, latitude, longitude in 006DV.004; kappa, stress drop, corner frequency, epicentral distance in kappawrap/caselsm4/db/lsm_8.srckappa columns 12, 22, 6, 37, and 18, respectively. Other subset details in Table 5.17. Unqualified, for corroboration only; not for use in quality-affecting work.

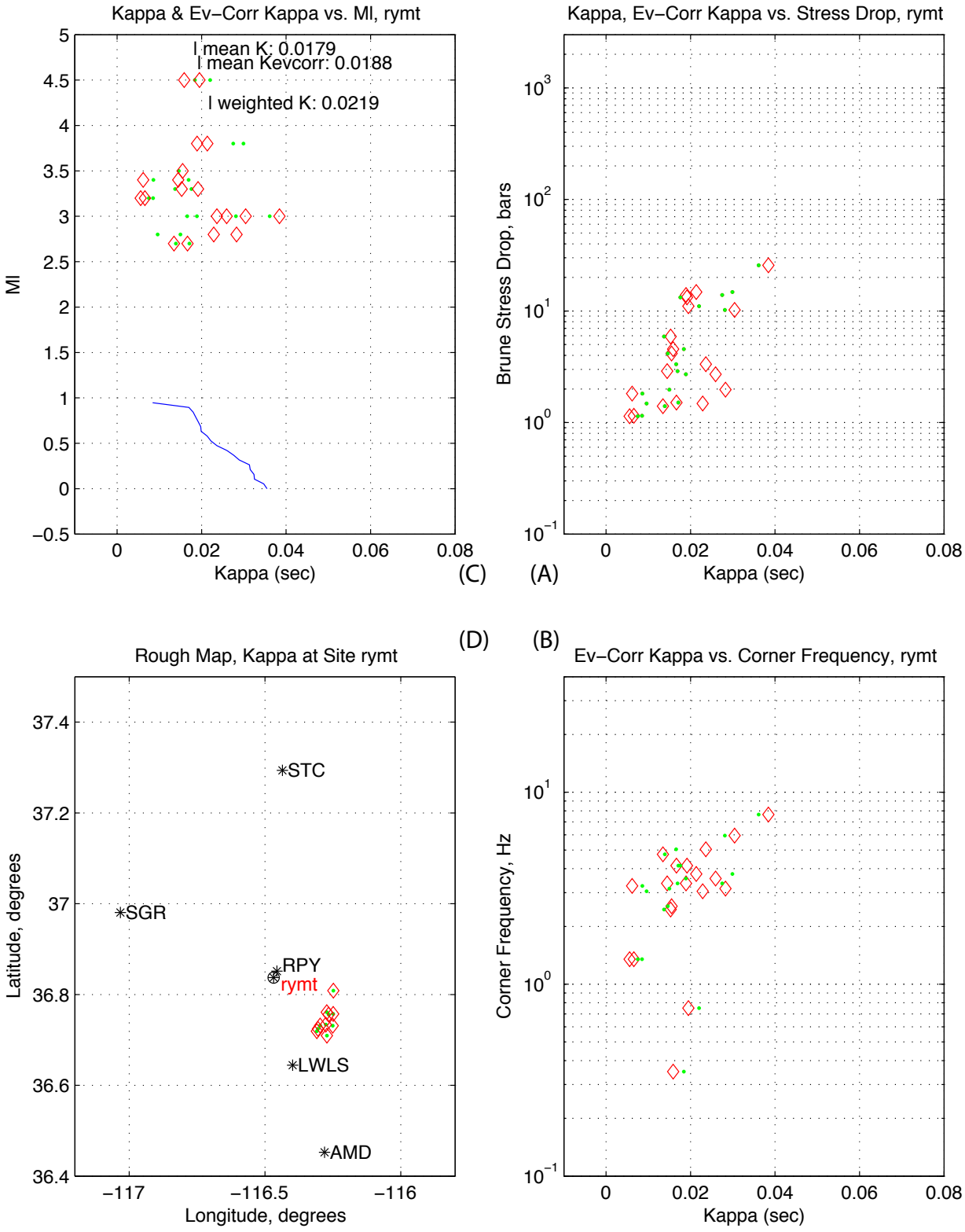

Figure 5.3.7.12. Station ryuc. Source: SN-UCCSN-UNR-097 v.1, Atch. 2, this figure: file kappawrap/caselsm4/Figs_summary/ml_vs_kcorr_40xsta.eps, where sta is the station name. Ml, latitude, longitude in 006DV.004; kappa, stress drop, corner frequency, epicentral distance in kappawrap/caselsm4/db/lsm_8.srckappa columns 12, 22, 6, 37, and 18, respectively. Other subset details in Table 5.17. Unqualified, for corroboration only; not for use in quality-affecting work.

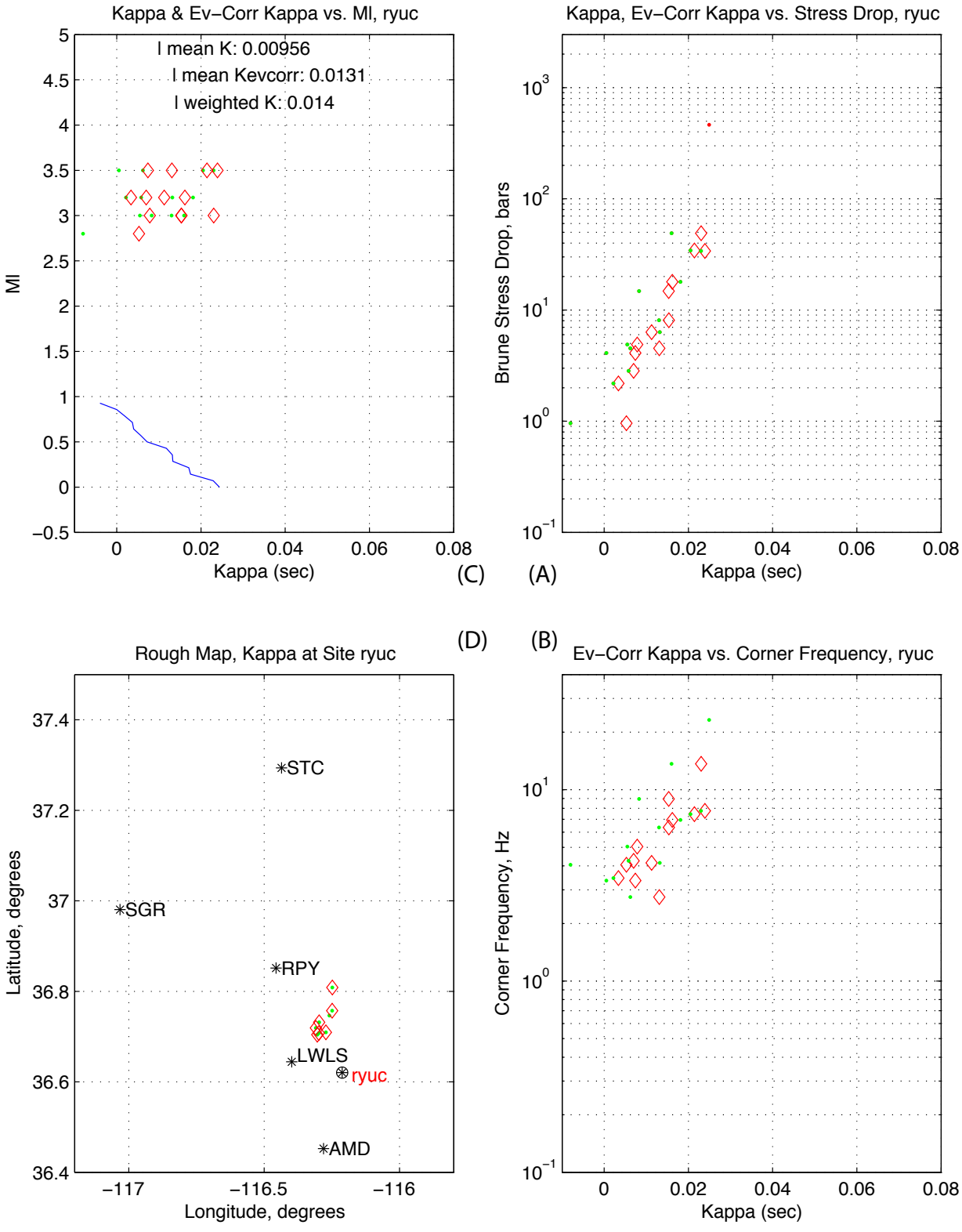

Figure 5.3.8 (a) Per-event average kappa and average from event-station records less than 40 km. (b) Kappa measurements by event for the LSM aftershocks.
Source: UCCSN-UNR-097, v. 1, Attachment 2, file kappawrap/caselsm4/Figs_summary/event_kappa_caselsm4.tbl. (upper figure), kappawrap/caselsm4/db/lsm_8.srckappa (lower). event origin-id=col. 1, kappa=col. 12, epicentral distance=col. 37. Unqualified., for corroboration purposes only; Not to for use in any quality-affecting work

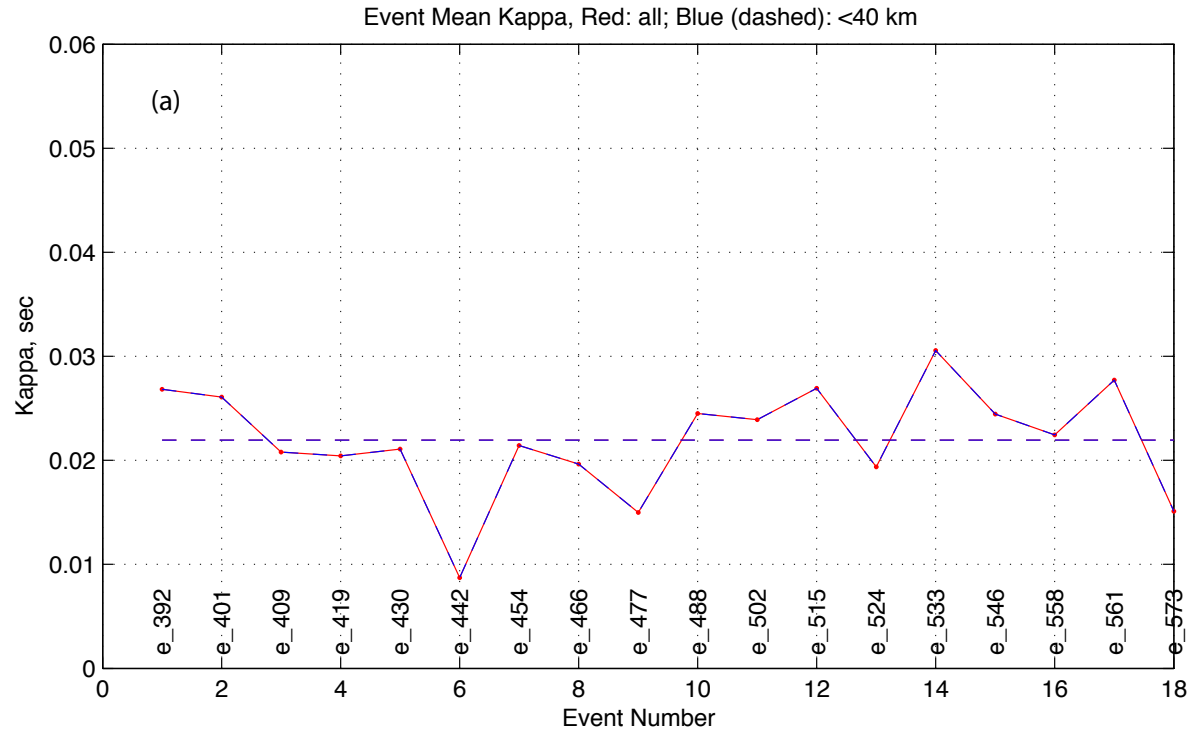

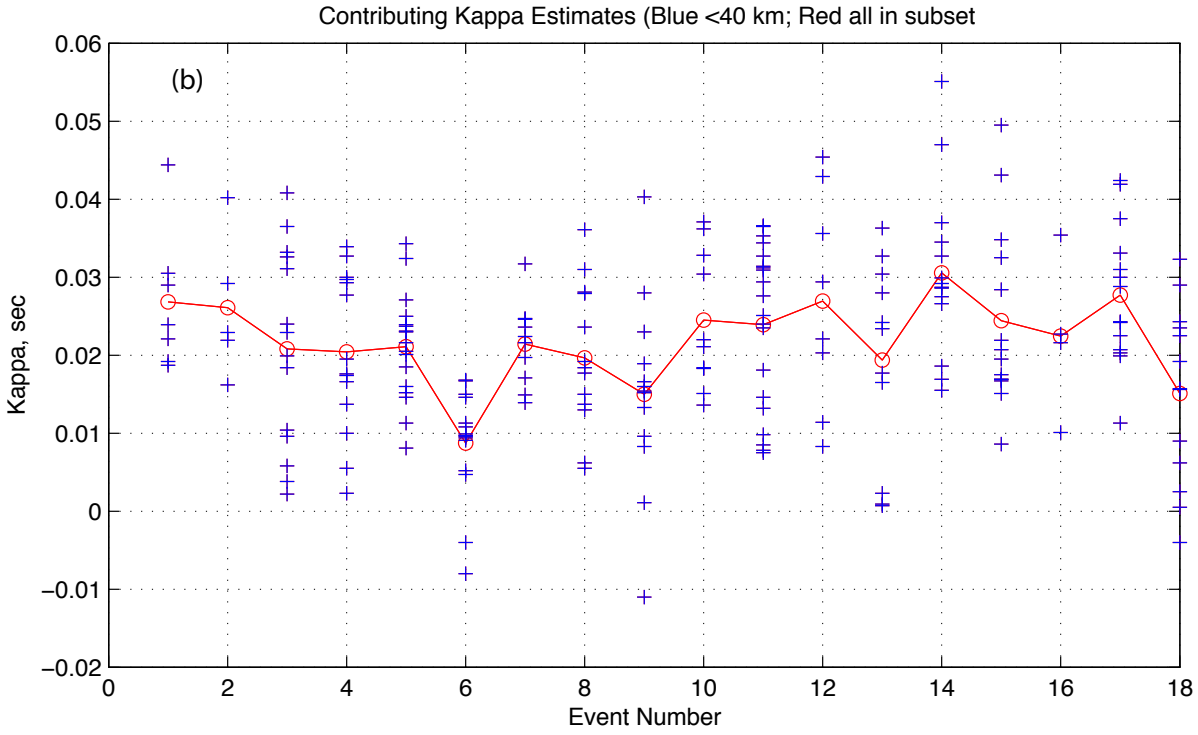

Figure 5.3.9.1 Stress drop is plotted versus corner frequency for every LSM moderate events (Table 5.5), caselsm4. X=epicentral distance>40 km.
Source: SN-UCCSN-UNR-097 v. 1, Atch 2, file kappawrap/caselsm4/Figs_summary/event_kappas1.eps, data in file kappawrap/caselsm4/db/lsm_8.srckappa. Stress drop=col 22, corner frequency= col 6; subset by event in col. 1, stress drop<100 MPa, squared error (col. 28)<0.151, SNRpct (col 43) >0.5; horizontal channels. Ml values from Table 5.5, source: Su, F., J. G. Anderson, J. N. Brune, and Y. Zeng. (1996). A comparison of direct S-wave and coda wave site amplification determined from aftershocks of the Little Skull Mountain earthquake, Bulletin of the Seismological Society of America, 86, 1006-1018. Table 2
Unqualified, for corroboration only. Not for use in any quality-affecting work.

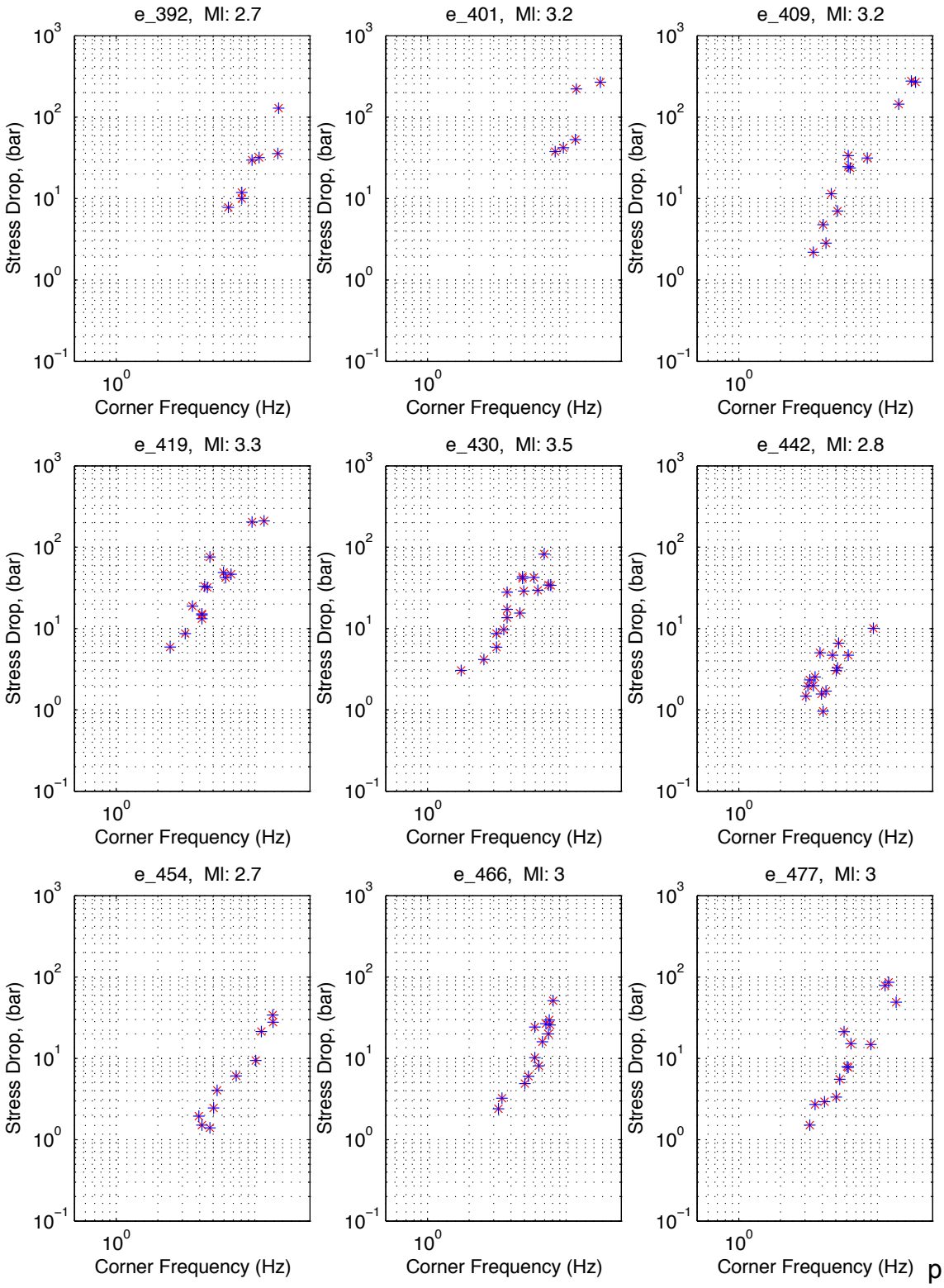

Figure 5.3.9.2 Stress drop is plotted versus corner frequency for every LSM moderate events (Table 5.5), caselsm4. X=epicentral distance>40 km.
Source: SN-UCCSN-UNR-097 v. 1, Atch 2, file kappawrap/caselsm4/Figs_summary/event_kappas1.eps, data in file kappawrap/caselsm4/db/lsm_8.srckappa. Stress drop=col 22, corner frequency= col 6; subset by event in col. 1, stress drop<100 MPa, squared error (col. 28)<0.151, SNRpct (col 43) >0.5; horizontal channels. Ml values from Table 5.5, source: Su, F., J. G. Anderson, J. N. Brune, and Y. Zeng. (1996). A comparison of direct S-wave and coda wave site amplification determined from aftershocks of the Little Skull Mountain earthquake, Bulletin of the Seismological Society of America, 86, 1006-1018. Table 2
Unqualified, for corroboration only. Not for use in any quality-affecting work.

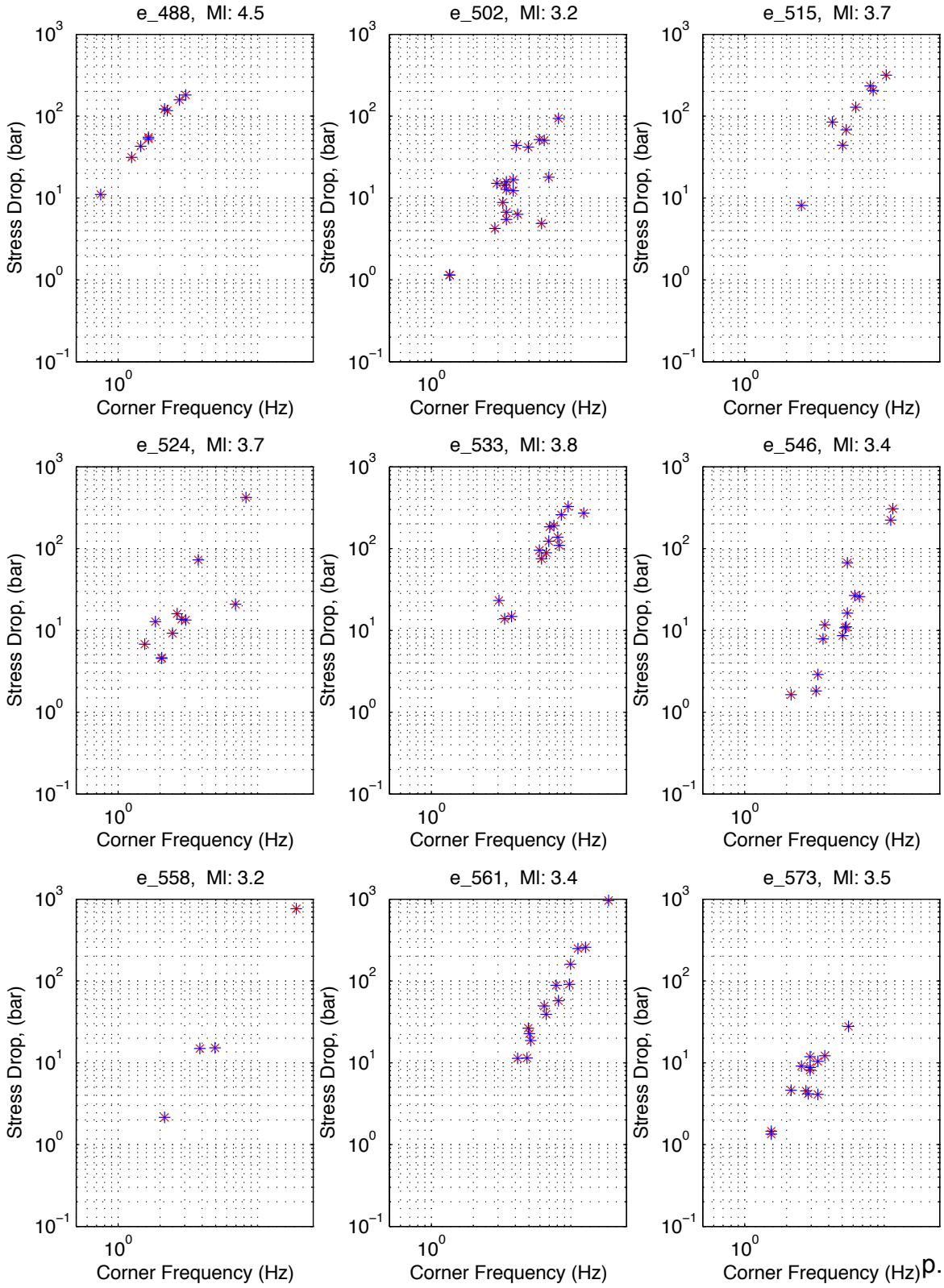

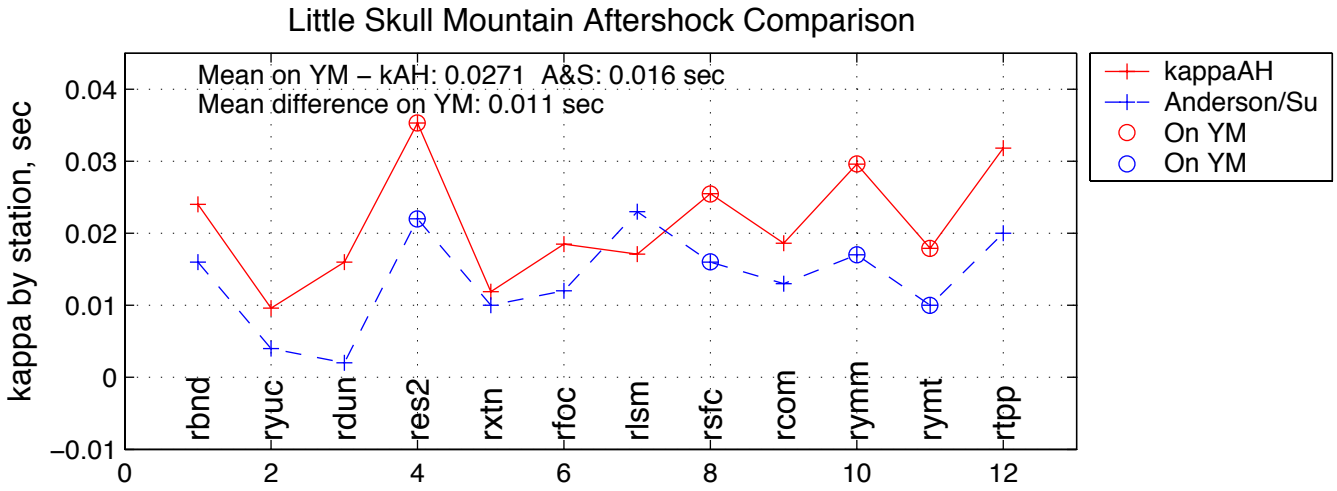

Figure 5.3.10. Comparison of kappaAH and Anderson and Su (MOL.20071203.0134) estimates. Sources: kappaAH data: UCCSN-UNR-097 v.1, Atch. 2, file kappawrap/caselsm4/Figs_summary/station_kappas_lsm.tbl, mean k column. Anderson/Su data: Anderson, J. G. and Su, F. (MOL.20071203.0134) Reevaluation of Kappa for Little Skull Mountain Earthquakes, University of Nevada Report, reference Work Plan WP# 14012210M3, Table 9.

Figure 5.3.11.1. Blume station LWLB spectral fitting - Lathrop Wells
Source: SN-UCCSN-UNR-097 v.1, Atch. 2, directory kappawrap/blume2/Figs
File: S00195_9218706522_LWLB_W2.eps
Unqualified, included for information only; Not for use in any quality-affecting work.

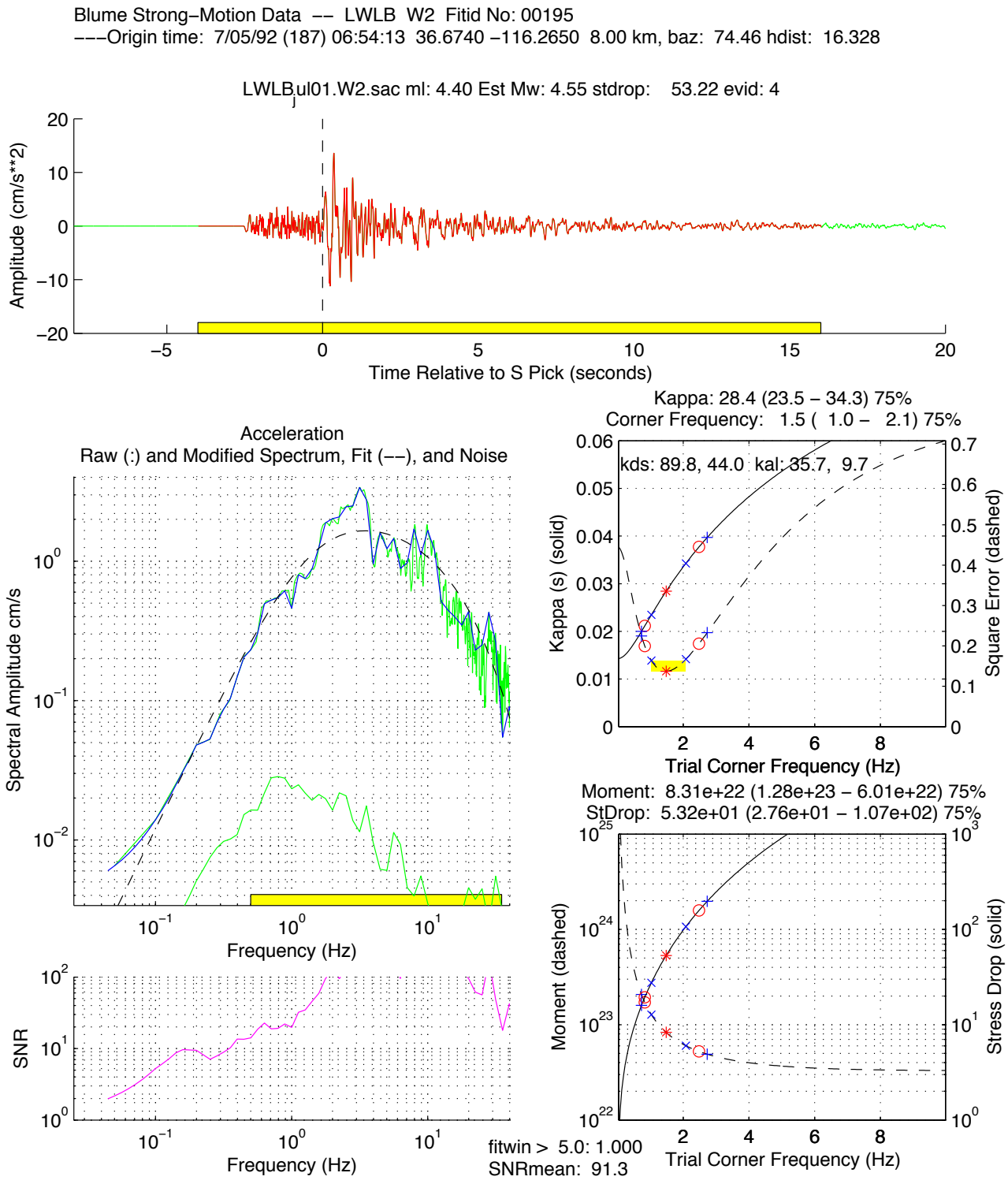

Kappa: 28.4 (23.5 – 34.3, 21.2–37.7, 20.0–39.7) Corner: 1.5 (1.0 – 2.1, 0.8– 2.5, 0.7– 2.7)
Mo: 8.31e+22 (1.28e+23– 6.01e+22, 1.72e+23– 5.24e+22, 2.07e+23– 4.91e+22) calib: 1.000e+07, silva: n
LF Spec: 3.09e–02 (4.75e–02– 2.23e–02, 6.38e–02– 1.95e–02, 7.71e–02– 1.82e–02) hdist: 16.3, logsp: y, 20.0
stress drop: 5.32e+01 (2.76e+01 – 1.07e+02, 1.94e+01– 1.58e+02, 1.59e+01– 1.97e+02) type: 2 scorr: n
mu: 3.20e+11 rho: 2.60 beta: 3.50e+05 Mwslope: 1.50 Mwint: 16.10 radf : 0.85 tocm: 1.00e–07 mtm: y nw: 4.0
siglvls: 1.230 1.500 1.700 dof: 40 prepk: 4.00 postpk: 16.00 minerr: 0.137 filter: n lo,hi,nr,ftype: 0.3 9999.0 2 high
taperlen: 0.05 smooth: 0 pass, 0.10 0.20 0.40 0.20 0.10, 2 Dbase: ./db/blume

Figure 5.3.11.2. Blume station LWLB spectral fitting - Lathrop Wells
Source: SN-UCCSN-UNR-097 v.1, Atch. 2, directory kappawrap/blume2/Figs
File: S00197_9218706522_LWLB_N2.eps
Unqualified, included for information only; Not for use in any quality-affecting work.

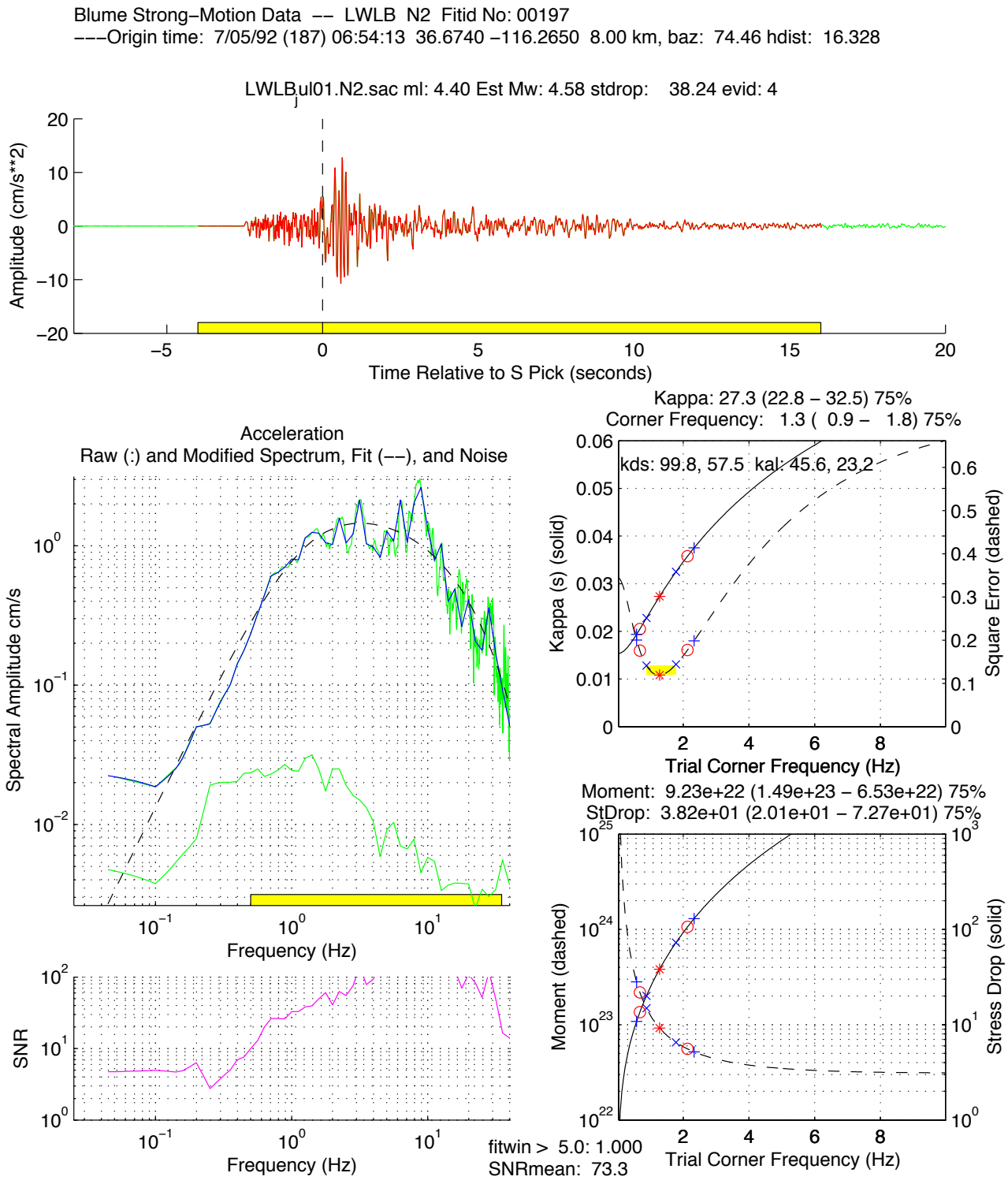

Kappa: 27.3 (22.8 – 32.5, 20.5–35.8, 19.4–37.5) Corner: 1.3 (0.9 – 1.8, 0.7– 2.1, 0.6– 2.3)
Mo: 9.23e+22 (1.49e+23– 6.53e+22, 2.18e+23– 5.57e+22, 2.81e+23– 5.19e+22) calib: 1.000e+07, silva: n
LF Spec: 3.43e–02 (5.55e–02– 2.43e–02, 8.12e–02– 2.07e–02, 1.05e–01– 1.93e–02) hdist: 16.3, logsp: y, 20.0
stress drop: 3.82e+01 (2.01e+01 – 7.27e+01, 1.36e+01– 1.06e+02, 1.08e+01– 1.30e+02) type: 2 scorr: n
mu: 3.20e+11 rho: 2.60 beta: 3.50e+05 Mwslope: 1.50 Mwint: 16.10 radf : 0.85 tocm: 1.00e–07 mtm: y nw: 4.0
siglvls: 1.230 1.500 1.700 dof: 40 prepk: 4.00 postpk: 16.00 minerr: 0.119 filter: n lo,hi,nr,ftype: 0.3 9999.0 2 high
taperlen: 0.05 smooth: 0 pass, 0.10 0.20 0.40 0.20 0.10, 2 Dbase: ./db/blume

Figure 5.3.11.3. Blume station LWLB spectral fitting - Lathrop Wells
Source: SN-UCCSN-UNR-097 v.1, Atch. 2, directory kappawrap/blume2/Figs
File: S00227_92181101422_LWLB_W2.eps
Unqualified, included for information only; Not for use in any quality-affecting work.

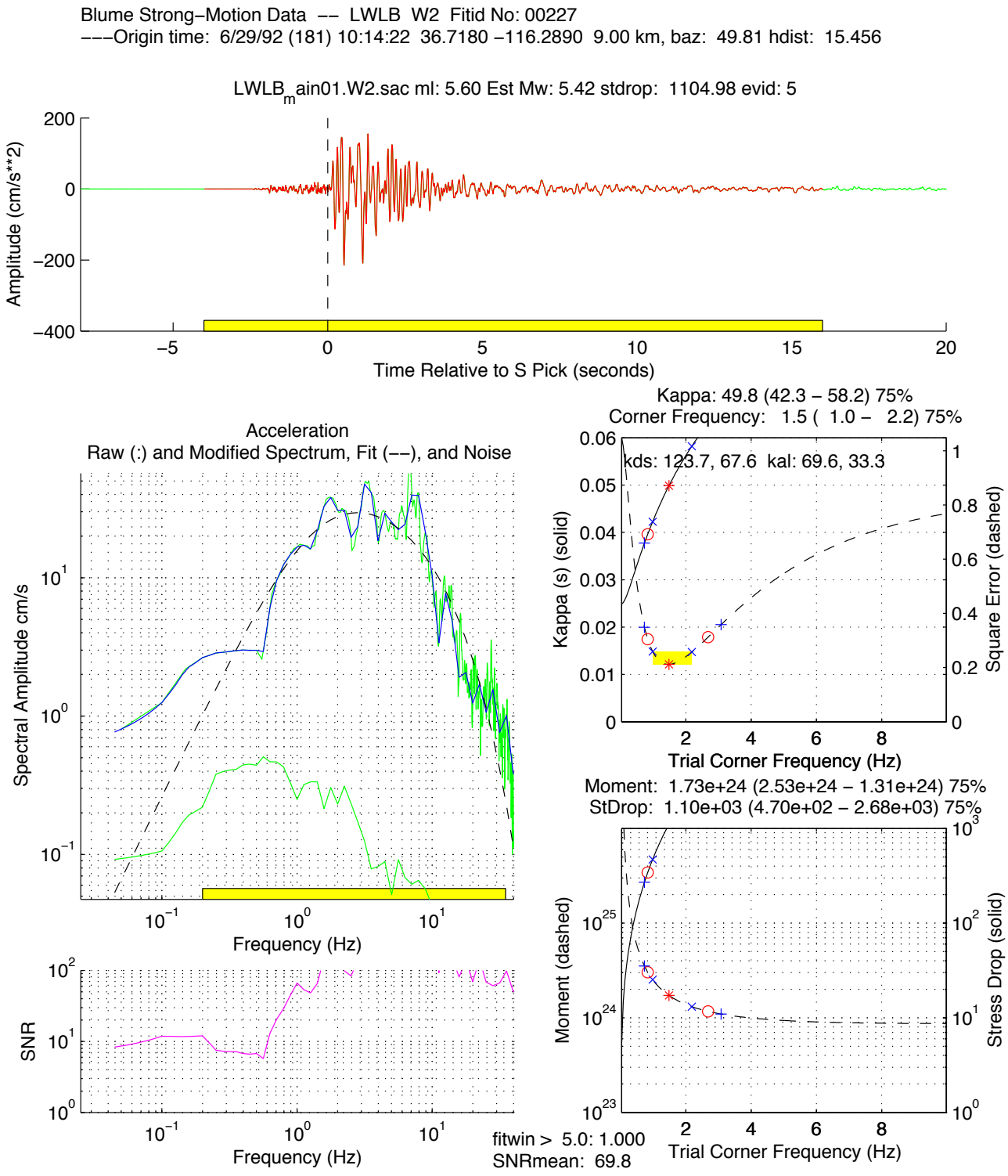

Kappa: 49.8 (42.3 – 58.2, 39.6–63.0, 37.7–66.4) Corner: 1.5 (1.0 – 2.2, 0.8– 2.7, 0.7– 3.1)
Mo: 1.73e+24 (2.53e+24– 1.31e+24, 3.03e+24– 1.17e+24, 3.52e+24– 1.10e+24) calib: 1.000e+07, silva: n
LF Spec: 6.77e–01 (9.93e–01– 5.15e–01, 1.19e+00– 4.59e–01, 1.38e+00– 4.30e–01) hdist: 15.5, logsp: y, 20.0
stress drop: 1.10e+03 (4.70e+02 – 2.68e+03, 3.42e+02– 4.45e+03, 2.71e+02– 6.33e+03) type: 2 scorr: n
mu: 3.20e+11 rho: 2.60 beta: 3.50e+05 Mwslope: 1.50 Mwint: 16.10 radf : 0.85 tocm: 1.00e–07 mtm: y nw: 4.0
siglvls: 1.230 1.500 1.700 dof: 40 prepk: 4.00 postpk: 16.00 minerr: 0.212 filter: n lo,hi,nr,ftype: 0.3 9999.0 2 high
taperlen: 0.05 smooth: 0 pass, 0.10 0.20 0.40 0.20 0.10, 2 Dbase: ./db/blume

Figure 5.3.11.4. Blume station LWLB spectral fitting - Lathrop Wells
Source: SN-UCCSN-UNR-097 v.1, Atch. 2, directory kappawrap/blume2/Figs
File: S00228_92181101422_LWLB_N2.eps
Unqualified, included for information only; Not for use in any quality-affecting work.

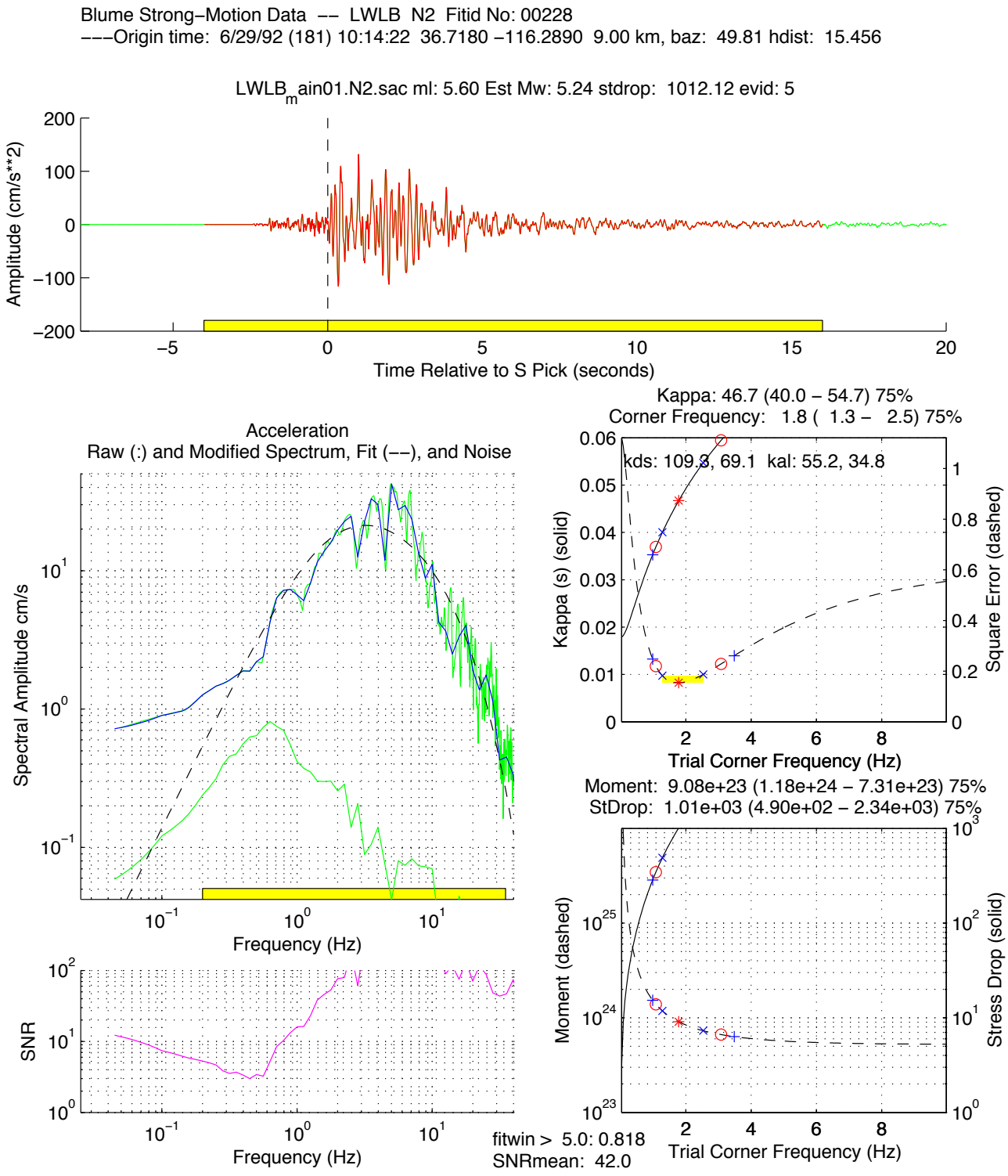

Kappa: 46.7 (40.0 – 54.7, 36.9–59.5, 35.3–62.5) Corner: 1.8 (1.3 – 2.5, 1.1– 3.1, 1.0– 3.5)
Mo: 9.08e+23 (1.18e+24– 7.31e+23, 1.39e+24– 6.65e+23, 1.53e+24– 6.33e+23) calib: 1.000e+07, silva: n
LF Spec: 3.57e–01 (4.65e–01– 2.87e–01, 5.45e–01– 2.61e–01, 6.02e–01– 2.48e–01) hdist: 15.5, logsp: y, 20.0
stress drop: 1.01e+03 (4.90e+02 – 2.34e+03, 3.46e+02– 3.84e+03, 2.85e+02– 5.27e+03) type: 2 scorr: n
mu: 3.20e+11 rho: 2.60 beta: 3.50e+05 Mwslope: 1.50 Mwint: 16.10 radf : 0.85 tocm: 1.00e–07 mtm: y nw: 4.0
siglvls: 1.230 1.500 1.700 dof: 40 prepk: 4.00 postpk: 16.00 minerr: 0.154 filter: n lo,hi,nr,ftype: 0.3 9999.0 2 high
taperlen: 0.05 smooth: 0 pass, 0.10 0.20 0.40 0.20 0.10, 2 Dbase: ./db/blume

Figure 5.3.11.5. Blume station LWLB spectral fitting - Lathrop Wells
Source: SN-UCCSN-UNR-097 v.1, Atch. 2, directory kappawrap/blume2/Figs
File: S00273_92257114622_LWLB_W1.eps
Unqualified, included for information only; Not for use in any quality-affecting work.

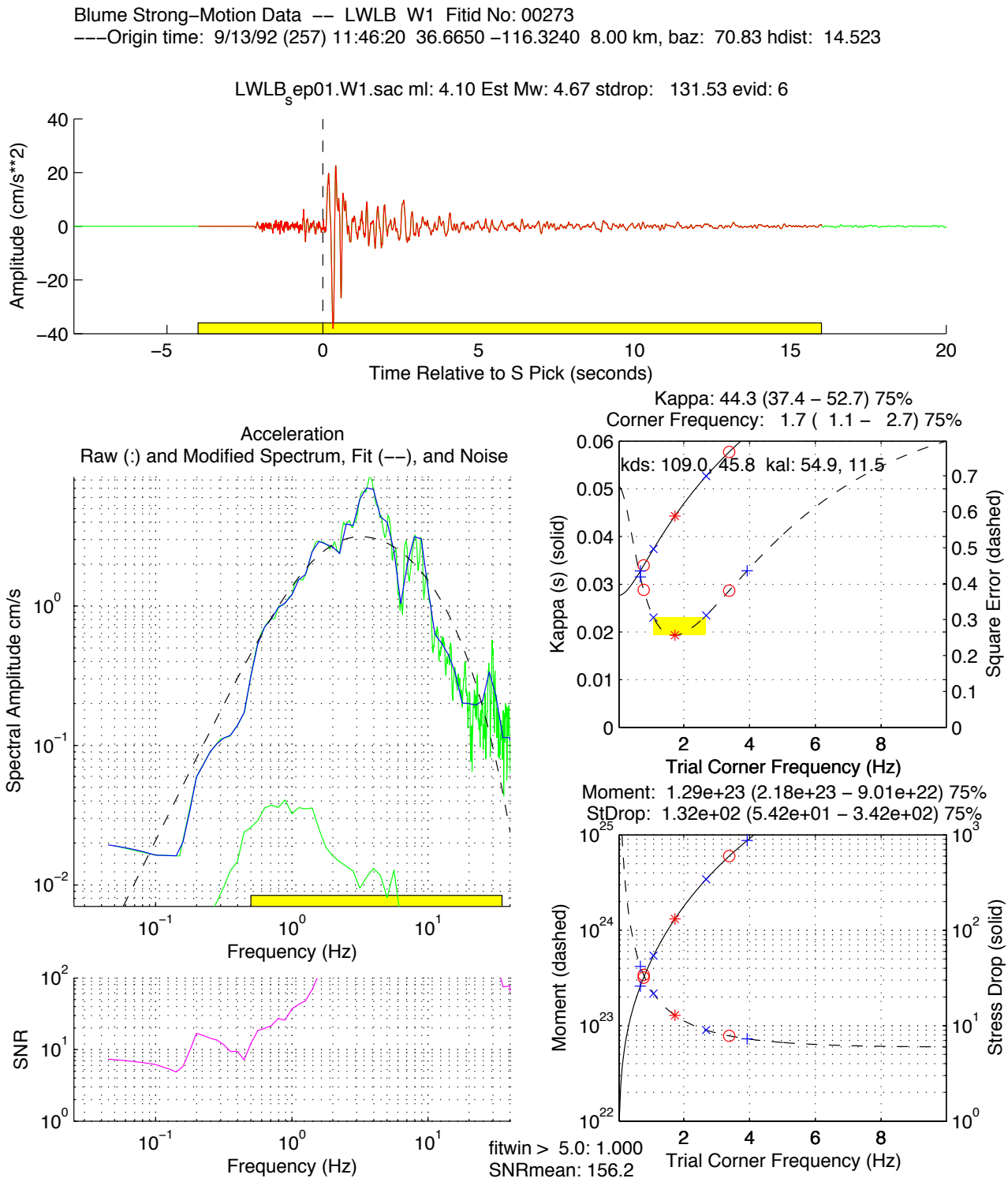

Kappa: 44.3 (37.4 – 52.7, 33.9–57.7, 32.8–61.2) Corner: 1.7 (1.1 – 2.7, 0.8– 3.4, 0.7– 3.9)
Mo: 1.29e+23 (2.18e+23– 9.01e+22, 3.41e+23– 7.84e+22, 4.19e+23– 7.29e+22) calib: 1.000e+07, silva: n
LF Spec: 5.37e–02 (9.10e–02– 3.76e–02, 1.42e–01– 3.28e–02, 1.75e–01– 3.05e–02) hdist: 14.5, logsp: y, 20.0
stress drop: 1.32e+02 (5.42e+01 – 3.42e+02, 3.19e+01– 5.98e+02, 2.60e+01– 8.74e+02) type: 2 scorr: n
mu: 3.20e+11 rho: 2.60 beta: 3.50e+05 Mwslope: 1.50 Mwint: 16.10 radf : 0.85 tocm: 1.00e–07 mtm: y nw: 4.0
siglvls: 1.230 1.500 1.700 dof: 40 prepk: 4.00 postpk: 16.00 minerr: 0.256 filter: n lo,hi,nr,ftype: 0.3 9999.0 2 high
taperlen: 0.05 smooth: 0 pass, 0.10 0.20 0.40 0.20 0.10, 2 Dbase: ./db/blume

Figure 5.3.11.6. Blume station LWLB spectral fitting - Lathrop Wells
Source: SN-UCCSN-UNR-097 v.1, Atch. 2, directory kappawrap/blume2/Figs
File: S00271_92257114622_LWLB_N1.eps
Unqualified, included for information only; Not for use in any quality-affecting work.

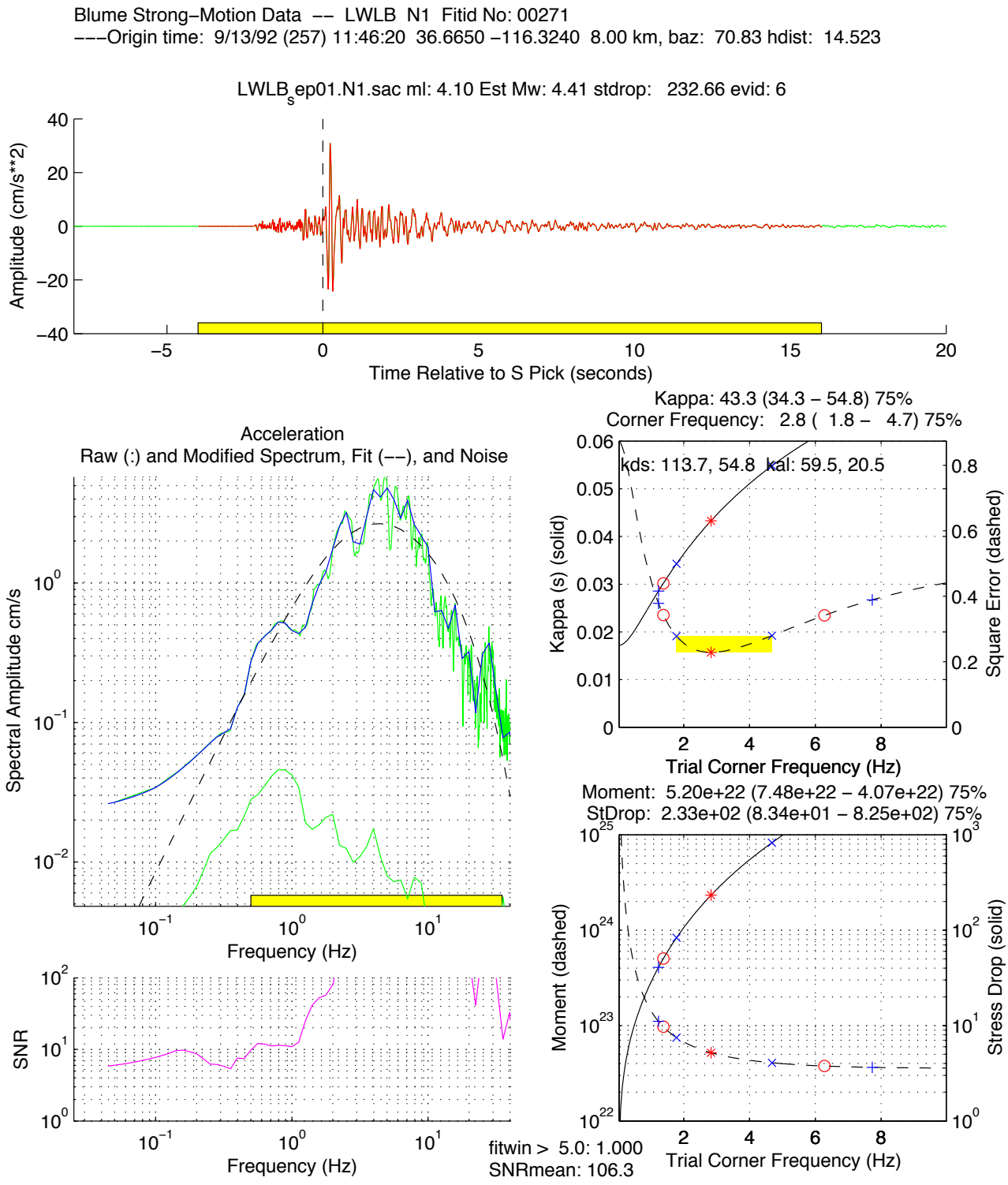

Kappa: 43.3 (34.3 – 54.8, 30.2–62.0, 28.6–67.0) Corner: 2.8 (1.8 – 4.7, 1.4– 6.3, 1.2– 7.7)
Mo: 5.20e+22 (7.48e+22– 4.07e+22, 9.72e+22– 3.77e+22, 1.11e+23– 3.65e+22) calib: 1.000e+07, silva: n
LF Spec: 2.17e–02 (3.13e–02– 1.70e–02, 4.06e–02– 1.57e–02, 4.63e–02– 1.52e–02) hdist: 14.5, logsp: y, 20.0
stress drop: 2.33e+02 (8.34e+01 – 8.25e+02, 5.04e+01– 1.84e+03, 4.08e+01– 3.33e+03) type: 2 scorr: n
mu: 3.20e+11 rho: 2.60 beta: 3.50e+05 Mwslope: 1.50 Mwint: 16.10 radf : 0.85 tocm: 1.00e–07 mtm: y nw: 4.0
siglvls: 1.230 1.500 1.700 dof: 40 prepk: 4.00 postpk: 16.00 minerr: 0.229 filter: n lo,hi,nr,ftype: 0.3 9999.0 2 high
taperlen: 0.05 smooth: 0 pass, 0.10 0.20 0.40 0.20 0.10, 2 Dbase: ./db/blume

Figure 5.3.12.1. Blume station CPTB spectral fitting - Control Point
Source: SN-UCCSN-UNR-097 v.1, Atch. 2, directory kappawrap/blume2/Figs
File: S00178_92187065403_CPTB_W1.eps
Unqualified, included for information only; Not for use in any quality-affecting work.

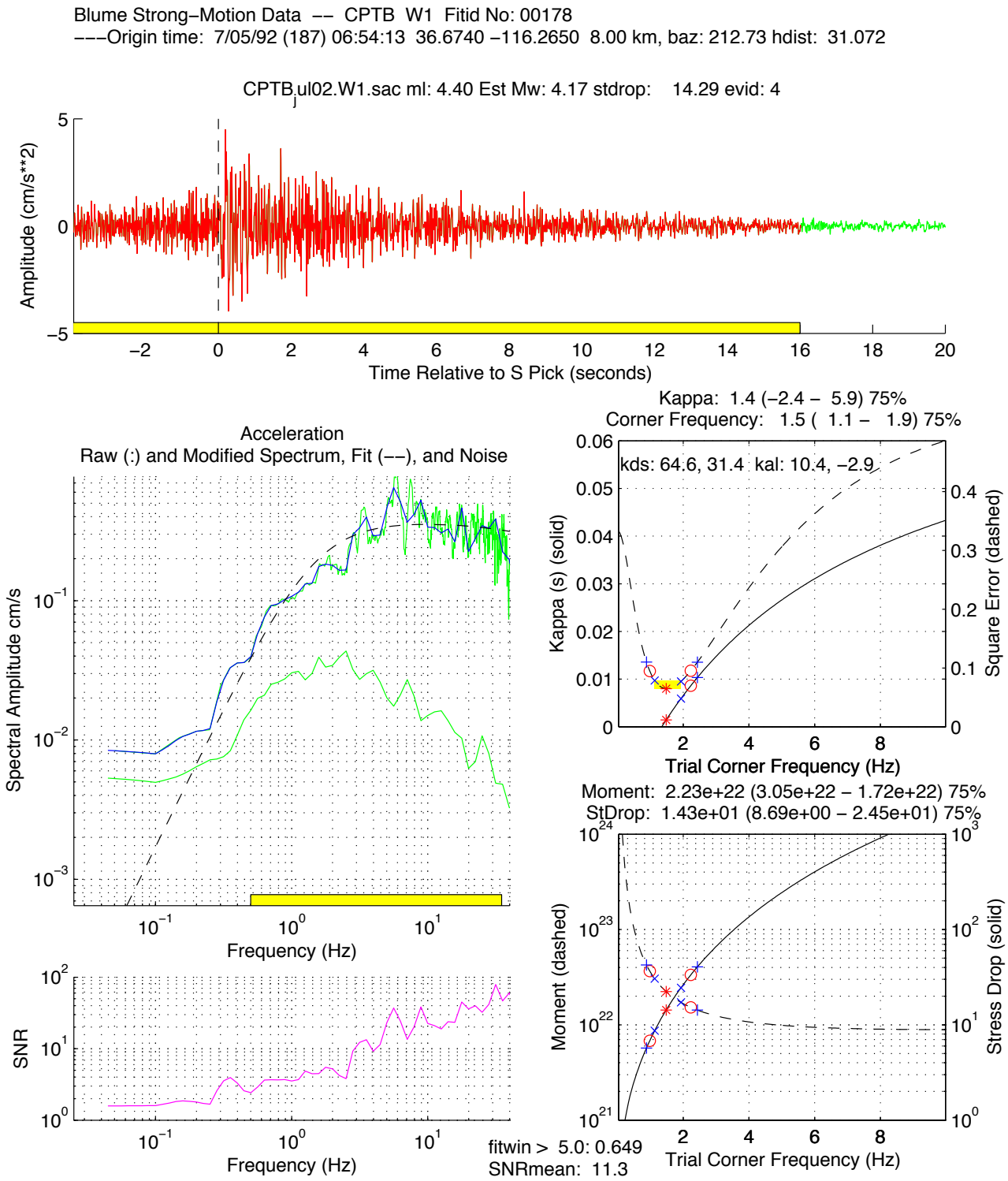

Kappa: 1.4 (–2.4 – 5.9, –4.1– 8.6, –5.2–10.3) Corner: 1.5 (1.1 – 1.9, 1.0– 2.2, 0.9– 2.4)
Mo: 2.23e+22 (3.05e+22– 1.72e+22, 3.66e+22– 1.53e+22, 4.24e+22– 1.43e+22) calib: 1.000e+07, silva: n
LF Spec: 4.36e–03 (5.95e–03– 3.36e–03, 7.15e–03– 2.98e–03, 8.29e–03– 2.79e–03) hdist: 31.1, logsp: y, 20.0
stress drop: 1.43e+01 (8.69e+00 – 2.45e+01, 6.81e+00– 3.34e+01, 5.71e+00– 4.05e+01) type: 2 scorr: n
mu: 3.20e+11 rho: 2.60 beta: 3.50e+05 Mwslope: 1.50 Mwint: 16.10 radf : 0.85 tocm: 1.00e–07 mtm: y nw: 4.0
siglvls: 1.230 1.500 1.700 dof: 40 prepk: 4.00 postpk: 16.00 minerr: 0.065 filter: n lo,hi,nr,ftype: 0.3 9999.0 2 high
taperlen: 0.05 smooth: 0 pass, 0.10 0.20 0.40 0.20 0.10, 2 Dbase: ./db/blume

Figure 5.3.12.2. Blume station CPTB spectral fitting - Control Point
Source: SN-UCCSN-UNR-097 v.1, Atch. 2, directory kappawrap/blume2/Figs
File: S00179_92187065403_CPTB_N1.eps
Unqualified, included for information only; Not for use in any quality-affecting work.

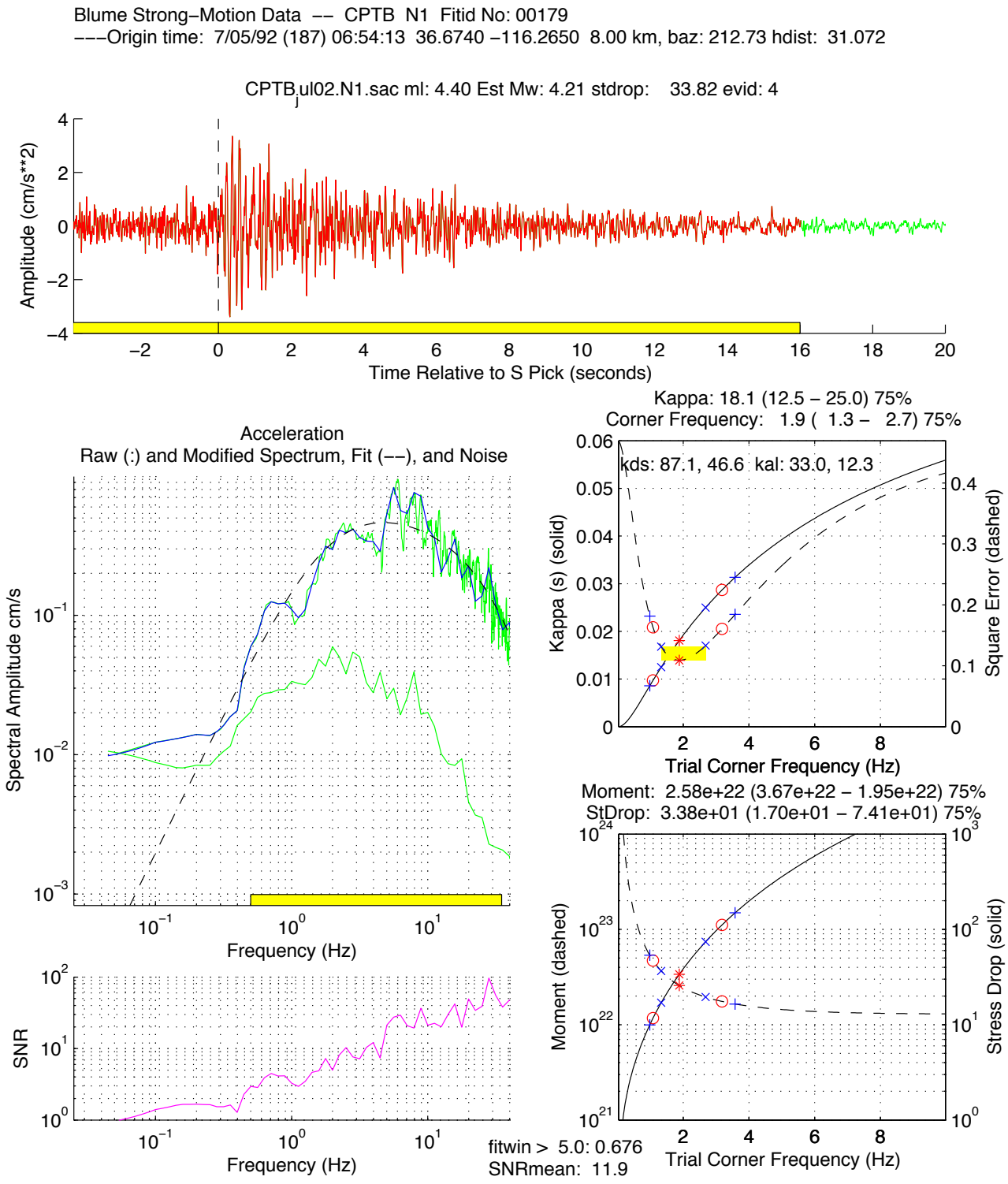

Kappa: 18.1 (12.5 – 25.0, 9.7–28.7, 8.6–31.3) Corner: 1.9 (1.3 – 2.7, 1.1– 3.2, 1.0– 3.6)
Mo: 2.58e+22 (3.67e+22– 1.95e+22, 4.71e+22– 1.75e+22, 5.35e+22– 1.65e+22) calib: 1.000e+07, silva: n
LF Spec: 5.03e–03 (7.16e–03– 3.81e–03, 9.20e–03– 3.43e–03, 1.04e–02– 3.22e–03) hdist: 31.1, logsp: y, 20.0
stress drop: 3.38e+01 (1.70e+01 – 7.41e+01, 1.17e+01– 1.11e+02, 9.95e+00– 1.49e+02) type: 2 scorr: n
mu: 3.20e+11 rho: 2.60 beta: 3.50e+05 Mwslope: 1.50 Mwint: 16.10 radf : 0.85 tocm: 1.00e–07 mtm: y nw: 4.0
siglvls: 1.230 1.500 1.700 dof: 40 prepk: 4.00 postpk: 16.00 minerr: 0.109 filter: n lo,hi,nr,ftype: 0.3 9999.0 2 high
taperlen: 0.05 smooth: 0 pass, 0.10 0.20 0.40 0.20 0.10, 2 Dbase: ./db/blume

Figure 5.3.12.3. Blume station CPTB spectral fitting - Control Point
Source: SN-UCCSN-UNR-097 v.1, Atch. 2, directory kappawrap/blume2/Figs
File: S00208_92181101424_CPTB_W2.eps
Unqualified, included for information only; Not for use in any quality-affecting work.

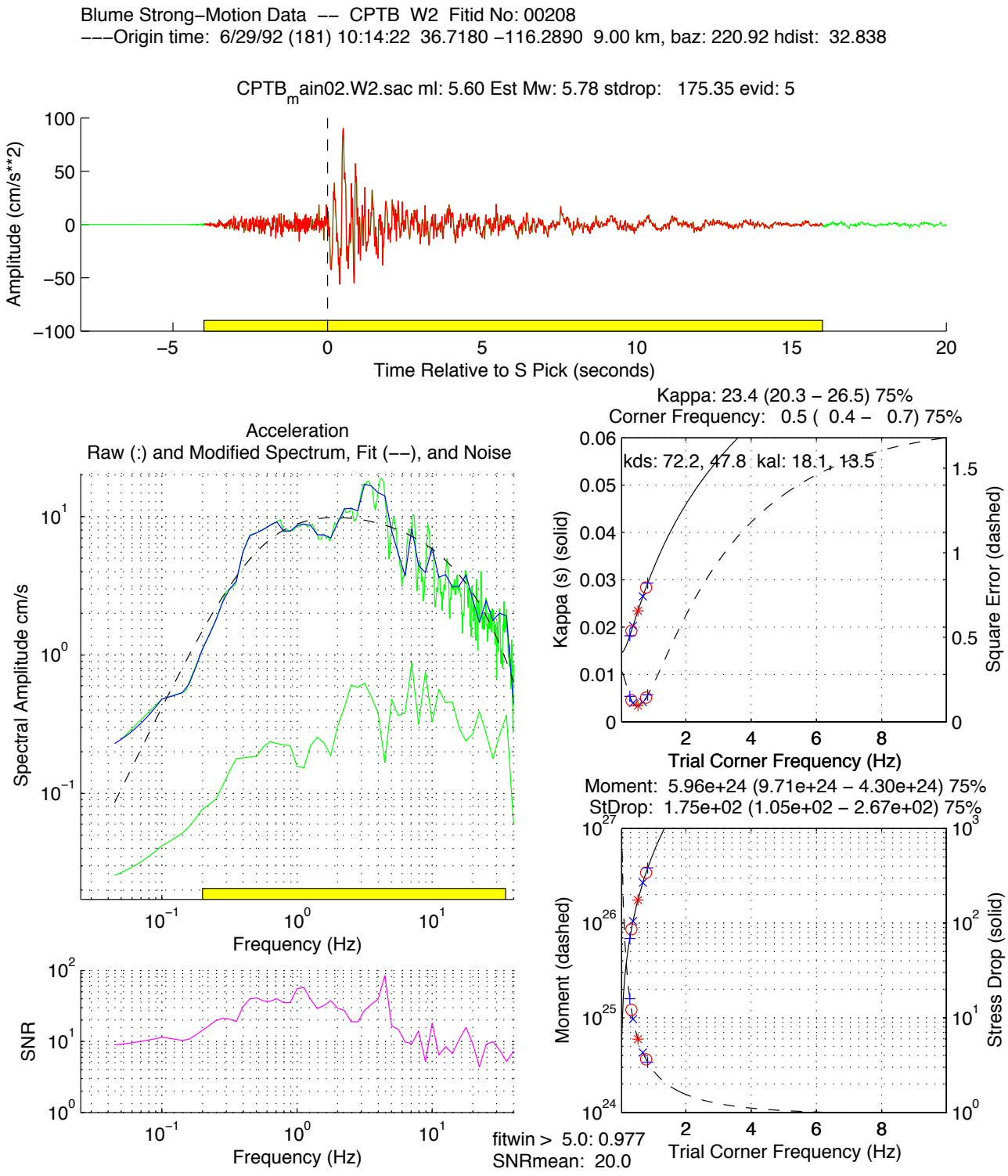

Kappa: 23.4 (20.3 – 26.5, 19.2–28.4, 18.2–29.3) Corner: 0.5 (0.4 – 0.7, 0.3– 0.8, 0.3– 0.8)
Mo: 5.96e+24 (9.71e+24– 4.30e+24, 1.21e+25– 3.64e+24, 1.59e+25– 3.39e+24) calib: 1.000e+07, silva: n
LF Spec: 1.10e+00 (1.79e+00– 7.94e–01, 2.24e+00– 6.73e–01, 2.94e+00– 6.26e–01) hdist: 32.8, logsp: y, 20.0
stress drop: 1.75e+02 (1.05e+02 – 2.67e+02, 8.62e+01– 3.41e+02, 6.90e+01– 3.83e+02) type: 2 scorr: n
mu: 3.20e+11 rho: 2.60 beta: 3.50e+05 Mwslope: 1.50 Mwint: 16.10 radf : 0.85 tocm: 1.00e–07 mtm: y nw: 4.0
siglvls: 1.230 1.500 1.700 dof: 40 prepk: 4.00 postpk: 16.00 minerr: 0.096 filter: n lo,hi,nr,ftype: 0.3 9999.0 2 high
taperlen: 0.05 smooth: 0 pass, 0.10 0.20 0.40 0.20 0.10, 2 Dbase: ./db/blume

Figure 5.3.12.4. Blume station CPTB spectral fitting - Control Point
Source: SN-UCCSN-UNR-097 v.1, Atch. 2, directory kappawrap/blume2/Figs
File: S00210_92181101424_CPTB_N2.eps
Unqualified, included for information only; Not for use in any quality-affecting work.

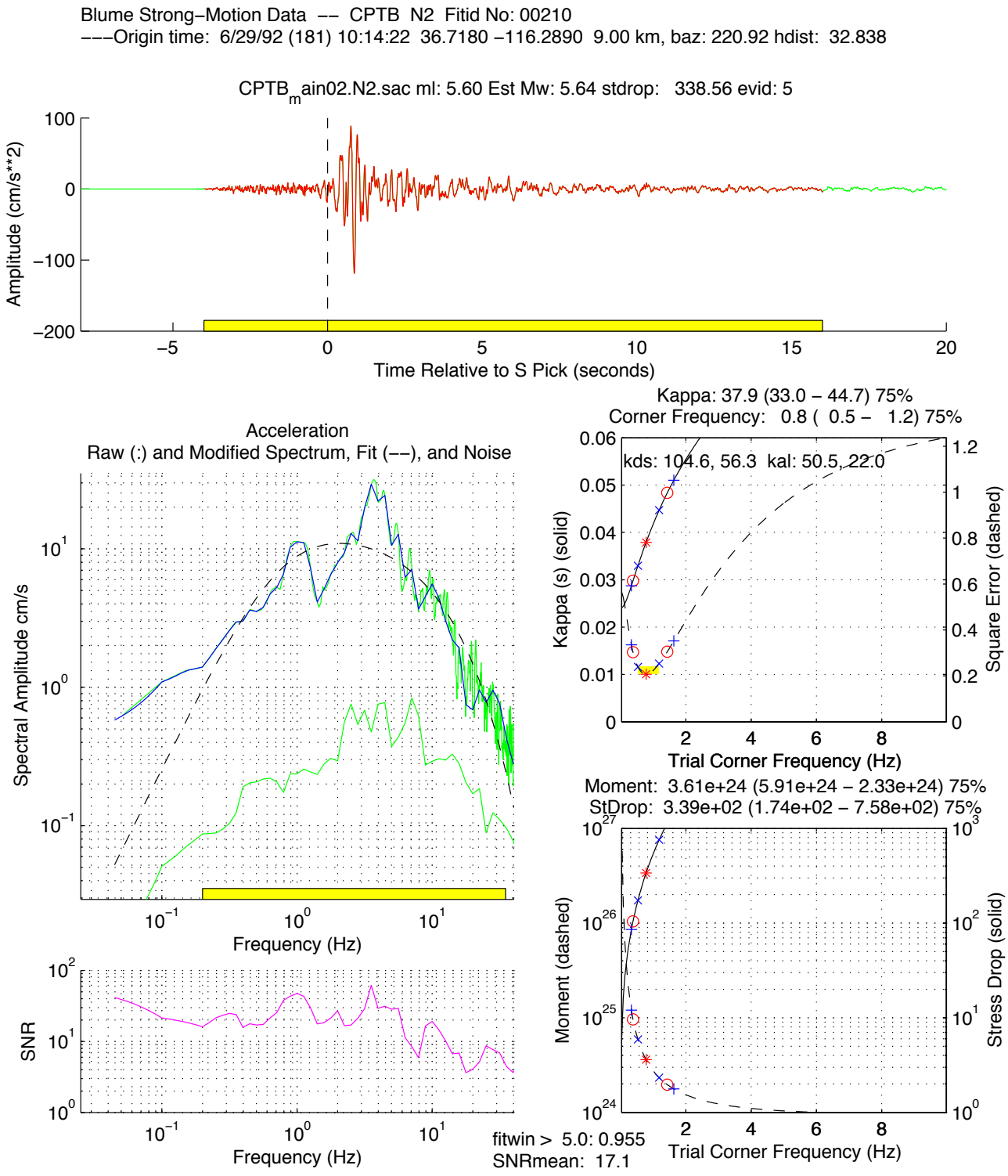

Kappa: 37.9 (33.0 – 44.7, 29.8–48.4, 28.7–51.0) Corner: 0.8 (0.5 – 1.2, 0.4– 1.4, 0.3– 1.6)
Mo: 3.61e+24 (5.91e+24– 2.33e+24, 9.63e+24– 1.97e+24, 1.20e+25– 1.77e+24) calib: 1.000e+07, silva: n
LF Spec: 6.67e–01 (1.09e+00– 4.31e–01, 1.78e+00– 3.64e–01, 2.22e+00– 3.28e–01) hdist: 32.8, logsp: y, 20.0
stress drop: 3.39e+02 (1.74e+02 – 7.58e+02, 1.04e+02– 1.14e+03, 8.55e+01– 1.52e+03) type: 2 scorr: n
mu: 3.20e+11 rho: 2.60 beta: 3.50e+05 Mwslope: 1.50 Mwint: 16.10 radf : 0.85 tocm: 1.00e–07 mtm: y nw: 4.0
siglvls: 1.230 1.500 1.700 dof: 40 prepk: 4.00 postpk: 16.00 minerr: 0.207 filter: n lo,hi,nr,ftype: 0.3 9999.0 2 high
taperlen: 0.05 smooth: 0 pass, 0.10 0.20 0.40 0.20 0.10, 2 Dbase: ./db/blume

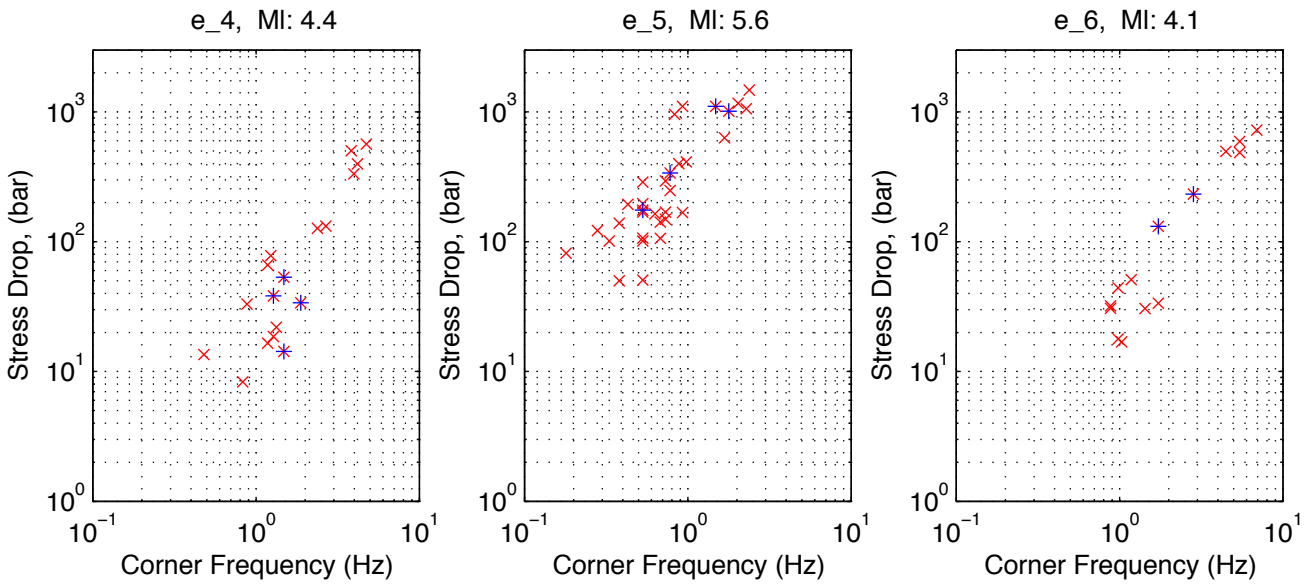

Figure 5.3.13 Blume network estimates of stress drop vs. corner frequency for the LSM mainshock and two aftershocks.
Source: SN-UCCSN-UNR-097 v. 1, Atch 2, directory kappawrap/blume2, figure in Figs_summary/event_kappas1.eps; data in file db/blume.srckappa. Stress drop=col 22, corner frequency= col 6; subset by event in col. 1, stress drop<100 MPa, squared error (col. 28)<0.151, SNRpct (col 43) >0.5; horizontal channels. Ml values from Table 5.6, sourced from Lum and Honda (1992,,1993).

Unqualified, for corroboration only. Not for use in any quality-affecting work.

Figure 5.3.14.1 Individual station plots for the Blume strong-motion network. Station LWLB. SGBDSN station LWLS is now sited where LWLB was in 1992 for these earthquakes, so only one station symbol seems to be present in (D).
Source: SN-UCCSN-UNR-097 v.1, Atch. 2, directory kappawrap/blume2/Figs_summary, file ml_vs_kcorr_40xLWLB.eps.pdf. Ml, latitude, longitude in Lum and Honda (1992, 1993; details in Tables 5.6 and 5.7) ; kappa, stress drop, corner frequency, epicentral distance in kappawrap/blume2/db, file blume.srckappa, columns 12, 22, 6, 37, and 18, respectively. Unqualified, for corroboration only; not for use in quality-affecting work.

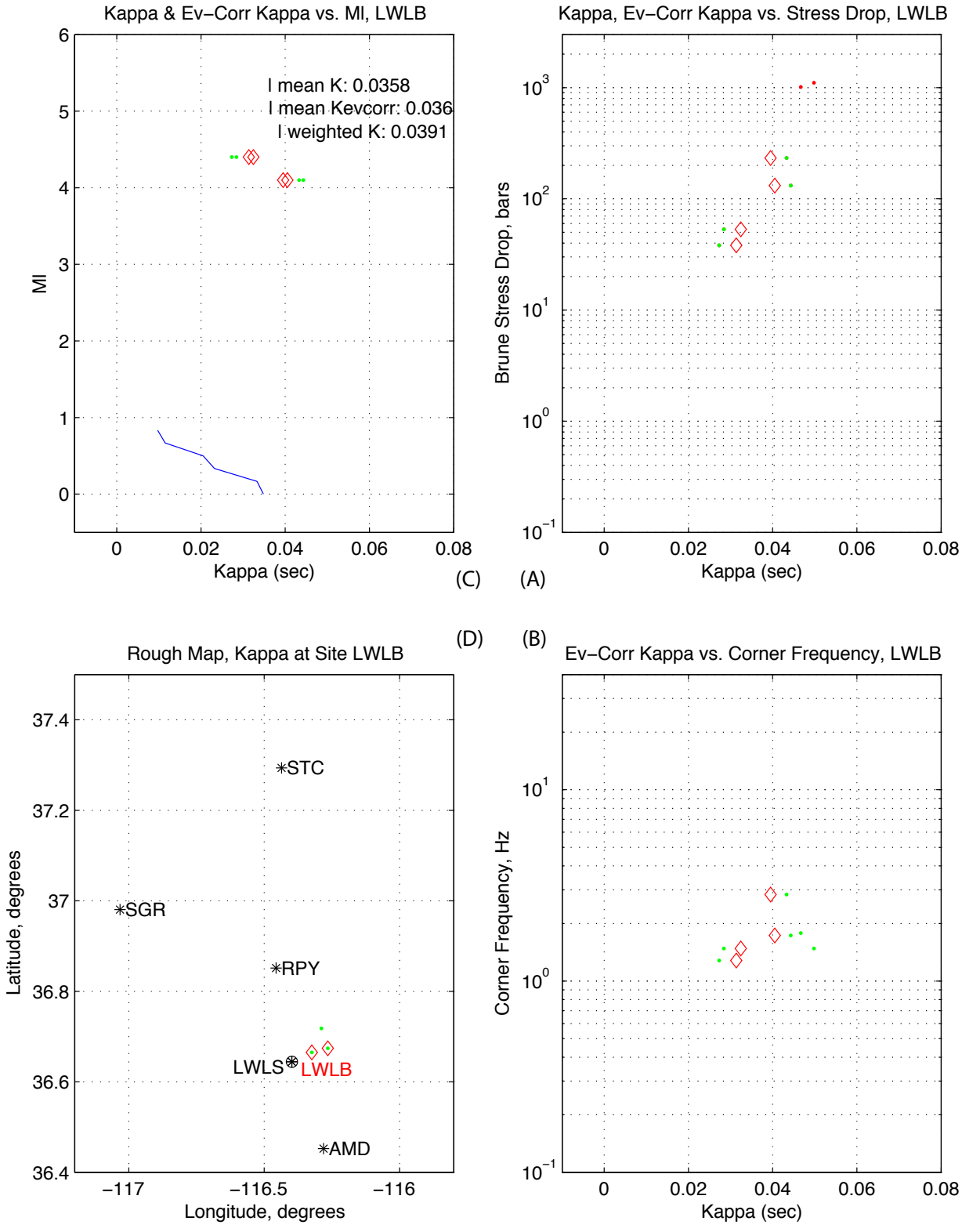

Figure 5.3.14.2 Individual station plots for the Blume strong-motion network. Station CPTB. Source: SN-UCCSN-UNR-097 v.1, Atch. 2, directory kappawrap/blume2/Figs_summary, file ml_vs_kcorr_40xCPTB.eps.pdf. Ml, latitude, longitude in Lum and Honda (1992, 1993; details in Tables 5.6 and 5.7) ; kappa, stress drop, corner frequency, epicentral distance in kappawrap/blume2/db, file blume.srckappa, columns 12, 22, 6, 37, and 18, respectively. Unqualified, for corroboration only; not for use in quality-affecting work.

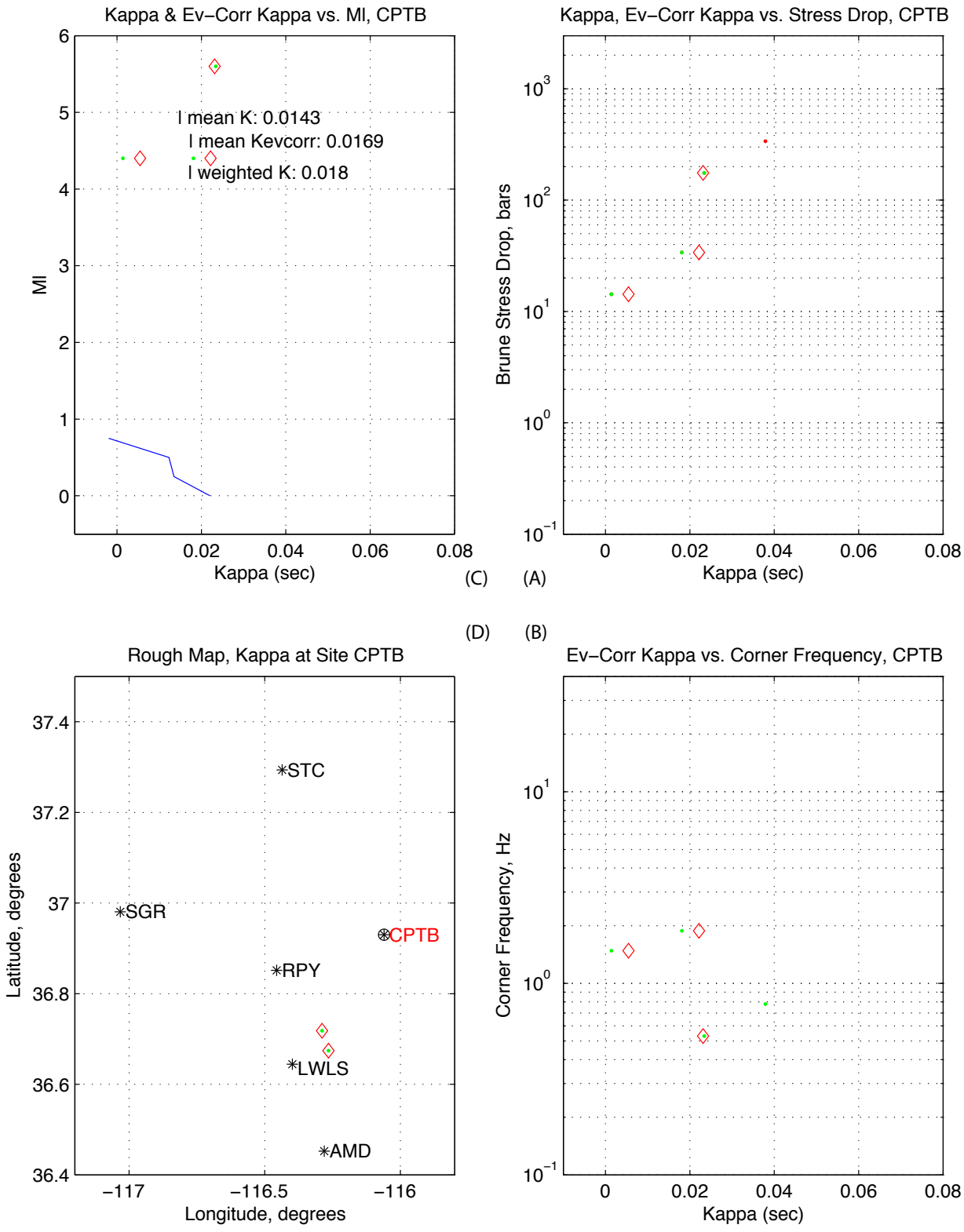

Figure 5.3.14.3 Individual station plots for the Blume strong-motion network. Station BTYB. Source: SN-UCCSN-UNR-097 v.1, Atch. 2, directory kappawrap/blume2/Figs_summary, file ml_vs_kcorr_40xBTYB.eps.pdf. Ml, latitude, longitude in Lum and Honda (1992, 1993; details in Tables 5.6 and 5.7) ; kappa, stress drop, corner frequency, epicentral distance in kappawrap/blume2/db, file blume.srckappa, columns 12, 22, 6, 37, and 18, respectively. Unqualified, for corroboration only; not for use in quality-affecting work.

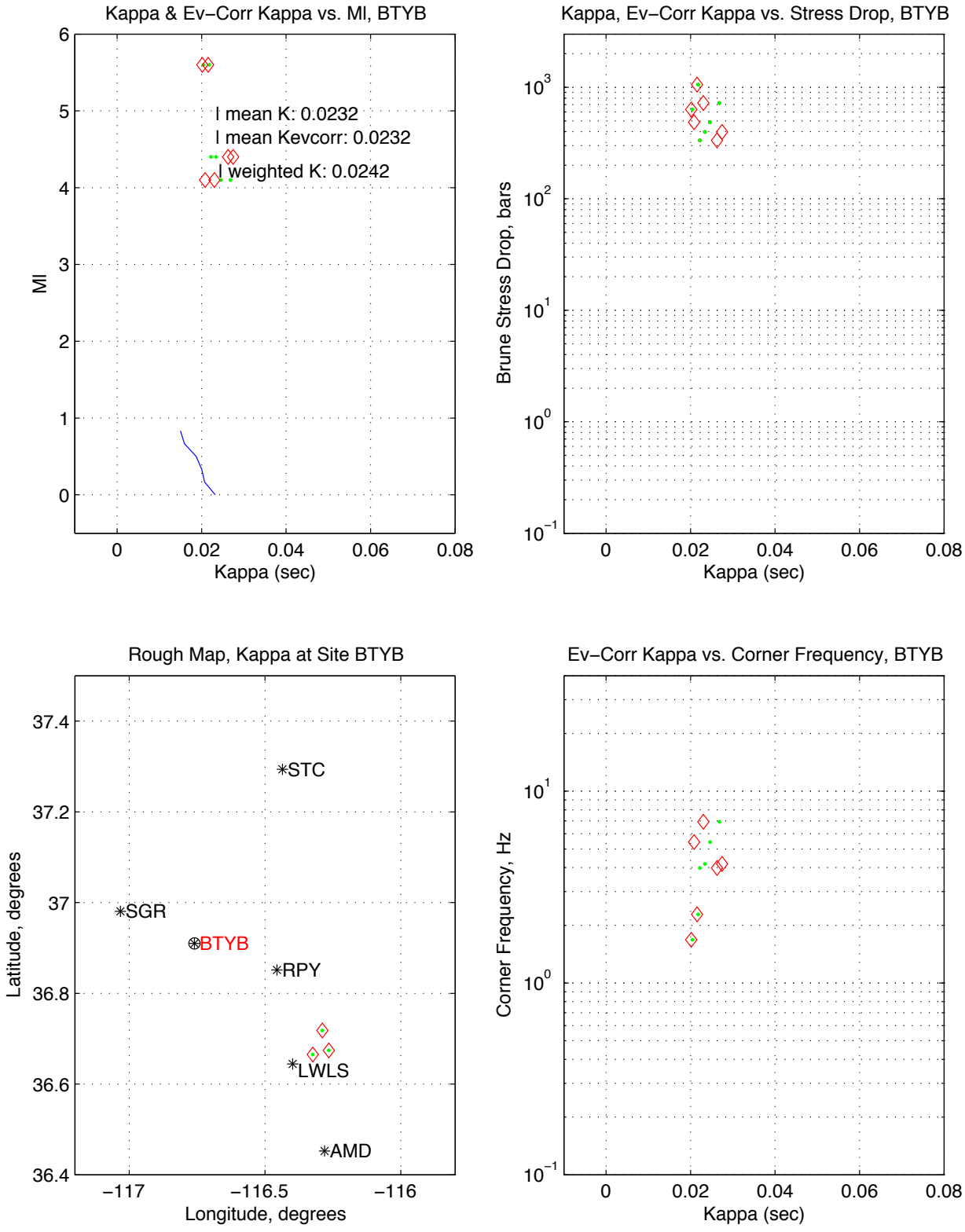

Figure 5.3.15. (Upper) Acceleration slope kappa vs. kappa from kappaAH for three events recorded by the Blume strong-motion network. The general correspondence of the two is clear, although slope kappas are approximately 15% higher. (Lower) Stress drop vs. kappa for the three Blume strong-motion network recordings.
Source: SN-UCCSN-UNR-097 v.1, Atch. 2, directory kappawrap/blume2/Figs_summary, file blume_kacc2_k.eps.pdf. Data in kappawrap/blume2/db/blume.srckappa; kappa=col 12, slope kappa=col 17 (the 5-25 Hz band estimate), and stress drop =col 22 (in MPa; bars=10*MPa). Points plotted if SNRpct (col 43)>=0.75 (i.e., good signal-to-noise) and corner frequency (col 6) >0.15 Hz (physical corner frequecies).

Unqualified, for information and corroboration only; not for use in any quality-affecting work.

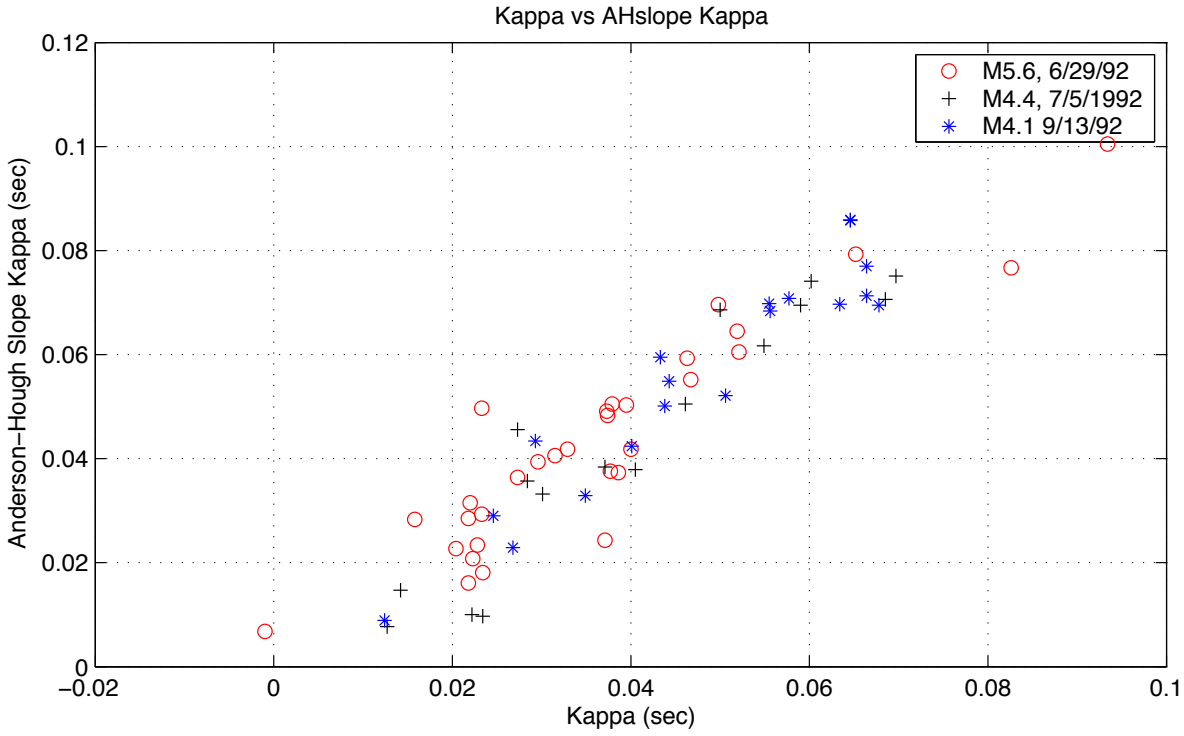

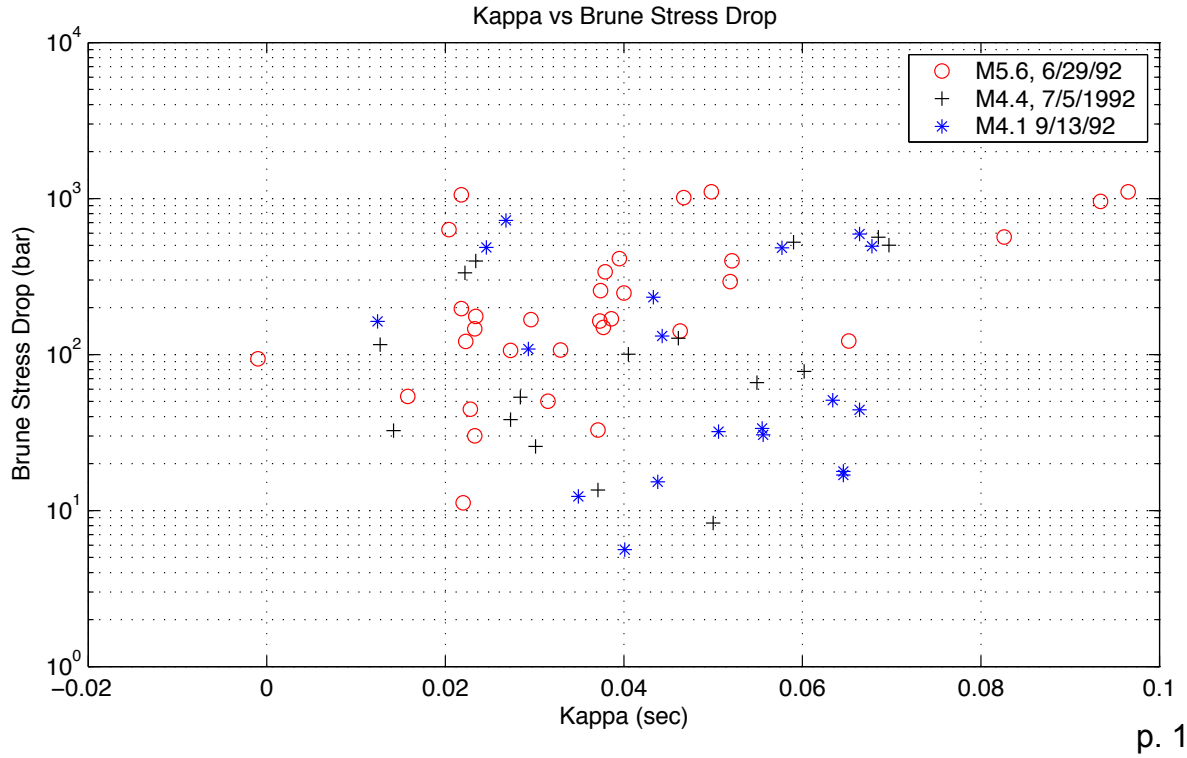

11. APPENDICES

Appendix A: Overview of the spectral fitting process

We have streamlined the calculation of *kappa* and other relevant parameters, using a *MATLAB* based program *kappaAH* (STN-UCCSN-003). The primary steps in the computational process include:

Step 1: We divide the data into manageable subsets (tens of earthquakes or a few thousand waveforms) in which each site recording has an analyst-determined S-wave arrival.

Step 2: We visually inspect the data to eliminate seismic waveforms that overprint one another. All overprinted events are removed from the analysis database.

Step 3: A set of input parameters are defined by the user to guide the computational process. Parameters include the window length for analysis, the spectral estimation method, the frequency range to fit, and the trial frequency range for spectral fitting. Table A1 provides a complete list.

Step 4: Two segments are excerpted from each waveform: one aligned on the body wave, and another sampling the pre-P noise.

Sept 5: We compute the signal-to-noise ratio for the portion of the spectrum to be fit and the percentage of the fitting window for which the signal-to-noise ratio exceeds a threshold value.

Step 6. We estimate *kappa* and M_o for all trial frequencies. Best-fitting values and their respective error limits are identified.

Step 7. We store all pertinent information in a *MATLAB* structure array as well as displaying the results graphically (Figure 5.1.3).

Step 8. Final data selection choices such as signal-to-noise ratios, error bounds, etc., are applied to select and display results. Because primary results are written to a relational database, final choices for analysis and display can be deferred.

Table A1. KappaAH input parameter list and example settings

Alphabetic list of input parameters to *MATLAB* program *kappaAH*. The particular choice parameters for any given case may vary.

Parameter	Example	Purpose/Description [Possible values]
beta	3.5e5	Assumed S-wave velocity (β) at the source (cm/s)
dbase	'lsm_8'	Database name
dbaseflag	'unr'	Seismic network Identifier [anza/unr]
dof	40	Degrees of freedom in Chi-squared test
f0hi	50.0	Maximum trial corner frequency (Hz)
f0inc	0.20	Frequency increment (Hz)
f0lo	0.2	Minimum trail corner frequency (Hz)
fslope1hi	25	Computation #1 of displacement & acceleration slope-*kappa* values: maximum frequency (Hz)
fslope1lo	5	Computation #1 of displacement & acceleration slope-*kappa* values: minimum frequency (Hz)
fslope2hi	30	Computation #2 of displacement & acceleration slope-*kappa* values: maximum frequency (Hz)
fslope2lo	10	Computation #2 of displacement & acceleration slope-*kappa* values: minimum frequency (Hz)
fthi	35.	Maximum frequency for spectrum fit (Hz)
ftlo	0.9	Minimum frequency for spectrum fit (Hz)
ftype	'high'	Type of Butterworth filter to apply
hi_corner	9999	Butterworth high frequency corner (Hz)
iddbase	'id'	Identification counter
kappaHigh	.060	Plotting range of *kappa*
kappaInc	.001	*Kappa* increment
kappaLo	-0.05	Low plotting range of *kappa*
lo_corner	0.3	Butterworth low frequency corner
magcol	'ml'	Network magnitude [*ml/mb/ms*]
Modist	1.0e5	Distance to which spectra will be normalized (cm)
mu	3.2e11	Rigidity (dyne/cm^2)
Mwintercept	16.1	Intercept of *Mo* vs. *Mw* relation
Mwslope	1.5	Slope of *Mo* vs. *Mw*
norder	2	Number of poles to use in the Butterworth filter.
nsmooth	0	Number of spectral smoothing passes (optional, assumed zero if usemultitaper = y)
nw	4	Time-bandwidth product used in the multitaper spectral method
phaseflag	'S'	Phase of interest [P/S]
postpk	4.0	data of interest: end-time in seconds after the phase

		arrival
postwf	8	Display window: end-time in seconds after the phase arrival
prepk	1.0	data of interest: start-time in seconds before the phase arrival
prewf	10	Display window: start-time in seconds before the phase arrival
radfactor	0.85	Radiation factor (Φ, Eqn 1)
rho	2.6	Assumed density at the source (ρ, Eqn 1, gm/cm^3)
sensor_correct	'y'	Apply sensor correction [Y/N]
smoothfn	[0.1 0.20 0.4 0.20 0.10]	Smoothing function coefficients
SNRmin	5	Minimum signal to noise (SNR) ratio (used only in results figures, this value can be changed in post processing)
taperlen	0.05	Cosine taper length as a fraction of data length (applies only if usemultitaper = 0)
titlestring	'ANZA: Toro at PFO (M>1)'	Identification title
type	1	Instrument type (γ in Eqn. 2) Used only if database does not indicate type. 2 == acceleration 1 == velocity 0 == displacement
usefilter	'y'	Preprocessing Butterworth filter [Y/N]. Note the Butterworth filter's main purpose is to remove low frequency 'noise' for small earthquakes.
usemultitaper	'y'	Y == multitaper N == FFT

Appendix B: Station summary plots showing horizontal component fitting results.

QA: Qualified.

Results here are from *case6a*, *kappaAH* analysis of SGBDSN station data. In DID 006GB.003, see kappawrap/case6a/Figs45. Stations are listed alphabetically in files that begin with the station code. Fixed stress-drop version has "fixed" in the filename.

Results were generated directly by *kappaAH* macro *byevent9* are included alphabetically by station. These figures reflect subsets implemented in *kappaAH v.1* macro *getgood2*. They include requiring horizontal channels only, corner frequency bounded at the 95% level below 45 Hz and a signal-to-noise ratio of 5:1 over 90% of the spectral fitting band from 0.9 to 35 Hz. Trial corner frequencies extended to 50 Hz. Stress drops over 5000 bars were also excluded, but this subset did not exclude any fits passed by the previous filters. The plots in Appendix B explore the constrained corner frequency subset and were used to decide how to develop best estimates. A second set of figures is included with each station that shows what other parameters would result if the stress drop is constrained to 45 bars. The value of 45 bars was chosen to be near the 47 bar average adopted for the Little Skull Mountain earthquake for use in the Yucca Mountain Probabilistic Seismic Hazard Analysis. Fixed stress drop cases of 30 and 60 bars were also developed, but are not included because it does not appear that fixing the stress drop materially improves our understanding of *kappa* or other parameters. They may be viewed on Electronic Supplement 2 of Scientific Notebook SN-UCCSN-UNR-097, v.1, files kappawrap/case6a/Figs30 and Figs60.

Caption and Discussion, Appendix B Figures:

In each plot, the *upper-left* panel shows corner frequency versus *kappa*. Trends toward higher *kappa* with increasing stress drop would be diagnostic of numerical artifacts in the spectral fitting phase. Stress drop is plotted versus corner frequency in the *middle-right* panel. Stress drops above a few hundred bars are rare in this set. The two panels together show that corner frequencies are rarely above ~8 Hz, and that the majority of measurements are obtained from corner frequencies smaller than about ~6 Hz. The fixed stress drop station plots have a predictably smaller range of corner frequencies. Site median *kappa* estimates (second title line) may increase or decrease if the stress drop is fixed, with the change typically being by 5-15 msec.

Stress drop $\Delta\sigma$ is plotted versus *kappa* in the *upper-right* panels. Some stations show a modest linear trend in $\Delta\sigma$ vs. *kappa*. Stress drop $\Delta\sigma \sim M_o f_c^3$, and linear trends have a slope of about 3 where they are present, so a trade-off of *kappa* with corner frequency is suggested. Usually, however, the corresponding trend in f_c vs. *kappa* (*upper-left)* is weak or absent, however. For the present, the cause of linear trends in $\Delta\sigma$ vs. f_c is not known.

The *middle-left* plot of moment vs. *kappa* and *lower-left* plot of network magnitude vs. *kappa* explore the magnitude dependence of *kappa*. A weak dependence could be expected

since larger earthquakes are well recorded to a greater distance, and they tend to lose high frequencies (increase in *kappa*) with distance. On the whole, however, *kappa* is not a function of moment or magnitude in the present data. Fixed stress drop plots show a greater central tendency in *kappa*.

In the *lower-right kappa* is plotted versus epicentral and hypocentral distance. Both distances are plotted because each have been used in interpretations pertaining to Yucca Mountain (Biasi and Smith, 2001 used epicentral distance; Su et al., 1996, used hypocentral). This plot gives one the opportunity to assess the consequences of distance correction κ_r. A correction of 0.0005 sec/km, similar to that used by Anderson and Su (MOL.20071203.0134), would lead to a decrease in *kappa* of 10 msec over 20 km. For many sites, however, the data are approximately consistent with a constant *kappa* out to 30-40 km, and increase at an inconsistent rate at greater distances. The formal inversion model estimates a single term from this data and applies it to all stations, either as a linear trend (model 4) or a bi-linear trend (model 9). Distance corrections were too inconsistent and often had the effect of contradicting *kappa* estimates from nearby earthquakes, and thus were not applied to the preferred *kappa* estimates.

Station summary estimates of *kappa*, stress drop, and corner frequency are shown in the second and third lines of the title block. Median values include events from all distances and should be treated with caution.

Figure B 1. Station AL5 parametric plot. Free stress drop.
Source: DID 006GB.003, directory kappawrap/case6a/Figs45
File AL5.85170_87586.NE.eps

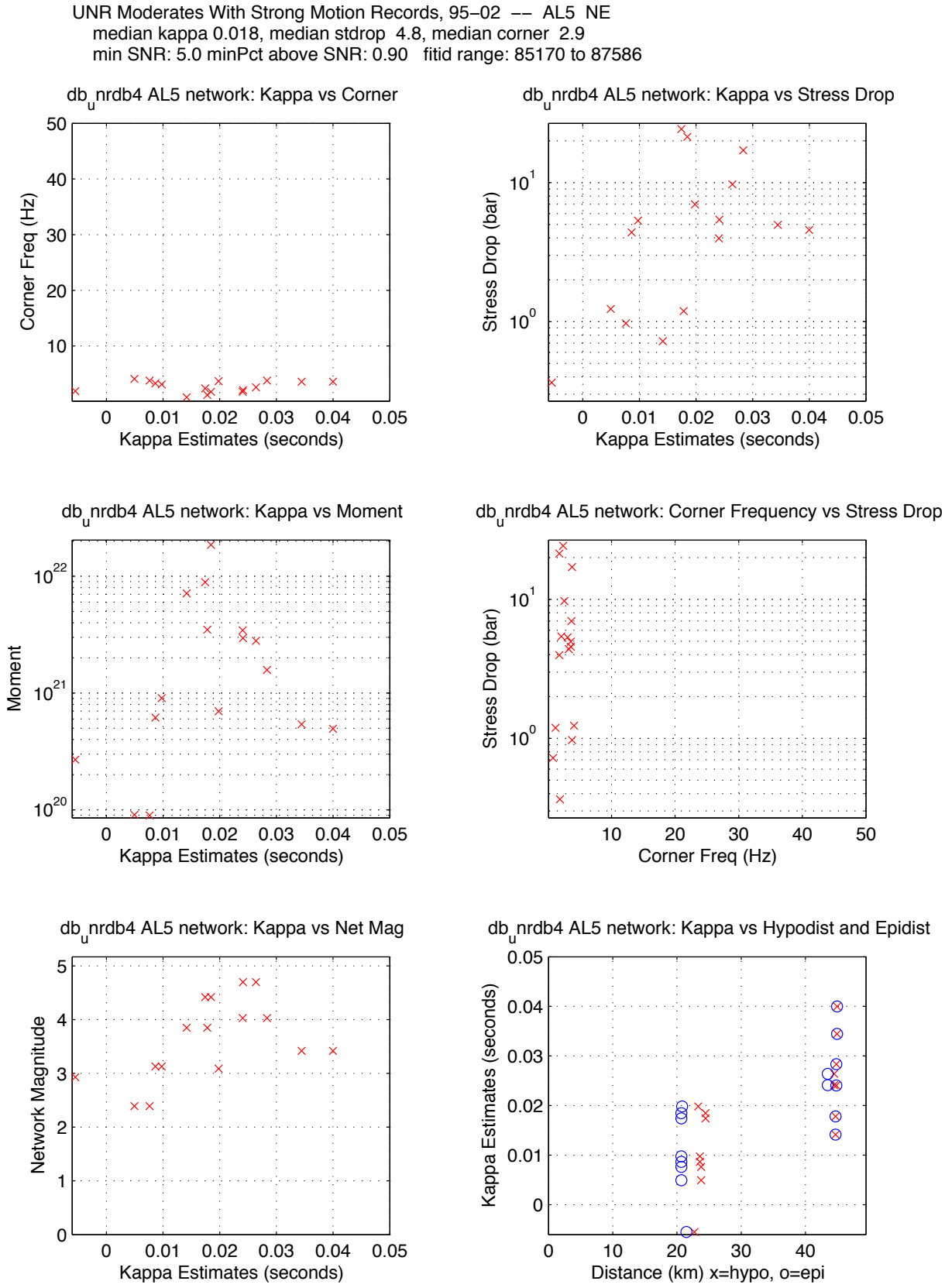

AL5:NE Passing: 16, Fail SNR: < 5 in 0.9 of freq range = 2, Fail SqErr: > 0.3 = 1, Fail StDrop: > 5000 = 0
AL5:NE Fail High Corner: > 45 Hz = 2

Figure B 2. Station AL5 parametric plot. Fixed stress drop.
Source: DID 006GB.003, directory kappawrap/case6a/Figs45
File AL5.85170_87586.NE.fixed.eps

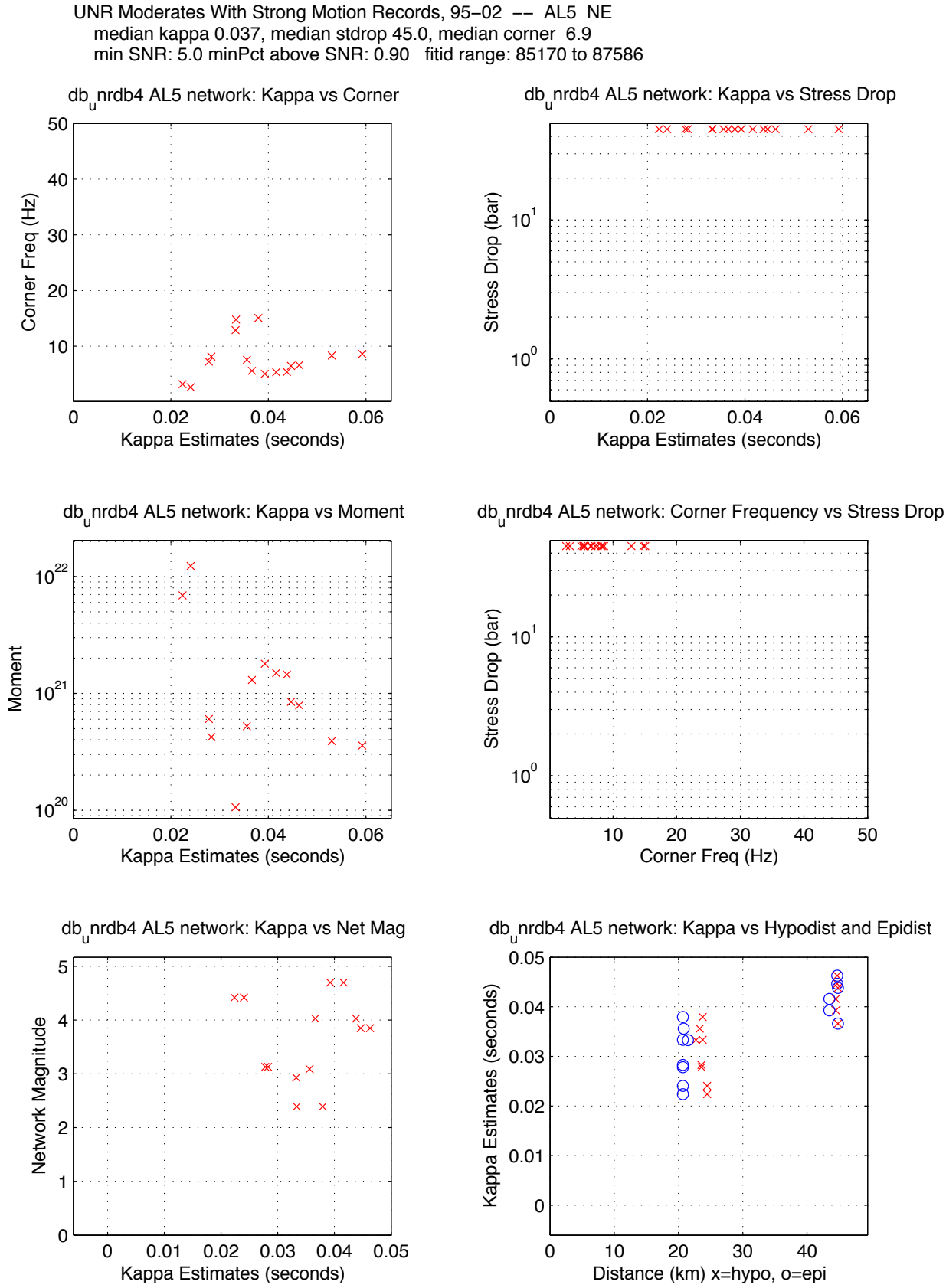

AL5:NE Passing: 16, Fail SNR: < 5 in 0.9 of freq range = 2, Fail SqErr: > 0.3 = 1, Fail StDrop: > 5000 = 0
AL5:NE Fail High Corner: > 45 Hz = 2

Figure B 3. Station AMD parametric plot. Free stress drop.
Source: DID 006GB.003, directory kappawrap/case6a/Figs45
File AMD.85170_87586.NE.eps

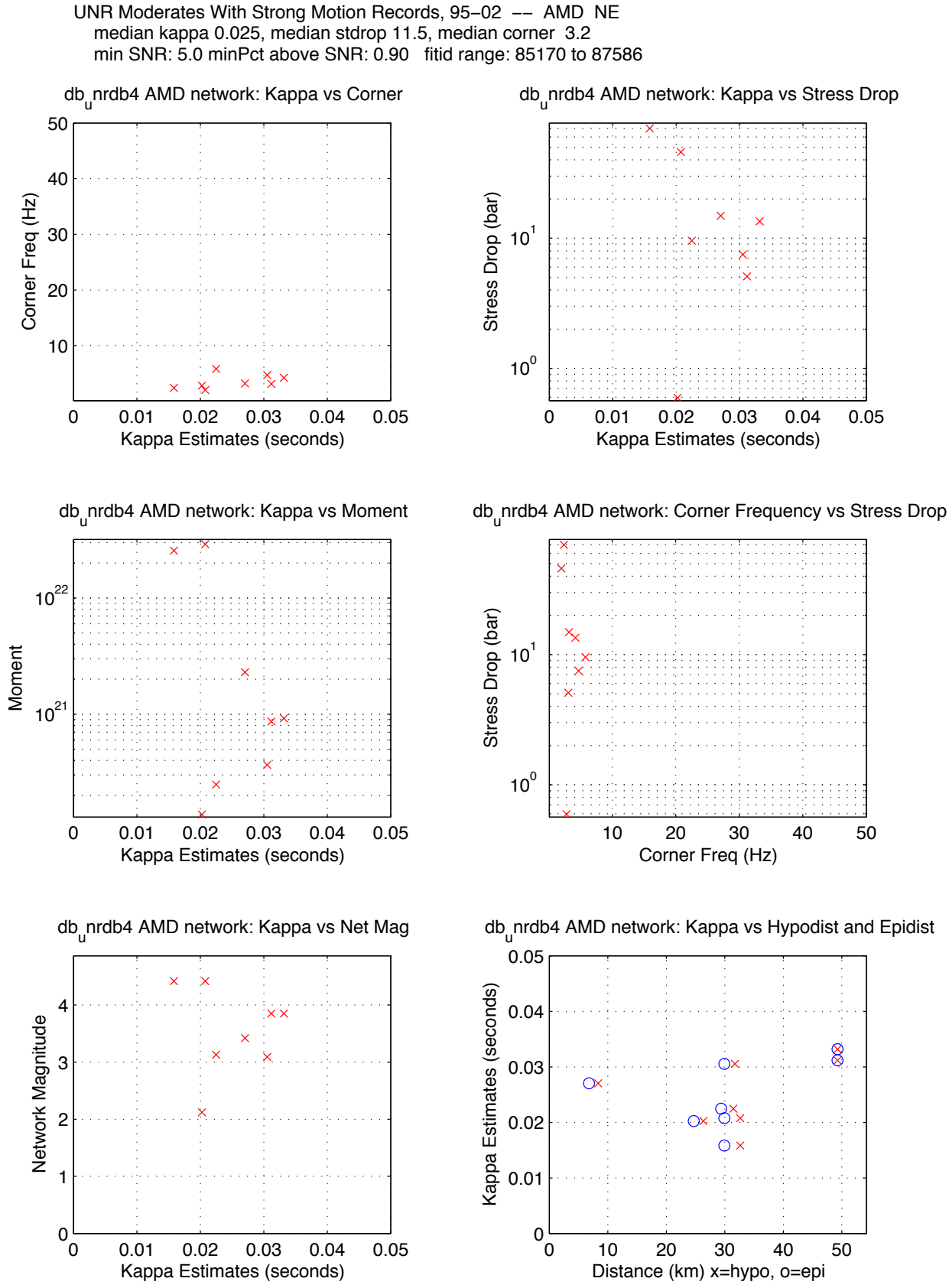

AMD:NE Passing: 8, Fail SNR: < 5 in 0.9 of freq range = 0, Fail SqErr: > 0.3 = 0, Fail StDrop: > 5000 = 0
AMD:NE Fail High Corner: > 45 Hz = 1

Figure B 4. Station AMD parametric plot. Fixed stress drop.
Source: DID 006GB.003, directory kappawrap/case6a/Figs45
File AMD.85170_87586.NE.fixed.eps

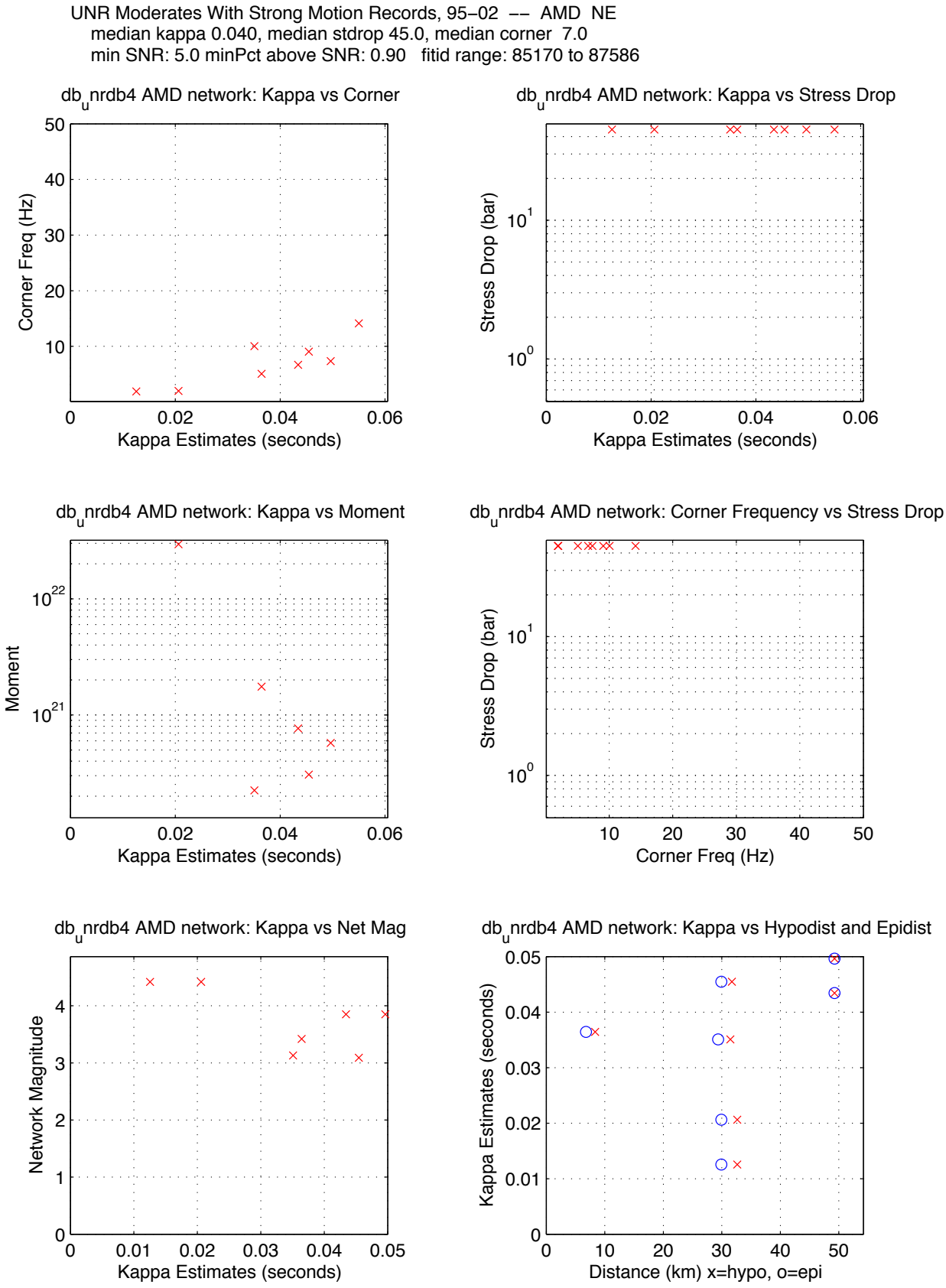

AMD:NE Passing: 8, Fail SNR: < 5 in 0.9 of freq range = 0, Fail SqErr: > 0.3 = 0, Fail StDrop: > 5000 = 0
AMD:NE Fail High Corner: > 45 Hz = 1

Figure B 5. Station BTW parametric plot. Free stress drop.
Source: DID 006GB.003, directory kappawrap/case6a/Figs45
File BTW.85170_87586.NE.eps

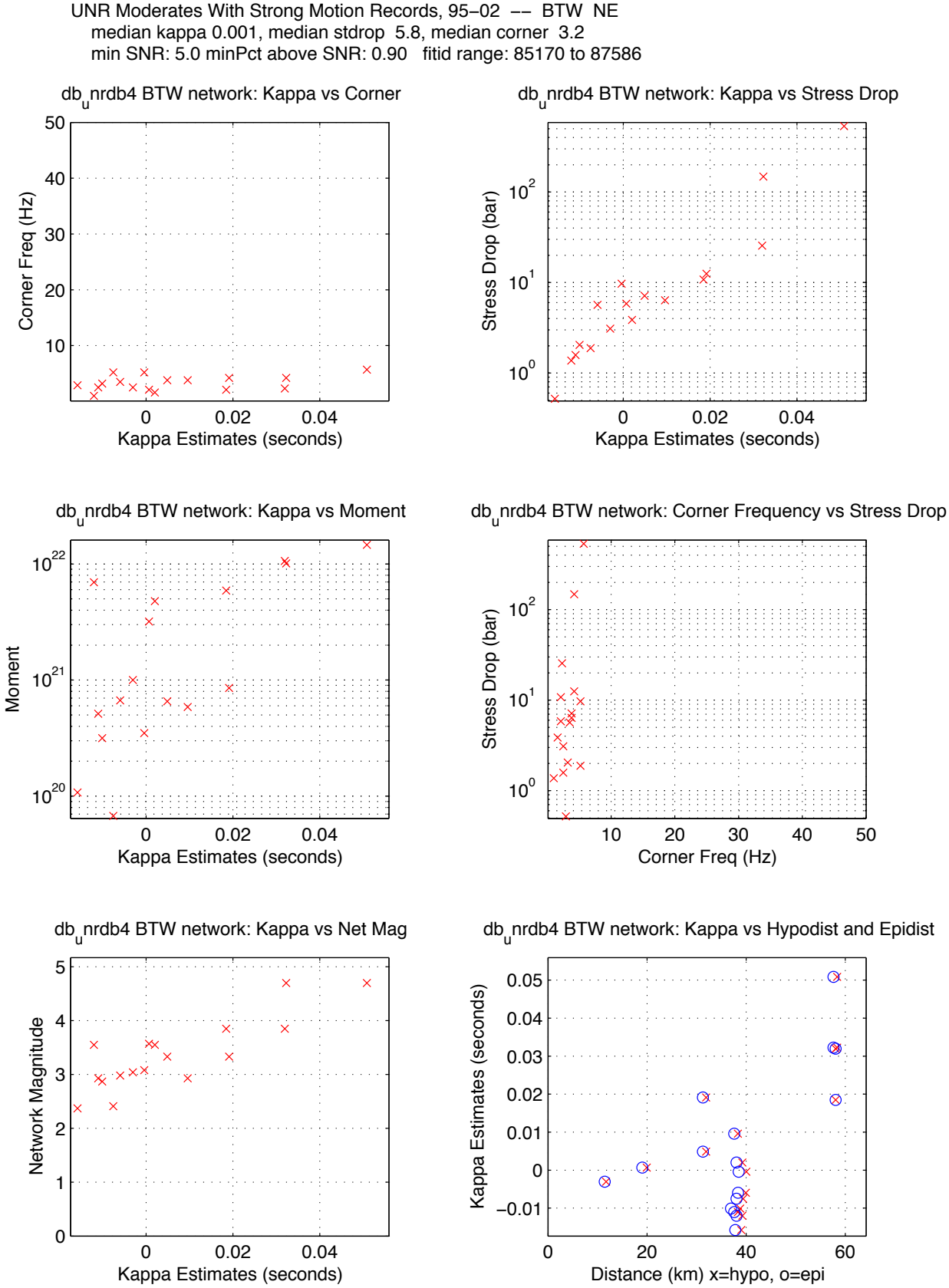

BTW:NE Passing: 17, Fail SNR: < 5 in 0.9 of freq range = 0, Fail SqErr: > 0.3 = 0, Fail StDrop: > 5000 = 0
BTW:NE Fail High Corner: > 45 Hz = 7

Figure B 6. Station BTW parametric plot. Free stress drop.
Source: DID 006GB.003, directory kappawrap/case6a/Figs45
File BTW.85170_87586.NE.eps

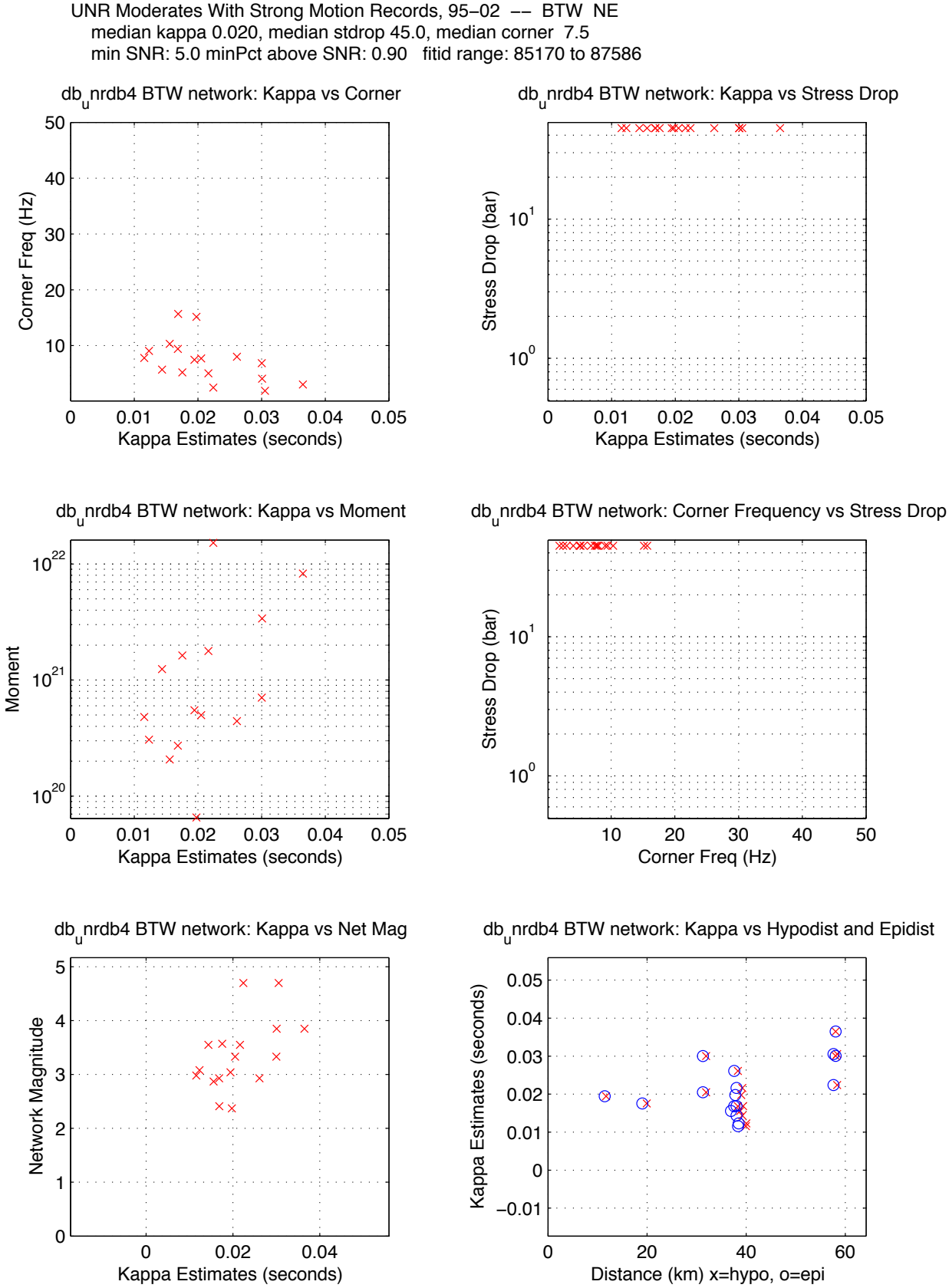

BTW:NE Passing: 17, Fail SNR: < 5 in 0.9 of freq range = 0, Fail SqErr: > 0.3 = 0, Fail StDrop: > 5000 = 0
BTW:NE Fail High Corner: > 45 Hz = 7

Figure B 7. Station BYMS parametric plot. Free stress drop.
Source: DID 006GB.003, directory kappawrap/case6a/Figs45
File BYMS.85170_87586.NE.eps

UNR Moderates With Strong Motion Records, 95–02 –– BYMS NE
median kappa 0.024, median stdrop 34.6, median corner 3.7
min SNR: 5.0 minPct above SNR: 0.90 fitid range: 85170 to 87586

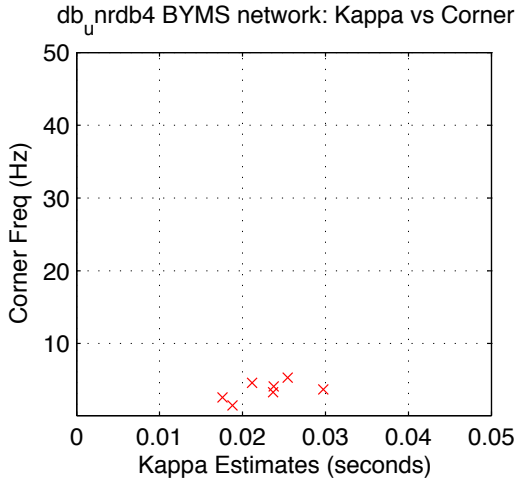

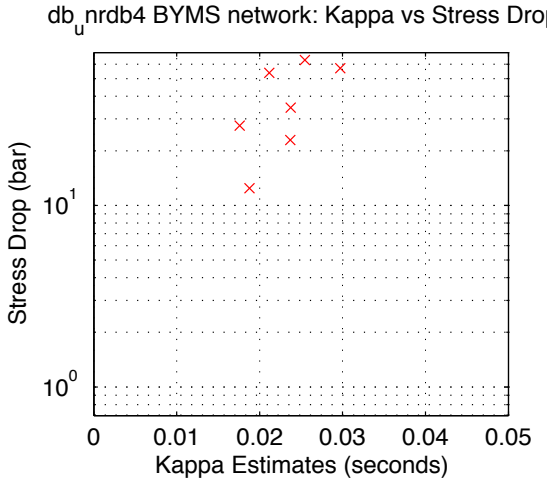

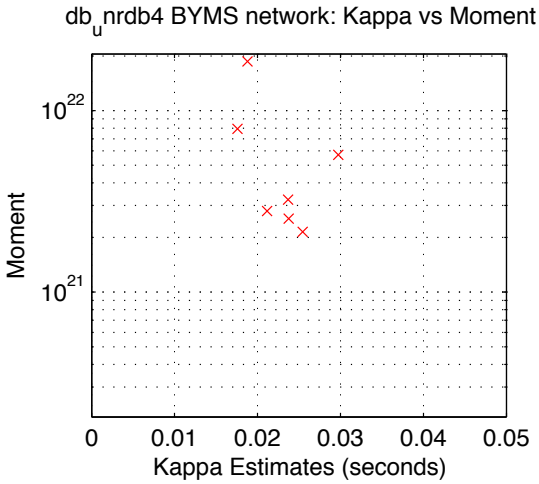

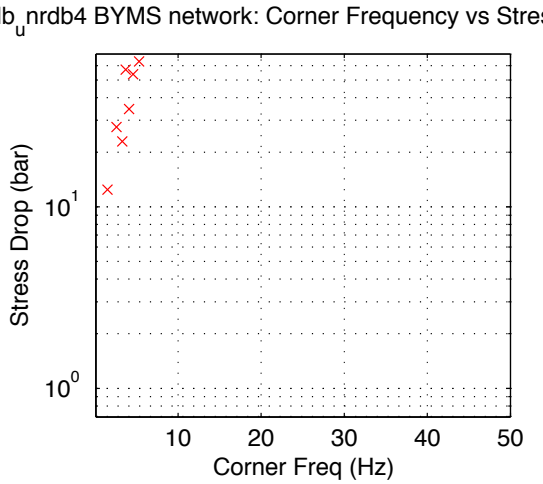

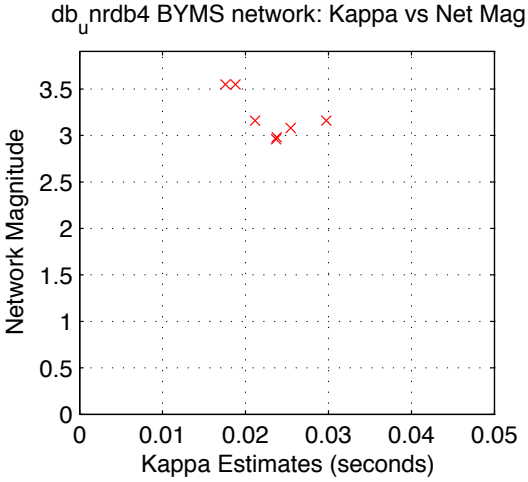

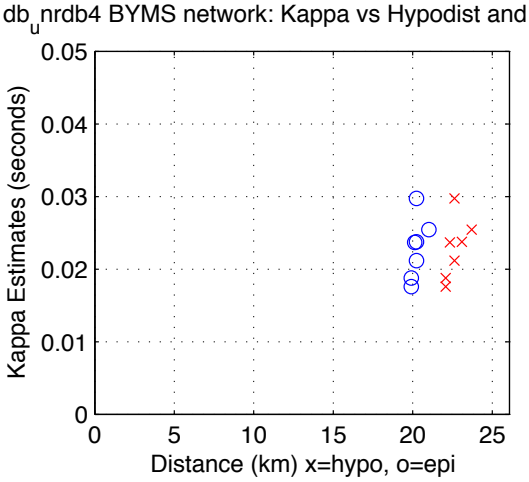

BYMS:NE Passing: 7, Fail SNR: < 5 in 0.9 of freq range = 15, Fail SqErr: > 0.3 = 0, Fail StDrop: > 5000 = 0
BYMS:NE Fail High Corner: > 45 Hz = 0

Figure B 8. Station BYMS parametric plot. Fixed stress drop.
Source: DID 006GB.003, directory kappawrap/case6a/Figs45
File BYMS.85170_87586.NE.fixed.eps

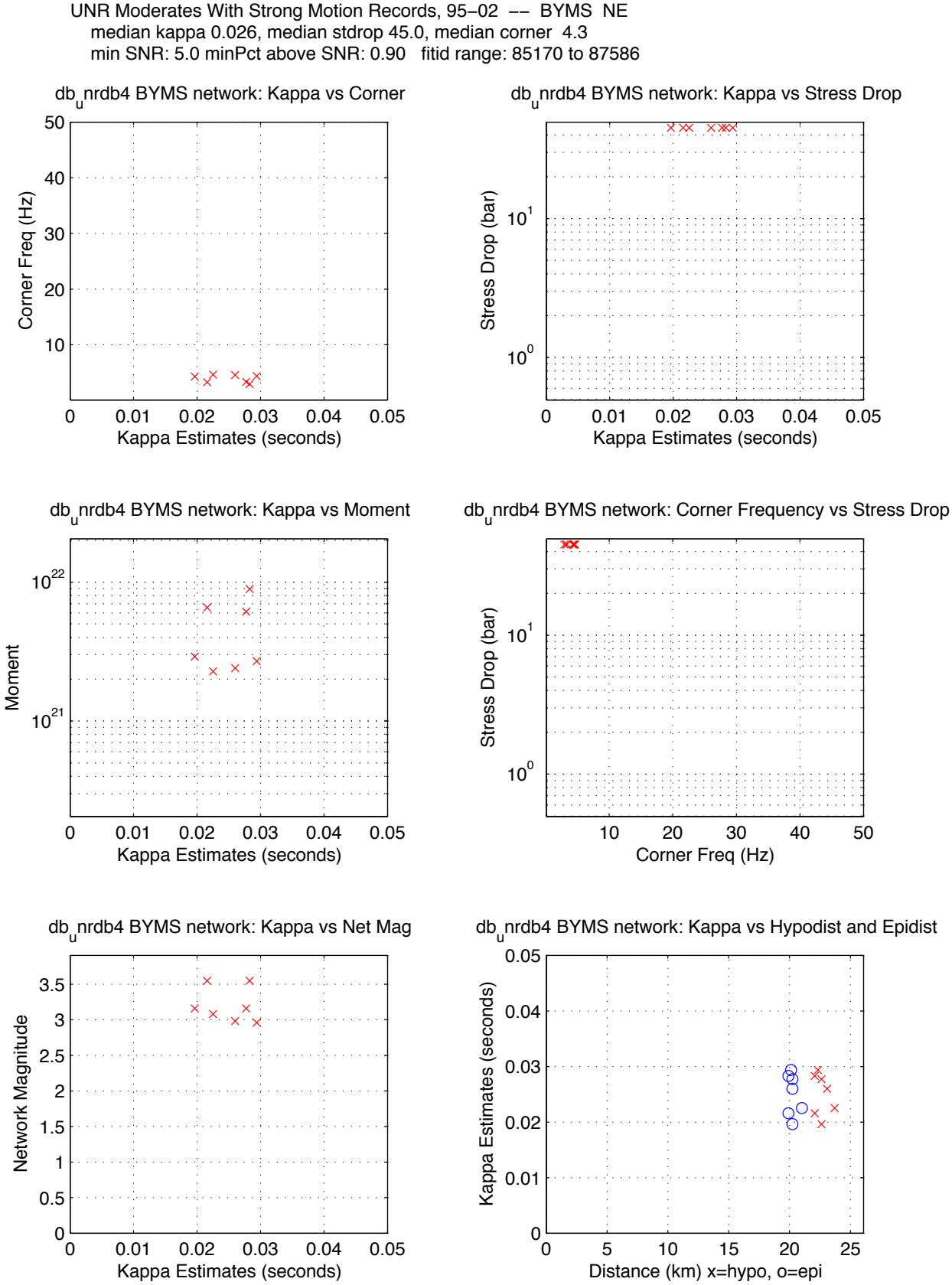

BYMS:NE Passing: 7, Fail SNR: < 5 in 0.9 of freq range = 15, Fail SqErr: > 0.3 = 0, Fail StDrop: > 5000 = 0
BYMS:NE Fail High Corner: > 45 Hz = 0

Figure B 9. Station CAF parametric plot. Free stress drop.
Source: DID 006GB.003, directory kappawrap/case6a/Figs45
File CAF.85170_87586.NE.eps

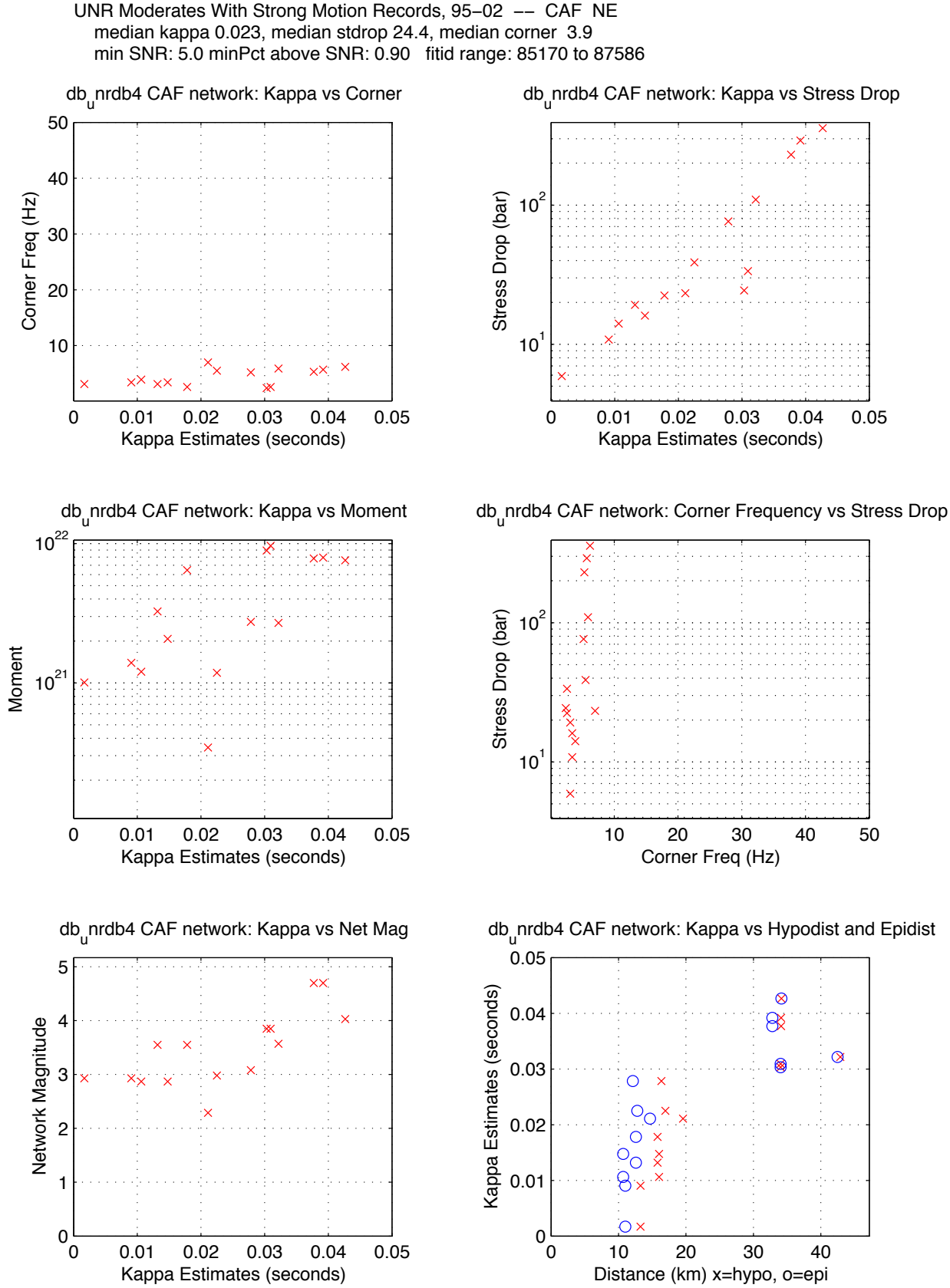

CAF:NE Passing: 15, Fail SNR: < 5 in 0.9 of freq range = 0, Fail SqErr: > 0.3 = 0, Fail StDrop: > 5000 = 0
CAF:NE Fail High Corner: > 45 Hz = 8

Figure B 10. Station CAF parametric plot. Fixed stress drop.
Source: DID 006GB.003, directory kappawrap/case6a/Figs45
File CAF.85170_87586.NE.fixed.eps

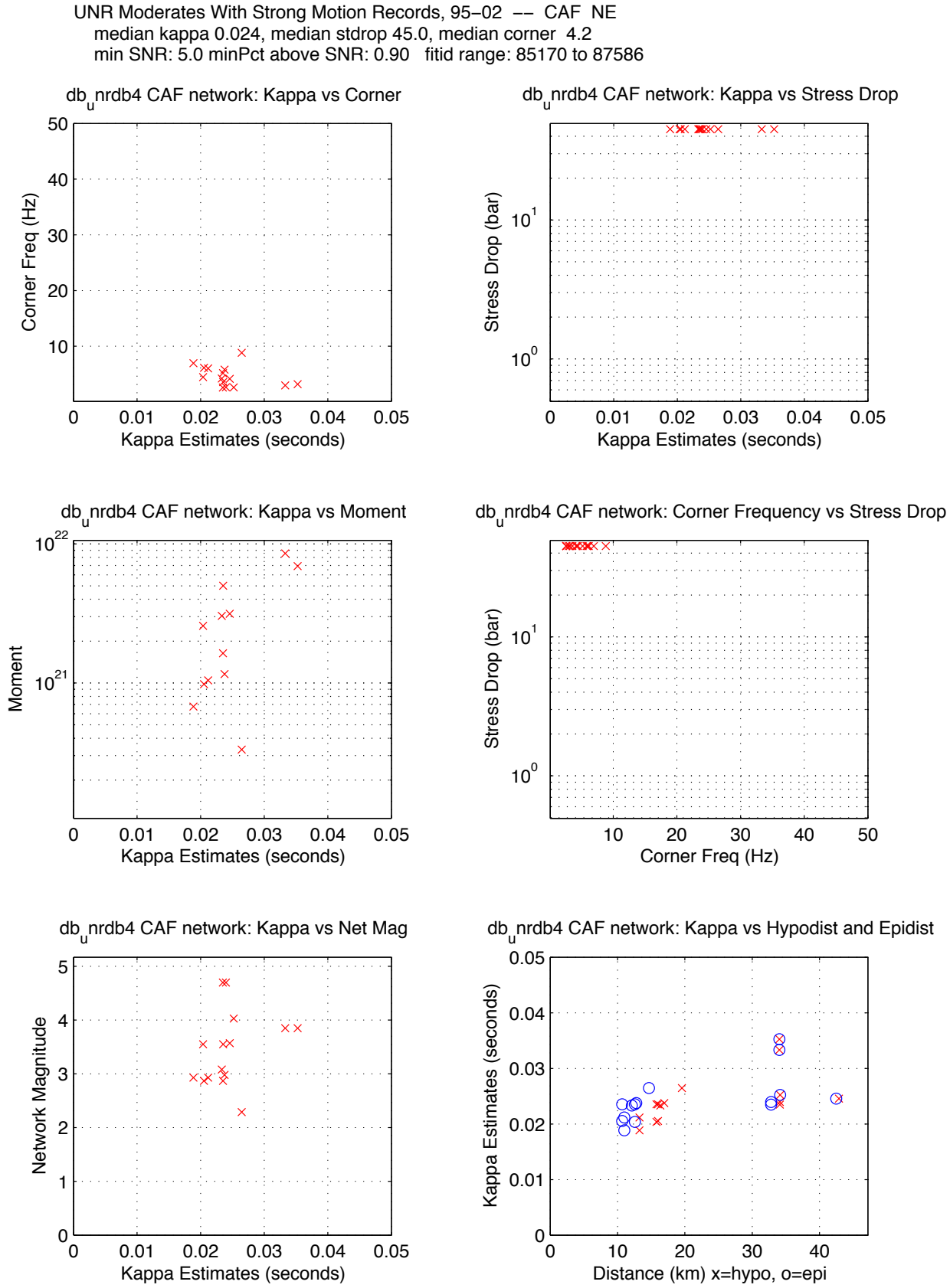

CAF:NE Passing: 15, Fail SNR: < 5 in 0.9 of freq range = 0, Fail SqErr: > 0.3 = 0, Fail StDrop: > 5000 = 0
CAF:NE Fail High Corner: > 45 Hz = 8

Figure B 11. Station CRF parametric plot. Free stress drop.
Source: DID 006GB.003, directory kappawrap/case6a/Figs45
File CRF.85170_87586.NE.eps

UNR Moderates With Strong Motion Records, 95–02 –– CRF NE
median kappa 0.030, median stdrop 6.3, median corner 3.5
min SNR: 5.0 minPct above SNR: 0.90 fitid range: 85170 to 87586

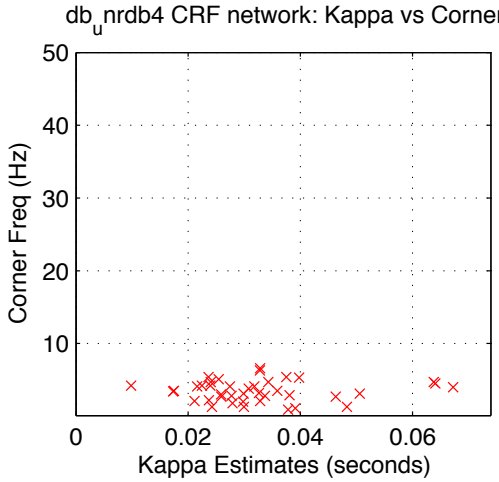

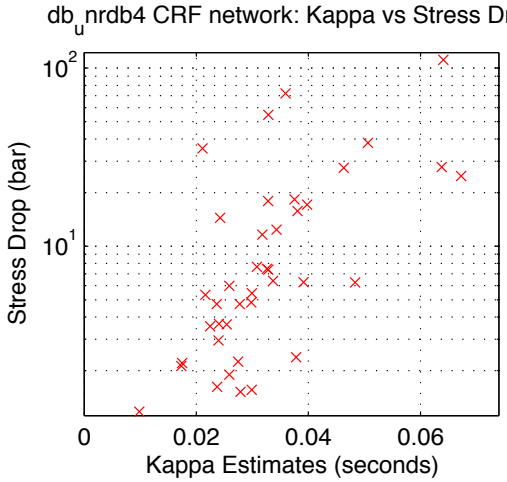

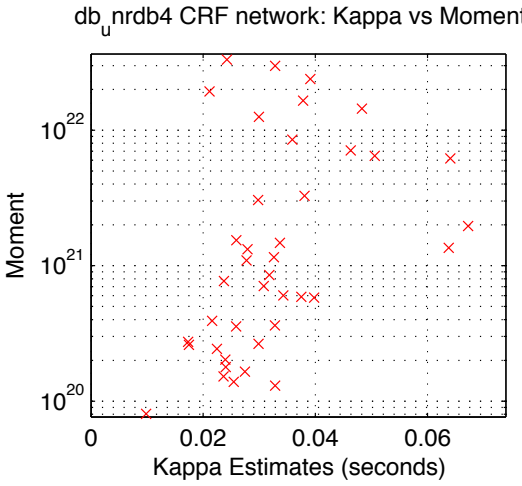

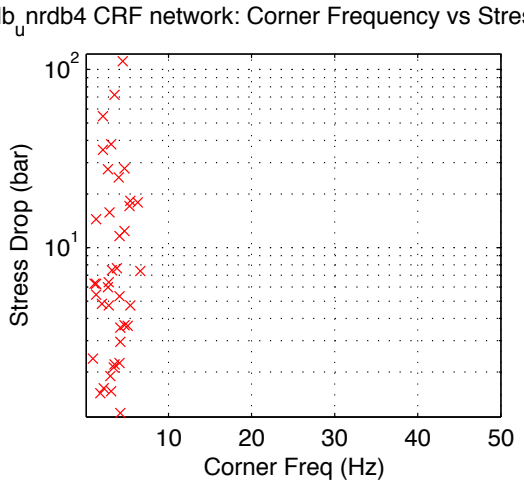

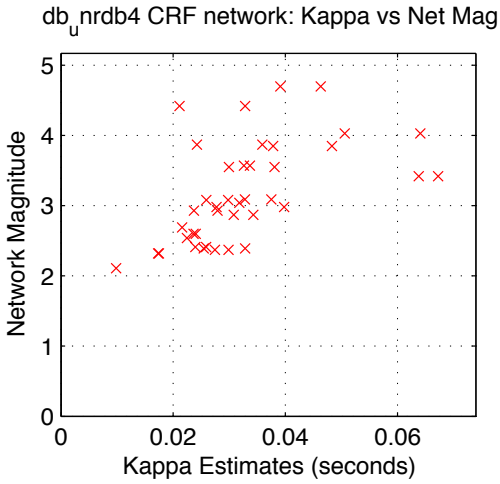

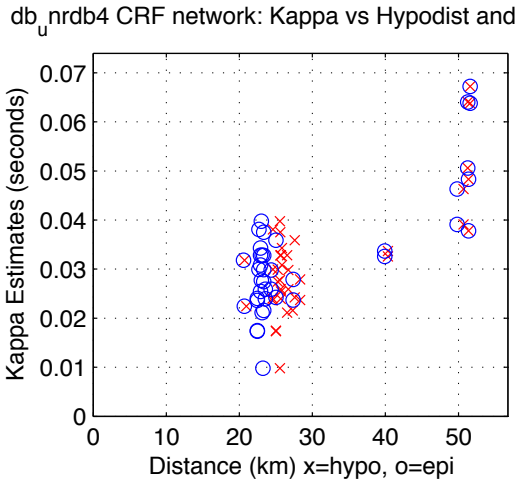

CRF:NE Passing: 40, Fail SNR: < 5 in 0.9 of freq range = 2, Fail SqErr: > 0.3 = 0, Fail StDrop: > 5000 = 0
CRF:NE Fail High Corner: > 45 Hz = 1

Figure B 12. Station CRF parametric plot. Fixed stress drop.
Source: DID 006GB.003, directory kappawrap/case6a/Figs45
File CRF.85170_87586.NE.fixed.eps

UNR Moderates With Strong Motion Records, 95–02 –– CRF NE
median kappa 0.046, median stdrop 45.0, median corner 7.2
min SNR: 5.0 minPct above SNR: 0.90 fitid range: 85170 to 87586

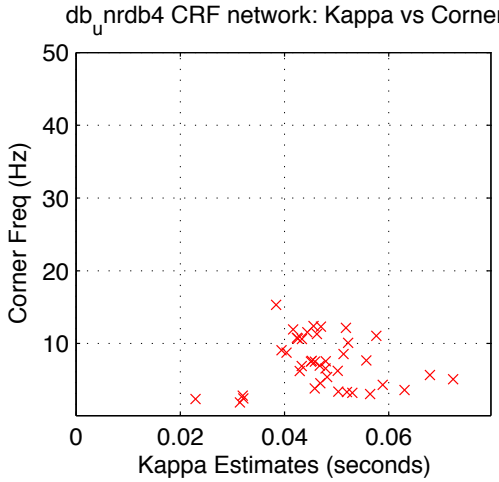

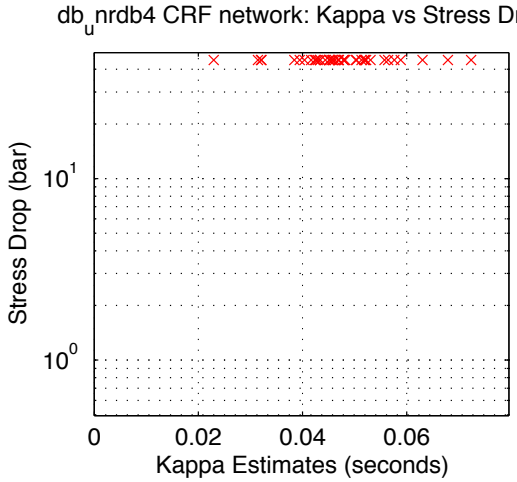

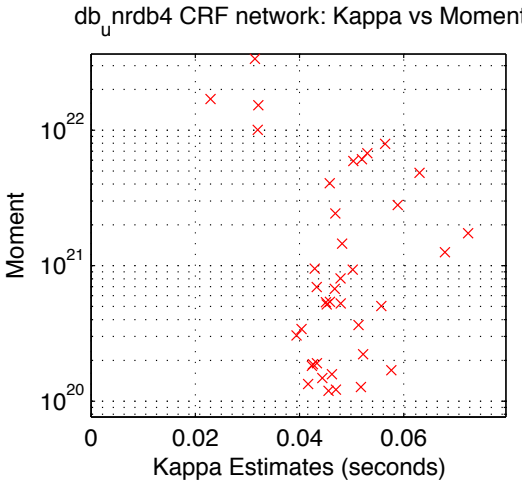

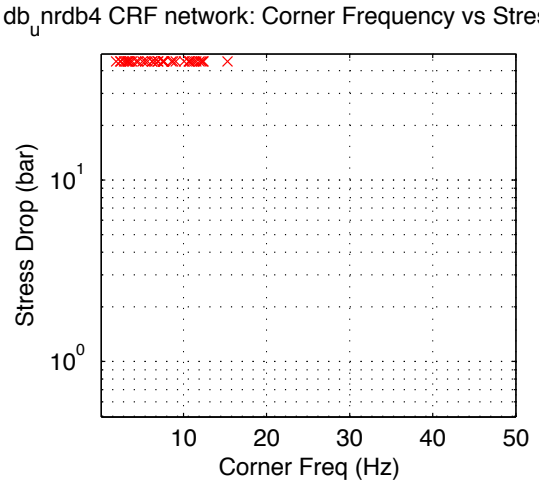

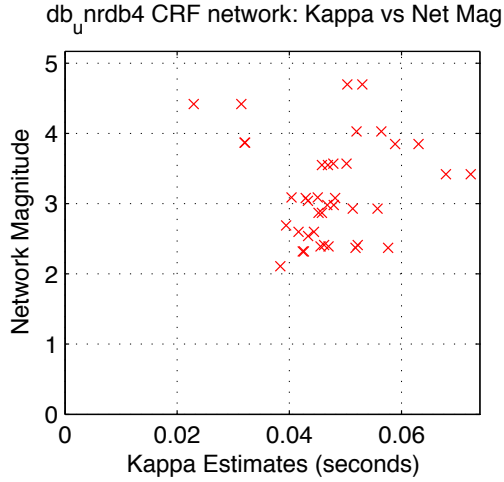

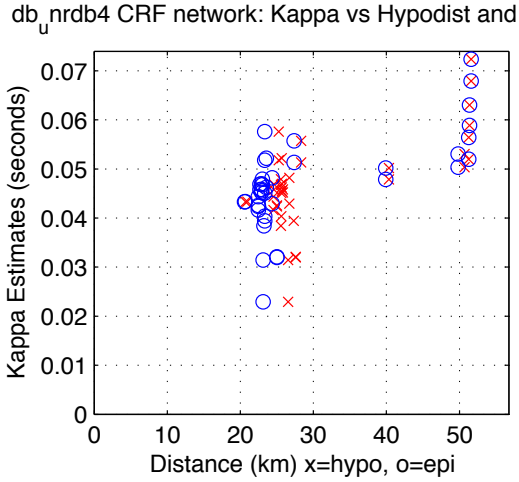

CRF:NE Passing: 40, Fail SNR: < 5 in 0.9 of freq range = 2, Fail SqErr: > 0.3 = 0, Fail StDrop: > 5000 = 0
CRF:NE Fail High Corner: > 45 Hz = 1

Figure B 13. Station DOM parametric plot. Free stress drop.
Source: DID 006GB.003, directory kappawrap/case6a/Figs45
File DOM.85170_87586.NE.eps

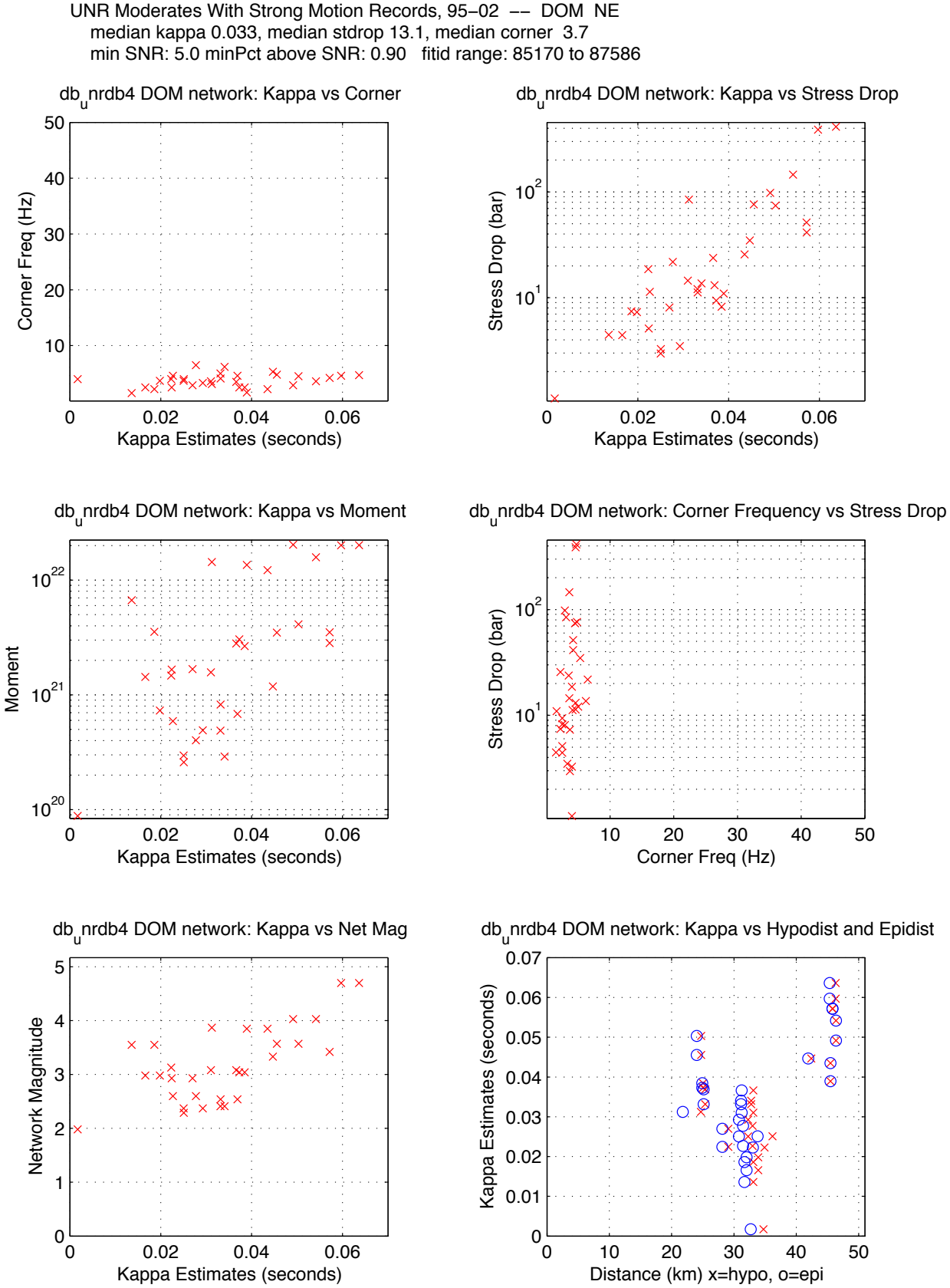

DOM:NE Passing: 33, Fail SNR: < 5 in 0.9 of freq range = 0, Fail SqErr: > 0.3 = 0, Fail StDrop: > 5000 = 0
DOM:NE Fail High Corner: > 45 Hz = 3

Figure B 14. Station DOM parametric plot. Fixed stress drop.
Source: DID 006GB.003, directory kappawrap/case6a/Figs45
File DOM.85170_87586.NE.fixed.eps

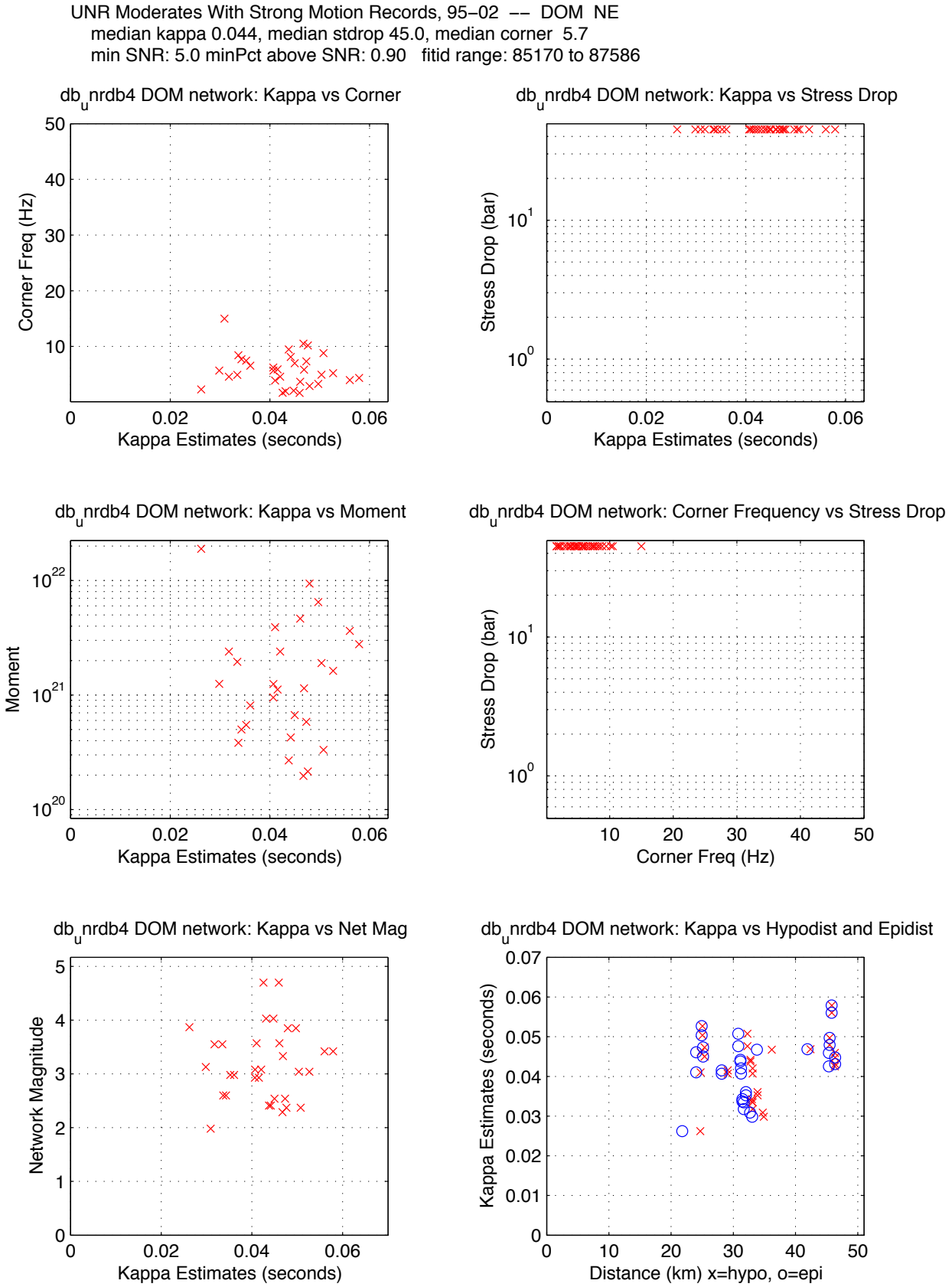

DOM:NE Passing: 33, Fail SNR: < 5 in 0.9 of freq range = 0, Fail SqErr: > 0.3 = 0, Fail StDrop: > 5000 = 0
DOM:NE Fail High Corner: > 45 Hz = 3

Figure B 15. Station EXHS parametric plot. Free stress drop.
Source: DID 006GB.003, directory kappawrap/case6a/Figs45
File EXHS.85170_87586.NE.eps

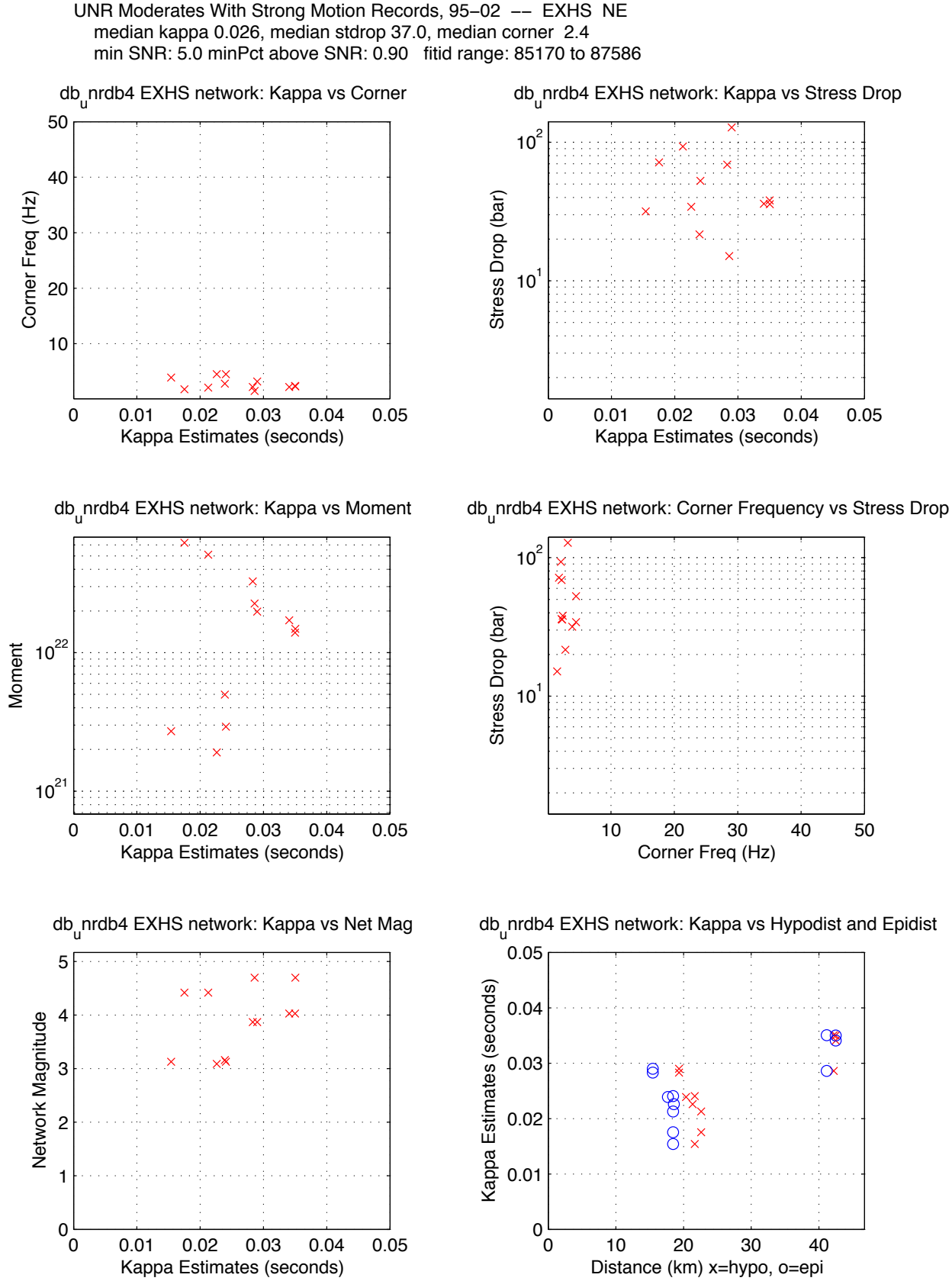

EXHS:NE Passing: 12, Fail SNR: < 5 in 0.9 of freq range = 0, Fail SqErr: > 0.3 = 0, Fail StDrop: > 5000 = 0
EXHS:NE Fail High Corner: > 45 Hz = 0

Figure B 16. Station EXHS parametric plot. Fixed stress drop.
Source: DID 006GB.003, directory kappawrap/case6a/Figs45
File EXHS.85170_87586.NE.fixed.eps

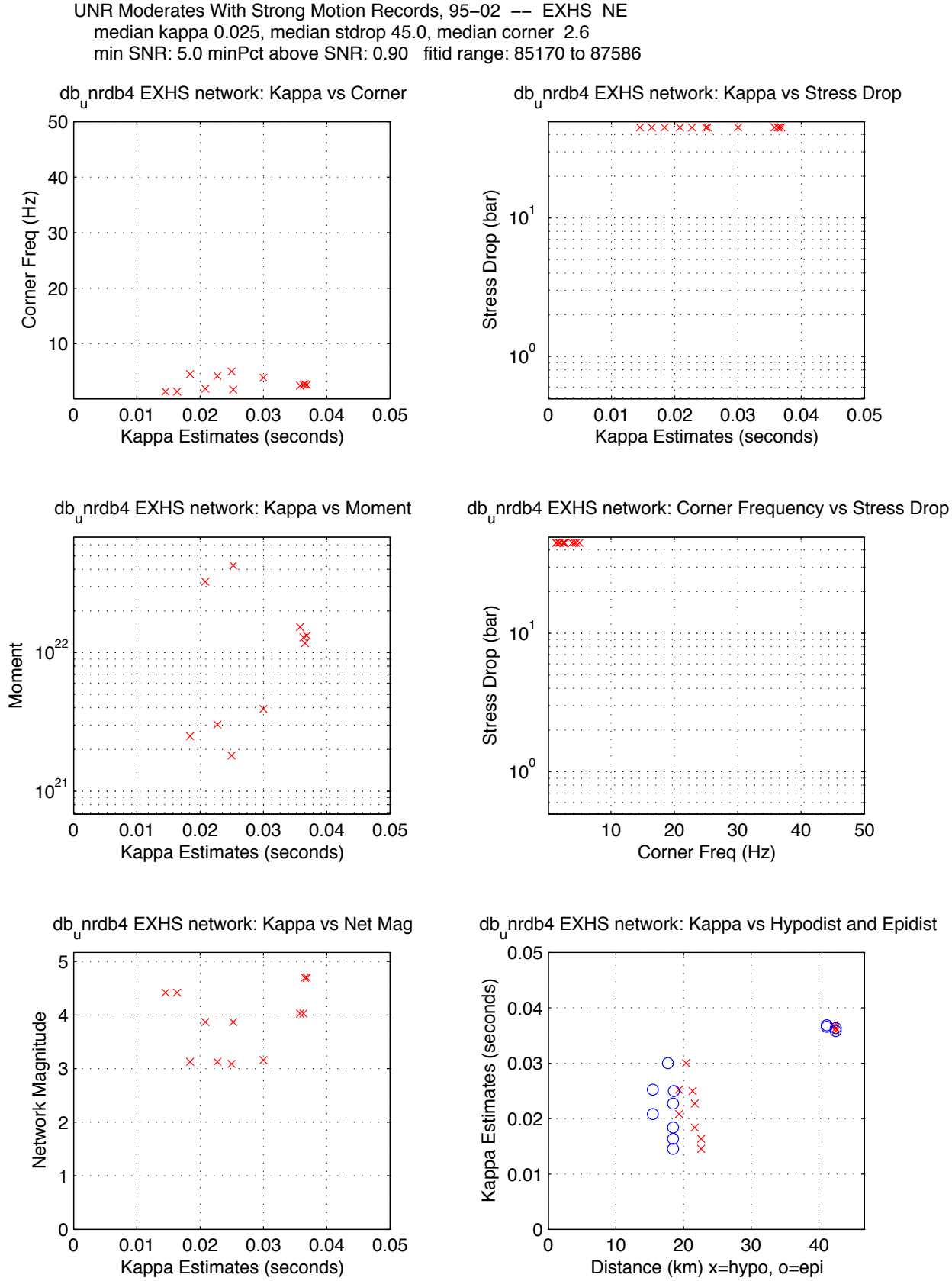

EXHS:NE Passing: 12, Fail SNR: < 5 in 0.9 of freq range = 0, Fail SqErr: > 0.3 = 0, Fail StDrop: > 5000 = 0
EXHS:NE Fail High Corner: > 45 Hz = 0

Figure B 17. Station FMW parametric plot. Free stress drop.
Source: DID 006GB.003, directory kappawrap/case6a/Figs45
File FMW.85170_87586.NE.eps

UNR Moderates With Strong Motion Records, 95–02 –– FMW NE
median kappa 0.016, median stdrop 3.4, median corner 3.6
min SNR: 5.0 minPct above SNR: 0.90 fitid range: 85170 to 87586

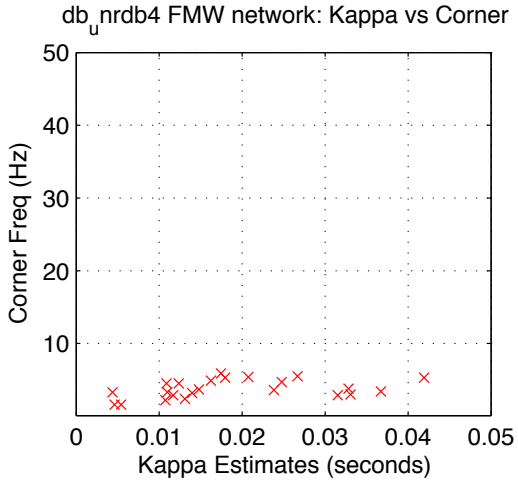

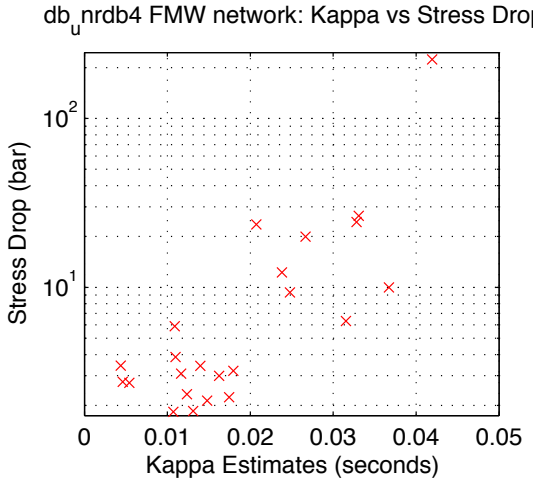

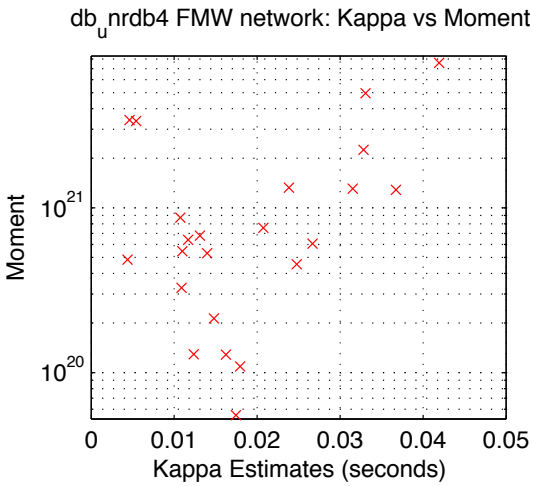

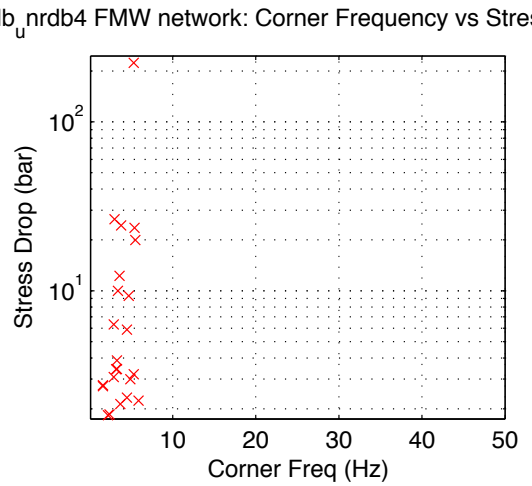

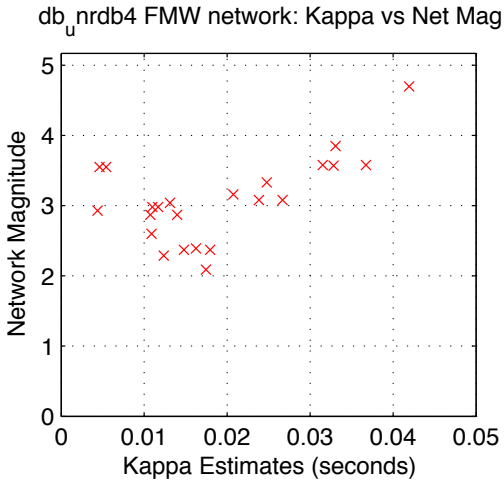

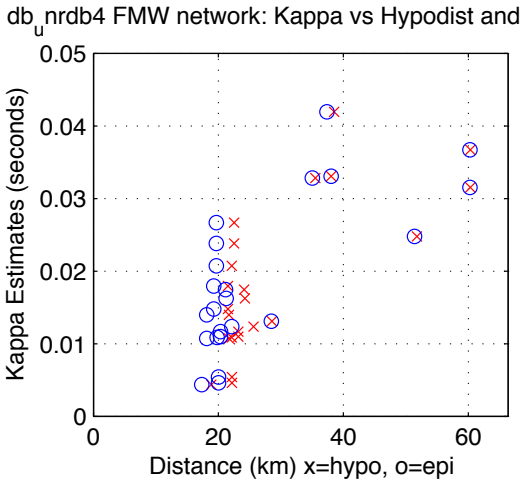

FMW:NE Passing: 23, Fail SNR: < 5 in 0.9 of freq range = 0, Fail SqErr: > 0.3 = 1, Fail StDrop: > 5000 = 0
FMW:NE Fail High Corner: > 45 Hz = 4

Figure B 18. Station FMW parametric plot. Fixed stress drop.
Source: DID 006GB.003, directory kappawrap/case6a/Figs45
File FMW.85170_87586.NE.fixed.eps

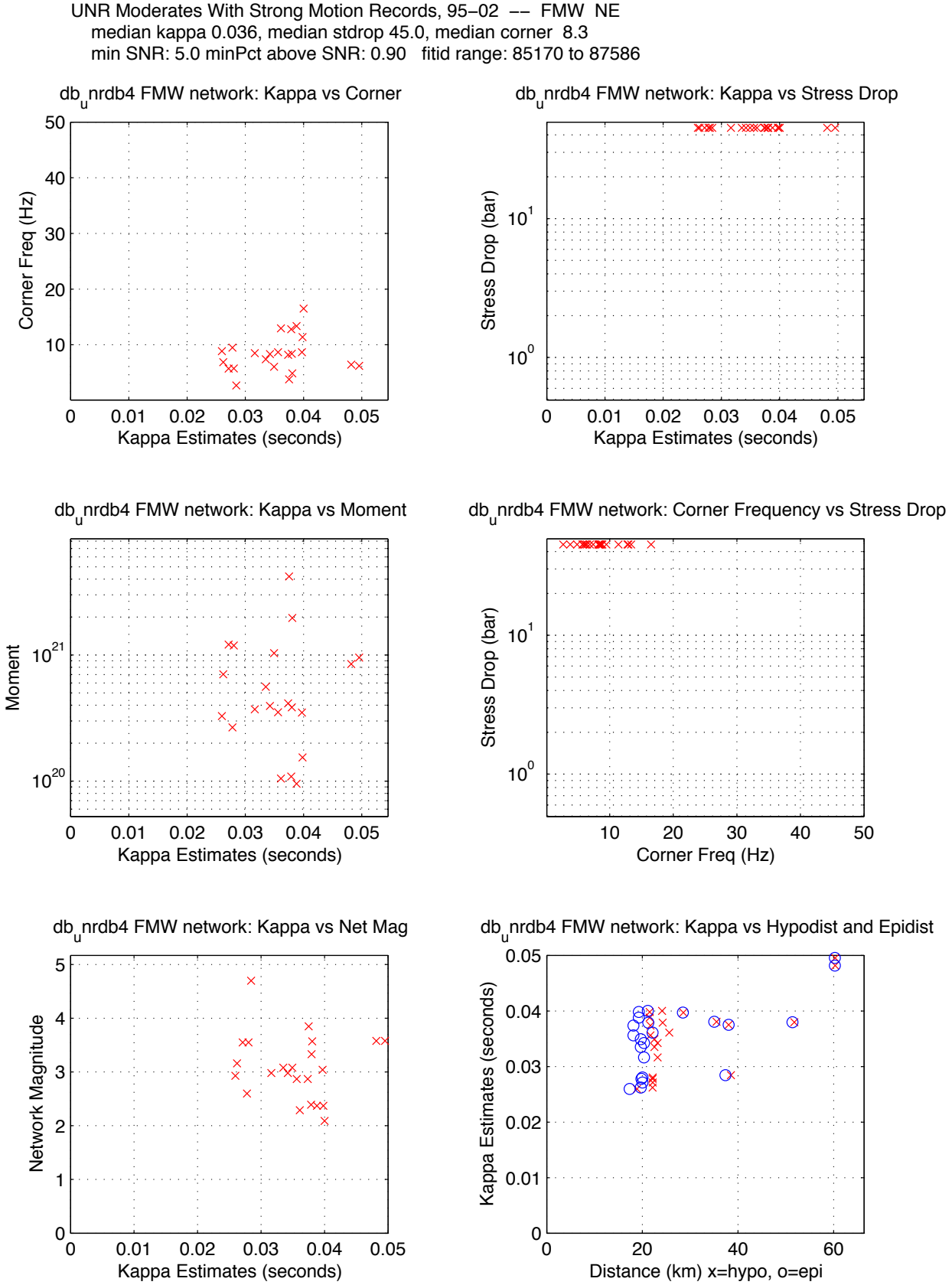

FMW:NE Passing: 23, Fail SNR: < 5 in 0.9 of freq range = 0, Fail SqErr: > 0.3 = 1, Fail StDrop: > 5000 = 0
FMW:NE Fail High Corner: > 45 Hz = 4

Figure B 19. Station FOCS parametric plot. Free stress drop.
Source: DID 006GB.003, directory kappawrap/case6a/Figs45
File FOCS.85170_87586.NE.eps

UNR Moderates With Strong Motion Records, 95–02 –– FOCS NE
median kappa 0.021, median stdrop 63.8, median corner 2.9
min SNR: 5.0 minPct above SNR: 0.90 fitid range: 85170 to 87586

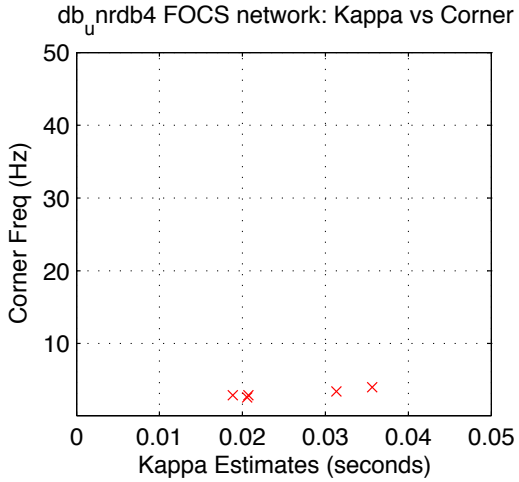

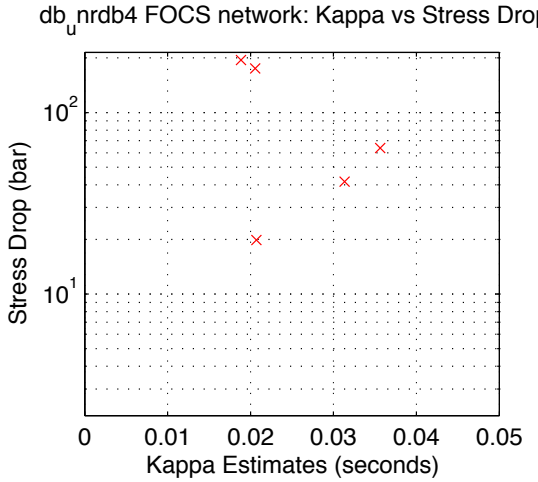

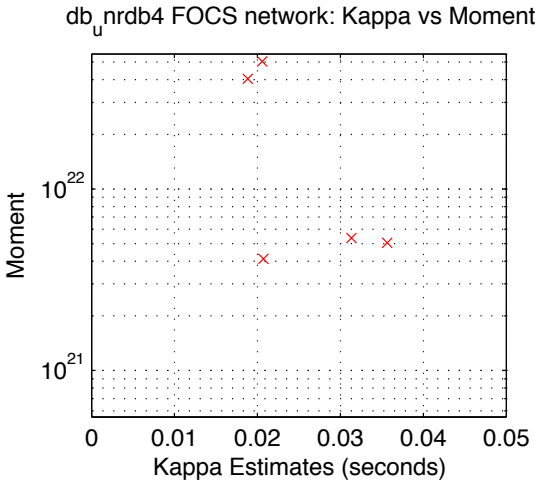

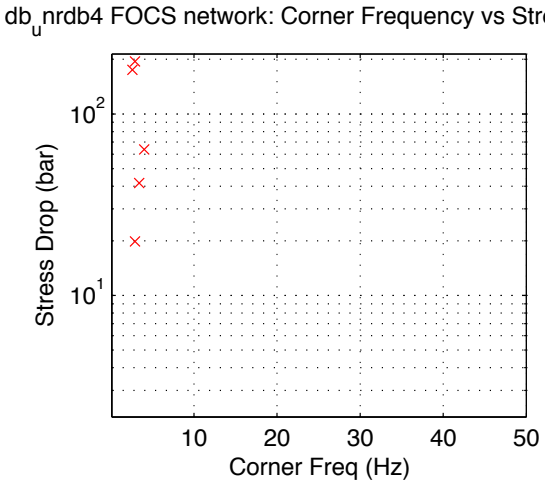

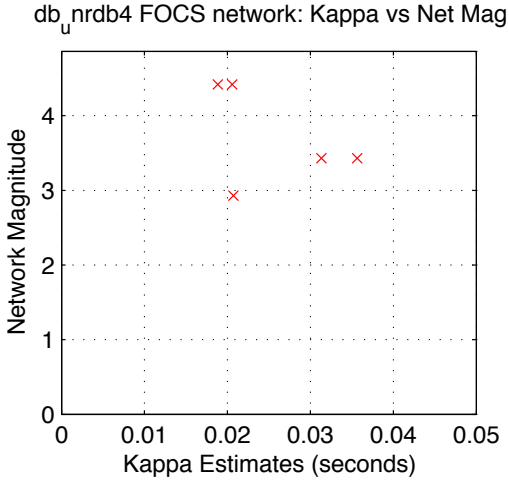

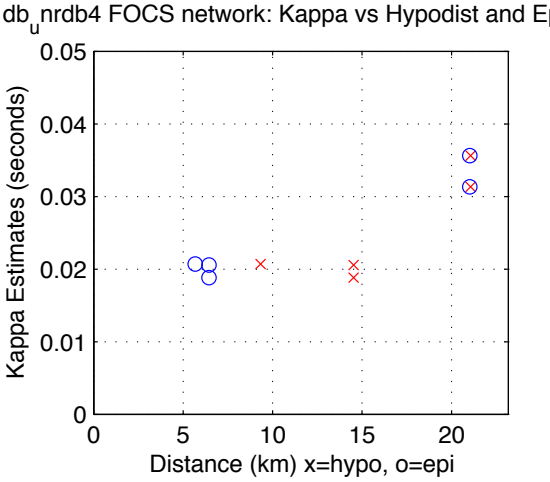

FOCS:NE Passing: 5, Fail SNR: < 5 in 0.9 of freq range = 8, Fail SqErr: > 0.3 = 0, Fail StDrop: > 5000 = 0
FOCS:NE Fail High Corner: > 45 Hz = 2

Figure B 20. Station FOCS parametric plot. Fixed stress drop.
Source: DID 006GB.003, directory kappawrap/case6a/Figs45
File FOCS.85170_87586.NE.fixed.eps

UNR Moderates With Strong Motion Records, 95–02 –– FOCS NE
median kappa 0.028, median stdrop 45.0, median corner 3.4
min SNR: 5.0 minPct above SNR: 0.90 fitid range: 85170 to 87586

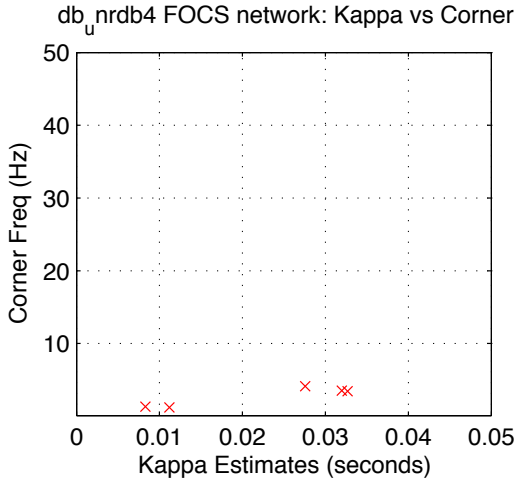

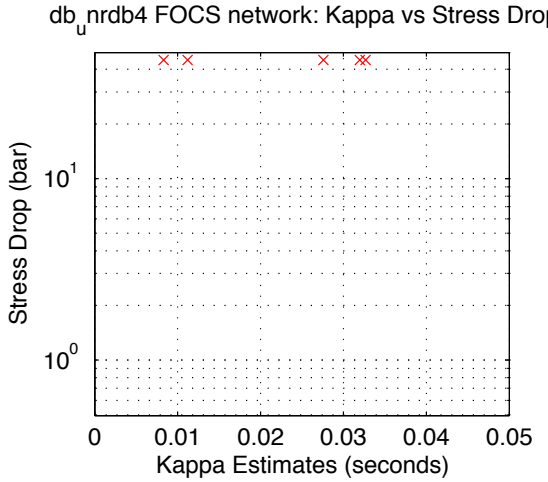

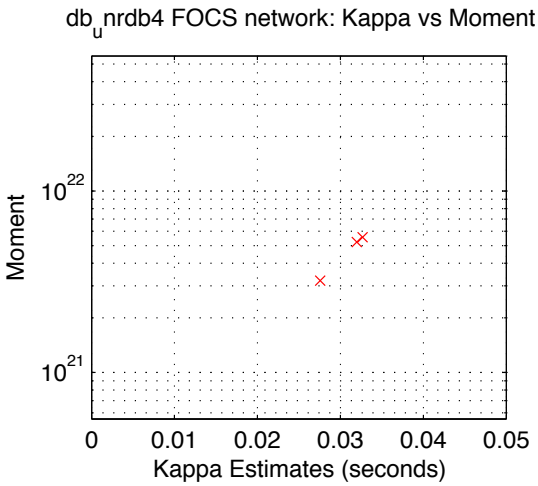

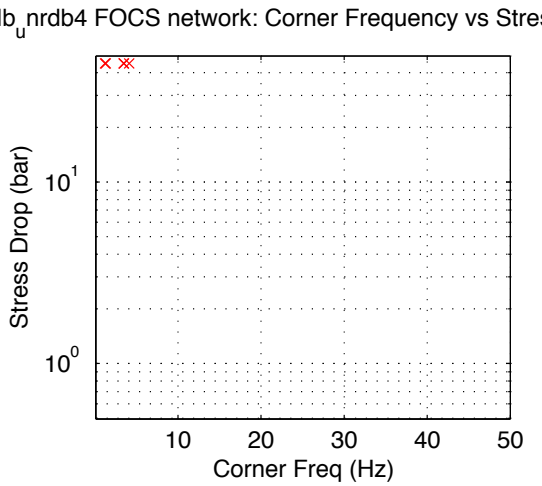

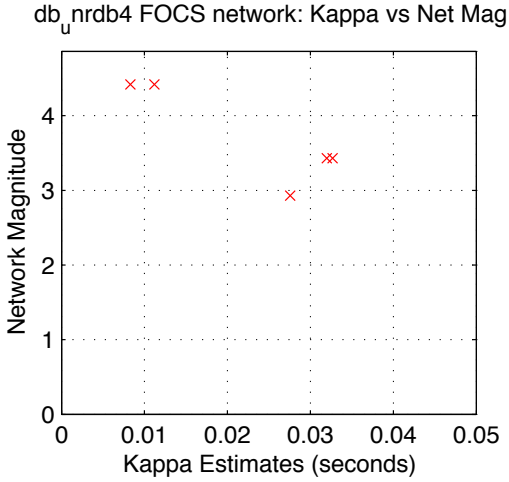

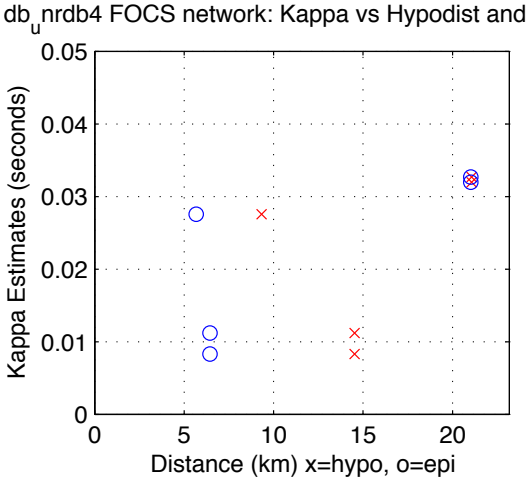

FOCS:NE Passing: 5, Fail SNR: < 5 in 0.9 of freq range = 8, Fail SqErr: > 0.3 = 0, Fail StDrop: > 5000 = 0
FOCS:NE Fail High Corner: > 45 Hz = 2

Figure B 21. Station FRG parametric plot. Free stress drop.
Source: DID 006GB.003, directory kappawrap/case6a/Figs45
File FRG.85170_87586.NE.eps

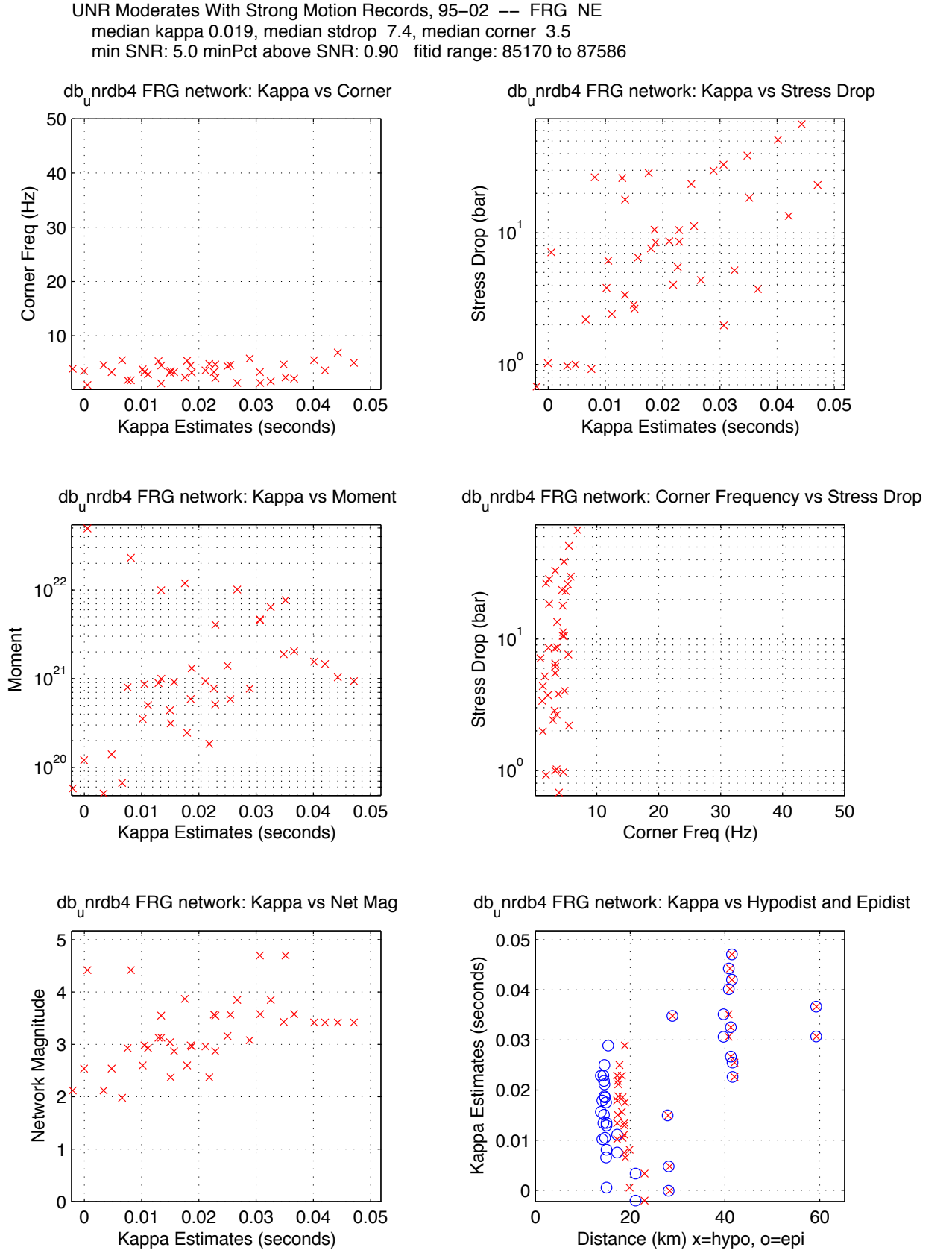

FRG:NE Passing: 40, Fail SNR: < 5 in 0.9 of freq range = 2, Fail SqErr: > 0.3 = 0, Fail StDrop: > 5000 = 0
FRG:NE Fail High Corner: > 45 Hz = 8

Figure B 22. Station FRG parametric plot. Fixed stress drop.
Source: DID 006GB.003, directory kappawrap/case6a/Figs45
File FRG.85170_87586.NE.fixed.eps

UNR Moderates With Strong Motion Records, 95–02 –– FRG NE
median kappa 0.035, median stdrop 45.0, median corner 6.6
min SNR: 5.0 minPct above SNR: 0.90 fitid range: 85170 to 87586

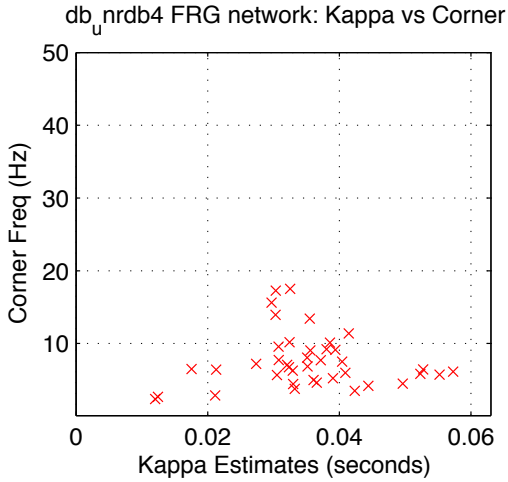

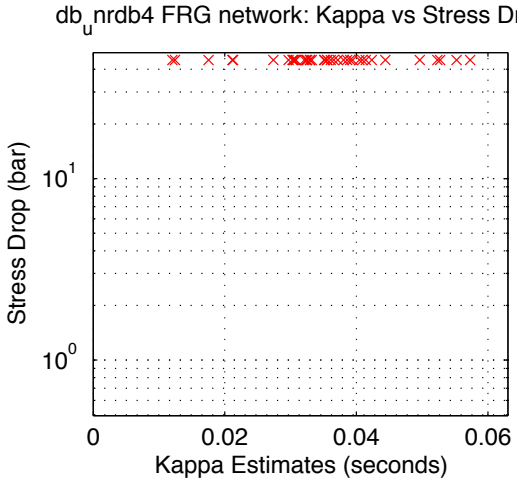

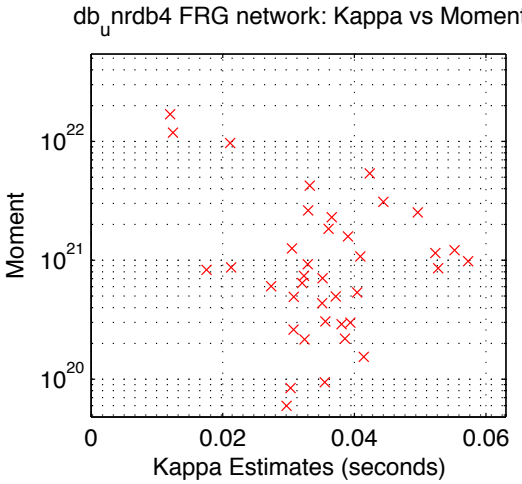

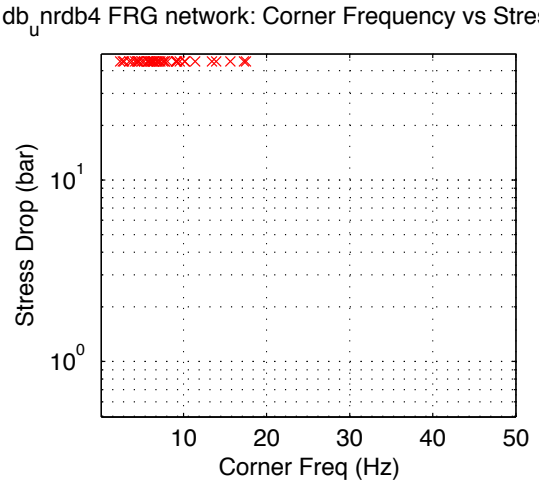

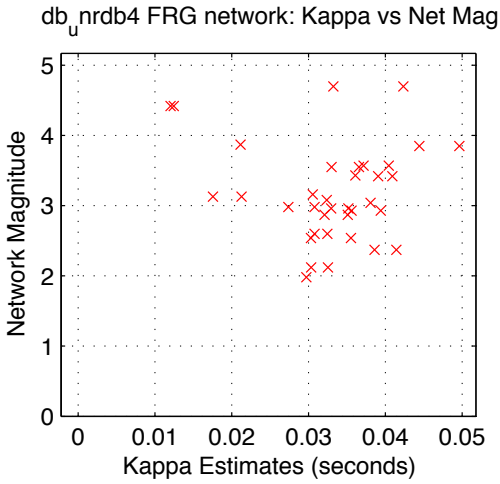

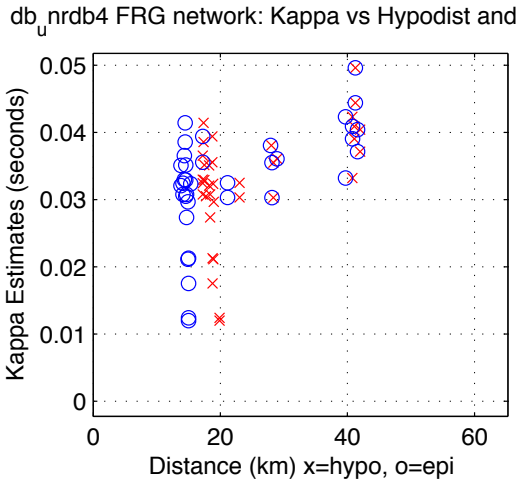

FRG:NE Passing: 40, Fail SNR: < 5 in 0.9 of freq range = 2, Fail SqErr: > 0.3 = 0, Fail StDrop: > 5000 = 0
FRG:NE Fail High Corner: > 45 Hz = 8

Figure B 23. Station LSC parametric plot. Free stress drop.
Source: DID 006GB.003, directory kappawrap/case6a/Figs45
File LSC.85170_87586.NE.eps

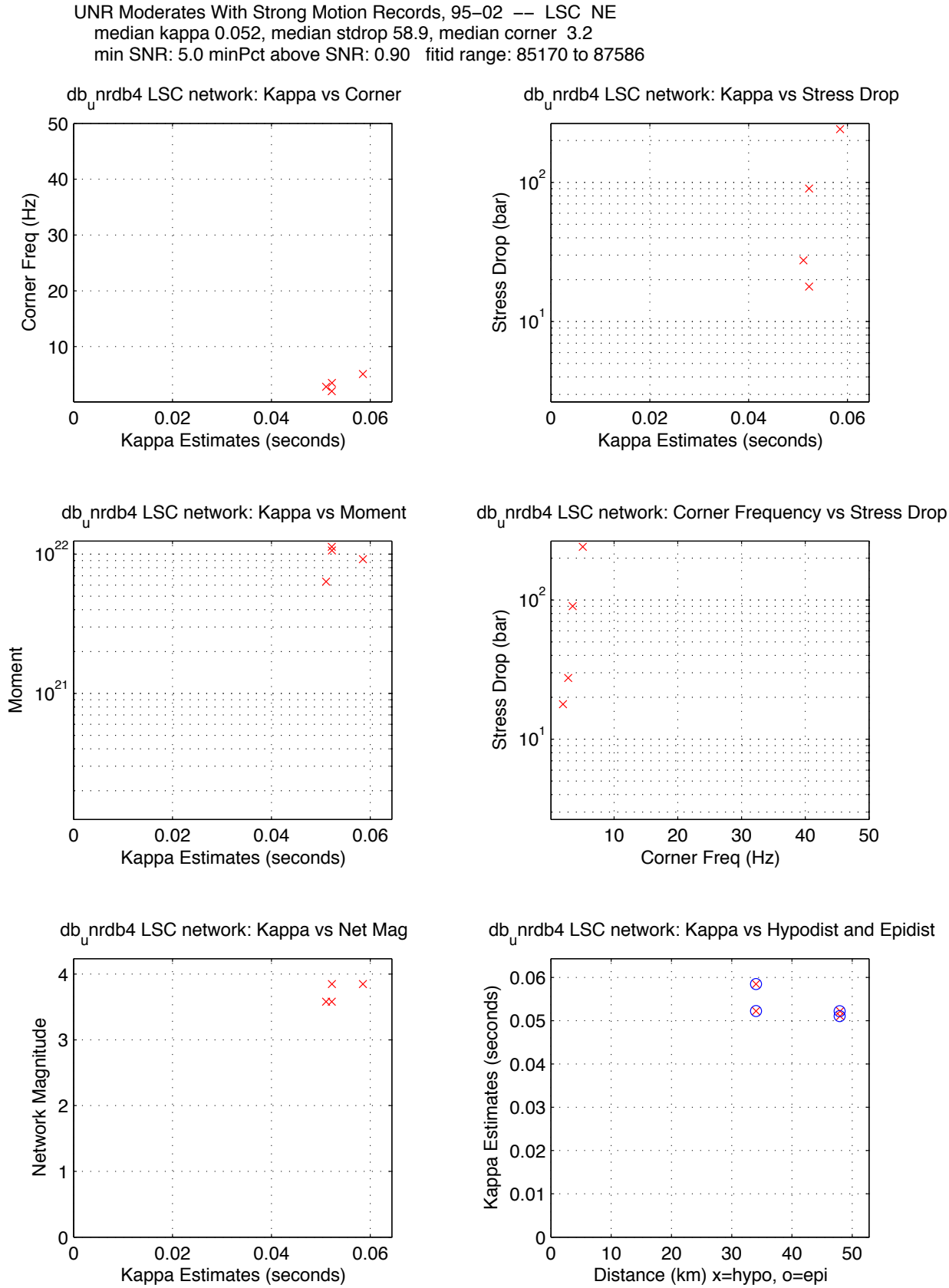

LSC:NE Passing: 4, Fail SNR: < 5 in 0.9 of freq range = 1, Fail SqErr: > 0.3 = 0, Fail StDrop: > 5000 = 0
LSC:NE Fail High Corner: > 45 Hz = 0

Figure B 24. Station LSC parametric plot. Fixed stress drop.
Source: DID 006GB.003, directory kappawrap/case6a/Figs45
File LSC.85170_87586.NE.fixed.eps

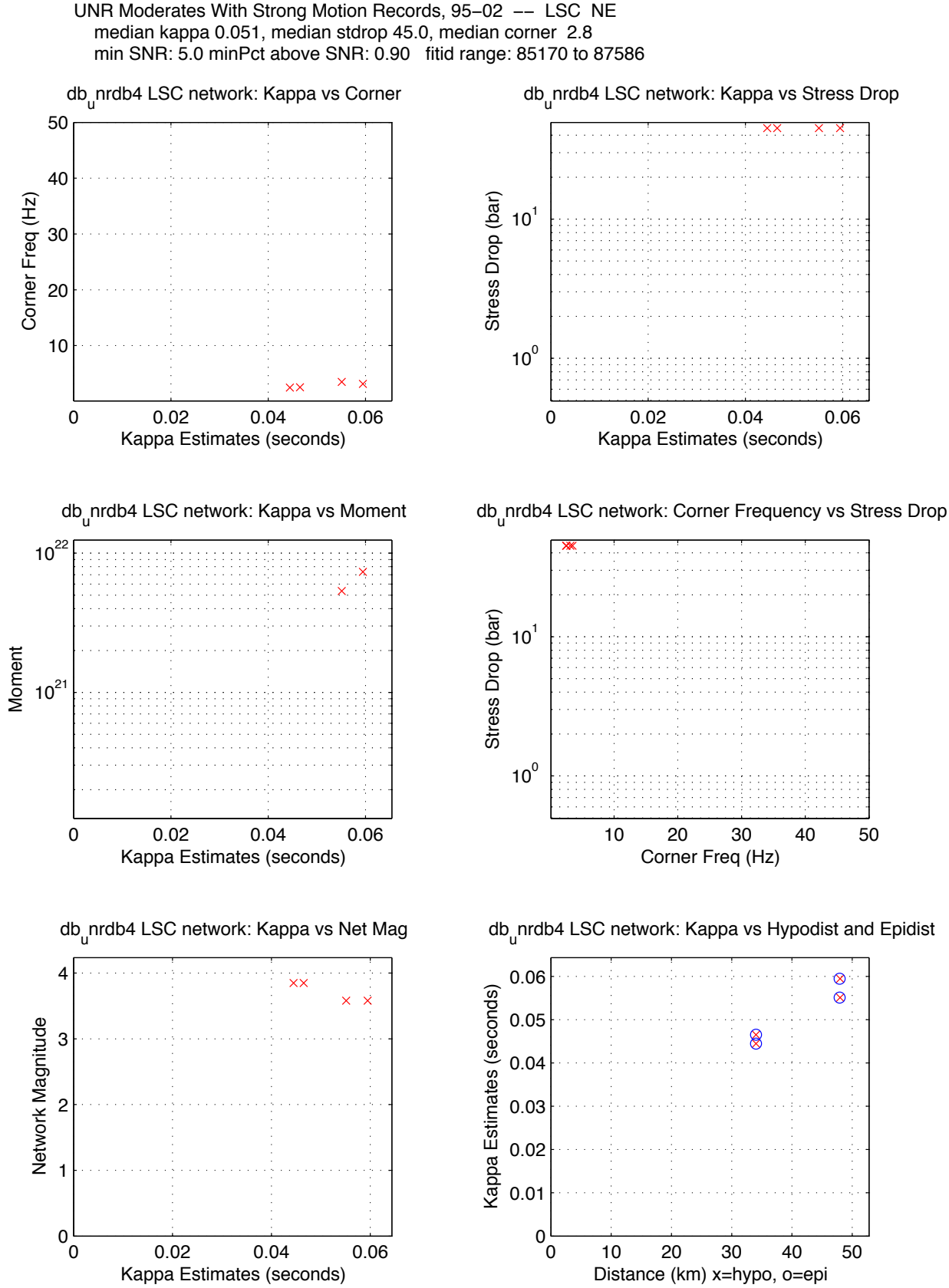

LSC:NE Passing: 4, Fail SNR: < 5 in 0.9 of freq range = 1, Fail SqErr: > 0.3 = 0, Fail StDrop: > 5000 = 0
LSC:NE Fail High Corner: > 45 Hz = 0

Figure B 25. Station LWLS parametric plot. Free stress drop.
Source: DID 006GB.003, directory kappawrap/case6a/Figs45
File LWLS.85170_87586.NE.eps

UNR Moderates With Strong Motion Records, 95–02 –– LWLS NE
median kappa 0.031, median stdrop 79.6, median corner 2.9
min SNR: 5.0 minPct above SNR: 0.90 fitid range: 85170 to 87586

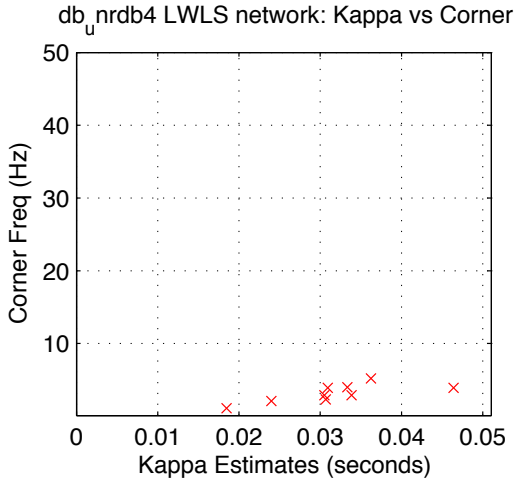

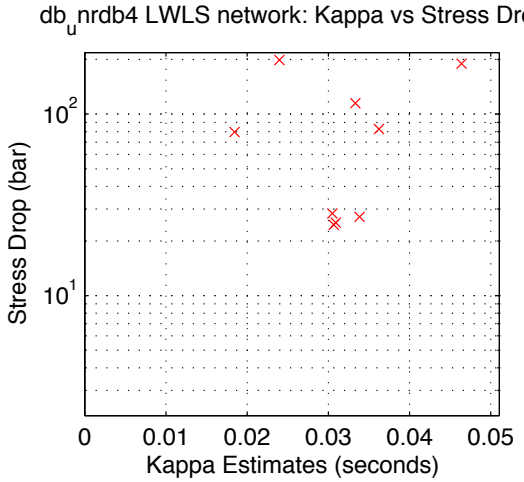

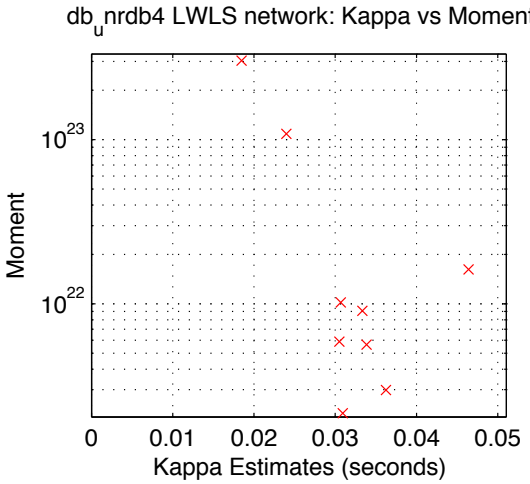

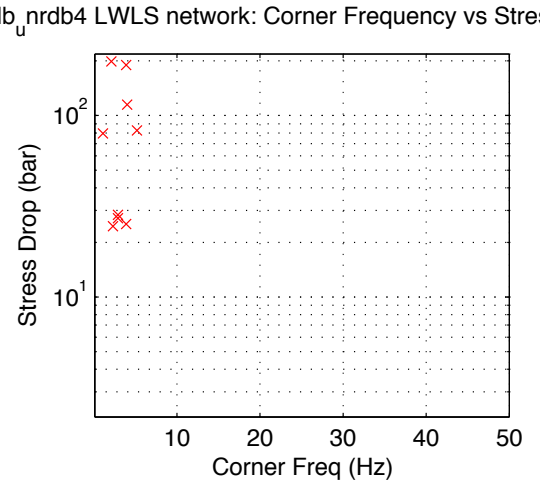

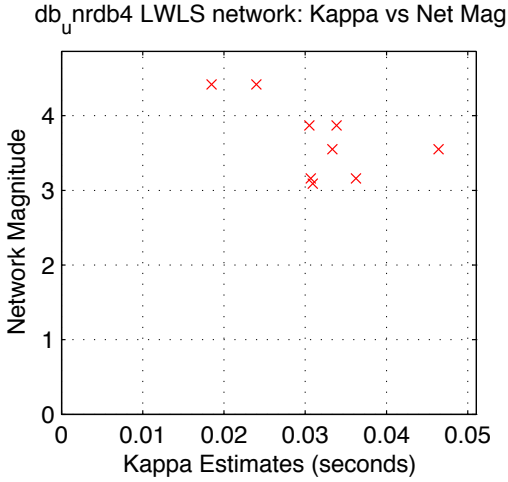

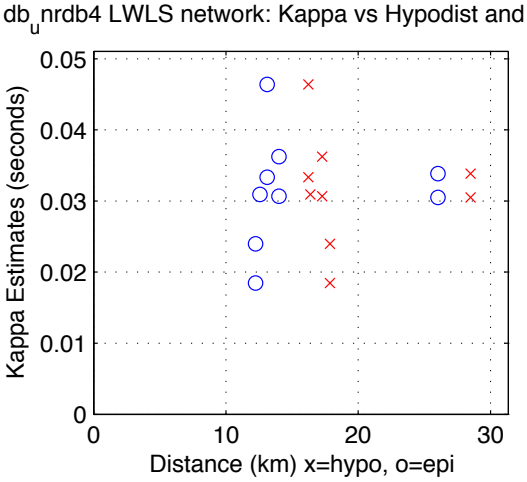

LWLS:NE Passing: 9, Fail SNR: < 5 in 0.9 of freq range = 15, Fail SqErr: > 0.3 = 0, Fail StDrop: > 5000 = 0
LWLS:NE Fail High Corner: > 45 Hz = 0

Figure B 26. Station LWLS parametric plot. Free stress drop.
Source: DID 006GB.003, directory kappawrap/case6a/Figs45
File LWLS.85170_87586.NE.eps

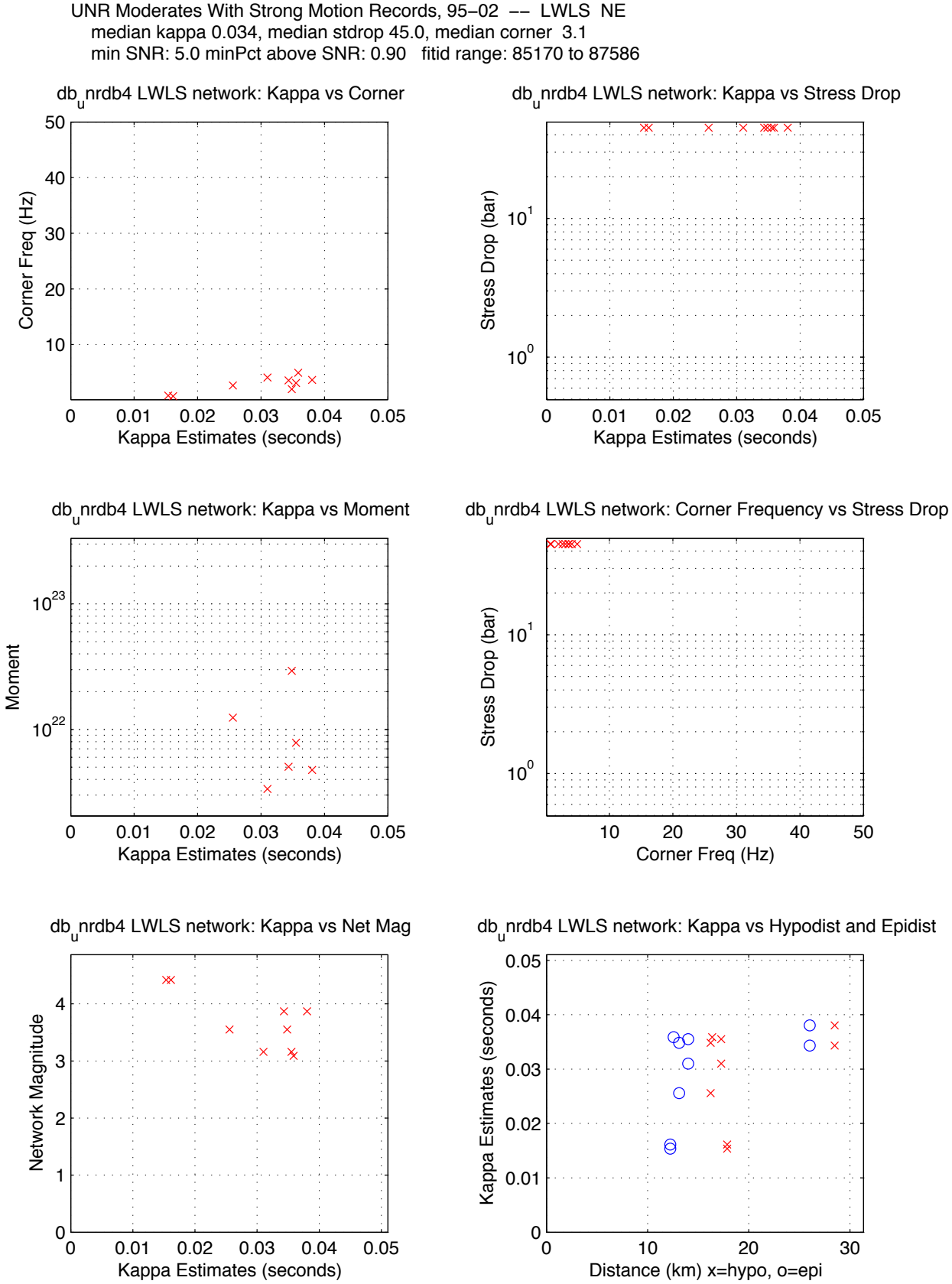

LWLS:NE Passing: 9, Fail SNR: < 5 in 0.9 of freq range = 15, Fail SqErr: > 0.3 = 0, Fail StDrop: > 5000 = 0
LWLS:NE Fail High Corner: > 45 Hz = 0

Figure B 27. Station MDVS parametric plot. Free stress drop.
Source: DID 006GB.003, directory kappawrap/case6a/Figs45
File MDVS.85170_87586.NE.eps

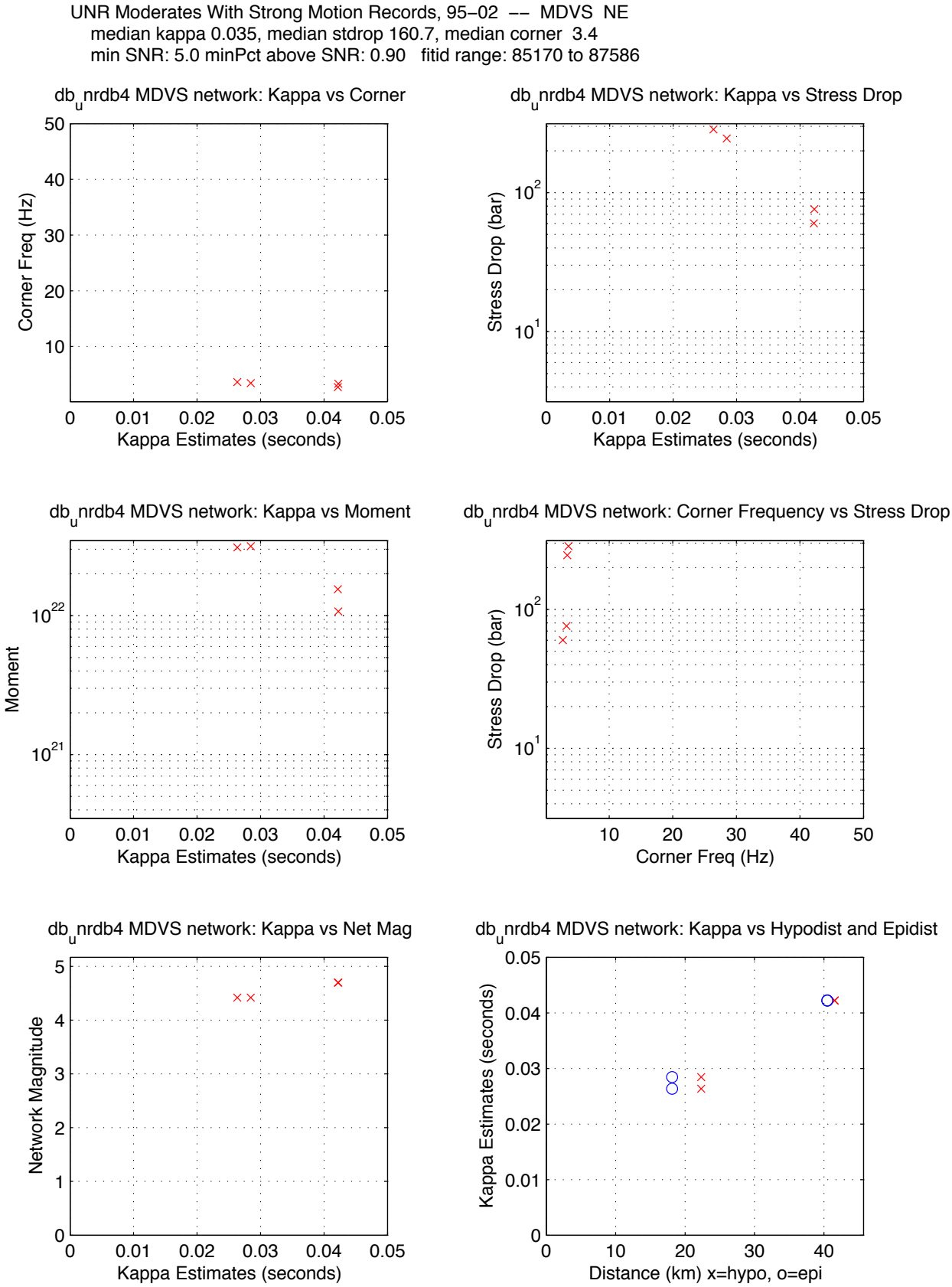

MDVS:NE Passing: 4, Fail SNR: < 5 in 0.9 of freq range = 5, Fail SqErr: > 0.3 = 0, Fail StDrop: > 5000 = 0
MDVS:NE Fail High Corner: > 45 Hz = 0

Figure B 28. Station MDVS parametric plot. Fixed stress drop.
Source: DID 006GB.003, directory kappawrap/case6a/Figs45
File MDVS.85170_87586.NE.fixed.eps

UNR Moderates With Strong Motion Records, 95–02 –– MDVS NE
median kappa 0.027, median stdrop 45.0, median corner 1.9
min SNR: 5.0 minPct above SNR: 0.90 fitid range: 85170 to 87586

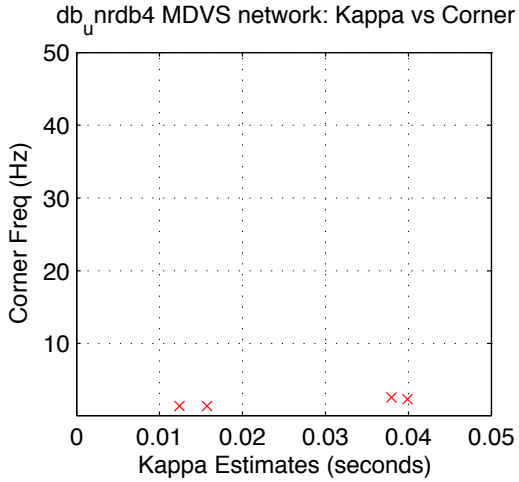

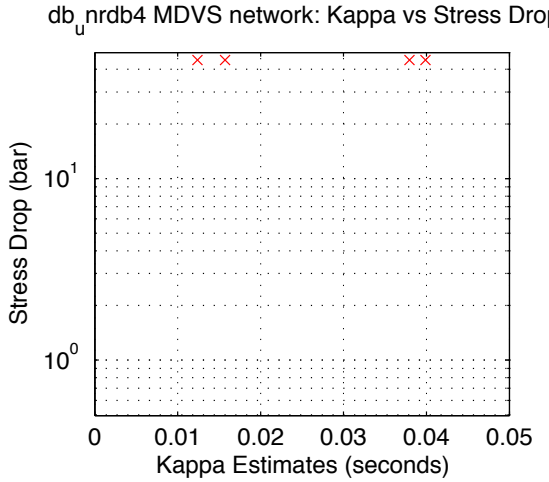

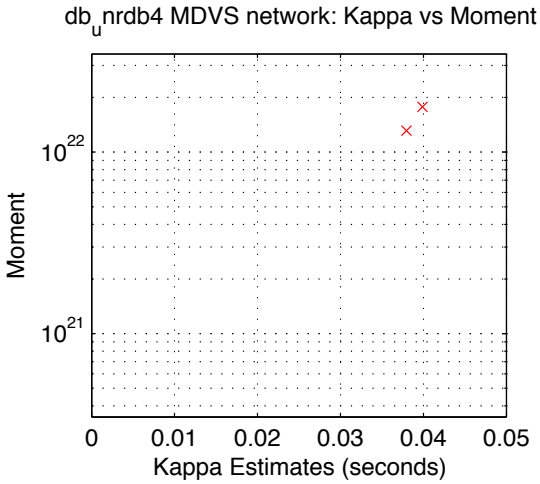

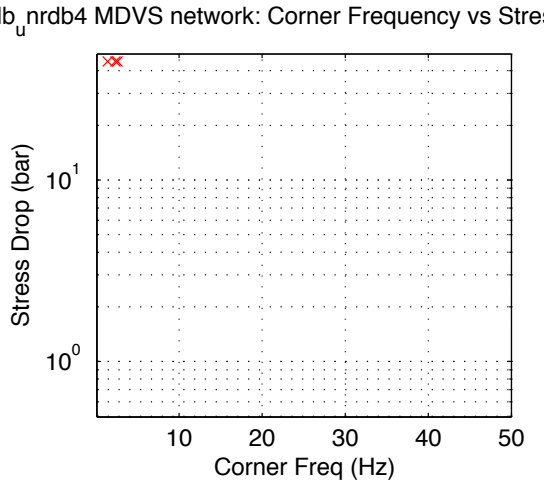

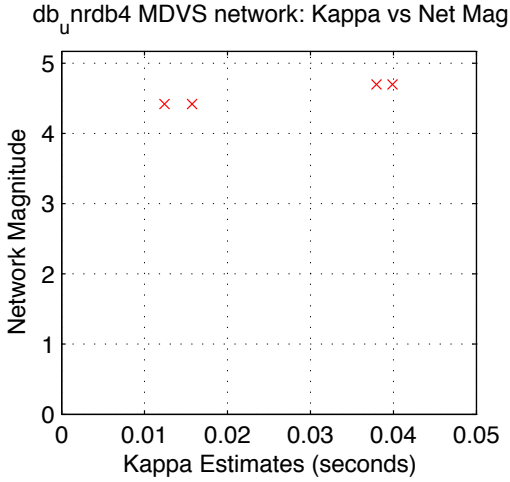

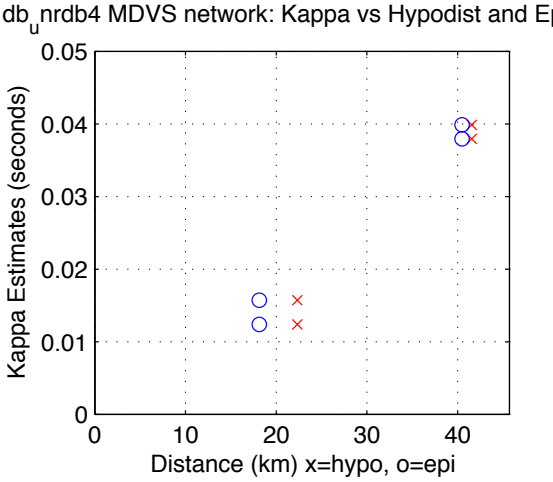

MDVS:NE Passing: 4, Fail SNR: < 5 in 0.9 of freq range = 5, Fail SqErr: > 0.3 = 0, Fail StDrop: > 5000 = 0
MDVS:NE Fail High Corner: > 45 Hz = 0

Figure B 29. Station NCF parametric plot. Free stress drop.
Source: DID 006GB.003, directory kappawrap/case6a/Figs45
File NCF.85170_87586.NE.eps

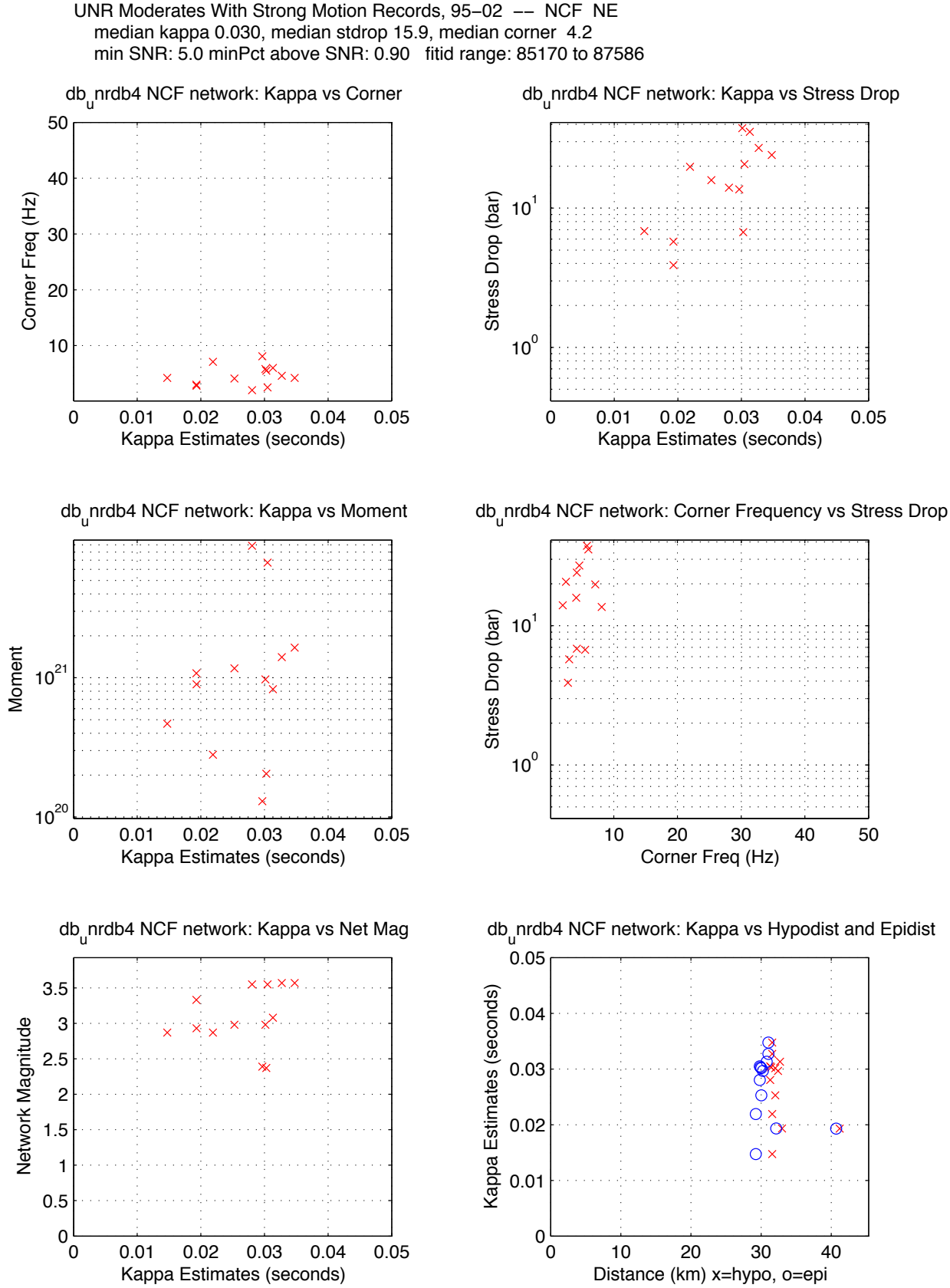

NCF:NE Passing: 13, Fail SNR: < 5 in 0.9 of freq range = 0, Fail SqErr: > 0.3 = 0, Fail StDrop: > 5000 = 0
NCF:NE Fail High Corner: > 45 Hz = 5

Figure B 30. Station NCF parametric plot. Fixed stress drop.
Source: DID 006GB.003, directory kappawrap/case6a/Figs45
File NCF.85170_87586.NE.fixed.eps

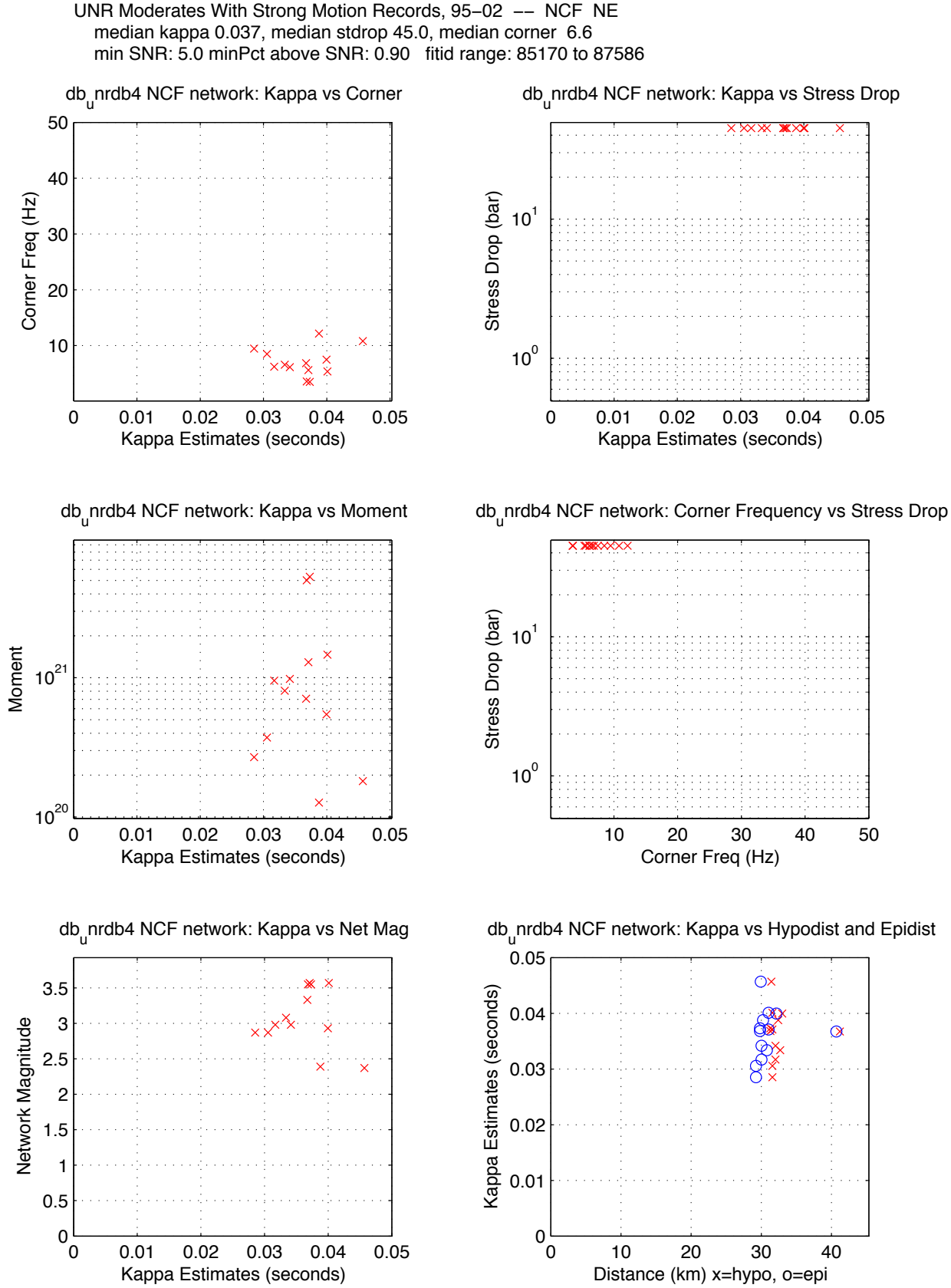

NCF:NE Passing: 13, Fail SNR: < 5 in 0.9 of freq range = 0, Fail SqErr: > 0.3 = 0, Fail StDrop: > 5000 = 0
NCF:NE Fail High Corner: > 45 Hz = 5

Figure B 31. Station PUV parametric plot. Free stress drop.
Source: DID 006GB.003, directory kappawrap/case6a/Figs45
File PUV.85170_87586.NE.eps

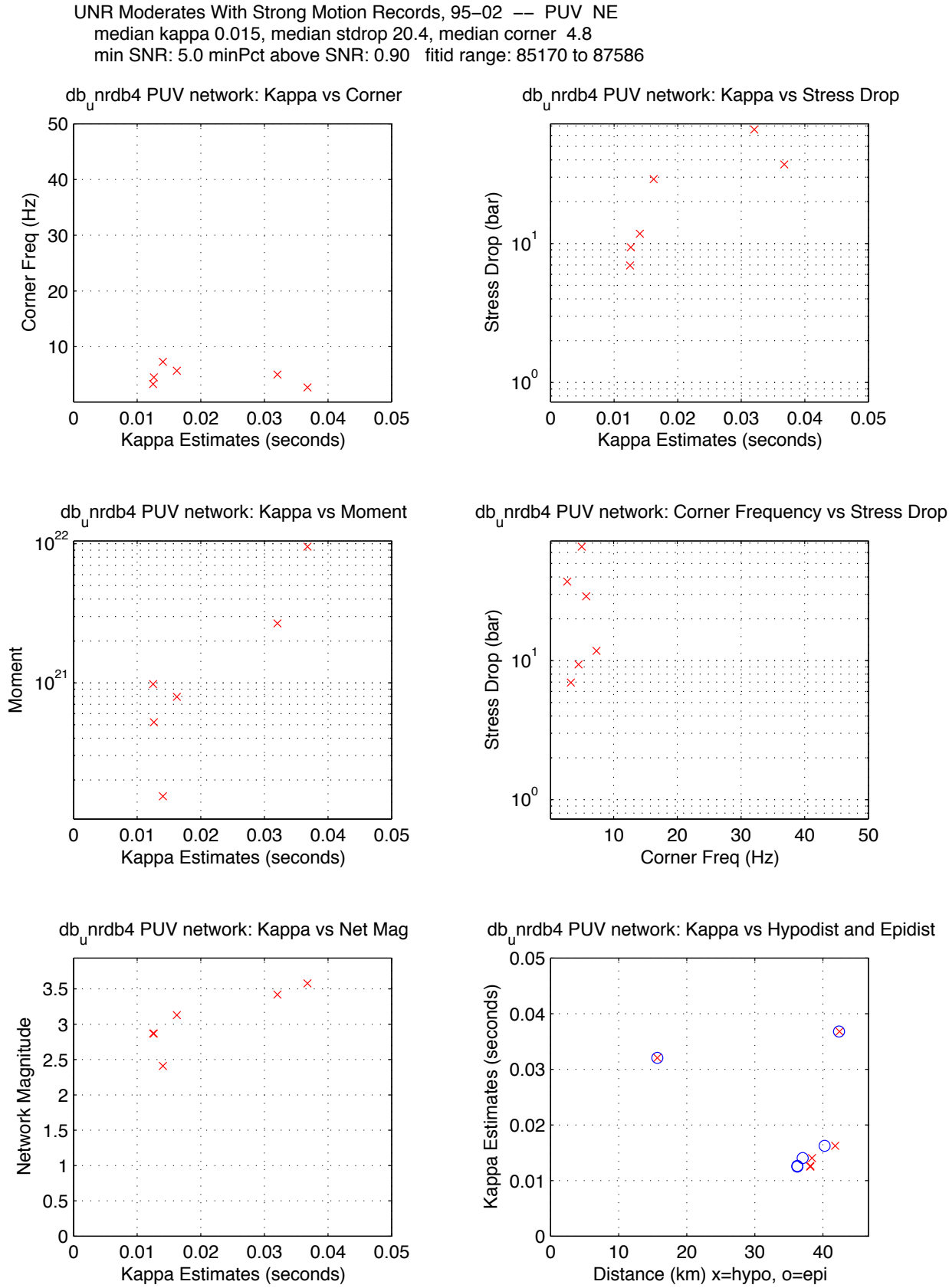

PUV:NE Passing: 6, Fail SNR: < 5 in 0.9 of freq range = 0, Fail SqErr: > 0.3 = 0, Fail StDrop: > 5000 = 0
PUV:NE Fail High Corner: > 45 Hz = 0

Figure B 32. Station PUV parametric plot. Fixed stress drop.
Source: DID 006GB.003, directory kappawrap/case6a/Figs45
File PUV.85170_87586.NE.fixed.eps

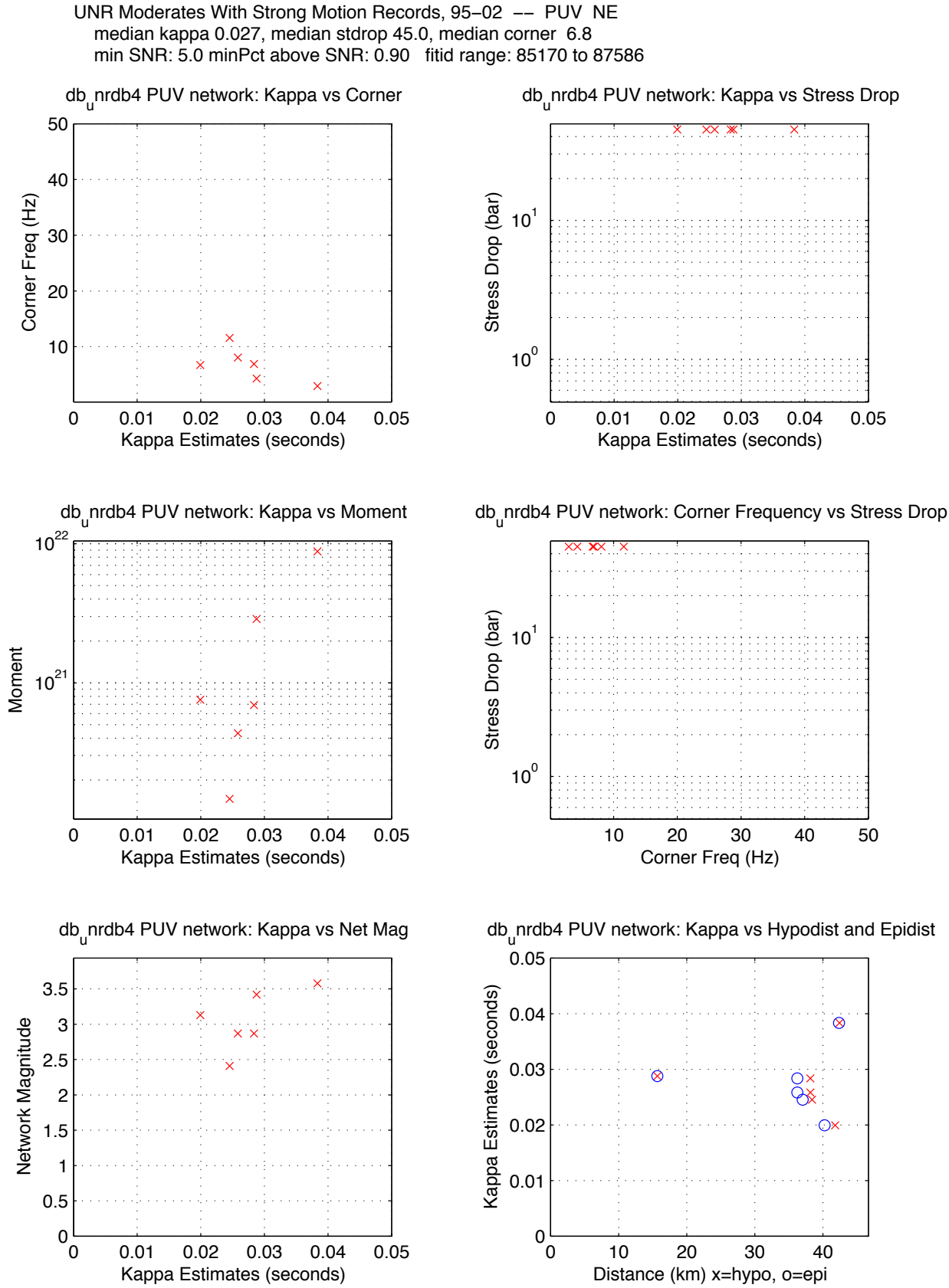

PUV:NE Passing: 6, Fail SNR: < 5 in 0.9 of freq range = 0, Fail SqErr: > 0.3 = 0, Fail StDrop: > 5000 = 0
PUV:NE Fail High Corner: > 45 Hz = 0

Figure B 33. Station RED parametric plot. Free stress drop.
Source: DID 006GB.003, directory kappawrap/case6a/Figs45
File RED.85170_87586.NE.eps

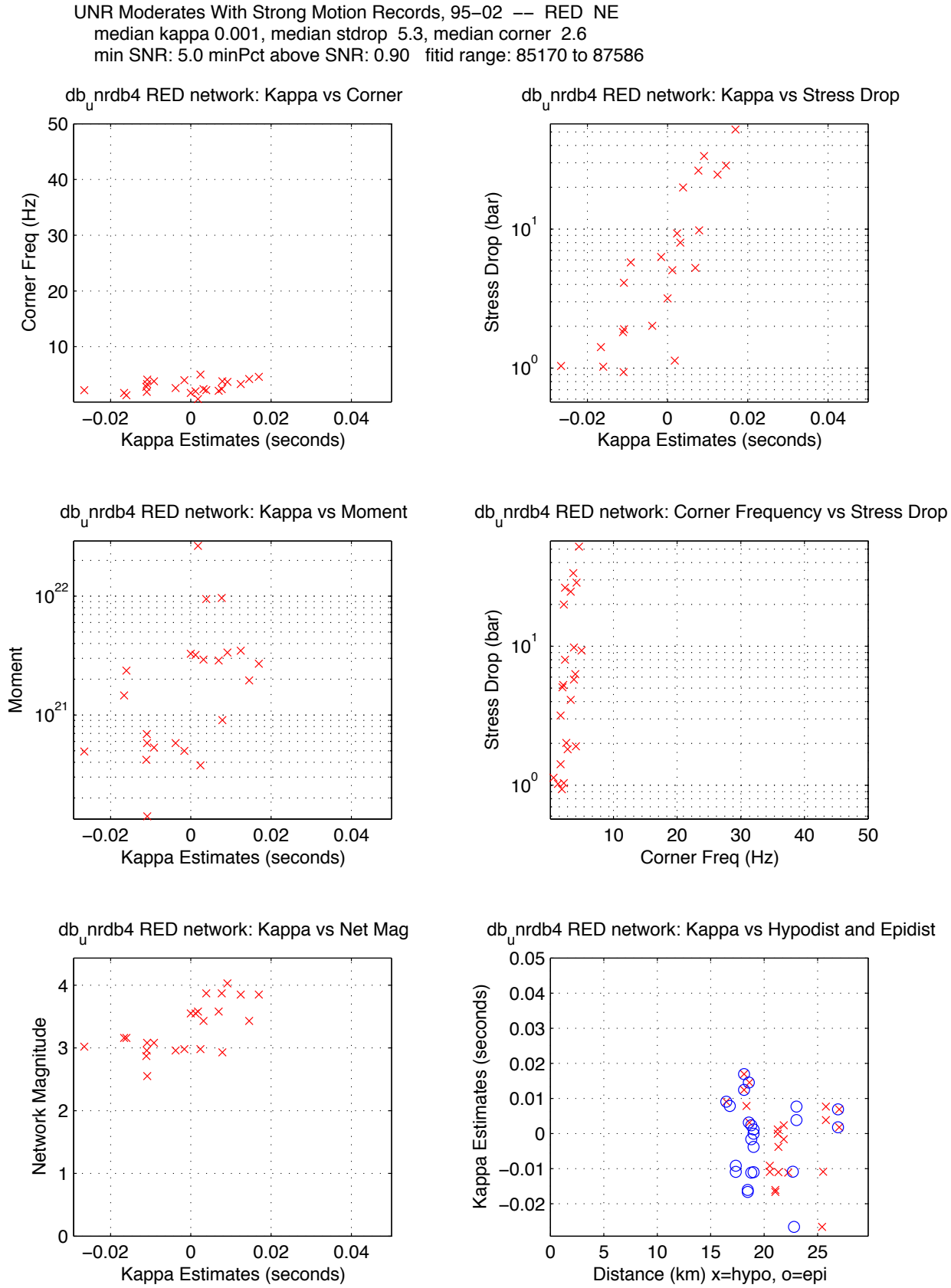

RED:NE Passing: 23, Fail SNR: < 5 in 0.9 of freq range = 0, Fail SqErr: > 0.3 = 1, Fail StDrop: > 5000 = 0
RED:NE Fail High Corner: > 45 Hz = 5

Figure B 34. Station RED parametric plot. Fixed stress drop.
Source: DID 006GB.003, directory kappawrap/case6a/Figs45
File RED.85170_87586.NE.fixed.eps

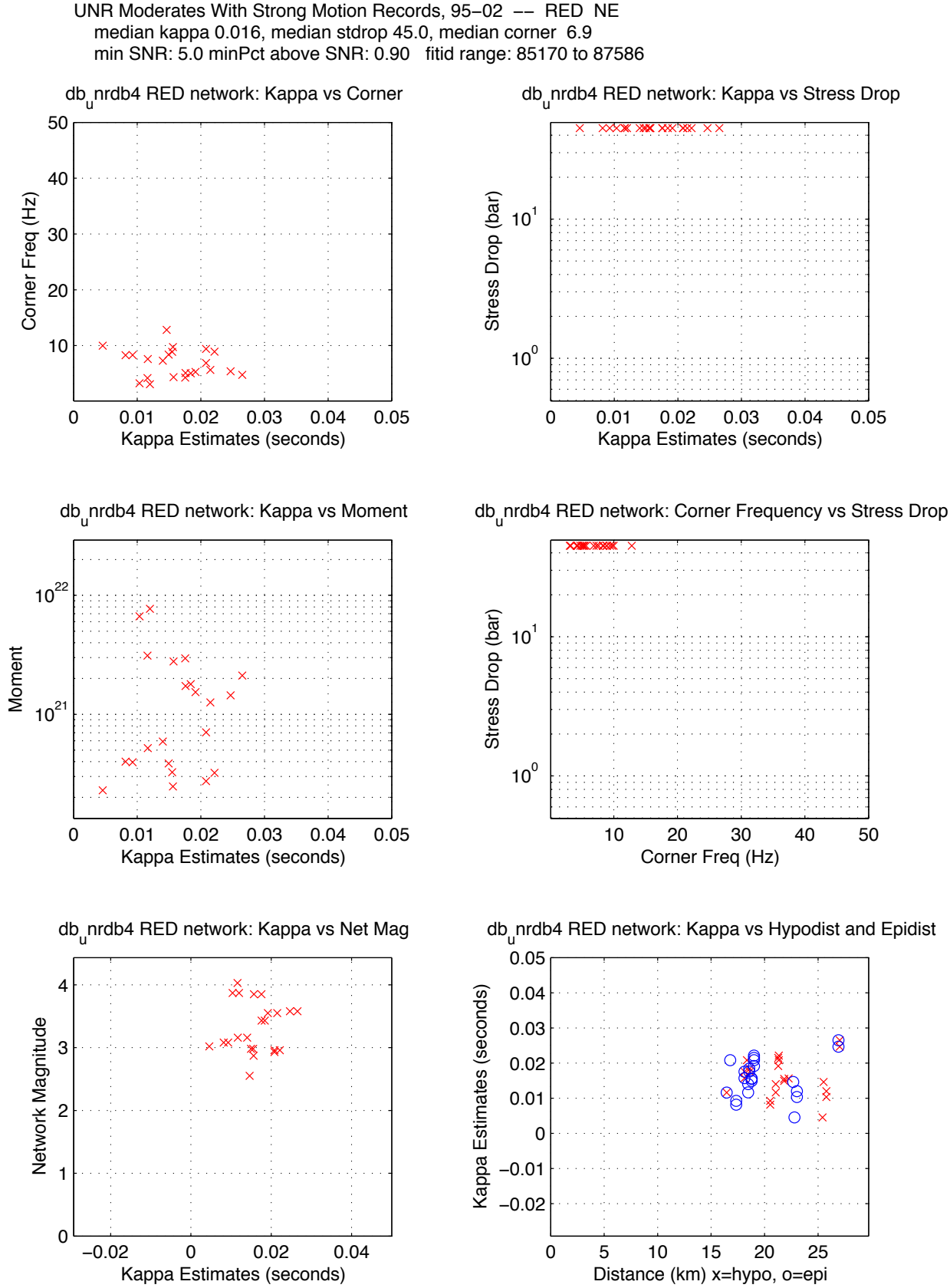

RED:NE Passing: 23, Fail SNR: < 5 in 0.9 of freq range = 0, Fail SqErr: > 0.3 = 1, Fail StDrop: > 5000 = 0
RED:NE Fail High Corner: > 45 Hz = 5

Figure B 35. Station RPY parametric plot. Free stress drop.
Source: DID 006GB.003, directory kappawrap/case6a/Figs45
File RPY.85170_87586.NE.eps

UNR Moderates With Strong Motion Records, 95–02 –– RPY NE
median kappa 0.036, median stdrop 19.5, median corner 3.6
min SNR: 5.0 minPct above SNR: 0.90 fitid range: 85170 to 87586

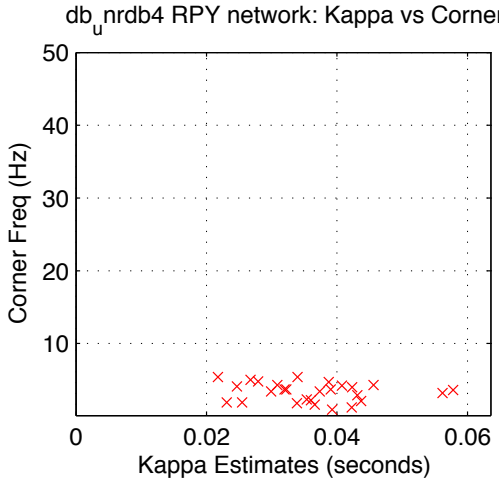

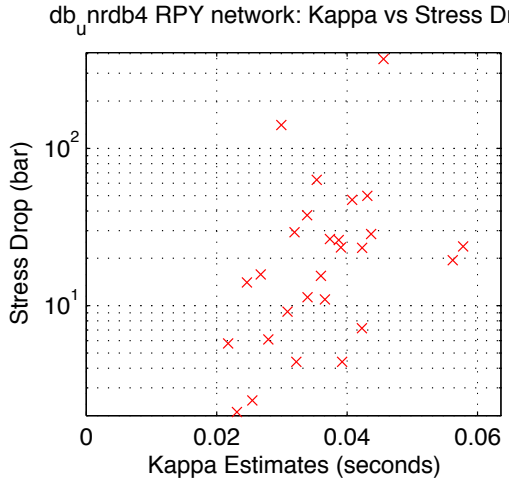

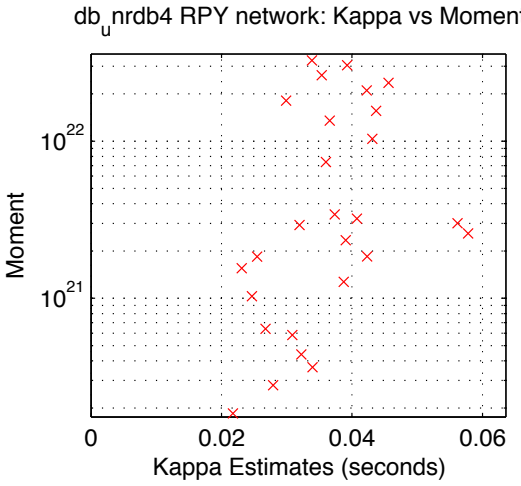

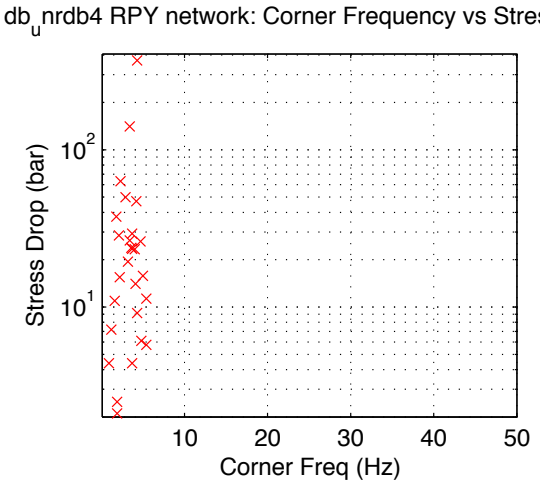

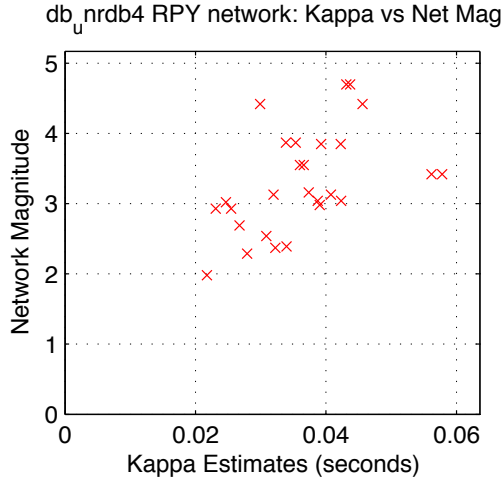

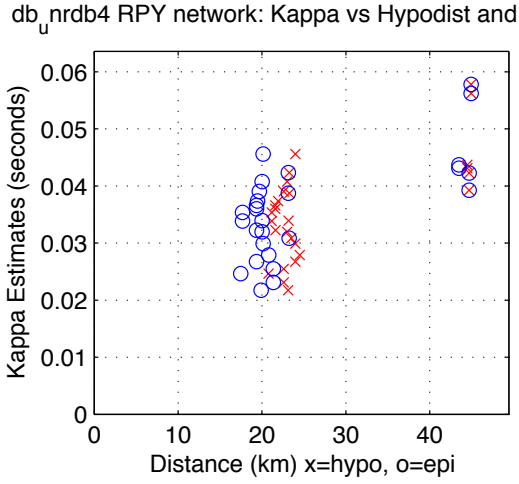

RPY:NE Passing: 27, Fail SNR: < 5 in 0.9 of freq range = 1, Fail SqErr: > 0.3 = 0, Fail StDrop: > 5000 = 0
RPY:NE Fail High Corner: > 45 Hz = 0

Figure B 36. Station RPY parametric plot. Fixed stress drop.
Source: DID 006GB.003, directory kappawrap/case6a/Figs45
File RPY.85170_87586.NE.fixed.eps

UNR Moderates With Strong Motion Records, 95–02 –– RPY NE
median kappa 0.044, median stdrop 45.0, median corner 4.6
min SNR: 5.0 minPct above SNR: 0.90 fitid range: 85170 to 87586

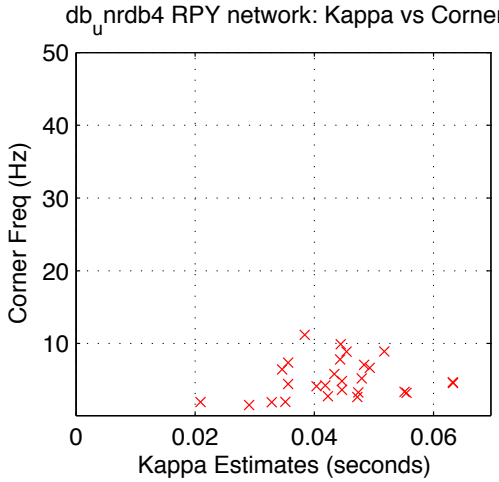

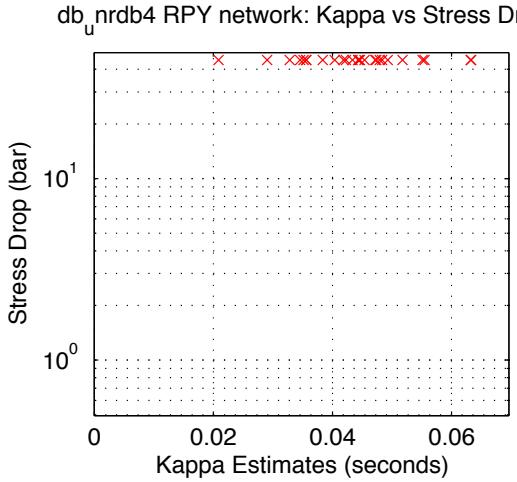

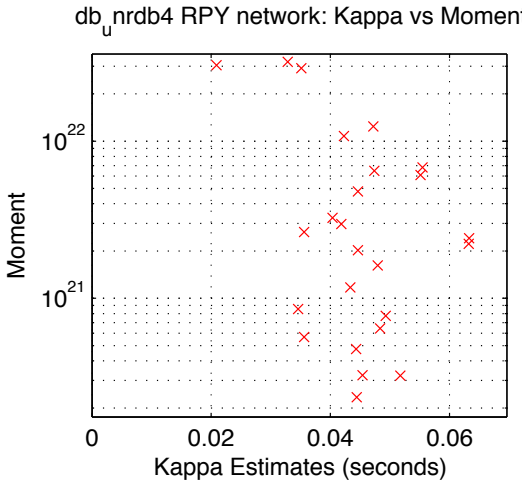

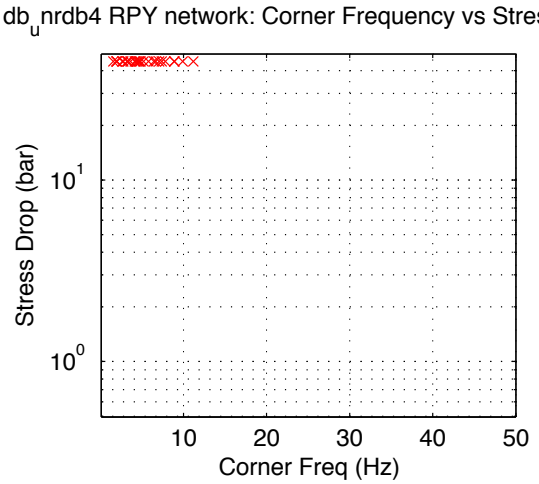

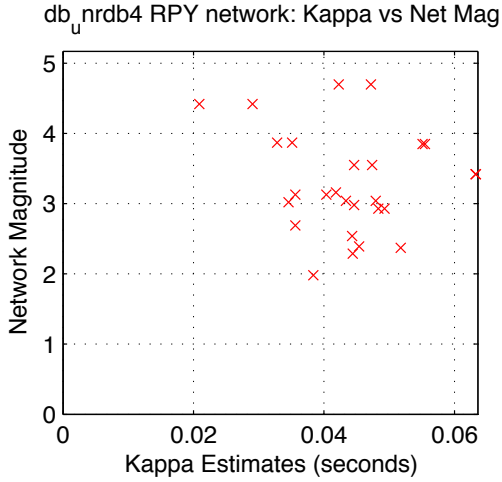

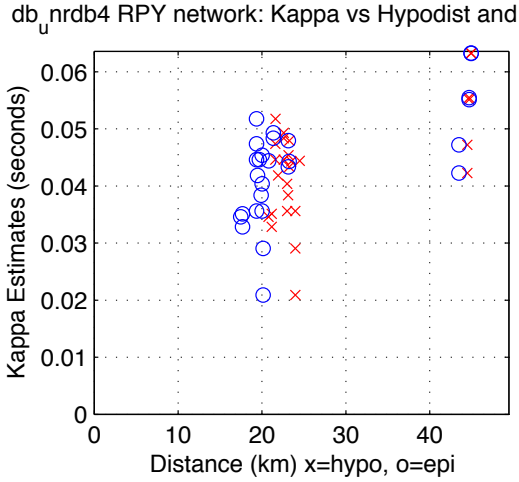

RPY:NE Passing: 27, Fail SNR: < 5 in 0.9 of freq range = 1, Fail SqErr: > 0.3 = 0, Fail StDrop: > 5000 = 0
RPY:NE Fail High Corner: > 45 Hz = 0

Figure B 37. Station SCF parametric plot. Free stress drop.
Source: DID 006GB.003, directory kappawrap/case6a/Figs45
File SCF.85170_87586.NE.eps

UNR Moderates With Strong Motion Records, 95–02 –– SCF NE
median kappa 0.035, median stdrop 7.5, median corner 4.0
min SNR: 5.0 minPct above SNR: 0.90 fitid range: 85170 to 87586

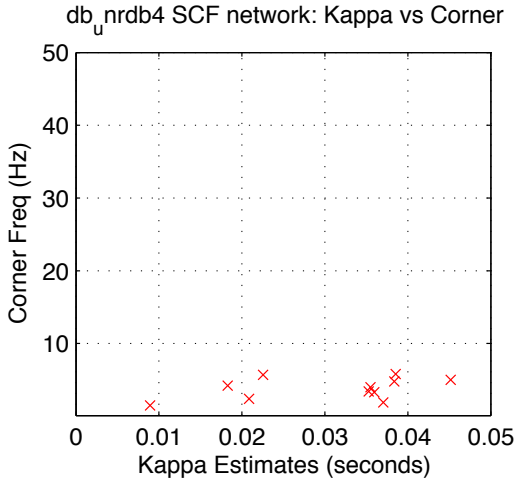

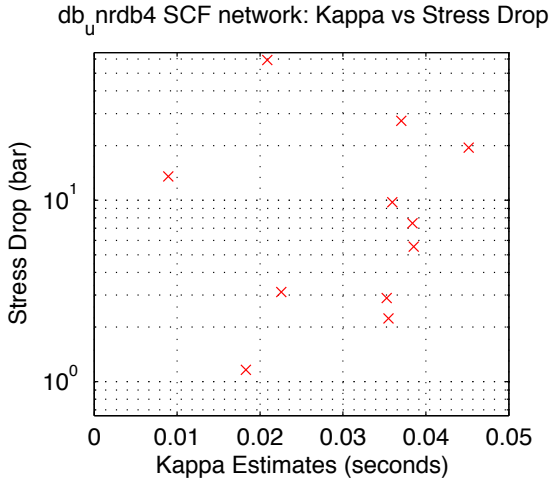

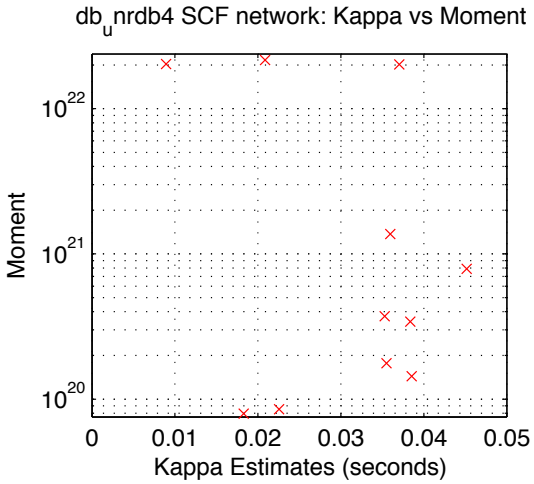

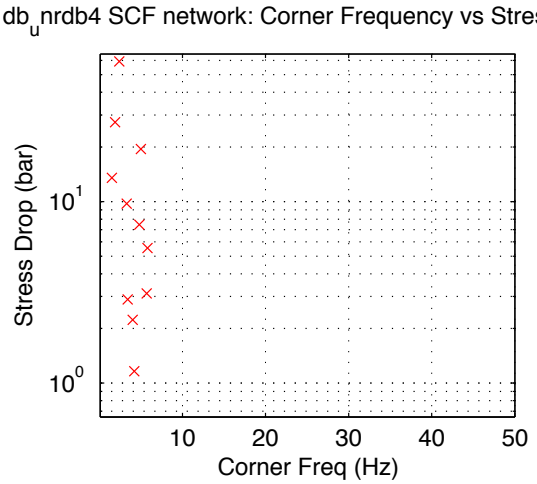

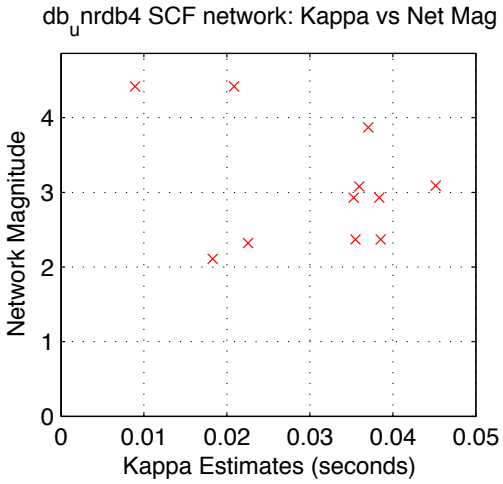

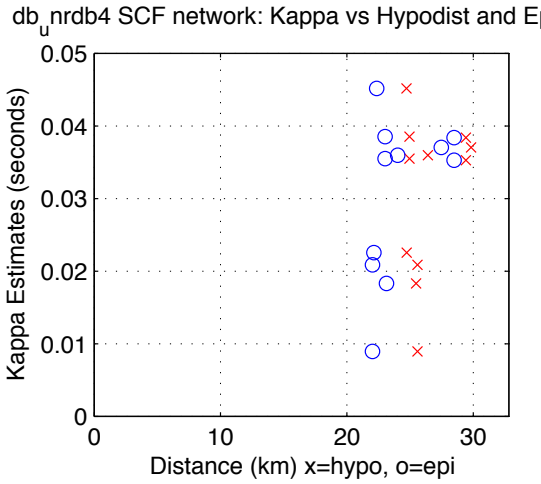

SCF:NE Passing: 11, Fail SNR: < 5 in 0.9 of freq range = 2, Fail SqErr: > 0.3 = 0, Fail StDrop: > 5000 = 0
SCF:NE Fail High Corner: > 45 Hz = 1

Figure B 38. Station SCF parametric plot. Fixed stress drop.
Source: DID 006GB.003, directory kappawrap/case6a/Figs45
File SCF.85170_87586.NE.fixed.eps

UNR Moderates With Strong Motion Records, 95–02 –– SCF NE
median kappa 0.049, median stdrop 45.0, median corner 9.2
min SNR: 5.0 minPct above SNR: 0.90 fitid range: 85170 to 87586

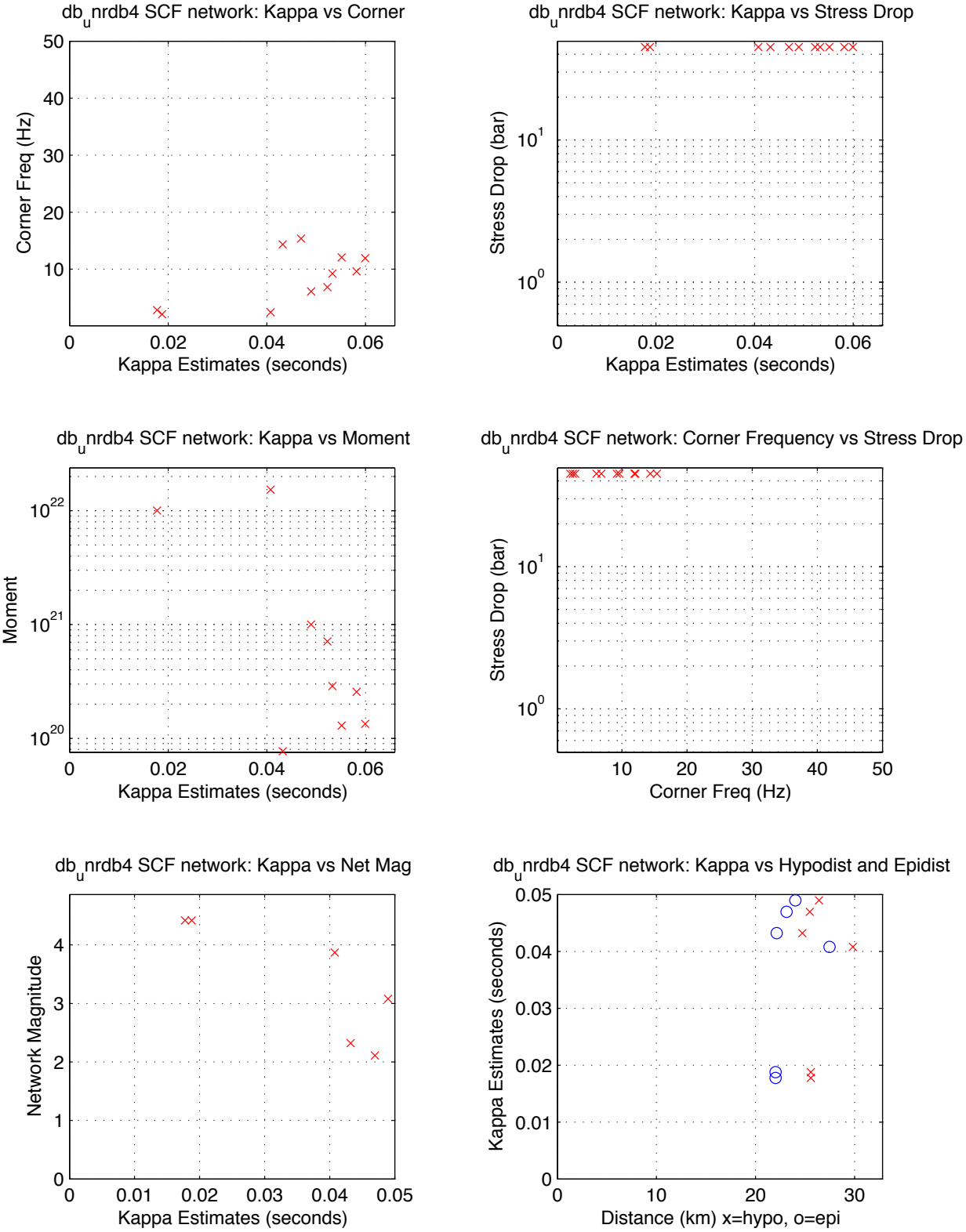

SCF:NE Passing: 11, Fail SNR: < 5 in 0.9 of freq range = 2, Fail SqErr: > 0.3 = 0, Fail StDrop: > 5000 = 0
SCF:NE Fail High Corner: > 45 Hz = 1

Figure B 39. Station SGR parametric plot. Free stress drop.
Source: DID 006GB.003, directory kappawrap/case6a/Figs45
File SGR.85170_87586.NE.eps

UNR Moderates With Strong Motion Records, 95–02 –– SGR NE
median kappa 0.022, median stdrop 5.5, median corner 2.7
min SNR: 5.0 minPct above SNR: 0.90 fitid range: 85170 to 87586

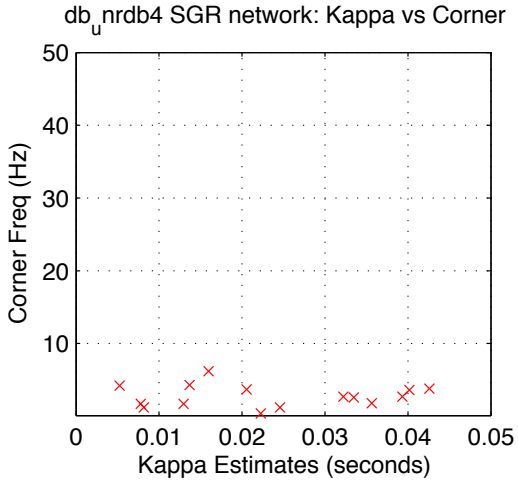

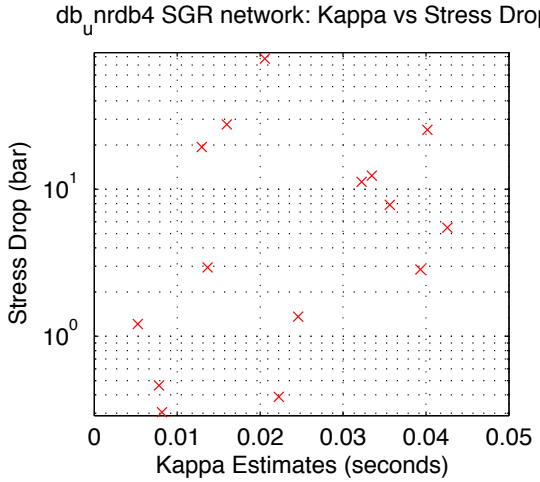

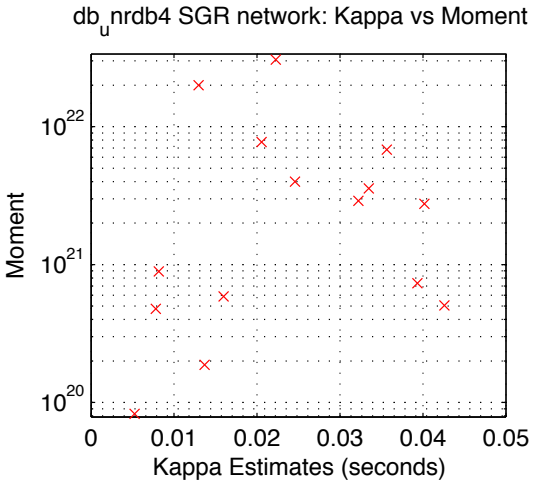

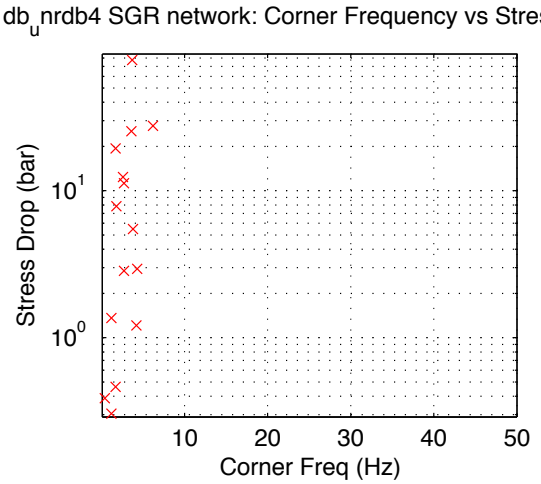

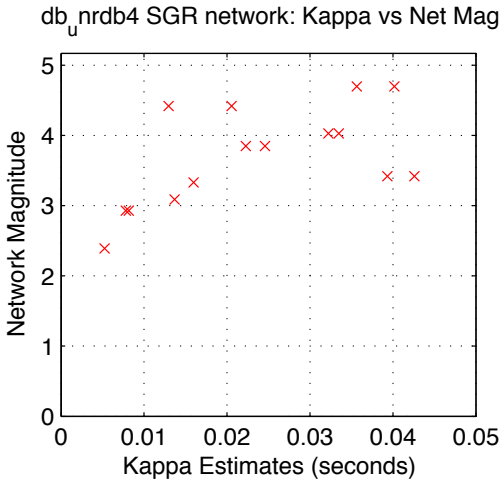

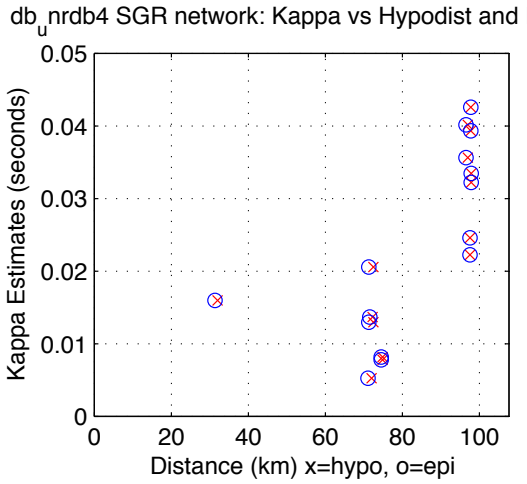

SGR:NE Passing: 15, Fail SNR: < 5 in 0.9 of freq range = 0, Fail SqErr: > 0.3 = 0, Fail StDrop: > 5000 = 0
SGR:NE Fail High Corner: > 45 Hz = 5

UNR Moderates With Strong Motion Records, 95−02 −− SGR NE
median kappa 0.045, median stdrop 45.0, median corner 6.3
min SNR: 5.0 minPct above SNR: 0.90 fitid range: 85170 to 87586

db$_u$nrdb4 SGR network: Kappa vs Corner

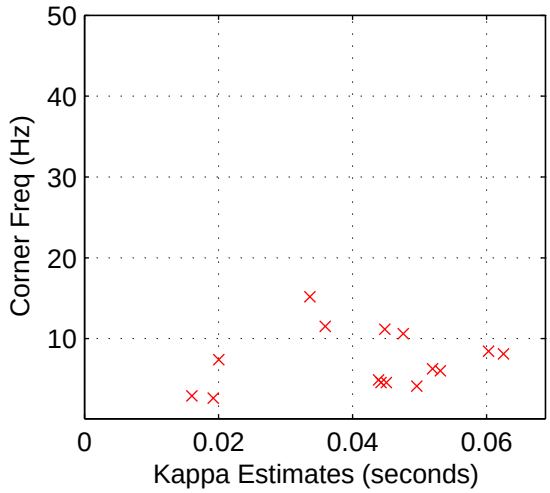

db$_u$nrdb4 SGR network: Kappa vs Stress Drop

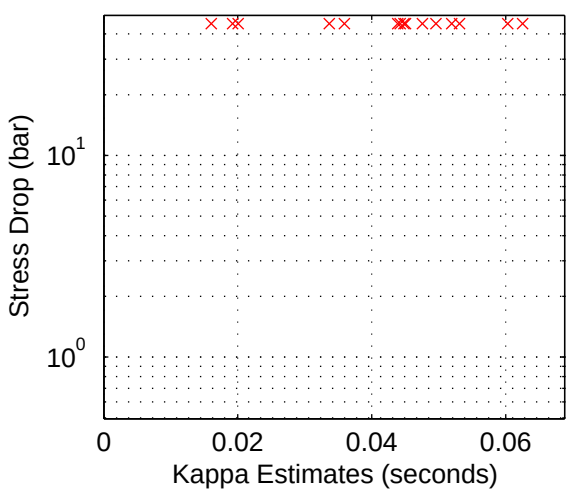

db$_u$nrdb4 SGR network: Kappa vs Moment

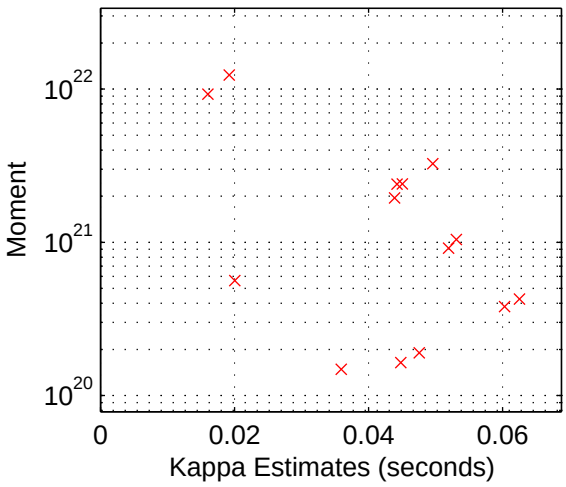

db$_u$nrdb4 SGR network: Corner Frequency vs Stress Drop

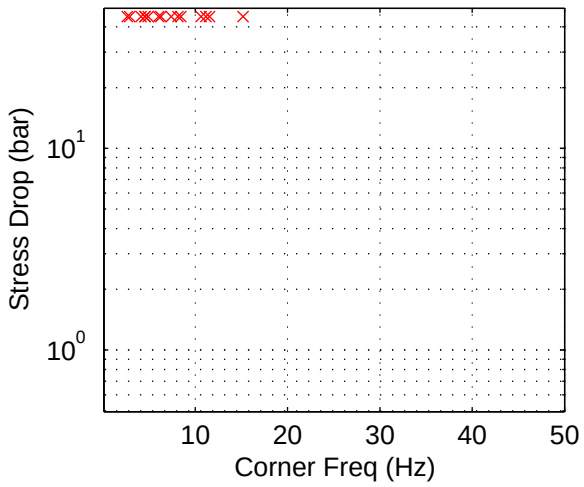

db$_u$nrdb4 SGR network: Kappa vs Net Mag

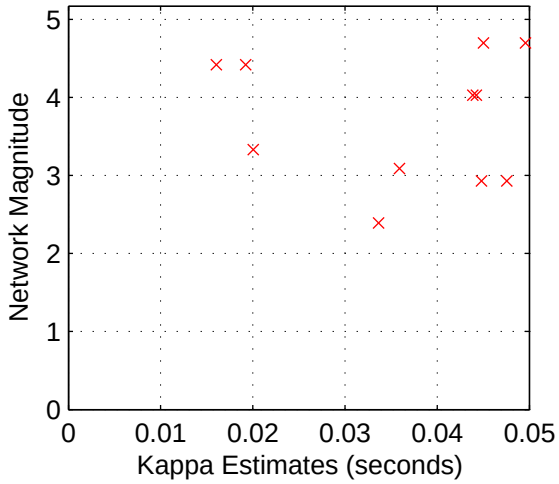

db$_u$nrdb4 SGR network: Kappa vs Hypodist and Epidist

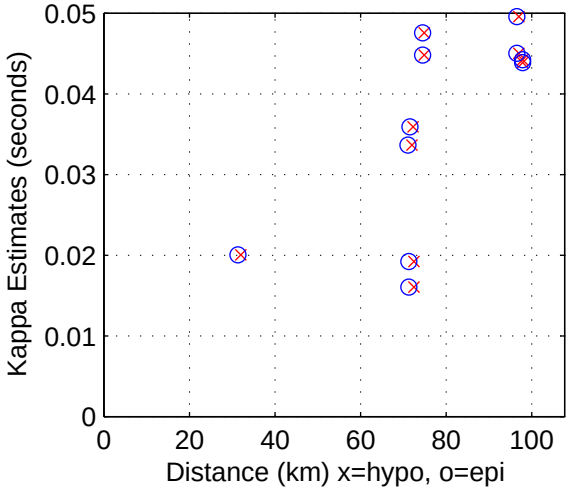

SGR:NE Passing: 15, Fail SNR: < 5 in 0.9 of freq range = 0, Fail SqErr: > 0.3 = 0, Fail StDrop: > 5000 = 0
SGR:NE Fail High Corner: > 45 Hz = 5

Figure B 41. Station SPC parametric plot. Free stress drop.
Source: DID 006GB.003, directory kappawrap/case6a/Figs45
File SPC.85170_87586.NE.eps

UNR Moderates With Strong Motion Records, 95–02 –– SPC NE
median kappa 0.036, median stdrop 19.6, median corner 3.4
min SNR: 5.0 minPct above SNR: 0.90 fitid range: 85170 to 87586

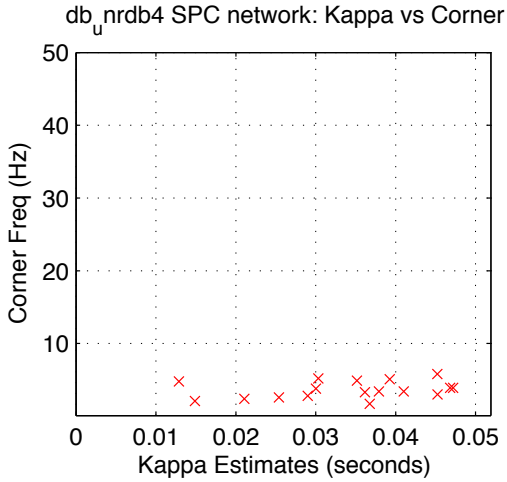

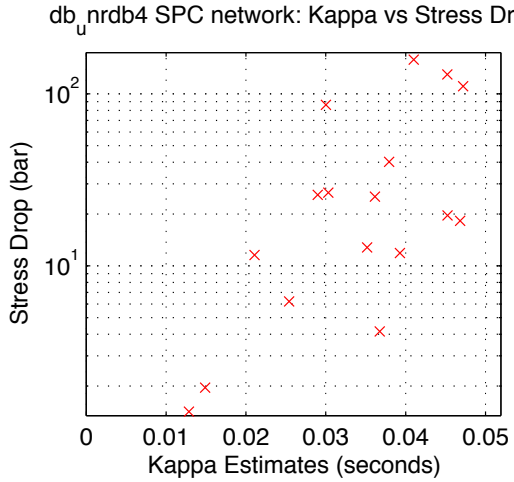

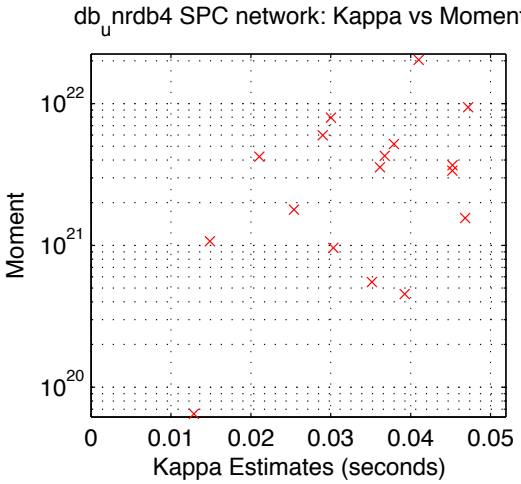

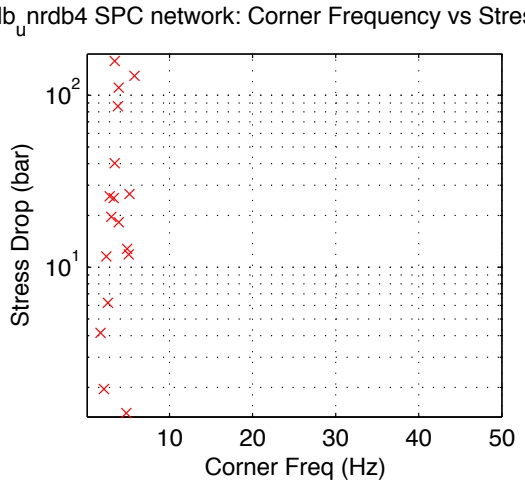

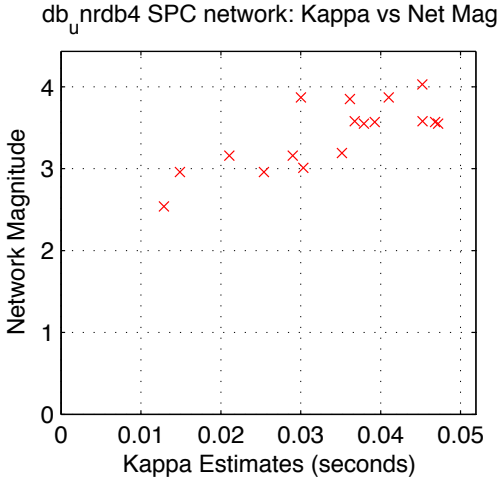

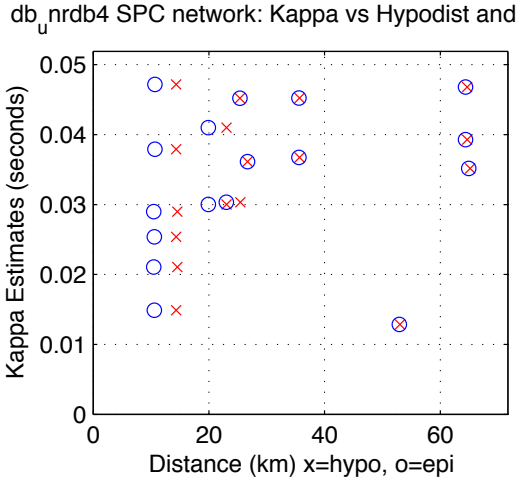

SPC:NE Passing: 17, Fail SNR: < 5 in 0.9 of freq range = 0, Fail SqErr: > 0.3 = 0, Fail StDrop: > 5000 = 0
SPC:NE Fail High Corner: > 45 Hz = 6

Figure B 42. Station SPC parametric plot. Fixed stress drop.
Source: DID 006GB.003, directory kappawrap/case6a/Figs45
File SPC.85170_87586.NE.fixed.eps

UNR Moderates With Strong Motion Records, 95–02 –– SPC NE
median kappa 0.040, median stdrop 45.0, median corner 4.4
min SNR: 5.0 minPct above SNR: 0.90 fitid range: 85170 to 87586

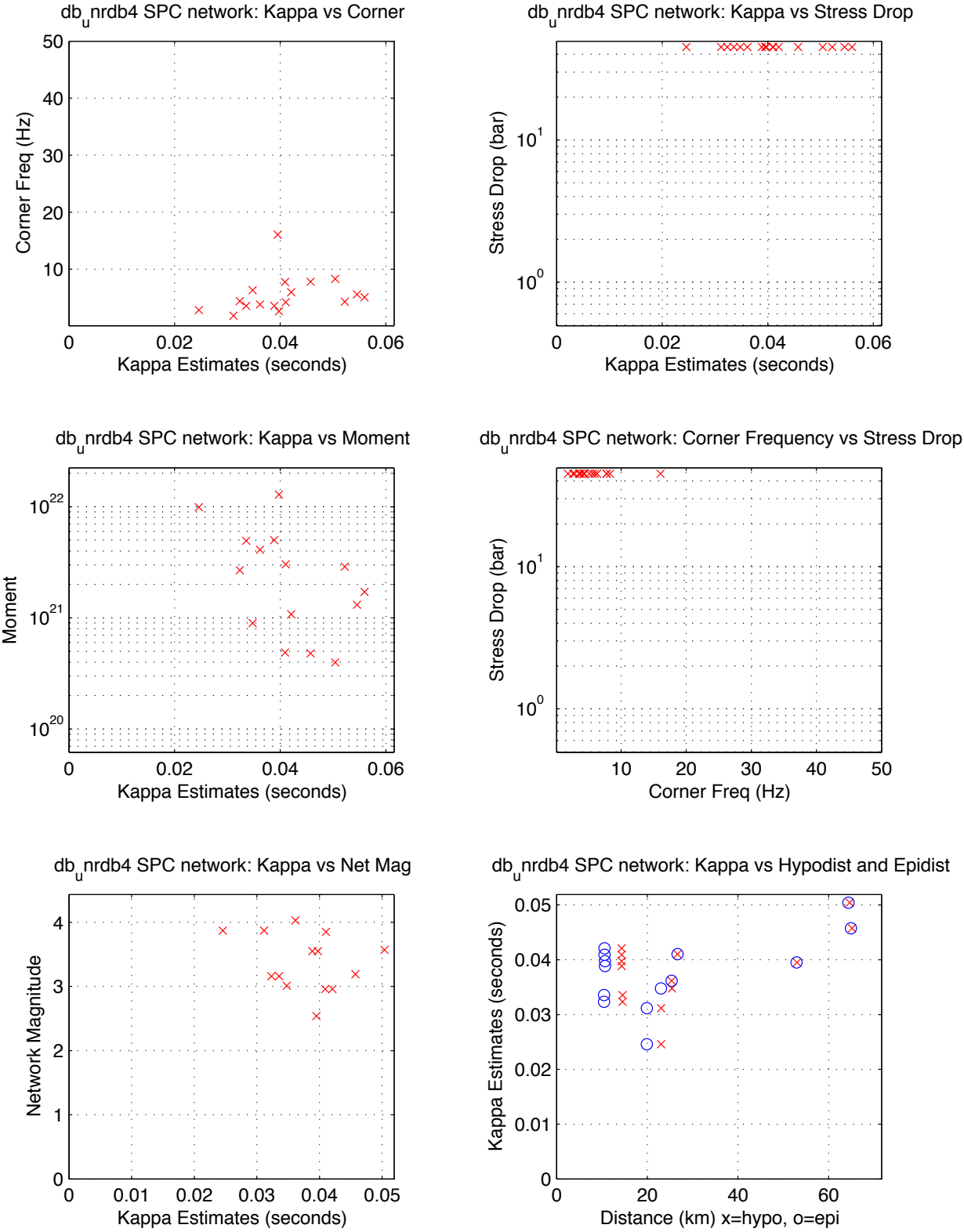

SPC:NE Passing: 17, Fail SNR: < 5 in 0.9 of freq range = 0, Fail SqErr: > 0.3 = 0, Fail StDrop: > 5000 = 0
SPC:NE Fail High Corner: > 45 Hz = 6

Figure B 43. Station SPRS parametric plot. Free stress drop.
Source: DID 006GB.003, directory kappawrap/case6a/Figs45
File SPRS.85170_87586.NE.eps

UNR Moderates With Strong Motion Records, 95–02 –– SPRS NE
median kappa 0.032, median stdrop 29.2, median corner 2.6
min SNR: 5.0 minPct above SNR: 0.90 fitid range: 85170 to 87586

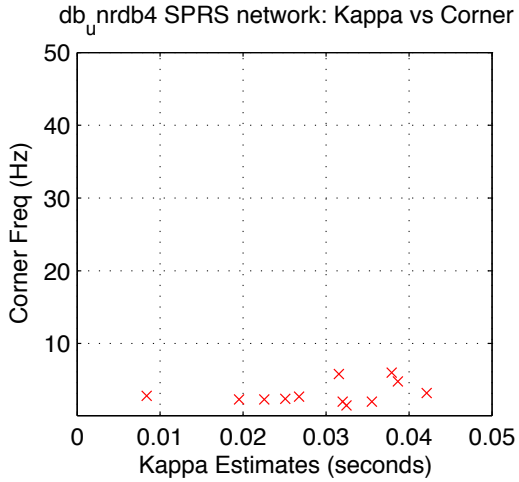

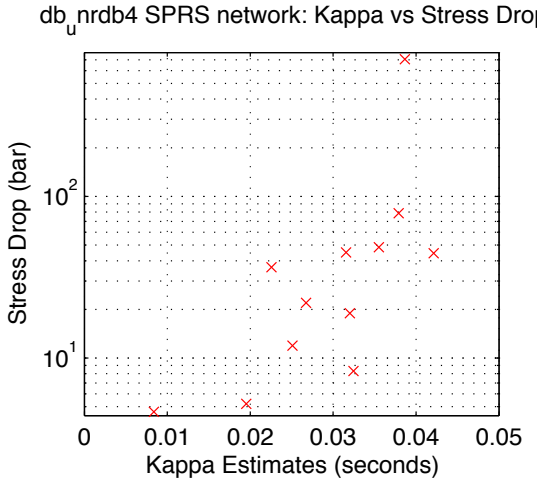

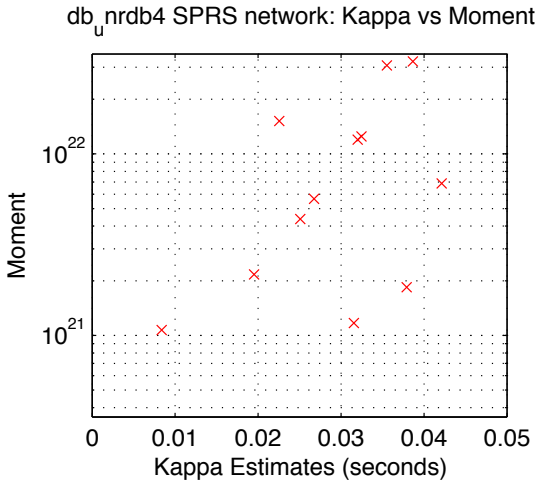

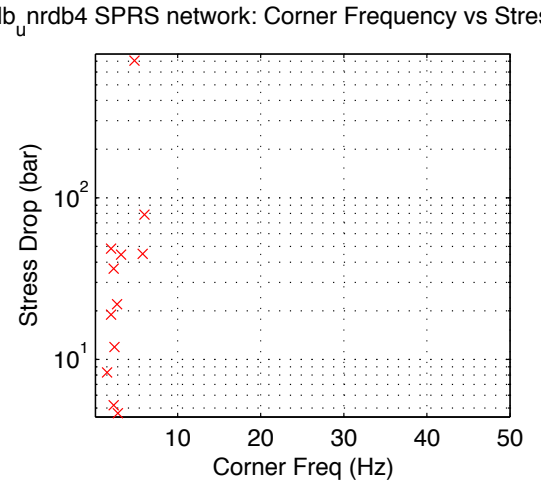

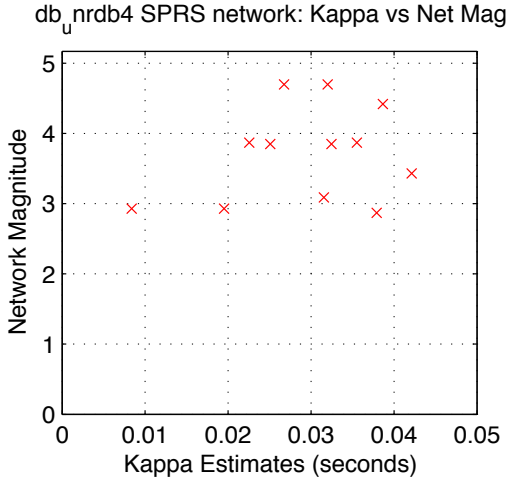

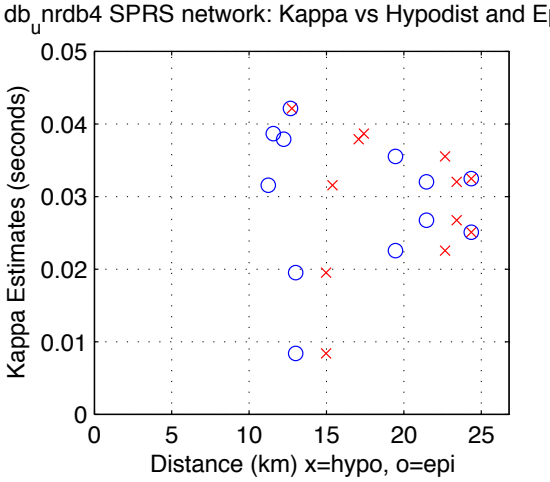

SPRS:NE Passing: 12, Fail SNR: < 5 in 0.9 of freq range = 24, Fail SqErr: > 0.3 = 0, Fail StDrop: > 5000 = 0
SPRS:NE Fail High Corner: > 45 Hz = 0

Figure B 44. Station SPRS parametric plot. Fixed stress drop.
Source: DID 006GB.003, directory kappawrap/case6a/Figs45
File SPRS.85170_87586.NE.fixed.eps

UNR Moderates With Strong Motion Records, 95–02 –– SPRS NE
median kappa 0.034, median stdrop 45.0, median corner 3.6
min SNR: 5.0 minPct above SNR: 0.90 fitid range: 85170 to 87586

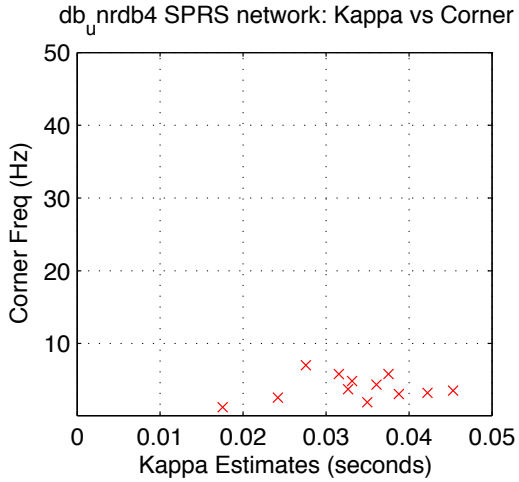

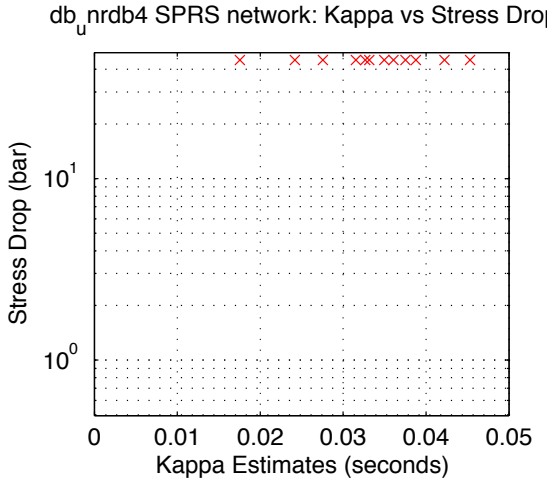

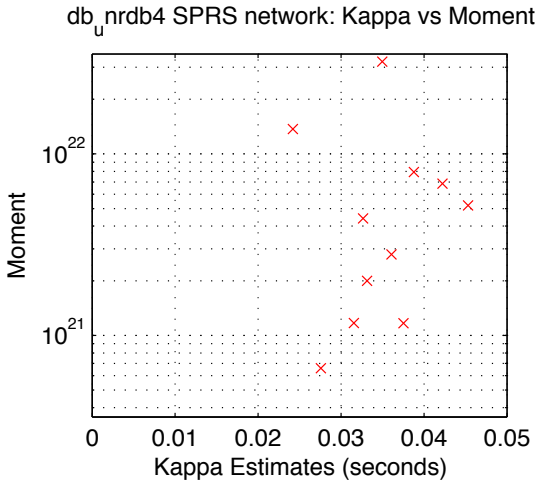

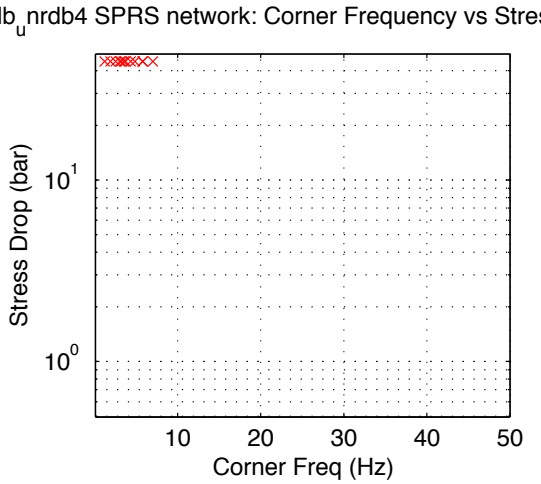

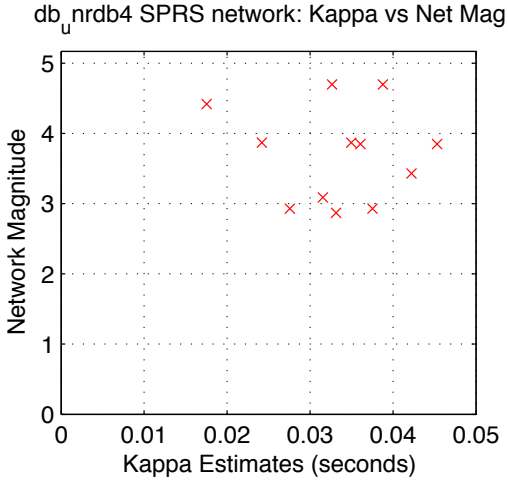

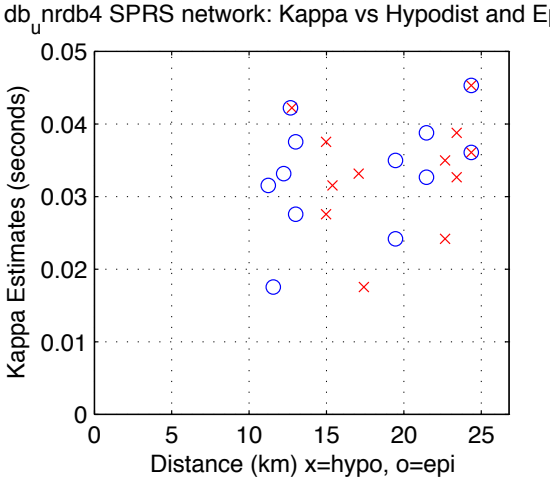

SPRS:NE Passing: 12, Fail SNR: < 5 in 0.9 of freq range = 24, Fail SqErr: > 0.3 = 0, Fail StDrop: > 5000 = 0
SPRS:NE Fail High Corner: > 45 Hz = 0

Figure B 45. Station STC parametric plot. Free stress drop.
Source: DID 006GB.003, directory kappawrap/case6a/Figs45
File STC.85170_87586.NE.eps

UNR Moderates With Strong Motion Records, 95–02 –– STC NE
median kappa 0.032, median stdrop 26.7, median corner 3.2
min SNR: 5.0 minPct above SNR: 0.90 fitid range: 85170 to 87586

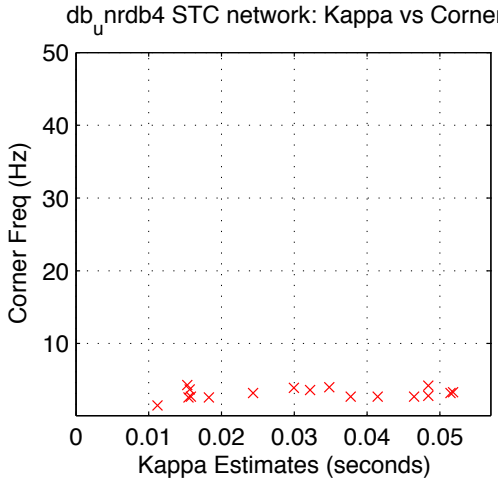

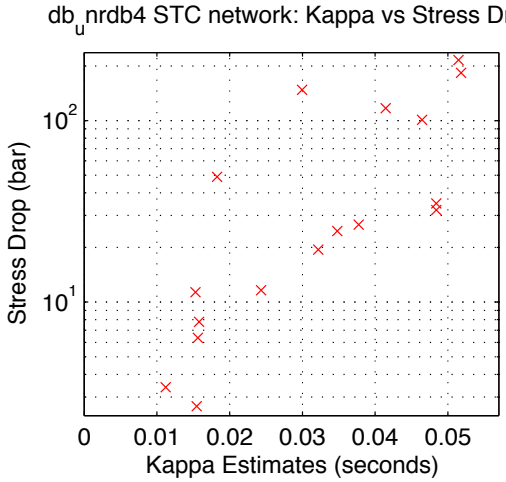

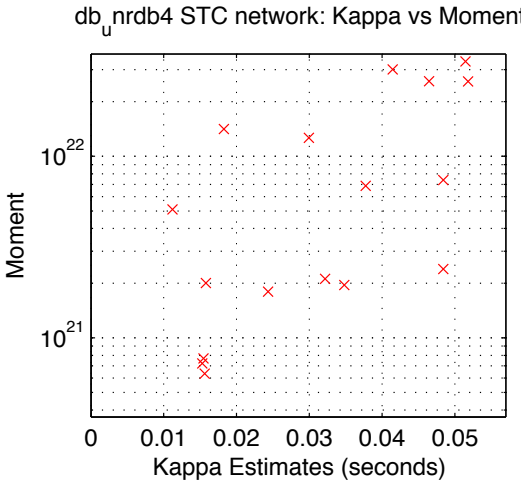

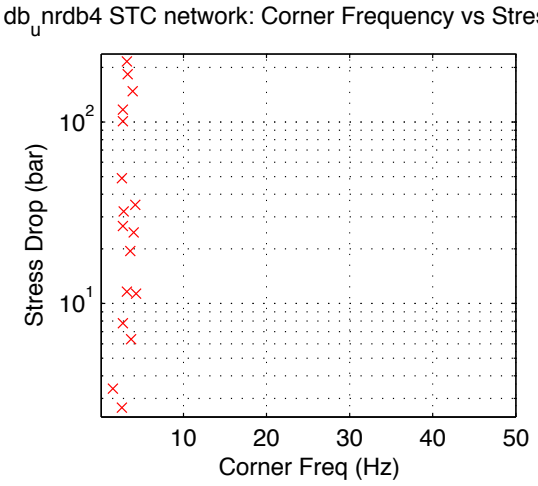

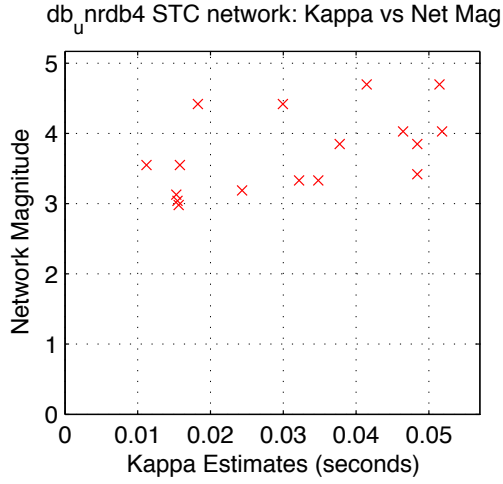

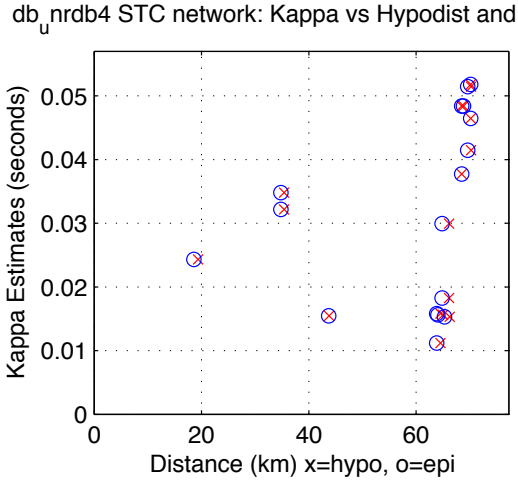

STC:NE Passing: 17, Fail SNR: < 5 in 0.9 of freq range = 0, Fail SqErr: > 0.3 = 1, Fail StDrop: > 5000 = 0
STC:NE Fail High Corner: > 45 Hz = 2

Figure B 46. Station STC parametric plot. Free stress drop.
Source: DID 006GB.003, directory kappawrap/case6a/Figs45
File STC.85170_87586.NE.eps

UNR Moderates With Strong Motion Records, 95–02 –– STC NE
median kappa 0.039, median stdrop 45.0, median corner 4.6
min SNR: 5.0 minPct above SNR: 0.90 fitid range: 85170 to 87586

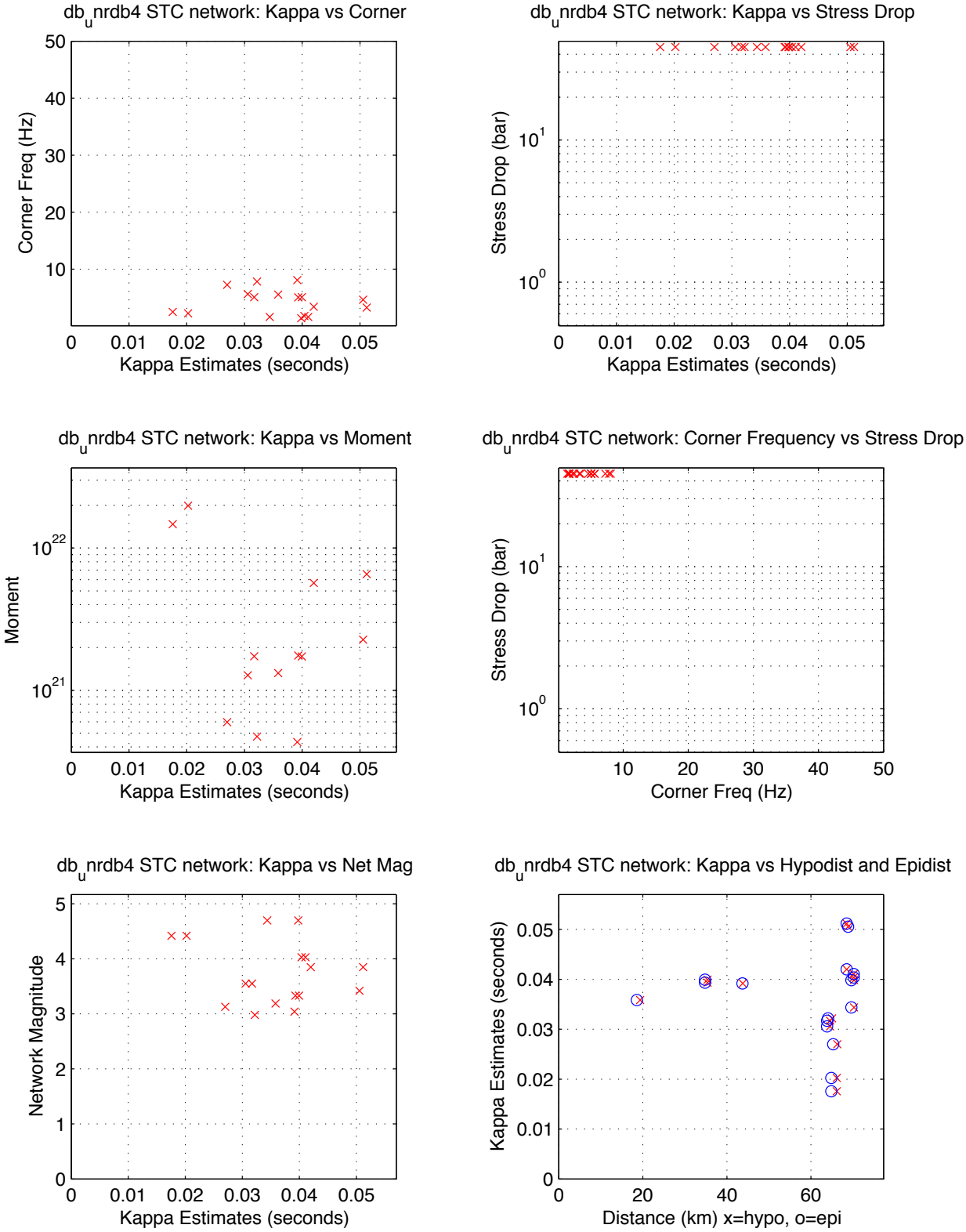

STC:NE Passing: 17, Fail SNR: < 5 in 0.9 of freq range = 0, Fail SqErr: > 0.3 = 1, Fail StDrop: > 5000 = 0
STC:NE Fail High Corner: > 45 Hz = 2

Figure B 47. Station STH parametric plot. Free stress drop.
Source: DID 006GB.003, directory kappawrap/case6a/Figs45
File STH.85170_87586.NE.eps

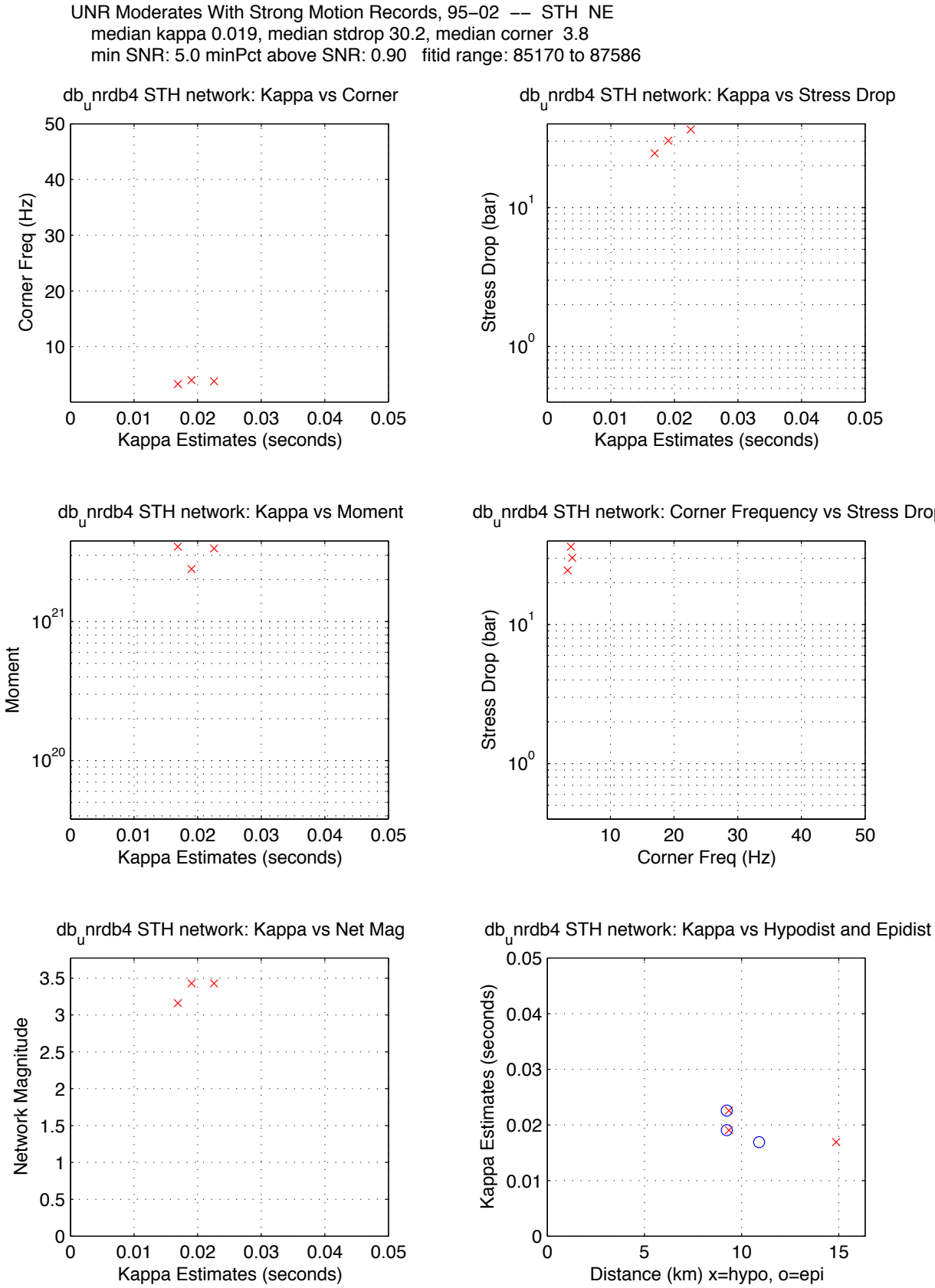

STH:NE Passing: 3, Fail SNR: < 5 in 0.9 of freq range = 0, Fail SqErr: > 0.3 = 0, Fail StDrop: > 5000 = 0
STH:NE Fail High Corner: > 45 Hz = 0

Figure B 48. Station STH parametric plot. Fixed stress drop.
Source: DID 006GB.003, directory kappawrap/case6a/Figs45
File STH.85170_87586.NE.fixed.eps

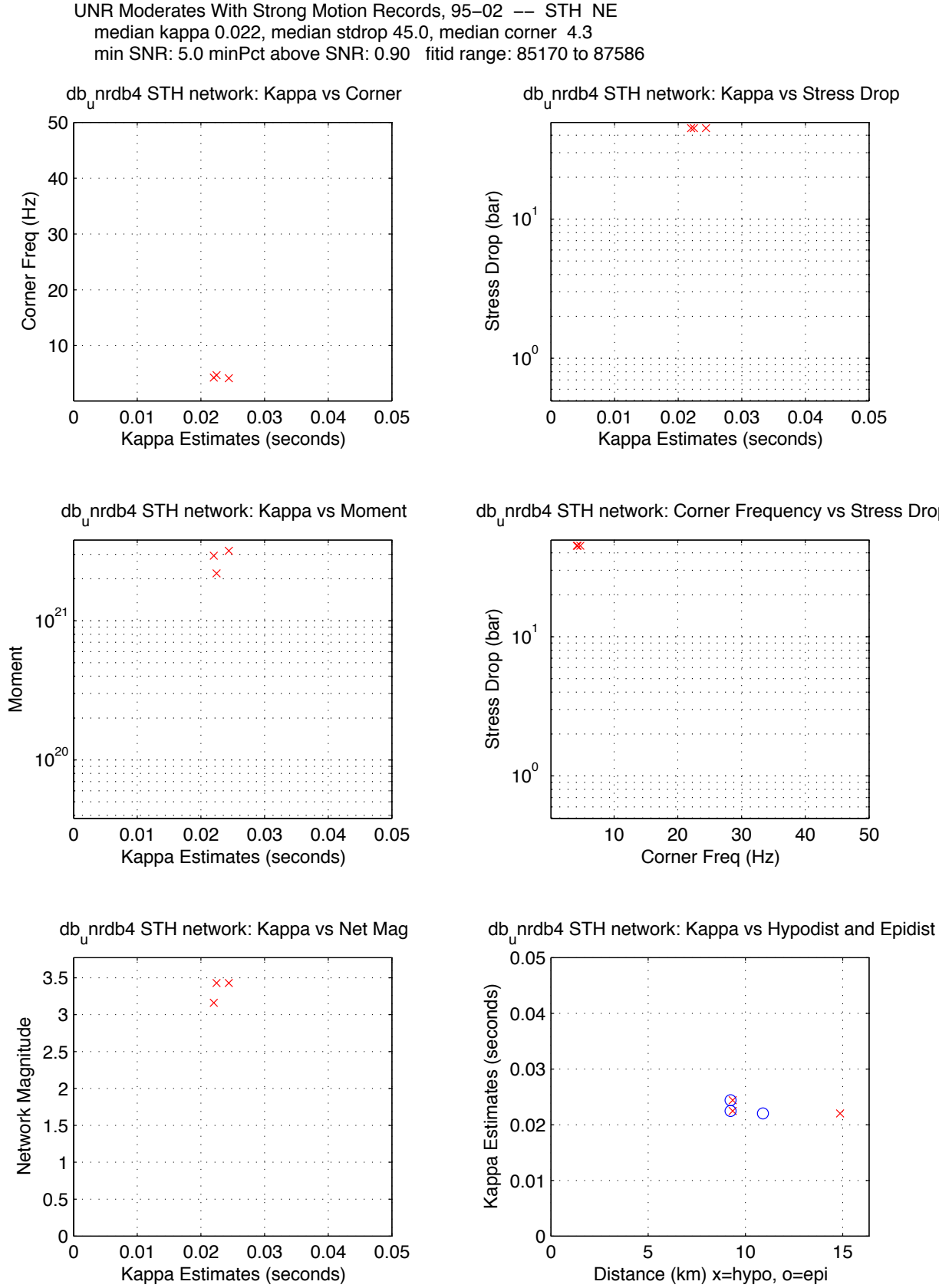

STH:NE Passing: 3, Fail SNR: < 5 in 0.9 of freq range = 0, Fail SqErr: > 0.3 = 0, Fail StDrop: > 5000 = 0
STH:NE Fail High Corner: > 45 Hz = 0

Figure B 49. Station STO parametric plot. Free stress drop.
Source: DID 006GB.003, directory kappawrap/case6a/Figs45
File STO.85170_87586.NE.eps

UNR Moderates With Strong Motion Records, 95–02 –– STO NE
median kappa 0.030, median stdrop 16.9, median corner 4.0
min SNR: 5.0 minPct above SNR: 0.90 fitid range: 85170 to 87586

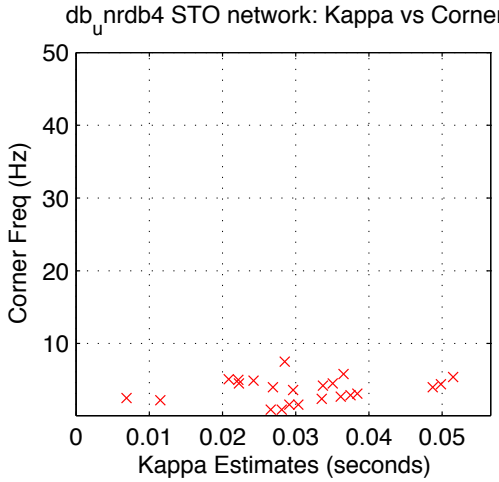

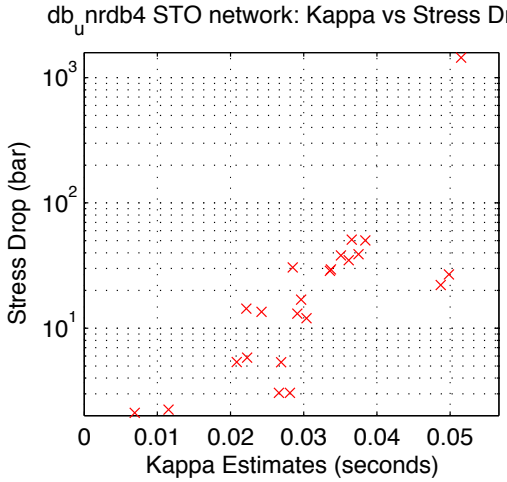

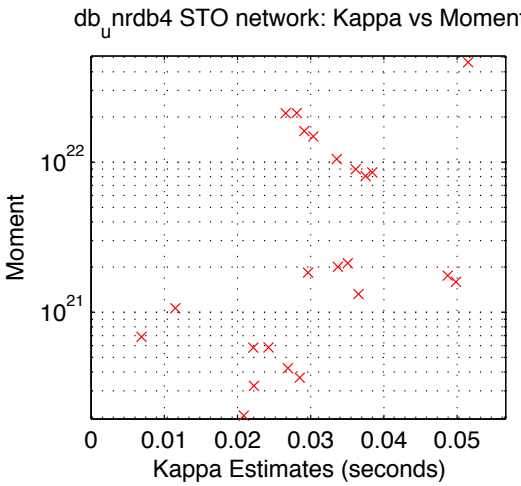

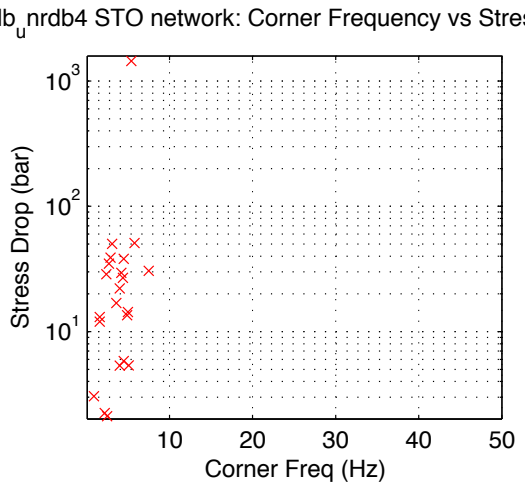

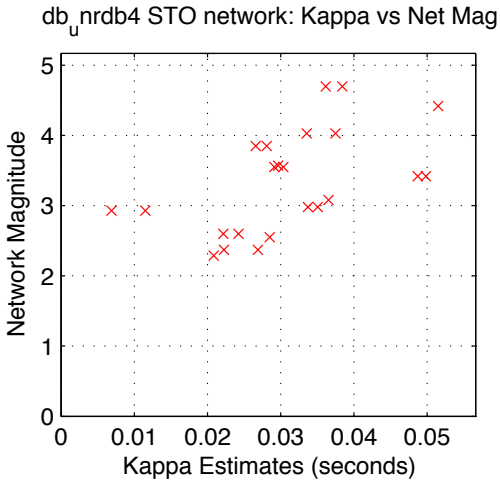

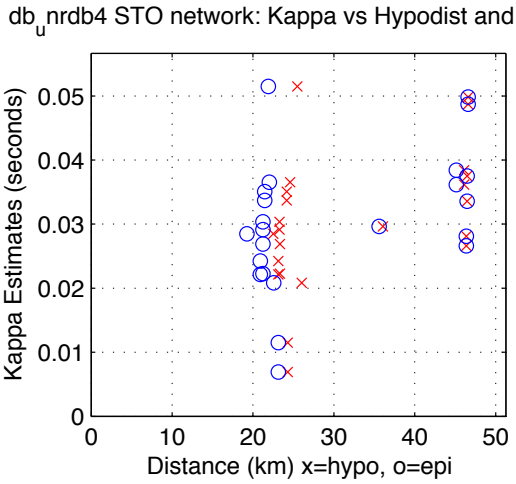

STO:NE Passing: 23, Fail SNR: < 5 in 0.9 of freq range = 1, Fail SqErr: > 0.3 = 0, Fail StDrop: > 5000 = 0
STO:NE Fail High Corner: > 45 Hz = 3

Figure B 50. Station STO parametric plot. Fixed stress drop.
Source: DID 006GB.003, directory kappawrap/case6a/Figs45
File STO.85170_87586.NE.fixed.eps

UNR Moderates With Strong Motion Records, 95–02 –– STO NE
median kappa 0.038, median stdrop 45.0, median corner 5.3
min SNR: 5.0 minPct above SNR: 0.90 fitid range: 85170 to 87586

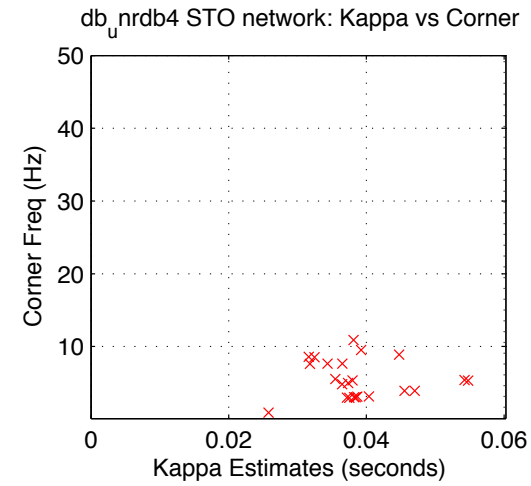

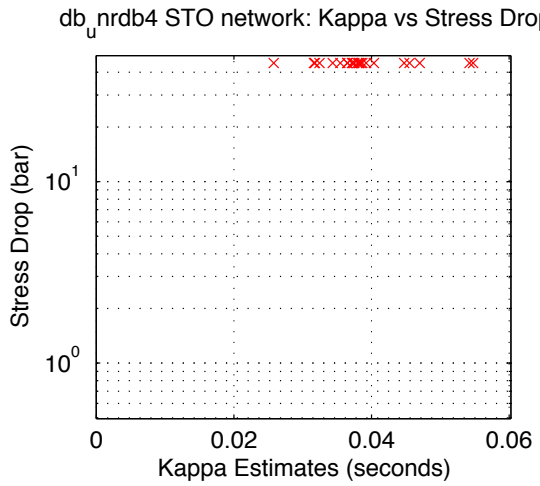

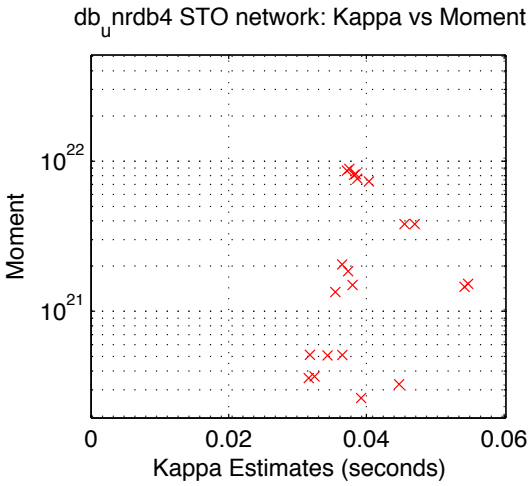

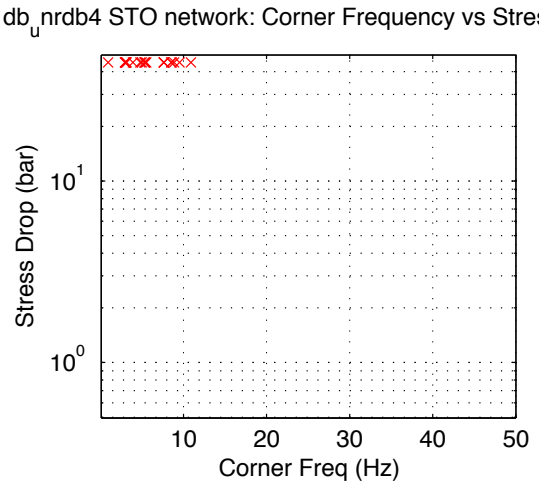

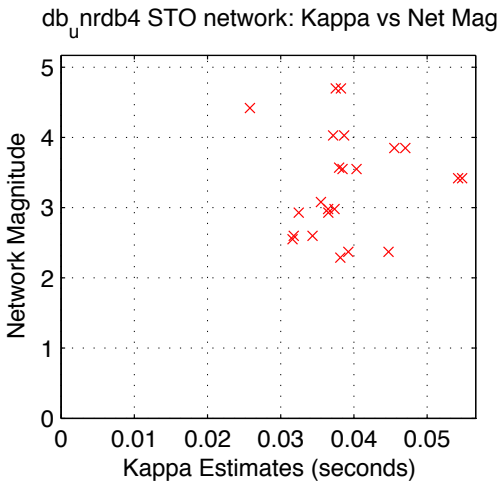

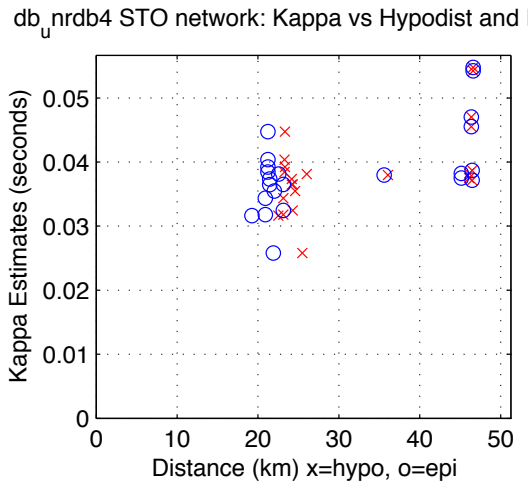

STO:NE Passing: 23, Fail SNR: < 5 in 0.9 of freq range = 1, Fail SqErr: > 0.3 = 0, Fail StDrop: > 5000 = 0
STO:NE Fail High Corner: > 45 Hz = 3

Figure B 51. Station SYM parametric plot. Free stress drop.
Source: DID 006GB.003, directory kappawrap/case6a/Figs45
File SYM.85170_87586.NE.eps

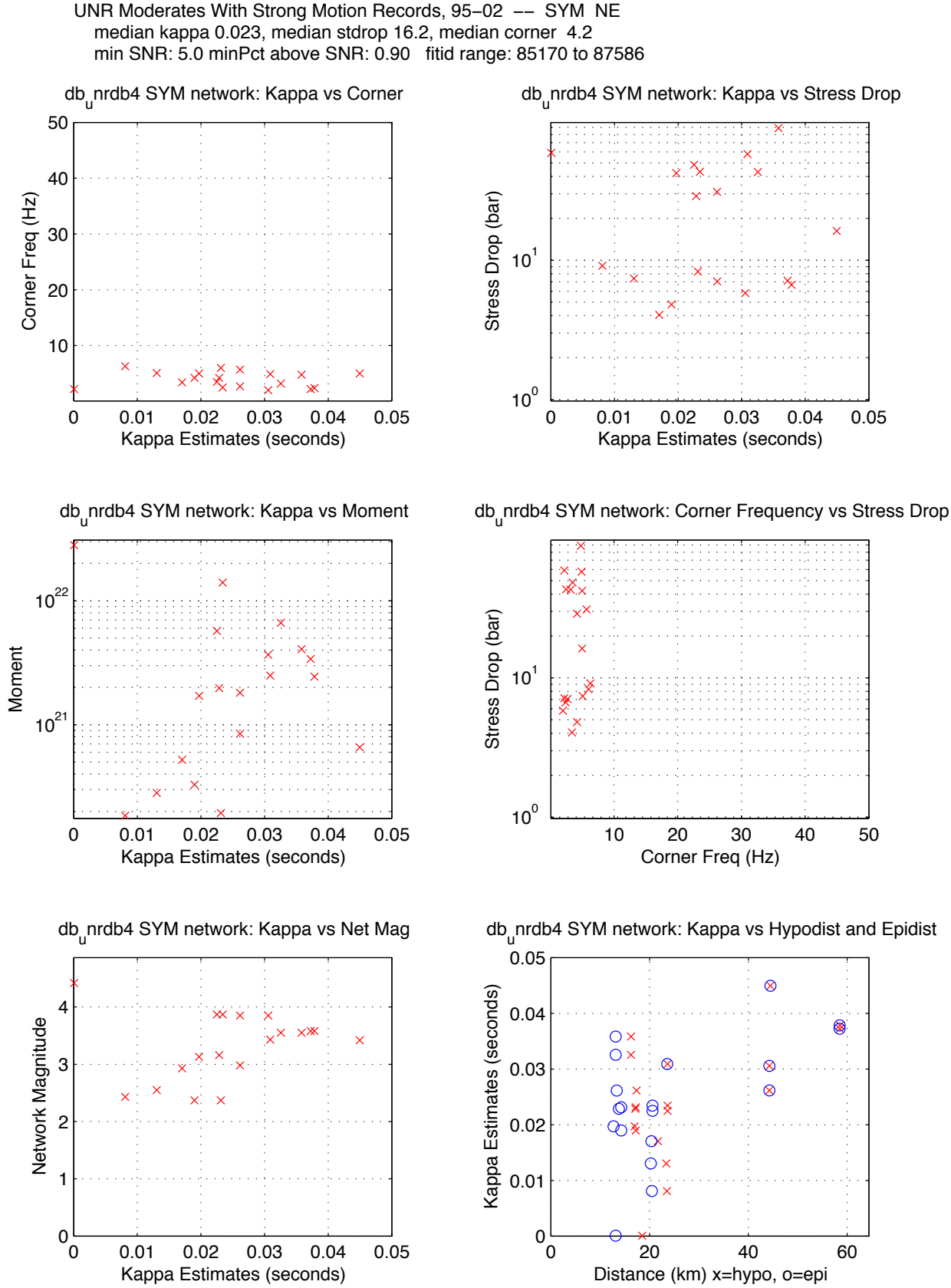

SYM:NE Passing: 19, Fail SNR: < 5 in 0.9 of freq range = 1, Fail SqErr: > 0.3 = 0, Fail StDrop: > 5000 = 0
SYM:NE Fail High Corner: > 45 Hz = 1

Figure B 52. Station SYM parametric plot. Fixed stress drop.
Source: DID 006GB.003, directory kappawrap/case6a/Figs45
File SYM.85170_87586.NE.fixed.eps

UNR Moderates With Strong Motion Records, 95–02 –– SYM NE
median kappa 0.030, median stdrop 45.0, median corner 5.1
min SNR: 5.0 minPct above SNR: 0.90 fitid range: 85170 to 87586

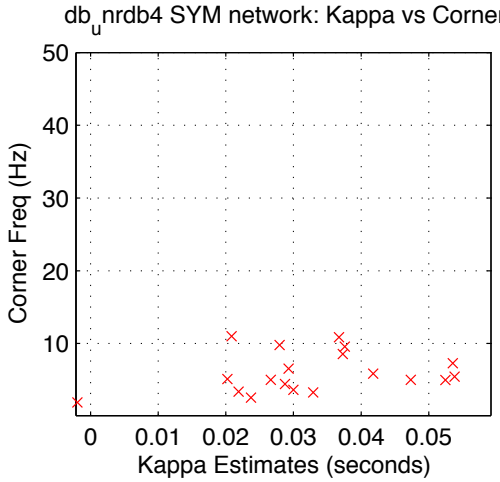

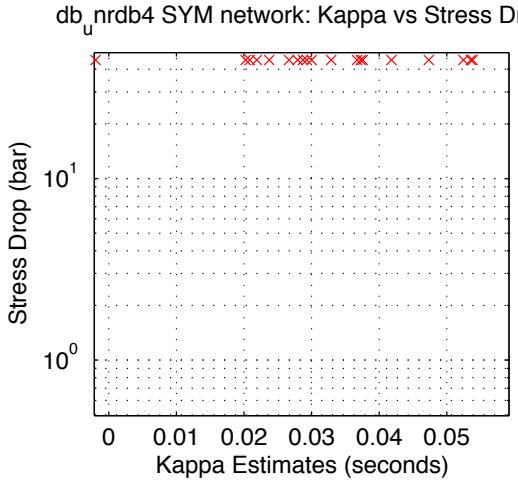

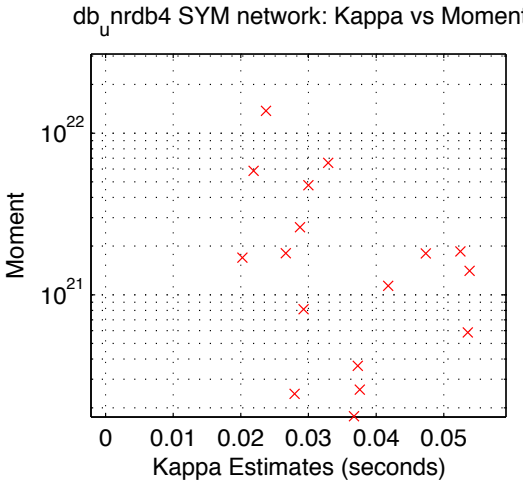

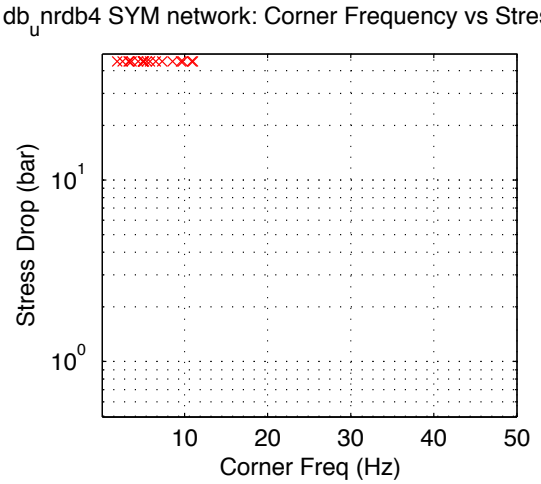

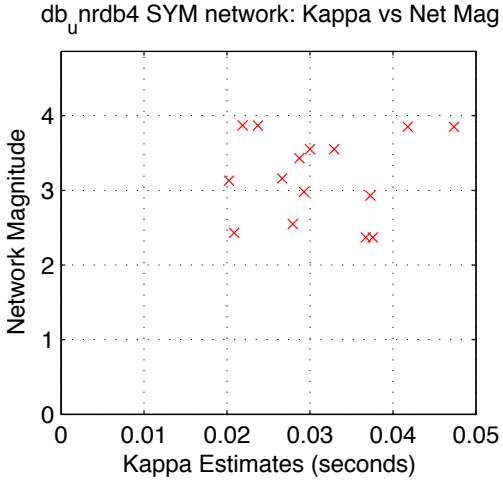

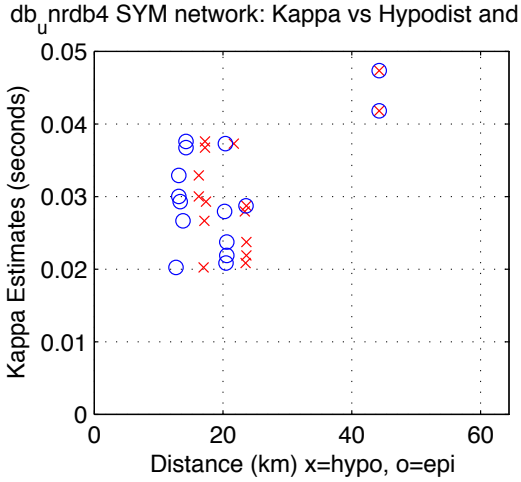

SYM:NE Passing: 19, Fail SNR: < 5 in 0.9 of freq range = 1, Fail SqErr: > 0.3 = 0, Fail StDrop: > 5000 = 0
SYM:NE Fail High Corner: > 45 Hz = 1

Figure B 53. Station SYMS parametric plot. Free stress drop.
Source: DID 006GB.003, directory kappawrap/case6a/Figs45
File SYMS.85170_87586.NE.eps

UNR Moderates With Strong Motion Records, 95–02 –– SYMS NE
median kappa 0.025, median stdrop 48.5, median corner 2.7
min SNR: 5.0 minPct above SNR: 0.90 fitid range: 85170 to 87586

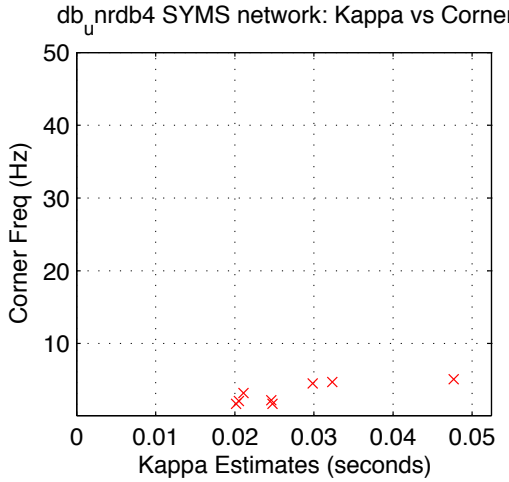

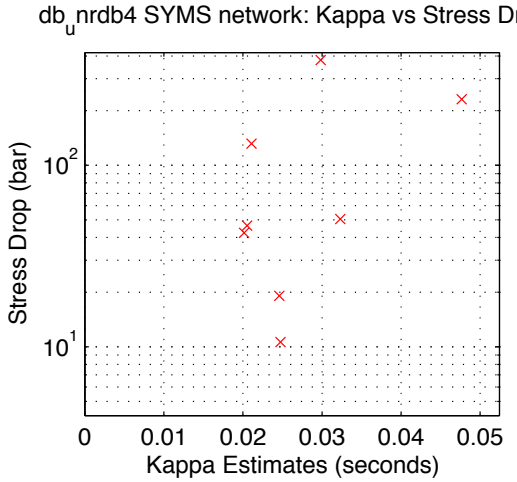

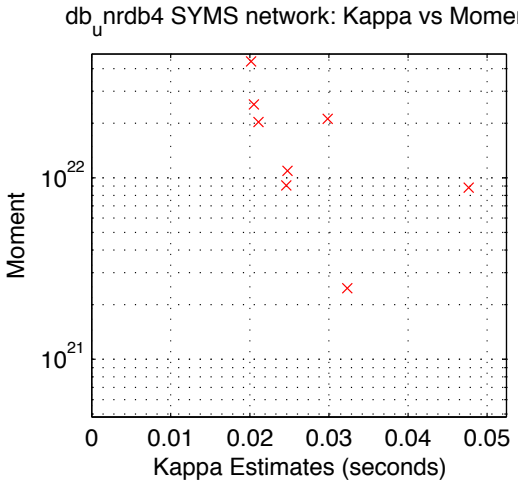

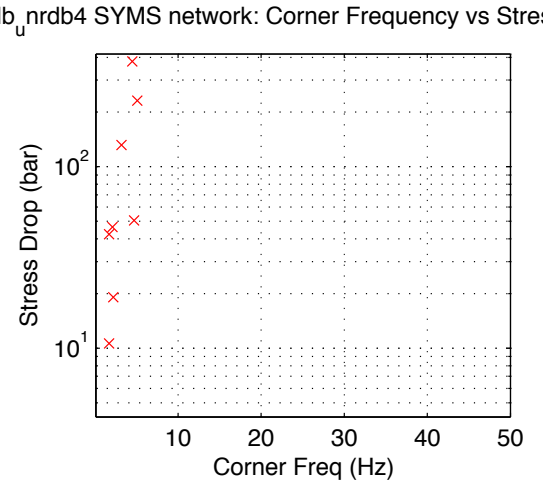

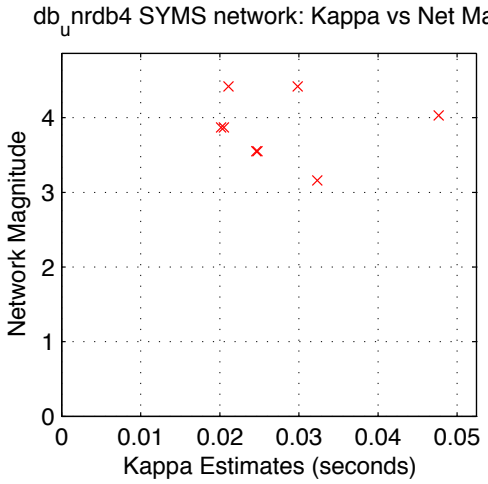

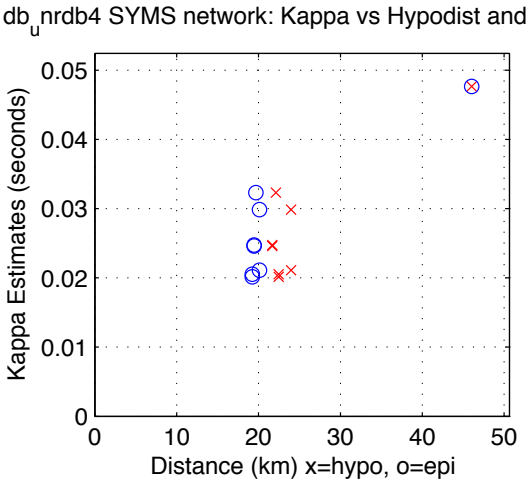

SYMS:NE Passing: 8, Fail SNR: < 5 in 0.9 of freq range = 30, Fail SqErr: > 0.3 = 0, Fail StDrop: > 5000 = 0
SYMS:NE Fail High Corner: > 45 Hz = 0

Figure B 54. Station SYMS parametric plot. Fixed stress drop.
Source: DID 006GB.003, directory kappawrap/case6a/Figs45
File SYMS.85170_87586.NE.fixed.eps

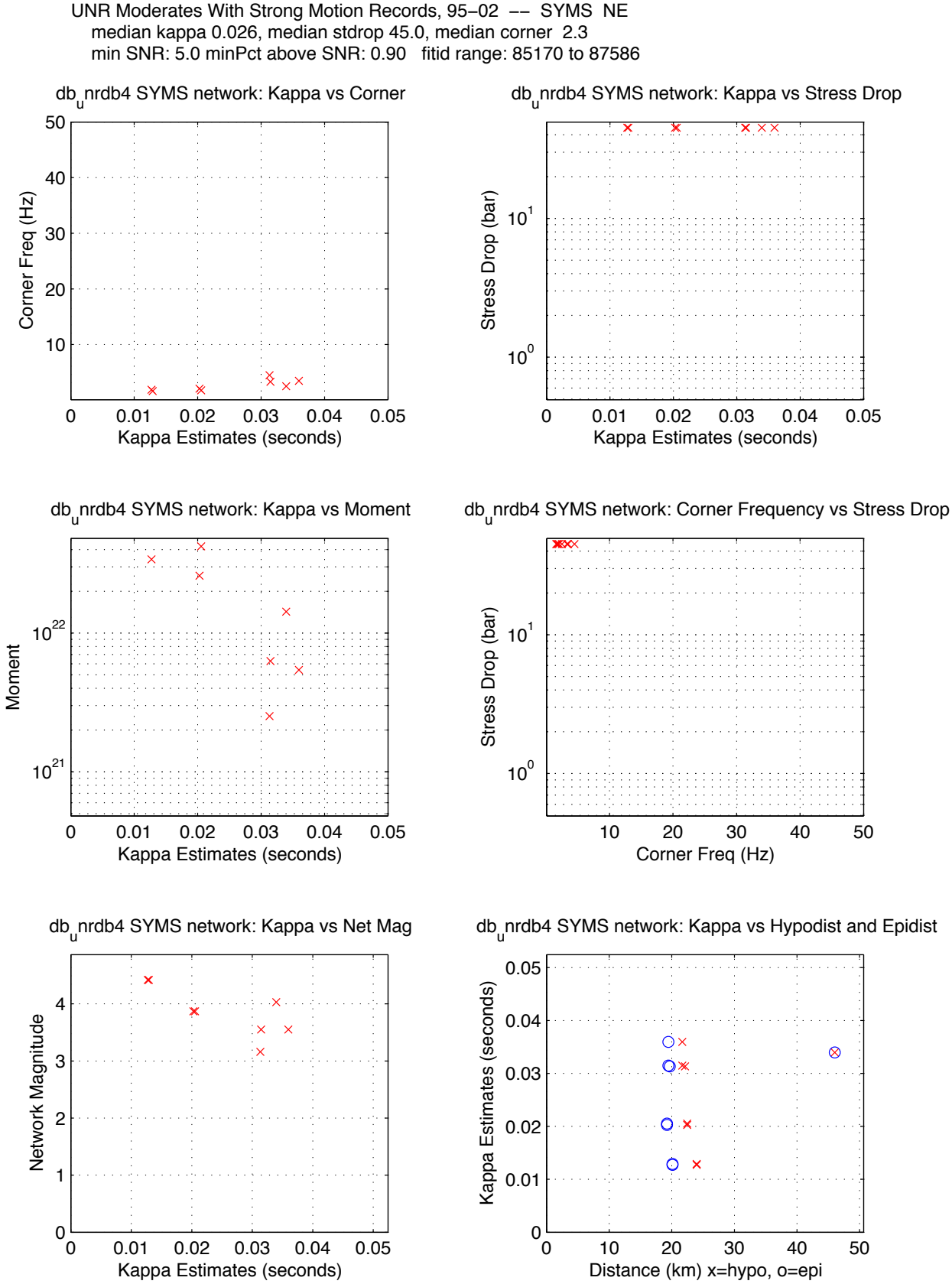

SYMS:NE Passing: 8, Fail SNR: < 5 in 0.9 of freq range = 30, Fail SqErr: > 0.3 = 0, Fail StDrop: > 5000 = 0
SYMS:NE Fail High Corner: > 45 Hz = 0

Figure B 55. Station TAR parametric plot. Free stress drop.
Source: DID 006GB.003, directory kappawrap/case6a/Figs45
File TAR.85170_87586.NE.eps

UNR Moderates With Strong Motion Records, 95–02 –– TAR NE
median kappa 0.022, median stdrop 3.3, median corner 2.3
min SNR: 5.0 minPct above SNR: 0.90 fitid range: 85170 to 87586

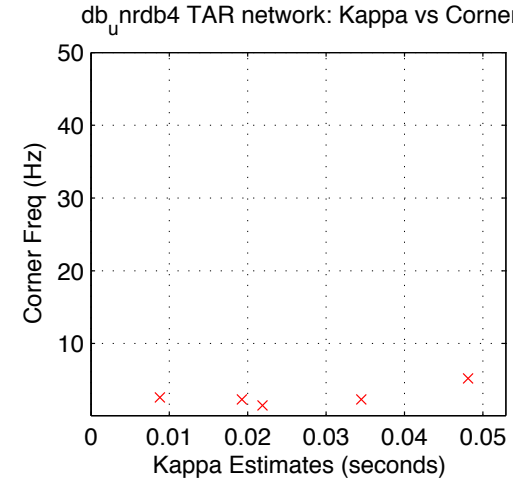

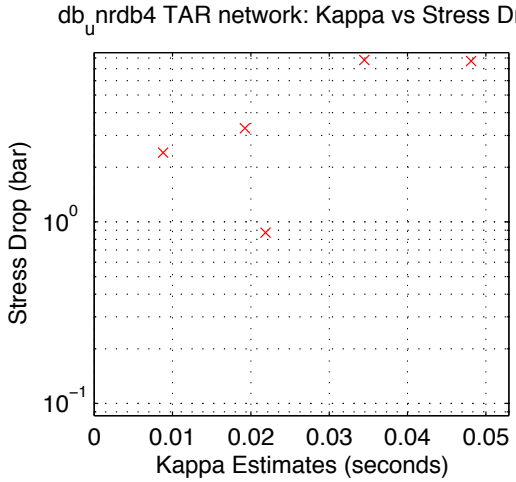

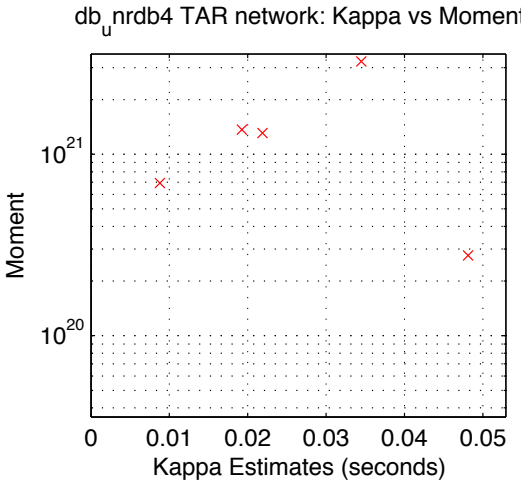

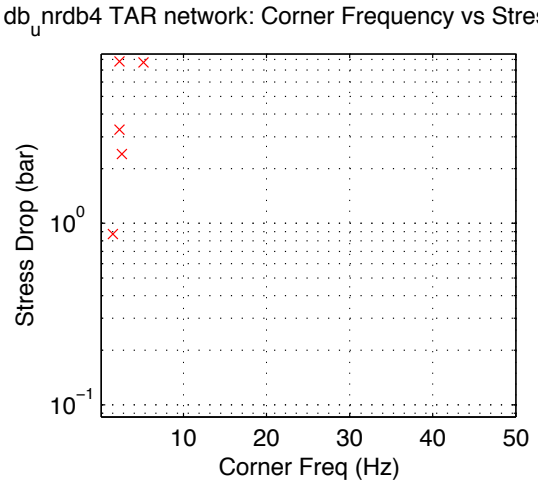

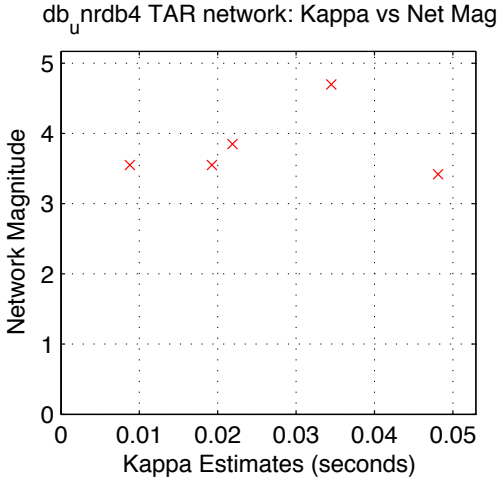

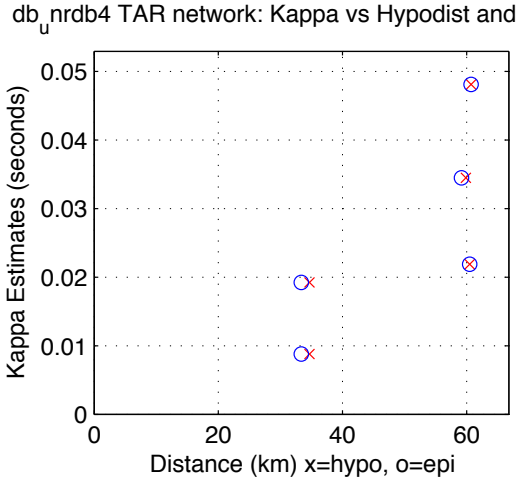

TAR:NE Passing: 5, Fail SNR: < 5 in 0.9 of freq range = 0, Fail SqErr: > 0.3 = 1, Fail StDrop: > 5000 = 0
TAR:NE Fail High Corner: > 45 Hz = 7

Figure B 56. Station TAR parametric plot. Fixed stress drop.
Source: DID 006GB.003, directory kappawrap/case6a/Figs45
File TAR.85170_87586.NE.fixed.eps

UNR Moderates With Strong Motion Records, 95–02 –– TAR NE
median kappa 0.049, median stdrop 45.0, median corner 8.4
min SNR: 5.0 minPct above SNR: 0.90 fitid range: 85170 to 87586

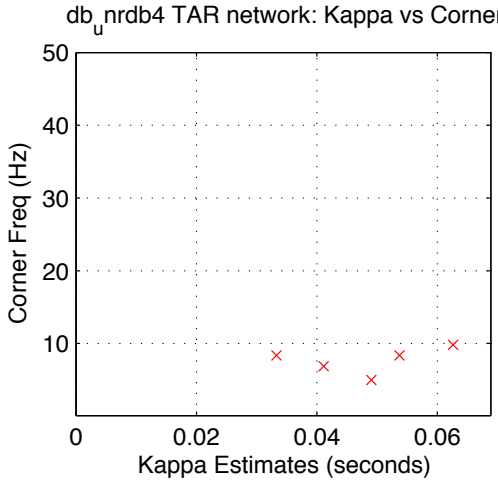

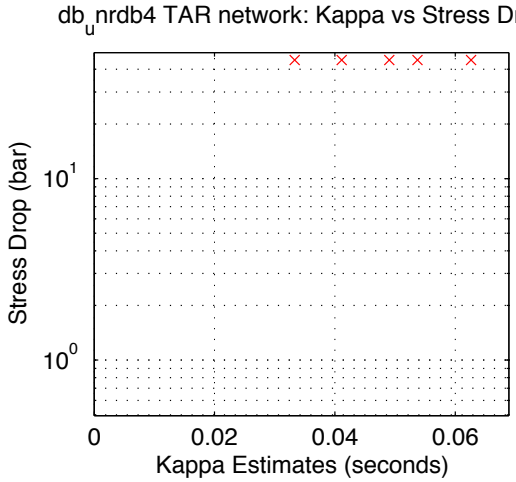

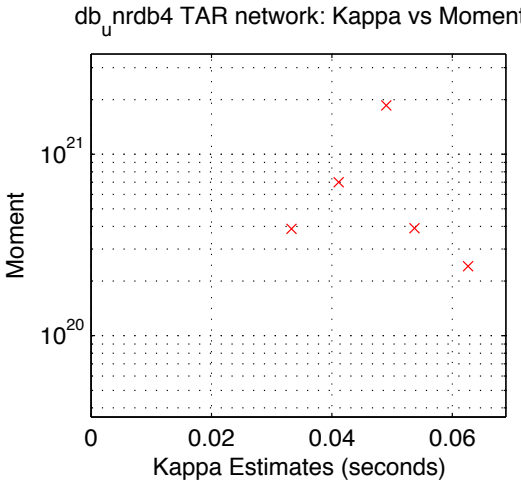

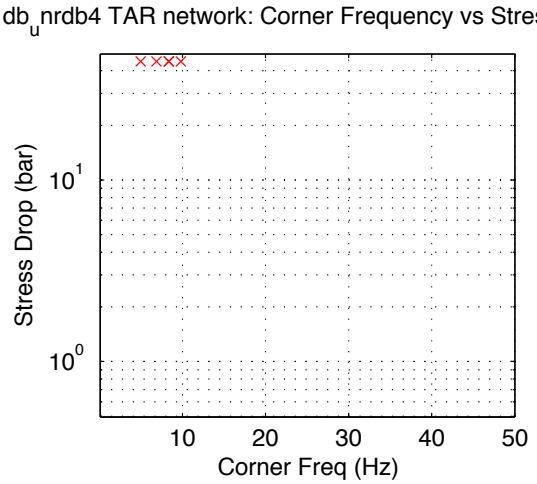

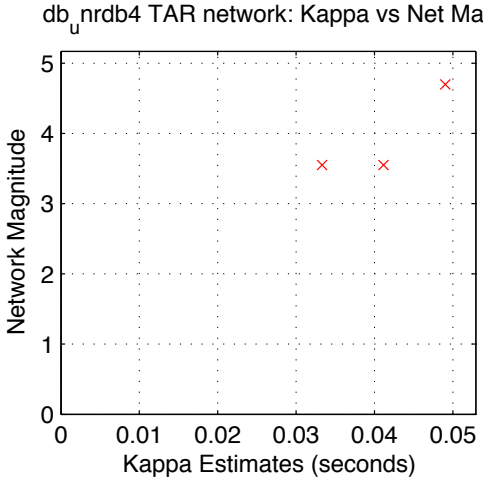

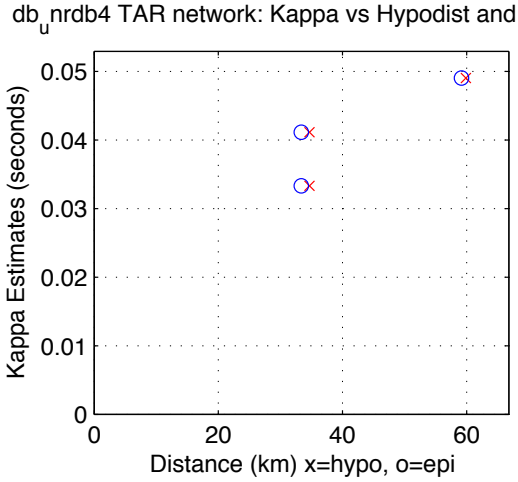

TAR:NE Passing: 5, Fail SNR: < 5 in 0.9 of freq range = 0, Fail SqErr: > 0.3 = 1, Fail StDrop: > 5000 = 0
TAR:NE Fail High Corner: > 45 Hz = 7

Figure B 57. Station TIM parametric plot. Free stress drop.
Source: DID 006GB.003, directory kappawrap/case6a/Figs45
File TIM.85170_87586.NE.eps

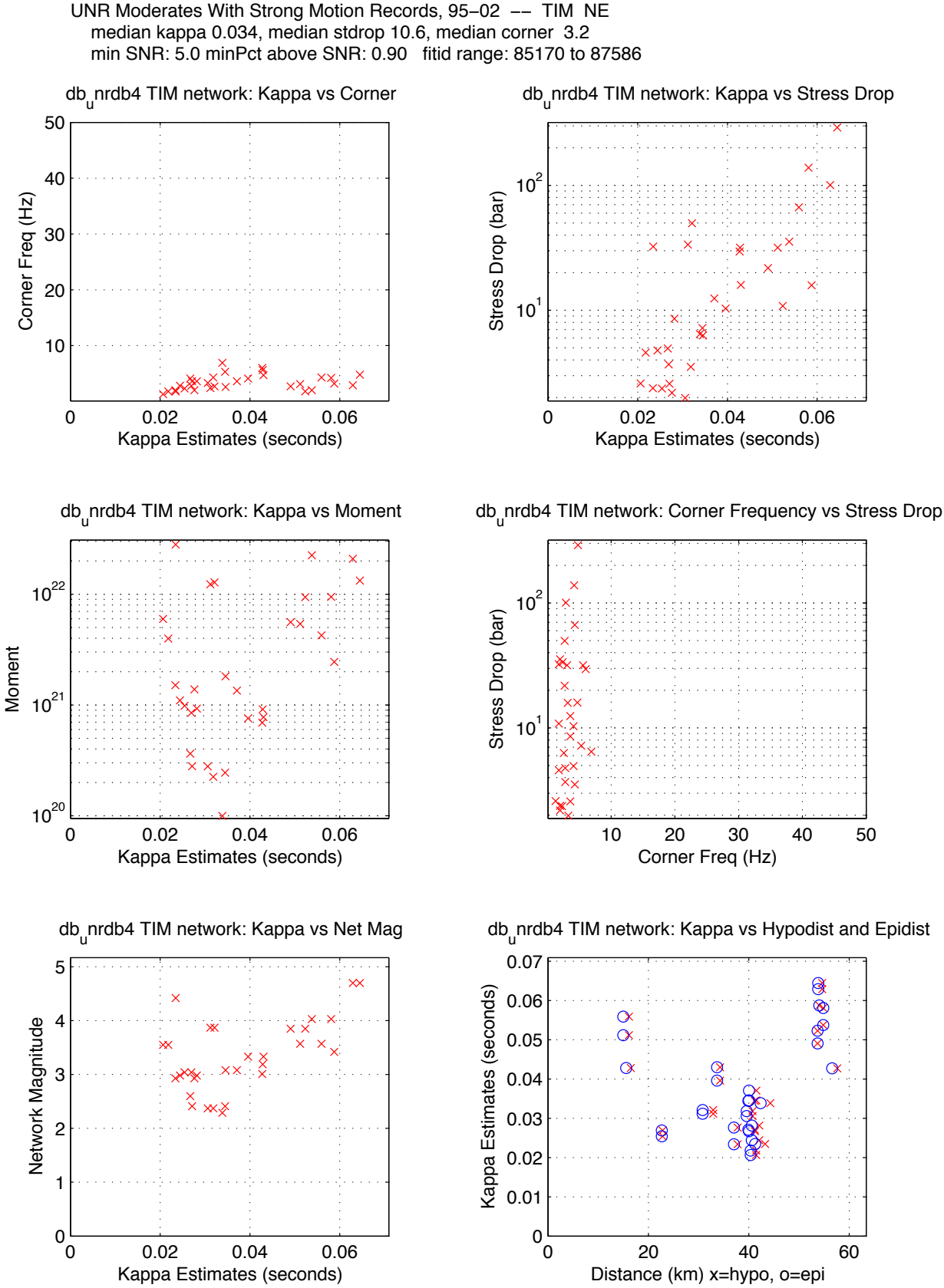

TIM:NE Passing: 32, Fail SNR: < 5 in 0.9 of freq range = 0, Fail SqErr: > 0.3 = 0, Fail StDrop: > 5000 = 0
TIM:NE Fail High Corner: > 45 Hz = 5

Figure B 58. Station TIM parametric plot. Fixed stress drop.
Source: DID 006GB.003, directory kappawrap/case6a/Figs45
File TIM.85170_87586.NE.fixed.eps

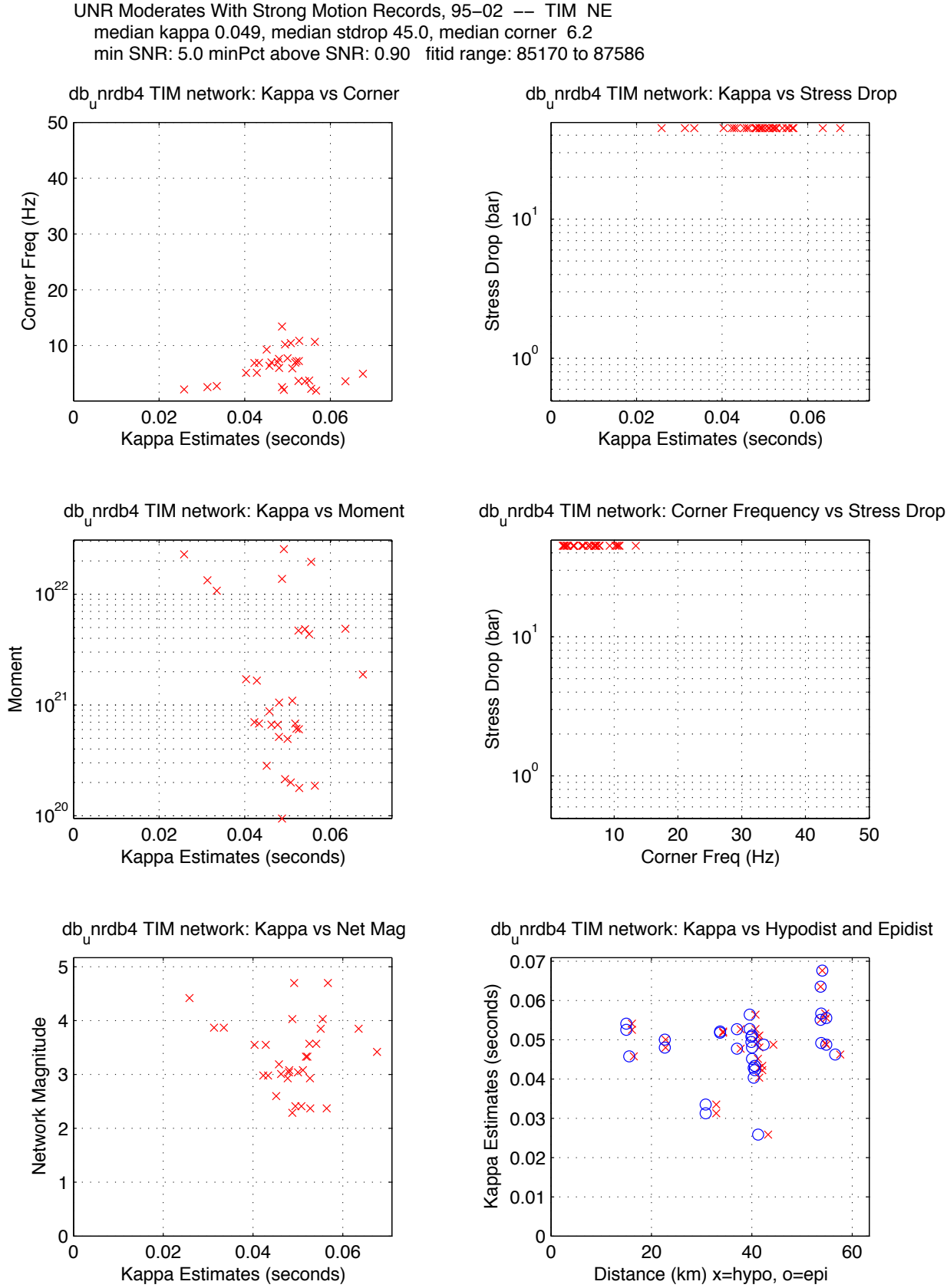

TIM:NE Passing: 32, Fail SNR: < 5 in 0.9 of freq range = 0, Fail SqErr: > 0.3 = 0, Fail StDrop: > 5000 = 0
TIM:NE Fail High Corner: > 45 Hz = 5

Figure B 59. Station TPW parametric plot. Free stress drop.
Source: DID 006GB.003, directory kappawrap/case6a/Figs45
File TPW.85170_87586.NE.eps

UNR Moderates With Strong Motion Records, 95–02 –– TPW NE
median kappa 0.019, median stdrop 3.1, median corner 3.3
min SNR: 5.0 minPct above SNR: 0.90 fitid range: 85170 to 87586

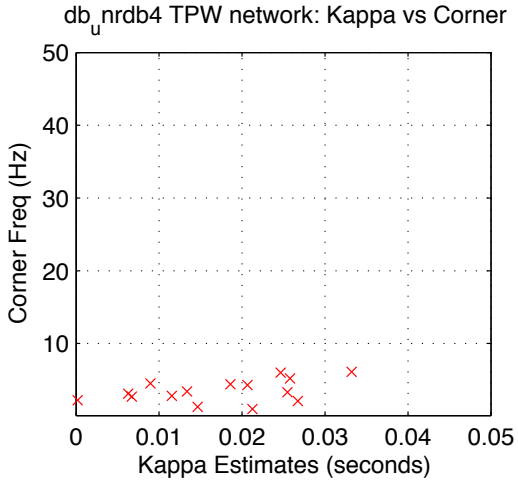

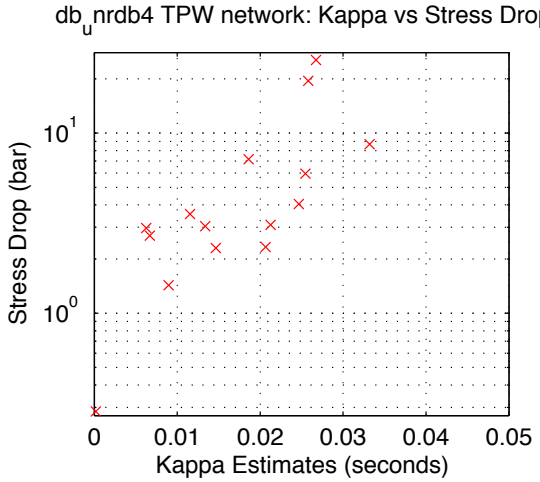

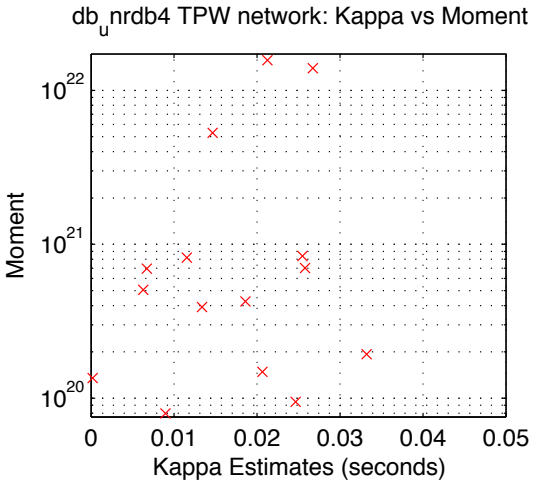

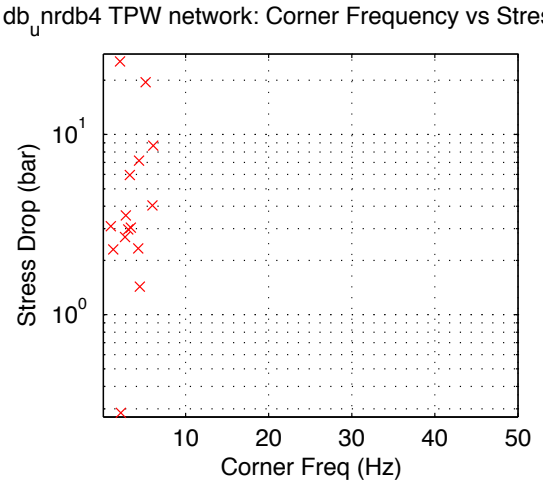

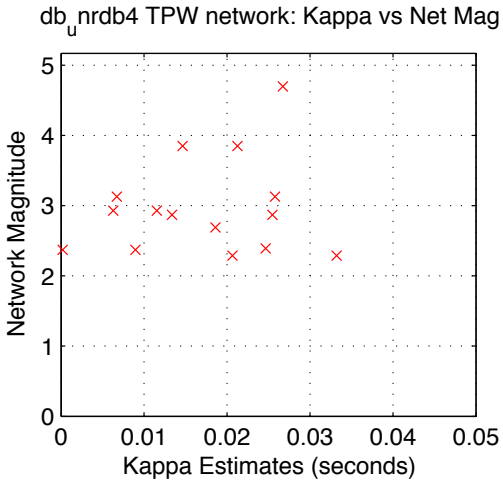

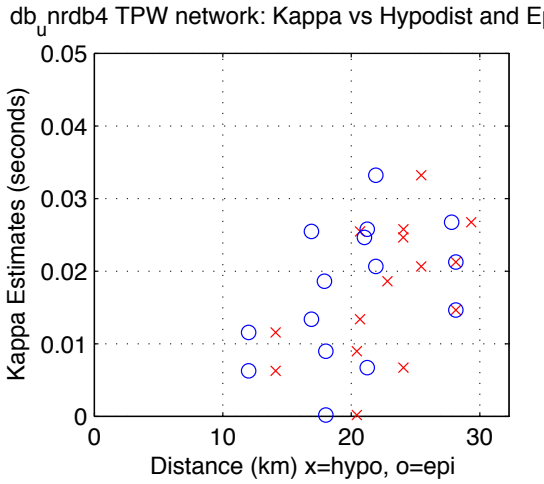

TPW:NE Passing: 15, Fail SNR: < 5 in 0.9 of freq range = 0, Fail SqErr: > 0.3 = 0, Fail StDrop: > 5000 = 0
TPW:NE Fail High Corner: > 45 Hz = 13

Figure B 60. Station TPW parametric plot. Fixed stress drop.
Source: DID 006GB.003, directory kappawrap/case6a/Figs45
File TPW.85170_87586.NE.fixed.eps

UNR Moderates With Strong Motion Records, 95–02 –– TPW NE
median kappa 0.036, median stdrop 45.0, median corner 8.7
min SNR: 5.0 minPct above SNR: 0.90 fitid range: 85170 to 87586

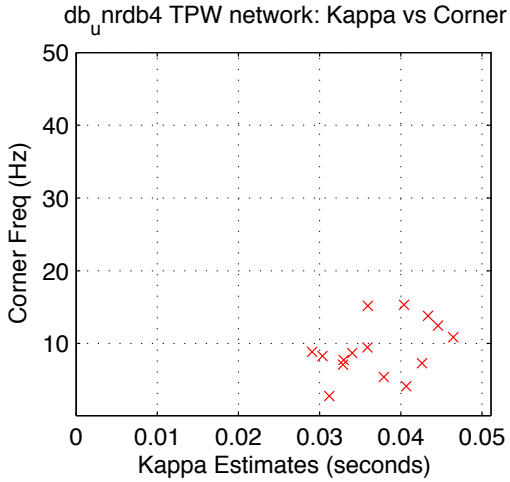

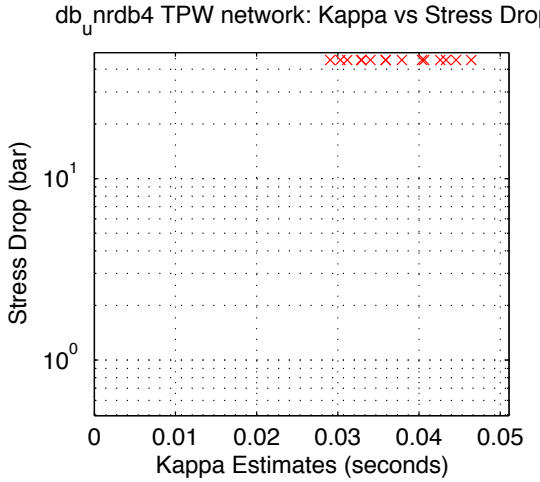

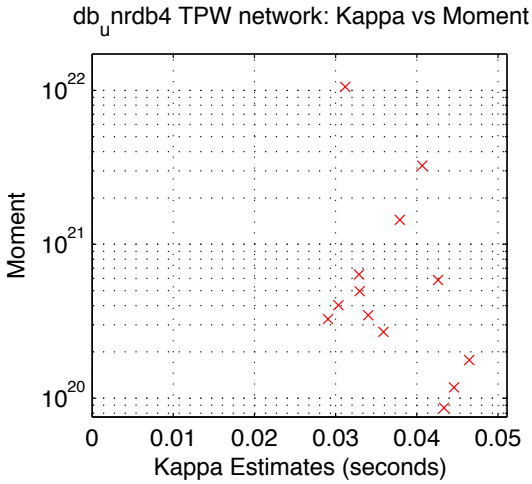

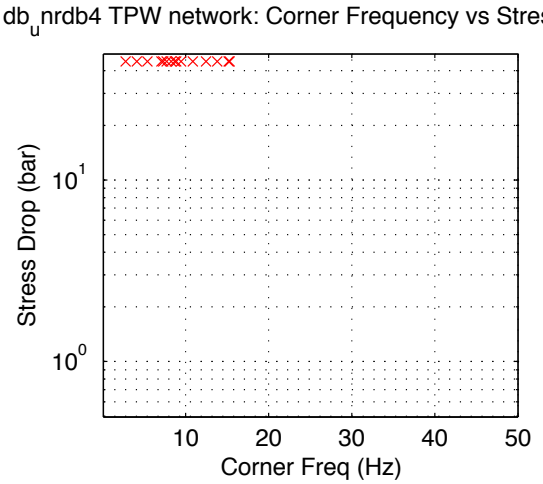

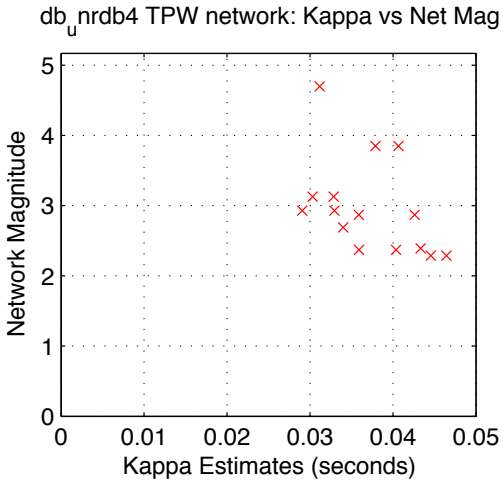

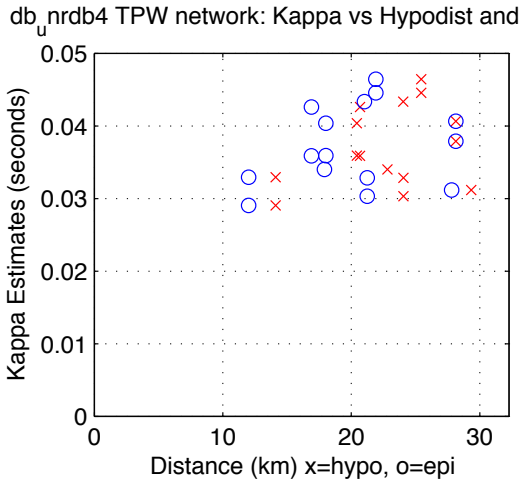

TPW:NE Passing: 15, Fail SNR: < 5 in 0.9 of freq range = 0, Fail SqErr: > 0.3 = 0, Fail StDrop: > 5000 = 0
TPW:NE Fail High Corner: > 45 Hz = 13

Figure B 61. Station TWP parametric plot. Free stress drop.
Source: DID 006GB.003, directory kappawrap/case6a/Figs45
File TWP.85170_87586.NE.eps

UNR Moderates With Strong Motion Records, 95–02 –– TWP NE
median kappa 0.016, median stdrop 4.3, median corner 3.8
min SNR: 5.0 minPct above SNR: 0.90 fitid range: 85170 to 87586

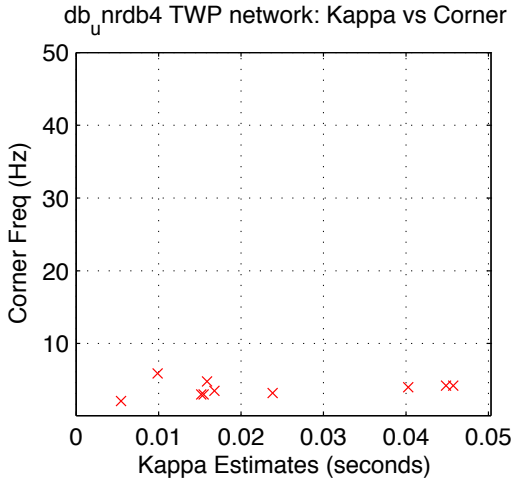

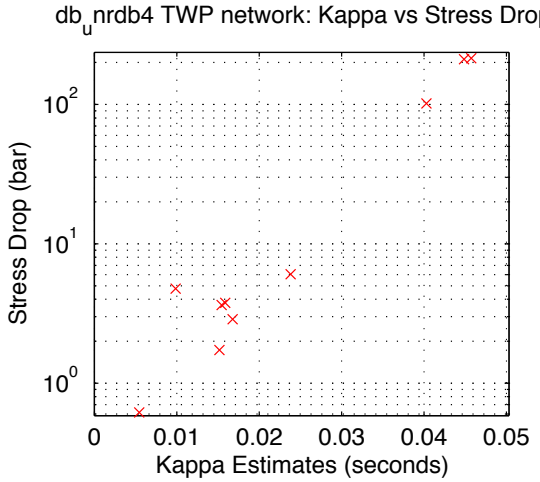

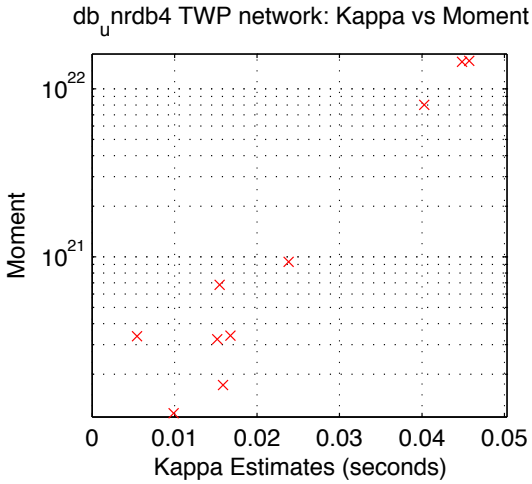

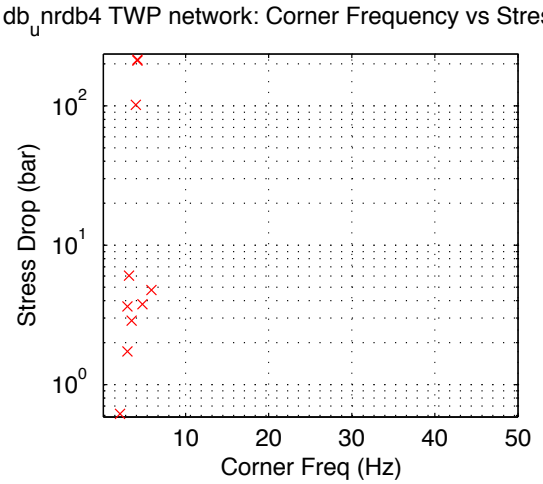

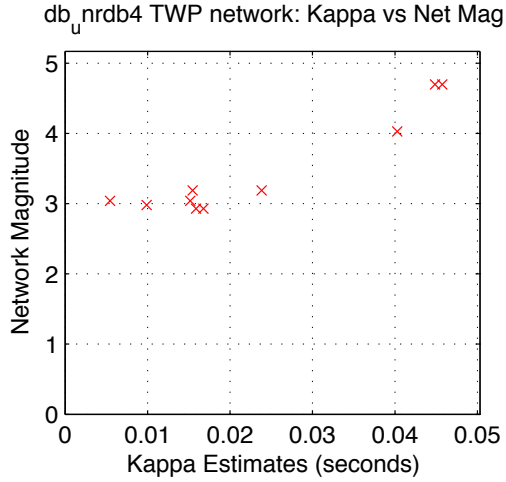

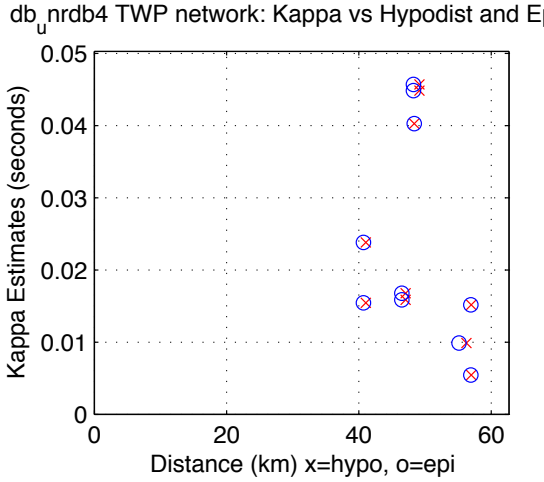

TWP:NE Passing: 10, Fail SNR: < 5 in 0.9 of freq range = 0, Fail SqErr: > 0.3 = 0, Fail StDrop: > 5000 = 0
TWP:NE Fail High Corner: > 45 Hz = 1

Figure B 62. Station TWP parametric plot. Fixed stress drop.
Source: DID 006GB.003, directory kappawrap/case6a/Figs45
File TWP.85170_87586.NE.fixed.eps

UNR Moderates With Strong Motion Records, 95–02 –– TWP NE
median kappa 0.036, median stdrop 45.0, median corner 9.0
min SNR: 5.0 minPct above SNR: 0.90 fitid range: 85170 to 87586

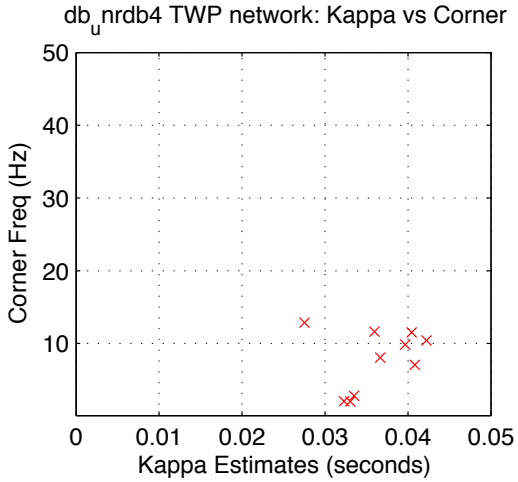

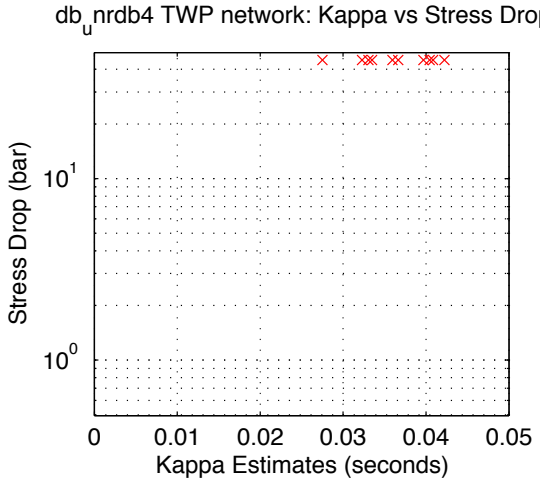

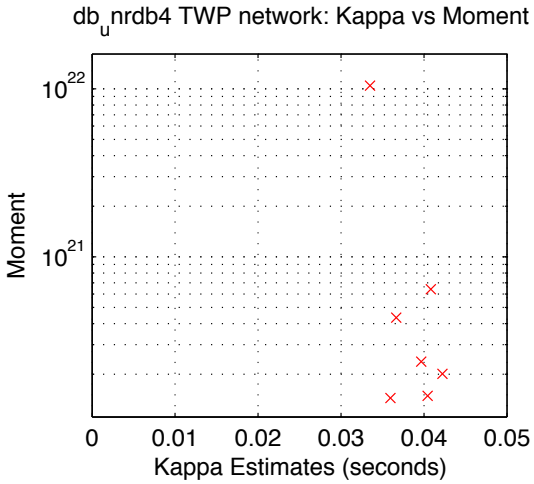

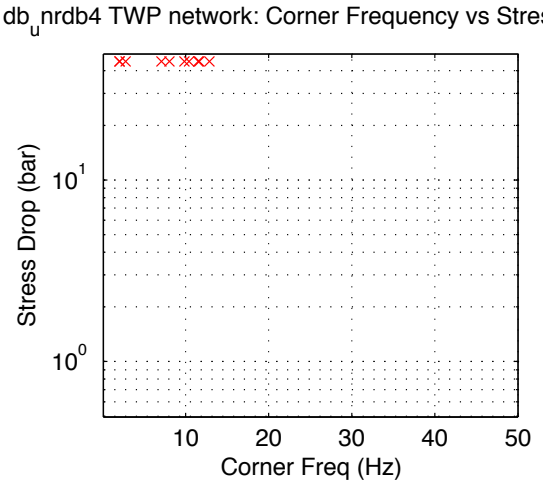

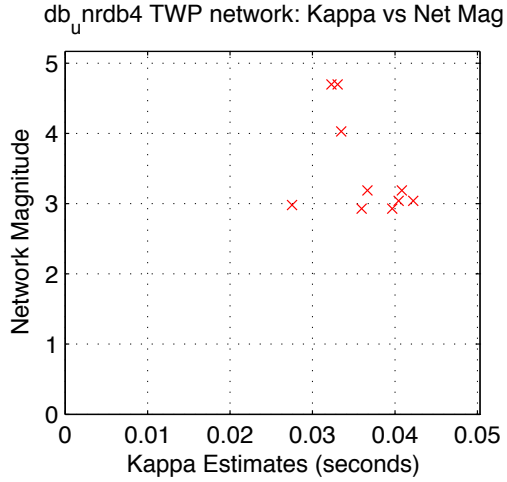

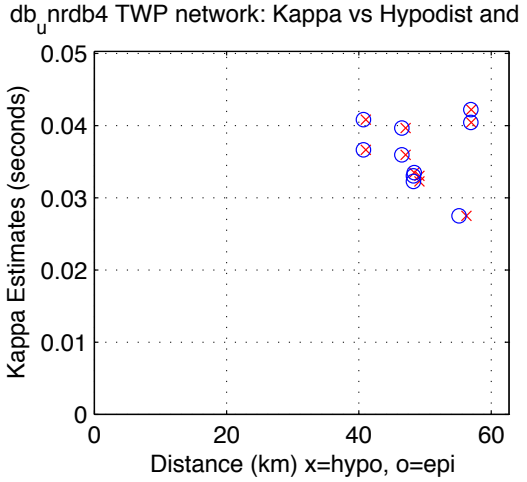

TWP:NE Passing: 10, Fail SNR: < 5 in 0.9 of freq range = 0, Fail SqErr: > 0.3 = 0, Fail StDrop: > 5000 = 0
TWP:NE Fail High Corner: > 45 Hz = 1

Figure B 63. Station TYM parametric plot. Free stress drop.
Source: DID 006GB.003, directory kappawrap/case6a/Figs45
File TYM.85170_87586.NE.eps

UNR Moderates With Strong Motion Records, 95–02 –– TYM NE
median kappa 0.027, median stdrop 3.7, median corner 3.7
min SNR: 5.0 minPct above SNR: 0.90 fitid range: 85170 to 87586

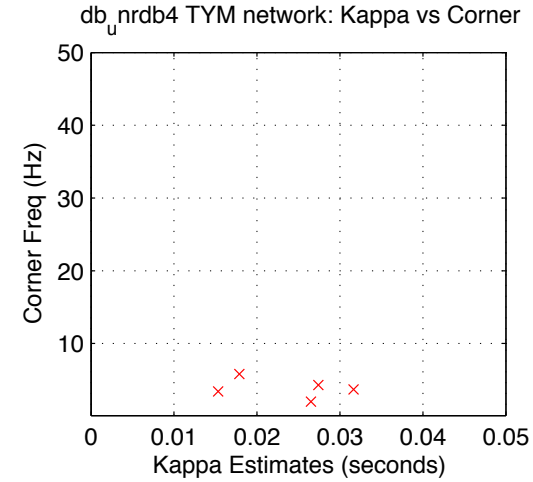

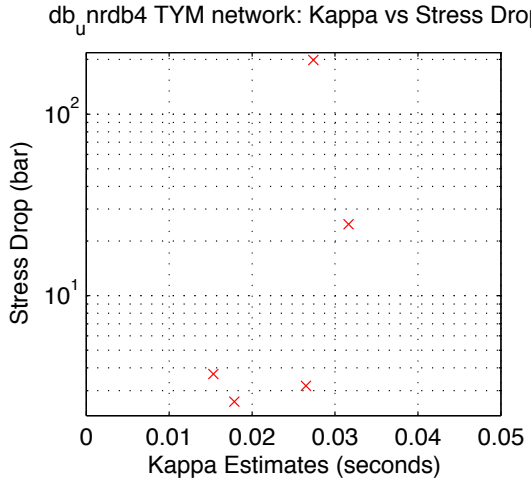

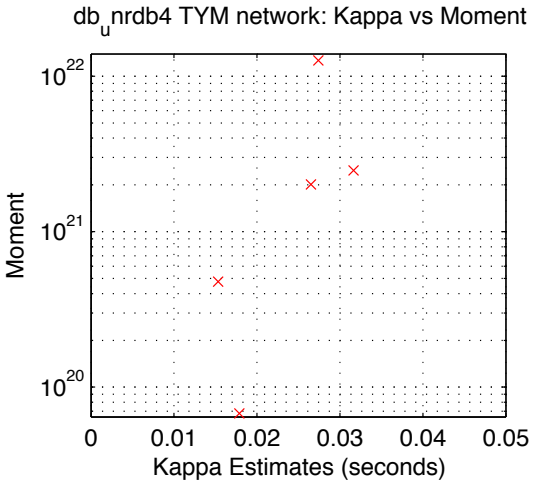

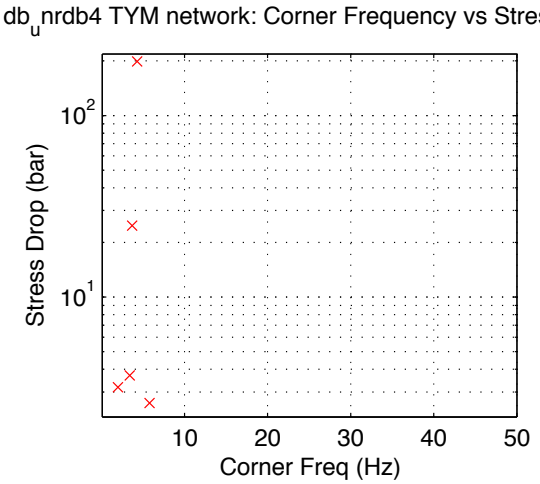

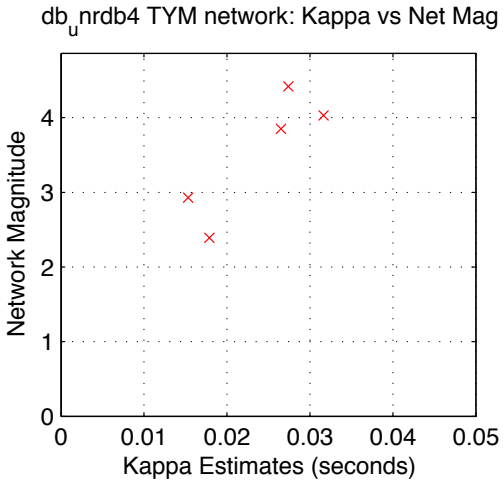

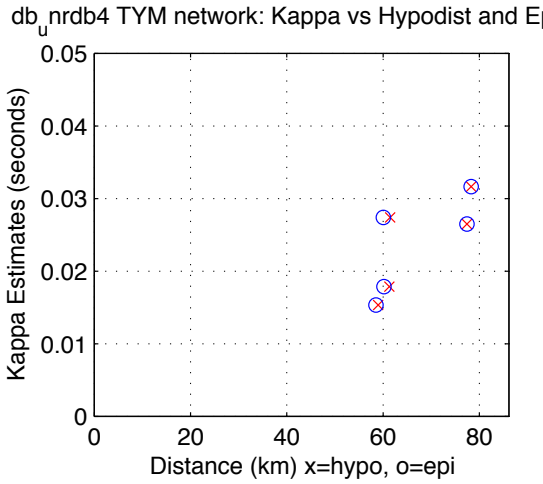

TYM:NE Passing: 5, Fail SNR: < 5 in 0.9 of freq range = 0, Fail SqErr: > 0.3 = 0, Fail StDrop: > 5000 = 0
TYM:NE Fail High Corner: > 45 Hz = 0

Figure B 64. Station TYM parametric plot. Fixed stress drop.
Source: DID 006GB.003, directory kappawrap/case6a/Figs45
File TYM.85170_87586.NE.fixed.eps

UNR Moderates With Strong Motion Records, 95–02 –– TYM NE
median kappa 0.037, median stdrop 45.0, median corner 6.3
min SNR: 5.0 minPct above SNR: 0.90 fitid range: 85170 to 87586

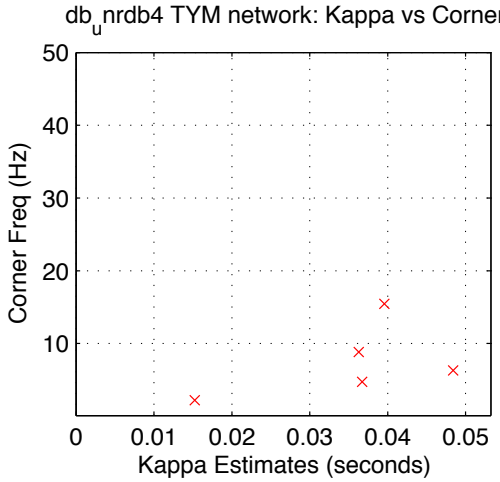

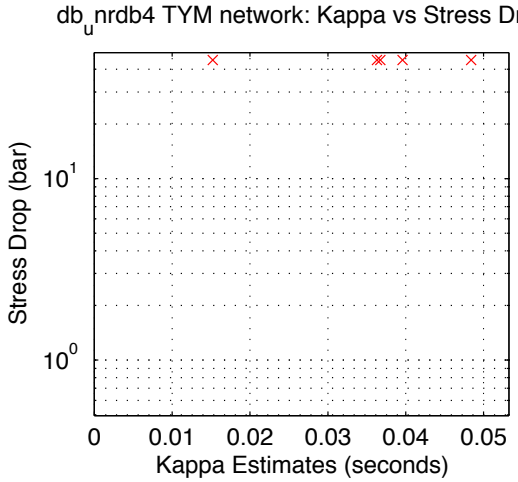

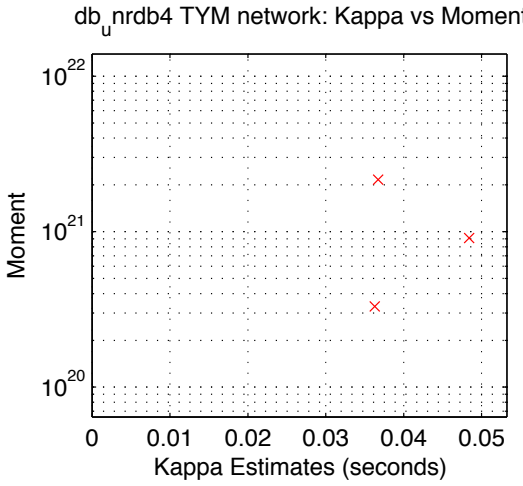

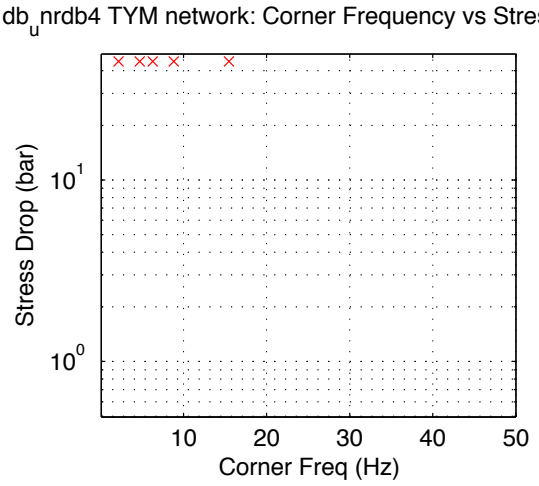

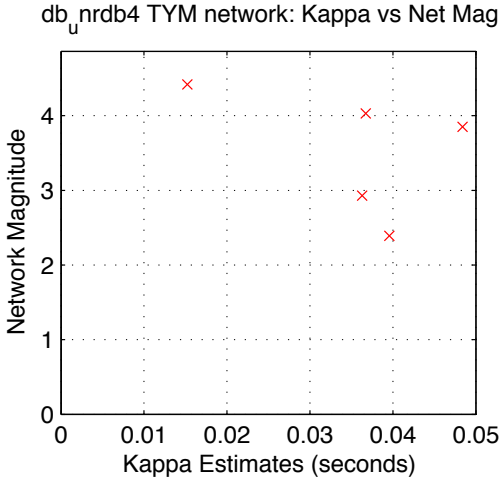

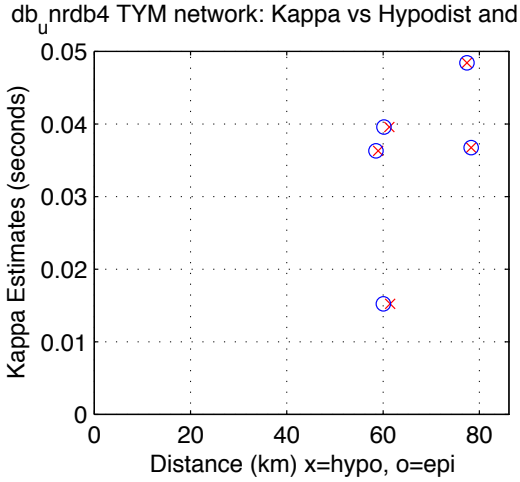

TYM:NE Passing: 5, Fail SNR: < 5 in 0.9 of freq range = 0, Fail SqErr: > 0.3 = 0, Fail StDrop: > 5000 = 0
TYM:NE Fail High Corner: > 45 Hz = 0

Figure B 65. Station TYMS parametric plot. Free stress drop.
Source: DID 006GB.003, directory kappawrap/case6a/Figs45
File TYMS.85170_87586.NE.eps

UNR Moderates With Strong Motion Records, 95–02 –– TYMS NE
median kappa 0.029, median stdrop 17.3, median corner 2.0
min SNR: 5.0 minPct above SNR: 0.90 fitid range: 85170 to 87586

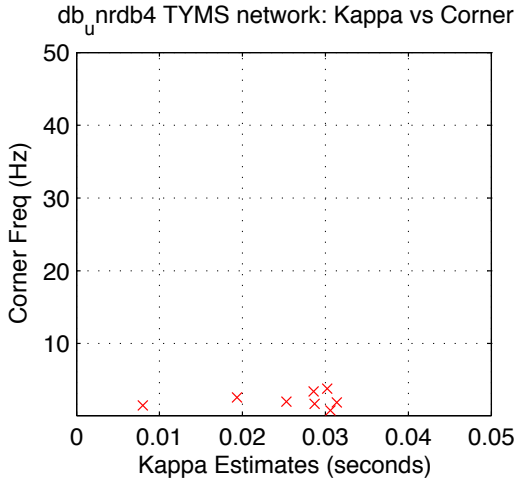

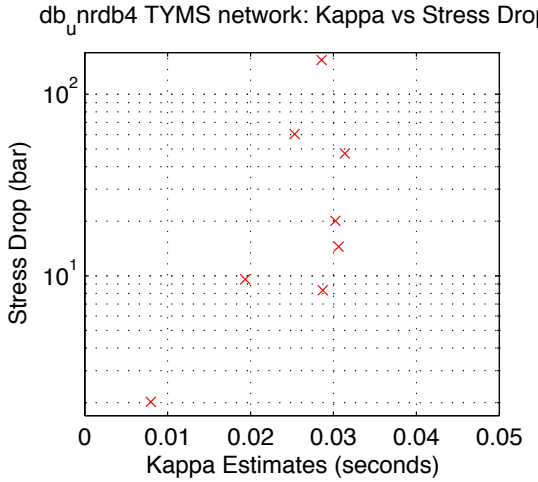

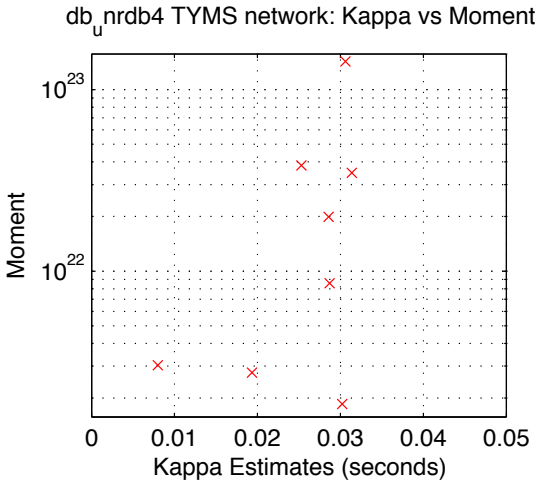

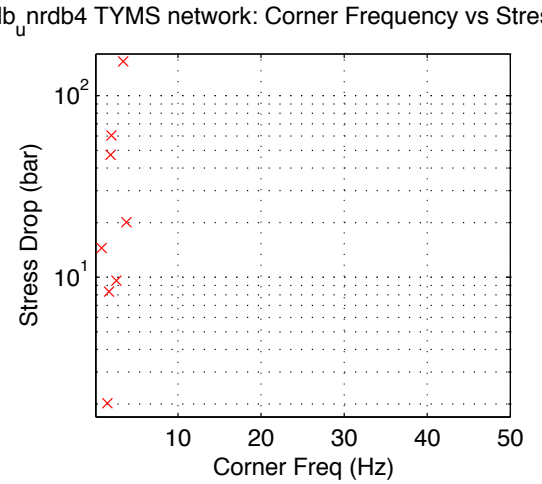

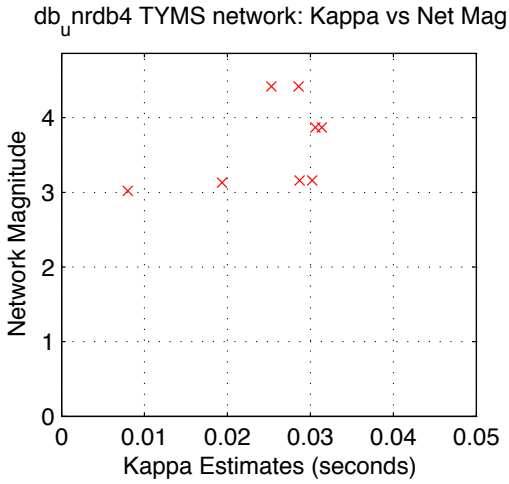

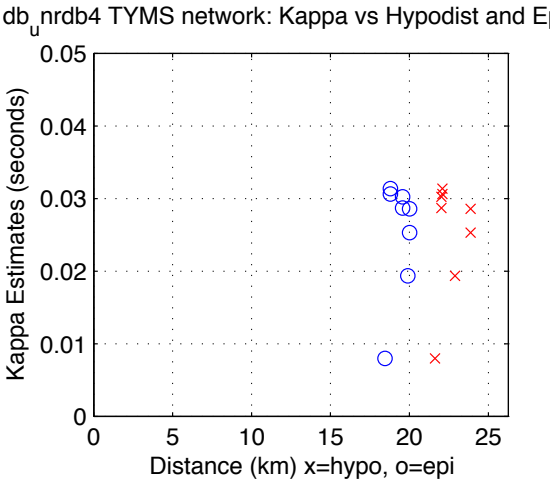

TYMS:NE Passing: 8, Fail SNR: < 5 in 0.9 of freq range = 14, Fail SqErr: > 0.3 = 0, Fail StDrop: > 5000 = 0
TYMS:NE Fail High Corner: > 45 Hz = 0

Figure B 66. Station TYMS parametric plot. Free stress drop.
Source: DID 006GB.003, directory kappawrap/case6a/Figs45
File TYMS.85170_87586.NE.eps

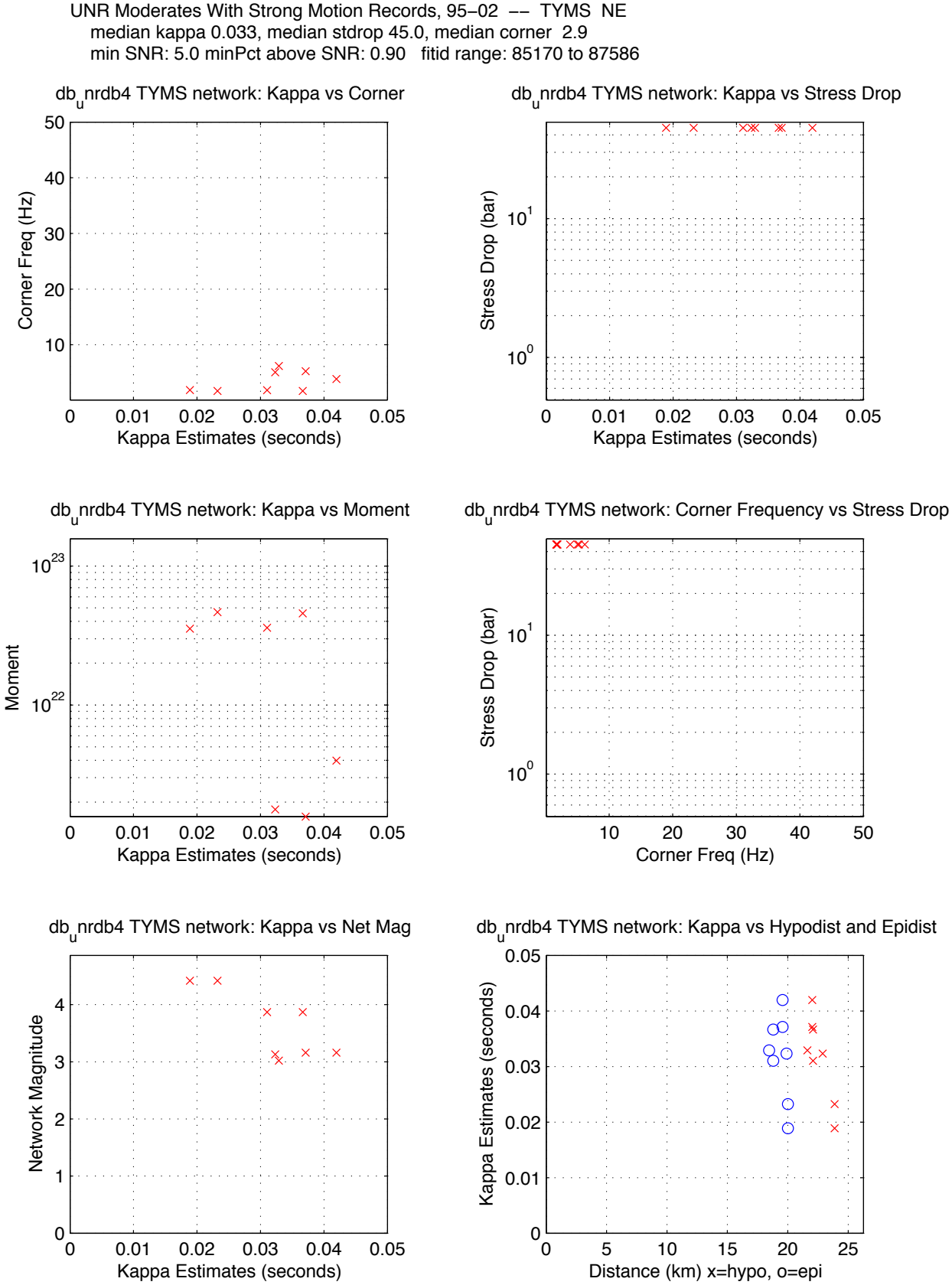

TYMS:NE Passing: 8, Fail SNR: < 5 in 0.9 of freq range = 14, Fail SqErr: > 0.3 = 0, Fail StDrop: > 5000 = 0
TYMS:NE Fail High Corner: > 45 Hz = 0

Figure B 67. Station WCTS parametric plot. Free stress drop.
Source: DID 006GB.003, directory kappawrap/case6a/Figs45
File WCTS.85170_87586.NE.eps

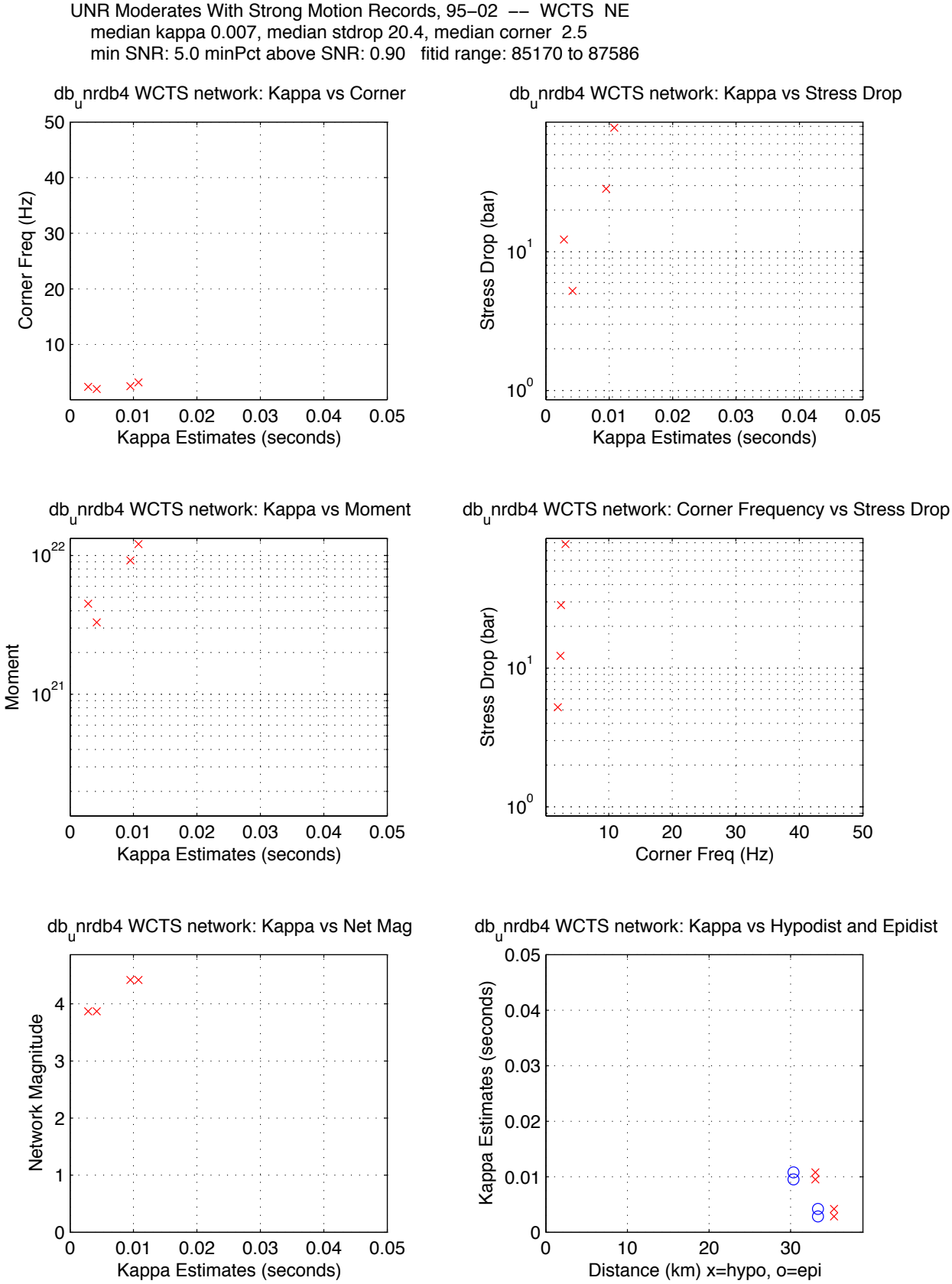

WCTS:NE Passing: 4, Fail SNR: < 5 in 0.9 of freq range = 9, Fail SqErr: > 0.3 = 0, Fail StDrop: > 5000 = 0
WCTS:NE Fail High Corner: > 45 Hz = 0

Figure B 68. Station WCTS parametric plot. Fixed stress drop.
Source: DID 006GB.003, directory kappawrap/case6a/Figs45
File WCTS.85170_87586.NE.fixed.eps

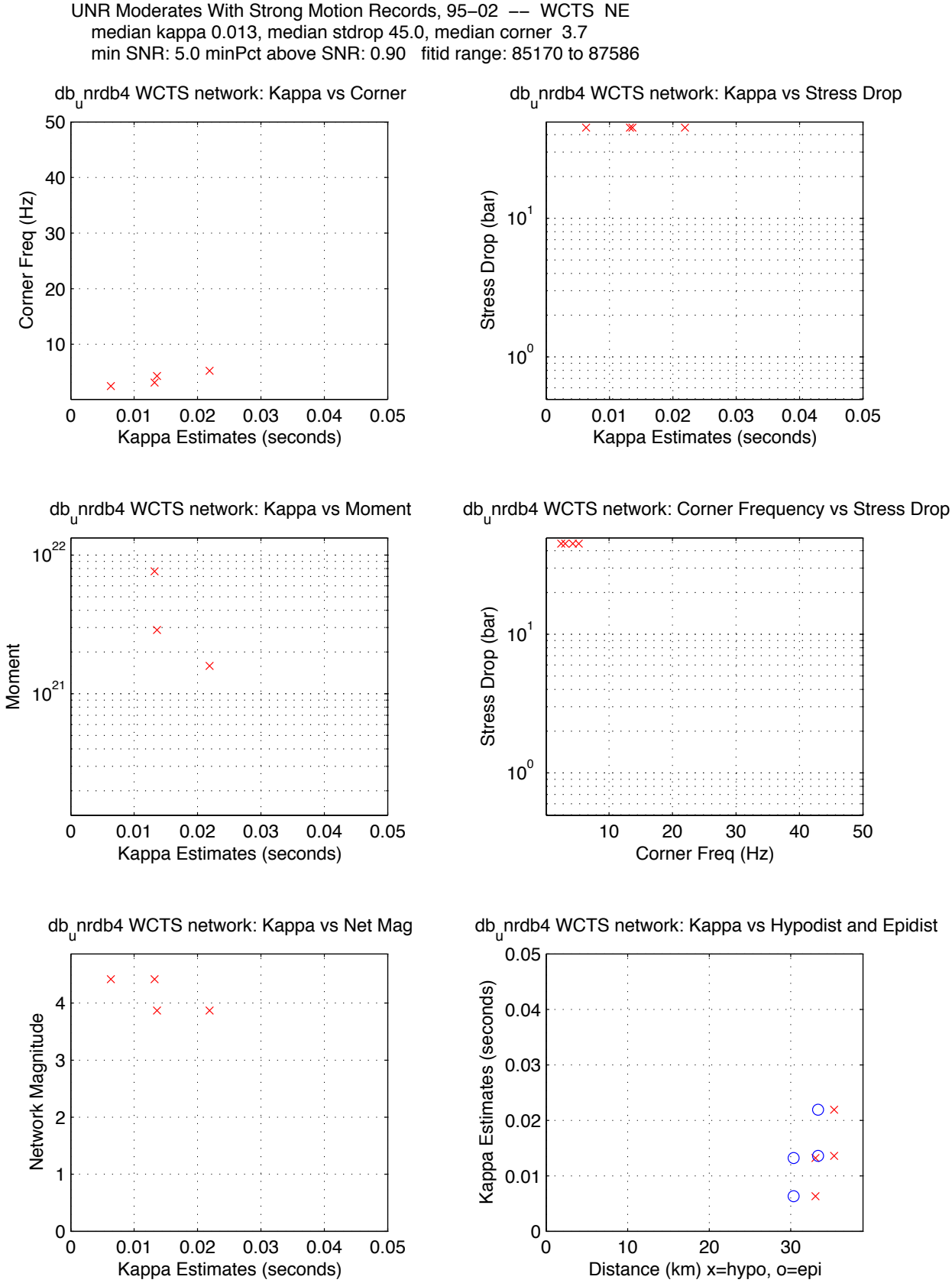

WCTS:NE Passing: 4, Fail SNR: < 5 in 0.9 of freq range = 9, Fail SqErr: > 0.3 = 0, Fail StDrop: > 5000 = 0
WCTS:NE Fail High Corner: > 45 Hz = 0

Figure B 69. Station WLD parametric plot. Free stress drop.
Source: DID 006GB.003, directory kappawrap/case6a/Figs45
File WLD.85170_87586.NE.eps

UNR Moderates With Strong Motion Records, 95–02 –– WLD NE
median kappa 0.015, median stdrop 1.9, median corner 3.8
min SNR: 5.0 minPct above SNR: 0.90 fitid range: 85170 to 87586

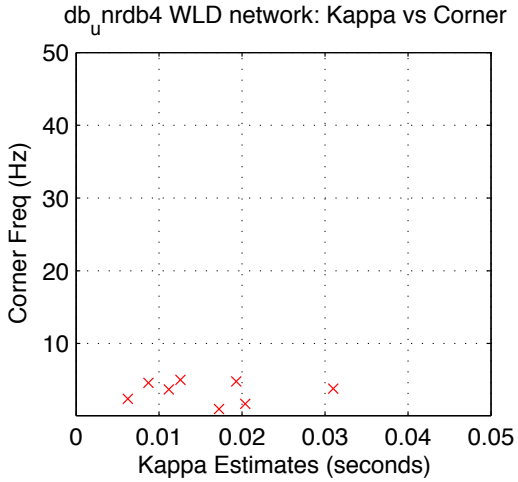

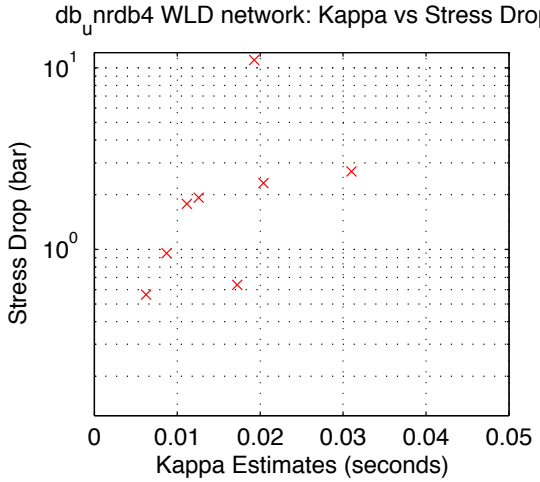

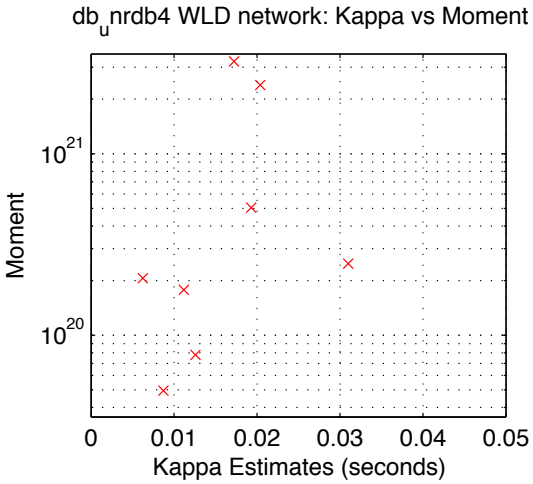

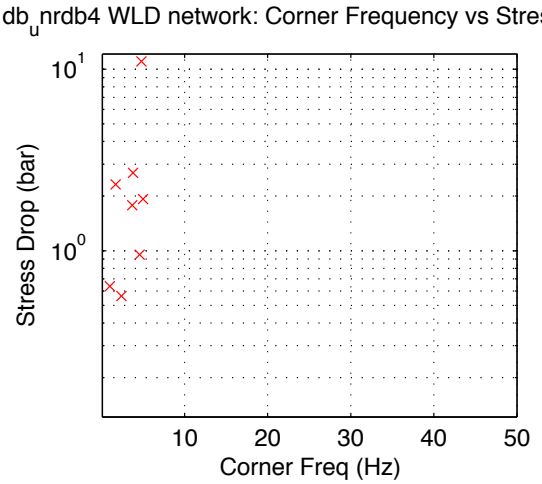

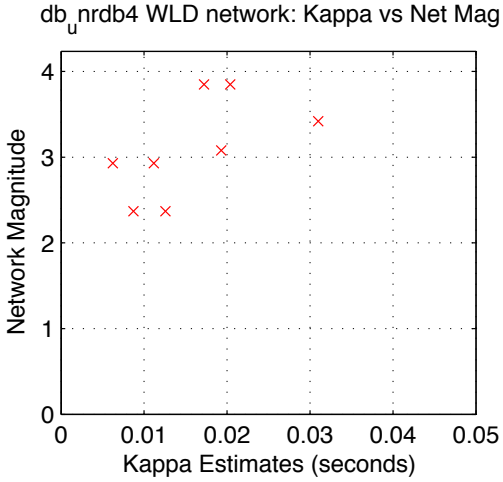

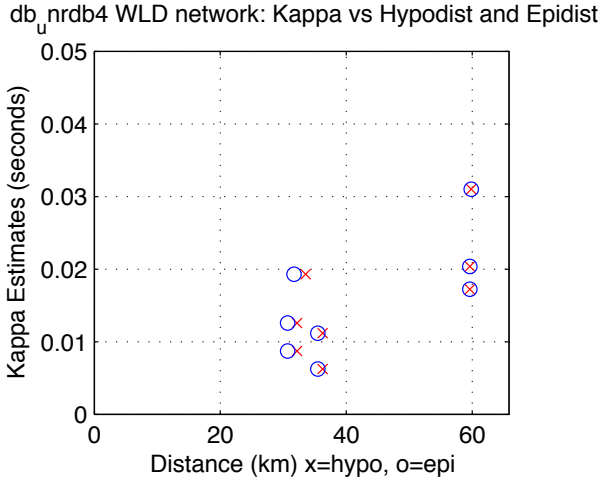

WLD:NE Passing: 8, Fail SNR: < 5 in 0.9 of freq range = 0, Fail SqErr: > 0.3 = 0, Fail StDrop: > 5000 = 0
WLD:NE Fail High Corner: > 45 Hz = 3

Figure B 70. Station WLD parametric plot. Fixed stress drop.
Source: DID 006GB.003, directory kappawrap/case6a/Figs45
File WLD.85170_87586.NE.fixed.eps

UNR Moderates With Strong Motion Records, 95–02 –– WLD NE
median kappa 0.040, median stdrop 45.0, median corner 11.4
min SNR: 5.0 minPct above SNR: 0.90 fitid range: 85170 to 87586

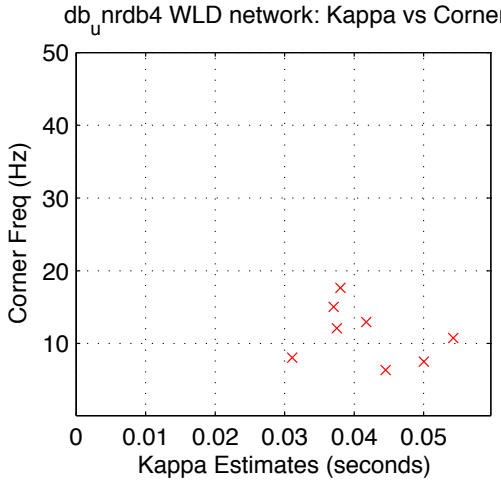

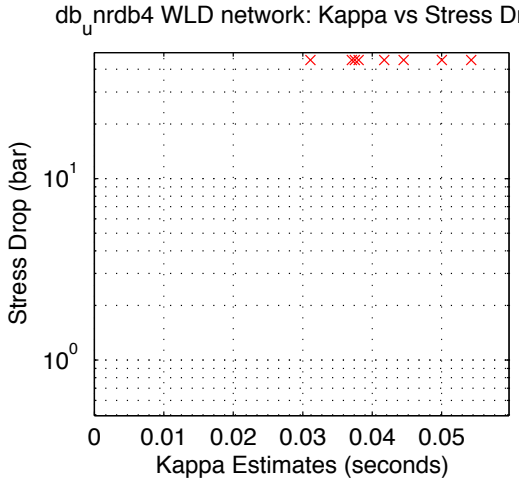

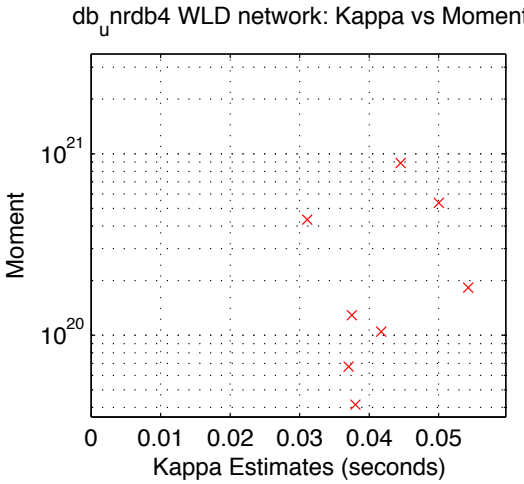

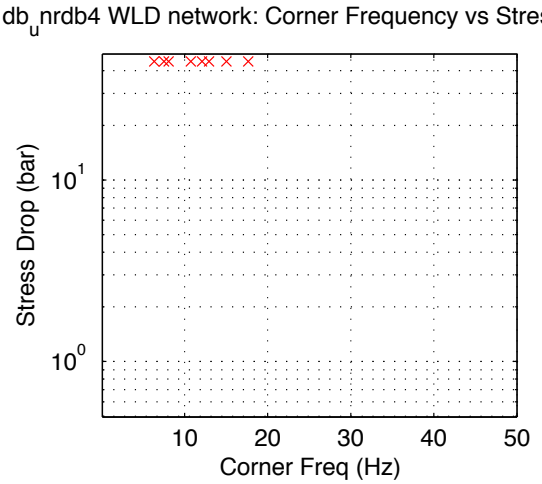

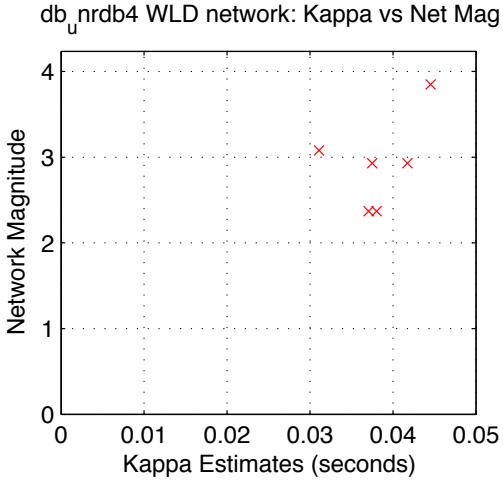

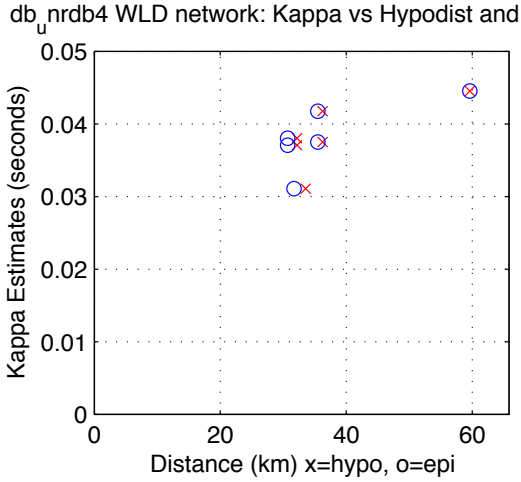

WLD:NE Passing: 8, Fail SNR: < 5 in 0.9 of freq range = 0, Fail SqErr: > 0.3 = 0, Fail StDrop: > 5000 = 0
WLD:NE Fail High Corner: > 45 Hz = 3

Figure B 71. Station YCW parametric plot. Free stress drop.
Source: DID 006GB.003, directory kappawrap/case6a/Figs45
File YCW.85170_87586.NE.eps

UNR Moderates With Strong Motion Records, 95–02 –– YCW NE
median kappa 0.023, median stdrop 6.6, median corner 3.3
min SNR: 5.0 minPct above SNR: 0.90 fitid range: 85170 to 87586

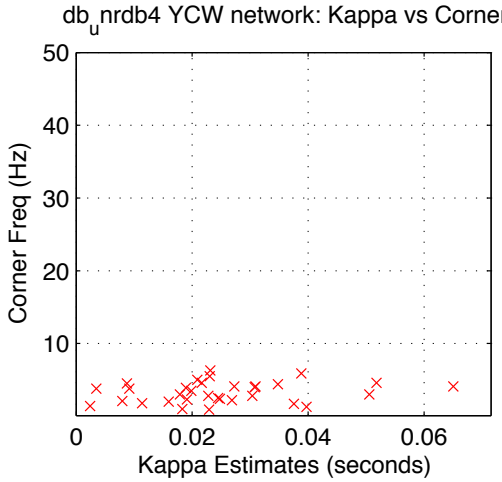

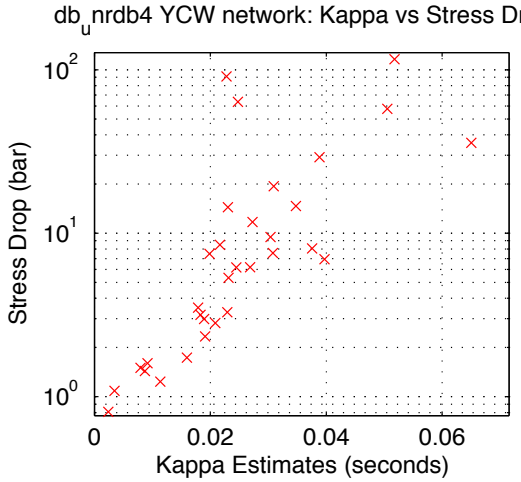

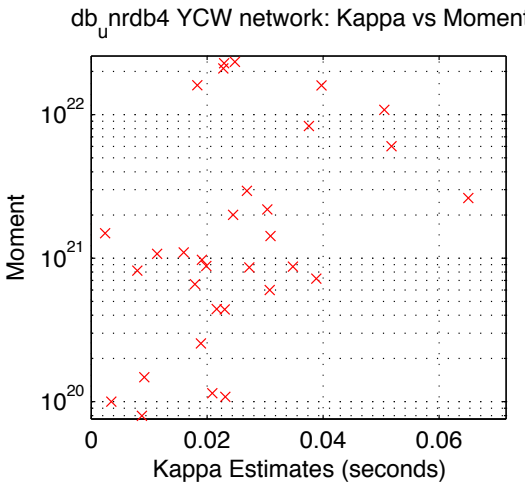

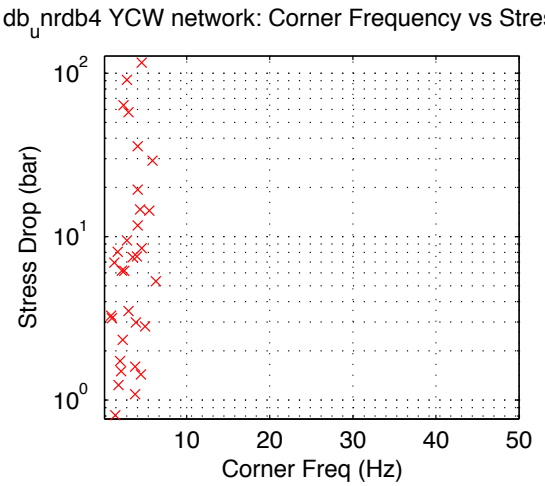

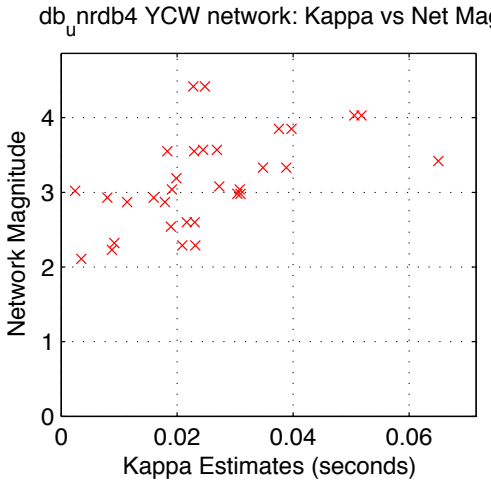

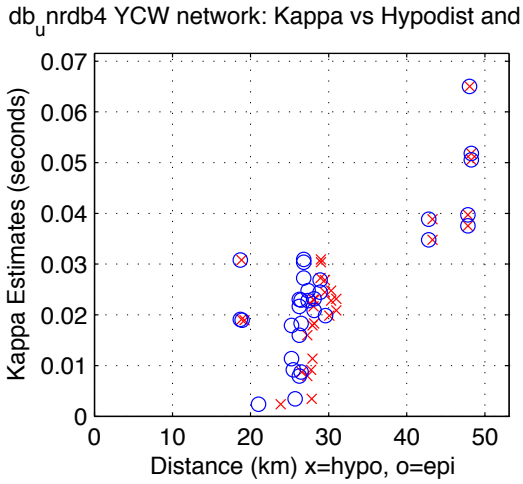

YCW:NE Passing: 32, Fail SNR: < 5 in 0.9 of freq range = 0, Fail SqErr: > 0.3 = 0, Fail StDrop: > 5000 = 0
YCW:NE Fail High Corner: > 45 Hz = 3

Figure B 72. Station YCW parametric plot. Fixed stress drop.
Source: DID 006GB.003, directory kappawrap/case6a/Figs45
File YCW.85170_87586.NE.fixed.eps

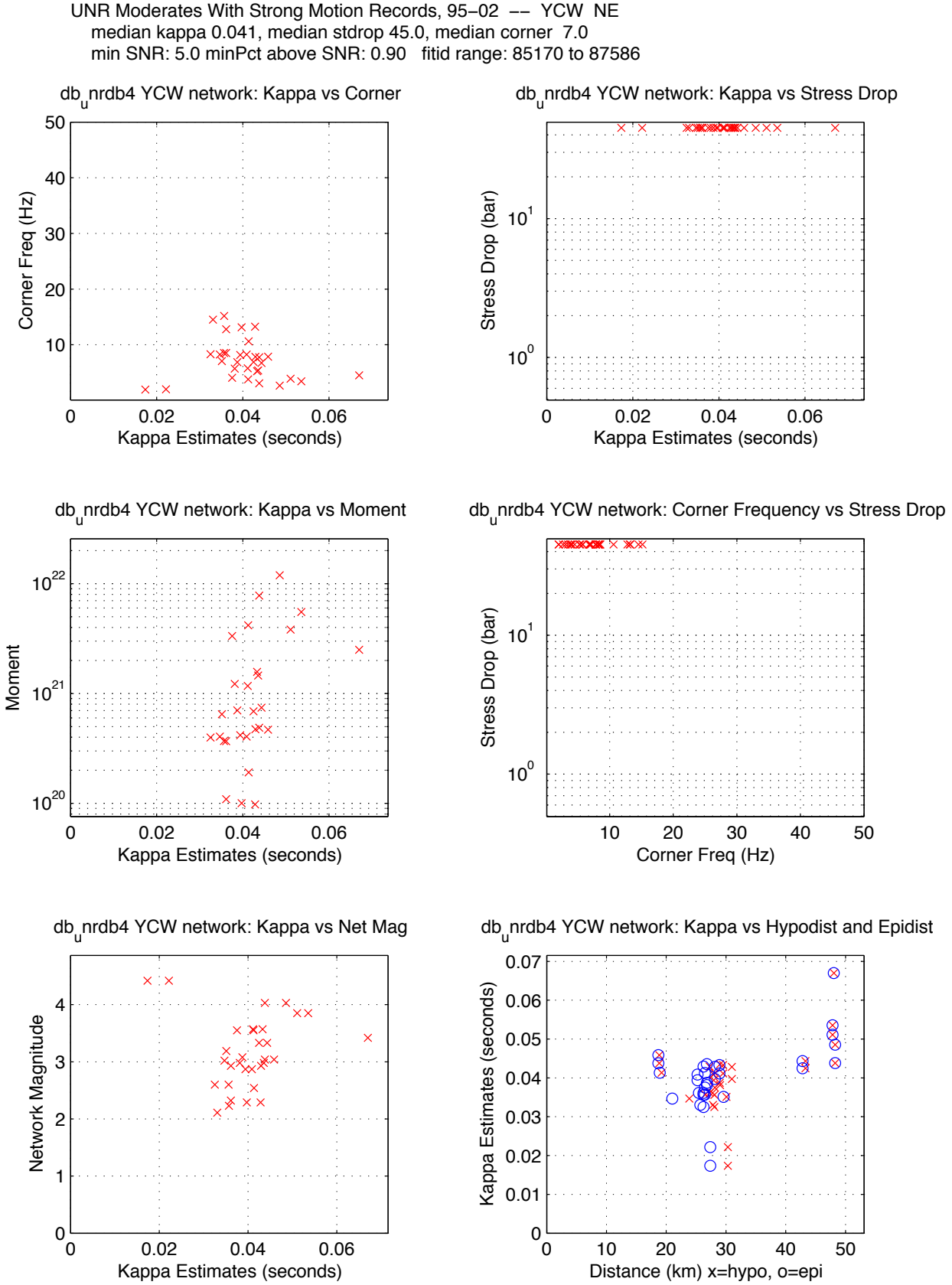

YCW:NE Passing: 32, Fail SNR: < 5 in 0.9 of freq range = 0, Fail SqErr: > 0.3 = 0, Fail StDrop: > 5000 = 0
YCW:NE Fail High Corner: > 45 Hz = 3